

Molecular Symmetry

David J. Willock

 WILEY

Molecular Symmetry

Molecular Symmetry

DAVID J. WILLOCK

Cardiff University



A John Wiley and Sons, Ltd, Publication

This edition first published 2009

© 2009 John Wiley & Sons Ltd

Registered office

John Wiley & Sons Ltd, The Atrium, Southern Gate, Chichester, West Sussex,
PO19 8SQ, United Kingdom

For details of our global editorial offices, for customer services and for information about how to apply for permission to reuse the copyright material in this book please see our website at www.wiley.com.

The right of the author to be identified as the author of this work has been asserted in accordance with the Copyright, Designs and Patents Act 1988.

All rights reserved. No part of this publication may be reproduced, stored in a retrieval system, or transmitted, in any form or by any means, electronic, mechanical, photocopying, recording or otherwise, except as permitted by the UK Copyright, Designs and Patents Act 1988, without the prior permission of the publisher.

Wiley also publishes its books in a variety of electronic formats. Some content that appears in print may not be available in electronic books.

Designations used by companies to distinguish their products are often claimed as trademarks. All brand names and product names used in this book are trade names, service marks, trademarks or registered trademarks of their respective owners. The publisher is not associated with any product or vendor mentioned in this book. This publication is designed to provide accurate and authoritative information in regard to the subject matter covered. It is sold on the understanding that the publisher is not engaged in rendering professional services. If professional advice or other expert assistance is required, the services of a competent professional should be sought.

The publisher and the author make no representations or warranties with respect to the accuracy or completeness of the contents of this work and specifically disclaim all warranties, including without limitation any implied warranties of fitness for a particular purpose. This work is sold with the understanding that the publisher is not engaged in rendering professional services. The advice and strategies contained herein may not be suitable for every situation. In view of ongoing research, equipment modifications, changes in governmental regulations, and the constant flow of information relating to the use of experimental reagents, equipment, and devices, the reader is urged to review and evaluate the information provided in the package insert or instructions for each chemical, piece of equipment, reagent, or device for, among other things, any changes in the instructions or indication of usage and for added warnings and precautions. The fact that an organization or Website is referred to in this work as a citation and/or a potential source of further information does not mean that the author or the publisher endorses the information the organization or Website may provide or recommendations it may make. Further, readers should be aware that Internet Websites listed in this work may have changed or disappeared between when this work was written and when it is read. No warranty may be created or extended by any promotional statements for this work. Neither the publisher nor the author shall be liable for any damages arising herefrom.

A catalogue record for this book is available from the British Library

ISBN 978-0-470-85347-4 (hbk) 978-0-470-85348-1 (pbk)

Set in 10/12pt Times by Integra Software Services Pvt. Ltd, Pondicherry, India

Printed and bound in Great Britain by CPI Antony Rowe, Chippenham, Wiltshire

Contents

<i>Preface</i>	xi
1 Symmetry Elements and Operations	1
1.1 Introduction	1
1.2 Symmetry Elements and Operations	6
1.2.1 <i>Proper Rotations: C_n</i>	6
1.2.2 <i>The Plane of Symmetry: σ</i>	9
1.2.3 <i>The Inversion Centre: i</i>	13
1.3 Examples of the Impact of Geometric Symmetry on Chemistry	17
1.3.1 <i>Oxygen Transfer via Metal Porphyrins</i>	17
1.3.2 <i>Nuclear Magnetic Resonance: Chemical Equivalence</i>	18
1.4 Summary	22
1.5 Self-Test Questions	23
Further Reading	24
2 More Symmetry Operations and Products of Operations	25
2.1 Introduction	25
2.2 Background to Point Groups	25
2.3 Closed Groups and New Operations	26
2.3.1 <i>Products of Operations</i>	26
2.3.2 <i>Fixed Symmetry Elements</i>	29
2.3.3 <i>The Final Missing Operation, Improper Rotations: S_n</i>	31
2.3.4 <i>Equivalences for Improper Rotation Operations</i>	34
2.4 Properties of Symmetry Operations	37
2.4.1 <i>Equivalent Operations and Equivalent Atoms</i>	37
2.4.2 <i>The Inverse of an Operation</i>	38
2.4.3 <i>The Order of the Product; Operations that Commute</i>	39
2.5 Chirality and Symmetry	41
2.6 Summary	42
2.7 Completed Multiplication Tables	43
2.8 Self-Test Questions	44
3 The Point Groups Used with Molecules	45
3.1 Introduction	45
3.2 Molecular Classification Using Symmetry Operations	45
3.3 Constructing Reference Models with Idealized Symmetry	47

3.4	The Nonaxial Groups: C_s , C_i , C_1	48
3.4.1	<i>Examples of Molecules for the Nonaxial Groups: C_s, C_i, C_1</i>	49
3.5	The Cyclic Groups: C_n , S_n	50
3.5.1	<i>Examples of Molecules for the Cyclic Groups: C_n, S_n</i>	52
3.6	Axial Groups Containing Mirror Planes: C_{nh} and C_{nv}	55
3.6.1	<i>Examples of Molecules for Axial Groups Containing Mirror Planes: C_{nh} and C_{nv}</i>	58
3.7	Axial Groups with Multiple Rotation Axes: D_n , D_{nd} and D_{nh}	59
3.7.1	<i>Examples of Axial Groups with Multiple Rotation Axes: D_n, D_{nd} and D_{nh}</i>	61
3.8	Special Groups for Linear Molecules: $C_{\infty v}$ and $D_{\infty h}$	64
3.9	The Cubic Groups: T_d and O_h	65
3.10	Assigning Point Groups to Molecules	69
3.11	Example Point Group Assignments	69
3.11.1	<i>Example 1: Conformations of Cyclohexane</i>	69
3.11.2	<i>Example 2: Six-Coordinate Metal Complexes</i>	72
3.12	Self-Test Questions	73
4	Point Group Representations, Matrices and Basis Sets	75
4.1	Introduction	75
4.2	Symmetry Representations and Characters	75
4.2.1	<i>Water; H_2O, C_{2v}</i>	75
4.2.2	<i>Direct Products</i>	79
4.3	Multiplication Tables for Character Representations	81
4.4	Matrices and Symmetry Operations	82
4.5	Diagonal and Off-Diagonal Matrix Elements	85
4.5.1	<i>Ammonia, NH_3, C_{3v}</i>	85
4.6	The Trace of a Matrix as the Character for an Operation	87
4.7	Noninteger Characters	88
4.7.1	<i>Boron Trifluoride, BF_3, D_{3h}</i>	88
4.8	Reducible Representations	91
4.8.1	<i>Water; H_2O, C_{2v}</i>	91
4.9	Classes of Operations	93
4.9.1	<i>[$Ni(CN)_4$]$^{2-}$, D_{4h}</i>	93
4.10	Degenerate Irreducible Representations	96
4.10.1	<i>Ammonia, NH_3, C_{3v}</i>	98
4.11	The Labelling of Irreducible Representations	100
4.12	Summary	102
4.13	Completed Tables	102
4.14	Self-Test Questions	102
	Further Reading	103
5	Reducible and Irreducible Representations	105
5.1	Introduction	105
5.2	Irreducible Representations and Molecular Vibrations	107

5.3	Finding Reducible Representations	110
5.4	Properties of Point Groups and Irreducible Representations	112
5.5	The Reduction Formula	118
5.5.1	<i>Applying the Reduction Formula</i>	120
5.6	A Complete Set of Vibrational Modes for H ₂ O	122
5.7	Choosing the Basis Set	126
5.7.1	<i>Carbonyl Stretching Modes of [Fe(CO)₅], D_{3h}</i>	126
5.8	The d-Orbitals in Common Transition Metal Complex Geometries	128
5.8.1	<i>Square Planar, D_{4h}</i>	132
5.8.2	<i>Tetrahedral, T_d</i>	137
5.8.3	<i>Octahedral, O_h</i>	142
5.8.4	<i>Trigonal Bipyramidal, D_{3h}</i>	147
5.9	Linear Molecules: Groups of Infinite Order	154
5.10	Summary	161
5.11	Self-Test Questions	162
6	Applications in Vibrational Spectroscopy	163
6.1	Introduction	163
6.2	Selection Rules	165
6.2.1	<i>Infrared Spectroscopy</i>	165
6.2.2	<i>Infrared Absorption and the Greenhouse Gases</i>	173
6.2.3	<i>Interstellar H₂</i>	177
6.2.4	<i>Raman Spectroscopy</i>	177
6.2.5	<i>Comparison of Infrared and Raman Selection Rules</i>	184
6.3	General Approach to Analysing Vibrational Spectroscopy	186
6.3.1	<i>Example: the C—H Stretch Bands of 1,4-Difluorobenzene</i>	187
6.4	Symmetry-Adapted Linear Combinations	190
6.5	Normalization	193
6.6	The Projection Operator Method	195
6.6.1	<i>Projection Operator Applied to the C—H Stretches of 1,4-Difluorobenzene</i>	196
6.6.2	<i>The Projection Operator and Degenerate Representations</i>	198
6.7	Linking Results for Symmetry-Inequivalent Sets of Atoms	202
6.7.1	<i>Sets of Atoms Differing in Mass or Chemical Bond Strength</i>	203
6.8	Additional Examples	206
6.8.1	<i>Benzene, D_{6h}</i>	206
6.8.2	<i>The fac and mer Isomers of Transition Metal Complexes</i>	212
6.9	Summary	215
6.10	Self-Test Questions	216
	Further Reading	217
7	Symmetry in Chemical Bonding	219
7.1	Introduction	219
7.1.1	<i>Wave Phenomena and Interference</i>	220
7.1.2	<i>The Born Interpretation of the Wavefunction</i>	222

7.2	Bond Energies	225
7.2.1	<i>The Symmetry-Adapted Linear Combinations for the Molecular Orbitals of H_2^+ and H_2</i>	228
7.2.2	<i>The Chemical Bond Energy from Molecular Orbitals</i>	232
7.2.3	<i>The Molecular Orbital Energy</i>	236
7.2.4	<i>Bond Order</i>	238
7.3	The Relative Energies of Hydrogen-Like Atomic Orbitals	239
7.3.1	<i>Radial Behaviour of Atomic Orbitals</i>	239
7.3.2	<i>The Relative Energies of Atomic Orbitals in Different Elements</i>	242
7.3.3	<i>The Relative Energies of Atomic Orbitals from Electronegativity</i>	244
7.4	The Molecules Formed by Other Second-Row Elements with Hydrogen	252
7.4.1	<i>BeH₂, Beryllium Hydride</i>	252
7.4.2	<i>BH₃, Boron Hydride</i>	253
7.4.3	<i>CH₄, Methane</i>	258
7.4.4	<i>NH₃, Ammonia</i>	264
7.4.5	<i>H₂O, Water</i>	269
7.5	The Second-Row Diatomic Molecules	270
7.5.1	<i>Homonuclear Diatomics</i>	270
7.5.2	<i>Heteronuclear Diatomics of Second-Row Elements</i>	276
7.6	More Complex Polyatomic Molecules	278
7.6.1	<i>Ethene</i>	278
7.7	Metal Complexes	284
7.7.1	<i>Complexes Containing σ-Donor Ligands</i>	284
7.7.2	<i>The Jahn–Teller Effect</i>	287
7.7.3	<i>Complexes Containing Ligand Orbitals of π-Symmetry</i>	291
7.8	Summary	295
7.9	Self-Test Questions	296
	Further Reading	297

Appendices

Appendix 1	H₂O Models for Identifying the Results of Symmetry Operation Products	299
Appendix 2	Assignment of Chiral Centre Handedness using Cahn–Ingold–Prelog Rules	303
Appendix 3	Model of a Tetrahedron and the Related Cube	307
Appendix 4	Model of an Octahedron	313

Appendix 5 Matrices and Determinants	317
A5.1 Matrices as Representations of Symmetry Operators	317
A5.1.1 <i>Products of Matrices</i>	318
A5.1.2 <i>Products of Matrices, Expressed as Summations</i>	319
A5.2 Matrices for Solving Sets of Linear Equations	321
Further Reading	324
Appendix 6 The Mathematical Background to Infrared Selection Rules	325
A6.1 Model Based on Classical Mechanics	325
A6.2 Model Based on Quantum Mechanics	328
A6.3 Excited Vibrational States	333
A6.4 Vibrational Modes for Polyatomic Molecules	335
A6.5 Generalization to Arbitrary Transitions	336
A6.6 Summary of Selection Rules	337
Further Reading	338
Appendix 7 The Franck–Condon Principle	339
Appendix 8 Classical Treatment of Stokes/Anti-Stokes Absorption	343
Appendix 9 The Atomic Orbitals of Hydrogen	345
A9.1 Choice of Coordinate System	347
A9.2 Separation of Variables	348
A9.3 The Angular Equation	349
A9.4 Physical Interpretation of the Angular Equation Solutions	354
A9.5 Angular Momentum	356
A9.6 The Radial Equation	359
A9.7 The Complete Atomic Orbitals	361
A9.8 Expectation Values	364
A9.9 Real Combinations to Form the Familiar Atomic Orbitals	367
A9.10 Cartesian Forms of the Real Angular Functions	369
A9.11 Endnote on Imaginary Numbers	370
Further Reading	373
Appendix 10 The Origin of Chemical Bonding in H₂⁺	375
A10.1 Chemical Bond Formation	376
A10.2 H Atom and H ⁺ Cation	376
A10.3 The Virial Theorem	379
A10.4 H ₂ ⁺ Molecule	381
A10.5 Choice of Coordinate System for H ₂ ⁺ : Cylindrical Polar Coordinates	383

A10.6	H_2^+ : the Electron Kinetic Energy	386
A10.7	H_2^+ : the Electronic Potential Energy	387
A10.8	The Chemical Bond Formation Energy Based on Rigid Atomic Orbitals	393
A10.9	Optimal Radial Decay of Molecular Orbitals Further Reading	396 399
Appendix 11	H_2O Molecular Orbital Calculation in C_{2v} Symmetry	401
	Further Reading	406
Appendix 12	Character Tables	407
A12.1	Non-Axial Groups	407
A12.2	Axial Groups	407
	A12.2.1 C_n Groups	407
	A12.2.2 S_n Groups	408
	A12.2.3 C_{nv} Groups	408
	A12.2.4 C_{nh} Groups	409
	A12.2.5 D_n Groups	410
	A12.2.6 D_{nd} Groups	411
	A12.2.7 D_{nh} Groups	412
A12.3	Cubic Groups	413
	A12.3.1 Tetrahedral, T_d	413
	A12.3.2 Rotational Subgroup of T_d, T	413
	A12.3.3 Octahedral, O_h	414
	A12.3.4 Rotational Subgroup of O_h, O	414
A12.4	Groups for Linear Molecules	414
<i>Index</i>		415

Preface

Symmetry is central to spectroscopy, chemical bonding theory and many other aspects of the molecular sciences. The idea of this book is to introduce the topic in a graduated way, from molecular structure, through point groups, leading into the powerful tools that group theory provides. Example models and applications are used at all stages to show how the sometimes abstract ideas are relevant to practical problems. It is designed to be a useful companion at all levels of undergraduate study and beyond.

Chapters 1 and 2 introduce the ideas of symmetry elements and operations for the description of molecular geometry; this sets up the required symbols through examples of particular molecules. Chapter 3 looks from a slightly different perspective, laying out all the sets of operations that are contained in the common point groups and discussing why only certain sets are possible. For all three chapters Appendices 1, 2 and 4 give some paper models that can be used for visualization of the shapes that are not easily built using a molecular modeling kit. These paper models will also be available from the website. The reader interested in the applications of symmetry, without too much detail of the background, may wish to skip over Chapter 3 on the first reading.

Chapters 4 and 5 introduce the concepts of group theory, which makes symmetry indispensable for understanding many areas of chemistry. This book concentrates on applications in vibrational spectroscopy and molecular orbital theory and so illustrative examples are drawn from these areas.

Chapter 6 covers applications in vibrational spectroscopy, specifically dealing with infra-red and Raman. The chapter explains how symmetry is used to rationalise experimental data to help determine the shape and structure of molecules. To do this some background on the physical origin of spectral bands and the role of symmetry in determining selection rules is given.

Finally, Chapter 7 deals with molecular orbital theory. Molecular orbital pictures are quite straightforward to produce with modern software and the results of such calculations are used as illustrations throughout. The aim of this chapter is to demystify how molecular orbitals are obtained from sets of atomic orbitals. Some fundamental concepts, such as the idea of electronegativity and the factors that influence the strength of bonding are reviewed.

Further appendices are linked to each chapter to provide a more detailed coverage of material such as spectroscopic selection rules, the mathematics of matrices and background quantum mechanics. The flow of the text will work without these, but curiosity should hopefully draw the reader to them.

Many people have helped me in the production of this book, most notably those that have reviewed various parts of the manuscript; Mike Hewlins, Peter Knowles, Massimo Mella, Jamie Platts and Edward Jeffery. They have been thorough in their reading of the

text and frank in their comments on it, for which I am very grateful. Dai Hibbs, Bernard Richardson and Mike Coogan also provided some images from their own research, which has notably enlivened the presentation of the practical implications of symmetry. I have also taught the topic for a number of years with Simon Aldridge and Chris Morley, and have benefited greatly from their ideas.

David J. Willock
Cardiff, November 2008.

Powerpoint slides of all figures from this book, along with other supplementary material can be found on this book's webpage at www.wileyeurope.com/college/willock

1

Symmetry Elements and Operations

1.1 Introduction

Symmetry and group theory provide us with a formal method for the description of the geometry of objects by describing the patterns in their structure. In chemistry, it is a powerful method that underlies many apparently disparate phenomena. Symmetry allows us to describe accurately the types of bonding that can occur between atoms or groups of atoms in molecules. It also governs the transitions that may occur between energy levels in molecular systems, which in turn allows us to predict the absorption properties of molecules and, hence, their spectra.

This book will lay out the formal language used in the area, using illustrative examples of particular molecules throughout. We will then apply the ideas of symmetry to describe molecular structure and bonding in molecules and to consider the implications in spectroscopy.

Even in our surroundings we often look for symmetry. Figure 1.1 shows a picture of a wood engraving entitled *Fish, Vignette* made in 1955 by the artist M.C. Escher. In this work, the intertwined fish are shown set inside a hexagonal border. All of the fish illustrated have the same shape and they are designed to fit together perfectly. Six of the fish touch fins in the centre of the image and each of these has a partner with a fin on a corner of the hexagon. If we imagine rotating the picture by 60° about the central point, each fish would move to a new position and exactly replace a fish of opposite colour. This property gives the picture an attractive quality, but it also tells us that we could reconstruct the whole image by knowing the shape of the fish and the initial position of any pair, simply using six equivalent sections placed according to the rotation. At each step all we need do is remember to change the colours of the fish. The image is said to have rotational symmetry, and the techniques of this book provide a concise method of stating the rules for the construction of the picture.



Figure 1.1 M.C. Escher's 'Fish, Vignette' Copyright 2008 The M.C. Escher Company-Holland. All rights reserved. www.mcescher.com.

Figure 1.2 shows the ceiling of the Arab Room of Cardiff Castle. It is clear that the decorators have gone to a lot of trouble to use symmetry. In this case, a rotation of the image through 90° would interchange the positions of the windows; but, since they are identical, the pattern would appear unchanged. Four such rotations are possible, with the last returning each part of the ceiling to exactly its initial location. This image also has additional symmetry properties not possessed by Escher's fish. Imagine a line drawn horizontally across the image so that it passes through the centre of the left- and right-hand windows. The two sections of the image are now reflections of each other, with each feature in the upper part of the picture repeated in the lower half, as if reflected in a mirror standing



Figure 1.2 Arab Room ceiling, Cardiff Castle. Copyright: Cardiff Council.

perpendicular to the line. The mirror can be thought of as a plane of symmetry, and this image contains four such planes.

We can also look for planes of symmetry in nature. The fern frond shown in Figure 1.3 looks perfectly normal at first glance. However, on close inspection it can be seen that the left side of the leaf is just a reflection of the right-hand side on the surface of a pond. The picture is shown with the water surface vertical, which enhances the illusion. From half the leaf and its reflected image we can easily imagine the complete structure.

In chemistry, symmetry is not simply to do with beauty. It affects the properties of molecules and, in particular, influences the spectra we observe. For instance, most people would say that benzene is a ‘more’ symmetric molecule than fluorobenzene (Figure 1.4), since the fluorinated carbon should be different to the other carbon atoms. Figure 1.5 shows that this simple substitution has a profound affect on the infrared (IR) spectra of the two molecules.

The IR spectrum of benzene is very simple, showing only four main bands. On substitution with a single fluorine atom to give fluorobenzene, the spectrum becomes much more complex, with many more bands appearing between 400 and 1600 cm^{-1} .

We know that IR spectra are the result of radiation exciting vibrational modes in a molecule. The number of possible lines is related to the number of vibrational modes for the molecule in question. Since each atom in a molecule can move in three dimensions (X , Y , Z), both benzene and fluorobenzene will have a total of 36 degrees of freedom. For



Figure 1.3 The frond of a fern imaged at the surface of a pond. Although we see a complete leaf, the left-hand side is actually a reflection. In fact, the segments (or pinna) on opposite sides of a frond are usually not quite mirror images of one another, as the points at which the pinna attach to the stem are staggered.

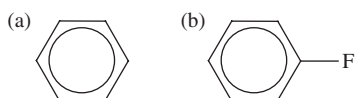


Figure 1.4 The structures of (a) benzene and (b) fluorobenzene.

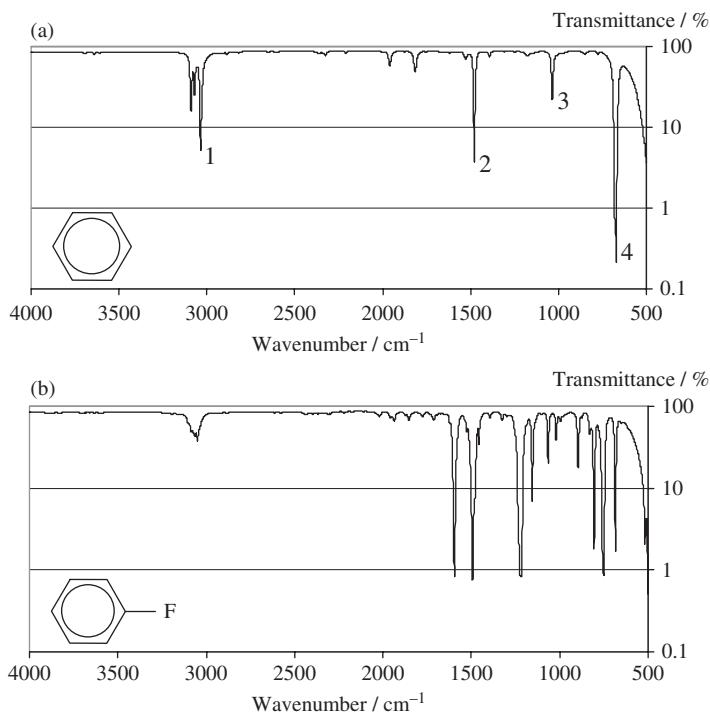


Figure 1.5 The infra-red spectra of (a) benzene and (b) fluorobenzene. Note that the transmittance scale is logarithmic and the drop in the base line between around 700 and 500 cm⁻¹ is a feature of the instrument. Data kindly provided by Dr Mike Coogan, School of Chemistry, Cardiff University.

a nonlinear molecule there are six degrees of freedom associated with the motion of the molecule as a whole (three translations and three rotations), and these are not vibrations. So, we expect the number of vibrational modes for a molecule containing N atoms to be $3N - 6$. Both benzene and fluorobenzene have 12 atoms, and so have 30 vibrational modes. The fact that this does not result in 30 IR absorptions is a result of the symmetry of the molecules; and because benzene is ‘more’ symmetric than fluorobenzene, fewer modes of vibration are detected in the spectrum of benzene than in that of fluorobenzene.

To understand and quantify these differences in spectra we need more rigorous definitions of symmetry than simply saying benzene is ‘more’ symmetric than fluorobenzene. The geometric constructs of molecular symmetry help us to define a molecule’s symmetry and the use of group theory allows us to predict the number of absorption lines that will be observed.

To achieve this we look for features in the geometry of a molecule that give rise to its symmetry. The most easily recognized of these features, or *symmetry elements*, are rotational axes (lines of symmetry) and mirror planes (planes of symmetry). These will be discussed in the remaining sections of this chapter, along with the inversion centre, which is a point of symmetry. There are other symmetry elements and operations that are possible, and we will meet these in Chapter 2. The symmetry elements imply that

there are symmetry operations: actions that can be carried out which appear to leave the molecule unchanged. If a molecule has multiple symmetry elements then there will be at least one point in space which lies within them all. For example, Figure 1.8 shows that all the rotation axes of ferrocene meet at the central point where the Fe atom is located. For this reason, the symmetry of molecules is often referred to as *point group symmetry*. The idea of this book is to introduce the ideas of point group symmetry and its application in vibrational spectroscopy and the molecular orbital (MO) description of chemical bonding.

In periodic systems (such as crystal structures), other symmetries exist to do with translation between equivalent molecules. See the Further Reading section at the end of this chapter for a book on this topic.

1.2 Symmetry Elements and Operations

1.2.1 Proper Rotations: C_n

The geometric properties of shapes that make them symmetric can be classified by their symmetry elements. The validity of a symmetry element can be checked by carrying out the corresponding operation and then comparing the object with the starting point. For example, imagine constructing an axis for a water molecule which runs through the oxygen atom, bisecting the H—O—H angle, with the axis in the plane of the molecule. This construction is shown in Figure 1.6, which also illustrates the result of rotating the molecule by 180° around the axis. After the rotation, we end up with a view of the water molecule identical to the starting point, so much so that if we had not labelled the hydrogen atoms it would be indistinguishable from the original. This result shows that the axis we have drawn is a symmetry element of the molecule and the act of rotating the molecule is the corresponding symmetry operation. The rotation operation also shows that the two hydrogen atoms in the water molecule are equivalent; if a symmetry operation can interchange two atoms, then the atoms must occupy identical chemical environments.

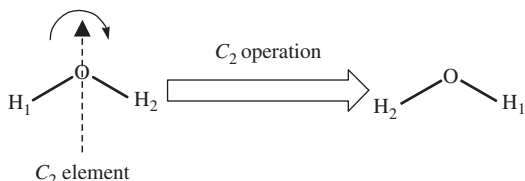


Figure 1.6 The C_2 symmetry element of water and the result of the C_2 operation.

Rotational elements and operations are labelled using a capital C . For rotations by 180° there are two positions of the molecule which appear identical, the starting point and the molecule after the rotation, so a subscript 2 is added to the label: C_2 . This subscript is known as the *order* of the rotation axis.

To emphasize the difference between elements and operations further, consider the structure of ammonia shown in Figure 1.7. A C_3 axis is present: the symmetry element is a line running through the nitrogen atom and the centre of the triangle formed by the three hydrogen atoms.

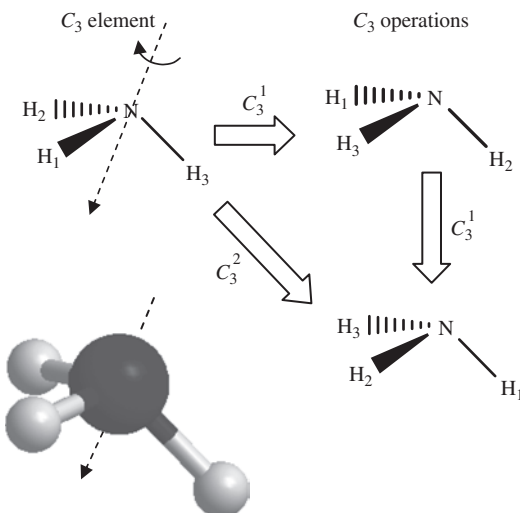


Figure 1.7 The C_3 axis of ammonia and the corresponding operations. The lower image shows a ball-and-stick model of ammonia in roughly the same orientation as the chemical drawing pictures above. The superscript on the operations gives the number of rotations starting from the initial configuration.

The C_3 axis actually has two symmetry operations associated with it, as can be seen in Figure 1.7: a rotation by 120° and a rotation by 240° . By convention, a rotation operation moves the atoms clockwise when looking down the axis direction. In the first step of the operation sequence shown in Figure 1.7, a clockwise rotation by 120° takes each hydrogen atom to the position of one of its neighbours. A second application of the operation takes each hydrogen atom to the original position of its other neighbour. To distinguish the two operations we add a superscript to indicate how many times the operation has been applied. So C_3^2 means that, starting from the original configuration, two successive rotations of 120° are applied, i.e. a total of 240° .

Molecules may contain more than one rotation axis, and those axes may have different orders. In this situation, the highest order axis is termed the *principal axis*. As an example, Figure 1.8 shows the structure of ferrocene (di-cyclopentadienyl iron(II)). This complex has a C_5 axis, which is the line joining the centres of the cyclopentadiene rings through the Fe centre (Figure 1.8a). In addition, there are five C_2 axes that run through the Fe atom parallel to the ring systems and perpendicular to the principal axis. These are best seen looking down the principal axis direction, as shown in Figure 1.8b. The C_2 rotation operations cause the exchange of the cyclopentadiene rings, whereas the C_5 operation simply rotates each cyclopentadiene ring around its centre. There is a convention that molecules are orientated so that the principal axis defines the vertical direction and that this is also aligned with the Cartesian Z-axis. This means that the vertical direction in Figure 1.8a runs up the page, whereas ‘vertical’ in Figure 1.8b is into the page.

The symmetry elements for a molecule are fixed in space: as we move the atoms under a given operation the symmetry elements are not shifted. For ferrocene, the atoms of the complex can be moved between any of five arrangements using the principal axis. In any

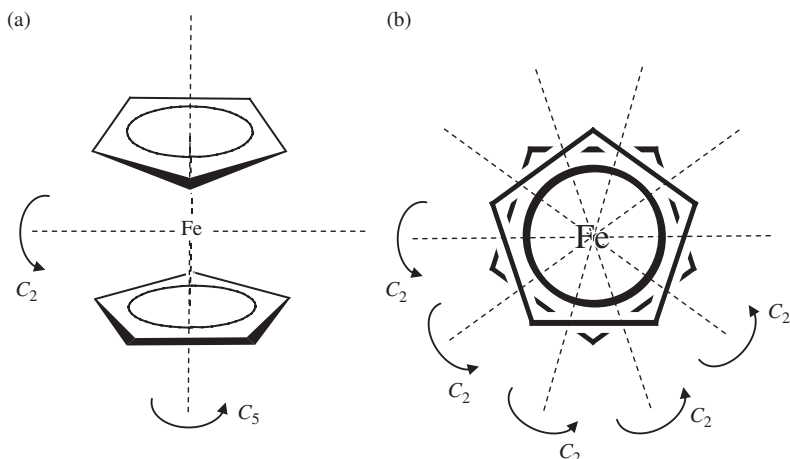


Figure 1.8 The structure of ferrocene, illustrating (a) the C_5 axis and an example C_2 axis; (b) a plan view of the molecule showing all five C_2 axes.

of these, each of the C_2 axes remains a symmetry element. The five C_2 axes meet at a point on the principal axis and they have an angular spacing of 72° , i.e. the angle of rotation for the C_5^1 operation. So, after a C_5^1 operation, the arrangement of the atoms around any of the C_2 axes is shifted to one of its neighbours; this implies that all the C_2 axes have an equivalent environment of atoms, and so they are treated as equivalent axes.

It is also possible for a molecule to contain axes of the same order that are not equivalent to one another. Figure 1.9 shows the structure of benzene, a molecule which has a C_6 principal axis perpendicular to the molecular plane. Each of the carbon atoms in benzene can be placed at any of the six positions by successive applications of the C_6 rotation and so all of the carbon atoms are in identical environments. Each C_6 operation rotates the molecule about its centre by 60° . Two C_6 operations, C_6^2 , will give a rotation of 120° , which we have already seen corresponds to a C_3^1 rotation. We will usually use the lowest order alternative when listing symmetry operations, so that the C_6 axis has associated with it:

$$C_6^1, \text{ which is unique}$$

$$C_6^2 = C_3^1$$

$$C_6^3 = C_2$$

$$C_6^4 = C_3^2$$

$$C_6^5, \text{ which is unique.}$$

This means that the C_6 axis gives rise to two C_6 operations, two C_3 operations and a C_2 operation, and so there must always be C_3 and C_2 axes collinear with a C_6 .

In the plane of the benzene molecule there are also C_2 axes that pass through opposite carbon atoms. The rotations about these axes must not be confused with the C_2 operation from the principal axis, and so the axes are labelled C_2' , as shown in Figure 1.9. The C_2'

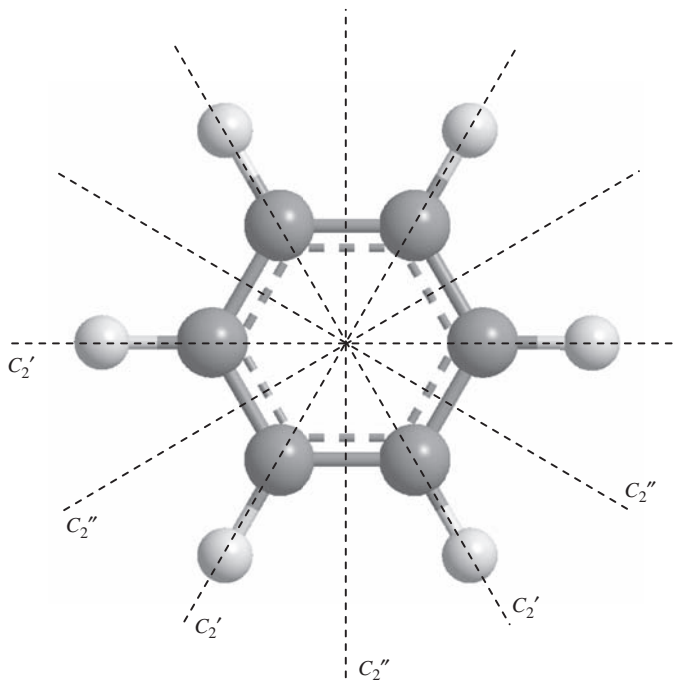


Figure 1.9 The structure of benzene showing the two sets of three C_2 axes in the molecular plane; the principal C_6 axis is perpendicular to the plane and passes through the centre of the molecule at the crossing point of the C_2' and C_2'' axes.

axes are 60° apart, and so successive C_6 operations will alter which particular atoms are on which C_2' axes. However, each C_2' axis always contains two C and two H atoms, and so the three axes are equivalent. There is a second set of axes which join opposite bond centres, and these are labelled C_2'' to distinguish them from the C_2' axes. We can tell that the C_2'' and C_2' axes form distinct sets both from their chemical environments (one set join bond centres and one set join atoms) and from the fact that the C_6 operations never interchange a bond centre and an atom position. We have made the choice that the axes joining opposite atoms should be labelled C_2' and that those between the bond centres that do not contain any atoms in the symmetry element are labelled C_2'' .

A further possibility for multiple rotation axes is to have more than one candidate for the principal axis. For example, the highest order axis for ethene is a twofold axis, but there are three nonequivalent C_2 axes, as shown in Figure 1.10. The choice of principal axis is now arbitrary, and it is usual to assign each axis a Cartesian label (X, Y or Z) so that they can be referred to explicitly.

1.2.2 The Plane of Symmetry: σ

If a plane exists for which reflection of each atom in a molecule gives an indistinguishable configuration, the molecule is said to have a plane of symmetry, which is given the label σ .

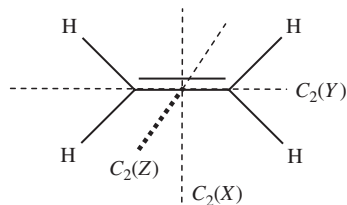


Figure 1.10 The structure of ethene showing three distinct C_2 axes.

The symmetry element is the plane itself, since all points in the plane remain unchanged by the operation of reflection. For the water molecule there are two planes of symmetry, as shown in Figure 1.11. These are distinguished by labelling the plane perpendicular to the molecule σ and the plane of the molecule itself σ' . The C_2 axis of water is the only axis, and so it is also the principal axis defining the vertical direction. This means that the mirror planes are standing vertically, and so a subscript is added to remind us of this, giving σ_v and $\sigma_{v'}$.

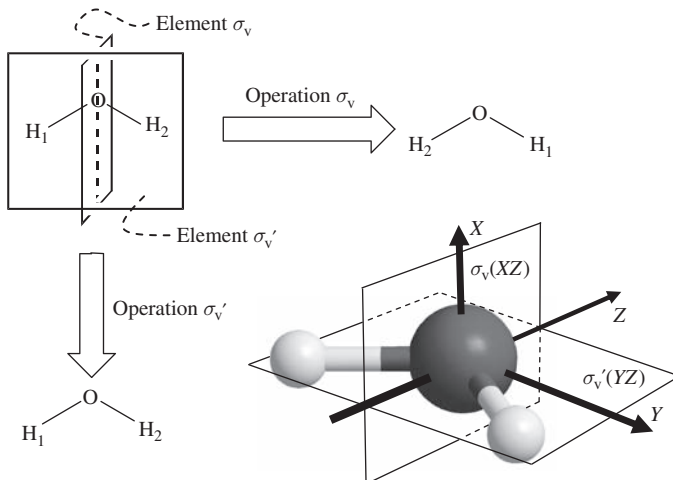


Figure 1.11 The two mirror planes for the H_2O molecule showing the difference between σ_v and $\sigma_{v'}$ operations. The inset shows the relationship between the mirror planes and a reference axis system.

Which plane is which is a somewhat arbitrary choice; however, the designation described here is quite widely used and is based on the alignment of the symmetry planes with the Cartesian axis system. Figure 1.11 shows that the two planes intersect in the line of the C_2 axis we identified earlier; the planes of symmetry are said to *contain* the rotational axis. The principal axis gives us the Cartesian Z -direction, which, in this case, is in

the molecular plane. We also take Y to be in the molecular plane, and so X must be perpendicular to it. The full labels for the mirror planes of water become $\sigma_v(XZ)$ and $\sigma_v'(YZ)$, but it is common to omit the Cartesian parts of these labels.

Some molecules have multiple axes and mirror planes. For example, boron trifluoride (BF_3) is a planar molecule with a C_3 axis perpendicular to the plane and passing through the boron atom, as shown in Figure 1.12. However, there are also C_2 axes in the plane of the molecule which run along each of the $\text{B}-\text{F}$ bonds.

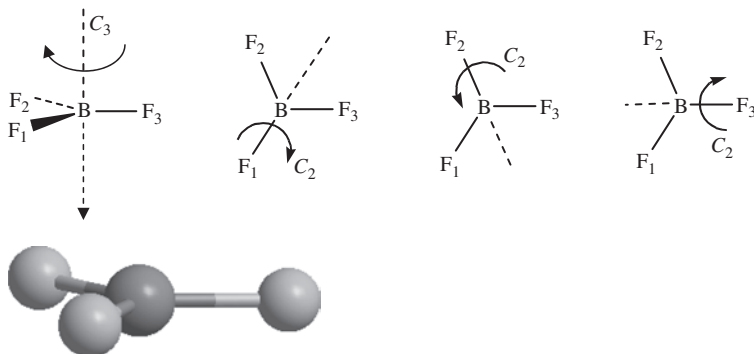


Figure 1.12 The rotational symmetry elements of BF_3 . To the left is a flying wedge drawing looking from the side of the molecule in the same orientation as the perspective ball-and-stick model below it. The C_2 axes are shown with the molecule viewed looking down on the molecular plane.

The highest order axis present is taken to be the principal axis and gives us the ‘vertical’ direction. So, BF_3 has three vertical mirror planes, each of which contains a $\text{B}-\text{F}$ bond; an example of a vertical mirror plane in BF_3 is shown in Figure 1.13a. The C_3 operations will move the fluorine atoms between these planes, but each will always contain one fluorine atom and reflect the other two into one another. So, although there are three vertical planes, they are identical, requiring only the single label σ_v , and there are three σ_v operations. The plane of the molecule for BF_3 is also a plane of symmetry, as illustrated in Figure 1.13b. This contains all three of the $\text{B}-\text{F}$ bonds, but not the principal axis. In fact, the plane is perpendicular to the C_3 axis, i.e. the plane is horizontal and so is labelled σ_h .

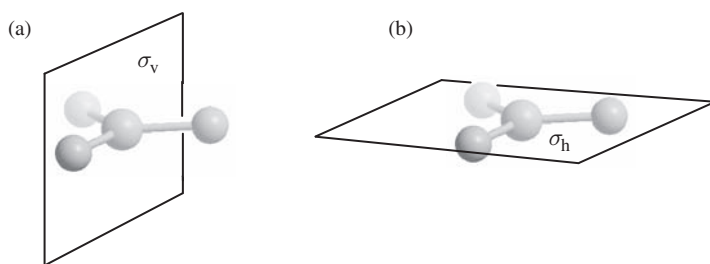


Figure 1.13 The two types of symmetry plane for BF_3 : (a) an example of a vertical plane; (b) the horizontal plane σ_h .

More complex collections of rotation axes and planes require the definition of an additional type of mirror plane. To illustrate this we can return to the case of benzene. In Figure 1.9 we showed that there are two sets of rotation axes in the molecular plane of benzene and labelled these C_2' , for the axes passing through opposite atoms, and C_2'' , for the axes passing through opposite bonds. There are also two sets of three mirror planes which each contain the principal axis and either a C_2' or C_2'' axis. Both types of mirror plane are vertical, but we need to distinguish them from one another. Each of the first set contain a C_2' axis and these are labelled σ_v . Planes in the second set are vertical, but are also in between the C_2' axes; this sort of vertical plane is called a dihedral plane and is given the symbol σ_d . The relationship of the σ_v and σ_d planes to the C_2' axes in benzene is shown in Figure 1.14.

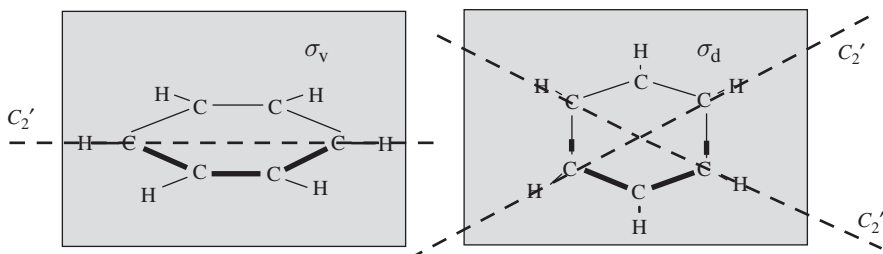


Figure 1.14 The vertical (σ_v) and dihedral (σ_d) planes of benzene and their relation to the C_2' axes. The bonds in front of the planes have been thickened.

The dihedral plane has been introduced using an example where there is more than one type of vertical plane. However, σ_d planes are defined by their relationship to the horizontal C_2' axes; this means that molecules do exist in which σ_d is the only type of vertical plane.

An example of a molecule with σ_d but no σ_v planes is ethane in its staggered conformation. The principal axis in this case is a C_3 axis running along the C–C bond, and the molecule is shown orientated vertically in Figure 1.15a. The illustrated dihedral plane of symmetry contains the two carbon atoms, H₁ and H₆. There are horizontal C_2 axes passing through the C–C bond centre, but they are not in the mirror planes, as can be seen from a Newman projection along the principal axis in Figure 1.15b. Figure 1.15a and b shows two of the three C_2 axes: one rotates the molecule so that H₁ and H₄ interchange, while with the other H₁ and H₅ are swapped. The mirror plane in the diagram bisects the angle between these two axes and so is labelled σ_d . The σ_d operation would swap H₅ with H₄ and H₂ with H₃. There are three C_2 axes for ethane and, correspondingly, there are three σ_d planes.

The dihedral plane also occurs when there is more than one type of vertical mirror plane even if there are no horizontal C_2 axes. Figure 1.15c shows a metal complex with four equivalent equatorial ligands. The internal structure of these ligands L will be assumed not to affect the symmetry properties of the complex. The complex has a principal axis of order 4, so there is a vertical C_2 axis ($C_4^2 = C_2$). However, the two axial halogen atoms are different (Cl and Br) and so there are no horizontal C_2 axes. There are two mirror planes that each contain two *trans*-L ligands; these are labelled σ_v . The figure also shows one

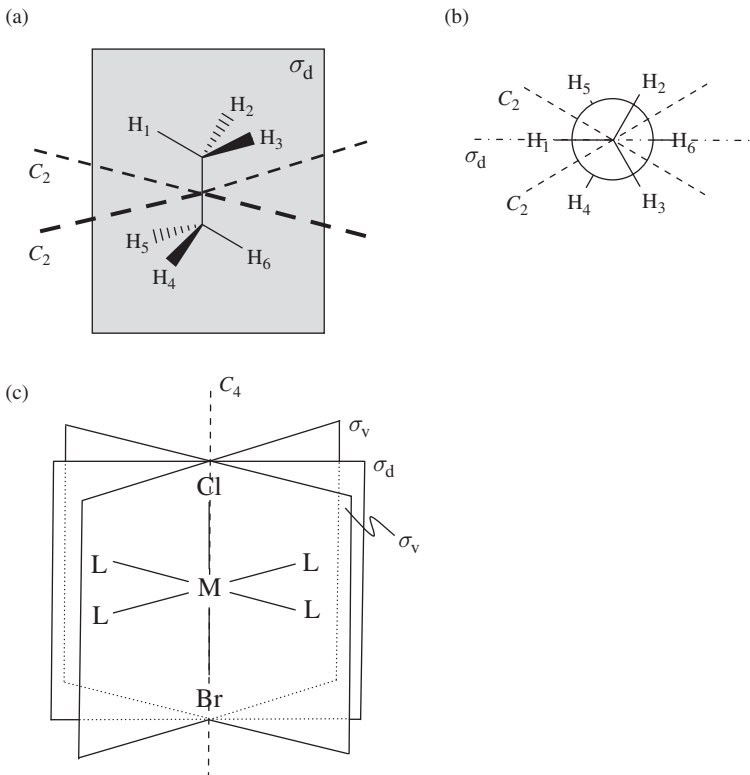


Figure 1.15 (a) An example dihedral plane σ_d for ethane in the staggered conformation and the two C_2 axes it lies between. (b) A Newman projection view showing the σ_d plane bisects the angle between the C_2 axes. (c) An example metal complex with no horizontal C_2 axes.

example of another pair of planes that only contain M and the halogen atoms, and reflect *cis*-L ligands into one another. This plane bisects the angle between the two σ_v planes and so is labelled σ_d . The other σ_d plane would be perpendicular to the page.

Problem 1.1: In Section 1.2.3, Figure 1.19 shows the structure of the square planar complex $[\text{PtCl}_4]^{2-}$, find and label all the proper rotation axes and planes of symmetry for this structure. Remember to consider the full set of operations for high-order axes.

1.2.3 The Inversion Centre: *i*

So far, we have looked at symmetry operations for which the corresponding elements are the plane (a reflection operation) and a line (the rotation operation). The next symmetry element is the *inversion centre*, labelled *i*. The operation of inversion leaves only a single point unchanged, and so it is often referred to as a centre, or point, of symmetry. The inversion operation is illustrated in Figure 1.16 with two pairs of points, A, A' and B, B', which represent atoms in a hypothetical molecule. For each pair, the points are equidistant

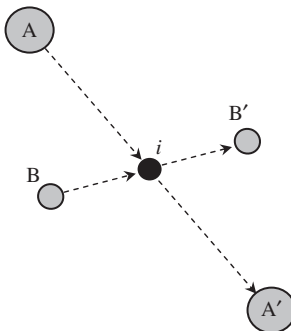


Figure 1.16 An illustration of the inversion centre operation. Under inversion, each point in a molecule is moved through the inversion centre to a position on the opposite side of the centre and at the same distance from the centre as the original point. In this case, atom pairs $A-A'$ and $B-B'$ are linked by the inversion centre i .

from the inversion centre, and the lines between A and A' and between B and B' include i . To perform the inversion operation we imagine moving each atom in the molecule along a straight line to the inversion centre and then moving them along the same line beyond the centre to a distance equivalent to their starting point. For the hypothetical example, A and A' would be interchanged, as would B and B' . If the inversion operation result is indistinguishable from the initial geometry, then the molecule has an inversion centre. The inversion operation can be thought of as similar to the reflection operation, but referred to a point rather than a plane.

In two dimensions, we can illustrate the difference between the inversion centre and a simple reflection using lens optics. In Figure 1.17a, a drinking glass is used as a cylindrical lens behind which a piece of paper carries the word ‘Reflect’ and is backlit in the set-up shown in Figure 1.17a. When viewed through the glass at a distance beyond the focus of the cylindrical lens the word is reversed, as shown in Figure 1.17b. This result is the same as if we had reflected the word through a plane perpendicular to the paper. The optical quality of the drinking glass is low, so distortion of the letters is also apparent. If we use a small pocket lens in a similar set-up (Figure 1.17c), then the result is not only the reversal of the word, but also the top and bottom of the letters are swapped over, as shown in Figure 1.17d. Figure 1.18 shows ray diagrams of the optics for the cylindrical and normal lens. In the cylindrical case (Figure 1.18a) the rays from the object (the word ‘Reflect’ in this case) are brought to a line focus because the lens has no curvature in the vertical direction. When the viewer is placed beyond the focus, rays from the left of the object appear to the right and *vice versa*, leading to the observed reversal. For the hand lens (Figure 1.18b) the focus is a point and so, in addition to left and right reversing, top and bottom are also swapped.

These are two-dimensional examples, because the words are planar; in fact, the third dimension, perpendicular to the paper, is used to carry out the operation using the optics. A square planar species, such as the $[\text{PtCl}_4]^{2-}$ ion shown in Figure 1.19a, has a centre of inversion, and the operation seems to act much like our optics example. On inversion, the chlorine atoms *trans* to each other in the original molecule are interchanged.

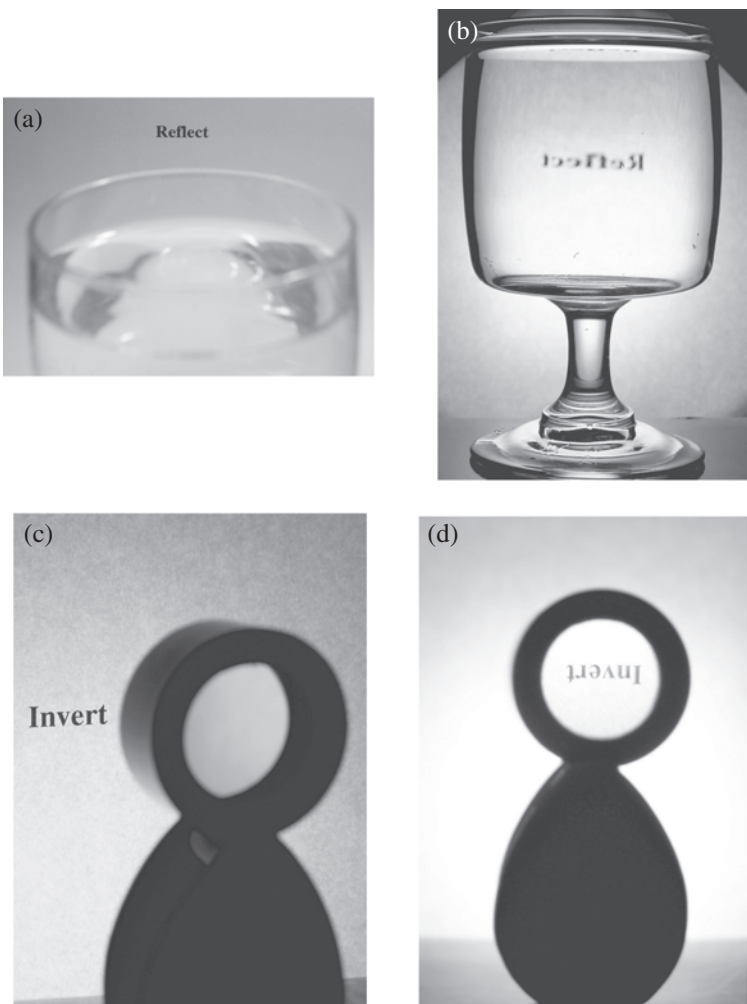


Figure 1.17 A two-dimensional illustration of the difference between reflection and inversion operations. (a) The set-up used and (b) the result of viewing the word ‘Reflect’ through a cylindrical lens. (c) The set-up and (d) result of viewing the word ‘invert’ beyond the focal point of a hand lens.

However, in three dimensions the inversion operation will swap left with right, top with bottom and back with front simultaneously. For this to be a symmetry operation which leaves the molecule unchanged, the centre of inversion symmetry element will always be at the centre of the structure. So the Pt atom in $[\text{PtCl}_4]^{2-}$ remains in the same position after the operation. Figure 1.19b shows the three-dimensional example SF_6 ; here, the central S atom is on the inversion centre and so remains in the same place after inversion, but, with the F atoms labelled, it can be seen that atoms *trans* to one another are again swapped over. The molecular models of these two structures in Figure 1.19c should help to visualize the process.

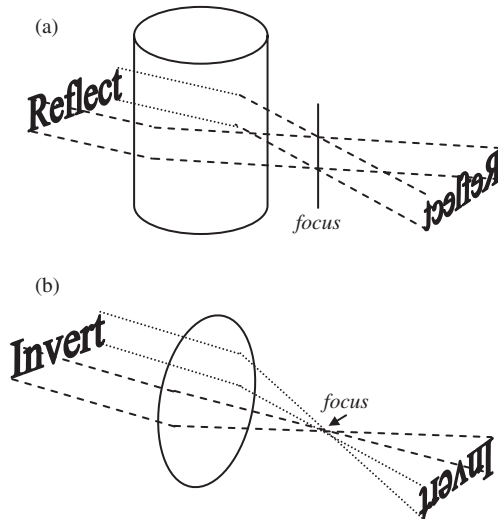


Figure 1.18 Ray tracing diagrams for (a) the reflection and (b) the inversion operations presented in Figure 1.17.

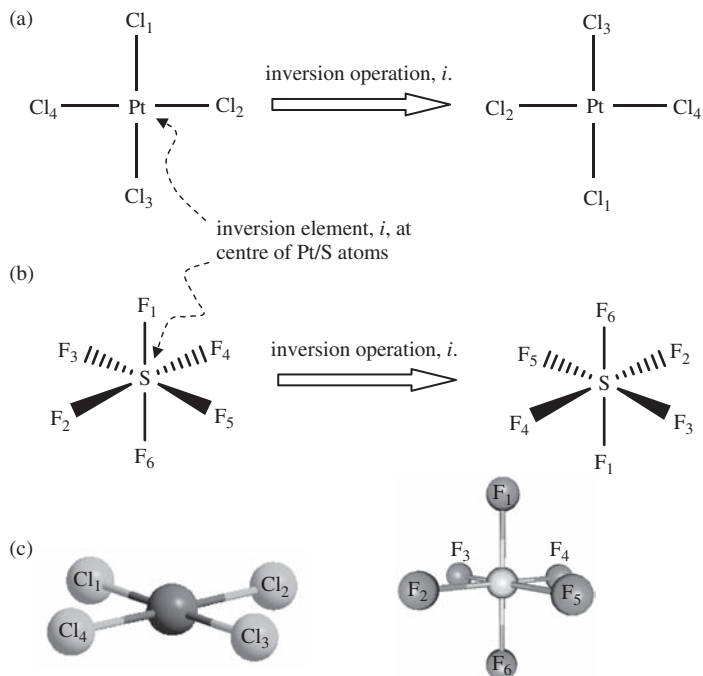


Figure 1.19 The inversion element and operation for (a) a chemical complex $[PtCl_4]^{2-}$ and (b) the molecule SF_6 . (c) Ball and stick representations of the two structures used in (a) and (b).

Problem 1.2: Square planar complexes have five planes of symmetry; using the structure of $[\text{PtCl}_4]^{2-}$ from Figure 1.19a, find these planes and sketch out the result of each associated operation on the positions of the Cl atoms. Hence, confirm that no mirror plane gives the arrangement shown after the inversion operation in Figure 1.19a.

1.3 Examples of the Impact of Geometric Symmetry on Chemistry

So far, we have only considered some of the geometric factors involved with symmetry. Even so, the use of symmetry to identify equivalent atoms or groups in molecules already allows some insight to be gained into the way symmetry can be used to interpret the chemical behaviour of molecules possessing, or lacking, the symmetry elements introduced so far. We can also start to explore how symmetry helps deduce chemical structure from experimental data.

1.3.1 Oxygen Transfer via Metal Porphyrins

Rotation axes and mirror planes are very common symmetry elements in molecules and can lend important properties to the structure. For example, in biology, the porphyrin ring (Figure 1.20) is the basic structure of an important class of tetra-dentate ligands. The idealized unsubstituted ring has a C_4 principal axis at its centre perpendicular to the plane of the ring. This will give rise to two C_4 (C_4 and C_4^3) and one C_2 (C_4^2) operations. Figure 1.20 also shows that there are four C_2 axes in the plane of the ring: two C_2' and two C_2'' . Each of these axes can be used to turn the planar molecule over so that the upper and lower faces are interchanged. Since this is achieved through symmetry operations, it implies

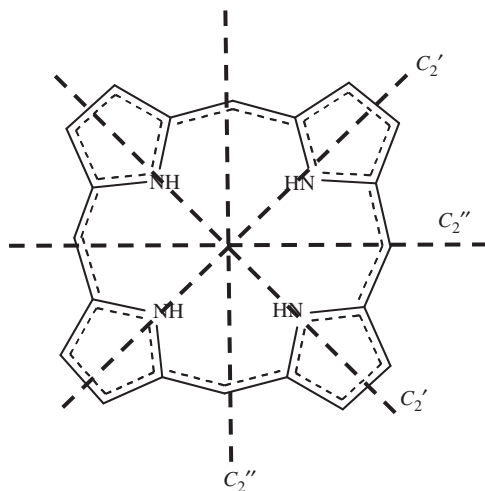


Figure 1.20 The porphyrin ring structure. A C_4 axis passes through the centre of the ligand perpendicular to the molecular plane; this is also a C_2 axis, since $C_2^1 = C_4^2$. The four C_2 axes shown in the molecular plane form two sets of two, labelled C_2' and C_2'' .

that the two faces of the ring are identical. This does have important consequences for the biological processes involving porphyrin rings. In particular, complexes of Fe^{2+} with more elaborate porphyrin ligands are essential for the function of haem, which is involved in oxygen storage in the haemoglobin component of blood. When it is oxygenated, the central Fe atom carries a single oxygen atom which sits above the plane of the ring and it is coordinated by part of the host protein structure from below. Since the two faces of the porphyrin ligand are linked by symmetry operations, it does not matter ‘which way up’ the porphyrin is orientated as it is incorporated into the protein.

1.3.2 Nuclear Magnetic Resonance: Chemical Equivalence

An important use of symmetry is as an aid in the determination of molecular structure from spectroscopic data. We often know the molecular formula of a new compound, but this does not tell us the molecular structure. In a nuclear magnetic resonance (NMR) experiment, a macroscopic sample of an unknown compound is exposed to a strong magnetic field. Magnetic nuclei in the sample will have different energies depending on the orientation of their magnetic moment with respect to the external field. According to quantum mechanics, the magnetic moment of a nucleus is dependent on its spin. For nuclei with a spin of $1/2$, such as ^1H or ^{13}C , two states will be possible: one with the spin aligned with the external field and one with the spin aligned opposite to the external field. The energy difference between these two states is small, of the same order of magnitude as the energy of a photon of radio-frequency electromagnetic radiation. This means that, if the sample is probed using radio-frequency waves, we will see an absorption when the photon energy exactly matches the energy difference between the two magnetic states of the nucleus.

In NMR spectroscopy, the probe frequency of the radio waves is actually held fixed and in the original approach the magnetic field applied was scanned through a range of values. The energy difference between the two spin states will be altered as the field is scanned, and a strong absorption will be observed when the energy difference exactly matches the probe radio-frequency. In most modern machines the ‘scanning’ process has been replaced by a pulsed approach, which allows all environments of a given nucleus to be analysed simultaneously.

In addition to the magnetic field applied in the experiment, the nuclei also experience the magnetic field created by the electrons and other magnetic nuclei in the molecule. The electronic effect tends to be larger than the nuclear influence on the local magnetic field at a given nucleus and so the nuclear effects are only resolved in high-resolution spectra. In the following examples we will only consider low-resolution spectra, and so will ignore the magnetic coupling between nuclei. The magnitude of the electronic contribution to the local magnetic field depends on how the electron density is distributed in the molecule; in particular, the field from the valence electrons will depend on the other elements present and the types of bonding holding the structure together. So, the energy separation between the spin states depends not just on the applied field from the NMR machine, but also on the local chemical environment of the nucleus being probed. This makes NMR an extremely useful technique in chemistry, because the positions of the NMR bands provide information on the molecular structure of the sample.

Generally, NMR spectra are plotted in terms of chemical shifts, which are the absorption frequency differences between the sample nuclei and the same element in a laboratory

standard. For carbon (^{13}C) and hydrogen (^1H) NMR experiments, a commonly used standard is tetramethylsilane (TMS). The chemical shift δ is defined as

$$\delta = \frac{\nu - \nu_{\text{TMS}}}{\nu_{\text{TMS}}} \times 10^6 \quad (1.1)$$

where ν is the absorption frequency of the sample atoms and ν_{TMS} is the absorption of the corresponding element (^{13}C or ^1H) in the standard. This chemical shift is dimensionless, since the reference absorption frequency appears in the denominator; this ensures that experiments on spectrometers with different probe frequencies give the same chemical shift values for a given sample. The difference in frequencies observed between samples and the standard is typically only a few kilohertz, whereas the probe frequency will be in the 200–1000 MHz range. Hence, the factor of 10^6 is introduced to give chemical shifts that can be quoted using simple numbers, typically 0–12 for ^1H NMR, and the shifts are quoted as parts per million (ppm).

The chemical shifts from a ^1H NMR spectrum are used as an indication of the chemical environment of each proton in the molecule of the sample. If two hydrogen atoms are linked by a symmetry operation, then they will have the same environment and are referred to as chemically equivalent. The line in the ^1H NMR spectrum for each will occur at exactly the same position, and so the intensity of the peak at this chemical shift will be twice that of a hydrogen atom in a unique environment, i.e. not linked to any other hydrogen atoms by symmetry operations. This allows us to use the intensity of the peaks as an indication of the number of equivalent hydrogen atoms in a molecule and so may help to determine the sample's molecular structure.

As an example, Figure 1.21 shows a computer-generated ^1H NMR spectrum for a compound with the chemical formula C_8H_{14} . There are several possibilities for the molecular structure of this sample, two of which are given in Figure 1.22. The spectrum shows two peaks with the lower chemical shift having a height six times that of the other signal.

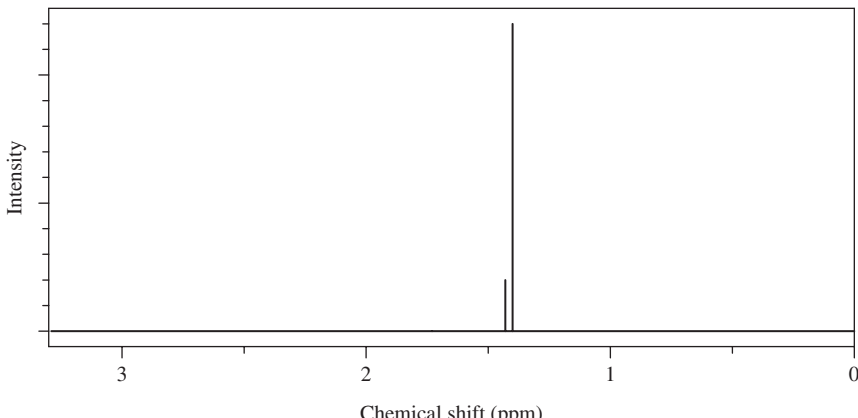


Figure 1.21 A ^1H NMR spectrum for a compound with the chemical formula C_8H_{14} generated using the ChemDraw package.

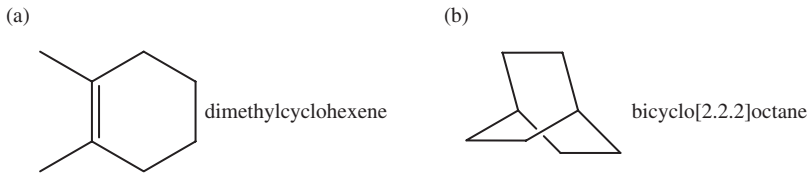


Figure 1.22 Two possible molecular structures for the chemical formula C_8H_{14} .

This implies that there are only two environments for the 14 hydrogen atoms and they are divided into a set of 2 and a set of 12. Three-dimensional structures of the two alternatives are shown in Figure 1.23, along with examples of the rotation axes and mirror planes that are symmetry elements of the structures.

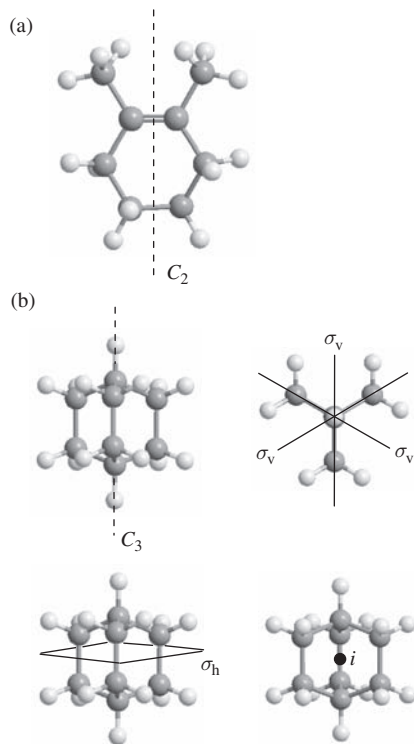


Figure 1.23 (a) The C_2 axis in dimethylcyclohexene and (b) the principal C_3 axis and example symmetry planes for bicyclo[2.2.2]octane.

Only bicyclo[2.2.2]octane has a structure consistent with the spectrum, since the two hydrogen atoms that lie on the principal axis (C_3) are linked by σ_h and by i and all of the other 12 hydrogen atoms are linked by combinations of σ_h , σ_v , C_3 and i operations. None of the symmetry operations would interchange the axial hydrogen atoms with any of the

hydrogen atoms in the CH_2 groups, and so there are two distinct sets of hydrogen atoms. This gives the same division of the hydrogen atoms between the two environments that was implied from the spectral data. The dimethylcyclohexene alternative has only a C_2 axis and no other symmetry axes or planes. As we shall see below, this means that it has hydrogen atoms in at least three different environments, and so would be expected to give a more complex ^1H NMR spectrum.

The absorption event in an NMR experiment takes a short, but finite, time. If the proton in a ^1H NMR experiment is moving rapidly, then it may experience more than one environment on the time scale of the experiment and only the average chemical shift will be observed. For example, methyl groups are usually undergoing rapid rotation at room temperature, and so the three hydrogen atoms will appear equivalent even though they may not be linked by symmetry operations. In the spectrum of dimethylcyclohexene we would see only a single chemical shift for all six of the methyl protons, since the two methyl groups are linked by symmetry operations in the static structure. Similarly, molecular motion would be expected to cause the hydrogen atoms of each CH_2 group in the ring to interchange rapidly from axial to equatorial as the ring changes its conformation. The C_2 axis implies that the two CH_2 groups adjacent to the methylated carbon atoms are equivalent and that the remaining CH_2 groups are also equivalent to one another. This gives at least three distinct ^1H NMR signals.

This type of analysis can also give some information on the dynamics of molecular motion. Figure 1.24 shows the structure of $\text{Al}_2(\text{CH}_3)_6$. The symmetry axes and mirror

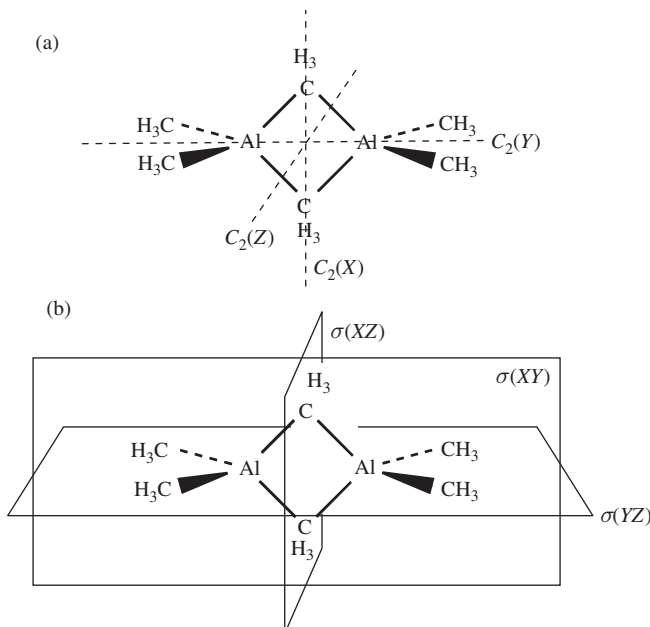


Figure 1.24 The structure of $\text{Al}_2(\text{CH}_3)_6$ showing (a) the rotation axes and (b) mirror planes assuming the structure of the methyl group can be ignored.

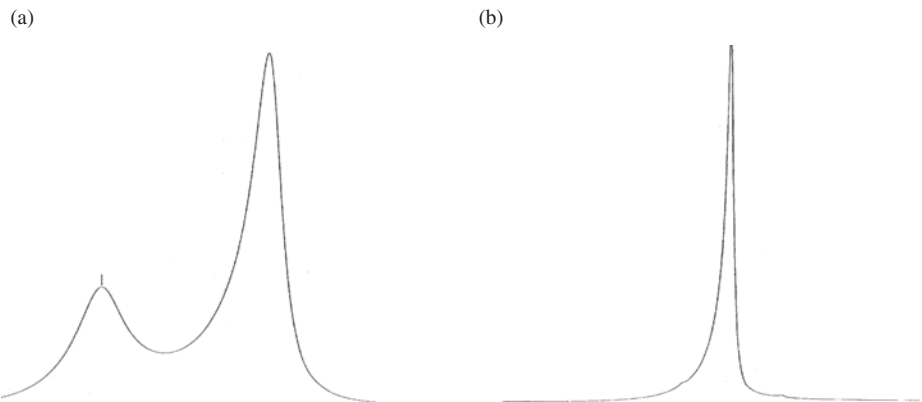


Figure 1.25 ^1H NMR spectra of $\text{Al}_2(\text{CH}_3)_6$: (a) at -40°C ; (b) at 20°C .

planes for the structure are illustrated assuming that the internal structure of the methyl groups can be ignored due to the rapid rotation discussed above. Using the symmetry operations, we see that the methyl groups form two sets: The four methyl groups that have only one bond to an Al atom (terminal methyl groups) and the two methyl groups that bridge between Al atoms. Figure 1.25a shows the ^1H NMR spectrum for $\text{Al}_2(\text{CH}_3)_6$ taken at a temperature of -40°C . As expected, we see two chemical shifts, with the signal for the terminal methyl hydrogen atoms more intense than that for the hydrogen atoms of the bridging methyl groups. However, a spectrum of the same sample taken at 20°C shows only a single peak, as illustrated in Figure 1.25b. This peak has a chemical shift in between the values found for the terminal and bridging methyl hydrogen atoms at lower temperature. This suggests that at 20°C there is a rapid interchange of the terminal and bridging methyl groups so that the hydrogen atoms sample both environments. A possible mechanism for this process is shown in Figure 1.26. Here, exchange is achieved without dissociation of the dimer, a bond between an Al and bridging methyl group is broken by thermal excitation and then a simple rotation converts the methyl group labelled C_1H_3 from terminal to bridging.

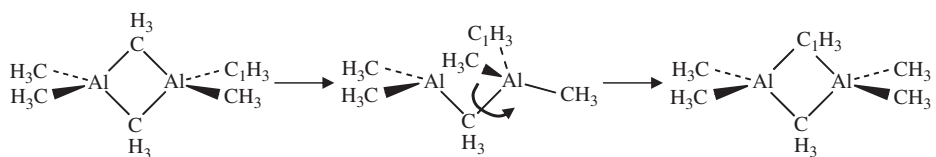


Figure 1.26 Possible mechanism for the rapid interchange of terminal and bridging methyl groups in $\text{Al}_2(\text{CH}_3)_6$.

1.4 Summary

Symmetry elements are imaginary geometrical entities that are the signature of symmetry properties in objects. So far, we have seen that a line of symmetry is required for a rotation

axis, a plane for a reflection and a single point for inversion. The symmetry element is the set of points that are not moved when the corresponding symmetry operation takes place.

Symmetry operations are the actions, such as rotations or reflections, that can be used to transform an object in such a way that, after the operation, it is indistinguishable from the starting point.

The symmetry elements and operations of a molecule are given standard symbols, including:

- *Proper rotation axes*, labelled C_n , where n is the axis order. The highest order axis present for a given molecule is called the principal axis and defines the vertical direction used to orientate the molecule in space.
- *Reflection planes*, labelled σ , with three possible subscripts:
 - σ_v , a vertical mirror plane, contains the principal axis – if there are horizontal C_2 axes, then σ_v will also contain those of highest priority;
 - σ_d , a dihedral mirror plane, also contains the principal axis – if there are horizontal C_2 axes, then σ_d will bisect the angle between those of highest priority;
 - σ_h , a horizontal mirror plane, is perpendicular to the principal axis.
- *Inversion centre*, labelled i , has a single point as the symmetry element. Inversion requires each point in the molecule to have an equivalent point on the opposite side of the centre of symmetry and equidistant from it. A molecule may have at most one point of inversion.

Atoms in a molecule that are linked by symmetry operations have identical chemical environments, and so identical NMR chemical shifts.

1.5 Self-Test Questions

These questions are designed to give you practice at applying the concepts learned in this chapter. Most of the questions for this chapter require you to visualize the geometry of a molecule, and you may find it useful to construct models. In the illustrations here, as in the rest of the text, we continue to use the convention that C atoms are not explicitly labelled in organic molecules and hydrogen atoms are omitted unless the geometry is ambiguous without them. The ‘flying wedge’ convention is also used to indicate bonds above and below the plane of the paper.

1. For each of the molecules in Figure 1.27 identify all of the rotation axes present, giving the order of each axis and describing any that form a set of identical axes. You should make sketches of the molecules viewed from different directions to illustrate your answer.
2. Give the orders of the principal axes for the molecules illustrated in Figure 1.27.
3. Identify all the mirror planes present in the molecules of Figure 1.27 and use the rotation axes you have found to label them as σ_v , σ_d or σ_h .

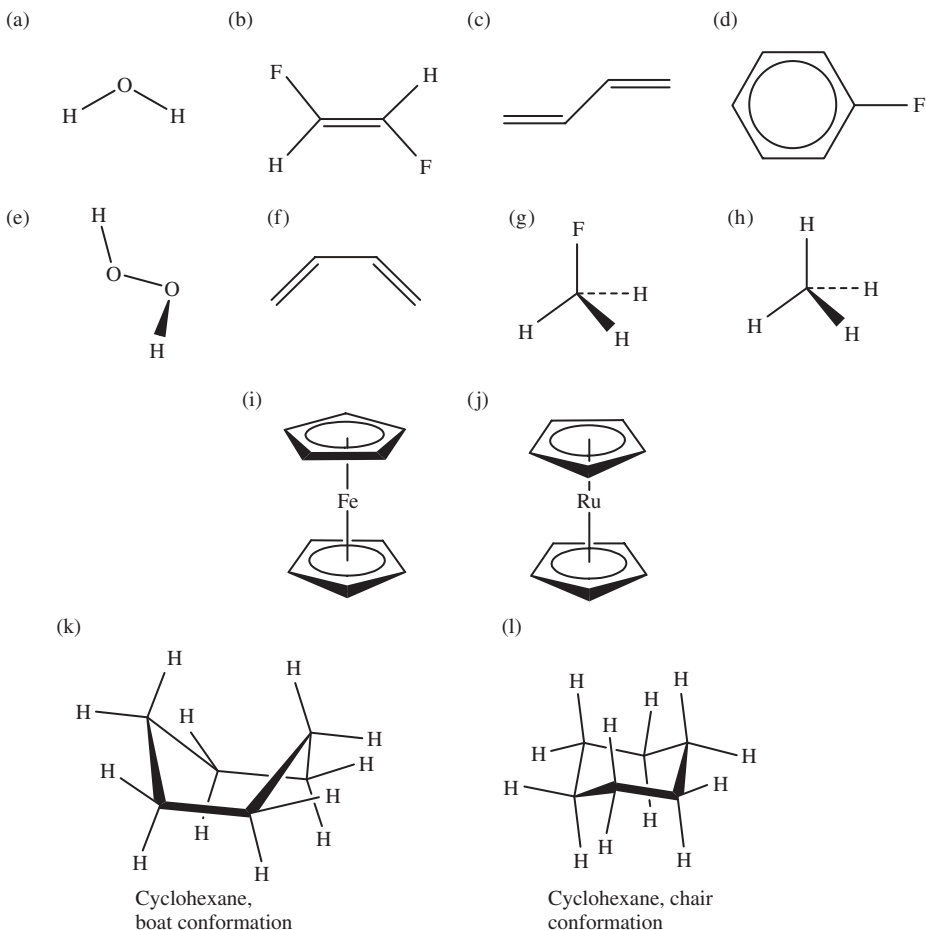


Figure 1.27 Example molecules for symmetry analysis.

4. How many distinct ^1H NMR peaks would you expect for each molecule containing H atoms in Figure 1.27?
5. Draw molecular structures of each of the isomers of difluorobenzene and identify all axes and mirror planes of symmetry for each case.

Further Reading

Crystal symmetry is covered in several texts, including:

Senechal, M. (1990) *Crystalline Symmetries: An Informal Mathematical Introduction*. Adam Hilger (ISBN 0-7503-0041-8).

Franzen HF (1994) *Physical Chemistry of Solids, Basic Principles of Symmetry and Stability of Crystalline Solids*. World Scientific Publishing (ISBN 9-8102-1154-6).

2

More Symmetry Operations and Products of Operations

2.1 Introduction

In this chapter we will explore further the symmetry operations that are used to describe molecular structure. New operations are introduced to complete the set used in molecular symmetry. Particular sets of operations often recur, with many molecules having the same collection of operations. Once we establish how the properties of a molecule depend on the set of valid operations, this will mean that we can actually infer the properties of many related molecules of the same symmetry. The sets of operations are referred to as point groups, and our main task in this chapter is to introduce the concept of a point group. The formal construction of the point groups most commonly used in chemistry is carried out in Chapter 3. The properties of the point groups, and their application in vibrational spectroscopy and MO theory, are then the subject of the remainder of the book.

The definition of a point group comes from the general idea of a group in mathematics. For molecular point groups to take advantage of general group theory we require two additional symmetry operations to be defined: the identity and the improper rotation. These operations are introduced in the first half of the chapter through the idea of a group being *closed*.

2.2 Background to Point Groups

In Chapter 1 we covered three types of symmetry operation: m rotations about an axis of order n , C_n^m ; reflection through a plane, σ_v , σ_d or σ_h ; and inversion through a point, i . Point groups arise from the observation that a given set of operations is valid for more than one molecule. For example, Figure 2.1 shows that both water and fluorobenzene have a single

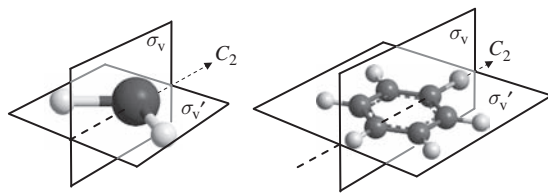


Figure 2.1 The symmetry elements of water and fluorobenzene; in this case, each element has only one corresponding operation.

C_2 axis and two vertical mirror planes, σ_v and σ_v' . These molecules do not have any other rotation axes or mirror planes and do not have an inversion centre; so, according to the operations met so far, this set completely describes the symmetry of both molecules. The two molecules are said to belong to the same symmetry point group because they have exactly the same set of valid symmetry operations.

2.3 Closed Groups and New Operations

2.3.1 Products of Operations

In general, the idea of a point group is a mathematical abstraction that helps us classify molecular geometry. A point group is a list of all symmetry operations that an object which belongs to the group can undergo and remain apparently unchanged. The set of operations that form a group must be complete, in the sense that if any two members of the group are applied in succession the result must also be a single operation which is a member of the group. This means that the group is ‘closed’, i.e. it is not possible to generate a new symmetry operation by combining those in the group. This property of groups can be useful: ensuring that the group of operations is closed is one way of checking that all the operations that are possible have been identified. The requirement for a group to be closed also leads to further symmetry operations, as will be shown in the following sections.

Multiplication Table for H_2O

To check that a group is closed we form the product of each pair of operations within the group and find the single equivalent operation that achieves the same end point. The product of a pair of symmetry operations is defined as the result of applying them in succession. Taking H_2O as an example, $C_2\sigma_v'$ is the product of a vertical reflection through the molecular plane and a 180° rotation and is achieved by carrying out the reflection followed by the rotation. This would be one possible combination of operations for the H_2O molecule; and if the group is closed, all such products should be equivalent to a single operation. A complication can arise in finding the single operation that is equivalent to the product. For the example of $C_2\sigma_v'$ the hydrogen atoms would be swapped but either the C_2 operation or the σ_v operation alone would also interchange them; so, by looking only at atom positions, it is impossible to tell which operation to chose. There is not enough information in just the atom positions to tell the operations apart; some way is needed to

orientate the atoms in space. To do this we can add a set of vectors to the oxygen atom of the molecule. These are initially aligned with the global coordinate system, for which we will use capital letters. By convention, the molecule is orientated with its principal axis (here the C_2 axis) along the Z-direction, the Y-direction is set in the molecular plane and the X-direction is then perpendicular to the plane.

The vectors on the oxygen atom are aligned with their respective directions in the starting diagram for each operation as shown in Figure 2.2. This differentiation between the global coordinate system and the atom-based vectors will become important when we consider multiple operations later in this chapter. Figure 2.2 illustrates how these vectors can be used to differentiate between the rotation and reflection operations. The C_2 operation leaves the z-vector unchanged because it is along the direction of the rotation axis, but x and y are both reversed. The σ_v operation, which is reflection in the XZ plane, only reverses

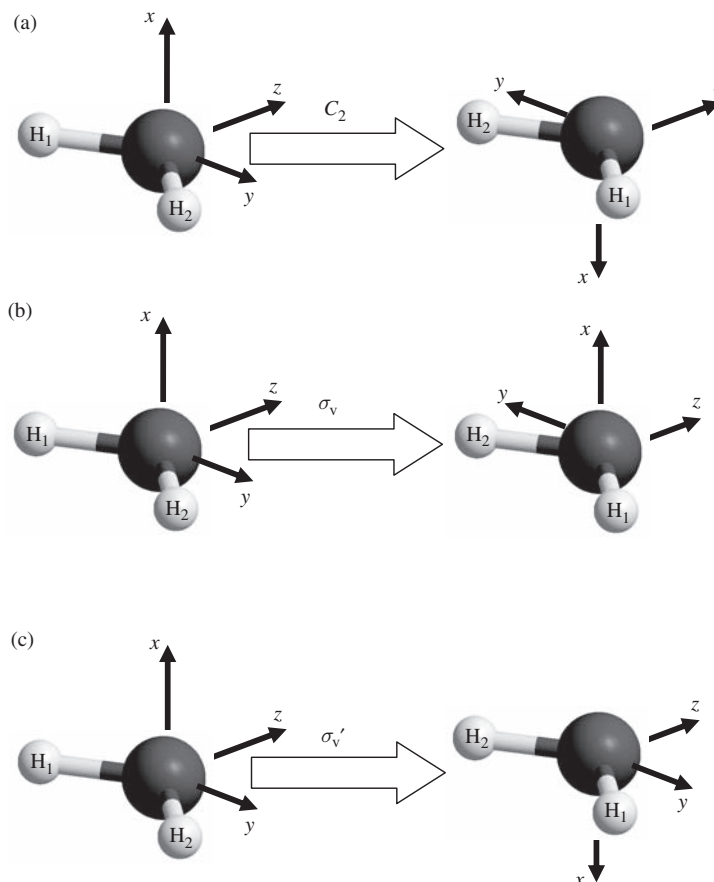


Figure 2.2 The symmetry operations for H_2O , including the result of the operations on a set of vectors added to the oxygen atom: (a) C_2 is along Z and so reverses only x and y; (b) σ_v contains x and z and so only reverses y; (c) σ_v' contains the y and z vectors so only reverses x.

the y -vector, while the σ_v' operation leaves both y and z unchanged and only reverses x . Once the vectors are taken into account, the operations do give different results.

To see exactly the result of successive operations, the end point of one operation is used as the start point of the next. Some products are easy to visualize; for example, the product $C_2^{-1}C_2^1$, i.e. a rotation by 360° , leaves the molecule unchanged and in exactly the same configuration as the starting point. If we are to have a closed group, then this combined operation must be the result of a single operation in the group, and so a new operation is introduced, the identity operation E .

On application of the identity operation E , nothing moves at all; so the entire molecule is the symmetry element. No matter what the shape of a molecule, a rotation of 360° about any axis would give an indistinguishable arrangement of the atoms. This is because a rotation of 360° is equivalent to *doing nothing* to the molecule. It does not matter what axis is used, or even if the operation is done at all, and so all molecules possess the identity symmetry element. We will see that other repeated applications of other symmetry operations can also lead to the case of an identical molecule.

For more complex sequences of operations it is helpful to use drawings or models including the vectors to understand the results of successive operations. Appendix 1 gives some templates for paper models of water illustrating the vectors used here for each end point shown in Figure 2.2.

To identify all the possible products systematically, a multiplication table of symmetry operations can be drawn up in which each row and column of the table has one of the symmetry operations as a heading; the body of the table then contains the operation resulting from the product of that row and column. The starting point for the case of H_2O is given in Table 2.1 and it is left to the reader to complete this following the instructions in Problem 2.1.

Problem 2.1: The results of the operation products for Table 2.1 have been left blank. Work out the single operation equivalent to each product and fill in the table. The paper models from Appendix 1 can be used to help in this exercise. Start with the model representing the result of the first operation and then carry out the second. Compare the configuration obtained with the three other models to identify the end point. You should find that for every pair of operations there is always a model that looks the same as the end point you have come up with. A completed table is included at the end of the chapter.

Table 2.1 The multiplication table for the H_2O symmetry operations.

		First operation →			
		E	C_2	$\sigma_v(XZ)$	$\sigma_v'(YZ)$
Second operation	E	E	C_2	$\sigma_v(XZ)$	$\sigma_v'(YZ)$
	C_2	C_2	E	$\sigma_v'(YZ)$	$\sigma_v(XZ)$
	$\sigma_v(XZ)$	$\sigma_v'(YZ)$	$\sigma_v(XZ)$	E	C_2
	$\sigma_v'(YZ)$	$\sigma_v(XZ)$	$\sigma_v'(YZ)$	C_2	E

The multiplication table for H_2O contains only operations we have already identified: E , C_2 , σ_v and σ_v' . This confirms that this set of operations forms a closed group and is a reassurance that no symmetry operations have been missed.

2.3.2 Fixed Symmetry Elements

Multiplication Table for NH_3

In the example of H_2O above we used the idea of a global axis system, X , Y , Z . This axis system is used to define the positions of the symmetry elements of the molecule and, once set, the global axis system is not moved by any operations that are carried out. This means that the symmetry elements should be considered immovable and symmetry operations only move the atoms in the molecule. This becomes especially important when molecules with more symmetry elements are considered. For example, ammonia (NH_3) has a principal axis of order 3 and three vertical mirror planes, as shown in Figure 2.3.

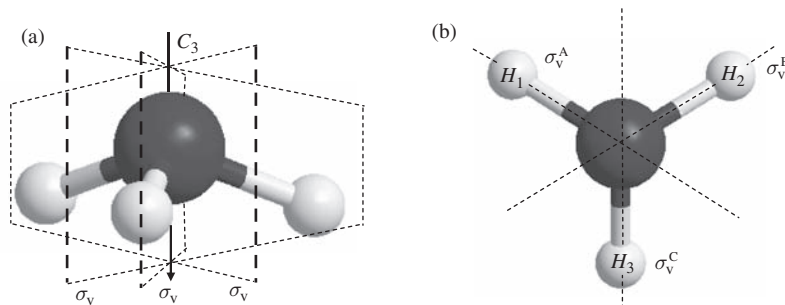


Figure 2.3 The symmetry elements for ammonia (NH_3): (a) viewed with the principal axis in the plane of the page; (b) viewed along the principal axis with the mirror planes labelled following the text.

In this case the vertical mirror planes are actually equivalent, since they each contain one $\text{N}-\text{H}$ bond. However, to carry out the multiplication of operations we will add an additional label to the mirror planes so that they can be distinguished. In the initial configuration, we have chosen σ_v^A , σ_v^B and σ_v^C to be the planes containing $\text{N}-\text{H}_1$, $\text{N}-\text{H}_2$ and $\text{N}-\text{H}_3$ respectively (Figure 2.3b).

This choice sets the location of each mirror plane in space; so, to work out the product of two operations, it is necessary to hold the planes in place during the whole manoeuvre. For example, the product $\sigma_v^A C_3^1$ is illustrated in Figure 2.4. This involves a rotation around the principal axis which brings H_3 into the σ_v^A plane. Reflection by the plane then swaps H_1 and H_2 . Comparing the final configuration with the start point, it can be seen that H_2 has returned to its original position but H_1 and H_3 have been interchanged, a result that can be achieved by σ_v^B alone, i.e.:

$$\sigma_v^A C_3^1 = \sigma_v^B \quad (2.1)$$

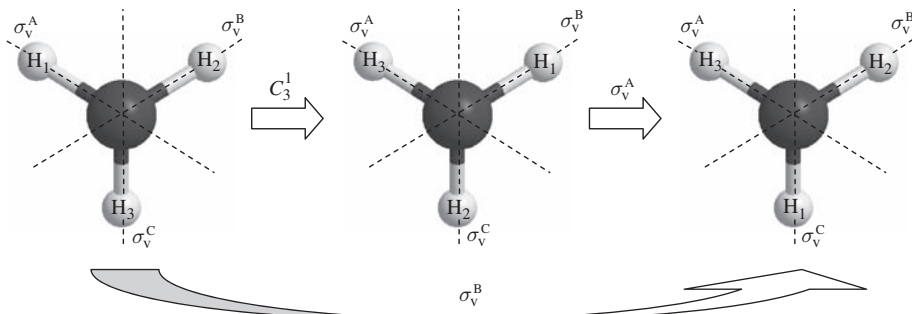


Figure 2.4 The $\sigma_v^A C_3^1$ operation product for NH_3 . Note that the positions of the symmetry planes are set in the global coordinate system and so remain constant throughout.

Before completing the multiplication table we will write down some observations on the types of answer to expect for these products; this will help narrow down the possibilities for this exercise and for more complex cases.

(i) A product between two rotation operations around a common axis is simply the sum of the individual rotations, here $C_3^1 C_3^1 = C_3^2$. If the total rotation exceeds the order of the axis, then the number of operations should be reduced by subtracting the order. This follows from the definition we used for the identity:

$$C_n^n = E, \quad \text{so} \quad C_3^2 C_3^2 = C_3^4 = C_3^3 C_3^1 = EC_3^1 = C_3^1 \quad (2.2)$$

(ii) The product of a rotation with a reflection through a vertical mirror plane will give another reflection. In this NH_3 example, the rotation does not change the order of the H atoms. A reflection swaps two H atoms and so the order is changed from clockwise to anticlockwise. The result cannot be the identity or a rotation, so another mirror plane is the only choice.

(iii) The product of two reflections in vertical mirror planes is the same as a rotation about the principal axis. Reflections swap the order of the H atoms, so two reflections will return them to the initial clockwise ordering. Reflection in the same mirror plane twice is the identity, which is included in this general statement through Equation (2.2).

Problem 2.2: The multiplication table for NH_3 has been left partially blank (Table 2.2); you should use the above rules to say what type of operation is possible in each case and then fill in the missing entries using a model of the molecule as described below.

The model should use different colours for the three hydrogen atoms to represent H_1 , H_2 and H_3 . Place the model on a piece of paper; use the initial positions of each hydrogen atom and define the mirror planes following Figures 2.3 and 2.4. Starting with the model aligned with the paper, carry out the two operations required for the particular product, keeping the paper reference fixed in place. To carry out a reflection simply swap the two hydrogen atoms that are not in the mirror plane. The single operation for each product can be found by comparing the final configuration of the model with the reference on the paper. Before doing the next product, realign the model with the original starting point. A completed table is included at the end of this chapter.

Table 2.2 The multiplication table for the NH_3 symmetry operations.

		First operation - - - - - →					
Second operation		E	C_3^1	C_3^2	σ_v^A	σ_v^B	σ_v^C
		E	C_3^1	C_3^2	σ_v^A	σ_v^B	σ_v^C
↓	C_3^1	C_3^1	C_3^2	E	σ_v^C	σ_v^B	
↓	C_3^2						
↓	σ_v^A	σ_v^A	σ_v^B	σ_v^C	E	C_3^2	
↓	σ_v^B	σ_v^B	σ_v^C	σ_v^A	C_3^2	C_3^1	
▼	σ_v^C	σ_v^C	σ_v^A	σ_v^B	C_3^1	E	

2.3.3 The Final Missing Operation, Improper Rotations: S_n

The Case of Ethane

Ethane in the staggered conformation belongs to a more complex symmetry group than water or ammonia. The elements of rotation, reflection and inversion present for staggered ethane are shown in Figure 2.5. The highest order axis present is the C_3 axis along the C—C bond (Figure 2.5a), and so this is the principal axis, defining the vertical direction. There are also three equivalent C_2 axes perpendicular to the planes that contain the C—C bond and each pair of *trans* hydrogen atoms (H_1 and H_6 in Figure 2.5b, for example). The C_2 axes pass through the centre of the C—C bond and the C_2 operations swap hydrogen atoms from either end of the molecule, as illustrated in Figure 2.5b. Each of the planes used to define the C_2 axis directions is also a mirror plane for the molecule. Comparing the position of the C_2 axes and the mirror planes in the Newman projection of Figure 2.5c shows that these planes are between the C_2 axes and so should be labelled σ_d . The molecule also contains an inversion centre which swaps the two carbon atoms over and moves hydrogen atoms from one end of the molecule to the other (Figure 2.5d). By comparing the result of the C_2 rotation in Figure 2.5b with that for the inversion in Figure 2.5d it can be seen that the rotation and inversion are indeed different operations leading to different arrangements of the labelled atoms. The Newman projection shows that the C_2 rotation leads to a reversal in the order of the hydrogen atoms within each methyl group from a clockwise arrangement of H_1 , H_2 and H_3 to an anticlockwise ordering, whereas the inversion centre preserves the clockwise order.

If the symmetry group of ethane is to be closed, then it must be possible to write down a single operation that can replace any combination of two other members of the group. Figure 2.6 shows the result of a C_3^1 rotation followed by inversion. The C_3 rotation moves the hydrogen atoms around by 120° but does not interchange them between the ends of the molecule or change the H ordering. After inversion, the hydrogen atoms are swapped between the ends and the ordering remains clockwise. However, this is clearly a different configuration from that for the i operation alone. The only other operations that swap hydrogen atoms from the top and bottom of the molecule are the C_2 rotations, and we have seen that these change the ordering of the hydrogen atoms from clockwise to anticlockwise. Accordingly, within the operations identified so far, no single operation can replace the iC_3^1 product, and so the group is not closed.

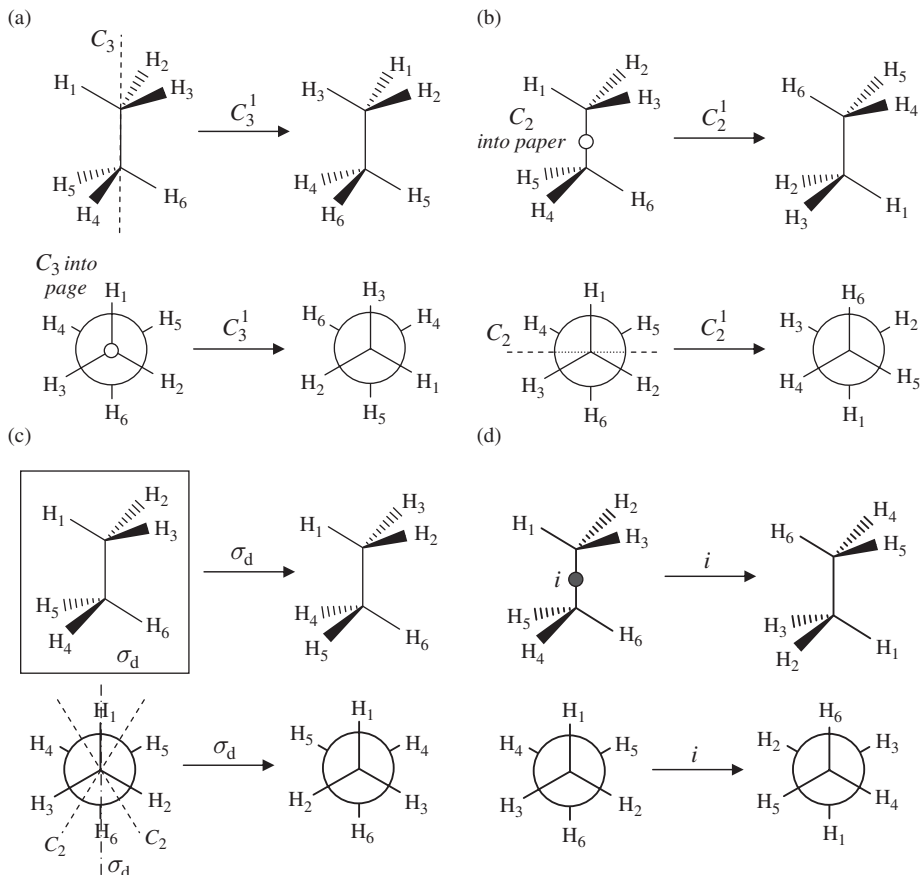


Figure 2.5 Symmetry elements and example operations for ethane in the staggered conformation; each example is shown both in flying wedge representation and in Newman projection. (a) The C_3 principal axis, defining the vertical direction; (b) C_2 axis for $H_1-C-C-H_6$ plane; there are three equivalent C_2 axes, (c) one of the three equivalent σ_d planes; in the Newman projection the plane is shown to be between the C_2 axes, hence the dihedral designation; (d) the inversion centre.

In fact, the reason that this problem has arisen is that we are still lacking one symmetry element and its corresponding operation, the improper rotation S_n .

An improper rotation S_n is actually a combination of two operations: a rotation about a C_n axis and then a reflection through a plane which is horizontal with respect to the axis. This operation is defined as the two procedures together. The molecule has an S_n axis of symmetry if the combined rotation-reflection gives a result indistinguishable from the start point. After just the rotation the structure may be completely different from the start point; neither the C_n axis nor the mirror plane need be symmetry elements themselves.

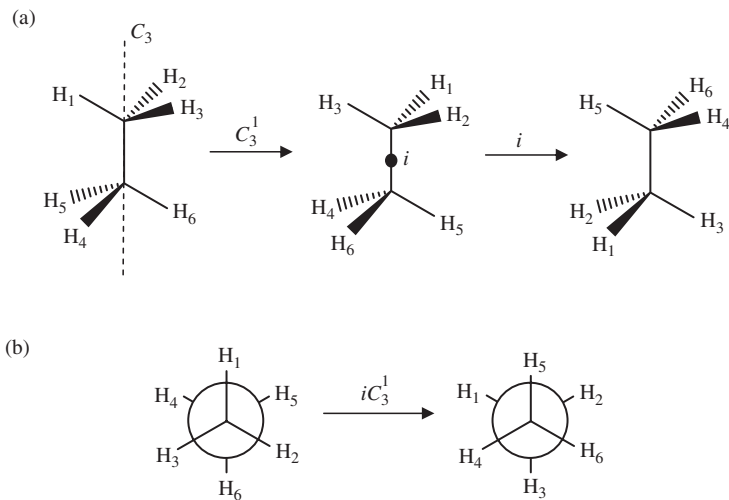


Figure 2.6 The compound operation iC_3 for ethane in the staggered conformation: (a) using flying wedge notation; (b) in the Newman projection.

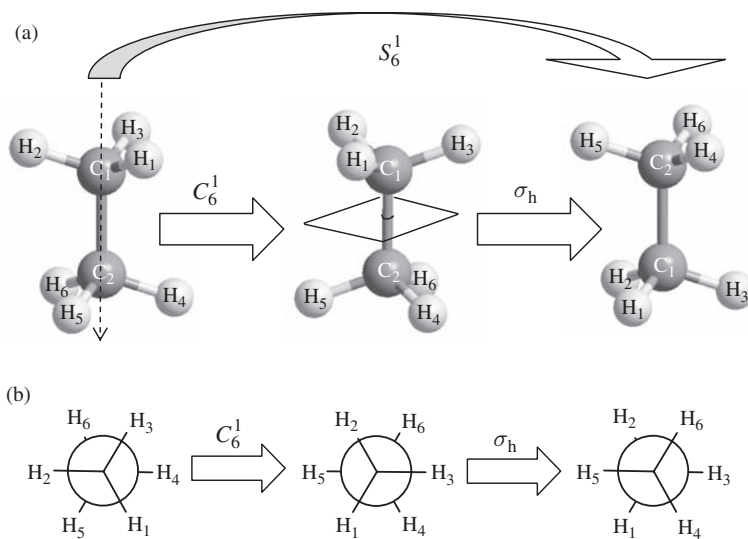


Figure 2.7 Summary of the improper rotation operation for ethane in the staggered conformation.

The missing symmetry operations for ethane in the staggered conformation are improper rotations. Ethane has an order 6 improper rotation axis, S_6 , which is illustrated along with the S_6^1 operation, in Figure 2.7. After describing the operations that the S_6 axis leads to, we will use them to close the symmetry point group of ethane.

The Newman projection in Figure 2.7b shows the ethane molecule looking directly down the C–C bond. If all the hydrogen atoms were in the same plane, we would

expect a C_6 axis to be present along the C—C direction. In fact, a rotation by C_6 changes the molecule and so is not a symmetry operation. For example, in the first picture in Figure 2.7a, H_1 appears at the top of the molecule and the C— H_1 bond points out of the page to the right of C_1 . After the C_6 rotation, H_1 is still at the top of the molecule but to the left of C_1 , where there was no hydrogen atom in the original molecule. However, in the Newman projection of Figure 2.7b, it can be seen that, after the rotation, H_1 is directly over the original position of H_5 . So, if we take the structure generated by the rotation and reflect it through a horizontal plane through the centre of the C—C bond we generate a new configuration which is indistinguishable from the first. This means that the combined rotation and reflection is a symmetry operation for the molecule. Note that the only point that is unaffected by the combined operation is the centre point of the C—C bond; so, like the inversion centre, the symmetry element for the operation is a point. However, the element of an S_n axis is often taken to be the rotation axis because this direction is required to perform the operation. The order of the axis in ethane is 6, and so the staggered conformation of ethane has an S_6 improper rotation symmetry element.

2.3.4 Equivalences for Improper Rotation Operations

The number of operations from an improper rotation axis depends on the order of the axis and on the removal of any operations that can be written more simply. The number of operations can be seen by repeatedly carrying out the improper rotation until the original configuration is obtained. For example, the result of six successive S_6 operations on ethane returns the molecule to its starting configuration, as shown in Figure 2.8.

Simpler operations which give the same result can be identified for some of the S_6 operations by comparing each of the intermediate structures with the starting point. For example, S_6^2 and S_6^4 involve an even number of applications of the horizontal mirror plane that is part of the improper rotation. This places the hydrogen atoms at the same ends of the molecule as in the original configuration, but rotated away from their original positions. These results can also be obtained by a simple rotation using the C_3 axis, and so we write the equivalences $S_6^2 = C_3^1$ and $S_6^4 = C_3^2$. Similarly, the S_6^3 operation gives the same result as the inversion centre, and so only the latter is included in the list of unique operations for the molecule. In addition, the S_6^6 operation is equivalent to the identity, and so the S_6 element leads to only two unique operations: S_6^1 and S_6^5 . These observations on the S_6 axis can be generalized to any improper rotation of even order.

When an improper rotation has *even* order:

- $S_n^{2m} = C_{n/2}^m$, $m = 1$ to $n/2$; that is, for any even number of operations there is an equivalent simple rotation.
- $S_n^{n/2} = i$ for $n/2$ odd, $S_n^{n/2} = C_2$, for $n/2$ even; that is, when the improper rotation is carried out half as many times as the order of the axis there is an equivalent ‘simple’ operation. Here, there are two scenarios. (i) If $n/2$ is odd, the repetition of the improper rotation implies an odd number of σ_h reflections and a C_2 rotation; the result is then the same as the inversion operation i . (ii) If $n/2$ is even, the molecule will not appear to have been reflected through σ_h and so $S_n^{n/2}$ is simply an instance of (1).
- $S_n^n = E$; that is, carrying out the even ordered improper rotation the same number of times as its order results in a configuration identical to the starting point.

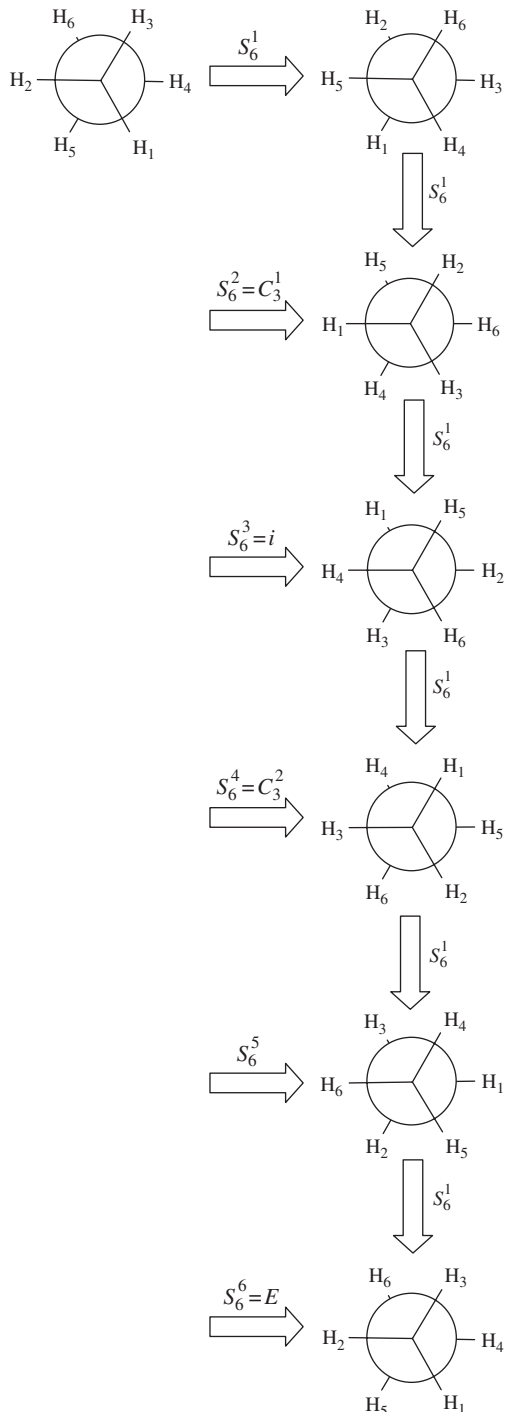


Figure 2.8 The complete set of S_6 operations illustrated using ethane viewed along the C-C bond in the Newman projection. Note that each operation is labelled by its relation to the starting point (top left).

These observations also imply that, if an improper axis of even order is found, there must be a rotation axis with half its order and an inversion centre. Also, for a molecule with an inversion centre, there must be an improper axis of rotation. In the case of a molecule with an inversion centre but without any simple rotation axes, the improper rotation is an S_2 axis. However, this S_2 axis is not usually quoted, since $S_2^1 = i$ and $S_2^2 = E$, so there are no unique operations associated with an S_2 axis.

The improper rotation consists of a rotation and reflection. Even though the axis and horizontal plane need not be elements themselves, if they are present then the improper rotation will also be a symmetry element. For example, the planar molecule BF_3 has a principal C_3 axis and a horizontal mirror plane σ_h , and so there is also an S_3 axis collinear with the C_3 . For planar molecules, the reflection in σ_h does not alter any atom positions; however, if we place a vertical arrow on one of the F atoms, then it will be reversed by the reflection. In later chapters, the addition of arrows like this will be used in the analysis of molecular vibrations and is referred to as a *basis*. A basis allows us to study the effect of symmetry operations not only on the atom positions but also their motion. In Figure 2.9 the idea is simpler: we add the arrow to highlight operations which turn the molecular

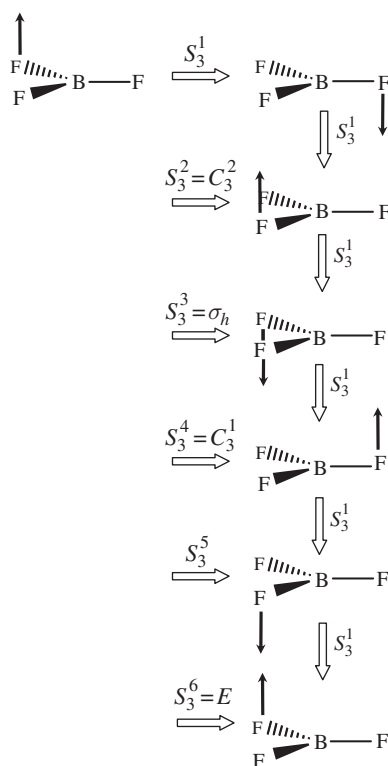


Figure 2.9 The complete set of S_3 operations illustrated using BF_3 . Note that to show the result of each operation fully requires an arrow perpendicular to the molecular plane. Each operation is labelled by its relation to the common starting point (top left).

plane over. The effect of repeated S_3 improper rotations on the BF_3 molecule can then be followed more clearly.

After even numbers of operations the arrow returns to the top face of the molecule, and so there is an equivalent simple rotation that can give the same result. Since the order of the axis is odd, S_3^3 does not return the molecule to its start point; although all the atoms are in the same place as in the original configuration, the arrow is pointing down, and so $S_3^3 = \sigma_h$. Only after six applications of the operation do we find that $S_3^6 = E$. In this case there are only two unique operations arising from the S_3 axis: S_3^1 and S_3^5 .

In general, for an *odd* ordered improper rotation:

1. $S_n^{2m} = C_n^p$, where m runs from 1 to $(n - 1)$ and $p = 2m$ for $2m < n$ or $p = 2m - n$ for $2m > n$; that is, an even number of applications of an odd-order improper rotation is the same as a related simple rotation. The operations with rotations less than 360° can also be described as the same number of simple rotations, and improper rotations involving angles greater than 360° are related to odd numbers of simple rotations.
2. $S_n^n = \sigma_h$; that is, carrying out the improper rotation a number of times equal to its order results in a simple reflection through the horizontal mirror plane.
3. $S_n^{2n} = E$; that is, it requires $2n$ applications of the operation to return the molecule to its starting configuration.

2.4 Properties of Symmetry Operations

2.4.1 Equivalent Operations and Equivalent Atoms

It is worth pausing at this point to think about what the symmetry operations are doing when used to describe the molecular geometry. As an example, we will return to the case of ethane, for which the operations E , C_3^1 , C_3^2 , $3C_2$ (three equivalent C_2 axes), i , S_6^1 , S_6^5 and $3\sigma_d$ have now been identified, i.e. a total of 12 unique operations. The results of these operations have been described in terms of the rearrangement of the hydrogen atoms around the framework of the ethane structure. The two methyl groups that form the molecule always remain with the same composition, even when the atom labelling is taken into account, so that C_1H_{1-3} forms one methyl and C_2H_{4-6} the other. However, the symmetry operations can change the end of the molecule occupied by each methyl group and can change the ordering of hydrogen atoms within the group, from clockwise to anticlockwise. The symmetry operations give a systematic way to rearrange the equivalent atoms within a molecule so that each atom ‘visits’ all chemically equivalent positions. This idea was used in the discussion of NMR spectroscopy in Chapter 1.

We limit the list of operations by identifying equivalences so that there is no redundancy; each arrangement of the labelled atoms in the molecule is generated only once. The hydrogen atoms of ethane are particularly useful for this. If we chose the carbon atoms, then there are only ever two arrangements: the carbon atoms sit on the C_3 axis and in the three mirror planes and so are unchanged by C_3^1 or C_3^2 rotations or any simple reflection. They are also swapped over by S_6^1 and S_6^5 any C_2 rotation or i . The carbon atoms do not show the full effect of these operations because they are at special symmetry positions. For the same reason, in planar molecules like BF_3 , no atom sets show the full effects of symmetry operations; in particular, the mirror plane containing all the atoms will always

appear to give the same result as E . This is why arrows need to be added to fully appreciate the result of the improper rotations illustrated in Figure 2.9.

2.4.2 The Inverse of an Operation

With the inclusion of the improper rotation the set of symmetry operations used in chemistry is complete and we may look at the relationships that occur between operations. Earlier in the chapter we introduced the identity operation E ; when this is used to form a product with any other operation, X say, the result is the same as if the operation was carried out alone:

$$EX = XE = X \quad (2.3)$$

E plays a role in symmetry operations similar to the number 1 in ordinary algebra, where the equivalent equation would be

$$1 \times X = X \times 1 = X \quad (2.4)$$

The existence of unity in normal algebra also implies that all numbers have an inverse, X^{-1} , with the property

$$X^{-1}X = 1 \quad (2.5)$$

For a number, $X^{-1} = 1/X$; however, it is not clear what ‘dividing by’ a symmetry operation means. We just require that there is an operation X^{-1} which has the property,

$$X^{-1}X = E \quad (2.6)$$

The identity operation is present in all point groups; so, if X is in a given point group, then so is X^{-1} . A list of operations and their inverses is given in Table 2.3.

Table 2.3 A list of operations and their inverses. Note that m and n are integers and the subscripts on the mirror planes indicate that any mirror plane is its own inverse.

Operation X	Inverse X^{-1}	Operation X	Inverse X^{-1}
E	E	$\sigma_{h,d,v}$	$\sigma_{h,d,v}$
C_n^m	C_n^{n-m}	S_n^m (n even)	S_n^{n-m}
i	i	S_n^m (n odd)	S_n^{2n-m}

The operations E , i and any mirror plane are their own inverses. The inverse for a rotation depends on the order of the axis. If an axis is of order n , then $C_n^n = E$ and so the inverse of a C_n^m rotation is simply the number of additional rotations required to complete 360° , i.e. C_n^{n-m} .

A similar argument applies to improper rotations of even order. However, improper rotations of odd order require two complete rotations before the original configuration is regained, and so a factor of 2 is introduced in the inverse.

Problem 2.3: Find and confirm (by forming $X^{-1}X$) the inverse operations for (i) S_4^3 , (ii) C_5^2 and (iii) S_6^3 .

2.4.3 The Order of the Product; Operations that Commute

Equipped with the full set of symmetry operations it is now possible to check that any group of molecular operations is closed, and so we return to the problem of ethane in its staggered conformation. Ethane contains a set of equivalent C_2 axes and a set of equivalent dihedral mirror planes σ_d . For the purposes of this exercise these must be distinguished so that the exact equivalence of the products of operations may be discerned. The notation to be used is given in Figure 2.10. From the diagram of the molecule in the space-filling representation (Figure 2.10a) the C_2 axes can be seen to be equivalent: they all go through the centre of the C–C bond and are perpendicular to it. Looking down the C_3 axes, it can also be seen that each C_2 axis lies in-between C–H bonds that are at opposite ends of the molecule. With the atoms labelled as shown in Figure 2.10b we can distinguish the result of each C_2 operation. For example C_2^A will cause H_3 to be swapped with H_6 , but C_2^B will cause H_3 to swap with H_4 .

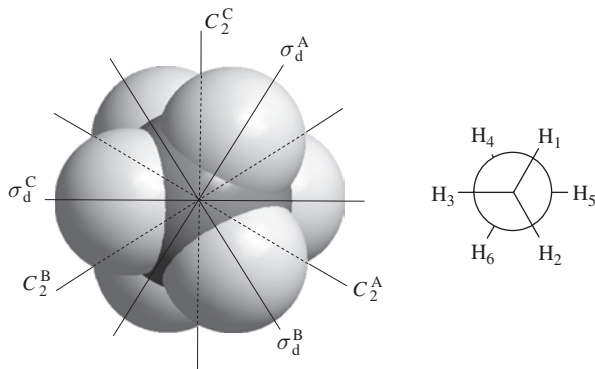


Figure 2.10 Labelling used for the sets of equivalent C_2 axes and dihedral mirror planes for the purposes of constructing the multiplication table for ethane. Note that the σ_d planes have been labeled so that A initially contains H_1 , B initially contains H_2 and C initially contains H_3 , the C_2 axes have also been labeled for the σ_d plane to which they are perpendicular.

As before, when generating products of operations for the multiplication table, the symmetry elements are thought of as fixed in space, set by the global axis system. For example, C_2^A will alter the positions of the hydrogen atoms but not the location of C_2^B .

Applying each pair of operations in turn gives the full multiplication table shown in Table 2.4. This table is considerably more complex than that for the examples of water and ammonia used earlier because the number of individual operations is greater. However, the rules set out for the products of the principal axis with vertically orientated mirror planes can also be seen to apply to the dihedral planes in this case.

Table 2.4 The full multiplication table for ethane in the staggered conformation. The additional labels on the C_2 axes and σ_d planes are defined in Figure 2.10.

First operation - - - - - →													
	E	C_3^1	C_3^2	C_2^A	C_2^B	C_2^C	i	S_6^1	S_6^5	σ_d^A	σ_d^B	σ_d^C	
2 nd	E	E	C_3^1	C_3^2	C_2^A	C_2^B	C_2^C	i	S_6^1	S_6^5	σ_d^A	σ_d^B	σ_d^C
op.	C_3^1	C_3^1	C_3^2	E	C_2^C	C_2^A	C_2^B	S_6^5	i	S_6^1	σ_d^C	σ_d^A	σ_d^B
	C_3^2	C_3^2	E	C_3^1	C_2^B	C_2^C	C_2^A	S_6^1	S_6^5	i	σ_d^B	σ_d^C	σ_d^A
	C_2^A	C_2^A	C_2^B	C_2^C	E	C_3^1	C_3^2	σ_d^A	σ_d^C	σ_d^B	i	S_6^5	S_6^1
	C_2^B	C_2^B	C_2^C	C_2^A	C_3^2	E	C_3^1	σ_d^B	σ_d^A	σ_d^C	S_6^1	i	S_6^5
	C_2^C	C_2^C	C_2^A	C_2^B	C_3^1	C_3^2	E	σ_d^C	σ_d^B	σ_d^A	S_6^5	S_6^1	i
	i	i	S_6^5	S_6^1	σ_d^A	σ_d^B	σ_d^C	E	C_3^2	C_3^1	C_2^A	C_2^B	C_2^C
	S_6^1	S_6^1	i	S_6^5	σ_d^B	σ_d^C	σ_d^A	C_3^2	C_3^1	E	C_2^B	C_2^C	C_2^A
	S_6^5	S_6^5	S_6^1	i	σ_d^C	σ_d^A	σ_d^B	C_3^1	E	C_3^2	C_2^C	C_2^A	C_2^B
	σ_d^A	σ_d^A	σ_d^B	σ_d^C	i	S_6^5	S_6^1	C_2^A	C_2^C	C_2^B	E	C_3	$^1C_3^2$
	σ_d^B	σ_d^B	σ_d^C	σ_d^A	S_6^1	i	S_6^5	C_2^B	C_2^A	C_2^C	C_3^2	E	C_3^1
↓	σ_d^C	σ_d^C	σ_d^A	σ_d^B	S_6^5	S_6^1	i	C_2^C	C_2^B	C_2^A	C_3^1	C_3^2	E

Table 2.4 also illustrates that the result of the product of two symmetry operations often depends on the order that they are executed. For example:

$$\sigma_d^B C_2^A = S_6^1, \text{ but } C_2^A \sigma_d^B = S_6^5, \text{ which means that } \sigma_d^B C_2^A \neq C_2^A \sigma_d^B \quad (2.7)$$

When the result of a pair of operations depends on the order in this way it is said that the operators do not *commute*. In the multiplication of real numbers, the product does not matter on the order used, and so multiplication of simple numbers is commutative, whereas the product of symmetry operations may not commute. In the earlier example of H_2O we did not see this order dependence of the products, and so there are some pairs of operations that do commute.

Pairs of operations that will always commute arise for any product involving the cases:

1. Two rotations around the same axis.
2. The inversion centre and any reflection or rotation, simple or improper.
3. Reflection through two planes which are perpendicular to one another.
4. C_2 rotations about perpendicular axes.
5. Rotation followed by reflection in a plane perpendicular to the rotation axis.

All of the operations for the H_2O molecule fall into one or other of these categories.

For each of the multiplication tables we have derived in this chapter, each row and column contains all of the symmetry operations with no repeats but in a different order to any of the other rows or columns. This is a general property of multiplication tables and should be borne in mind when checking results.

2.5 Chirality and Symmetry

Chiral molecules have the property that they cannot be superimposed on their own mirror images. This means that a chiral molecule can exist in at least two forms which have identical connectivity between the atoms but which are different geometrically. The two forms will be mirror images of one another and are referred to as enantiomers. The properties of the enantiomers are identical unless we probe with a second chiral object. For example, pure, single enantiomer, samples of a chiral compound will have identical melting points and solubilities in nonchiral solvents. However, they will react differently with a single enantiomer of another compound.

Many naturally occurring organic molecules are chiral. For example, limonene (1-methyl-4-isopropenylcyclohex-1-ene) has two enantiomers. These are labelled *S*-limonene and *R*-limonene, from the Latin words for left (*Sinister*) and right (*Rectus*). The assignment of these labels follows a set of rules devised by Cahn, Ingold and Prelog, which is discussed in Appendix 2. Both enantiomers of limonene are formed naturally and are a large part of the molecular mixture determining the smell of citrus fruits. The two chiral forms are sensed differently: *S*-limonene smells of lemons, whereas the mirror image compound *R*-limonene smells of oranges. The left-handed structure, *S*-limonene, is shown in Figure 2.11a and the right-handed structure, *R*-limonene, is shown in Figure 2.11b.

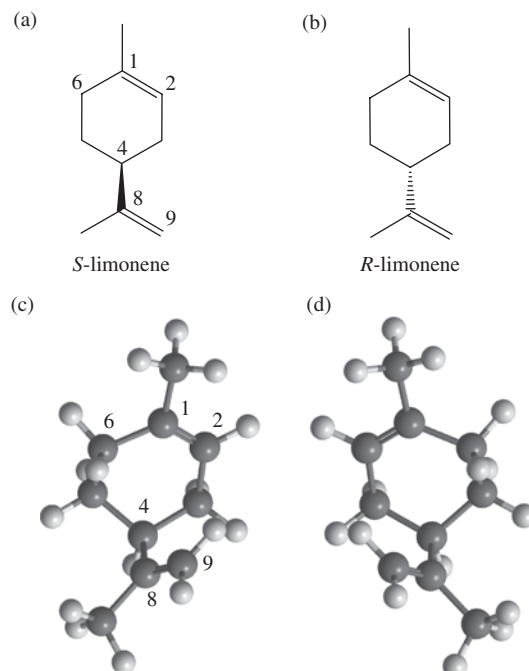


Figure 2.11 The molecular structure of the enantiomers of limonene: (a, c) the chemical structure and ball-and-stick three-dimensional model of *S*-limonene; (b, d) corresponding illustrations for *R*-limonene.

Figure 2.11c and d show three-dimensional representations of the two enantiomers orientated to emphasize that they are reflections of one another. If you have a modelling kit you should construct models of the two enantiomers shown in Figure 2.11c and d and confirm that they cannot be superimposed on one another.

Inspection of Figure 2.11 should concentrate on carbon 4 (C4), which is at the bottom of the cyclohexene ring in each diagram. If we move from C4 around the ring in a clockwise direction, we arrive at C6 after two bonds; this is a saturated ($>\text{CH}_2$) carbon centre. Moving around the ring in the anticlockwise direction from C4 we arrive at C2, which is a carbon atom in the double bond of the ring, so that the two sections of the six-carbon ring either side of C4 are different. The other two substituents on C4 are an isopropyl group and a hydrogen atom, so that the four substituents on C4 are different to one another. This is one way of generating a chiral molecule; if a molecule contains one centre that has four different groups attached, in such away that the four groups are not coplanar, the molecule will be chiral. Since the chirality in this case arises from the substitution patterns possible at a single atom, e.g. C4 in our example, the atom which is substituted is called a chiral centre. Swapping any two of the groups at the chiral centre will give the other enantiomer. However, for carbon centres, the energy required to swap two groups is usually large and so if a single enantiomer is created it will be stable and so observable.

The use of symmetry in determining which molecules can be chiral can be discussed based on the fact that enantiomers are related to one another by reflection. Any object has only one mirror image; it does not matter where the mirror is positioned to reflect the object. This immediately tells us that a molecule with a plane of symmetry cannot be chiral, because we generate an identical molecule when it is reflected in the symmetry plane and so the molecule must be indistinguishable from its mirror image. In fact, if there is any symmetry operation that links a molecule with its mirror image, then the molecule cannot be chiral.

Simple mirror planes are not the only symmetry elements that use reflection. If a molecule possesses an improper rotation axis, then the reflection through the mirror plane used in the symmetry operation will also link the mirror images. So any molecule containing an improper rotation axis as a symmetry element cannot be chiral. Also, since $S_2^2 = i$, the inversion centre also precludes chirality.

So, the most general statement for identifying molecules that are chiral is that:

Chiral molecules must belong to a point group without mirror planes, improper rotation axes or the inversion centre.

2.6 Summary

1. Molecules that can undergo an identical set of operations belong to the same symmetry point group. The idea of a group is really a mathematical abstraction, and for a set of operations to form a proper group the following must apply:

- (i) The product of any two members must also be a member of the group; this means that the group is ‘closed’, i.e. a new symmetry operation cannot be generated by combining the ones in the group.
 - (ii) There must be an identity operation E ; this is just a matter of remembering to write it down, since all objects have the identity element. Any molecule is unchanged by the identity operation (i.e. doing nothing), and so all molecules have at least E .
 - (iii) Every member of a group must have an inverse, i.e. if you carry out an operation there must be another member of the group that undoes that operation. This is one reason for having the identity operator; for example, the inverse to σ_v is σ_v itself, since $\sigma_v\sigma_v = E$. Reflections and the inversion operation are their own inverses in this way, but operations involving rotations have more complex inverses, as detailed in Table 2.3.
2. The symmetry elements of a point group are defined with respect to a global axis system and so do not move under any of the operations of the group.
 3. To check that a group is closed, a multiplication table should be constructed giving all the products of operations in the group.
 4. Symmetry operations need not commute: In general, the order in which two symmetry operations are applied will affect the result, giving different equivalent single operations. The conditions under which operations do commute (i.e. the result is the same irrespective of order) is discussed in Section 2.4.3.

2.7 Completed Multiplication Tables

Tables 2.5 and 2.6 give the completed multiplication tables for H_2O and NH_3 .

Table 2.5 A completed multiplication table for the H_2O symmetry operations.

		First operation - - - - - →			
		E	C_2	$\sigma_v(XZ)$	$\sigma'_v(YZ)$
Second operation	E	E	C_2	$\sigma_v(XZ)$	$\sigma'_v(YZ)$
	C_2	C_2	E	$\sigma'_v(YZ)$	$\sigma_v(XZ)$
	$\sigma_v(XZ)$	$\sigma_v(XZ)$	$\sigma'_v(YZ)$	E	C_2
	$\sigma'_v(YZ)$	$\sigma'_v(YZ)$	$\sigma_v(XZ)$	C_2	E

Table 2.6 A completed multiplication table for the NH_3 symmetry operations.

		First operation - - - - - →					
		E	C_3^1	C_3^2	σ_v^A	σ_v^B	σ_v^C
Second operation	E	E	C_3^1	C_3^2	σ_v^A	σ_v^B	σ_v^C
	C_3^1	C_3^1	C_3^2	E	σ_v^C	σ_v^A	σ_v^B
	C_3^2	C_3^2	E	C_3^1	σ_v^B	σ_v^C	σ_v^A
	σ_v^A	σ_v^A	σ_v^B	σ_v^C	E	C_3^1	C_3^2
	σ_v^B	σ_v^B	σ_v^C	σ_v^A	C_3^2	E	C_3^1
	σ_v^C	σ_v^C	σ_v^A	σ_v^B	C_3^1	C_3^2	E

2.8 Self-Test Questions

- The principal axis direction is usually used as the Z -direction when orientating a molecule in space. For the case of BF_3 , draw the molecule with the fluorine atoms labelled 1–3 and sketch a p_z orbital on each fluorine atom.
 - By considering the effect of the symmetry operations on each orbital show that:
 - the C_3^1 and σ_h operations lead to different results to the S_3^1 operation they make up;
 - the S_3^4 operation leads to an identical result to the C_3^1 operation.
 - The orientation of the orbitals in part (a) can be represented by a single arrow on any of the atoms in the molecule. Using this representation, draw up a multiplication table for the BF_3 case. It will help to use a model and a piece of paper to mark the reference frame, as described in Problem 2.2. In addition, some feature, such as an additional plastic ‘bond’ should be added perpendicular to the plane of the molecule to represent the orientation of the orbitals.
- If we orientate a water molecule as in Figure 2.1 and then move one of the hydrogen atoms in the Z -direction, which way would each of the symmetry operations expect the other hydrogen to go? Draw diagrams to support your answer. What happens if we move the hydrogen in the X -direction (perpendicular to the plane of the molecule)?
- We have seen that $C_2^2 = E$. This is equivalent to saying that a C_2 rotation followed by another C_2 rotation is the same as the identity operation. Using the example molecules suggested, work out the single operation which gives the same result as each of the operation products listed below. In each case, apply the rightmost operation first, number the atoms and add any vectors required to help you identify the configuration generated.
 - $C_4^1 C_2^A$ using the square planar complex $[\text{PtCl}_4]^{2-}$, take C_2^A to be along $\text{Cl}_1\text{-Pt-Cl}_3$.
 - $C_6^5 i$ using benzene.
 - $S_{10}^1 C_5^2$ using ferrocene, refer to Figure 1.8 for the structure.
 - $C_2(Z) \sigma(XZ)$ using ethene, refer to Figure 1.10 for structure and orientation.
- In the main text of Chapters 1 and 2 we have looked at some aspects of the symmetry for the following molecules:
 - H_2O
 - NH_3
 - benzene
 - fluorobenzene
 - BF_3
 - $[\text{PtCl}_4]^{2-}$
 - C_2H_6 (staggered).

Write out all the symmetry elements and operations for each molecule and make a note of any that have exactly the same set.

3

The Point Groups Used with Molecules

3.1 Introduction

In this chapter we will review the common point groups found in chemistry and arrive at a simple methodology to assign any molecule to a point group. Example molecules will then be discussed in Chapter 4. The properties of each point group are encapsulated in the character tables listed in Appendix 12. Each table contains the point group symbol and a listing of the symmetry operations on the top line of the table. The meaning of the rest of the symbols in these tables will become clear in later chapters. Here, we just point out that, once a molecular point group assignment has been made, the operations that are allowed for the molecule can be checked by reference to the point group character table.

3.2 Molecular Classification Using Symmetry Operations

The fact that molecules have a three-dimensional structure and shape was shown by Louis Pasteur in 1848 in some critical experiments on crystalline salts of tartaric acid that formed part of his doctoral studies. Tartaric acid is a naturally occurring compound that is extracted from grape juice and sometimes crystallizes as potassium bitartrate from solution in wine. Pasteur concentrated on the related compound sodium ammonium tartrate. The two forms of tartrate were chemically identical, but a solution of potassium bitartrate would rotate the plane of polarization of plane polarized light to the right whereas a solution of sodium ammonium tartrate would not. Pasteur studied the crystal structures of tartaric acid salts and found the crystallites themselves were chiral, i.e. the facets of the crystals occur in two forms that are mirror images of one another, so that the two crystallite forms cannot be superimposed. In the pure potassium bitartrate, only ‘right-handed’ facets were

observed; however, the sodium ammonium tartrate consisted of a mixture of left- and right-handed crystals. By picking out the two forms from the mixture (using tweezers), Pasteur was able to make solutions of only left-handed or only right-handed crystals and showed that the solution of left-handed crystals gave the opposite optical rotation to that from the right-handed crystals. This demonstrated that the building blocks of the crystals in the two crystal forms were different from one another, since the crystal structure is lost in solution. The conclusion that Pasteur drew was that tartaric acid molecules themselves have a three-dimensional shape and can be left- or right-handed. This type of molecule he classified as asymmetric, and he inferred that molecules that do not rotate the plane of polarized light must be symmetric. We now know that naturally occurring tartaric acid occurs as either the *R,R* or *S,S* molecular structures, as shown in Figure 3.1, and that Pasteur was fortunate to find an example where the crystallization process itself separates the two enantiomers.

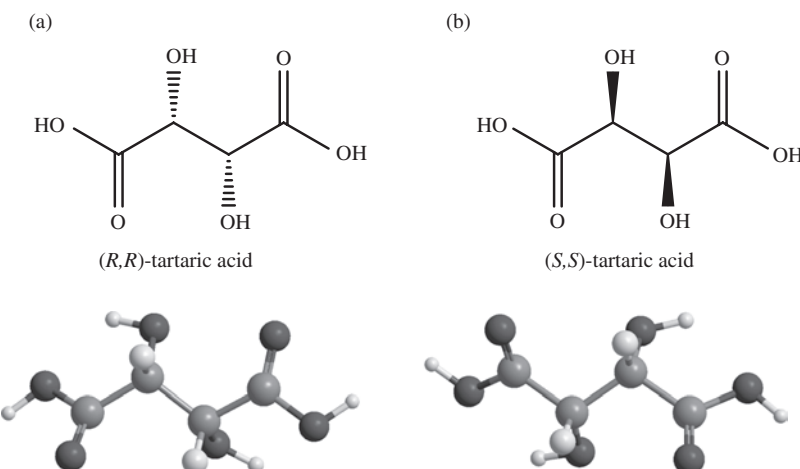


Figure 3.1 The naturally occurring chiral forms of tartaric acid: (a) *R,R* and (b) *S,S*. The molecular models in the lower part of the figures are both set with the OH groups pointing backward so that the mirror image relationship between the two forms can be readily seen.

This was the first example of classification based on molecular shape and gave some indication of the physical properties of molecules that were classified as symmetric compared with those that were labelled asymmetric. However, chirality is not the only manifestation of molecular symmetry, and so a more complete classification of molecular shape has been developed; the system of point groups. To classify the symmetry of a molecule we derive its point group, which carries much more geometric information than Pasteur's symmetric or asymmetric designation.

The system of labels used for molecular point groups comes from the work of Schönflies (1853–1928). The symbols are designed to carry information on the symmetry elements present in the object being discussed. The symmetry of a molecule is governed by the bonding geometries that are preferred by the particular atoms or chemical groups from

which it is formed. This means that the point groups which contain symmetry operations that coincide with the preferred geometries are more popular than others. For example, small symmetric molecules based on four-coordinate carbon atoms often have C_2 or C_3 axes, as shown in the examples of Figure 3.2. However, for this type of molecule, C_4 axes are less common.

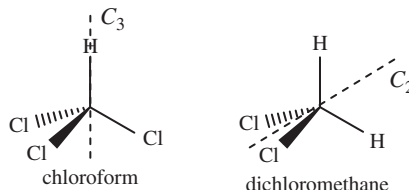


Figure 3.2 Example molecules based on a four-coordinate carbon atom: trichloromethane (chloroform) has a C_3 axis and dichloromethane has only a C_2 axis.

The point groups we will consider can be linked into families, and the groups that are not very common in their own right form important subgroups of more ubiquitous family members. In this chapter, each family of point groups will be considered in turn by looking at the operations in the group itself using idealized model structures. Once the general form of the set of point groups is outlined, some example molecules from particular members of the family will be presented.

3.3 Constructing Reference Models with Idealized Symmetry

The symmetry operations of a group relate equivalent atoms for any molecule conforming to the group symmetry. So far, we have looked for the presence of an operation by imagining the result of carrying it out and checking that atom positions interchange correctly. In this chapter we will look for the possible combinations of operations that can form proper, closed, groups, and this exercise can be carried out in a slightly different way. If we take a single atom and apply a symmetry operation, then the atom will, in general, move to a different position. This movement will occur provided the atom is not at a special symmetry point: on the axis of a rotation or in a mirror plane, etc. In a molecule for which the symmetry operation is valid, the new position will be occupied by an equivalent atom. If we wish to see what a molecule in a particular point group should look like, this movement of one particular atom, or set of atoms, can be used to generate a ‘typical’ object for the point group. The application of all of the operations of the group to such a set of generating atoms will produce a model object conforming to the point group. As examples we will consider simple cases with up to four generating atoms; one or two of these will be positioned at any special symmetry points and the remainder will be at general positions. After each section on a particular set of symmetry point groups we will discuss examples of molecules that belong to those groups. We start with the simplest groups containing either no principal axis or a single rotation axis. These are given group symbols beginning with capital C .

3.4 The Nonaxial Groups: C_s , C_i , C_1

If there are no symmetry axes present, then there are only a few options for the symmetry elements that can be used in a group. The simplest of these is the group C_1 . The symbol C_1 implies that the principal axis is of order 1. That is a rotation by 360° , and so really only E is present, but the symbol is used for consistency with groups containing more symmetry elements. Clearly, many molecules belong to this group, and it is a trivial subgroup of all other point groups.

A C_1 symmetric molecule must contain at least four atoms. This is because any three atoms can be used to define a plane, which would be a symmetry plane for the triatomic. Similarly diatomic molecules always contain a symmetry axis joining the centres of the two atoms and these belong to a special pair of symmetry groups, $C_{\infty v}$ and $D_{\infty h}$, which we will meet later in this chapter. Figure 3.3a shows a three-dimensional set of points that form an object with C_1 symmetry. The points are shaded differently to indicate that they represent different chemical elements and so cannot be related to each other by symmetry. They are also joined by lines to emphasize that they are not coplanar, and the triangular face of the object which is closest to the viewer is marked with a line.

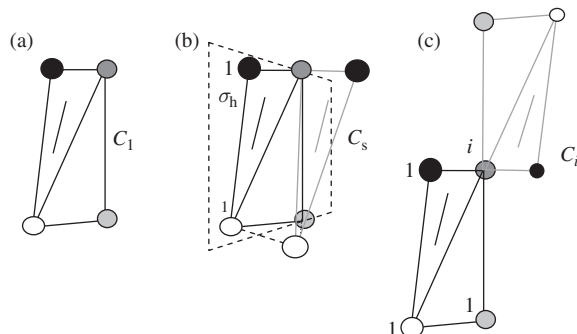


Figure 3.3 Example objects with (a) C_1 , (b) C_s and (c) C_i symmetry. The differently shaded points should be thought of as atoms of different chemical elements. The label 1 has been added to suggest points that are the initial positions used to generate symmetry images of the same shading.

The other two point groups in this section contain only a single additional operation. This operation must be its own inverse to ensure that the group is closed and so the choices are a single mirror plane or the inversion centre. The case of a single C_2 axis comes under the cyclic groups C_n discussed below.

If a molecule contains only a symmetry plane it has C_s symmetry, and by convention the plane is labelled as horizontal, σ_h . In Figure 3.3b we have introduced a mirror plane into the C_1 object of Figure 3.3a, so that it contains the points that are shaded grey. With the mirror plane present the black and white points each have a reflection image on the opposite side of the mirror plane and so a real object with a plane placed in this way must have equivalent atoms at the new positions shown. The points shaded grey are in the plane

and so do not generate any images. The resulting six-point object has C_s symmetry. It is not the simplest case; we could have chosen a plane containing three of the points for example, but it illustrates the relationship between the new structure and the C_1 object we used as the starting point.

The third nonaxial group contains only the identity operator and inversion centre i , and this point group is given the symbol C_i . An example of a C_i object generated from the C_1 structure of Figure 3.3a is shown in Figure 3.3c. We have chosen to place the inversion centre at the top right point in the generating structure, and so this point occurs only once in the resulting object. The other three points generate new positions in the C_i object through the action of the inversion operation. Each of these pairs of points would hold an atom of the same chemical element, and it is an arbitrary choice which we consider as the ‘original’ and which the ‘generated’ point.

3.4.1 Examples of Molecules for the Nonaxial Groups: C_s , C_i , C_1

There are many molecules that conform to the C_s point group; for example, dichlorofluoromethane (Figure 3.4a) and secondary amines such as $\text{N}(\text{CH}_3)_2\text{H}$ (Figure 3.4b). More complex examples include tropinone, Figure 3.4c and d, which is a natural product used

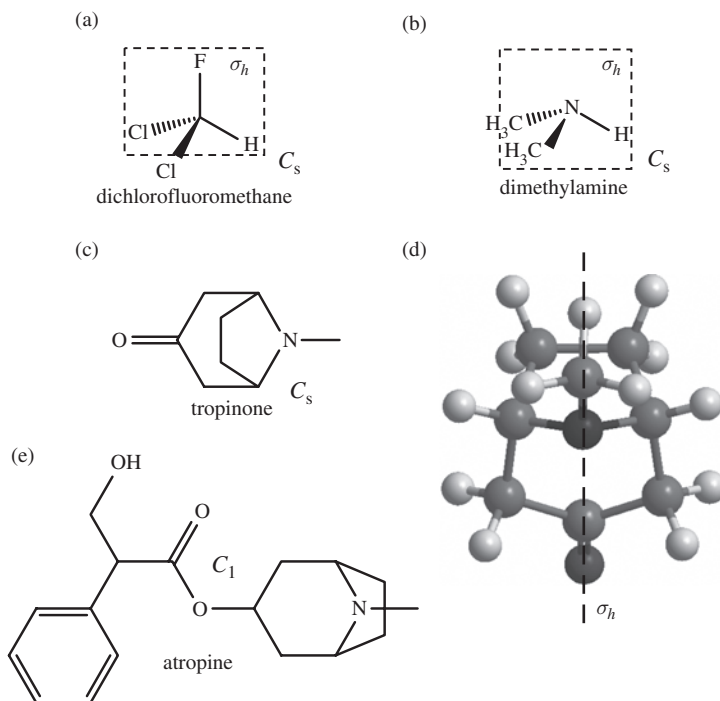


Figure 3.4 Example molecules conforming to the nonaxial group C_s ; each molecule has only a mirror plane and E as symmetry element. Tropinone, structure (c), is shown as a three-dimensional model in (d) and is a precursor to the C_1 (only symmetry element E) molecule shown as (e).

as a precursor for the production of the C_1 molecule atropine, Figure 3.4e. Atropine is an auxiliary drug used in anaesthesia to control secretions by the salivary and gastric glands during operations on these areas of the body.

If a molecule has only an inversion centre present it has C_i symmetry. Examples of this point group are less common, but substituted ethanes such as $(1S,2R)$ -1,2-dichloro-1,2-difluoroethane (Figure 3.5a) can take on conformations with C_i symmetry, and some bimetallic complexes, such as the general structure shown in Figure 3.5b, also fall into this classification.

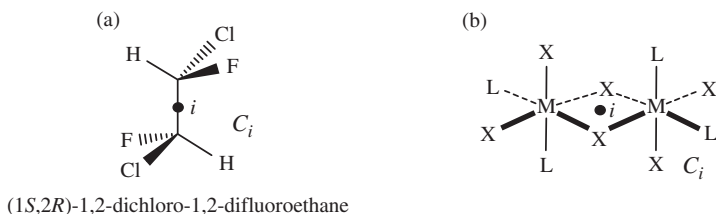


Figure 3.5 Molecular structures with C_i symmetry: (a) a particular conformation of $(1S,2R)$ -1,2-dichloro-1,2-difluoroethane; (b) a bridged transition metal complex shown with nonspecific metal centre M and ligand L,X labels.

3.5 The Cyclic Groups: C_n, S_n

Cyclic groups contain only operations derived from the repeated application of a single rotational symmetry operation. The point group is C_n if the repeated operation is a simple rotation, and we have the point group S_n if it is an improper rotation axis. In both cases the subscript denotes the order of the axis.

All the operations in a cyclic group commute with one another, because a product of two operations can easily be written as the root operation applied multiple times. For example:

$$C_n^m C_n^l = C_n^{m+l} = C_n^l C_n^m \quad (3.1)$$

A group with this property is termed Abelian.

C_2 , the simplest of the C_n groups, is another example in which there is only a single operation other than E present, since C_2 is its own inverse.

For groups containing axes we will use a group order of 4 to generate our typical objects. The C_4 example is shown in Figure 3.6a and the S_4 object is shown in Figure 3.6b. The identification convention for the points introduced for the earlier examples is also used here. However, the points are arranged so that the light and dark grey shaded ones are on the symmetry axis and the black and white points are not. Since the points on the axis are not affected by the rotation operation, the grey points do not generate any new images. However, the black and white points form sets of four points: the initial one (marked 1 in Figure 3.6a) and three symmetry images that correspond to the C_4^1 , $C_2 = C_4^2$ and C_4^3 operations which define the columns of the character table (Figure 3.7a). The C_4^1 , rotation by 90° clockwise, and C_4^3 , rotation by 90° anticlockwise, turn out to have equivalent effects

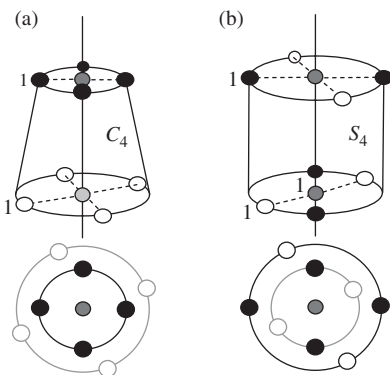


Figure 3.6 Objects generated for (a) C_4 and (b) S_4 symmetry groups. Grey atoms have been placed on the symmetry axis and atoms marked as 1 are suggested initial points for the generation of the set of atoms with the same colouring. The lower diagrams are plan views looking at the upper diagrams from above; lighter lines are used to indicate points further from the viewer. In the plan view for (b) the base is drawn smaller than the top of the figure for clarity.

(a)	C_4	E	$2C_4$	C_2
(b)	S_4	E	$2S_4$	C_2

Figure 3.7 The top lines of the character tables for (a) C_4 and (b) S_4 point groups.

in the symmetry analysis of molecular vibrations or orbitals. In the character table, the column headed $2C_4$ is shorthand for these two C_4 operations. In general, the columns of a character table can refer to more than one operation; these are referred to as *classes* of operations.

The whole set of operations produces an axial ‘molecule’ in which there are four equivalent substituents at either end. The black and white points are at different distances from the axis, and so the radii of the circles drawn to show the relationship between images in Figure 3.6a are different, emphasizing that there are no symmetry-equivalent points at opposite ends of the object. Below the three-dimensional sketch is a plan view of the same structure. For the points at either end of the object, we could also think to introduce vertical mirror planes relating the points to their opposite images within the same terminal group. However, the offset in orientation between the two ends is such that these mirror planes would not be symmetry elements of the object as a whole.

Groups containing only S_n axes must be of even order. This is because point groups containing odd-order improper rotation axes will always have the associated horizontal mirror plane as an additional symmetry element through the equivalence, $S_n^n = \sigma_h$ (n odd), defined in Section 2.3.3. The S_2 group is synonymous with the C_i group, since $S_2^1 = i$, and so the group character table listings in Appendix 12 begin with S_4 . The top line of the S_4 character table is reproduced in Figure 3.7b. The equivalences for the improper rotation axes also lead to the inclusion of simple rotations in these character table headings, since an even-order S_n axis implies the presence of a $C_{n/2}$ rotation axis.

An example of an object belonging to the point group S_4 is constructed from our four generating points in Figure 3.6b. The plan view in Figure 3.6b is drawn looking from above the object, and the lower atoms are drawn on the inner circle for clarity. In this example, we have placed the grey atoms on the S_4 axis and put the black and white generating points at the same distance from the axis at opposite ends of the object. The S_4 operation involves a rotation by 90° followed by a reflection through a mirror plane perpendicular to the axis. The mirror plane is at the midpoint on the axis joining the two grey atoms. This means they must be equivalent to one another, and so they are shaded the same and one is marked as a generator. The black and white points are off axis, and so generate three images each. The reflection part of the S_4 operation results in atoms being swapped from one end of the ‘molecule’ to the other, so that the two ends have an equal number of each type. This also means that the related substituents at either end of the molecule must be equidistant from the axis.

3.5.1 Examples of Molecules for the Cyclic Groups: C_n, S_n

There are several examples of simple C_2 symmetric molecules, including hydrogen peroxide (H_2O_2 , Figure 3.8a) and (1S,2S)-1,2-dimethylcyclopropane (Figure 3.8b). By definition, C_n groups do not contain improper rotation axes, and so molecules in these

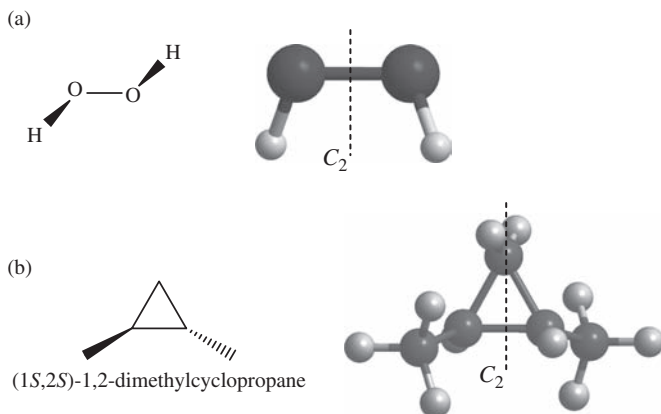


Figure 3.8 Example molecules from the C_2 point group. (a) The O–H bonds of hydrogen peroxide are not coplanar; the only symmetry operations for this molecule are E and C_2 . (b) (1S,2S)-1,2-Dimethylcyclopropane. Three-dimensional models of each molecule are shown to the right of the chemical drawings.

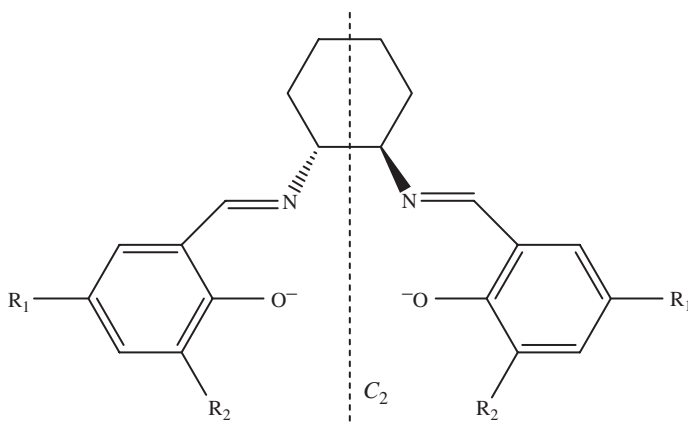


Figure 3.9 The C_2 symmetric Salen ligand. This tetra-dentate anionic ligand is an example of a chiral molecule used as a metal ligand in enantioselective catalysis. The (R,R) form of the ligand is shown here. A variety of groups can be used in the positions marked R_1 and R_2 , including phenyl ($-C_6H_5$) and tert-butyl ($-C(CH_3)_3$).

groups may be chiral, as shown by the second of these examples. One important case is that of chiral salen ligands, such as the example shown in Figure 3.9. This molecule is C_2 symmetric and can be used as a tetra-dentate ligand for a transition metal centre such as Mn or Cr; the conformation in the figure is that expected for the ligand coordinated to a metal centre. Salen ligands contain two chiral centres at the substituted carbon atoms of the cyclohexane ring. Complexes using the salen ligand are important homogeneous catalysts for the epoxidation of alkenes. In these reactions, the chirality of the ligand influences the chirality of the product, and so enantioselective epoxidation is possible.

Problem 3.1: Check the assignment of the chiral centres made in the caption to Figure 3.9 is correct.

C_n groups of higher order are less common than C_2 . One notable example is triphenylphosphine, (PPh_3 , Ph = phenyl group, C_6H_5) a ligand used widely in the chemistry of metal complexes. The three phenyl rings can avoid steric interactions by orientating like propeller blades in the C_3 symmetric structure shown in Figure 3.10.

Examples of molecules with S_n symmetry are relatively rare. An example in organic chemistry is 1,3,5,7-tetramethylcyclooctatetraene (Figure 3.11a and b). This structure contains an eight-membered ring with alternating single and double bonds between carbon atoms. This ring system is not aromatic; the bonds are localized as shown in the chemical drawing picture of Figure 3.11a. The localization of the bonds leads to a nonplanar structure with the geometry shown in Figure 3.11b. The 1,3,5,7-methyl substituents frustrate the horizontal C_2 axes and vertical mirror planes that are present for the unsubstituted ring, and

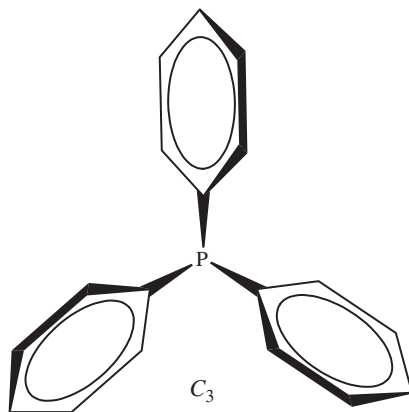


Figure 3.10 The structure of PPh_3 , a molecule with C_3 symmetry.

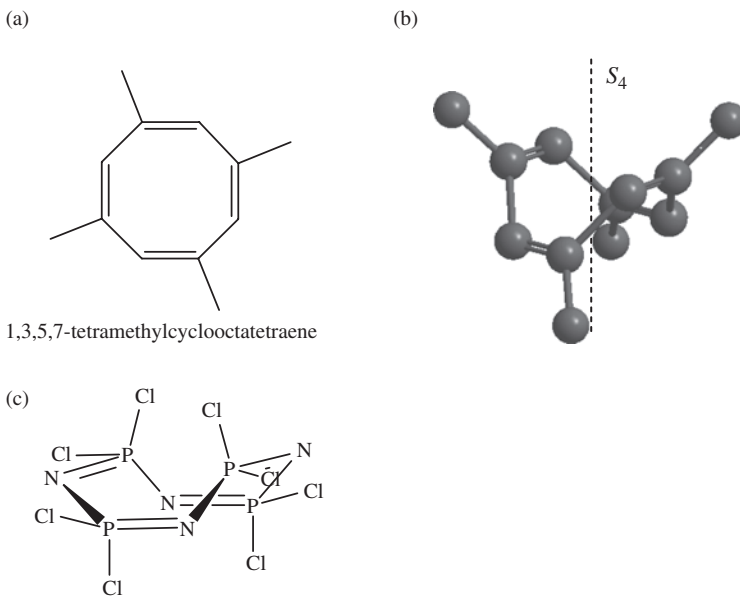


Figure 3.11 Chemical compounds with S_4 symmetry: (a) chemical structure and (b) three-dimensional model of 1,3,5,7-tetramethylcyclooctatetraene; in both cases H atoms are omitted for clarity. (c) A cyclic phosphazene with the formula $\text{N}_4\text{P}_4\text{Cl}_8$ also belongs to the S_4 point group.

so this structure has S_4 symmetry. Similar molecular structures are found for cyclic phosphazenes, which are inorganic compounds containing alternating N and P atoms with two substituents on each P atom. An example with the molecular formula $\text{N}_4\text{P}_4\text{Cl}_8$, which also has S_4 symmetry, is shown in Figure 3.11c.

3.6 Axial Groups Containing Mirror Planes: C_{nh} and C_{nv}

In these groups there is only one axis and the subscript n in the group label is used to indicate its order. The single axis must be the principal axis and defines the vertical direction for the molecule. The C_{nh} point groups contain a single horizontal plane, while the C_{nv} groups have n vertical planes as discussed below.

We begin with an idealized C_{4v} object created from four generating points. Two of these are placed on the axis and two off axis, as shown in the two alternative settings in Figure 3.12a and b. The points are positioned so that one of the vertical mirror planes is the plane of the paper, as shown by the dotted rectangle labelled σ_v . In Figure 3.12a, the mirror plane is valid for both sets of off-axis points, since the generating points at either end of the molecule are also in one of the two σ_v planes; this is reminiscent of a molecule in an eclipsed conformation.

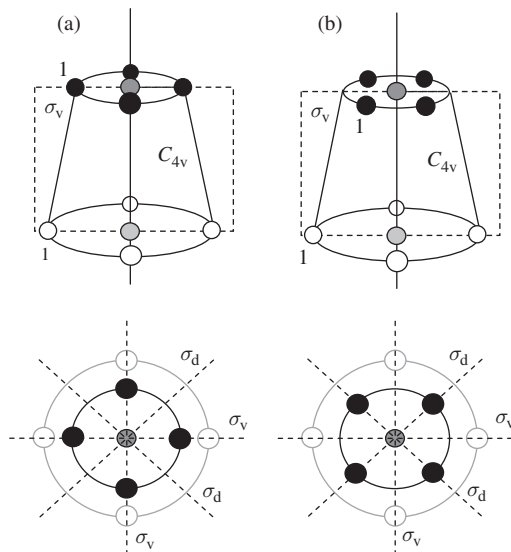


Figure 3.12 Objects in the C_{4v} point group generated to give (a) eclipsed and (b) staggered geometry. The points marked '1' are suggested start points for generating the figures. The lower diagrams are plan views with shading used to give a sense of depth.

The alternative arrangement, shown in Figure 3.12b, is to have one generating point in the σ_v mirror plane and one placed in the σ_d plane. Figure 3.12b shows that this implies a staggered conformation for the imaginary molecule, with, in this C_{4v} example, an angle of 45° between the σ_v and σ_d . Any other relation between the positions of the sets of points at either end of the object would not be consistent with this arrangement of the mirror planes, and so the symmetry of the object would reduce to C_4 .

From Figure 3.12a and b we can also see that any atom which is away from the principal axis of a C_{nv} molecule will have n symmetry-related atoms by virtue of the n rotational

operations around the axis. If we assume an atom is in one of the vertical mirror planes, then it must follow that all of the symmetry-related atoms are also in mirror planes. In the example of Figure 3.12a this leads to two σ_v . We can also position vertical planes as the bisectors of the angles between the two σ_v planes. These new planes are in a different environment: in Figure 3.12a they contain no atoms and in Figure 3.12b they contain atoms from the other set. Since the new planes bisect the angles between the σ_v planes, they are labelled σ_d .

If we generate an example object for an odd-order axis, such as the C_{3v} case shown in Figure 3.13, then the distinction between σ_v and σ_d is no longer relevant. All mirror planes contain only one of each type of point and also bisect the angle between other planes. In this case the vertical planes are all identical and are simply labelled σ_v . This difference is seen in the listing of the point group operations at the top of the corresponding point group tables (Figure 3.14).

Equivalent mirror planes are another example of a class containing more than one symmetry operation in a group. They have identical arrangements of atoms around them and

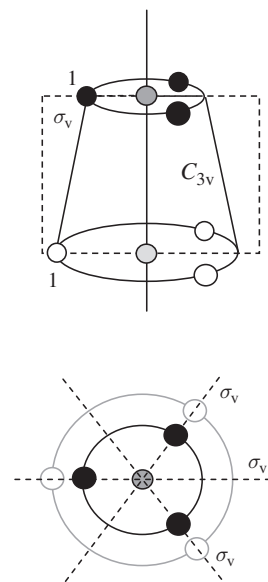


Figure 3.13 An object in the C_{3v} point group; in this case, all vertical mirror planes are equivalent, as can be seen in the plan view, and so only the label σ_v is used.

(a)	C_{4v}	E	$2C_4$	C_2	$2\sigma_v$	$2\sigma_d$
(b)	C_{3v}	E	$2C_3$	$3\sigma_v$		

Figure 3.14 The headings used in (a) the C_{4v} and (b) the C_{3v} character tables.

so give equivalent results for any property of the molecule, as we will see in later chapters. The character tables require only one column for each class of operations, but the number of equivalents is noted in the column heading; hence, for example, $2\sigma_v$ appears as a heading in the C_{4v} character table.

In general, C_{nv} point groups have n -mirror planes each of which contain the principal axis. For even-order axes these are split into two groups, σ_v and σ_d , but for groups with odd-order principal axes the planes are all equivalent and are labelled σ_v .

The objects generated from our three generating points for the C_{nh} point groups are shown for the even- and odd-order axis cases in Figure 3.15a and b respectively. The tops of the corresponding character tables are given in Figure 3.16. Again, we consider the examples of an order 4 axis for the even example and order 3 for the odd. With the horizontal mirror plane placed equidistant from the two grey points which define the axis, these points become symmetry equivalent and so have been shaded similarly. The off-axis generating points are now part of a $2n$ set, because each point above the plane must have an equivalent point below. In the C_{nh} point groups the mirror plane is perpendicular to the axis, and so there must also be an improper S_n axis collinear with the principal axis. For

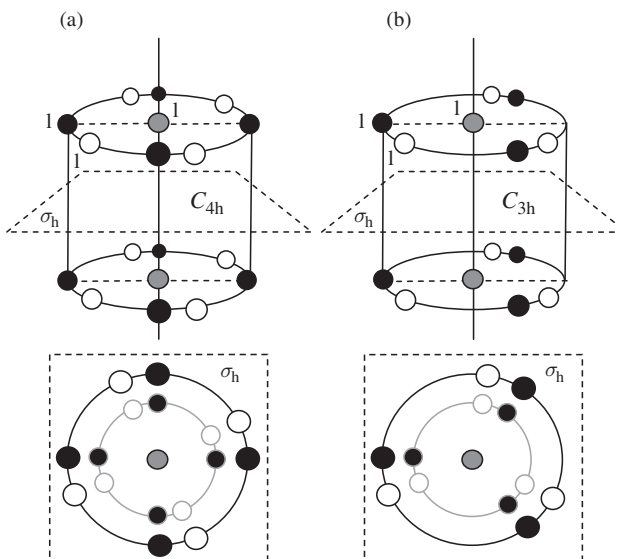


Figure 3.15 A general object generated from the three points marked '1' and the symmetry operations of the (a) C_{4h} and (b) C_{3h} point groups.

(a)	C_{4h}	E	$2C_4$	C_2	i	$2S_4$	σ_h	
(b)	C_{3h}	E	$2C_3$	σ_h	$2S_3$			

Figure 3.16 The headings of (a) the C_{4h} and (b) the C_{3h} point groups.

the even axis case (Figure 3.15a) the principal axis must also be a C_2 axis, which means that there will also be an inversion centre ($i = S_2^{-1}$).

For the odd-order axis case the only operations in the group are the principal axis rotations, the horizontal mirror plane reflection and the improper rotations generated by taking these two together.

Since these groups contain mirror planes, molecules belonging to C_{nh} or C_{nv} are not chiral.

3.6.1 Examples of Molecules for Axial Groups Containing Mirror Planes: C_{nh} and C_{nv}

The C_{2v} point group is extremely common; we have already met water and mono-substituted benzene rings such as fluorobenzene (Figure 2.2), which fall into this point group. There are many other examples, such as urea and furan shown in Figure 3.17a and b respectively. C_{3v} is also a common point group, claiming molecules such as chloroform (CHCl_3) and 1,1,1-trichloroethane, which are shown in Figure 3.17c and d respectively.

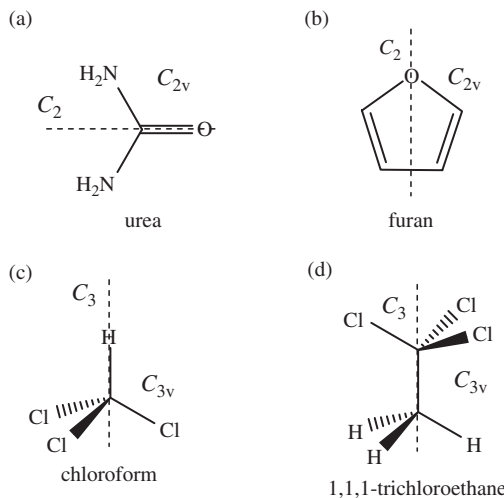


Figure 3.17 Molecules belonging to (a) the C_{2v} and (b) the C_{3v} point groups.

It is less easy to find examples for the C_{nh} point groups; there are several C_{2h} molecules, such as (*E*)-1,2-diphenylethene (common name stilbene), shown in Figure 3.18. This molecule is planar due to conjugation between the ethene double bond and phenyl substituents. Any planar molecule must have the plane of the molecule as a symmetry element, and in this case this is the only symmetry plane present. The principal axis is C_2 and is perpendicular to the plane, which must, therefore, be labelled σ_h . Since C_2 and σ_h are present we must have an S_2 axis, but the only resulting operation is equivalent to an inversion ($i = S_2^{-1}$) and so only i is quoted.

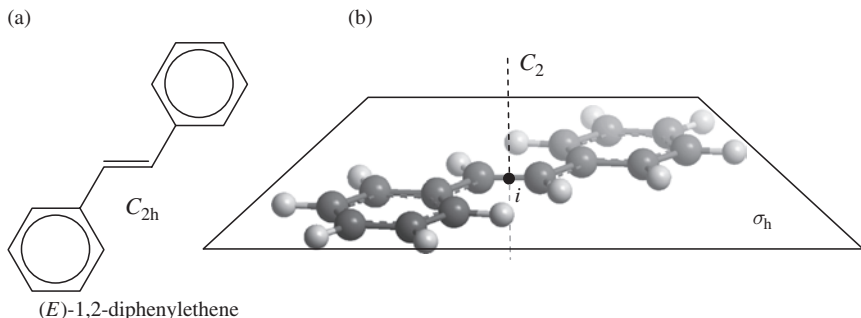


Figure 3.18 (a) The structure of (E)-1,2-diphenylethene, which belongs to the C_{2h} point group, and (b) a ball-and-stick model showing the C_{2h} symmetry elements.

3.7 Axial Groups with Multiple Rotation Axes: D_n , D_{nd} and D_{nh}

Groups containing multiple rotation axes which do not fall into the cubic groups that we meet later on are given point group labels beginning with D . The first set of these contains only rotation axes and are simply referred to as D_n groups, for which the subscript n gives the order of the principal axis. The second set of axes is always C_2 and perpendicular to the principal axis passing through the centre of the molecule. This arrangement means that there are nC_2 axes, since there will be n equivalent orientations of the molecule around the principal axis and each of these must also have a C_2 rotation that is a valid symmetry operation.

There are very few examples of molecules belonging to the D_n point groups, but they provide important subgroups of the more common D_{nd} and D_{nh} point groups. The D_n groups can be thought of as distortions of molecules in these higher symmetry point groups that destroy the mirror planes present. We can, of course, use the generation method to construct a D_4 object as an example of this type of point group. This is shown in Figure 3.19a: the grey points are placed on the principal axis equidistant from the centre of the object and so they become symmetry equivalent. The principal axis in this example is even ordered, and so is also the first C_2 axis we would identify ($C_4^2 = C_2^1$). Looking at the plan view, there are two distinct sets of C_2 axes perpendicular to the principal. The first are directly under two of the points generated from the black circle, and these are labelled C_2' . The second pair of C_2 axes bisect the angles between the C_2' pair and are not under any points in the plan view. Since they are in a different environment to either the C_2 or C_2' axes, they are labelled C_2'' . The generating points off axis are now members of sets of eight, since the two ends of the structure are linked by the horizontal C_2' axes.

The D_{nd} groups are extensions of the related D_n groups by the introduction of dihedral mirror planes in between the horizontal C_2 axes, as shown in Figure 3.19b. To continue with four generating points and a principal axis of order 4 would lead to highly cluttered diagrams, so we have reduced the number of generating points to two: an on-axis grey point and an off-axis black point. The grey point on the axis is not central, and so the C_2' or C_2'' operations will generate a second grey point. However, because the principal axis operations leave points on the axis unaffected, only two points are generated. Off-axis

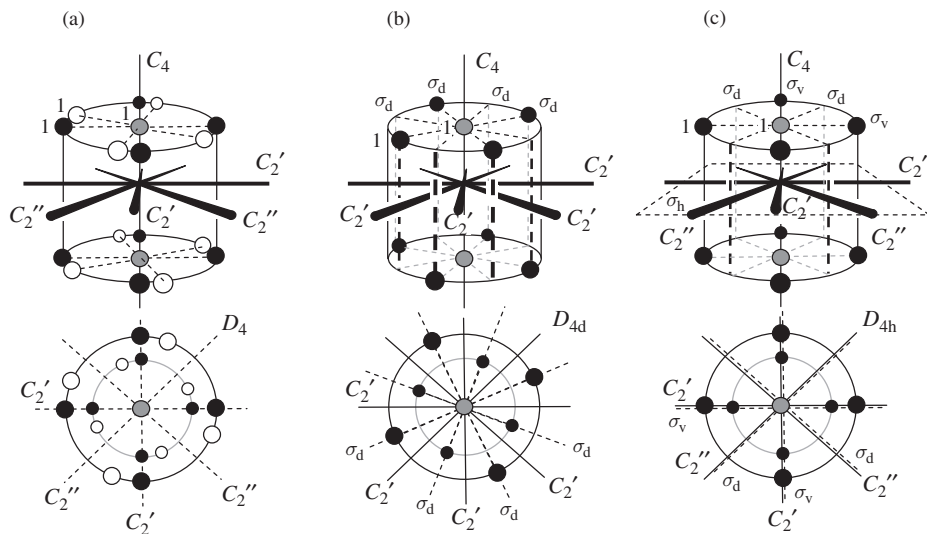


Figure 3.19 Illustrative constructions for (a) D_4 , (b) D_{4d} and (c) D_{4h} point groups. In each case the points marked '1' can be thought of as generating points, and all symmetry-equivalent points have identical shading.

points that are not on the C_2' or C_2'' axes lead to $2n$ symmetry-equivalent points, and so the black circle in the D_{4d} example has spawned seven images. The dihedral mirror planes require that the off-axis points are arranged either on the mirror planes or in pairs of points equidistant from the planes. We saw in the C_{4v} examples of Figure 3.12 that this requirement in that case leads to molecules that are either in an eclipsed or staggered conformation. Here, D_{nd} is the point group for molecules in a staggered conformation in which the two ends of the molecule are equivalent.

We have already discussed an example of this sort of point group in Chapter 2, where the product table for ethane (D_{3d}) in the staggered conformation was derived, resulting in Table 2.4. Referring back to that table, it can be seen that the section based on products of simple rotations only ever generates other simple rotations or the identity. This shows that C_3 and D_3 are self-contained, closed, subgroups of D_{3d} . This can be a useful property to exploit in a symmetry problem. We can initially work in a simpler subgroup requiring less operations to be considered and then check that our results are consistent with the complete group. This approach is used in many of the problems tackled in Chapters 6 and 7.

If a molecule with the symmetry elements of D_3 also has a horizontal mirror plane then it belongs to the D_{3h} point group. The general structure for this case is shown in Figure 3.19c, where again we have used one on-axis (grey) and one off-axis (black) generating point. The horizontal mirror plane implies that the two ends of the object have equivalent points which are eclipsed in the plan view of the molecule looking down the principal axis. The presence of the horizontal plane and C_2 axes also implies that there must be vertical and dihedral mirror planes present for the group to be closed. For example, Figure 3.20 shows

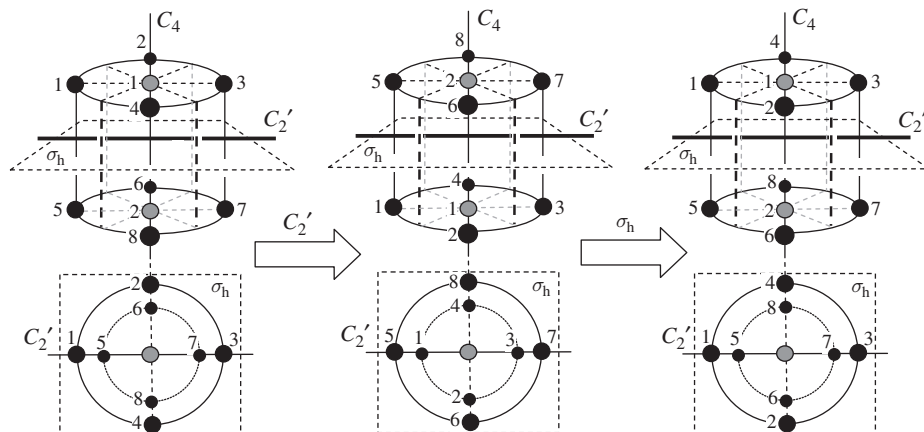


Figure 3.20 A combined $\sigma_h C_2'$ operation in the D_{4h} point group, showing that $\sigma_h C_2' = \sigma_v$. The vertical plane is the plane of the paper containing the off-axis points 1, 3, 5, 7; comparing the start point and the end, these points are in their original positions, whereas the pairs 2, 4 and 6, 8 have been swapped as expected for the single reflection through σ_v .

that the product of a C_2' axis and the horizontal mirror plane is equivalent to a reflection in a vertical mirror plane, i.e.

$$\sigma_h C_2' = \sigma_v \quad (3.2)$$

Since the group must be closed, the σ_v planes must also be possible operations in the group. These sorts of relationships limit the number of point groups that are possible.

Problem 3.2: Show that the product of a C_2'' axis and the σ_h plane in the D_{4h} point group implies that there are also σ_d mirror planes.

3.7.1 Examples of Axial Groups with Multiple Rotation Axes: D_n , D_{nd} and D_{nh}

In the previous section we noted that the D_n point group is quite rare. However, it does form a subgroup of the much more ubiquitous D_{nd} and D_{nh} point groups.

Figure 3.21 shows two examples of molecules in the D_{nd} point groups. Allene is the common name for the molecule propa-1,2-diene (C_3H_4), which has a bond angle of 180° at the central C atom (Figure 3.21a). The two double bonds form at right angles to one another, and so the terminal CH_2 groups are staggered. This gives an S_4 axis along the same line as the C_2 axis containing the three C atoms, and this C_2 axis is accordingly taken as the principal axis. The improper rotation and the additional C_2' axes can be seen more clearly in the view down the principal axis shown to the right in Figure 3.21a. This view also shows the σ_d mirror planes which are in between the axes.

Symmetry operations for ethane in the staggered conformation were covered in Section 2.3.3, including the illustration of example operations in Figure 2.5. It should now be clear that these are just the operations required to classify ethane as belonging to the D_{3d} point group.

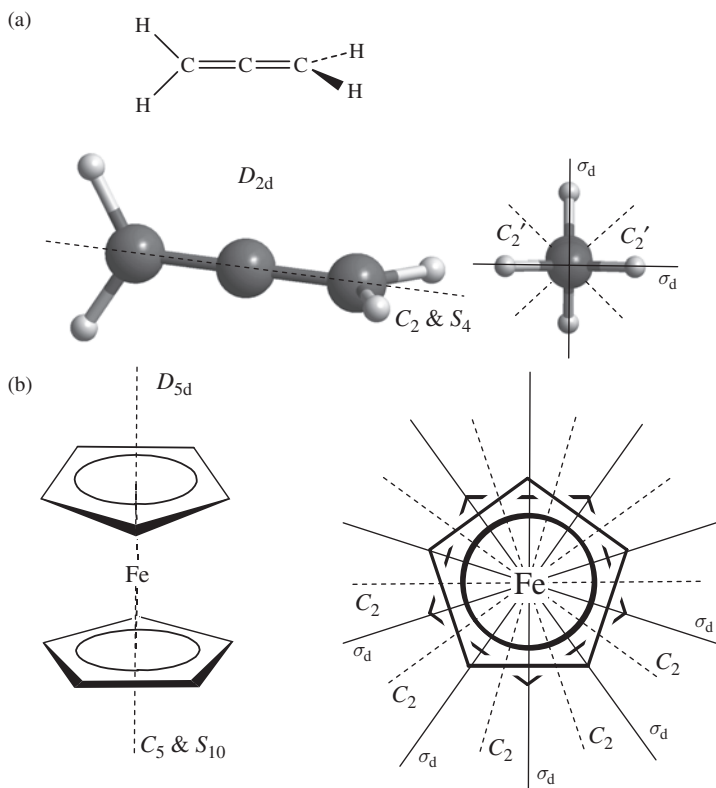


Figure 3.21 Example molecules belonging to D_{nd} point groups (a) propa-1,2-diene, D_{2d} , (b) ferrocene, D_{5d} .

The axial symmetry elements for ferrocene are shown in Figure 3.21b along with the dihedral mirror planes. Since the principal axis in this case is C_5 , ferrocene belongs to the D_{5d} point group.

It should be noted that if any of our example molecules had a slightly different ‘twist’ along the principal axis, then the dihedral mirror planes would no longer be valid and the symmetry would be reduced to D_n .

Molecules in D_{nh} point groups are shown in Figure 3.22. Ethene is a classic example of D_{2h} symmetry, and the C_2 axes and mirror planes are overlaid on this molecule in Figure 3.22a. This group contains only C_2 axes, and none has the collinear S_4 axis we used to identify the principal axis in the D_{2d} example. Hence, the designation of the vertical direction for the ethene molecule is an arbitrary choice from the three possibilities. This is recognized in the headings of the character table by assigning each of the C_2 axes to a Cartesian axis direction, X, Y or Z , rather than giving one a higher priority than the other two. The usual convention with planar molecules, when such ambiguity arises, is to set Z perpendicular to the molecular plane and then X and Y are set as shown in Figure 3.22a. Labelling of the mirror planes follows the same convention and all planes and axes meet at a central point, which is the site of an inversion centre.

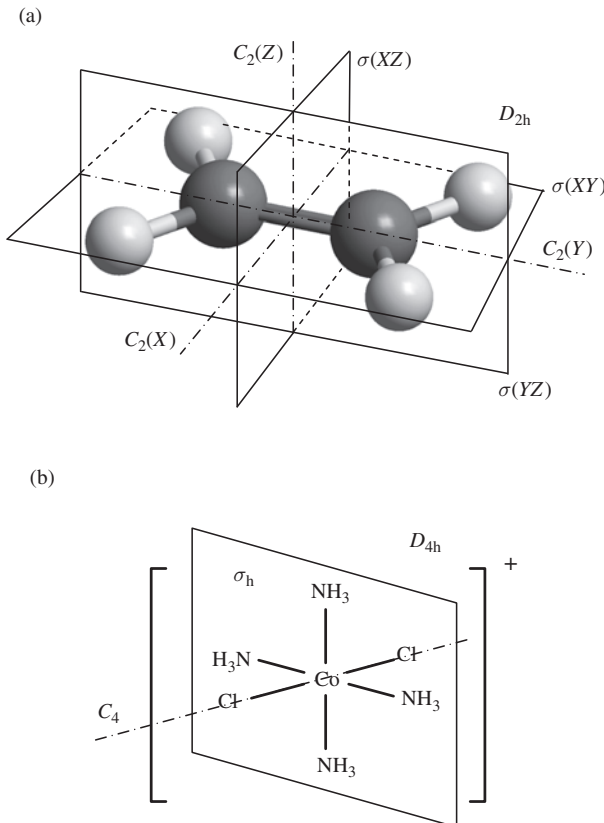


Figure 3.22 Example molecules belonging to D_{nh} point groups: (a) ethene, D_{2h} ; (b) the trans-isomer of $[\text{Co}(\text{NH}_3)_4\text{Cl}_2]^+$, D_{4h} .

The trans-isomer of $[\text{Co}(\text{NH}_3)_4\text{Cl}_2]^+$ has a C_4 axis defined by the $\text{Cl}-\text{Co}-\text{Cl}$ line, as shown in Figure 3.22b. The four amine ligands are in the horizontal mirror plane, which also contains four C_2 axes (two, C_2' , along $\text{Co}-\text{NH}_3$ bonds and two, C_2'' , bisecting $\text{H}_3\text{N}-\text{Co}-\text{NH}_3$ angles). The complex is shown with the principal axis running from front left to back right of the diagram, but remember that this axis sets the vertical reference direction used in discussing the geometry. This complex is an example of the D_{4h} point group. Note that in this assignment we have ignored the amine H atoms. The amine ligands are able to rotate freely around the $\text{Co}-\text{NH}_3$ bonds, and so the orientations of the H atoms will be dynamically averaged out and will not influence the properties of the complex.

Problem 3.3: Elemental sulfur can form molecular S_8 ring structures which belong to the D_{4d} point group. Sketch out the conformation of S_8 this implies.

Problem 3.4: Benzene (C_6H_6) is a planar molecule with a principal C_6 axis. Assign its point group and illustrate the positions of the symmetry elements on sketches of the

molecule. Remember that, once the point group is assigned, the full list of symmetry operations can be read from the top of the character table in Appendix 12.

3.8 Special Groups for Linear Molecules: $C_{\infty v}$ and $D_{\infty h}$

To construct general objects for the axial groups, we have used points on the principal axis to show that operations involving this axis leave these points unaffected. In groups with an axis of order infinity, any off-axis points would generate an infinite number of new atom positions under the rotation operation. This means that any molecule belonging to these groups must be linear. The principal axis will then contain all the atoms in the molecule, and so any rotation will leave the atom coordinates unaffected. The order of the axis is infinite, since there are an infinite number of possible angles of rotation which leave the molecule in an identical state. In a similar way, any plane containing the axis must be a valid symmetry element for the object, since it will contain all the points belonging to the structure. So, there are also an infinite number of vertical mirror planes present.

Figure 3.23 shows the two point groups that arise for linear molecules. If the two ends of the molecule are different, then the only symmetry elements are C_∞ and the vertical mirror planes, so the point group is $C_{\infty v}$ by analogy with C_{2v} , C_{3v} , etc. If the molecule has equivalent points at either end of the axis then it will also have a horizontal mirror plane σ_h and an infinite number of C_2 axes perpendicular to the principal axis. In this case the point group will be $D_{\infty h}$, since the same types of element are present as for D_{nh} point groups. The character table titles for these two groups are shown in Figure 3.24. The presentation

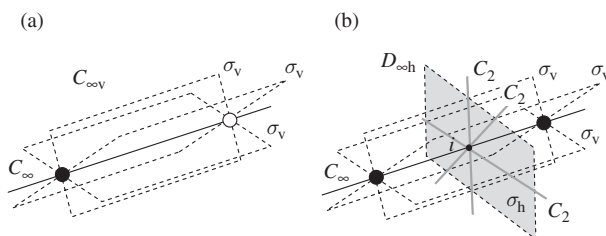


Figure 3.23 Objects constructed for (a) the $C_{\infty v}$ and (b) $D_{\infty h}$ point groups. In each case, only a small selection of the infinite number of possible σ_v planes is shown.

(a)	$C_{\infty v}$	E	$2C_\infty^\Phi$	\dots	$\infty\sigma_v$	
(b)	$D_{\infty h}$	E	$2C_\infty^\Phi$	\dots	$\infty\sigma_v$	i

Figure 3.24 The headings used for the character tables for linear molecules: (a) $C_{\infty v}$; (b) $D_{\infty h}$. In each case, the column heading ‘...’ indicates an infinite number of similar operations to the preceding column and the superscript Φ refers to the angle of rotation for the operation.

of the character table data requires the infinite number of operations to be noted, and this is done by adding lines of dots to the title line to indicate that a sequence of related operations is present. The notation C_{∞}^{Φ} is used for the rotation operations about the infinite axis, where Φ indicates the angle of rotation for the operation. There are two operations for each angle, since clockwise and anticlockwise rotations belong to the same class.

Linear molecules are rather straightforward to visualize and so we will not provide illustrative examples here. Diatomic molecules, such as O_2 , Cl_2 and N_2 , provide good examples of molecules in the $D_{\infty h}$ point group, alongside the linear molecules ethylene, C_2H_2 and CO_2 . Diatomics formed from two different elements, such as CO , NO and HF , belong to the $C_{\infty v}$ point group, along with more complex linear molecules such as hydrogen cyanide (HCN).

3.9 The Cubic Groups: T_d and O_h

The point groups covered so far, with the exception of the simple C_1 , C_s and C_i cases, have had a principal axis which is straightforward to define and no other axes of order higher than 2. Those point groups describe well the wide range of molecules that can be considered to be axial or planar. In this section we turn to cases that are often regarded as higher symmetry objects in which there are multiple axes of order higher than 2. This set of related groups is best thought of as the symmetry groups for simple solid shapes. We will deal with two common cases of tetrahedral and octahedral molecules and show how these relate to the symmetry of the cube. There are some molecules of very high symmetry, such as buckminsterfullerene (C_{60}) in which all 60 C atoms are symmetry equivalent, but the consideration of such cases is beyond the scope of this introductory text.

The tetrahedron is an important shape in chemistry. Methane, the complex $[Ni(CO)_4]$ and many other molecules in which a central atom has four equivalent bonds take on this geometry. The symmetry of the tetrahedron is best discussed with reference to a solid model, and a paper template is provided in Appendix 3 from which a tetrahedron and the related cube can be constructed. This paper model also has some representative symmetry elements drawn on it which are also illustrated in Figure 3.25. The highest order axes are C_3 which join each corner of the tetrahedron to the centre of the opposite face. There are four corners, and so there are four axes; each gives rise to two operations (C_3^{-1} and C_3^2), and so $8C_3$ appears in the title line of the character table (Figure 3.26a).

Figure 3.25b shows that there are also C_2 axes which run through the centres of opposite edges of the tetrahedron; for methane, these axes bisect two of the H—C—H angles. The tetrahedron has six edges and so there are $3C_2$ operations. The lines of the C_2 axes are shared by S_4 axes; these are best seen by looking down an axis direction, as shown in Figure 3.25c, in which the mirror plane used in the improper rotation is also given. The S_4^2 operations are identical to the C_2 rotations we have already identified, and so only S_4^{-1} and S_4^3 are counted at the head of the character table; with three axes this shows $6S_4$. Finally, there are six mirror planes, each of which contains an edge of the tetrahedron and bisects the opposite edge, as shown in Figure 3.25d. This means that each plane contains two of the C_3 and one of the C_2 axes. Since the C_3 is the highest order axis, we would expect it to define vertical; however, there is now no clear choice between the C_3 axes to be made, as they are all equivalent. This influences the designation of the six equivalent mirror planes,

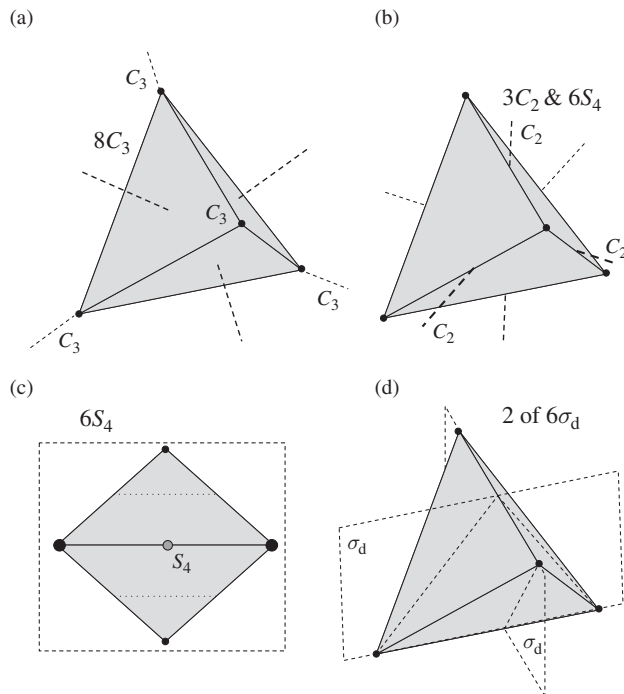


Figure 3.25 The symmetry elements for the operations of tetrahedral T_d symmetry. (a) The $8C_3$ axes giving $8C_3$ operations, (b) the $3C_2$ axes, (c) a view down one of the three S_4 axes and the mirror plane that is used as part of the improper rotation and (d) two of the six dihedral mirror planes.

(a)	T_d	E	$8C_3$	$3C_2$	$6S_4$	$6\sigma_d$					
(b)	O_h	E	$8C_3$	$6C_2$	$6C_4$	$3C_2 (= C_4^2)$	i	$6S_4$	$8S_6$	$3\sigma_h$	$6\sigma_d$

Figure 3.26 The headings from (a) the T_d and (b) the O_h character table.

two of which are shown in Figure 3.25d. Each mirror plane contains two of the C_3 axes, and so a given mirror plane will have a vertical orientation with respect to either of these. The angle between the other two C_3 axes is bisected by our example plane, and so the designation σ_d is used.

The tetrahedron symmetry elements can be thought of as a subset of those of a related cube. If we draw a cube and place atoms at half of the eight corners such that on any face they are diagonally opposite to one another, then the atoms will define a tetrahedron, as shown in Figure 3.27a. The paper model of a cube from Appendix 3 is made with one open side so that the tetrahedral model can be inserted into it in the same orientation. This relationship between the cube and the tetrahedron shows how the tetrahedron can be

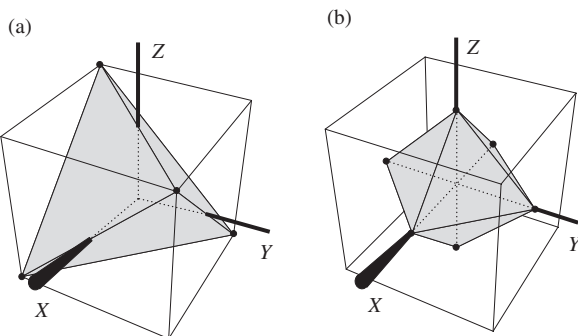


Figure 3.27 The relationship between the cube and (a) the tetrahedron and (b) the octahedron. The axis system shown can be used as a common reference frame for all three figures.

orientated with respect to an axis system. The axis system marked on the models and in Figure 3.27 have X , Y and Z each emerging from the centre of a cube face with the origin of the axis system at the cube centre. This places each axis along a C_4 symmetry axis for the cube. The tetrahedron and the cube share the same centre, but the X , Y and Z axes each pass through the centre of an edge of the tetrahedron, i.e. along the C_2 axes. We will use this axis system in later chapters to orientate basis functions, such as the atomic orbitals (AOs) of the central atom of a tetrahedron.

Figure 3.27b shows how an octahedron can also be constructed inside the cube. This time, the corners of the octahedron are at the centre of the faces of the cube and so the X , Y and Z axes are along the lines from the centre of the figure to its corners; in an octahedral complex, this would be along the metal centre–ligand bonds. These lines are C_4 axes for the octahedron and the cube; in fact, all the symmetry elements of the cube are also valid for the octahedron and both belong to the O_h point group. The symmetry elements for the operations listed in the character table headings (Figure 3.26b) are illustrated in Figure 3.28 using the two objects nested in the same way as shown in Figure 3.27b. The highest order axes are C_4 , which pass through the centres of opposite faces of the cube and through opposite corners of the octahedron (Figure 3.28a). These are collinear with the X , Y and Z axes defined in Figure 3.27b. Each C_4 axis gives rise to two C_4 operations (C_4^1 , C_4^3) and there must also be a C_2 axis along the same line, since $C_4^2 = C_2^1$. So these three axes account for the $6C_4$ and $3C_2 (= C_2^2)$ column headings in the O_h character table (Figure 3.24b). Joining opposite corners of the cube are the C_3 axes shown in Figure 3.28b; these axes also pass through the centre of opposite faces in the octahedron. There are eight corners to the cube, so there are four such axes; each gives two operations (C_3^1 and C_3^2), and so $8C_3$ heads up the second column of the character table. Figure 3.28c shows that there are a further set of C_2 axes joining the centres of opposite edges of the cube which also pass through opposite edges of the octahedron. There are 12 edges in each figure, and so $6C_2$ axes with associated $6C_2$ operations.

The improper S_6 axes are more difficult to see than the C axes, but it helps to look directly along the C_3 axis of the three-dimensional model as shown in Figure 3.28d. From this view it is clear that a rotation by C_6^1 would bring the three foreground corners (marked

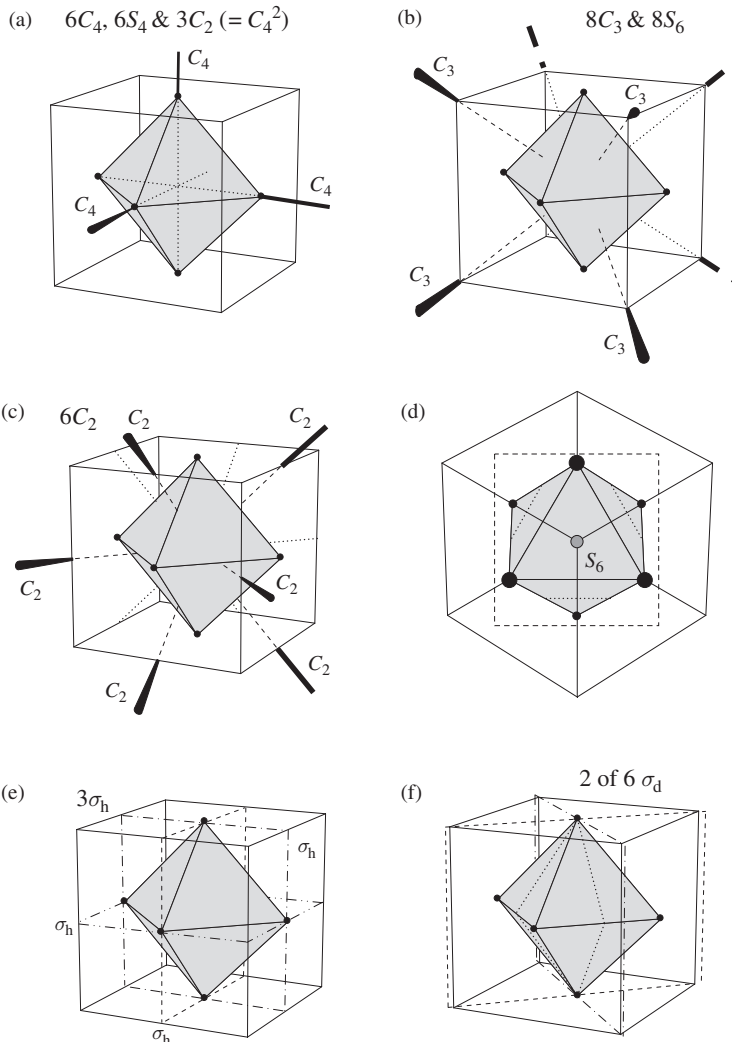


Figure 3.28 The symmetry elements of O_h to which the cube and octahedron belong. (a) C_3 axes, (b) C_4 axes, (c) C_2 axes, (d) an S_6 axis and the mirror plane that forms part of the operation; there are four such axes collinear with the C_3 axes. (e) The $3\sigma_h$ planes and (f) two of the $6\sigma_d$ planes; these contain the C_4 axis along Z; the other σ_d planes are in identical pairs containing X or Y.

with large points in the diagram) directly over the three background points. A reflection through the plane perpendicular to the C_3 axis and passing through the cube centre would then produce a geometry indistinguishable from the starting point. This means that the S_6 axes are collinear with the C_3 axes. We saw in Chapter 2 that any S_6 axis only leads to two operations that cannot be written more simply (S_6^1 and S_6^5), and so the character table contains a heading $8S_6$.

The fact that there are three C_4 axes means that there is no single ‘correct’ choice of principal axis, and so the direction of ‘vertical’ is an arbitrary selection from three equivalent possibilities in O_h symmetry. This leads to the curious situation that there are three σ_h planes. These planes are shown in Figure 3.28e; they pass through the centre of the cube, each parallel to two cube faces, and would contain four of the six ligands in an octahedral complex. This designation of $3\sigma_h$ just reinforces the idea that the three mutually perpendicular C_4 axes are equally valid ‘vertical’ directions. There are also six further mirror planes, each of which contains two opposite edges of the cube and bisects four of the faces of the octahedron. Two of these planes are shown in Figure 3.28f. These are designated σ_d , since they each bisect the angles between the two C_4 axes that are ‘horizontal’ for their own particular choice of ‘vertical’. The improper S_4 symmetry elements are simply compounded operations of each C_4 and its corresponding σ_h .

3.10 Assigning Point Groups to Molecules

In discussing the point groups that are used to described the geometry of molecules we have moved from simple cases containing only a single operator, through the various axial groups and finally to the high-symmetry tetrahedron, octahedron and cube. A first step in studying the symmetry properties of any molecule is to assign its point group correctly. The systematic presentation allows us to break this task down into a series of questions to aid the assignment process. The basic questions that should be asked when confronted with a molecular structure are:

1. Does the molecule belong to a high-symmetry group such as O_h or T_d ?
2. Does the molecule have any symmetry axes? If not, it must be in a nonaxial group and can be classified as C_s , C_i or C_1 .
3. If the molecule is axial, is the principal axis the only proper rotation? If yes, then it must belong to a C or S type group. Or are there horizontal C_2 axes which place it in a classification of D type?

More detailed questions can be added to these broad categorizations to allow a point group assignment to be made. One strategy is summarized in the flow diagram shown in Figure 3.29, and in the following sections we will apply this approach to some example structures.

3.11 Example Point Group Assignments

3.11.1 Example 1: Conformations of Cyclohexane

The simple chemical drawing picture for cyclohexane shown in Figure 3.30a gives the impression of a planar ring. However, each carbon in the ring has four bonds, and so the ring is puckered. One possible conformation for cyclohexane is the chair form shown in Figure 3.30b. The ring puckering is best appreciated by building a three-dimensional molecular model or using a graphical ball-and-stick representation (Figure 3.30c). The advantage of the three-dimensional model is that the molecule can be viewed from many

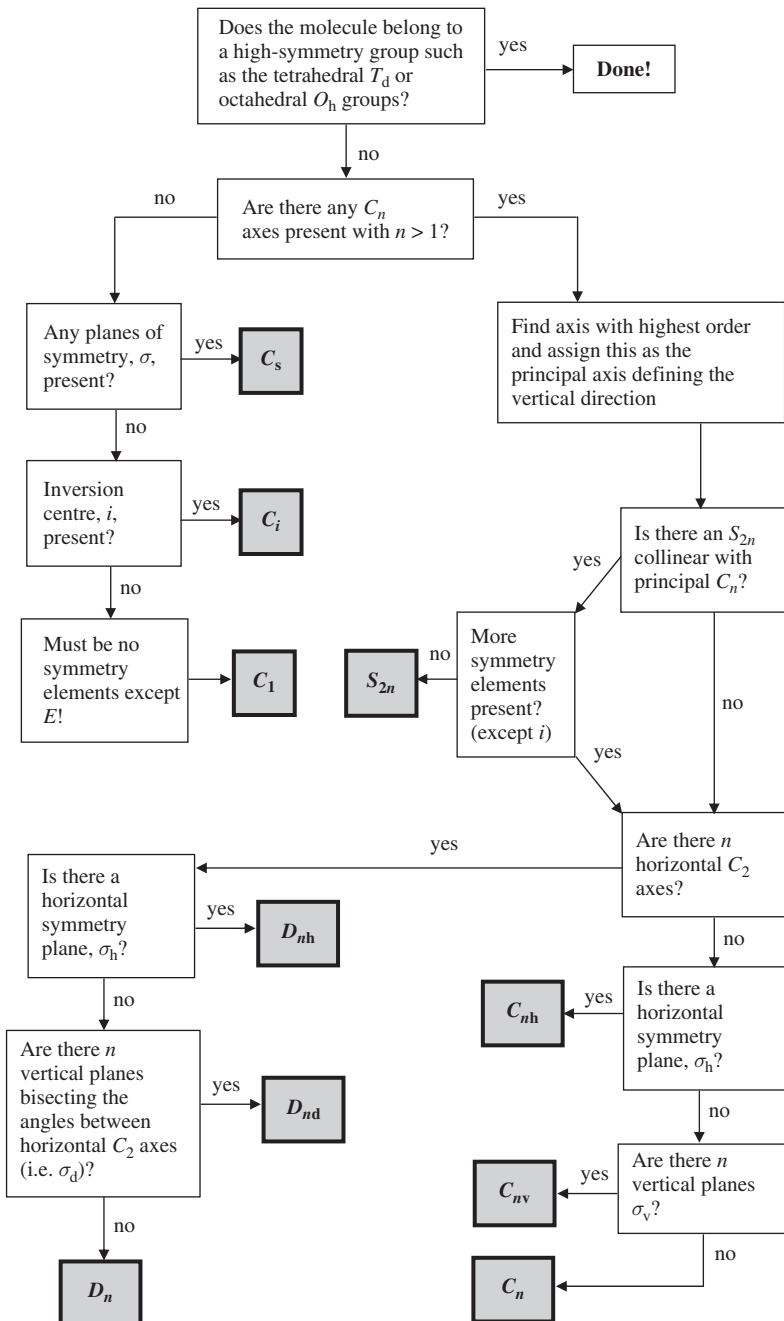


Figure 3.29 Flow diagram for point group assignment.

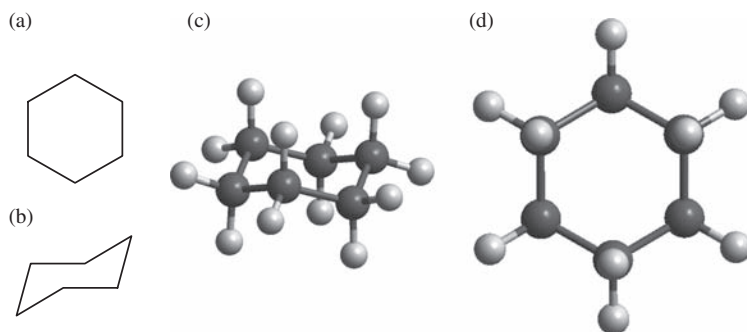


Figure 3.30 The structure of cyclohexane: (a) standard chemical drawing diagram, (b) ball-and-stick model showing ring puckering in chair conformation and (c) view down C_3 principal axis.

alternative angles and so it is much easier to pin down the symmetry elements. For example, in the cyclohexane case, looking down on to the six ring to give the view shown in Figure 3.30d reveals that the principal axis is C_3 , so we are on the right-hand branch of the flow diagram (Figure 3.29) with $n = 3$. Still looking down the principal axis, it appears that a C_6 rotation will bring each carbon atom to the position of one of its neighbours. However, due to the ring pucker, alternate carbon atoms are actually on opposite sides of the average C atom plane. This means that a C_6 rotation followed by a reflection is a symmetry operation but a simple C_6 rotation is not, i.e. we have an S_6 axis collinear with the C_3 . This S_6 operation can also be seen from the positions of the H atoms in the side view of Figure 3.30c, since the vertical C—H bonds alternate from pointing up to pointing down around the ring. The next question on the flow diagram asks if there are further elements other than i (remember $i = S_2^{-1}$). There are other elements; in particular, there are three horizontal C_2 axes which run between opposite bond centres, and so we must have one of the D point groups. There is no horizontal plane of symmetry, but there are vertical planes which contain opposite CH_2 groups. These bisect the angle between the horizontal C_2 axes and so are labelled σ_d . With a principal axis order of 3 we have the point group D_{3d} .

Another possible conformation for cyclohexane is the boat structure shown in Figure 3.31. This structure is slightly higher in energy than the chair conformer, but is still accessible at room temperature and above. In the boat conformation, the ring puckering

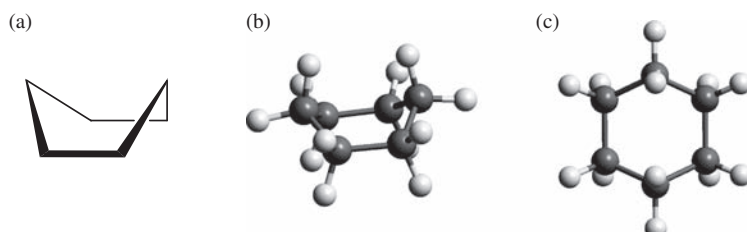


Figure 3.31 Cyclohexane in the boat conformation: (a) chemical drawing representations, (b) side view and (c) view down C_2 axis of ball-and-stick model.

is less regular and the principal axis becomes C_2 , as can be seen in the plan view of Figure 3.31c. There is no improper rotation axis this time and there are no horizontal C_2 axes. Since the principal axis is the only axis present, we have one of the C_n point groups with $n = 2$. Following the flow diagram of Figure 3.29, there are no horizontal mirror planes, but there are two vertical mirror planes. The first contains the two CH_2 groups that are ‘up’ in Figure 3.31b (forming the prow and stern of the ‘boat’) and the second is perpendicular to this and runs through the centre of the two $\text{C}—\text{C}$ bonds formed by the other four C atoms (reflecting the prow into the stern). These planes are both vertical, but they are in different environments and so are labelled σ_v and σ_v' . So, we arrive at the point group C_{2v} .

The fact that the same molecule can have conformations in different point groups is extremely common. Symmetry does not dictate which conformation should be preferred, since it only describes the structure. However, by working out the spectroscopic properties of each conformation with the restrictions imposed by symmetry taken into account we can identify whether a particular conformation is dominant based on experimental data.

3.11.2 Example 2: Six-Coordinate Metal Complexes

Transition metal complexes with six ligands are very common; for example, the hexaaquo complexes of Ni^{2+} and Cu^{2+} shown in Figure 3.32. The Ni complex (Figure 3.32a) is very regular with all the $\text{Ni}—\text{O}$ distances at 2.07 \AA and all $\text{O}—\text{Ni}—\text{O}$ angles at 90° . Ignoring the detailed structure of the water molecules, we can immediately assign this Ni complex as belonging to the octahedral O_h point group. The Cu^{2+} complex in Figure 3.32b, on the other hand, is not quite a regular octahedron. The $\text{Cu}—\text{O}$ distances for the axial ligands are 2.38 \AA and the four equatorial $\text{Cu}—\text{O}$ distances are around 1.95 \AA . This means that the C_4 axes present in an octahedral complex along the lines joining opposite equatorial ligands are not valid in this case; the symmetry is different to the Ni^{2+} example. This is often viewed as a reduction in the symmetry for the copper complex, i.e. we may imagine that with six ligands the complex will adopt O_h but in fact we find some of the symmetry elements are not valid for the structure; the complex has ‘reduced’ its symmetry for some reason. In this case the reason is electronic in nature and is commonly referred to as the Jahn–Teller effect. The electronic background to this will be covered later, but for now we

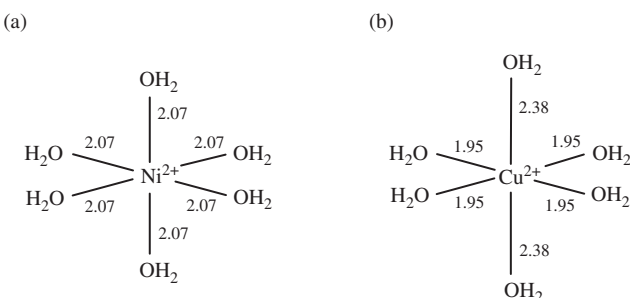


Figure 3.32 Two hexaaquo transition metal complexes: (a) $[\text{Ni}(\text{H}_2\text{O})]^2+$; (b) $[\text{Cu}(\text{H}_2\text{O})]^2+$. Distances are given in Ångstrøms.

will just assign the point group to allow a description of the symmetry reduction. Although the C_4 axes across the equatorial ligands have been lost, the C_4 axis joining the axial ligands remains, and so this is the principal axis. The flow diagram in Figure 3.29 next requires us to look for S_{2n} collinear with the C_4 . There is no S_8 axis, but there are four horizontal C_2 axes which fall into two sets. The first are the axes running between opposite equatorial ligands (they would be C_4 in perfect O_h); these are labelled as C_2' , as the highest priority C_2 axis is along the principal axis ($C_4^2 = C_2$). The second set of horizontal C_2 axes bisects the O—Cu—O angles in the equatorial plane, and these are referred to as C_2'' . The presence of these axes places us in a D -type point group. In this case there is a horizontal mirror plane, the equatorial plane, and so the point group is D_{4h} .

In transforming from our imaginary octahedral hexaaquo Cu^{2+} complex to the observed structure; two of the ligands that are opposite to one another have moved further away from the copper centre than the other four and the symmetry of the structure has become axial in nature. To describe this sort of axial distortion, therefore, we would say that the complex symmetry is reduced from O_h to D_{4h} .

3.12 Self-Test Questions

1. We now have all the information required to be able to place any molecule in its point group by using the flow chart in Figure 3.29. Assign the point groups of the molecules shown in Figure 1.27 that have not been covered in the text. You should build models of any but the simplest structure.
2. Sketch the three isomers of difluoroethene and assign the point group of each.
3. The molecule B_2Cl_4 consists of planar BCl_2 units joined via a $\text{B}=\text{B}$ bond. Rotation about the $\text{B}-\text{B}$ bond is possible. Using the flow chart given in Figure 3.29, determine the point group of the molecule if the two BCl_2 groups are:
 - (a) eclipsed;
 - (b) staggered;
 - (c) half-way between ideal eclipsed and staggered conformations.
4. The molecules shown in Figure 3.33 are labelled according to their point groups. Each one has an improper rotation axis, as labelled below the structure.

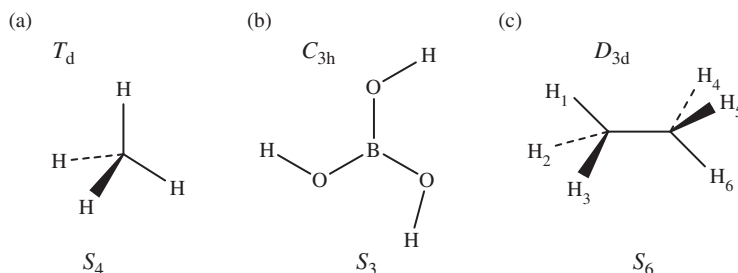


Figure 3.33 S_n axes present in the point groups for (a) methane, CH_4 , (b) $\text{B}(\text{OH})_3$ and (c) the staggered conformation of ethane.

- (a) Draw a sketch of each molecule with the hydrogen atoms labelled showing the appropriate S_n axis/axes.
 - (b) For each molecule, draw the result of successive operations (S_n^1 , S_n^2 , S_n^3 , etc.) for the improper rotations and show the results of multiple applications. To do this you should use the approach from Figures 2.8 and 2.9. In the case of the planar molecule H_3BO_3 you will need to add a vertical arrow on one of the H atoms, to illustrate the effect of the reflection component of the S_3 operation.
 - (c) From your drawings, identify any equivalent operations (e.g. $S_6^2 = C_3^1$). Hence, explain why the T_d group contains six S_4 operations, the C_{3h} group contains two S_3 operations and the D_{3d} group contains two S_6 operations.
5. In the main text we showed that the *trans*-isomer of $[\text{Co}(\text{NH}_3)_4\text{Cl}_2]^+$ belongs to the D_{4h} point group; assign the point group of the *cis*-isomer, ignoring the structure of the amine ligands.
6. Draw the structure of (1*R*,2*S*)-1,2-dimethylcyclopropane and assign its point group. You should recognize from your result that this molecule is not chiral. Explain why this is from both a symmetry and a structural point of view.
7. BF_3 is a planar molecule with a C_3 principal axis and three vertical mirror planes. Use the products of the operations accompanying these symmetry elements to show that the point group for the molecule contains a total of 12 operations and list them.
Identify the point group of BF_3 and compare your list with the class headings in the corresponding character table in Appendix 12.

4

Point Group Representations, Matrices and Basis Sets

4.1 Introduction

The painting in Figure 4.1 is called *Bowl of Fruit, Violin and Bottle* and was created by Picasso in 1914. At first glance it is difficult to see the three items of the title; but as the picture is studied, elements of each emerge. The painting is not the sort of image of the subject matter that a photograph would give; rather, it provides an abstract representation of the items. In this example, even the method of production is a representation; the picture looks like a collage, but is in fact an oil painting.

Representations have a special place in the symmetry of molecules. Up to now we have concentrated on the effect of symmetry operations on the atom positions in a molecule. It is this that defines the point group to which a molecule belongs. Representations give information about the effect of symmetry operations not only on the atom positions, but also on other attributes of a molecule, such as molecular orbitals or vibrational modes. The representations that are possible for any of these additional properties are fixed by the point group, and we can define the complete set of representations for a point group prior to examining a particular molecule. The main aim of this chapter is to explore the definition and origins of representations in molecular symmetry. To do this we will also delve a little deeper into the idea of a basis in symmetry analysis.

4.2 Symmetry Representations and Characters

4.2.1 Water, H_2O , C_{2v}

In Chapters 1–3, the symmetry operations which lead to identical atomic arrangements for a wide range of point groups have been discussed. In a few cases, additional objects such as vectors on particular atom centres were used to highlight the differences between

Publisher's Note:
Permission to reproduce this image
online was not granted by the
copyright holder. Readers are kindly
requested to refer to the printed version
of this chapter.

Figure 4.1 'Bowl of Fruit, Violin and Bottle' by Picasso. Reproduced with permission.
Copyright Succession Picasso/DACS 2008.

symmetry operations. For example, H_2O belongs to the point group C_{2v} with the symmetry elements illustrated in Figure 4.2. Based on the atom positions alone we cannot tell the difference between the C_2 rotation and the σ_v reflection, because either operation swaps the positions of the hydrogen atoms. To distinguish the operations requires additional information.

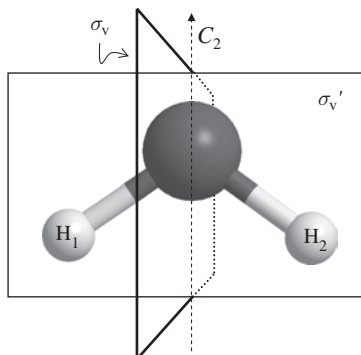


Figure 4.2 The symmetry elements of the C_{2v} point group of H_2O .

Figure 4.3 shows the effect of each C_{2v} operation on the $O(2p_x)$ orbital, demonstrating that the orbital is reversed by C_2 but not by σ_v ; so, although the atom positions are indistinguishable after these operations, the $O(2p_x)$ orbital is transformed differently.

Problem 4.1: Figure 4.3 also contains pictures of the $O(2s)$, $O(2p_z)$ and $O(2p_y)$ orbitals; insert the result of each symmetry operation for these in the appropriate position. The paper models of H_2O (from Appendix 1) may be useful for this exercise, as they can be used to find the effect of each symmetry operation on the x , y and z vectors at the O atom. A completed version of the figure is included at the end of the chapter.

It is clear that each of the p-orbitals on the O atom in the H_2O example responds differently to the symmetry operations: sometimes they are unaffected and sometimes they are reversed. Rather than draw out each orbital every time, it is possible to use a simple numerical scheme to *represent* the effect of each symmetry operation on each orbital. These numbers are known as the *characters* of the operation in the representation.

The characters give numerical factors relating each transformed orbital to its original form. If it is unchanged by the operation we write 1 and if it is reversed we write -1 .

For example, from Figure 4.3 it can be seen that the $O(2p_x)$ orbital is unaltered by the operations E and σ_v ; so, under these operations, $O(2p_x)$ has character 1. For the operations C_2 and σ'_v the phase of the $O(2p_x)$ orbital is reversed, giving a character of -1 .

The characters for all of the orbitals shown in Figure 4.3 are given in Table 4.1. The $O(2s)$ and $O(2p_z)$ orbitals transform identically under all four of the C_{2v} operations, and so Table 4.1 is overly long. In fact, the position of the O atom itself transforms in the same way: it is unaffected by all symmetry operations and so would have a character of 1 in each column. Since many properties of the molecule may transform in similar ways, we introduce labels for each of the possible standard sets of characters. These standard sets of characters are referred to as *irreducible representations* for the group and the pattern of characters for each of them forms the body of the character tables in Appendix 12.

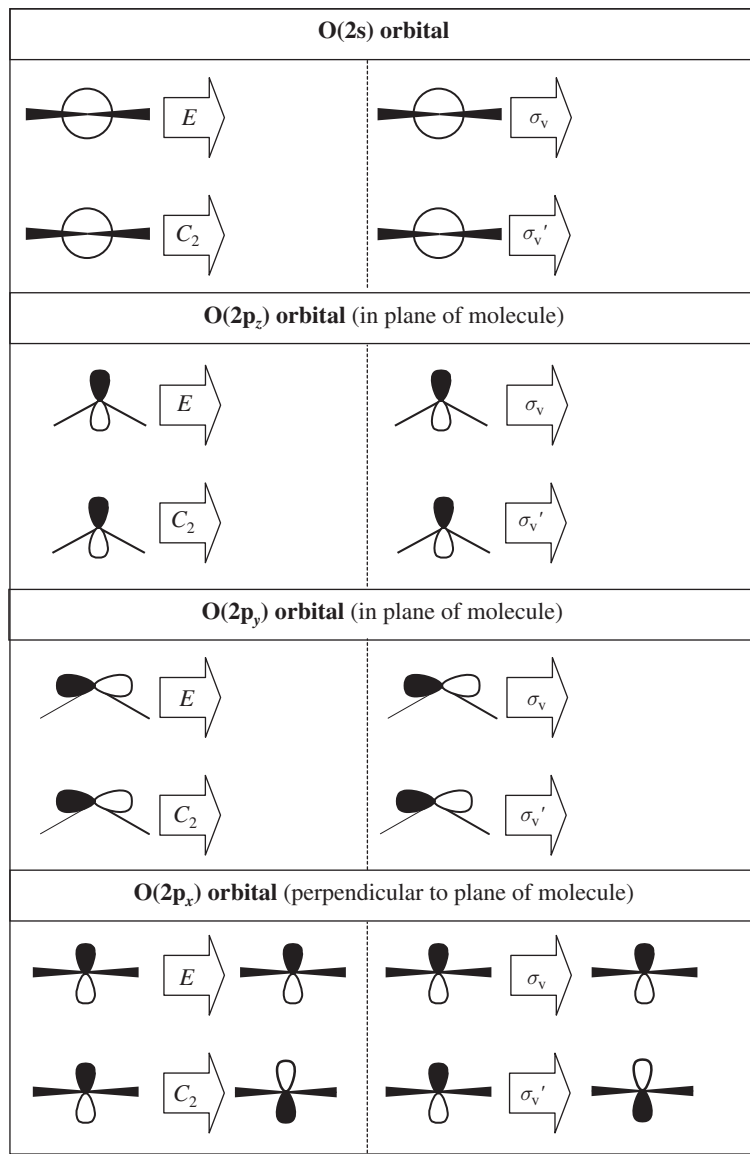


Figure 4.3 The transformations of the valence atomic orbitals on O in H_2O under the operations of the C_{2v} point group for the reader to complete. Note that the $2p_y$ and $2p_z$ orbitals are viewed looking down onto the molecular plane so that the atoms and principal axis are in the plane of the page. Flying wedges for the O—H bonds in the diagrams for the $2s$ and $2p_x$ orbitals indicate the view is down the principal axis with the H atoms above the plane of the paper. The symmetry elements for each operation can be seen in Figure 4.2. A completed table is included at the end of the chapter as Figure 4.12.

Table 4.1 Character representations for the transformations of the 2s and 2p orbitals in C_{2v} .

C_{2v}	E	C_2	$\sigma_v(XZ)$	$\sigma_v'(YZ)$	Orbital
	1	1	1	1	2s
	1	1	1	1	2p _z
	1	-1	1	-1	2p _x
	1	-1	-1	1	2p _y

The character table required for the 2s and 2p orbitals of O in C_{2v} water is shown in Table 4.2. The representation for O(2s) and O(2p_z) is A_1 ; this label is used in most point groups to indicate the representation for features that are unaffected by any operation. For the O(2p_x) orbital, the C_2 rotation and the σ_v' reflection operation each cause a change in sign, leading to characters of -1. This orbital is accordingly assigned a different label: B_1 . The O(2p_y) orbital also changes sign with the C_2 rotation, but is inverted by σ_v while σ_v' leaves it unchanged. The set of characters appropriate to O(2p_y) are generally referred to as the B_2 representation.

Table 4.2 Labelled representations for orbital transformations of the 2s and 2p orbitals on O in the C_{2v} molecule H_2O . Note that 2s and 2p_z have the same A_1 representation.

C_{2v}	E	C_2	$\sigma_v(XZ)$	$\sigma_v'(YZ)$	Orbital
A_1	1	1	1	1	2s, 2p _z
B_1	1	-1	1	-1	2p _x
B_2	1	-1	-1	1	2p _y

4.2.2 Direct Products

There is a further representation possible in the C_{2v} group, but none of the orbitals considered so far transform in the correct way for us to have found it. To see why a new representation is required we will consider the O(d_{xy}) orbital. Looking back at the p-orbital results, it can be seen that orbitals O(2p_x) and O(2p_y) transform in the same way as vectors along the corresponding Cartesian axes. The d_{xy} orbital can also be constructed from the corresponding function: xy . Figure 4.4a shows a plan view of the orbital with the positive and negative phase lobes shaded white and black respectively; Figure 4.4b shows the same orbital plotted using a computer simulation package in three dimensions. The phase of the orbital depends on which quadrant of the XY plane we look at: when both x and y of a point are positive, the function xy will be positive; when either is negative, xy is negative; and when both are negative, the product xy will give a positive value. Also, along the X-axis, the y-coordinate of any point is zero and so $xy = 0$; similarly, along the Y-axis $x = 0$ and so $xy = 0$. This is just the behaviour pattern of the orbital, and so we have constructed the d_{xy} orbital from the product xy .

So will O(d_{xy}) in H₂O have transformation characters that follow the product of the characters for O(p_x) and O(p_y)? This idea is tested in Table 4.3, which shows the characters we have already obtained for the x and y functions and the result when they are multiplied

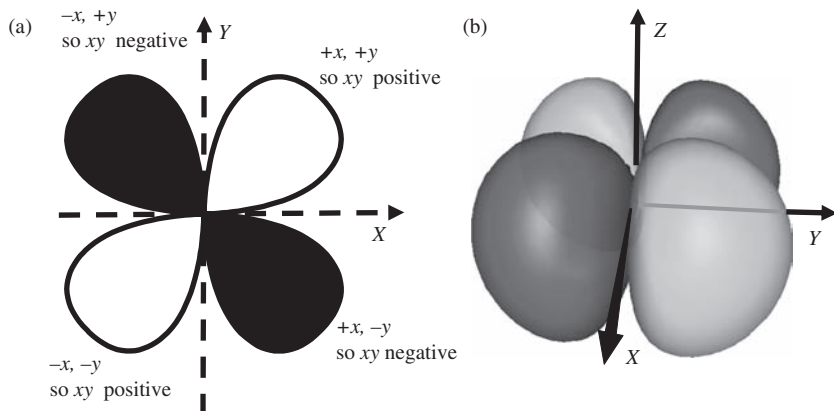


Figure 4.4 The d_{xy} orbital. (a) Sketch looking down the Z-axis showing how the function xy gives the phase of the orbital in the four quadrants of the XY plane; xy is also zero along each axis (along X , $y = 0$; along Y , $x = 0$) and so the nodes along the X and Y axes are also given. (b) A calculated iso-density surface.

Table 4.3 Transformation of d_{xy} in C_{2v} , from the direct product of characters for the x and y functions.

C_{2v}	E	C_2	$\sigma_v(XZ)$	$\sigma_v'(YZ)$	Orbital
B_1	1	-1	1	-1	$2p_x$
B_2	1	-1	-1	1	$2p_y$
$B_1 \times B_2 (= A_2)$	1	1	-1	-1	$3d_{xy}$

together to calculate the characters of the xy function. To show that these characters are correct for $O(d_{xy})$ we can look at the effect of each symmetry operation on the $O(d_{xy})$ orbital itself and obtain the characters independently. The result of each operation is illustrated in Figure 4.5, which shows that the values obtained using the product approach in Table 4.3 are indeed correct. The phase pattern of the orbital is not changed by the E or C_2 operations,

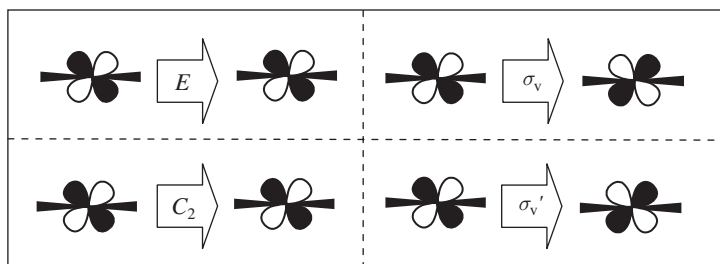


Figure 4.5 The effect of C_{2v} operations on a d_{xy} orbital placed on the O atom of H_2O . The flying wedge representation indicates the molecule is viewed down the C_2 axis.

but is reversed by either σ_v or σ_v' . The new set of characters is given the label A_2 , and this completes the standard set of representations for the C_{2v} point group.

The use of a character by character multiplication of two representations to obtain the characters for a new function is referred to as a *direct product*. In this example we have found that the representation for the d_{xy} function is the direct product of the representations for p_x and p_y . This is another property of groups that we will make use of in future chapters; in general, the direct product of any two representations in a group can be expressed as a sum of representations from the group. In this case we have found that

$$B_1 \times B_2 = A_2 \quad (4.1)$$

so the resulting summation requires only a single term, A_2 . We will find in Chapter 6 that direct products of this type are useful in calculating the properties of integrals required by spectroscopic selection rules. In that chapter we will meet more complex examples of direct products.

Problem 4.2: The $O(p_z)$ orbital in the H_2O example has a representation A_1 . Show that this implies that the $O(d_{xz})$ and $O(d_{yz})$ orbitals will have the same representation as the $O(p_x)$ and $O(p_y)$ functions respectively. Check your solutions by drawing diagrams for the result of each C_{2v} operation with the $O(d_{xz})$ and $O(d_{yz})$ orbitals.

Problem 4.3: By considering the direct products show that:

1. The direct product of A_1 with any representation in C_{2v} simply gives the representation back again.
2. The direct products $A_2 \times B_1 = B_2$ and $A_2 \times B_2 = B_1$ are correct in C_{2v} .

We will look more closely at the origin of the representation labels in Section 4.11, but first we have to consider the types of character that can occur and their relationship to the more complete matrix representations for point group operations.

4.3 Multiplication Tables for Character Representations

To be valid representations, the sets of numbers we have produced for the A_1, A_2, B_1 and B_2 representations must each act in the same way as the symmetry operations themselves. For example, we found in Chapter 2 that $C_2\sigma_v = \sigma_v'$ for the C_{2v} point group of H_2O . In the A_1 representation, both C_2 and σ_v have character 1 and so the character product is 1, which is also the character of σ_v' . This must hold for the whole multiplication table between the symmetry operators. For A_1 , the table is quite trivial, since it contains only 1s. However, the other representations must also give consistent multiplication tables.

The C_{2v} group multiplication table was constructed from the group operations in Problem 2.1 and the result is reproduced in Table 4.4a. The same table using the B_1 representation characters is given in Table 4.4b. In this representation version, the operation symbols for the row and column headings are replaced by the corresponding B_1 characters. The result of a product of operations then becomes a simple numerical multiplication of

Table 4.4 The complete multiplication table for (a) the C_{2v} group operations and (b) the B_1 representation.

C_{2v}	E	C_2	$\sigma_v(XZ)$	$\sigma_v'(YZ)$
E	E	C_2	σ_v	σ_v'
C_2	C_2	E	σ_v'	σ_v
$\sigma_v(xz)$	σ_v	σ_v'	E	C_2
$\sigma_v'(yz)$	σ_v'	σ_v	C_2	E

$C_{2v}:B_1$	1	-1	1	-1
1	1	-1	1	-1
-1	-1	1	-1	1
1	1	-1	1	-1
-1	-1	1	-1	1

the characters, with the only possible outcomes in this example being ± 1 . To check that the table is consistent with the results of the full operations, you should confirm that the numerical value obtained in each case in Table 4.4b is the correct value for the operation in the equivalent position in Table 4.4a.

Problem 4.4: Write out multiplication tables for the A_2 and B_2 representations in C_{2v} and confirm that they are also consistent with Table 4.4a.

4.4 Matrices and Symmetry Operations

Although the simple single number representations for a group, such as the example of B_1 in C_{2v} , do reproduce the multiplication table, we have lost some information by using characters as representations. From the B_1 character multiplication table it is not possible to say whether $C_2\sigma_v = \sigma_v'$ or C_2 , since Table 4.4b shows that both possibilities have character -1.

We have met this type of problem before: in Section 2.3.4, the equivalences of some improper rotations could not be understood from the atom positions alone. In the example of the planar molecule BF_3 , the results of C_3^{-1} and S_3^{-1} appeared to be equivalent if only the atom positions are considered. However, the two operations do give different results for objects not in the molecular plane. To show this difference we added a basis vector perpendicular to the plane of the molecule on one atom. After C_3^{-1} the orientation of this vector remained the same as the starting point, but after S_3^{-1} it was reversed.

In Table 4.4b there is not enough information in the single representation to distinguish the operations. Effectively, by only looking at the B_1 representation we are concentrating only on the $2p_x$ orbital. If we were to consider the $2p_x$ and $2p_y$ orbitals at the same time, then Table 4.3 shows we would get the results $E(1, 1)$, $C_2(-1, -1)$, $\sigma_v(1, -1)$ and $\sigma_v'(-1, 1)$, where the characters are written as $(2p_x, 2p_y)$. Now the pairs of characters are different and the use of multiple basis vectors at the same time allows the four C_{2v} operations to be differentiated.

So, if the results of operations on sets of basis vectors are considered collectively, we gain more information than when they are considered in isolation. This approach is formalized in the matrix representation of symmetry operations. The matrices are mathematical objects that contain enough information to carry out the symmetry operations on a whole set of basis vectors simultaneously.

To show how the matrix approach works, we will go over the ($2p_x$, $2p_y$) example more formally. We have used an equivalent set of basis vectors for the water problem before. Figure 2.2 shows a set of vectors labelled x , y and z on the O atom of H_2O along with the transformation that occurs after each of the symmetry operations in C_{2v} is applied. These vectors have exactly the same symmetry properties as the p-orbital set on the O atom, since they are their functional forms. The paper models from Appendix 1 can also be used to follow the transformations discussed with this basis. If we consider the x and y vectors together, the C_2 transformation can be written as,

$$\begin{pmatrix} x \\ y \end{pmatrix} \Rightarrow \begin{pmatrix} -x \\ -y \end{pmatrix} \quad (4.2)$$

since the C_2 rotation reverses both x and y . In this equation, we have brought together the transformation of x and y into a single relation by writing them in column vector form. To obtain characters, we would now identify factors which relate the rotated vectors to the original set, i.e. how to write the new vectors in terms of the old. In this case both vectors are reversed, so the result in Equation (4.2) could be written,

$$\begin{aligned} x' &= -1 \times x + 0 \times y \\ y' &= 0 \times x + -1 \times y \end{aligned} \quad (4.3)$$

where the prime has been added to indicate the vectors after transformation. This way of writing the equations is more complete than Equation (4.2) because it allows for the possibility that the new vectors are composed of any combination of the original ones; the zero terms are included to show that x' has no component along the old y -direction and y' no component along the old x .

Formulae such as Equation (4.3) are written using matrix notation by making the square block of the coefficients from the right-hand side into a matrix and writing the co-ordinates as column vectors:

$$\begin{pmatrix} x' \\ y' \end{pmatrix} = \begin{pmatrix} -1 & 0 \\ 0 & -1 \end{pmatrix} \begin{pmatrix} x \\ y \end{pmatrix} \quad (4.4)$$

The matrix given in Equation (4.4) is another possible way to write the C_2 axis operation. It actually contains the characters for both the B_1 and B_2 representations we identified earlier for the $2p_x$ and $2p_y$ orbitals. The manipulation of matrices and vectors is covered in Appendix 5, where the rules for multiplying the matrix into the vector on the right-hand side of Equation (4.4) are discussed.

A matrix representation for each symmetry operation in C_{2v} can now be written down and the results checked by constructing a multiplication table from the matrices rather than the characters.

Problem 4.5: Show that the matrix representations for the operations in C_{2v} acting on the x, y basis centred on the O atom of H_2O are;

$$E = \begin{pmatrix} 1 & 0 \\ 0 & 1 \end{pmatrix} \quad C_2 = \begin{pmatrix} -1 & 0 \\ 0 & -1 \end{pmatrix} \quad \sigma_v = \begin{pmatrix} 1 & 0 \\ 0 & -1 \end{pmatrix} \quad \sigma_v' = \begin{pmatrix} -1 & 0 \\ 0 & 1 \end{pmatrix} \quad (4.5)$$

It can be seen straight away from the solution of Problem 4.5 that there is no ambiguity in the matrix representation: the four matrices are different from one another, and so we can tell the operations apart.

For the matrices to be proper representations of the operations their products should reproduce the group multiplication table (Table 4.4a). The product of two operations, such as $C_2\sigma_v$, means take the original vectors, transform by the vertical reflection and then apply a C_2 rotation to this intermediate result. We could carry this out in two steps:

$$\begin{aligned} \begin{pmatrix} x' \\ y' \end{pmatrix} &= \sigma_v \begin{pmatrix} x \\ y \end{pmatrix} = \begin{pmatrix} 1 & 0 \\ 0 & -1 \end{pmatrix} \begin{pmatrix} x \\ y \end{pmatrix} = \begin{pmatrix} x \\ -y \end{pmatrix} \\ \begin{pmatrix} x'' \\ y'' \end{pmatrix} &= C_2 \begin{pmatrix} x' \\ y' \end{pmatrix} = \begin{pmatrix} -1 & 0 \\ 0 & -1 \end{pmatrix} \begin{pmatrix} x \\ -y \end{pmatrix} = \begin{pmatrix} -x \\ y \end{pmatrix} = \sigma_v' \begin{pmatrix} x \\ y \end{pmatrix} \end{aligned} \quad (4.6)$$

Here, a double prime is used to indicate the vectors after both transformations. In the last step we have found that the two operations result in x being reversed and y returning to its original state. This is just the same as the single σ_v' reflection, and so the equivalence $C_2\sigma_v = \sigma_v'$ is shown without the earlier confusion.

Appendix 5 shows how the multiplication rules for matrices and vectors can be extended to arrive at this conclusion more rapidly. We can write the $C_2\sigma_v$ product directly as

$$\begin{pmatrix} x'' \\ y'' \end{pmatrix} = C_2\sigma_v \begin{pmatrix} x \\ y \end{pmatrix} = \begin{pmatrix} -1 & 0 \\ 0 & -1 \end{pmatrix} \begin{pmatrix} 1 & 0 \\ 0 & -1 \end{pmatrix} \begin{pmatrix} x \\ y \end{pmatrix} = \begin{pmatrix} -1 & 0 \\ 0 & 1 \end{pmatrix} \begin{pmatrix} x \\ y \end{pmatrix} \quad (4.7)$$

The product matrix is the same as that for σ_v' from Problem 4.5, confirming the result we found by applying the matrices sequentially: $C_2\sigma_v = \sigma_v'$.

Table 4.5 gives the full multiplication table for C_{2v} using this matrix representation. Because the product of any operation with E is the same as the operation alone, the first row and first column of this table are simply the matrix representations for the four operations. Using these as references it is easy to check that the other six matrix products correspond exactly with the result for the operations given in Table 4.4a.

This section has shown that the matrix representation, used with a suitable set of basis vectors, can remove the difficulty of finding exactly which operation results from a given product in the same way as the introduction of basis vectors showed the difference between apparently equivalent operations. In fact, the matrix representation allows us to follow exactly what happens to a given basis under a symmetry transformation. In the next few sections we will explore the use of matrices in symmetry more fully and define the relationship between the matrix and simpler character representations.

Table 4.5 The multiplication table for the C_{2v} point group using the matrix representation of operators for the x and y basis.

C_{2v}	E	C_2	$\sigma_v(XZ)$	$\sigma_v'(YZ)$
E	$\begin{pmatrix} 1 & 0 \\ 0 & 1 \end{pmatrix}$	$\begin{pmatrix} -1 & 0 \\ 0 & -1 \end{pmatrix}$	$\begin{pmatrix} 1 & 0 \\ 0 & -1 \end{pmatrix}$	$\begin{pmatrix} -1 & 0 \\ 0 & 1 \end{pmatrix}$
C_2	$\begin{pmatrix} -1 & 0 \\ 0 & -1 \end{pmatrix}$	$\begin{pmatrix} 1 & 0 \\ 0 & 1 \end{pmatrix}$	$\begin{pmatrix} -1 & 0 \\ 0 & 1 \end{pmatrix}$	$\begin{pmatrix} 1 & 0 \\ 0 & -1 \end{pmatrix}$
$\sigma_v(XZ)$	$\begin{pmatrix} 1 & 0 \\ 0 & -1 \end{pmatrix}$	$\begin{pmatrix} -1 & 0 \\ 0 & 1 \end{pmatrix}$	$\begin{pmatrix} 1 & 0 \\ 0 & 1 \end{pmatrix}$	$\begin{pmatrix} -1 & 0 \\ 0 & -1 \end{pmatrix}$
$\sigma_v'(YZ)$	$\begin{pmatrix} -1 & 0 \\ 0 & 1 \end{pmatrix}$	$\begin{pmatrix} 1 & 0 \\ 0 & -1 \end{pmatrix}$	$\begin{pmatrix} -1 & 0 \\ 0 & -1 \end{pmatrix}$	$\begin{pmatrix} 1 & 0 \\ 0 & 1 \end{pmatrix}$

Problem 4.6: By forming matrix products, check each of the entries in Table 4.5 and confirm that each product gives the matrix for the operation expected from Table 4.4a.

4.5 Diagonal and Off-Diagonal Matrix Elements

4.5.1 Ammonia, NH_3 , C_{3v}

In the H_2O example the basis is set up to represent the $2p_x$ and $2p_y$ orbitals on the oxygen atom. The operations on this basis only ever give a character of +1 or -1 for each orbital, because the orbitals are either unaffected or have the phase pattern reversed. We now move on to examples in which the basis set is changed in more complex ways.

Figure 4.6 shows the basis of N–H bond vectors in the ammonia molecule, which belongs to the point group C_{3v} . These vectors give the direction of movement for the H atoms in vibrational modes of the molecule involving N–H stretching motion. From the figure we can see that the C_3^1 operation causes each basis vector to move to the position of one of its neighbours. In Figure 4.6, the basis vectors after the transformation have been marked with a prime, and comparing these to the original set we can write,

$$\begin{aligned} b'_3 &= b_1 \\ b'_1 &= b_2 \\ b'_2 &= b_3 \end{aligned} \quad \text{after } C_3^1 \quad (4.8)$$

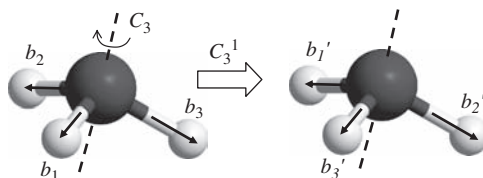


Figure 4.6 The ammonia molecule (point group C_{3v}) with a basis of N–H bonds marked.

The result is that b_3' has replaced the original b_1 , while b_1' is in the position previously occupied by b_2 and b_2' has the original b_3 position and direction.

This is more complex than in the H₂O example, since vectors are now interchanged. This makes it difficult to write down exactly what the operation does in terms of single characters, because any of the new functions could be composed from any of the original set. The matrix representation allows for this: each new vector is written as a linear combination of the original basis vectors. Figure 4.6 can be used to construct the relationships required by inspection:

$$\begin{aligned} b'_1 &= 0 \times b_1 + 1 \times b_2 + 0 \times b_3 \\ b'_2 &= 0 \times b_1 + 0 \times b_2 + 1 \times b_3 \\ b'_3 &= 1 \times b_1 + 0 \times b_2 + 0 \times b_3 \end{aligned} \quad (4.9)$$

The column vector notation can now be used to combine all three equations into one matrix equation.

The position of an element in the column is set by the starting point of the initial basis vectors. After a transformation, the positions in the column are filled by working out the vector that is now aligned with the reference for each element, i.e. we write the column vector

$$\begin{pmatrix} \text{vector now along original } b_1 \\ \text{vector now along original } b_2 \\ \text{vector now along original } b_3 \end{pmatrix} \quad (4.10)$$

So, the observed transformation of the basis for the C₃¹ operation in Figure 4.6 would be written

$$\begin{pmatrix} b_1 \\ b_2 \\ b_3 \end{pmatrix} \Rightarrow \begin{pmatrix} b_3 \\ b_1 \\ b_2 \end{pmatrix} \quad (4.11)$$

In this formula, an arrow, rather than an equals sign, is used to show that a transformation has taken place. The primes for the transformed column vector can be dropped because the position of the b -vectors in the column indicates the transformation that has taken place.

The representation of the symmetry operation by a matrix allows all three of the transformation equations in Equation (4.9) to be written down in one go based on the column vector notation:

$$\begin{pmatrix} 0 & 0 & 1 \\ 1 & 0 & 0 \\ 0 & 1 & 0 \end{pmatrix} \begin{pmatrix} b_1 \\ b_2 \\ b_3 \end{pmatrix} = \begin{pmatrix} b_3 \\ b_1 \\ b_2 \end{pmatrix} \quad (4.12)$$

Comparing this transformation matrix with the earlier H₂O examples, we see that the O atom orbital cases contained only elements on the diagonal positions in the square matrix, whereas the diagonal elements here are all zero. In the H₂O case, basis vectors were either left alone or reversed, and in Section 4.2 these results were given characters +1 and -1 respectively. In this example, the transformation results in each of the basis vectors moving to the position of one of the others, and so they completely lose their original ‘character’. Correspondingly, the diagonal element in the matrix for the vector will be zero.

In general, the diagonal terms in a transformation matrix tell us how much of each original basis function is retained. The off-diagonal terms give additional information on exactly how to build the new functions from the old.

So, the character for a particular operation and basis function is just the associated diagonal element in the matrix. In the NH₃ example, the C₃¹ rotation would have a character of 0 for each of the basis vectors.

A zero character for a basis function simply implies that it has been transformed into some combination of the other members of the basis set.

4.6 The Trace of a Matrix as the Character for an Operation

The character we assign for a particular basis vector has been linked to the diagonal element in the operation's matrix. This can be generalized to say that the sum of the diagonal elements of a matrix representing an operation on a particular basis is the sum of the characters for the basis under that operation. In matrix algebra, the sum of the diagonal elements of a matrix A is known as the trace of the matrix, Tr(A), i.e.

$$A = \begin{pmatrix} a_{11} & a_{12} & a_{13} \\ a_{21} & a_{22} & a_{23} \\ a_{31} & a_{32} & a_{33} \end{pmatrix} \quad \text{Tr}(A) = \sum_{i=1}^3 a_{ii} = a_{11} + a_{22} + a_{33} \quad (4.13)$$

This example shows the trace for a 3 × 3 matrix, but the idea of taking the sum of diagonal terms can be extended to matrices of any order.

Using the trace rather than picking out particular elements of the matrix allows a single character to be assigned for the result of the operation on the entire set of basis functions being considered. This will turn out to be a useful tactic in dealing with symmetry problems, since it allows whole sets of basis vectors to be considered together.

For example, the ammonia molecule belongs to the point group C_{3v} and so, in addition to the principal axis, there are three vertical mirror planes. The result of a reflection operation is shown in Figure 4.7; to see the how the transformation affects the basis set, one of the three degenerate mirror planes has been chosen as an example. The mirror contains the b₃ vector, and so the superscript C has been added to the mirror plane symbol following the convention employed in earlier chapters.

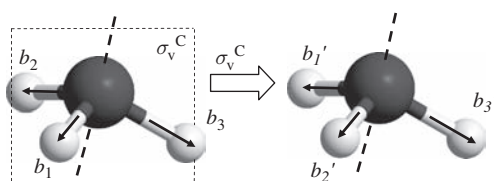


Figure 4.7 The effect of the σ_v^C plane reflection on the basis of N—H bonds on ammonia.

From Figure 4.7, the reflection has swapped b_1 and b_2 but has left b_3 unchanged. The matrix corresponding to this operation can be deduced from this result:

$$\sigma_v^C \begin{pmatrix} b_1 \\ b_2 \\ b_3 \end{pmatrix} = \begin{pmatrix} 0 & 1 & 0 \\ 1 & 0 & 0 \\ 0 & 0 & 1 \end{pmatrix} \begin{pmatrix} b_1 \\ b_2 \\ b_3 \end{pmatrix} = \begin{pmatrix} b_2 \\ b_1 \\ b_3 \end{pmatrix} \quad (4.14)$$

The other two vertical mirror planes have similar matrices:

$$\begin{aligned} \sigma_v^A \begin{pmatrix} b_1 \\ b_2 \\ b_3 \end{pmatrix} &= \begin{pmatrix} 1 & 0 & 0 \\ 0 & 0 & 1 \\ 0 & 1 & 0 \end{pmatrix} \begin{pmatrix} b_1 \\ b_2 \\ b_3 \end{pmatrix} = \begin{pmatrix} b_1 \\ b_3 \\ b_2 \end{pmatrix} \\ \sigma_v^B \begin{pmatrix} b_1 \\ b_2 \\ b_3 \end{pmatrix} &= \begin{pmatrix} 0 & 0 & 1 \\ 0 & 1 & 0 \\ 1 & 0 & 0 \end{pmatrix} \begin{pmatrix} b_1 \\ b_2 \\ b_3 \end{pmatrix} = \begin{pmatrix} b_3 \\ b_2 \\ b_1 \end{pmatrix} \end{aligned} \quad (4.15)$$

Here, σ_v^A and σ_v^B are the planes containing vectors b_1 and b_2 respectively in the original configuration. In all three cases the matrices swap two of the basis vectors and leave one unchanged. If we add up the diagonal elements of each matrix we find that the trace is 1 in each case, and so the total character of the three N—H bonds under any of the reflection operations is 1. The three matrices differ in which of the diagonal elements is 1, but the trace has the same value in each case; this is a consequence of the equivalence of the three mirror planes and means that only one heading, $3\sigma_v$, needs to appear in the C_{3v} character table for all three mirror planes (see Appendix 12).

Problem 4.7: Using the basis of N—H bonds defined in Figure 4.6, write down the matrix representation for a C_3^2 operation. Take the trace of this matrix and, hence, show that C_3^2 and C_3^1 operations have the same character for this basis.

4.7 Noninteger Characters

The examples up to now have been chosen so that each operation causes a given basis vector to be unaffected, reversed or transformed into a different basis function. In the analysis, we have shown that the matrix representation allows us to describe each of these transformations leading to the characters of +1, -1 and 0 respectively. However, if the basis vectors are not arranged to fit nicely with the symmetry elements, then the character assignment may not be so straightforward.

4.7.1 Boron Trifluoride, BF_3 , D_{3h}

For example, Figure 4.8 shows the result of the C_3^1 operation on a $p_x(\text{B})$ orbital in the BF_3 molecule. The orbital is no longer aligned with either the X or Y direction after the operation, so assigning its character requires some additional attention. The new orbital is in between the X and Y axes and so could also be constructed by some mixture of the

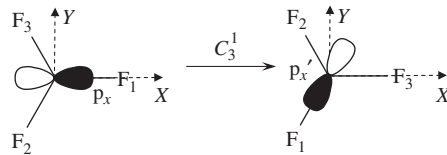


Figure 4.8 The effect of a C_3^1 rotation on the p_x orbital of B in BF_3 . Note that the principal C_3 axis is pointing into the page, along the negative Z-direction.

original p_x and p_y orbitals. The character is just the amount of the original $p_x(B)$ orbital present in such a linear combination.

The proportions of p_x and p_y orbitals can be calculated using trigonometry, and the process is easier to follow if the orbitals themselves are replaced with vectors to represent their functional forms, as shown in Figure 4.9a. The direction of a vector in this diagram

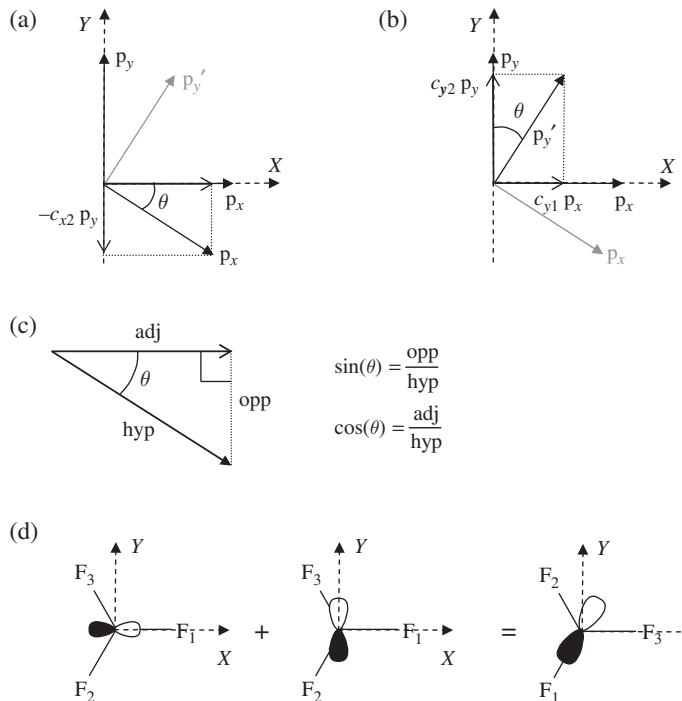


Figure 4.9 A simplified representation showing the result of a rotation through θ° about the Z axis on (a) a p_x orbital and (b) a p_y orbital (---: the global axes; —→: the vectors representing p -orbitals; →: vector components). Note that the Z-axis is perpendicular to the page (c) The general definitions of sine and cosine functions based on a right-angle triangle with the hypotenuse (hyp) opposite the right angle, and adjacent (adj) and opposite (opp) sides defined with respect to θ . (d) A graphical illustration of the sum $-(1/2)p_x - (\sqrt{3}/2)p_y = p_x'$ using the same shading of phases as Figure 4.8.

should be thought of as the orientation of the orbital and the length of the vector as its size. The original p_x and p_y vectors are aligned with their respective axes. Figure 4.9a shows that, for an arbitrary rotation of the p_x orbital by an angle θ , the new vector p_x' will not usually be perfectly aligned with either the original p_x or p_y vectors. In fact, only $\theta = 0$ or 180° will align p_x' with p_x to give characters of $+1$ and -1 , and only $\theta = 90^\circ$ or 270° will align p_x' with p_y , either giving a character of 0 . For any other values of θ we can use a linear combination of the original basis functions to produce the new p-orbital orientation. In the BF_3 example, $\theta = 120^\circ$, but for now we will continue with the general case and insert this angle for θ at the end.

The general formula for the linear combination can be written:

$$p_x' = c_{x1}p_x + c_{x2}p_y \quad (4.16)$$

where c_{x1} and c_{x2} control the amount of the original p_x and p_y orbitals used in the transformed function and are coefficients we have to find. In this case c_{x1} is the character for the p_x orbital, and the diagram shows that it represents the component of p_x' along the p_x direction. This limits the range of characters that are possible for the p_x orbital to between -1 and $+1$, because the component of a vector can never be greater than its magnitude.

The length of the vectors representing p_x and p_y are the same and are not affected by the rotation. With this in mind we can use the trigonometry of the diagram in Figure 4.9a to find the coefficients. Figure 4.9c is a reminder of the general definitions of the sine and cosine functions; applying these to the right-angle triangle with θ marked in Figure 4.9a gives

$$\cos(\theta) = \frac{c_{x1}|p_x|}{|p_x'|} = c_{x1} \quad \text{and} \quad \sin(\theta) = \frac{c_{x2}|p_y|}{|p_x'|} = c_{x2} \quad (4.17)$$

Here, we have used the convention that vertical lines mean the length or magnitude of a vector. Equation (4.16) now becomes

$$p_x' = p_x \cos(\theta) - p_y \sin(\theta) \quad (4.18)$$

Here the minus sign indicates that the opposite edge of the triangle in Figure 4.9a is in the opposite direction to p_y , the c_{x2} coefficient in the linear combination must take this into account. Similar considerations using Figure 4.9b show that the p_y' vector can be written as

$$p_y' = p_x \sin(\theta) + p_y \cos(\theta) \quad (4.19)$$

Equations (4.18) and (4.19) can be combined into a single form using matrix algebra:

$$\begin{pmatrix} p_x' \\ p_y' \end{pmatrix} = \begin{pmatrix} \cos(\theta) & -\sin(\theta) \\ \sin(\theta) & \cos(\theta) \end{pmatrix} \begin{pmatrix} p_x \\ p_y \end{pmatrix} \quad (4.20)$$

For the particular example of the p-orbitals on B in BF_3 , θ is 120° ; so:

$$\begin{pmatrix} p_x' \\ p_y' \end{pmatrix} = \begin{pmatrix} \cos(120) & -\sin(120) \\ \sin(120) & \cos(120) \end{pmatrix} \begin{pmatrix} p_x \\ p_y \end{pmatrix} = \begin{pmatrix} -1/2 & -\sqrt{3}/2 \\ \sqrt{3}/2 & -1/2 \end{pmatrix} \begin{pmatrix} p_x \\ p_y \end{pmatrix} \quad (4.21)$$

So, this rotation gives a p_x' -orbital which can also be generated as the sum:

$$p_x' = -\frac{1}{2}p_x - \frac{\sqrt{3}}{2}p_y \quad (4.22)$$

which contains a contribution from the original p_x orbital that is half the size and opposite in phase to the original. This equation is illustrated graphically in Figure 4.9d.

Now, using the rule that the character of the transformation is the diagonal element of the matrix, we find a character of $\cos(120) = -1/2$ for each orbital. From the trace of the matrix in Equation (4.21) we obtain a combined character for the p_x and p_y orbitals of $2\cos(120) = -1$.

Problem 4.8: The BF_3 molecule also contains three vertical mirror planes, each containing a $\text{B}-\text{F}$ bond. Using the geometry of Figure 4.8, draw the result of the reflection through the mirror planes containing each of the $\text{B}-\text{F}$ bonds. From your diagrams, write down the matrices for the effect on the p_x and p_y orbitals. Hence, derive the reflection matrices for this basis and show that the three matrices have the same trace and so these equivalent operations have the same total character.

4.8 Reducible Representations

A set of basis functions set up to analyze a problem will usually contain more objects than any of the standard representations listed in the character tables. The standard character sets are referred to as irreducible representations; this is because they describe the simplest symmetry behaviour of orbitals or vibrations in the point group. In general, it is easy to set up a basis to describe the problem in hand and work out a representation for the set as a whole by summing the characters of each basis function. Then we need to break down this reducible representation into a set of standard irreducible representations.

4.8.1 Water, H_2O , C_{2v}

In the H_2O example used in Section 4.3, for instance, the x and y vectors used as a basis on the O atom would have a matrix representation for C_{2v} point group operations as follows:

$$E = \begin{pmatrix} 1 & 0 \\ 0 & 1 \end{pmatrix} \quad C_2 = \begin{pmatrix} -1 & 0 \\ 0 & -1 \end{pmatrix} \quad \sigma_v(XZ) = \begin{pmatrix} 1 & 0 \\ 0 & -1 \end{pmatrix} \quad \sigma_v'(YZ) = \begin{pmatrix} -1 & 0 \\ 0 & 1 \end{pmatrix} \quad (4.23)$$

Trace :	2	−2	0
---------	---	----	---

We have now seen that the trace of each of these matrices is the summed characters for the basis vectors under their respective operations. In fact, it would be possible to write down the sum of characters for the basis without knowing the entire matrix representation. For any basis, we could just consider each vector in turn and ask the question: ‘How much of the original basis vector remains after the transformation?’ Under the identity E , the x and y vectors are both unchanged, giving a total character of 2, the C_2 rotation

reverses both vectors, a character of -2 , and each of the reflections leaves the vector it contains unchanged but reverses the other one, $1 - 1 = 0$. So we have found the trace of the matrices by inspection. This is the approach we will adopt in the remaining chapters of this book. What we need to do now is show that the trace is sufficient to identify the appropriate irreducible representations.

For the C_{2v} point group, we have already found all the standard labels, and the characters for the irreducible representations are given in the character table shown in Table 4.6. None of these standard representations have a 2 under the E column; in fact, they all have 1 . This is not a surprise, since we have already shown that x belongs to the B_1 representation and y to the B_2 representation by inspecting each basis vector in turn in Section 4.2. So the totalled character for the basis obtained above could be reduced to those for B_1 and B_2 , i.e. the characters for the individual vectors. Table 4.7 shows that the sum of the characters $B_1 + B_2$ agrees with the totals laid out in Equation (4.23). The reducible representation is usually given the symbol Γ , and so in this case we have shown that

$$\Gamma = B_1 + B_2 \quad (4.24)$$

In general, it will be possible to simplify the total representation for a basis of our choosing into a sum of the standard irreducible representations from the point group character table. The reducible and irreducible representations are linked by the fact that the sum of characters of the irreducible representations for a basis must give the characters of their reducible representation:

$$\chi_{\Gamma}(C) = \sum_i n_i \chi_i(C) \quad (4.25)$$

Here, we use the symbol χ for a character, the subscripts Γ and i indicating that the character is taken from the reducible representation and the i th irreducible representation respectively, for a given class of operations C . This formula simply says that the diagonal

Table 4.6 The C_{2v} character table.

C_{2v}	E	C_2	σ_v	σ_v'		
A_1	1	1	1	1	z	x^2, y^2, z^2
A_2	1	1	-1	-1	R_z	xy
B_1	1	-1	1	-1	x, R_y	xz
B_2	1	-1	-1	1	y, R_x	yz

Table 4.7 The sum of the characters from the B_1 and B_2 representations in the C_{2v} point group.

C_{2v}	E	C_2	σ_v	σ_v'
B_1	1	-1	1	-1
B_2	1	-1	-1	1
$B_1 + B_2$	2	-2	0	0

elements of the matrices for the full basis set must sum to the same value as those of the set of irreducible representations from which it is composed. The value of n_i in Equation (4.25) is set to the number of times we have to use irreducible representation i in forming the reducible representation Γ .

In Chapter 5 we will exploit this relationship between the reducible and irreducible representations further and find a general formula for obtaining the n_i values that control the composition of Γ for any basis and any point group. This chapter finishes with a few more examples of reducible and irreducible representations.

4.9 Classes of Operations

In the previous sections we have seen how the matrix representation allows us to follow the transformation of a set of basis vectors under the operations of a point group. We have also linked the characters that were introduced at the start of this chapter to the diagonal elements of the matrix for a given operation. A particular basis vector can have characters ranging from -1 to $+1$, corresponding to it being reversed by the operation or left alone, and any value in between. Fractional values correspond to the transformed basis function retaining part of their original form when we think about building the new vector from a linear combination of the initial basis set.

The character tables listed in Appendix 12 give standard sets of these characters for the irreducible representations of each point group. We saw in Chapter 3 that the top row of the character table gives a list of the unique operations in the point group. In many cases the operation symbol is preceded by a number which gives the number of equivalent operations of that type. These equivalent sets of operations are referred to as classes of operations, and now we can see how the same character arises for any operation within a class.

4.9.1 $[\text{Ni}(\text{CN})_4]^{2-}, D_{4h}$

Table 4.8 shows the standard character table for the D_{4h} point group. The top row of the character table is the list of the operations valid in this point group. This list always begins with the identity operator, and in groups like D_{4h} , which contains a rotational subgroup, the rotational operations are given next. The principal axis is the C_4 axis and the corresponding

Table 4.8 The D_{4h} character table.

D_{4h}	E	$2C_4$	C_2	$2C_2'$	$2C_2''$	i	$2S_4$	σ_h	$2\sigma_v$	$2\sigma_d$		
A_{1g}	1	1	1	1	1	1	1	1	1	1		$x^2 + y^2, z^2$
A_{2g}	1	1	1	-1	-1	1	1	1	-1	-1	R_z	
B_{1g}	1	-1	1	1	-1	1	-1	1	1	-1		$x^2 - y^2$
B_{2g}	1	-1	1	-1	1	1	-1	1	-1	1		xy
E_g	2	0	-2	0	0	2	0	-2	0	0	(R_x, R_y)	(xz, yz)
A_{1u}	1	1	1	1	1	-1	-1	-1	-1	-1		
A_{2u}	1	1	1	-1	-1	-1	-1	-1	1	1	z	
B_{1u}	1	-1	1	1	-1	-1	1	-1	-1	1		
B_{2u}	1	-1	1	-1	1	-1	1	-1	1	-1		
E_u	2	0	-2	0	0	-2	0	2	0	0	(x, y)	

column heading is $2C_4$. The number 2 signifies that the group contains two C_4 rotations, which have the same character for all irreducible representations. These are the C_4^1 and C_4^3 operations. The C_4^2 operation can also be written C_2^1 and this is the heading of the next column.

A typical molecule belonging to the D_{4h} point group is a square planar transition metal complex such as $[\text{Ni}(\text{CN})_4]^{2-}$, and the two rotations are illustrated in Figure 4.10. The figure also shows the result of the rotation using a basis consisting of x , y and z vectors on the central Ni atom of the complex. Note that this set of basis vectors is initially aligned with the corresponding reference directions, X , Y and Z , but that after the operations the reference axes remain fixed and only the basis vectors have rotated. This emphasizes that the symmetry elements are not shifted during symmetry operations. From inspection of Figure 4.10, the transformation matrices for the C_4^1 and C_4^3 operations in this basis are

$$C_4^1 = \begin{pmatrix} 0 & -1 & 0 \\ 1 & 0 & 0 \\ 0 & 0 & 1 \end{pmatrix} \quad \text{and} \quad C_4^3 = \begin{pmatrix} 0 & 1 & 0 \\ -1 & 0 & 0 \\ 0 & 0 & 1 \end{pmatrix} \quad (4.26)$$

Although the C_4^1 and C_4^3 matrices have different off-diagonal elements, the trace of each is 1. In fact, the trace of the matrices for these operations would be equal irrespective of the basis chosen. A character table only lists the characters for the standard sets of representations, and so the C_4^1 and C_4^3 operations can be put together in a single column. In this way the columns of the character tables may contain more than one operation and the operations contained in any column are linked by having the same character. The columns of the character table contain classes of operations which may be sets of one or more actual operations. This example shows that, in D_{4h} , a 90° rotation clockwise (C_4^1)

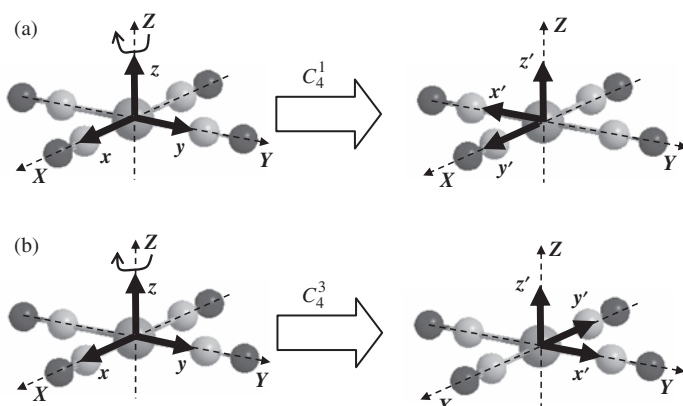


Figure 4.10 The D_{4h} complex $[\text{Ni}(\text{CN})_4]^{2-}$, showing a basis of x , y , z functions representative of the p -orbitals on Ni^{2+} . The effects on the basis of (a) the C_4^1 operation and (b) the C_4^3 operation are illustrated.

is equivalent to a 90° rotation anticlockwise (C_4^3). However, as noted earlier, the C_4^2 operation is listed separately, as the first C_2 rotation. The corresponding matrix is

$$C_2 = \begin{pmatrix} -1 & 0 & 0 \\ 0 & -1 & 0 \\ 0 & 0 & 1 \end{pmatrix} \quad (4.27)$$

which means that the 180° rotation reverses x and y but leaves z unchanged and so has a total character of -1 for this basis.

As a further example, we can see from Table 4.8 that the two vertical reflection planes in D_{4h} are in the same class. Figure 4.11 shows the two σ_v planes, which are labelled σ_v^A and σ_v^B ; from the diagram, we can write down the operation matrices as

$$\sigma_v^A = \begin{pmatrix} 1 & 0 & 0 \\ 0 & -1 & 0 \\ 0 & 0 & 1 \end{pmatrix} \quad \text{and} \quad \sigma_v^B = \begin{pmatrix} -1 & 0 & 0 \\ 0 & 1 & 0 \\ 0 & 0 & 1 \end{pmatrix} \quad (4.28)$$

In this case, either x or y is reversed by the reflection and the other two vectors are left unchanged, so the trace of the matrix is 1 in both cases. This allows the two mirror planes to be placed in the same class and gives the $2\sigma_v$ heading in the point group table.

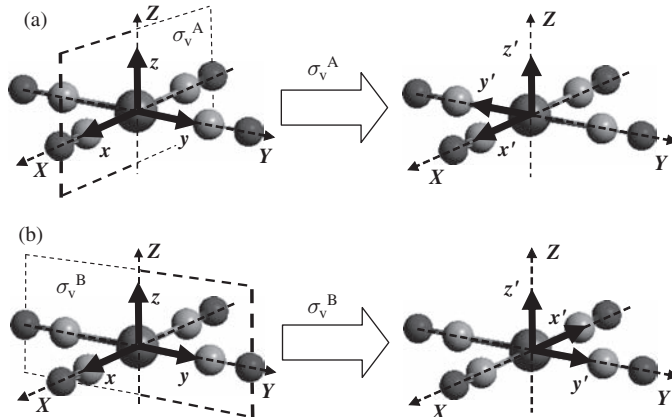


Figure 4.11 The D_{4h} complex $[\text{Ni}(\text{CN})_4]^{2-}$, showing a basis of x, y, z functions representative of the p -orbitals on Ni^{2+} . The effects on the basis of (a) the σ_v^A operation and (b) the σ_v^B operation are illustrated.

Problem 4.9: Draw sketches similar to Figures 4.10 and 4.11 showing the symmetry elements for each of the remaining D_{4h} operations listed as classes in Table 4.8. From your sketches, write down a matrix representation for each operation and then from the matrices:

1. Confirm that each of the $2C'_2$, $2C''_2$, $2S_4$, $2\sigma_v$ and $2\sigma_d$ classes contain two operations which in each case have the same character.
2. Show that the traces of the set of matrices give the character set shown in Table 4.9.

Table 4.9 The reducible character representation for the x, y, z basis on the central Ni atom of the D_{4h} complex as $[Ni(CN)_4]^{2-}$.

D_{4h}	E	$2C_4$	C_2	$2C_2'$	$2C_2''$	i	$2S_4$	σ_h	$2\sigma_v$	$2\sigma_d$	
Γ	3	1	-1	-1	-1	-3	-1	1	1	1	x, y, z

Problem 4.10: Using the matrices derived for the D_{4h} point group in Problem 4.9 check that the matrix product method gives the correct result for the following compound operations:

- (i) $C_4^{-1}C_2$; (ii) $C_2'(X)\sigma_d(AZ)$; (iii) $S_4^3\sigma_h$; (iv) iS_4^{-1} .

Here A indicates the line $X + Y$, i.e. the line in the XY plane at 45° to both the X and Y axes.

To do this, first refer to the basis defined in Figure 4.10 and write down the result you expect in terms of the operations themselves, then compare the result of the matrix product with the corresponding single operation matrix.

4.10 Degenerate Irreducible Representations

In the characters listed for the x, y, z basis in Table 4.9 there is an entry of 3 under the identity operation E . The identity operation leaves all basis vectors unchanged, so this just shows that there are three basis vectors. However, in the standard character table for the D_{4h} point group (Table 4.8) there are no entries with 3 under the identity class column, so this must be another example of a reducible representation. If we wish to assign standard labels from the character table to the x, y, z vectors, then we must simplify the situation by breaking the basis down into smaller sets in the hope of identifying which standard labels to use.

The complete set of matrices we have built up for the D_{4h} operations with the central atom x, y, z basis of Figures 4.10 and 4.11 show that it is possible to interchange x and y , but z is always left alone or reversed. For example, the C_4^{-1} and C_4^3 operations have the matrices shown in Equation (4.26) and these lead to the transformations $(x \rightarrow -y, y \rightarrow x)$ and $(x \rightarrow y, y \rightarrow -x)$ respectively. This linking of the x and y basis vectors can also be seen from the diagonal elements of the matrices. Equation (4.28) also shows that the vertical mirror plane σ_v^A has a -1 contribution to the trace of the matrix from the y basis function and a $+1$ from x , while σ_v^B has a -1 contribution from x and -1 from y . If we tried to separate x from y the two operations will no longer fall into the same class, since the individual basis functions have different characters for a particular mirror plane. Only for the two basis functions together is it valid to have a single class for the vertical reflections, since the total character for x and y is then zero for both mirror planes. The character for z is the same in both matrices, and so it would not matter if we treated this basis vector separately.

In fact, the x and y functions are never interchanged with z by any of the operations in D_{4h} , and so we can split them off together and consider z on its own. For example, the C_4^{-1} operation would become

$$C_4^{-1} \begin{pmatrix} x \\ y \\ z \end{pmatrix} = \begin{pmatrix} 0 & -1 & 0 \\ 1 & 0 & 0 \\ 0 & 0 & 1 \end{pmatrix} \begin{pmatrix} x \\ y \\ z \end{pmatrix} = \begin{pmatrix} 0 & -1 & 0 \\ 1 & 0 & 0 \\ 0 & 0 & z \end{pmatrix} \begin{pmatrix} x \\ y \\ z \end{pmatrix} \quad (4.29)$$

This splitting down of the matrix from a 3×3 form to a $2 \times 2 + 1 \times 1$ has reduced the size of the problem. The full set of 3×3 matrices for each of the operations in D_{4h} could be made simpler in this way, but we cannot break down the relationship between x and y any further, since some of the operations interchange them.

So the $2 \times 2 + 1 \times 1$ representations are the irreducible representations we seek. In the D_{4h} character table (Table 4.8) there are two irreducible representations with 2 under the identity class, E_g and E_u . The pair of p_x and p_y orbitals are reversed by the inversion operation, and so the character under the i column in the table has to be -2 ; this suggests that we should assign the irreducible representation E_u to the x, y part of our basis.

The x, y, z basis centred on the point of the group (here occupied by the Ni atom) is quite a common problem, and so the right-hand column of the character table indicates which representation to use. In this case (x, y) occurs in the right-hand end of the E_u row, indicating that we have correctly assigned these two vectors as contained, together, within the E_u representation.

What the E_u representation assignment is showing is that the x and y basis vectors on the central atom of a D_{4h} complex have identical environments. This has implications for any molecular objects that have the same character set. For example, it tells us that the p_x and p_y orbitals will form a degenerate pair in this molecular geometry, i.e. any molecular orbital containing p_x will have an identical partner involving p_y and the two molecular orbitals will have the same energy.

Table 4.9 gives the total characters for x, y and z , the set of which has been labelled Γ ; this is the convention for any reducible representation. We have assigned x, y to the E_u irreducible representation. The E_u characters give the x, y contribution to the character for the reducible x, y, z basis, so the z characters are simply the difference between the values for x, y, z and those for E_u as set out in Table 4.10. We could also have obtained this result from the matrices for the x, y, z basis directly; however, this type of manipulation using only the characters of operations becomes easier as the basis set size increases. Table 4.10 gives a difference with character 1 under the E operation, since it represents a single object, the z basis vector. If we compare the whole character set with the standards

Table 4.10 Subtraction of the E_u irreducible representation characters from Γ for the x, y, z basis on the central Ni atom of the D_{4h} complex as $[Ni(CN)_4]^{2-}$.

D_{4h}	E	$2C_4$	C_2	$2C_2'$	$2C_2''$	i	$2S_4$	σ_h	$2\sigma_v$	$2\sigma_d$	
Γ	3	1	-1	-1	-1	-3	-1	1	1	1	x, y, z
E_u	2	0	-2	0	0	-2	0	2	0	0	(x, y)
$\Gamma - E_u$	1	1	1	-1	-1	-1	-1	-1	1	1	z

listed in Table 4.8, then an exact match occurs with the A_{2u} irreducible representation and, indeed, the right-hand column contains the z symbol.

The reduction we have deduced can be summarized by the equation

$$\Gamma = E_u + A_{2u} \quad (4.30)$$

which simply means that the reducible representation Γ for the x, y, z basis set can be reduced to $E_u + A_{2u}$ and that none of the other standard irreducible representations listed in Table 4.8 is relevant for this basis.

Problem 4.11: The 2×2 matrices for the D_{4h} operations on the irreducible x, y basis are simply the upper left section of the 3×3 matrices from Problem 4.9. Use these matrices to confirm that the x, y basis has the same characters as the standard E_u in Table 4.8 for all classes of operations.

4.10.1 Ammonia, NH₃, C_{3v}

Another example of degeneracy is found in the C_{3v} example of the N—H bonds of ammonia that we used in Sections 4.5–4.8. From Figure 4.7, the vertical reflection plane σ_v^C swaps the N—H bond basis vectors b_1 and b_2 but leaves b_3 unchanged. Similar diagrams can be drawn for reflections through the equivalent planes σ_v^A and σ_v^B . Each of the planes contains one of the N—H bonds and causes the other two to be swapped over. The matrices corresponding to these operations can be deduced from this result:

$$\sigma_v^A = \begin{pmatrix} 1 & 0 & 0 \\ 0 & 0 & 1 \\ 0 & 1 & 0 \end{pmatrix} \quad \sigma_v^B = \begin{pmatrix} 0 & 0 & 1 \\ 0 & 1 & 0 \\ 1 & 0 & 0 \end{pmatrix} \quad \sigma_v^C = \begin{pmatrix} 0 & 1 & 0 \\ 1 & 0 & 0 \\ 0 & 0 & 1 \end{pmatrix} \quad (4.31)$$

In the standard C_{3v} character table shown in Table 4.11 there is only the single heading $3\sigma_v$ for reflections, i.e. the three planes belong to the same class. If we add up the diagonal elements of each matrix we find that the trace is 1 in each case, and so the total character of the three N—H bonds under any of the reflection operations is 1, consistent with this grouping of the mirror planes into a single class. In this case, the equivalent operations arise from the fact that three mirror planes are drawn in three identical environments; each contains one N—H bond and the associated operation causes the other two N—H bonds to be swapped over. The off-diagonal elements in the matrices allow each of the N—H basis

Table 4.11 The C_{3v} character table.

C_{3v}	E	$2C_3$	$3\sigma_v$		
A_1	1	1	1	z	$x^2 + y^2, z^2$
A_2	1	1	-1	R_z	
E	2	-1	0	$(x, y), (R_x, R_y)$	$(x^2 - y^2, xy), (xz, yz)$

vectors to visit any of the three positions in the original configuration of the molecule. This means that the three basis vectors are indistinguishable; anything we can say about b_1 will also be true of b_2 and b_3 . Also, if we use one N—H bond in a basis then we must include all three; a basis of just b_2 and b_3 would involve transformations that would require us to include b_1 also.

We cannot tell the three N—H bonds apart in the molecule, and so observables to do with the individual bonds or H atoms, such as the proton NMR shifts, will be identical. However, we show below that the vibrations due to N—H stretching motions need not form three degenerate modes.

Problem 4.12: Using the basis of N—H bonds defined in Figure 4.6, show that the reducible representation for the three N—H bond vectors b_1 , b_2 and b_3 is as shown in Table 4.12.

Table 4.12 The reducible representation for the basis of N—H bonds defined for the C_{3v} molecule ammonia in Figure 4.6.

C_{3v}	E	$2C_3$	$3\sigma_v$
Γ	3	0	1

There is no need to use full matrix expressions for the operators in this case. Consider an example operation from each class and arrive at the character using the rules:

1. if a basis vector is unchanged, add 1;
2. if a basis vector is swapped with another member of the basis, add 0.

In this case, no basis vectors which stay in position are ever reversed.

The reducible representation for the three N—H bonds is shown in Table 4.12. The irreducible representations from which this is composed must be from the standard set of Table 4.11. To obtain the correct match we can use the property given by Equation (4.25): that for each class of operations the appropriate standard irreducible characters sum to give that of the reducible representation.

In relatively simple cases, such as the three N—H bonds in ammonia, we can deduce the values of n_i that govern how many of each irreducible representation are present by inspection:

1. Under the identity operation E , Γ has a total character 3. There are several combinations of the irreducible representations that could give this character; for example:

$$3A_1 \text{ or } 3A_2 \text{ or } A_2 + E \dots \quad (4.32)$$

However, the sum must work with the same values of n_i for all classes of operation.

2. Under the $2C_3$ class we have $\chi_\Gamma = 0$, and so the only combinations which satisfy both the E and $2C_3$ classes are

$$A_1 + E \quad \text{and} \quad A_2 + E \quad (4.33)$$

To distinguish between these we can use the final character.

3. Under $3\sigma_v$ we have found 1, and so only $A_1 + E$ will satisfy all three of the symmetry classes simultaneously.

We have shown that, for the three basis vectors from Figure 4.6:

$$\Gamma = A_1 + E \quad (4.34)$$

So, although the three basis functions in this problem are equivalent, this result means that they can be used to construct three irreducible representations, only two of which are degenerate (in the E representation).

We will see later that the irreducible representations found here provide descriptions of the molecular vibrations that involve the N—H stretching modes of the ammonia molecule. The vibration of the molecule is a collective motion of all the atoms that make it up, and these irreducible representations are describing these collective motions. The vibrations fall into three patterns: two are a doubly degenerate pair (E) and the third a separate single vibration (A_1).

Before we deal with drawing out these molecular vibrations in Chapter 6, we will look at a more general way to decompose reducible representations into their irreducible constituents in Chapter 5.

Problem 4.13: Using the basis of N—H bonds defined in Figure 4.6, write down the matrix representation for C_3^1 and C_3^2 operations. Take the trace of these matrices and, hence, show that the two operations have the same character for this basis. This confirms that the two C_3 rotations belong to the same class.

4.11 The Labelling of Irreducible Representations

In this section we make some general comments on the labels used for irreducible representations. The labelling scheme now commonly adopted for irreducible representations was put forward by R.S. Mulliken. We have met some of the symbols used in the preceding sections, but have just taken their assignment directly from the relevant character tables. However, Mulliken did have a logical structure to the assignment of the labels, and an overview of this may help in understanding the behaviour of the irreducible representations in later chapters. Below is a simple summary of the meaning of the symbols used:

1. All representations for single objects (nondegenerate) are designated either A or B . Doubly degenerate representations are given the symbol E and triply degenerate representations T .
2. A representations have character 1 with respect to the principal axis primary operation, while B representations have character -1 for the principal axis.

3. Subscripts 1 and 2 are attached to A and B labels to indicate those that are symmetric (subscript 1) and antisymmetric (subscript 2) with respect to a C_2 axis perpendicular to the principal axis or, if the axis is absent, to a vertical mirror plane. Symmetric means a character +1 and antisymmetric a character of -1.
4. In groups with a centre of inversion i , the subscripts 'g' and 'u' are added to symbols of representations which are symmetric and antisymmetric respectively for the inversion operation. These symbols come from the German words *gerade* meaning 'even' and *ungerade* meaning 'odd'.
5. Primes and double primes are attached to letters to indicate those that are symmetric and antisymmetric with respect to σ_h in groups that do not contain i .

Points 4 and 5 come about from the idea of subgroups. For example, in Chapter 2, the multiplication table for ethane in the staggered conformation was considered, which we now recognize as an example in the D_{3d} point group. The D_{3d} multiplication table (Table 2.4) shows that the identity operator and the simple rotations could be taken for a group in their own right, because no other operations result from their products. This type of subgroup, in this case D_3 , is called a pure rotational group, since it contains only simple rotations.

Looking along the row of the multiplication table for the inversion centre, it is also clear that all the other members of the full D_{3d} point group occur as a product of one of the simple rotational operations and the inversion centre. In the D_{3d} character table there are three different possibilities for the characters under the pure rotation subgroup: labels A_1 , A_2 and E . For each of these there are then two possibilities for the behaviour of an object under the inversion operation:

1. If the object has even symmetry under i , then the product of each member of the subgroup with i will lead to the same character as the subgroup member itself. These are the even irreducible representations given the additional subscript 'g'. For the *gerade* representations in D_{3d} , the first three characters for the rotational subgroup are simply repeated under the operations generated by their product with i , so that the E , $2C_3$, $3C_2$ characters are repeated under i , $2S_6$ and $3\sigma_d$.
2. If an object has *ungerade* symmetry with respect to inversion, then it will have a negative character in the i column and the operations generated from combinations of the rotational subgroup members and i will have the opposite sign to that of the simple rotation involved. These are the representations labelled 'u'.

In groups without an inversion centre but containing a horizontal mirror plane, a similar argument can be put forward based on the combination of the pure rotational subgroup with the σ_h plane.

The points listed above still do not give a complete set of explanations for Mulliken's symbols. For example, the numerical subscripts used on E and T representations are not covered. However, these require mathematical explanations that are beyond the scope of this introductory text, and so we shall regard them simply as standard labels.

4.12 Summary

In this chapter, we have covered the idea of symmetry representations in terms of characters and matrices. The highlights are:

1. A representation of a set of symmetry operations allows the operations to be manipulated algebraically. The representation must give the same multiplication table as the operations themselves.
2. Matrices allow the effect of operations on sets of basis vectors to be written down algebraically and show exactly how basis vectors are transformed under each operation.
3. The character for a basis function under a given operation is a single number that describes how much of the original function remains after the transformation. For a single basis function it will be in the range -1 to $+1$.
4. Total characters for sets of basis functions are the trace of the corresponding matrix.
5. Character tables for the point groups give the sets of characters for the simplest representations in the group. These are the irreducible representations.
6. For a basis set of our choosing we will usually arrive at a set of characters that are not present in the character table. This is a reducible representation given the symbol Γ , and it will always be possible to express Γ as a sum of the irreducible representations.
7. Any reducible representation can be constructed as a linear sum of the standard irreducible representations. For the correct linear combination, the sum of the characters for the irreducible representations in each class will give the reducible character, i.e.

$$\chi_{\Gamma}(C) = \sum_i n_i \chi_i(C)$$

where the symbol χ is used for a character and the subscripts Γ and i signify the reducible representation and the i th irreducible representation for a given class C respectively. n_i is a positive integer (which can be zero) that gives the number of times the irreducible representation i is present in the reducible representation Γ .

4.13 Completed Tables

Figure 4.12 gives the completed table for Problem 4.1.

4.14 Self-Test Questions

1. Derive a reducible representation for the four CN bonds in the D_{4h} complex $[\text{Ni}(\text{CN})_4]^{2-}$ pictured in Figure 4.11. By comparing your results with possible combinations of the irreducible representations given in Table 4.8 identify the set that are equivalent to your reducible representation.
2. Write out matrices for all the operations in C_{3v} for the basis of N—H bonds shown in Figures 4.6 and 4.7. Using your matrices, derive a multiplication table for the operations in the C_{3v} point group and check your results against operations carried out on a model of the molecule. Remember that the symmetry elements are fixed in space and do not move when operations are carried out.

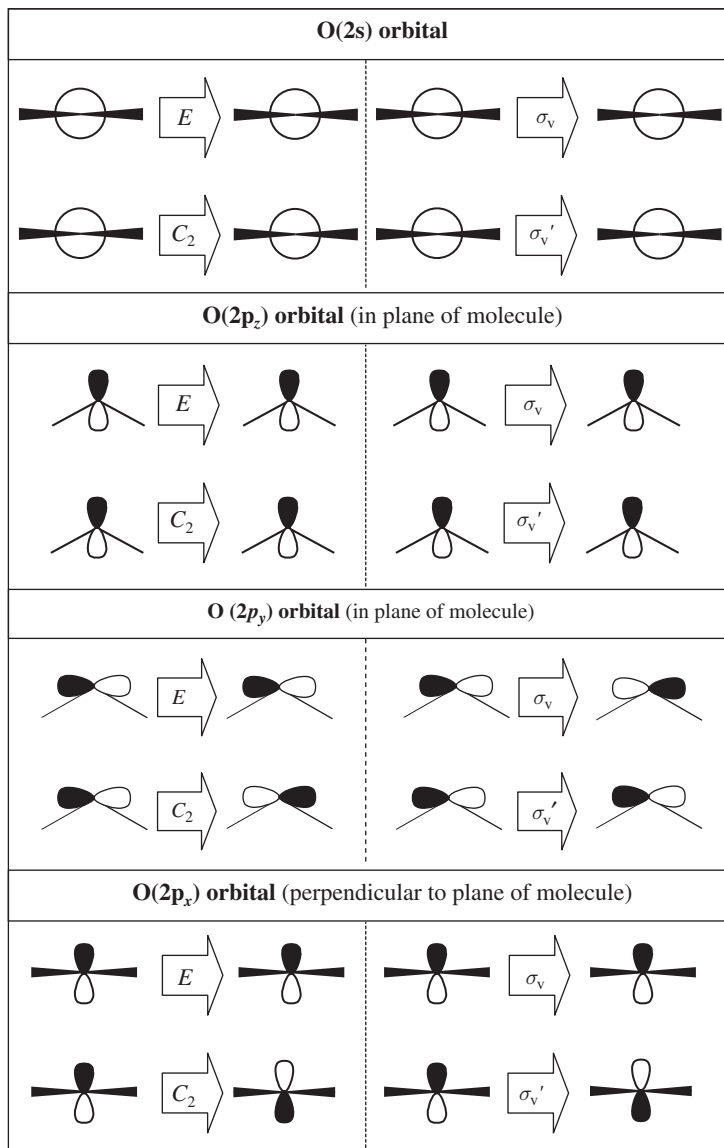


Figure 4.12 A completed version of the transformations of the valence AOs on O in H_2O under the operations of the C_{2v} point group for Problem 4.1.

Further Reading

The original paper by R.S. Mulliken including his assignment of irreducible representation labels:

Mulliken RS (1933) *Physical Review* **43**: 279.

5

Reducible and Irreducible Representations

5.1 Introduction

Figure 5.1 shows the fundamental vibrations of the sound board of a guitar. The motions of the sound board as it vibrates have been resolved using a laser interferometer to give a contour plot of the distortions of the surface caught at an instant in time. These vibrational motions are sustained because they correspond to the resonant frequencies of the sound board. For the listener, the correct resonance of the instrument gives the guitar the mixture of tones and overtones that distinguishes it from other instruments.

From a symmetry point of view the sound board of the guitar would be classified as belonging to the point group C_{2v} : there is a C_2 axis which runs along the line defined by the finger board (vertical in the images of Figure 5.1), a vertical mirror plane perpendicular to the board σ_v and the plane of the board itself σ_v' . However, the shape of the distortion due to the vibrations does not follow all of the symmetry operations in the point group in the same way. For example, the second vibration in Figure 5.1 involves the left- and right-hand sides of the sound board moving in opposite directions at a given instant: if the left-hand side is moving toward the viewer, then the right-hand side will be moving away. This is why the centre of the sound board, along the line of the C_2 axis, stays stationary at all times: it is a node in this vibrational mode. If the distortion were taken into account, both of the vertical mirror planes would no longer be symmetry elements; but rather than assign a new point group to the distortion, we will use the irreducible representations of the point group to describe it.

The characters under the operations of the C_{2v} point group for the Figure 5.1b vibration are set out in Figure 5.1g. This shows that the C_2 rotation leaves the distortion of the sound board apparently unchanged, giving character 1, while for a reflection through either mirror plane the motion of the vibrating sound board would appear to be reversed. This is equivalent to multiplying the original distortions by -1 , and so this is the character for the σ_v and σ_v' operations. Along with the character of 1 under the identity operation,

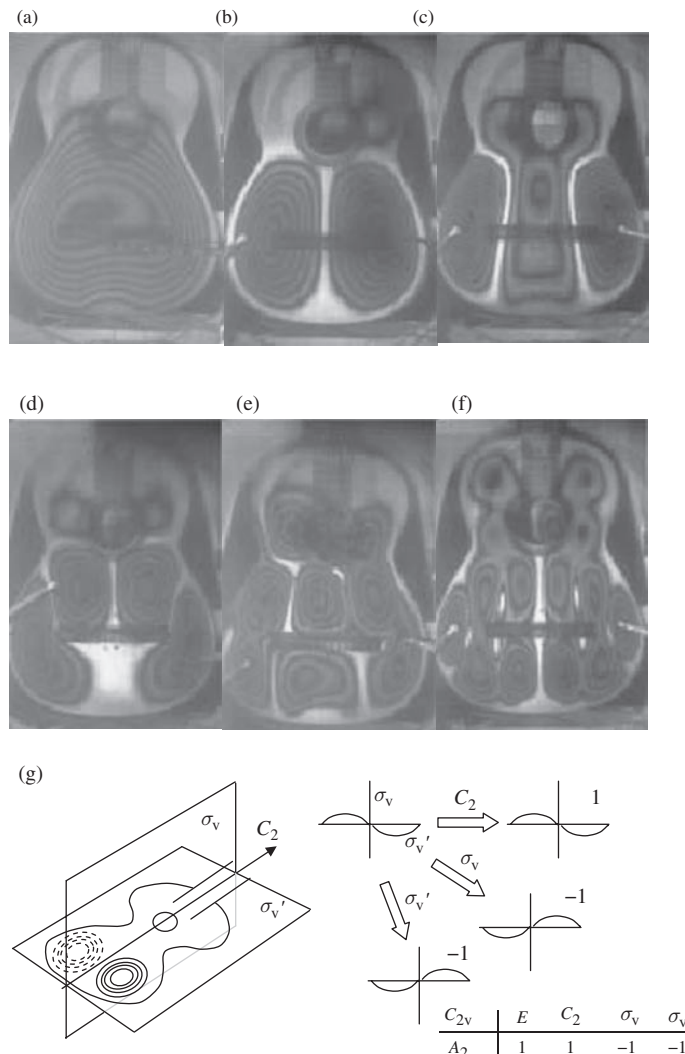


Figure 5.1 The fundamental modes of a guitar sound board photographed using laser interferometry. As the instrument vibrates, the distortions of the board perpendicular to its surface effectively amplify the sound of the vibrating string. The contour patterns are caused by the differing path lengths of the laser light reflected from the sound board. The frequency of vibration increases from (a) to (f). (g) Assignment of characters to mode (b) using the C_{2v} point group operations; the diagrams to the right give the shape of the distortion of the sound board looking down the C_2 axis. (Source: These images were kindly provided by Dr Bernard E. Richardson, School of Physics, Cardiff University.)

this character set is identical to the standard irreducible representation A_2 ; the vibration of Figure 5.1b is an A_2 vibration.

To generate the pictures of the guitar in Figure 5.1, the board was excited in a precise way to allow only a single resonant vibration in each case. Any vibration of the board while

the guitar is being played will be a mixture of all the possible resonances. For a given note the resonance for that particular pitch is dominant, but the others are still present to a smaller extent. The motion of the sound board while the guitar is played will be much more complex than the fundamental modes shown in Figure 5.1. However, any motion can be built up from a combination of the fundamental modes, and so the identification of these modes, particularly their symmetry properties, is important in the vibrational analysis of any object. Our main concern will be molecular vibrations for which the fundamental modes can be described in terms of atomic displacements.

In Section 4.8 we found how the matrix representation of a set of basis vector transformations for a point group can sometimes be made simpler. For example, the 2×2 matrix representation for x, y at O in H_2O can be reduced to two ' 1×1 ' matrices (i.e. a simple number for each operation) for x and y . This process of simplifying a representation to a set of irreducible standard representations is central to the application of symmetry in chemistry and corresponds to finding the fundamental modes of vibration that underlie molecular motion.

In this chapter we will use examples from the vibrational modes of H_2O and NH_3 , amongst others. The other application area discussed in this book is the derivation of molecular orbitals (MOs) from sets of atomic orbitals (AOs). To illustrate the application of the reduction formula in this area we turn to the AOs of transition metal centres in complexes of various geometries, to illustrate the link between the reducible and irreducible representations. The goal is to be able to work out the appropriate set of irreducible representations for any basis without resorting to the matrix representation. We saw at the end of Chapter 4 that the reduction process is actually possible using only the characters for each class of operations. These are straightforward to define by inspection of a suitable basis, as we show in the example of Section 5.2. The reduction process in Chapter 4 was carried out by inspection, but a more solid link between reducible and irreducible representations is provided by the reduction formula. This will be derived in Section 5.5 from the general properties of the character representation in any point group presented in Section 5.4. The formula's application is then outlined using examples in Sections 5.6–5.9. Here, we will find that the irreducible representations give the fundamental symmetry labels for vibrational modes or AOs/MOs. The identification of the pattern formed by each mode in terms of atomic motion for vibrations, and the construction of MOs from linear combinations of AOs, will be the subject of Chapters 6 and 7.

Problem 5.1: Confirm that the vibrations in Figure 5.1a and c can be assigned to the B_2 irreducible representation.

5.2 Irreducible Representations and Molecular Vibrations

In Chapter 1, the number of degrees of freedom for a molecule was calculated by considering the motion of each atom in the X, Y and Z directions. Each atom can move in three dimensions, and so a molecule containing N atoms has $3N$ degrees of freedom. The discussion of the guitar vibrations above shows that the actual motion of the atoms in a

vibration is likely to involve the whole molecule rather than just particular atoms. Each of these fundamental collective motions can be assigned an irreducible representation from the molecular point group. The motion of symmetry-related atoms will respond to the group operations following the corresponding characters.

Figure 5.2 shows an H_2O molecule with a basis of nine vectors included to allow us to describe the motion of each atom. These basis vectors are labelled x, y, z with the appropriate atom label as a subscript and are initially aligned with the reference axis system, X, Y, Z .

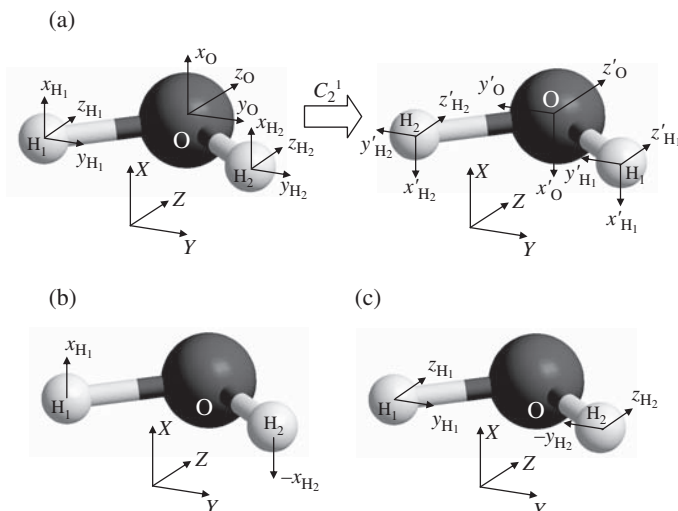


Figure 5.2 (a) Basis vectors for describing the motion of atoms in H_2O along the X, Y and Z directions and the effect of a C_2^1 rotation. (b) A combination of H_1 and H_2 movements along X that has a character of 1 for C_2^1 . (c) Combinations of H_1 and H_2 in the molecular plane can be obtained which have character 1 for all operations in C_{2v} and so are compliant with an A_1 vibration. The reference axis system is shown in the foreground of each diagram and is orientated using the convention that the Z -direction aligns with the principal symmetry axis. Note that the reference axis does not move during the rotation, all symmetry elements are referred to this axis system.

The direction of motion of an atom as part of a vibration is usually restricted by the symmetry properties of the irreducible representation. For example, imagine that the O atom in Figure 5.2a is moving in the X or Y directions along the basis vectors x_O or y_O respectively. The basis vectors shown in the figure are the same as those defined for the paper models in Appendix 1, and so it may help to have those to hand here. We can ask would this type of motion be compliant with a molecular vibration belonging to the A_1 representation? The A_1 representation has character 1 for all four of the symmetry elements of the C_{2v} group. However, Figure 5.2a shows that a rotation around C_2 would alter the directions x_O and y_O to $-x_O$ and $-y_O$ and so motion of O in these directions would appear reversed, giving a character of -1 . This means that motion of the O atom in the x_O or y_O directions is not possible in an ' A_1 vibration'.

Movement along z_O is unaltered by any of the operators in the group, and so an A_1 vibration can have the O atom moving only in the Z -direction. Note also that the right-hand

column of the C_{2v} character table in Appendix 12 contains the symbol z against A_1 , but x and y are elsewhere.

For H_1 and H_2 we have to consider the movement of both atoms together, because they are linked by the symmetry operations of the C_{2v} point group. What if H_1 were to move out of the molecular plane upward in the direction of the basis vector x_{H_1} in the starting configuration of Figure 5.2? The C_2 rotation would swap H_1 with H_2 and its motion would then be downward, following x'_{H_1} . In the molecular vibration, we could have a character of 1 for the C_2 rotation if H_2 were also moving in the $-X$ direction in the original orientation of the molecule; then, the motion as a whole would appear unchanged. This arrangement of H_1 and H_2 is shown in Figure 5.2b. However, we need characters of 1 for all symmetry operations for an A_1 vibration, and the Figure 5.2b combination has -1 for both $\sigma_v(XZ)$ and $\sigma_v'(YZ)$ and so contravenes the restrictions of the irreducible representation. It is actually a similar motion to the sound board in Figure 5.1b and g. So, motion of the H atoms out of the molecular plane is not possible for an A_1 vibration.

Now let us take H_1 moving in the YZ plane so that it moves toward the O atom, i.e. it has motion in the (Y, Z) direction (Figure 5.2c). In this case the C_2 axis leaves the motion unchanged only if H_2 moves in the $(-Y, Z)$ direction. This is also the set of H movements required by $\sigma_v(XZ)$ and $\sigma_v'(YZ)$ for a character of 1. Provided the two H atoms move together in this way, this would be consistent with the A_1 irreducible representation.

The molecular structure suggests that one possible A_1 vibration consists of both H atoms moving toward the O atom in unison and the O atom only moving only along the Z -axis. This would cause the O—H bonds to be compressed and stretched in phase with one another, a vibration commonly referred to as the symmetric stretch mode (Figure 5.3a).

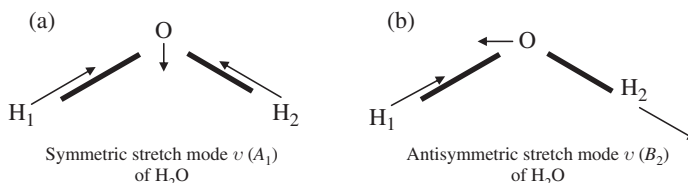


Figure 5.3 Vibrational O—H stretching modes of H_2O which fall into the (a) A_1 representations and (b) B_2 representation.

The molecule as a whole never actually moves during a vibration, so the motion of the H atoms and the O atom must be balanced with no net centre of mass motion. As the H atoms move toward the O atom, the O moves down the principal axis in such a way that the centre of mass of the molecule is held fixed. This is shown by the arrangement of the arrows in Figure 5.3a, with a shorter arrow on O due to its higher mass.

Problem 5.2: The antisymmetric stretch mode of H_2O is shown in Figure 5.3b. Show that this conforms to the B_2 irreducible representation. You should use the same molecular orientation as Figure 5.2a. The C_{2v} character table can be found in Appendix 12.

5.3 Finding Reducible Representations

In the previous section we deduced irreducible representation labels for two of the vibrational modes of H_2O by inspecting the molecular geometry and thinking about the possible movements of the atoms. This is easy enough for simple molecules but the representation for a particular atomic motion may not be so straightforward for more complex cases. Also, if there are many vibrational modes, it is unlikely that we would find them all by inspection. What is required is a general method to find the representations for all possible molecular vibrations. The approach we will use is first to identify all the irreducible representations that are present for a given basis and then interpret each of them in terms of combinations of the basis functions. The rest of this chapter is dedicated to the first part of this process and the second part is the subject of Chapter 6.

Staying with the vibrational analysis problem, for a molecule with N atoms we would expect $3N$ degrees of freedom, since each atom can move in three dimensions. For non-linear molecules, such as H_2O , the molecule as a whole will have six degrees of freedom: three translations and three rotations. This means that we would expect $3N - 6$ vibrations. Each of these vibrations will be a collective motion, potentially involving all of the atoms in the molecule.

However, we can derive the irreducible representations before the patterns of atomic motion in the vibrational modes are actually identified. This is done by first imagining that each individual atom is independent of the others. For example, Figure 5.2a shows a basis of nine vectors for the atoms in the H_2O molecule. This gives us the expected number of degrees of freedom, since $3N = 9$ for H_2O . If we were to set up a matrix representation for, say, the C_2 operation in the C_{2v} group for this basis, then we would have to use the 9×9 matrix shown in Figure 5.4a.

We saw in Figure 5.2 that because the H atoms are swapped over by the C_2^1 rotation so are their basis vectors. This shows up in the matrix representation as the two sets of nonzero off-diagonal elements in the lines for H_1 and H_2 . These are off-diagonal elements because the axes are moved to different atom positions by the rotation. Application of the matrix to the nine basis vectors is shown in Figure 5.3b, confirming that it correctly reproduces the operation.

The character for the C_2^1 operation using this basis is given by trace of the matrix, i.e. the sum of the diagonal terms, which is -1 . This is the last time we will resort to the matrix representation, because this example establishes the following simple rule:

If an operation moves an atom to a symmetry-equivalent position, then all basis vectors to do with that atom will give rise to only off-diagonal elements in the transformation matrix and so contribute zero to the character for the operation.

The $\sigma_v(XZ)$ operation also swaps the H atoms, and so we need only consider the basis vectors on the O atom to derive the total character for this operation. This plane causes the transformation

(a)

$$C_2 = \begin{pmatrix} -1 & 0 & 0 & 0 & 0 & 0 & 0 & 0 & 0 \\ 0 & -1 & 0 & 0 & 0 & 0 & 0 & 0 & 0 \\ 0 & 0 & 1 & 0 & 0 & 0 & 0 & 0 & 0 \\ 0 & 0 & 0 & 0 & 0 & 0 & -1 & 0 & 0 \\ 0 & 0 & 0 & 0 & 0 & 0 & 0 & -1 & 0 \\ 0 & 0 & 0 & 0 & 0 & 0 & 0 & 0 & -1 \\ 0 & 0 & 0 & 0 & 0 & 0 & 0 & 0 & 1 \\ 0 & 0 & 0 & -1 & 0 & 0 & 0 & 0 & 0 \\ 0 & 0 & 0 & 0 & -1 & 0 & 0 & 0 & 0 \\ 0 & 0 & 0 & 0 & 0 & 1 & 0 & 0 & 0 \end{pmatrix}$$

Lines for O vectors

Lines for H₁ vectors

Lines for H₂ vectors

(b)

$$\begin{pmatrix} -1 & 0 & 0 & 0 & 0 & 0 & 0 & 0 & 0 \\ 0 & -1 & 0 & 0 & 0 & 0 & 0 & 0 & 0 \\ 0 & 0 & 1 & 0 & 0 & 0 & 0 & 0 & 0 \\ 0 & 0 & 0 & 0 & 0 & 0 & -1 & 0 & 0 \\ 0 & 0 & 0 & 0 & 0 & 0 & 0 & -1 & 0 \\ 0 & 0 & 0 & 0 & 0 & 0 & 0 & 0 & -1 \\ 0 & 0 & 0 & 0 & 0 & 0 & 0 & 0 & 1 \\ 0 & 0 & 0 & -1 & 0 & 0 & 0 & 0 & 0 \\ 0 & 0 & 0 & 0 & -1 & 0 & 0 & 0 & 0 \\ 0 & 0 & 0 & 0 & 0 & 1 & 0 & 0 & 0 \end{pmatrix} \begin{pmatrix} x_O \\ y_O \\ z_O \\ x_{H_1} \\ y_{H_1} \\ z_{H_1} \\ x_{H_2} \\ y_{H_2} \\ z_{H_2} \end{pmatrix} = \begin{pmatrix} -x_O \\ -y_O \\ z_O \\ -x_{H_2} \\ -y_{H_2} \\ z_{H_2} \\ -x_{H_1} \\ -y_{H_1} \\ z_{H_1} \end{pmatrix}$$

Figure 5.4 A full matrix for the C_2 rotation of H_2O shown in Figure 5.2 accounting for the transformation of all nine basis vectors.

$x_O \rightarrow x_O$		character = 1
$y_O \rightarrow -y_O$		character = -1
$z_O \rightarrow z_O$		character = 1
<hr/>		
Total = 1		

So the total character for all nine basis vectors under the $\sigma_v(XZ)$ operation is 1. For the $\sigma_v'(YZ)$, which is the plane of the molecule, none of the atoms are moved and we find the following characters:

$x_{H_1} \rightarrow -x_{H_1}$, ch. = -1	$x_0 \rightarrow -x_0$, ch. = -1	$x_{H_2} \rightarrow -x_{H_2}$, ch. = -1
$y_{H_1} \rightarrow y_{H_1}$, ch. = 1	$y_0 \rightarrow y_0$, ch. = 1	$y_{H_2} \rightarrow y_{H_2}$, ch. = 1
$z_{H_1} \rightarrow z_{H_1}$, ch. = 1	$z_0 \rightarrow z_0$, ch. = 1	$z_{H_2} \rightarrow z_{H_2}$, ch. = 1
<hr/>		
Total H_1 = 1	Total O = 1	Total H_2 = 1
<hr/>		
Grand Total = 3		

Because y and z basis vectors are in the plane, they are unaffected by the operation and contribute 6 to the total character for the basis. However, all the x basis vectors are reversed, contributing -3. So the total character for the basis is $6 - 3 = 3$.

Finally, the E operator will leave all the vectors in the basis unchanged and so has character 9. The E operation always does nothing to the basis vectors, and so the E column in a character table gives the number of basis objects in the representation. The characters for the nine basis vectors are summarized in Table 5.1. In the C_{2v} group there are no

Table 5.1 The character set for the representation of the nine basis vectors used to represent the degrees of freedom of H_2O defined by the basis of Figure 5.2.

C_{2v}	E	C_2	$\sigma_v(XZ)$	$\sigma_v'(YZ)$
Γ	9	-1	1	3

degenerate representations and so, clearly, this representation using three vectors per atom is reducible.

In the leftmost column of Table 5.1 the symbol Γ (Greek capital Gamma) is used for the representation summed over all basis vectors. Γ is the general symbol employed for a reducible representation.

In Chapter 4 we found all the irreducible representations for the C_{2v} point group, the possible labels are A_1 , A_2 , B_1 and B_2 . Each of these has a character of 1 under the E operation column of the character table, and so each irreducible representation deals with only one object.

Γ must contain the two fundamental vibrations we found in Section 5.2 and seven other motions of the molecule. Several different motions can have the same symmetry label, provided each conforms to the character set for that irreducible representation. However, it is a daunting task to try to find all nine molecular motions by inspection. In the next two sections we derive an equation that automatically pulls out the irreducible representations from a reducible set of characters. We will then apply the formula to this particular case of H_2O .

5.4 Properties of Point Groups and Irreducible Representations

To obtain the reduction formula we first need to look at the general properties of point groups a little more closely by defining a few general properties and some useful terms.

Property 1: The set of allowed operations in a point group are split into *classes* of the same type. The operations in a class have the same character for all irreducible representations, and so only one heading entry occurs for each class in a character table.

The *number of operations in a given class* is denoted g_c .

The idea of classes was introduced in Section 4.9, where we found that related operations in a group can have the same trace in the matrix representation. If this is the case for any choice of basis, then the same character will always arise whichever operation from the class is selected, and so only a single column is required in the character table.

To illustrate further how operations can fall into the same class, we will look at the D_{3h} point group, for which cyclopropane (Figure 5.5) serves as an example molecule. Figure 5.5 also shows some example symmetry elements from D_{3h} . The principal C_3 axis is perpendicular to the plane of the three C atoms and passes through the centre of the triangle they define. This axis leads to two operations, C_3^1 and C_3^2 . We can use as a basis the

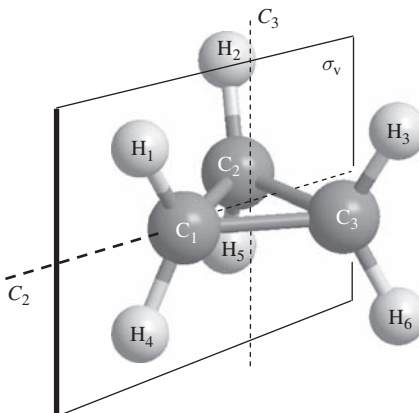


Figure 5.5 Cyclopropane as an example molecule belonging to the D_{3h} point group.

positions of the six H atoms to think about the transformations caused by these operations. For C_3^1 and C_3^2 , each of the hydrogen atoms would move as follows:

$$C_3^1 : \quad H_1 \rightarrow H_2, H_2 \rightarrow H_3, H_3 \rightarrow H_1 \quad \text{and} \quad H_4 \rightarrow H_5, H_5 \rightarrow H_6, H_6 \rightarrow H_4$$

$$C_3^2 : \quad H_1 \rightarrow H_3, H_2 \rightarrow H_1, H_3 \rightarrow H_2 \quad \text{and} \quad H_4 \rightarrow H_6, H_5 \rightarrow H_4, H_6 \rightarrow H_5$$

Since all the atoms are relocated, both of these operations have a total character of 0 and so may be grouped into the same class. This class consists of two symmetry operations, and so $g_c = 2$ giving a column heading of $2C_3$ in the D_{3h} character table (Appendix 12). In this case, both symmetry operations arise from a single symmetry element.

If we consider the vertical mirror plane shown in Figure 5.5, there is a single associated operation:

$$\sigma_v : \quad H_1 \rightarrow H_1, H_2 \rightarrow H_3, H_3 \rightarrow H_2 \quad \text{and} \quad H_4 \rightarrow H_4, H_5 \rightarrow H_6, H_6 \rightarrow H_5$$

In this case there are two H atoms left unaffected (the two in the mirror plane), and so the total character would be 2. However, the plane shown is only one choice of three possibilities; there is also a σ_v plane containing H_2 and H_5 and one containing H_3 and H_6 . The three planes are indistinguishable from one another and so give the same total character in our basis, or any other that we could choose. Accordingly, the σ_v planes form a class with $g_c = 3$. This is a case in which a class consists of three symmetry operations from three indistinguishable symmetry elements.

The grouping of symmetry operations into classes must imply that the character is the same for all operations in the class irrespective of the basis used. For example, from the D_{3h} example, rotation around the horizontal C_2 axis shown in Figure 5.5 gives the following result:

$$C_2^1 : \quad H_1 \rightarrow H_4, H_2 \rightarrow H_6, H_3 \rightarrow H_5 \quad \text{and} \quad H_4 \rightarrow H_1, H_5 \rightarrow H_3, H_6 \rightarrow H_2$$

which again has a total character of 0, and so we may consider grouping the C_2 and C_3 operations. However, selecting the C atom positions as a basis, the two operations give different characters:

$$C_3^1 : \quad C_1 \rightarrow C_2, C_2 \rightarrow C_3, C_3 \rightarrow C_1 \quad \text{total character } 0$$

$$C_3^2 : \quad C_1 \rightarrow C_3, C_2 \rightarrow C_1, C_3 \rightarrow C_2 \quad \text{total character } 0$$

$$C_2^1 : \quad C_1 \rightarrow C_1, C_2 \rightarrow C_3, C_3 \rightarrow C_2 \quad \text{total character } 1$$

So, while the C_3 operations still give the same character as each other, for the C_2^1 rotation the C atom on the axis is unaffected and we find a total character of 1. This means that the C_2 operation cannot be in the same class as C_3^1 and C_3^2 .

The C_2 axis is one of a set of three (each passes through a C atom and the centre of the opposite C—C bond). Rotation around any of these axes leaves one C unaffected but swaps around all the H atoms; so, in either basis set, any of the three axes gives the same total character. The three C_2 axes form another class within the D_{3h} point group; so, in the corresponding character table heading we see $3C_2$ and would assign $g_c = 3$ when considering this class.

In Section 5.5 it will be shown that any set of characters we obtain for a basis of our choice can be reduced to a summation of the standard irreducible representations from the character tables. This means that a sufficient condition for putting a given set of operations in the same class is that they have the same character for all irreducible representations. In general, operations that can be collected together fall into one of the two types we have discussed here.

The first type has operations that are linked to the same symmetry element, such as C_3^1 and C_3^2 . However, operations linked to the same element will not always fall into the same class; for example, in D_{4h} the C_4^1 and C_4^3 rotations associated with the principal axis are in the same class, but the C_4^2 operation is listed separately in the character table as C_2 . The second types of operation that fall into the same class are those for sets of symmetry-equivalent elements, such as the three equivalent mirror planes in D_{3h} .

It is also possible that symmetry-equivalent elements each give more than one operation to a class. For example, in the octahedral point group O_h there are four equivalent C_3 axes, each of which contributes two operations which are in the same class (C_3^1 and C_3^2), and so the heading in the character table reads $8C_3$. One of these C_3 axes is marked on the paper model of an octahedron from Appendix 4.

Problem 5.3: Show that each operation below belongs to a class with $g_c > 1$ and assign the value of g_c . Illustrate your answer with sketches of the result for each operation and derive the relevant total characters using the suggested structure and basis:

1. σ_d , in the D_{3d} point group, using a basis of the hydrogen atoms in staggered ethane (e.g. see Figure 2.5c).
2. S_4^1 , in the D_{4h} point group, using a basis of x, y, z vectors on the central atom of a square planar complex (e.g. see Figure 4.10);
3. all C_3^1 and C_3^2 operations in the T_d point group, using as a basis the C—H bond vectors in methane (see also the model tetrahedron from Appendix 3).

Property 2: The *order of the group* is the *total number of operations* that are in the group and is given the symbol h .

Finding the order of a point group is simply a matter of totalling the number of unique operations. In the previous section we considered the C_{2v} point group with H_2O as an example; this contains the operations E , C_2 , $\sigma_v(\text{XZ})$ and $\sigma_v'(\text{YZ})$, and so $h = 4$.

In Chapter 4 we also considered the D_{4h} group, which has the following operations:

$$E, 2C_4, C_2, 2C_2', 2C_2'', i, 2S_4, \sigma_h, 2\sigma_v, 2\sigma_d$$

Notice that in this list the equivalences discussed in Chapters 1 and 2 have been accounted for so that only unique operations are listed. Multiple operations in the same class are written as a single entry in the list; the number of operations within each class g_c is noted by a number in front of the symbol for the operation. This is the list that appears at the top of the character table in Appendix 12.

Counting up the total number of operations shows that the order of the D_{4h} group is 16. From a standard character table, the value of h can be calculated from the total number of operations given in the column headings. Mathematically, this summation process can be written:

$$h = \sum_c g_c \quad (5.3)$$

where the C under the summation sign indicates that the sum is over all classes of operations within the point group. Equation (5.3) means that the order of a group is the sum of the number of operations in each class. This makes calculating the order of the group when we have the point group table a simple matter of adding the numbers at the head of each column. For example, the character table for the D_{3h} group in Appendix 12 has the class headings E , $2C_3$, σ_h , $2S_3$ and $3\sigma_v$, making the g_c values 1, 2, 1, 2 and 3 respectively. Summing these gives the order of the group, $h = 9$.

Property 3: The number of irreducible representations in a point group is equal to the number of classes, i.e. all character tables are square.

Property 3 can be confirmed by inspecting any of the character tables in Appendix 12. For example, the D_{3d} point group for molecules such as ethane in the staggered conformation has the headings

$$E, 2C_3, 3C_2, i, 2S_6, 3\sigma_d$$

so that there are six classes.

The irreducible representations listed for D_{3d} are

$$A_{1g}, A_{2g}, E_g, A_{1u}, A_{2u}, E_u$$

so there are six of these as well.

Property 4: The sum of squares of the characters of an irreducible representation for all operations is equal to the order of the group. Since g_c gives the number of operations in a class, this can be written

$$\sum_c g_c [\chi_i(C)]^2 = h \quad (5.4)$$

where $\chi_i(C)$ is the character for the i th representation and C th class of operators.

To illustrate Property 4, we begin with the C_{2v} point group; since there are no equivalent operations, all the values of g_c are 1 and the totals are straightforward to calculate:

$$\text{for } A_1: \sum_c g_c [\chi_{A_1}(C)]^2 = 1 \times 1^2 + 1 \times 1^2 + 1 \times 1^2 + 1 \times 1^2 = 4$$

$$\text{for } A_2: \sum_c g_c [\chi_{A_2}(C)]^2 = 1 \times 1^2 + 1 \times 1^2 + 1 \times (-1)^2 + 1 \times (-1)^2 = 4$$

$$\text{for } B_1: \sum_c g_c [\chi_{B_1}(C)]^2 = 1 \times 1^2 + 1 \times (-1)^2 + 1 \times 1^2 + 1 \times (-1)^2 = 4$$

$$\text{for } B_2: \sum_c g_c [\chi_{B_2}(C)]^2 = 1 \times 1^2 + 1 \times (-1)^2 + 1 \times (-1)^2 + 1 \times 1^2 = 4$$

from class:

$$\overbrace{\quad\quad\quad}^E \quad \overbrace{\quad\quad\quad}^{C_2} \quad \overbrace{\quad\quad\quad}^{\sigma_v(XZ)} \quad \overbrace{\quad\quad\quad}^{\sigma_v'(YZ)}$$

(5.5)

The order of the group is 4, and so this property is confirmed for all of the irreducible representations of the C_{2v} point group.

For groups with equivalent sets of operations the corresponding values of g_c will be greater than 1. For example, in the tetrahedral point group, T_d , the character table in Appendix 12 states that there is one operation in the identity class, 8 operations in the C_3 class, 3 in the C_2 and so on. If we sum the number of operations in all classes we obtain the order of the group, i.e.:

$$h = \sum_c g_c = 1 + 8 + 3 + 6 + 6 = 24 \quad (5.6)$$

Taking the irreducible representations A_2 and E as examples, the sums for Property 4 are

$$\text{for } A_2: \sum_c g_c [\chi_{A_2}(C)]^2 = 1 \times 1^2 + 8 \times 1^2 + 3 \times 1^2 + 6 \times (-1)^2 + 6 \times (-1)^2 = 24$$

$$\text{for } E: \sum_c g_c [\chi_E(C)]^2 = 1 \times 2^2 + 8 \times (-1)^2 + 3 \times 2^2 + 6 \times 0^2 + 6 \times 0^2 = 24$$

from class :

$$\overbrace{\quad\quad\quad}^E \quad \overbrace{\quad\quad\quad}^{8C_3} \quad \overbrace{\quad\quad\quad}^{3C_2} \quad \overbrace{\quad\quad\quad}^{6S_4} \quad \overbrace{\quad\quad\quad}^{6\sigma_d}$$

(5.7)

In both cases the sum gives the order of the group, and so Property 4 is confirmed again.

Property 5: Any two different irreducible representations are *orthogonal*, this can be summarized by the formula

$$\sum_C g_c \chi_i(C) \chi_j(C) = 0 \quad i \neq j \quad (5.8)$$

where $\chi_i(C)$ and $\chi_j(C)$ are the characters for the i th and j th representations for the C th class of operators.

To demonstrate the orthogonality property we will use some more examples from the character tables in Appendix 12. The C_{2h} point group has no equivalent operations, so all four classes have $g_c = 1$. Applying Equation (5.8) to the B_g and A_u representations, we find

$$\begin{aligned} \sum_C g_c \chi_{B_g}(C) \chi_{A_u}(C) &= 1 \times 1 \times 1 + 1 \times (-1) \times 1 + 1 \times 1 \times (-1) + 1 \times (-1) \times (-1) \\ &= \underbrace{1}_{E} - \underbrace{1}_{C_2} - \underbrace{1}_i + \underbrace{1}_{\sigma_h} = 0 \end{aligned} \quad (5.9)$$

from class :

For point groups with multiple operations in the same class the values of g_c may be greater than 1. Using an example from the irreducible representations A_2' and E' in D_{3h} :

$$\begin{aligned} \sum_C g_c \chi_{A_2'}(C) \chi_{E'}(C) &= 1 \times 1 \times 2 + 2 \times 1 \times (-1) + 3 \times (-1) \times 0 \\ &+ \underbrace{1 \times 1 \times 2}_{\sigma_h} + 2 \times 1 \times (-1) + 3 \times (-1) \times 0 = 0 \\ &\quad \underbrace{2C_3}_{2S_3} \quad \underbrace{3C_2}_{3\sigma_v} \end{aligned} \quad (5.10)$$

from class :

We have seen some instances in which the characters are noninteger and so some additional care is required with the summations of Properties 4 and 5. For example, in D_{5h} , the doubly degenerate representations have characters expressed as cosines of angles for the operations involving the principal axis. The summation for the orthogonality condition of the irreducible representations E_1' and E_2' then becomes

$$\begin{aligned} \sum_C g_c \chi_{E_1'}(C) \chi_{E_2'}(C) &= 4 + 8 \cos(72) \cos(144) + 8 \cos(144) \cos(72) + 4 \\ &+ 8 \cos(72) \cos(144) + 8 \cos(144) \cos(72) \\ &= 8 + 32 \cos(72) \cos(144) \\ &= 8 - 32 \times \frac{1}{4} \\ &= 0 \end{aligned} \quad (5.11)$$

where angles are given in degrees.

Property 4 for these two representations can also be demonstrated:

$$\begin{aligned} \text{for } E_1' \sum_c g_c [\chi_{E_1'}(C)]^2 &= 4 + 8 \cos^2(72) + 8 \cos^2(144) + 4 + 8 \cos^2(72) + 8 \cos^2(144) \\ &= 8 + 16 \cos^2(72) + 16 \cos^2(144) \\ &= 8 + 16[\cos^2(72) + \cos^2(144)] \\ &= 8 + 16 \times \frac{3}{4} \\ &= 20 \end{aligned} \quad (5.12)$$

$$\begin{aligned} \text{for } E_2' \sum_{C \in \text{classes}} g_c [\chi_{E_2'}(C)]^2 &= 4 + 8 \cos^2(144) + 8 \cos^2(72) + 4 + 8 \cos^2(144) + 8 \cos^2(72) \\ &= 8 + 16 \times \frac{3}{4} \\ &= 20 \end{aligned} \quad (5.13)$$

The order of the D_{5h} point group is 20 and so Equation (5.8) is seen to hold.

The orthogonality condition is linked to the idea that the fundamental vibrations of a molecule should be independent of one another. If the fundamental vibrations each have the symmetry properties of one or other of the irreducible representations, then those which belong to different representations will naturally be orthogonal. Looking back at Figure 5.3, we assigned the symmetric stretch of H_2O to A_1 and the asymmetric stretch to B_2 . The orthogonality condition means that there is no way to scale the A_1 vibration and generate the B_2 or vice versa. Both are required for a full description of the stretching modes of H_2O , but any other vibration that only involves O—H stretch could be written as a combination of these two.

Later on we will meet vibrations that have the same symmetry labels as one another; however, the combination of basis functions (pattern of basis set arrows) used will differ in such a way that these modes, too, are orthogonal to each other.

The next section shows how properties 4 and 5 can be used to help us find out how many times an irreducible representation occurs in any reducible representation for which we have the character set. This will allow us to calculate the irreducible representations contained in any reducible set of characters without recourse to the matrix representation of Chapter 4.

Problem 5.4: Show that the following irreducible representations are orthogonal to one another:

1. B_{1g} with all *ungerade* representations in D_{2h} ;
2. A_{2u} with each of the triply degenerate representations in O_h ;
3. E_1 and the other doubly degenerate representations in D_{4d} .

5.5 The Reduction Formula

In Chapter 4 we saw how a representation could be used to mimic the symmetry properties of a molecule by describing the interaction of group operations with a particular basis.

Any collection of basis vectors that complies with the molecular symmetry can generate a character representation of the group, but in most cases it will be a reducible one and so can be simplified. In this section we will show that the simplification of a reducible representation Γ can be made using the data for the set of irreducible representations available in the standard character tables.

Section 4.11 used the matrix representation to deal with a set of three basis vectors x, y, z on the central atom of a square planar D_{4h} complex. It was shown that this basis can be reduced to $E_u + A_{2u}$ by inspection of the matrices for the operations in the D_{4h} group. The characters for the reducible and irreducible representations are shown in Table 5.2.

Table 5.2 The reducible representation for the x, y, z basis on a central atom in a D_{4h} complex, and its composite irreducible representations.

D_{4h}	E	$2C_4$	C_2	$2C_2'$	$2C_2''$	i	$2S_4$	σ_h	$2\sigma_v$	$2\sigma_d$	
Γ	3	1	-1	-1	-1	-3	-1	1	1	1	x, y, z
A_{2u}	1	1	1	-1	-1	-1	-1	-1	1	1	z
E_u	2	0	-2	0	0	-2	0	2	0	0	x, y

The breakdown of the 3×3 matrices into 2×2 and 1×1 does not affect any of the diagonal elements, which are the characters of our irreducible representations. This means that the irreducible characters in each class must add up to the character in the reducible representation they were derived from.

By inspection of Table 5.2, it can be seen that this is indeed the case. For any class of operations in the group, the characters of the irreducible representations sum to give that of Γ .

Writing characters from the irreducible representations in class C as $\chi_{E_u}(C)$ and $\chi_{A_{2u}}(C)$ and that for the reducible representation as $\chi_\Gamma(C)$ we have

$$\chi_\Gamma(C) = \chi_{E_u}(C) + \chi_{A_{2u}}(C) \quad (5.14)$$

This is a special case for the basis used. In general, any of the irreducible representations available in D_{4h} could have been present, and the sum for $\chi_\Gamma(C)$ is

$$\chi_\Gamma(C) = \sum_j n_j \chi_j(C) \quad (5.15)$$

where n_j is the number of times that the j th irreducible representation occurs. These n_j values may be 0; from Table 5.2 in our D_{4h} example, we expect all values to be 0 except those for the E_u and A_{2u} representations, which will each be 1. In this case, Equation (5.15) would become Equation (5.14).

So far, this is just a recap of the discussion leading to Equation (4.25). Now, Equation (5.15) will be used along with Properties 4 and 5 to obtain an expression for the set of n_j for the general case. This makes it possible to write down the make-up of any reducible representation in terms of the irreducible ones.

Properties 4 and 5 are embodied in Equations (5.4) and (5.8), which require a sum over classes and involve products of characters. Equation (5.15) can be converted to a similar form by multiplying the left- and right-hand sides by a character from an irreducible representation i and then summing over all classes. This will give

$$\sum_c g_c \chi_i(C) \chi_\Gamma(C) = \sum_c g_c \chi_i(C) \sum_j n_j \chi_j(C) \quad (5.16)$$

Changing the order of summations on the right-hand side produces

$$\sum_c g_c \chi_i(C) \chi_\Gamma(C) = \sum_j n_j \sum_c g_c \chi_i(C) \chi_j(C) \quad (5.17)$$

We now have a sum over classes for two reducible representations, i and j . The outer sum on the right hand side says that all values of j , from 1 to the number of irreducible representations in the group, must be considered. However, because the irreducible representations are orthogonal (Property 5), this sum is zero if i and j are different.

As each of the terms in the sum over j are considered, the case $i = j$ will naturally occur. In that instance, the sum over classes will be h (Property 4). This means that, whatever representation we chose for i , the only term in the sum over classes that survives is that with $i = j$, so that Equation (5.17) becomes

$$\sum_c g_c \chi_i(C) \chi_\Gamma(C) = n_i h \quad (5.18)$$

A small rearrangement gives the *reduction formula*:

$$n_i = \frac{1}{h} \sum_c g_c \chi_i(C) \chi_\Gamma(C) \quad (5.19)$$

Equation (5.19) gives the number of times, n_i , an irreducible representation i occurs within a reducible representation Γ . It is based only on information obtained from the standard character table (h , g_c and $\chi_i(C)$) and the characters for the reducible representation ($\chi_\Gamma(C)$) which can be derived from a suitable basis. This is an extremely useful equation and is known as the reduction formula, since it allows any Γ to be reduced to a set of standard irreducible representations.

5.5.1 Applying the Reduction Formula

To see how the reduction process works we can return to the x, y, z basis in the D_{4h} example, taking the i th representation to be each of the irreducible representations for the point group in turn. Table 5.3 shows all the terms in the summation for each irreducible representation and demonstrates that the summation in Equation (5.19) gives zero for every one

Table 5.3 The terms required for the application of the reduction formula to the x, y, z basis on a central atom in a D_{4h} complex.

D_{4h}	E	$2C_4$	C_2	$2C_2'$	$2C_2''$	i	$2S_4$	σ_h	$2\sigma_v$	$2\sigma_d$	$h = 16$
Γ	3	1	-1	-1	-1	-3	-1	1	1	1	
	$g_c \chi_i(C) \chi_\Gamma(C)$										$\sum_C g_c \chi_i(C) \chi_\Gamma(C)$
A_{1g}	3	2	-1	-2	-2	-3	-2	1	2	2	0
A_{2g}	3	2	-1	2	2	-3	-2	1	-2	-2	0
B_{1g}	3	-2	-1	-2	2	-3	2	1	2	-2	0
B_{2g}	3	-2	-1	2	-2	-3	2	1	-2	2	0
E_g	6	0	2	0	0	-6	0	-2	0	0	0
A_{1u}	3	2	-1	-2	-2	3	2	-1	-2	-2	0
A_{2u}	3	2	-1	2	2	3	2	-1	2	2	16
B_{1u}	3	-2	-1	-2	2	3	-2	-1	-2	2	0
B_{2u}	3	-2	-1	2	-2	3	-2	-1	2	-2	0
E_u	6	0	2	0	0	6	0	2	0	0	16

except A_{2u} and E_u , for which the summation gives 16. The order of the group is also 16, and so Equation (5.19) shows that

$$\Gamma = 1A_{2u} + 1E_u \quad (5.20)$$

i.e. the reducible representation Γ contains $1A_{2u}$ and $1E_u$ irreducible representations, as we found using matrices in Chapter 4. The representation Γ was constructed from three basis functions and we have found irreducible representations which are for a single object (A_{2u}) and a degenerate pair of objects (E_u).

For any application of the reduction formula we will always find that the number of objects in the irreducible set of representations is equal to the number used in the definition of the reducible representation, i.e. the number of basis functions.

Problem 5.5: BF_3 is a molecule in the D_{3h} point group. Show that the basis of $F(p_z)$ -orbitals shown in Figure 5.6 has the reducible representation given in Table 5.4.

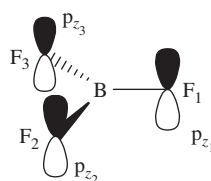


Figure 5.6 A basis of $F(p_z)$ orbitals in BF_3 .

Table 5.4 also gives another illustration of the application of the reduction formula to the basis of three $F(p_z)$ -orbitals for BF_3 , shown in Figure 5.6. In the reducible representation,

Table 5.4 The reducible representation for the $F(p_z)$ basis on BF_3 shown in Figure 5.6 and the application of the reduction formula to it.

D_{3h}	E	$2C_3$	$3C_2$	σ_h	$2S_3$	$3\sigma_v$	$h = 12$
Γ	3	0	-1	-3	0	1	
	$g_c \chi_\Gamma \chi_i$						$\sum_C g_c \chi_i(C) \chi_\Gamma(C)$
A_1'	3		-3	-3		3	0
A_2'	3		3	-3		-3	0
E'	6		0	-6		0	0
A_1''	3		-3	3		-3	0
A_2''	3		3	3		3	12
E''	6		0	6		0	12

the $2C_3$ and $2S_3$ classes have character 0 in Γ , and so the terms for these columns in the reduction formula must always be zero. The order of the D_{3h} point group is 12, and so summation over classes shows that

$$\Gamma = 1A_2'' + 1E'' \quad (5.21)$$

This means that the three p_z orbitals can be taken together in one pattern conforming to A_2'' and two degenerate patterns following E'' . In mathematical terms, the patterns are symmetry-adapted linear combinations (SALCs) of the orbitals that conform to the irreducible representations. The three orbitals taken together as drawn in Figure 5.6 would give an SALC with a character of -1 for any operation that flips the molecule plane over and +1 for all others. This is exactly the character set for A_2'' , and so we have found a pictorial representation of the SALC. Finding the two degenerate E'' SALCs is more complex and is left to Chapter 7, where MOs are discussed in more detail.

5.6 A Complete Set of Vibrational Modes for H_2O

In Chapter 1 it was noted that the number of vibrational modes of a molecule can be calculated by counting the degrees of freedom of the atoms (three per atom for X, Y and Z movement) and subtracting the degrees of freedom for motion of the molecule as a whole, three for its translation and (for nonlinear molecules) three for rotation. This was used in Section 5.2 to arrive at a reducible representation for the basis of nine atomic degrees of freedom for H_2O , the classic C_{2v} molecule. The characters for this representation were given in Table 5.1. We can now apply the reduction formula to identify the irreducible representations for the three vibrations of H_2O .

Table 5.5 gives the terms generated by the reduction formula for each of the irreducible representations in C_{2v} . This shows that

$$\Gamma = 3A_1 + A_2 + 2B_1 + 3B_2 \quad (5.22)$$

As expected, the nine basis vectors have produced nine irreducible representations, but only $9 - 6 = 3$ of these can correspond to molecular vibrations. The others are motions of the molecule as a whole.

Table 5.5 The application of the reduction formula to the nine basis vector representation of H_2O atomic degrees of freedom defined in Figure 5.2.

C_{2v}	E	C_2	$\sigma_v(XZ)$	$\sigma_v'(YZ)$		$h = 4$
Γ	9	-1	1	3		
			$g_c \chi_r(C) \chi_i(C)$		\sum_c	$\frac{1}{h} \sum_c$
A_1	9	-1	1	3	12	3
A_2	9	-1	-1	-3	4	1
B_1	9	1	-1	3	8	2
B_2	9	1	1	-3	12	3

There are three translations and three rotations of the molecule as if it were a rigid body. For any molecule in the point group, the rigid body motions will have the same irreducible representations. In the standard character tables of Appendix 12 the symbols x, y, z and R_x, R_y, R_z are written in the rightmost columns and can be used to identify the representations for rigid-body movement and rotation respectively. So, most of the time, it is just a matter of referring to the character table to find the irreducible representations that should be removed and so isolate the vibrational mode symbols.

However, to demonstrate how the rigid-body motion conforms to the irreducible representations, in this example we will go over the effect of symmetry operations on the translational and rotational motion of H_2O .

The three translations are motions along the axes of the coordinate system which follow the symbols x, y or z in the right-hand column of the character table. The standard C_{2v} table is reproduced in Table 5.6 and the assignments made for translation are easily checked. For example, the molecule moving as a whole along the Y -axis direction is assigned to the B_2 representation. To see this we could place a basis vector y at the centre of mass of the molecule parallel to the Y reference axis in Figure 5.2, which would represent the motion. The centre of mass of the molecule lies on the C_2 axis nearer to the O atom than either of the two H atoms due to the greater mass of the former.

Table 5.6 The standard character table for the C_{2v} point group.

C_{2v}	E	C_2	$\sigma_v(XZ)$	$\sigma_v'(YZ)$		
A_1	1	1	1	1	z	x^2, y^2, z^2
A_2	1	1	-1	-1	R_z	xy
B_1	1	-1	1	-1	x, R_y	xz
B_2	1	-1	-1	1	y, R_x	yz

A y -vector placed at the centre of mass responds to the symmetry operations in the same way as the y -vector on O in Figure 5.2a: after a C_2 rotation or reflection in the $\sigma_v(XZ)$ plane it would be reversed, corresponding to a character of -1, while the y -vector would be unaffected by the identity operator E or a $\sigma_v'(YZ)$ reflection so that these have a character of 1. This set of characters is just the B_2 representation, and so we have confirmed that motion in the Y direction should be assigned to the B_2 representation.

Problem 5.6: Confirm that movement of the H_2O molecule as a whole in the X and Z directions follows the B_1 and A_1 representations respectively.

Translations of the molecule as a whole are clearly not vibrations, so we remove them from the list of irreducible representations found for the full basis

$$\Gamma(R, v) = 2A_1 + A_2 + B_1 + 2B_2 \quad (5.23)$$

Now $\Gamma(R, v)$ contains the remaining representations for the rotational and vibrational degrees of freedom.

The rotations of the molecule as a whole are shown in Figure 5.7. In the character tables of Appendix 12 and in Table 5.6 these are given the labels R_x , R_y and R_z next to their respective irreducible representations. The effect of operations on rotations is a little harder to visualize and it is useful to refer to the paper models from Appendix 1 at this point.

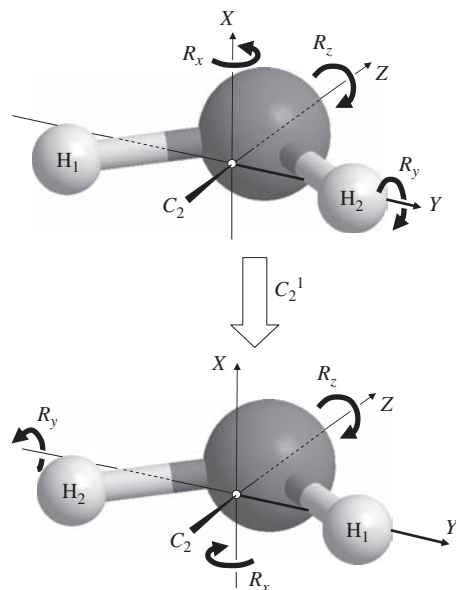


Figure 5.7 The affect of a C_2 symmetry operation on the rotational motion of the H_2O molecule.

Figure 5.7 shows the result of a C_2^1 operation on the rotational motions around each axis. To assign a character we have to image what would happen to the direction of the rotation when the operation is carried out. For example, taking the clockwise rotation around the Y -axis in the starting structure, at the instant shown we would expect the H atoms to be moving toward the top of the diagram while the O atom moves downward. After the C_2 rotation these movements would be reversed, so the direction of rotation would change from clockwise to anticlockwise, giving a character of -1 . In Figure 5.7, this is shown by the curved arrow around the Y -axis changing direction after the operation. To emphasize

the operation has taken place, the arrows indicating rotation around X and Y have also been moved, but, as usual, the reference X , Y and Z axes are kept fixed. Rotation around X is also reversed, but that around Z is not affected by the operation as it involves rotation around the symmetry axis.

Figure 5.8 shows the rotations around the three reference axes and the result of a $\sigma_v'(YZ)$ operation: reflection through the molecular plane. In this case, rotation around either Y or Z appears reversed, giving a character of -1 . The X axis is perpendicular to the plane, and while the arrow indicating the direction of rotation has been relocated by the operation, its direction is unaltered, giving a character of 1 .

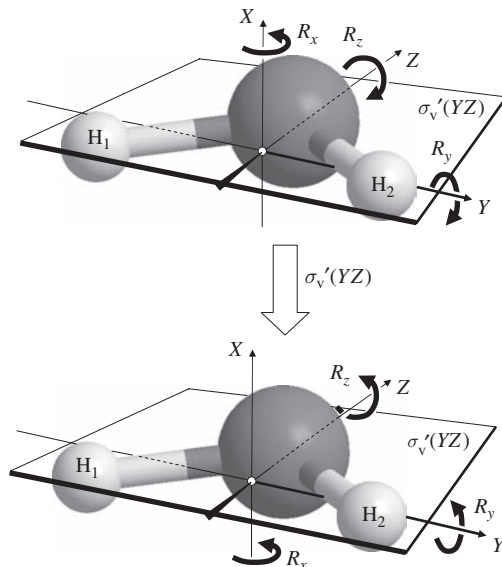


Figure 5.8 The effect of a $\sigma_v'(YZ)$ symmetry operation on the rotational motion of the H_2O molecule.

Problem 5.7: Drawing diagrams similar to Figures 5.7 and 5.8, show that the $\sigma_v(XZ)$ operation gives the expected characters for R_x (from B_2), R_y (from B_1) and R_z (from A_2).

So, the irreducible representations for the rigid-body movement and rotation of H_2O have now been identified and we can remove them from the total set of irreducible representations derived from the atomic degrees of freedom. This leaves us with

$$\Gamma(v) = 2A_1 + B_2 \quad (5.24)$$

These are the three irreducible representations for the vibrational degrees of freedom for H_2O . Two of these we have already met in Section 5.2: the A_1 symmetric stretch and the B_1 antisymmetric stretch shown in Figure 5.3. The remaining vibration also has an A_1 representation; this is the bending mode illustrated in Figure 5.9. This collective motion of

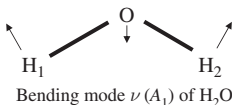


Figure 5.9 The A_1 symmetric bending mode of H_2O .

the molecule is not affected by any of the operations of the point group and so conforms to the A_1 irreducible representation.

The O—H bonds do not change length in the bending mode, while the H—O—H angle is constant in the A_1 stretching vibration. So, although we have found two A_1 vibrations, they are still orthogonal to one another.

The method of obtaining pictures of the vibrational modes which conform to the irreducible representations, such as those of Figures 5.3 and 5.9, will be discussed more fully in Chapter 6. In the remainder of this chapter we cover some more examples of the application of the reduction formula to find the irreducible representations for modes of vibration and for atomic orbitals.

5.7 Choosing the Basis Set

The basis set size is determined by the particular problem in hand. In the analysis of H_2O in Section 5.2 we concentrated on the stretching vibrations of the O—H bonds. This is a problem which could be approached using a basis as simple as the two bond vectors. However, with that basis we would miss the bending mode that was identified by using the nine basis vectors that represent the full atomic degrees of freedom.

In general, the basis vectors to use for an analysis should be capable of describing the motions or orbitals which are sought. For example, in Figure 4.6, the basis vectors placed on the three N—H bonds of NH_3 were used to illustrate the result of a C_3^1 rotation. As in our H_2O example, this choice of basis set would be suitable for studying the vibrational stretching modes of the NH_3 molecule, but it would not allow any bending modes involving changes of H—N—H angles to be described. This would require a different or extended basis set with vectors arranged perpendicular to the N—H bonds. The important thing to consider when choosing the basis set is that enough basis functions are included to cope with the problem without overcomplicating the analysis.

If we wish to carry out a full vibrational mode analysis on a molecule containing N atoms, then there will be $3N$ degrees of freedom. To be sure of capturing all modes of vibration, a $3N$ set of basis vectors would be required. However, if the molecule has particular vibrational modes that we know will be in a distinct region of the spectrum, then this can be reduced.

5.7.1 Carbonyl Stretching Modes of $[Fe(CO)_5]$, D_{3h}

A notable case in which the region of the spectrum to be dealt with is known is that of carbonyl ligands in transition metal complexes. The carbonyl ligand stretching modes occur in the range $2100\text{--}1700\text{ cm}^{-1}$. This region is usually not shared with other functional

groups in a compound, so that bands observed here can be assigned to the C=O stretching modes.

For example, the trigonal bipyramidal pentacarbonyl-iron complex $[\text{Fe}(\text{CO})_5]$ shown in Figure 5.10 belongs to the D_{3h} point group. The complex contains 11 atoms, and so a full vibrational analysis would require $3 \times 11 = 33$ basis vectors. However, if we are only interested in the C=O bond stretching modes, then a suitable basis set would only require the five C=O bond vectors shown in Figure 5.10. The basis vectors have been drawn to the side of the C=O bonds for clarity, but should be treated as lying directly along each bond.

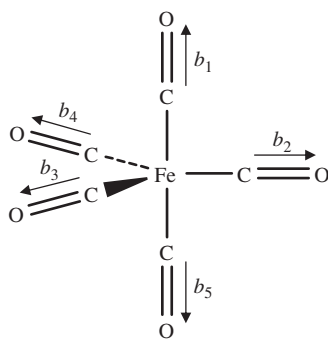


Figure 5.10 The trigonal bipyramidal complex $[\text{Fe}(\text{CO})_5]$, point group D_{3h} . A suitable basis for obtaining the irreducible representations of the carbonyl stretching modes is shown.

The set of total characters form a reducible representation which is summarized in the first row of Table 5.7. These are obtained by considering an example operation from each class in turn:

Table 5.7 The reduction formula is applied to the basis of five C=O bonds in the D_{3h} complex $[\text{Fe}(\text{CO})_5]$, shown in Figure 5.10.

D_{3h}	E	$2C_3$	$3C_2$	σ_h	$2S_3$	$3\sigma_v$	$h = 12$
Γ	5	2	1	3	0	3	
				$g_c \chi_i(C) \chi_\Gamma(C)$		\sum_C	
A_1'	5	4	3	3	0	9	24
A_2'	5	4	-3	3	0	-9	0
E'	10	-4	0	6	0	0	12
A_1''	5	4	3	-3	0	-9	0
A_2''	5	4	-3	-3	0	9	12
E''	10	-4	0	-6	0	0	0

The identity operator, as always, leaves all basis vectors unchanged, and we simply count the number in the basis to arrive at a character of 5.

The C_3 axis contains the two basis vectors on the axial carbonyl ligands, and so these remain in place after any C_3 rotation. However, the equatorial ligands are moved by either

the C_3^1 or C_3^2 operation, contributing 0. This gives a total character of 2 for the basis in the $2C_3$ class.

There are three C_2 axes, each of which contains one of the equatorial $\text{C}=\text{O}$ ligands; thus, on rotation, one ligand will stay in place while each of the other four ligands is exchanged with a partner. For example, rotation around the axis containing basis vector b_2 will result in b_3 swapping with b_4 and b_1 swapping with b_5 . This gives a total character of 1, whichever axis we choose.

The horizontal mirror plane contains the three equatorial ligands, and so reflection simply exchanges b_1 and b_5 , giving a total character of 3.

The improper rotation moves the equatorial ligand positions in the same way as the simple rotation around the principal axis; however, the additional σ_h reflection also swaps b_1 with b_5 , so that the total character is 0.

Finally, the three equivalent vertical mirror planes each contain the axial ligands and one of the equatorial $\text{C}=\text{O}$ groups, contributing 3 to the total character for this operation. Each σ_v reflection swaps the remaining two basis vectors, and so they contribute 0.

Taking the values of $\chi_i(C)$ for each of the irreducible representations from the standard D_{3h} character table in Appendix 12, we can now apply the reduction formula to this problem. The values of the individual triple products required in the summation are written out in Table 5.7, which shows that the reducible representation has the composition

$$\Gamma = 2A_1' + E' + A_2'' \quad (5.25)$$

From five basis vectors we have identified only four irreducible representations, but E' is doubly degenerate and so contains two different vibrational modes, i.e. the five basis vectors have been used to generate five vibrations. These will occur at four different frequencies, since the two modes within E' must have the same vibrational frequency. However, this does not tell us that there will be four vibrational bands in an IR spectrum, because to observe a spectral band we require vibrations that absorb light. To find out which vibrations are IR active requires the use of selection rules, and that will be covered in Chapter 6.

5.8 The d-Orbitals in Common Transition Metal Complex Geometries

The d-orbitals of transition metal atoms in the gas phase are degenerate with one another, meaning that a d-electron has the same energy irrespective of which particular d-orbital it occupies. This degeneracy is lifted when a transition metal is part of a complex, so that the energies of the orbitals will differ according to their disposition with respect to the ligands of the complex. There are two common ways to discuss the bonding in transition metal complexes.

In the first, d-orbitals on the metal centre are viewed as interacting with the field generated by the ligands. This field is not spherically symmetric, since the ligands are arranged in a particular geometry and so electrons in the d-orbitals on the metal can experience different effective environments. This leads to the splitting of the d-orbitals into sets of energy levels, some of which may be degenerate if two or more d-orbitals have an equivalent environment in the complex. This level of degeneracy can be discussed based on the symmetry of the complex without specific consideration of the orbitals

on the ligands themselves. This is the starting point for ligand field theory, which will be used here to discuss the symmetry of the p- and d-orbitals for an atom at the centre of a complex in a few common geometries. An s-orbital is spherically symmetric and so, for the central atom in a complex, always has the totally symmetric representation of the point group (character 1 for all classes!). A more complete picture of the bonding in metal complexes is provided by molecular orbital (MO) theory, in which the mixing of ligand and metal orbitals is considered explicitly, but we will leave that until Chapter 7.

In the following examples, the point group of a variety of complexes is used to derive the symmetry labels for the atomic orbitals (AOs) of the central atom. The central atom orbitals are at the intersection of all the symmetry elements in the point groups considered and so are never moved through space by an operation. However, they may be reorientated, and so we will work out the characters for each AO set (p, d) and then apply the reduction formula to find the appropriate irreducible representation labels. These results will be used in Chapter 7 when assembling MOs for some of the complexes, and there we will use the fact that the standard character tables have the p and d functions written in the rightmost columns. For the central atom, this means that we can simply read off the symmetry label from the table.

The following pages demonstrate how these assignments are made, but first we will review the functional forms of the d-orbitals.

The Schrödinger equation can be solved for the case of a single electron bound to a positively charged nucleus to give the familiar s, d, p, ... energy levels. These solutions are exact for the H atom, but electron-electron interactions complicate matters for heavier elements. As a starting point, we can treat each electron in the heavy atom system as if it interacts only with a nuclear charge adjusted for shielding due to the other electrons. The origin of these ‘hydrogen-like’ orbitals from solutions of the Schrödinger equation is covered in Appendix 9, and we meet them again in Chapter 7.

Each AO function can be thought of as the product of a radial and an angular part. The radial part describes the shape of the wavefunction as we move away from the nuclear centre. The angular part describes the shape of the wavefunction as we move around the nuclear centre. The d-orbitals are generally labelled according to their angular functional forms; for example, as we saw briefly in Section 4.2.2 d_{xy} means that the orbital has its largest amplitude in the XY plane with a phase pattern that follows the xy function. Figure 5.11a shows that the amplitude of the d_{xy} function is zero when either x or y is zero, and the d_{xy} function has its greatest amplitude for a given distance from the origin when x and y are of equal size. The phase of the d_{xy} function depends on the signs of x and y , so that d_{xy} has a positive phase if both are positive (xy) or both are negative ($-x \times -y$), whereas the phase of d_{xy} is negative if only one of x or y is negative (e.g. $-x \times y$). If we start from any point and move round the nuclear centre we see that the phase changes for each quadrant of the xy plane.

The $d_{x^2-y^2}$ function (Figure 5.11b) also has its largest amplitude in the XY plane, but now the function has a positive maximum on the X-axis and a negative maximum on the Y-axis.

The d_{xz} and d_{yz} orbitals have shapes analogous to d_{xy} , but based on their different coordinate functions.

The d_z^2 orbital does not have the same appearance as the other four d-orbitals: it has positive lobes along the z and $-z$ directions and a toroidal (‘doughnut’-like) shaped lobe

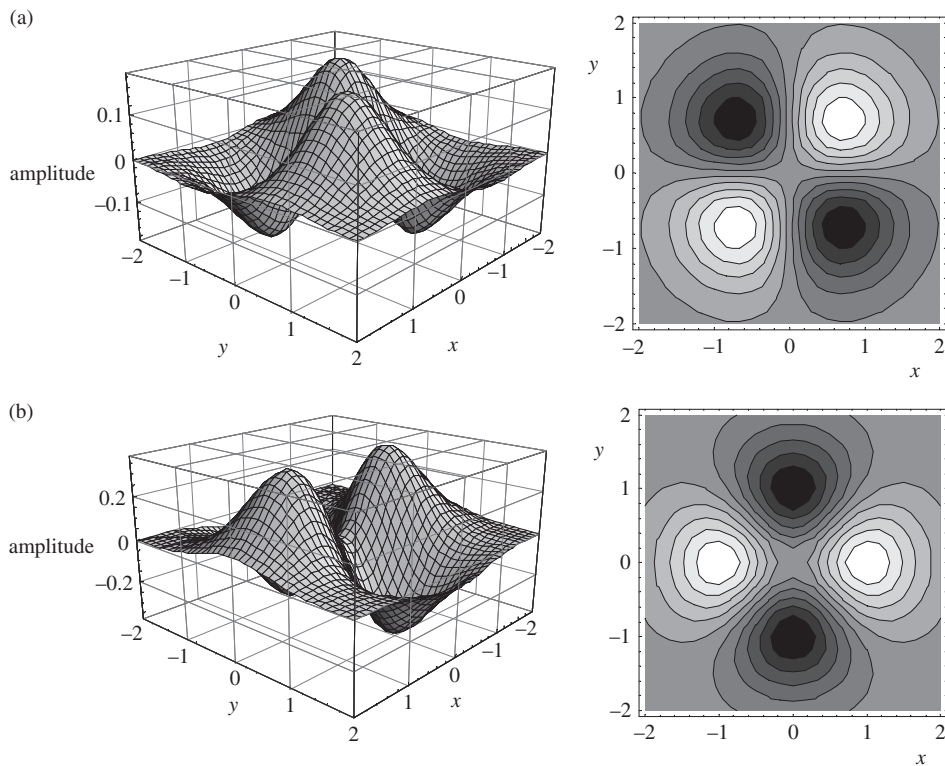


Figure 5.11 The phase pattern for (a) a d_{xy} orbital and (b) a $d_{x^2-y^2}$ orbital. These diagrams show slices through the orbitals in the XY plane; to the left the amplitude of the function in the plane is shown on the Z-axis, while to the right a contour representation is shown with light areas representing positive phase and dark areas negative phase.

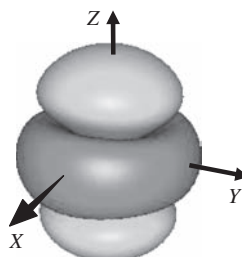


Figure 5.12 The d_{z^2} orbital.

in the xy plane, as shown in Figure 5.12. The reason behind this difference is the way the d-orbital functions are conventionally constructed in the Cartesian axis system. We know that there are 10 transition elements in the third row of the periodic table. Since each orbital can hold up to two electrons, this means there must be five d-orbitals. However,

the Cartesian axis system would naturally yield six angular functions that are suitable for d-orbitals, namely:

$$\frac{xy}{x^2 - y^2} \quad \frac{xz}{z^2 - x^2} \quad \frac{yz}{z^2 - y^2} \quad (5.26)$$

The first four of these we have already discussed. To make the fifth d-orbital, a linear combination of the remaining two is taken, i.e.

$$z^2 - x^2 + z^2 - y^2 = 2z^2 - x^2 - y^2 \quad (5.27)$$

which gives the familiar orbital shape. This construction is illustrated in Figure 5.13.

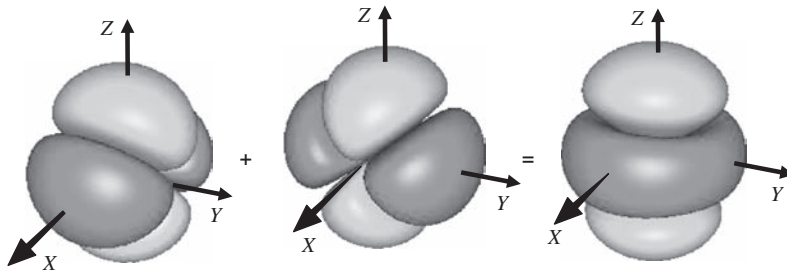


Figure 5.13 The construction of the d_{z^2} orbital as a linear combination of $d_{z^2-x^2}$ and $d_{z^2-y^2}$.

The linear combination for d_{z^2} has one drawback: the orbital now contains more volume than the other d-orbitals, since it is the sum of two functions. The volume of the orbital relates to the probability of finding an electron; in fact, an integral of the square of the wavefunction over a given volume gives this probability. The five d-orbitals must each give a total probability of 1, and so an additional factor is used to scale the d_{z^2} orbital back down to size.

With this normalization factor included, the angular d_{z^2} function becomes

$$\frac{1}{\sqrt{3}}(2z^2 - x^2 - y^2) \quad (5.28)$$

To see how the normalization factor works, consider squaring this function starting from it written as its constituent $z^2 - x^2$ and $z^2 - y^2$ functions:

$$\left\{ \frac{1}{\sqrt{3}}[(z^2 - x^2) + (z^2 - y^2)] \right\}^2 = \frac{1}{3}[(z^2 - x^2)^2 + (z^2 - y^2)^2 + 2(z^2 - x^2)(z^2 - y^2)] \quad (5.29)$$

The first two terms in this expression are the squares of the orbitals we have combined to form d_{z^2} ; since these contain the same volume as all the other d-orbitals, an integration over all space will give 1 for each. The third term contains the product of the $d_{z^2-x^2}$ and $d_{z^2-y^2}$ orbitals, and so is the volume that they have in common; their overlap. As can be seen in Figure 5.13, these orbitals share space only on the Z axis but have separate lobes

in the XY plane. This will give an integral of $1/2$, and so the three terms sum to 3 and the normalization factor then reduces this total volume to 1, as required.

In this exercise we have found a normalization factor that brings the z^2 orbital onto the same scale as $x^2 - y^2$. In Appendix 9 (Table A9.1) it is shown that the normalized functions for all five d-orbitals are,

$$\begin{aligned} & \frac{1}{2} \left(\frac{15}{\pi} \right)^{\frac{1}{2}} \frac{xz}{r^2} \\ & \frac{1}{2} \left(\frac{15}{\pi} \right)^{\frac{1}{2}} \frac{yz}{r^2} \\ & \frac{1}{2} \left(\frac{15}{\pi} \right)^{\frac{1}{2}} \frac{xy}{r^2} \\ & \frac{1}{4} \left(\frac{15}{\pi} \right)^{\frac{1}{2}} \frac{(x^2 - y^2)}{r^2} \\ & \frac{1}{4} \left(\frac{5}{\pi} \right)^{\frac{1}{2}} \frac{2z^2 - x^2 - y^2}{r^2} \end{aligned} \quad (5.30)$$

Where r is the distance from the nuclear centre. These functions also show that to bring $x^2 - y^2$ to the same scale as xy etc., requires a future factor of 2 to be included. To carry the full normalization constants in the calculations of the next few sections would be cumbersome since symmetry is really only concerned with how the functional forms change after symmetry operations and the proportions of the original basis set required to obtain the same result. Hence we will only use relative scaling factors when required. We will meet normalization factors again in Chapters 6 and 7.

To work out how the d-orbitals are affected by the symmetry of their environment, we will first analyse a basis of the x , y and z vectors at the central metal atom of each complex geometry. This will automatically show how the p-orbitals respond to each operation.

The results can then be used to deduce the functional form of each d-orbital after the transformation and so find the required character set for the d-orbitals. In general, the p- and d-orbitals will give reducible representations to which we can apply the reduction formula to find the irreducible representations for the point group.

5.8.1 Square Planar, D_{4h}

The x , y , z basis vectors on the central atom in a D_{4h} complex have already been considered in Section 4.9, where the orientation of the basis is defined in Figure 4.10. It was shown that the three vectors, and so the corresponding p-orbitals at a central metal atom, reduce to the A_{2u} and E_u irreducible representations.

Table 5.8 gives the transformations of the x , y and z vectors for a representative operation of each class of D_{4h} . We now know that the operations in a class give identical characters for any irreducible representation. This means that only one example from each class of

Table 5.8 The transformations of the p - and d -orbital functions under a symmetry operation from each class in D_{4h} . C_2 is the same axis as C_4 , C_2' are the axes through the metal-ligand bonds which are contained in the σ_v planes, and C_2'' are the axes bisecting the metal-ligand angles which are contained in the σ_d planes. L is taken as the direction of the $X + Y$ i.e. the line at 45° to both the X and Y axes. The shorthand z' is used for the d_{z^2} orbital rather than the full functional form, since it is unaffected by all symmetry operations.

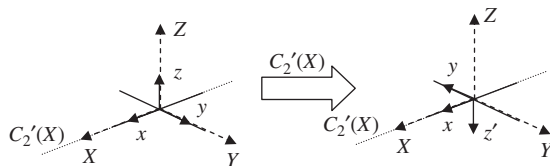


Figure 5.14 The $C_2(X)$ operation for the x, y, z basis of a D_{4h} square planar complex.

operations need be considered when looking for the transformation of a given basis, and suitable choices have been made in Table 5.9.

The d-orbital functions xy , xz , yz , $x^2 - y^2$ and $2z^2 - x^2 - y^2$ are treated by constructing them from the results for x , y and z . For instance, the change to the x, y, z basis after the $C'_2(X)$ operation is illustrated in Figure 5.14. Algebraically this can be written:

$$x \rightarrow x, \quad y \rightarrow -y \quad \text{and} \quad z \rightarrow -z \quad (5.31)$$

These formulae use arrows rather than equals signs to indicate the result of a transformation. They interpret the result of the operation (the vectors marked x' , y' and z' in Figure 5.14) in terms of the initial basis. Immediately, Equation (5.31) demonstrates that p_x has a character of 1 while p_y and p_z each have character -1 .

For the d-orbitals we simply obtain the transformed functions using the behaviour of the x, y, z basis so that:

$xy \rightarrow x(-y) = -xy$	character -1
$xz \rightarrow -xz$	character -1
$yz \rightarrow (-y)(-z) = yz$	character 1
$x^2 - y^2 \rightarrow x^2 - (-y)^2 = x^2 - y^2$	character 1
and	
$2z^2 - x^2 - y^2 \rightarrow 2z^2 - x^2 - y^2$	character 1

(5.32)

From this example and Table 5.8 there are three possible outcomes for the d_{xy} , d_{yz} and d_{xz} -orbital functions:

1. *A function is unaffected by the operation.* This can be the case even though the x , y and z vectors have altered; for example, following the C_2 operation x and y become $-x$ and $-y$, but for their product the two minus signs give a plus and so xy is unaffected. In these cases a character of 1 for the function is assigned.
2. *A function is transformed to its own negative.* This means that the areas of positive and negative phase will have been switched for the function. This could also have been achieved by a multiplication by -1 . Hence, the character in this situation is -1 , e.g. yz under the $\sigma_v(XZ)$ operation.
3. *A function is transformed into one of the other d-functions.* The d-functions are effectively our basis set in this analysis; so, if a function is transformed completely into another basis function, then a character of 0 is taken, e.g. xz under the $\sigma_d(LZ)$ operation becomes yz and so would have character 0.

The $d_{x^2-y^2}$ and d_{z^2} orbitals can be treated similarly, so long as the full functional form for d_{z^2} is used. For example, under $C_2''(L)$ using the x, y, z transformations from Table 5.8:

$$x^2 - y^2 \rightarrow y^2 - x^2 \quad (5.33)$$

and

$$\frac{1}{\sqrt{3}}(2z^2 - x^2 - y^2) \rightarrow \frac{1}{\sqrt{3}}(2z^2 - y^2 - x^2) \quad (5.34)$$

This means that the $x^2 - y^2$ orbital will be assigned a character of -1 and z^2 will be given a character of 1 . Based on the axis transformations of Table 5.8, we can now work out the characters for any of the d-functions, and these are given in Table 5.9.

Table 5.9 The characters for each orbital function under the operations defined in Table 5.8 and their sum to give $\Gamma(d)$.

D_{4h}	E	C_4^1	C_2	$C_2'(X)$	$C_2''(L)$	i	S_4^1	σ_h	$\sigma_v(XZ)$	$\sigma_d(LZ)$
xy	1	-1	1	-1	1	1	-1	1	-1	1
xz	1	0	-1	-1	0	1	0	-1	1	0
yz	1	0	-1	1	0	1	0	-1	-1	0
$x^2 - y^2$	1	-1	1	1	-1	1	-1	1	1	-1
z^2	1	1	1	1	1	1	1	1	1	1
$\Gamma(d)$	5	-1	1	1	1	5	-1	1	1	1

Because the z -vector is never interchanged with x or y in the D_{4h} point group, the character for d_{z^2} will be 1 for all operations. Similarly, x and y can only be left alone or interchanged, so $x^2 - y^2$ will give either +1 or -1, but not 0.

The characters for the individual orbitals in Table 5.9 are dependent on the choice of operation within a class. For example, from the $2C_2'$ class we chose the $C_2'(X)$ rotation axis and obtained the characters -1 and $+1$ for d_{xz} and d_{yz} respectively. Had we chosen $C_2'(Y)$, then the result for the individual orbitals would be reversed: $+1$ for d_{xz} and -1 for d_{yz} . However, the sum of these characters is the same for both choices of axis, and so the character totals for $\Gamma(d)$ in Table 5.9 would be the same for any choice of operations.

This reducible representation contains five objects, and so a total character of 5 appears under the E operator column. In addition, each of the d-orbitals has *gerade* symmetry, since they are unchanged by the inversion operation, so there is also a total character of 5 under i .

In Table 5.10, the reduction formula is applied to $\Gamma(d)$ in the D_{4h} point group, with the result that

$$\Gamma(d) = a_{1g} + b_{1g} + b_{2g} + e_g \quad (5.35)$$

where we have followed the convention of using lower case letters for the symmetry representation labels of orbitals. This convention allows the upper case letters to be reserved

Table 5.10 Application of the reduction formula to $\Gamma(d)$ in D_{4h} . The \sum_C column gives the summation required for the reduction formula: $\sum_C g_C \chi_i(C) \chi_r(C)$.

D_{4h}	E	$2C_4$	C_2	$2C_2'$	$2C_2''$	i	$2S_4$	σ_h	$2\sigma_v$	$2\sigma_d$		$h = 16$
$\Gamma(d)$	5	-1	1	1	1	5	-1	1	1	1		
							$g_C \chi_r(C) \chi_i(C)$				\sum_C	$h^{-1} \sum_C$
A_{1g}	5	-2	1	2	2	5	-2	1	2	2	16	1
A_{2g}	5	-2	1	-2	-2	5	-2	1	-2	-2	0	0
B_{1g}	5	2	1	2	-2	5	2	1	2	-2	16	1
B_{2g}	5	2	1	-2	2	5	2	1	-2	2	16	1
E_g	10	0	-2	0	0	10	0	-2	0	0	16	1
A_{1u}	5	-2	1	2	2	-5	2	-1	-2	-2	0	0
A_{2u}	5	-2	1	-2	-2	-5	2	-1	2	2	0	0
B_{1u}	5	2	1	2	-2	-5	-2	-1	-2	2	0	0
B_{2u}	5	2	1	-2	2	-5	-2	-1	2	-2	0	0
E_u	10	0	-2	0	0	-10	0	2	0	0	0	0

for the multi-electron states (also known as term states) that are used in the description of electronic spectroscopy.

The e_g label indicates a doubly degenerate level, it represents two d-orbitals, and so the right-hand side of this equation does contain five orbitals as required. The four irreducible representations all have *gerade* symmetry, in line with the d-orbitals that underlie them.

This symmetry analysis indicates that the five d-orbitals, which are all equivalent for the isolated metal ion, will split into four levels in a square planar D_{4h} environment, with one of these levels doubly degenerate.

Symmetry alone cannot give the energetic ordering of the orbital energy levels, since this is determined by their physical interaction with the ligand environment. In a ligand field model, the orbitals are ordered such that those with strong interactions with the ligands are highest in energy, the argument being that electrons in these AOs would be repelled by the ligand based electrons. We can use this to sketch out the orbital energy diagram as shown in Figure 5.15.

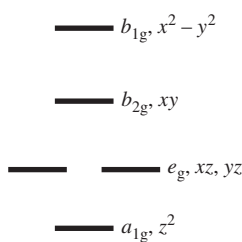


Figure 5.15 The d-orbital energy levels for the central atom of a D_{4h} complex.

The highest energy orbitals are those in the XY plane, with $x^2 - y^2$ above xy because its orbital lobes are pointing along the axes toward the ligands.

The xz and yz orbitals are lower in energy; an electron occupying either of these orbitals does not enter the XY plane because this is also a nodal plane. These two degenerate orbitals are in the e_g irreducible representation, since X and Y are equivalent directions in the complex.

Finally, the d_{z^2} orbital has the lowest energy of the set, since the lobe along the Z -axis avoids the ligands altogether.

5.8.2 Tetrahedral, T_d

To see how p- and d-orbitals on a central atom in a molecule or complex with T_d symmetry transform, we can use the same approach as covered above for D_{4h} .

First, we write down the effect of an example operation from each class on an x , y , z basis and then use this to obtain the transformed functional forms for the p-orbitals. Once the x , y , z basis has been dealt with, the products required for the d-orbital functions can be deduced and a reducible representation obtained from the set of example operations. Application of the reduction formula then gives the irreducible labels for the p- and d-orbitals.

Complexes with four identical ligands arranged around a central metal ion, such as the Co^{2+} complex $[\text{CoCl}_4]^{2-}$, fall into the T_d point group. Figure 5.16 shows this complex and also illustrates the outline of the tetrahedron formed by sketching lines between the Cl ligands. The T_d point group contains four equivalent C_3 axes and three equivalent C_2 axes along with six σ_d planes, which were discussed in Section 3.9. The choice of symmetry element for this exercise will follow those illustrated in Figure 5.16 and on the paper model of the tetrahedron and its associated cube from Appendix 3. By placing the tetrahedron inside the cube, the positioning of the reference axis system can be seen in the three-dimensional model.

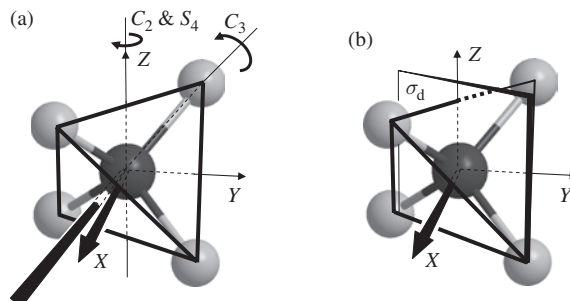


Figure 5.16 An example tetrahedral complex, $[\text{CoCl}_4]^{2-}$, overlaid with the reference axes in their standard orientation. (a) The symmetry axes and (b) the σ_d plane used in the symmetry analysis of the main text.

Table 5.11 gives the result of each selected operation on the x , y , z basis and the resulting d-orbital functional forms. The xy , yz and xz functions are unaffected, transformed

Table 5.11 The transformations of the p - and d -orbital functional forms under a symmetry operation from each class in T_d . The symmetry elements that were used are those shown on the paper model from Appendix 3. The normalization factor for the d_{z^2} orbital has been omitted for the sake of clarity.

T_d	E	C_3^1	C_2	S_4^1	σ_d
x	x	$-y$	$-x$	$-y$	y
y	y	z	$-y$	x	x
z	z	$-x$	z	$-z$	z
xy	xy	$-yz$	xy	$-xy$	xy
xz	xz	xy	$-xz$	yz	yz
yz	yz	$-xz$	$-yz$	$-xz$	xz
$x^2 - y^2$	$x^2 - y^2$	$y^2 - z^2$	$x^2 - y^2$	$y^2 - x^2$	$y^2 - x^2$
$2z^2 - x^2 - y^2$	$2z^2 - x^2 - y^2$	$2x^2 - y^2 - z^2$	$2z^2 - x^2 - y^2$	$2z^2 - x^2 - y^2$	$2z^2 - x^2 - y^2$

into -1 times the original function, or changed into a different product altogether. This makes the assignment of a character for these three functions straightforward. For example, xy becomes $-yz$ under C_3^1 , and so because the transformation has taken xy into another member of the d-orbital basis set we assign a character of 0.

In most of the entries of Table 5.11 the functional form for the d_{z^2} and $d_{x^2-y^2}$ functions can be seen as simply unchanged or multiplied by -1 and so character assignment can be made accordingly.

However, for d_{z^2} and $d_{x^2-y^2}$ under the C_3^1 rotation, the character assignment is a little less clear-cut. In this case, the $x^2 - y^2$ function follows

$$x^2 - y^2 \rightarrow y^2 - z^2 \quad (5.36)$$

The result indicates that the orbital has changed, but it is not instantly recognizable as another member of the basis set. This transformation is shown in Figure 5.17a, and comparison with Figure 5.13 shows that one of the orbitals used to create the d_{z^2} orbital has been produced. So, we may expect some part of the $2z^2 - x^2 - y^2$ function to now be present at the expense of the $x^2 - y^2$.

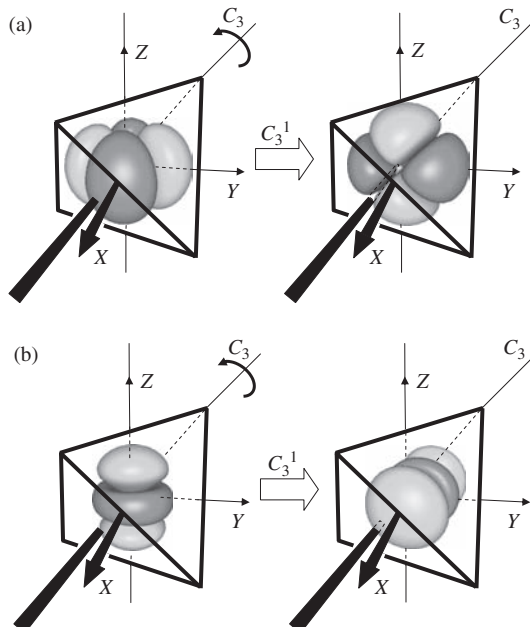


Figure 5.17 The C_3^1 operation in T_d showing the result for (a) the $d_{x^2-y^2}$ and (b) the d_{z^2} orbitals.

The new function contains y and z squared, but no products such as xy , yz or xz , and so its composition in terms of the d-orbital basis will only contain contributions from $2z^2 - x^2 - y^2$ and the original $x^2 - y^2$ function. So we can write

$$y^2 - z^2 = \frac{a}{\sqrt{3}}(2z^2 - x^2 - y^2) + b(x^2 - y^2) \quad (5.37)$$

in which the factor of $\sqrt{3}$ is required to normalize the z^2 when mixing with $x^2 - y^2$, see Equations (5.28) and (5.29). The coefficients a and b control how much of each basis function is used. To find the appropriate character we must obtain the amount of the $x^2 - y^2$ function remaining after the transformation, i.e. the value of b . Equation (5.37) links two orbitals that have a value at every point in space and so the left and right sides must be the same for any choice of x , y and z . For this to be the case the coefficients of x^2 must be balanced and those of y^2 and those of z^2 , so that

$$\begin{aligned} 0 &= \frac{-a}{\sqrt{3}} + b && \text{from } x^2 \text{ coefficients} \\ 1 &= \frac{-a}{\sqrt{3}} - b && \text{from } y^2 \text{ coefficients} \\ -1 &= \frac{2a}{\sqrt{3}} && \text{from } z^2 \text{ coefficients} \end{aligned} \quad (5.38)$$

This comparison of coefficients gives three equations for two unknowns, and so we can solve for a and b . From the z^2 coefficients we obtain

$$a = -\frac{\sqrt{3}}{2} \quad (5.39)$$

Then, from either the x^2 or y^2 coefficients:

$$\begin{aligned} 0 &= \frac{1}{2} + b && \text{from } x^2 && 1 = \frac{1}{2} - b && \text{from } y^2 \\ b &= -\frac{1}{2} && && b &= -\frac{1}{2} & \end{aligned} \quad (5.40)$$

So the character for the $x^2 - y^2$ orbital with the C_3^1 operation is $-1/2$.

Similarly, for the d_{z^2} function, the C_3^1 operation leads to

$$\frac{1}{\sqrt{3}}(2z^2 - x^2 - y^2) \rightarrow \frac{1}{\sqrt{3}}(2x^2 - y^2 - z^2) \quad (5.41)$$

Again, the result is not recognizable as one of the basis functions and so must be constructed from a linear combination of the original set. As before, we can exclude xy , yz and xz , as these products do not occur in the new function. So, the required linear combination must obey the relationship

$$\frac{1}{\sqrt{3}}(2x^2 - y^2 - z^2) = \frac{a}{\sqrt{3}}(2z^2 - x^2 - y^2) + b(x^2 - y^2) \quad (5.42)$$

Now there is a fresh pair of coefficients a and b . This time the character will be how much of the d_{z^2} orbital remains in the new function, and so we are looking for the value of a . Comparing coefficients of z^2 allows this to be obtained directly:

$$\frac{-1}{\sqrt{3}} = \frac{2a}{\sqrt{3}}$$

$$a = -\frac{1}{2} \quad (5.43)$$

So the character for d_{z^2} under C_3^{-1} is also $-1/2$.

The full set of characters for the p- and d-orbital functions in T_d are given in Table 5.12, along with their sums that give the reducible representations.

Table 5.12 The characters generated by the transformations of the p- and d-orbital functional forms under a symmetry operation from each class in T_d and the summation giving the total representations for p- and d-orbitals.

T_d	E	C_3^{-1}	C_2	S_4^{-1}	σ_d
x	1	0	-1	0	0
y	1	0	-1	0	0
z	1	0	1	0	0
$\Gamma(p)$	3	0	-1	-1	1
xy	1	0	1	-1	1
xz	1	0	-1	0	0
yz	1	0	-1	0	0
$x^2 - y^2$	1	-1/2	1	-1	-1
$2z^2 - x^2 - y^2$	1	-1/2	1	1	1
$\Gamma(d)$	5	-1	1	-1	1

For the p-orbitals the character set obtained for $\Gamma(p)$ is identical to that for t_2 in the T_d character table, so:

$$\Gamma(p) = t_2 \quad (5.44)$$

This means that all three p-orbitals are degenerate. In the model of the tetrahedron, X, Y and Z each pass through the centre of an edge, and so this result confirms that these three directions are symmetrically identical.

Application of the reduction formula to $\Gamma(d)$ is summarized in Table 5.13, where we find that

$$\Gamma(d) = e + t_2 \quad (5.45)$$

So the five d-orbitals are split into a set of three degenerate orbitals (t_2) and a degenerate pair (e).

Table 5.13 Application of the reduction formula to $\Gamma(d)$ in T_d .

T_d	E	$8C_3$	$3C_2$	$6S_4$	$6\sigma_d$			$h = 24$
$\Gamma(d)$	5	-1	1	-1	1	$g_c \chi_{\Gamma}(C) \chi_i(C)$	\sum_c	\sum_c
A_1	5	-8	3	-6	6		0	0
A_2	5	-8	3	6	-6		0	0
E	10	8	6	0	0	24	1	
T_1	15	0	-3	-6	-6	0	0	
T_2	15	0	-3	6	6	24	1	

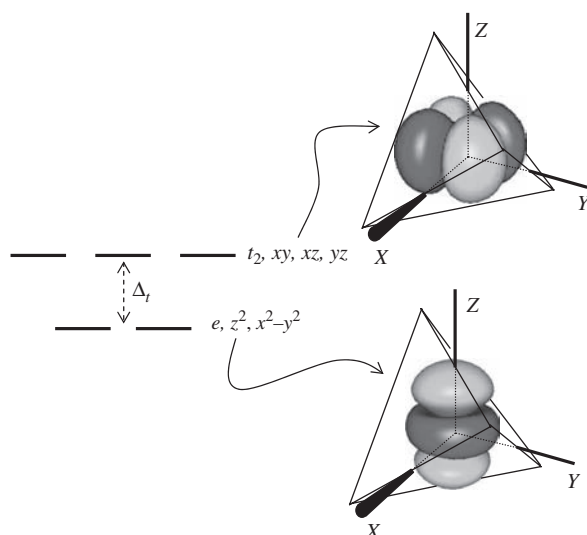


Figure 5.18 The d-orbital energy levels for the central atom of a T_d complex; the diagram to the right shows the reference axis system for the tetrahedron, with illustrations of the xy and z^2 orbitals.

Table 5.11 shows that the functions xy , yz and xz can be transformed into one another but are never mixed with $2z^2 - x^2 - y^2$ or $x^2 - y^2$. The latter two orbitals have lobes which point along the reference axis directions, i.e. at the edges of the tetrahedron and between the ligands of any complex. So, according to ligand field theory, the e orbitals (d_{z^2} and $d_{x^2-y^2}$) are lower in energy than the t_2 orbitals, xy , yz and xz , as shown in Figure 5.18. The energy gap between the e and t_2 levels is given by the symbol Δ_t and the size of this gap depends on the ligand field strength for the particular complex.

5.8.3 Octahedral, O_h

A complex with octahedral O_h symmetry has six identical ligands equidistant from a metal centre. An example of the Mn^{2+} complex, $[Mn(H_2O)_6]^{2+}$, is shown in Figure 5.19a, and the symmetry elements to be used in the analysis in this section are illustrated in

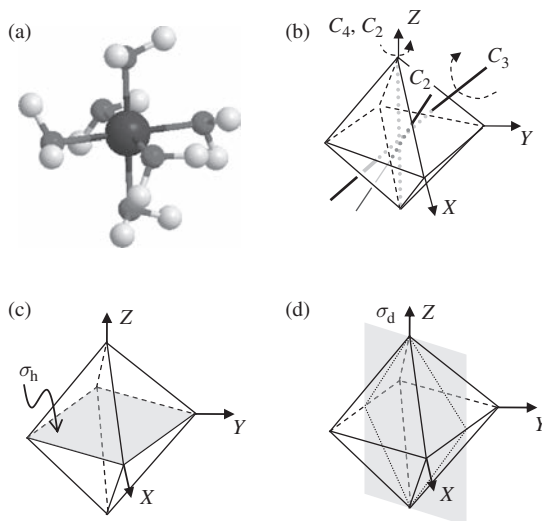


Figure 5.19 (a) An example octahedral complex, $[\text{Mn}(\text{H}_2\text{O})_6]^{2+}$, belonging to the O_h point group. The example symmetry axes (b), σ_h plane (c) and σ_d plane (d) used in the analysis of the main text.

Figures 5.19b–d. In the assignment of $[\text{Mn}(\text{H}_2\text{O})_6]^{2+}$ to the O_h point group we have ignored the positions of the H atoms on the H_2O ligands. This is justified because the structure shown is just one possibility for the positioning of the H atoms; rapid rotation of the ligands will lead to a ligand field which averages all possible H locations, giving the complex effective O_h symmetry.

The symmetry elements for O_h were discussed in Section 3.9. To set up the reference frame for the complex it is usual to align the axis system with the metal ligand bonds so that the ligands can be thought of as lying at the corners of the standard octahedral shape. This arrangement is also used in the three-dimensional model from Appendix 4, which also has the same set of example symmetry elements drawn on the paper octahedron.

Table 5.14 shows the result of operations using the selected symmetry elements on an x, y, z basis which is initially aligned with the reference axis system. The effect on the d-orbital functions is obtained by forming the appropriate products after the transformation. As we found in the D_{4h} and T_d point groups, the xy , xz and yz functions are linked by several of the symmetry operations, with the result that we can assign a character of +1 (function unaffected), -1 (function transformed to negative form of same product) or 0 (function transformed to different product).

However, under C_3^1 , C_2 and S_6^1 we find that the $x^2 - y^2$ and $2z^2 - x^2 - y^2$ are changed into functions that are not present in the original basis set. For example, under C_3^1 we find

$$x^2 - y^2 \rightarrow z^2 - x^2 \quad (5.46)$$

and

$$\frac{1}{\sqrt{3}}(2z^2 - x^2 - y^2) \rightarrow \frac{1}{\sqrt{3}}(2y^2 - z^2 - x^2) \quad (5.47)$$

Table 5.14 The transformations of the p - and d -orbital functions under example symmetry operations from each class in O_h . The symmetry elements that were used are those shown on the paper model from Appendix 4. The normalization factor for the d_{z^2} orbital has been omitted for the sake of clarity.

O_h	E	C_3^1	C_2	C_4^1	$C_2 (= C_4^2)$	i	S_4^1	S_6^1	σ_h	σ_d
x	x	z	z	-y	-x	-x	-y	-y	x	y
y	y	x	-y	x	-y	-y	x	-z	y	x
z	z	y	x	z	z	-z	-z	-x	-z	z
xy	xy	xz	$-yz$	$-xy$	xy	xy	$-xy$	yz	xy	xy
xz	xz	yz	xz	$-yz$	$-xz$	xz	yz	xy	$-xz$	yz
yz	yz	xy	$-xy$	xz	$-yz$	yz	$-xz$	xz	$-yz$	xz
$x^2 - y^2$	$x^2 - y^2$	$z^2 - x^2$	$z^2 - y^2$	$y^2 - x^2$	$x^2 - y^2$	$x^2 - y^2$	$y^2 - x^2$	$y^2 - z^2$	$x^2 - y^2$	$y^2 - x^2$
$2z^2 - x^2 - y^2$	$2z^2 - x^2 - y^2$	$2y^2 - z^2 - x^2$	$2x^2 - z^2 - y^2$	$2z^2 - x^2 - y^2$	$2x^2 - y^2 - z^2$	$2z^2 - x^2 - y^2$	$2z^2 - x^2 - y^2$			

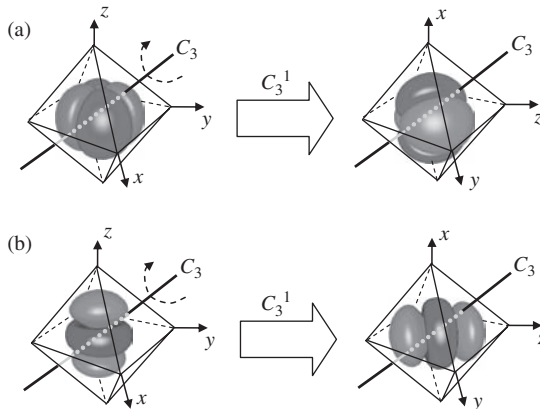


Figure 5.20 The effect of a C_3^1 rotation in O_h on (a) $d_{x^2-y^2}$ and (b) d_{z^2} .

These transformations are illustrated in Figure 5.20, which shows that the corresponding orbitals are orientated in a nonstandard way.

To find the characters for these orbitals we need to form linear combinations of the original basis set that are equivalent to the transformed functions. The functions we seek contain no products of axes; so, in a similar manner to the earlier T_d example, the xy , xz and yz functions can be disregarded. Taking the $z^2 - x^2$ case first:

$$z^2 - x^2 = \frac{a}{\sqrt{3}}(2z^2 - x^2 - y^2) + b(x^2 - y^2) \quad (5.48)$$

for which b is the amount of the original $x^2 - y^2$ remaining after the transformation, i.e. the character. This appears in the coefficient of both x^2 and y^2 ; however, these coefficients will also contain the unknown coefficient a , so this must be obtained first. From the z^2 coefficients we have

$$1 = \frac{2a}{\sqrt{3}} \quad \text{i.e.} \quad a = \frac{\sqrt{3}}{2} \quad (5.49)$$

Now, from the y^2 coefficients:

$$0 = -\frac{a}{\sqrt{3}} - b \quad \text{giving} \quad b = -\frac{a}{\sqrt{3}} \quad \text{and so} \quad b = -\frac{1}{2} \quad (5.50)$$

i.e. the character for the transformation of $x^2 - y^2$ by the selected C_3^1 operation is $-1/2$.

For the $2z^2 - x^2 - y^2$ case we start from the result of Equation (5.47) and form a new linear combination with unknown coefficients:

$$\frac{1}{\sqrt{3}}(2y^2 - z^2 - x^2) = \frac{a}{\sqrt{3}}(2z^2 - x^2 - y^2) + b(x^2 - y^2) \quad (5.51)$$

This time the coefficient a is the required character, so we can use the z^2 coefficient to obtain it directly:

$$-\frac{1}{\sqrt{3}} = \frac{2a}{\sqrt{3}} \quad \text{so that} \quad a = -\frac{1}{2} \quad (5.52)$$

The characters for all functions under each example operation are listed in Table 5.15, which also gives the total characters for the reducible representations of the sets of p- and d-orbitals.

Table 5.15 The characters generated by the transformations of the p- and d-orbital functional forms under a symmetry operation from each class in O_h and the summation giving the total representations for p- and d-orbitals.

O_h	E	C_3^1	C_2	C_4^1	$C_2 (= C_4^2)$	i	S_4^1	S_6^1	σ_h	σ_d
x	1	0	0	0	-1	-1	0	0	1	0
y	1	0	-1	0	-1	-1	0	0	1	0
z	1	0	0	1	1	-1	-1	0	-1	1
$\Gamma(p)$	3	0	-1	1	-1	-3	-1	0	1	1
xy	1	0	0	-1	1	1	-1	0	1	1
xz	1	0	1	0	-1	1	0	0	-1	0
yz	1	0	0	0	-1	1	0	0	-1	0
$x^2 - y^2$	1	-1/2	1/2	-1	1	1	-1	-1/2	1	-1
$2z^2 - x^2 - y^2$	1	-1/2	-1/2	1	1	1	1	-1/2	1	1
$\Gamma(d)$	5	-1	1	-1	1	5	-1	-1	1	1

Problem 5.8: In Table 5.14 under the S_6^1 operation we find the transformations

$$x^2 - y^2 \rightarrow y^2 - z^2 \quad \text{and} \quad \frac{1}{\sqrt{3}}(2z^2 - x^2 - y^2) \rightarrow \frac{1}{\sqrt{3}}(2x^2 - y^2 - z^2) \quad (5.53)$$

The corresponding characters in Table 5.15 are both $-1/2$. By finding the appropriate linear combination coefficients, confirm that this assignment is correct.

Because we have assembled the reducible representations for complete sets of orbitals, the character totals obtained are independent of the choice of symmetry elements or operations from each class in the point group. We can now proceed to using the reduction formula to find the irreducible labels for p- and d-orbitals in O_h . For the p-orbitals, inspection of the standard character table from Appendix 12 shows that

$$\Gamma(p) = t_u \quad (5.54)$$

The p-orbitals are each reversed by the inversion centre, since the positive- and negative-phase regions are swapped by this operation. This leads to a -3 total character under

i and implies that the irreducible representation is *ungerade*. The three p-orbitals each point along a reference axis direction, i.e. along equivalent metal–ligand bonds, and so they remain degenerate in this complex geometry, as confirmed by this irreducible representation assignment.

For the d-orbitals we will apply the reduction formula. To make the job easier note that these functions are not changed by the inversion centre, since they all contain only even products of the *x*, *y* and *z* basis. This means that the d-orbitals have *gerade* symmetry, and so we only include irreducible representations with the ‘g’ subscript in the reduction. The application of the reduction formula is laid out in Table 5.16, which shows that

$$\Gamma(\text{d}) = e_g + t_{2g} \quad (5.55)$$

As we found in the T_d case, the five d-orbitals are split into a degenerate set of three (t_{2g}) and a degenerate pair (e_g). In this case, however, the reference axis system is aligned with the metal–ligand bonds, and so the e_g orbitals interact more strongly with the ligand set than those of the t_{2g} , making the former higher in energy, as shown in Figure 5.21. The energy gap between the t_{2g} and e_g levels is referred to as the ligand field splitting parameter and is given the symbol Δ_o , and the size of this gap depends on the type of ligand used in the complex.

5.8.4 Trigonal Bipyramidal, D_{3h}

Complexes formed with five identical ligands may have the trigonal bipyramidal structure shown in Figure 5.22a. This geometry belongs to the D_{3h} point group and the set of example symmetry elements we will employ for the following analysis are defined in Figure 5.22b. In the complex, two of the ligands are opposite, or *trans*, to one another, defining the principal C_3 symmetry axis, which is assigned as the Z-direction. The other three ligands are in the equatorial plane with L–M–L angles of 120° . The choice of the reference *X* and *Y* directions is less clear for D_{3h} than in the earlier examples, and here we make the choice that *X* will be along an M–L bond with *Y* placed to complete the right-handed axis system.

We begin with the effect of each operation on an *x*, *y*, *z* basis which is initially aligned with the reference axis system at the central M atom. The C_3 axis is along the Z direction, and so the *z* basis function is unaffected by the rotation. However, the *x* and *y* basis vectors are rotated by 120° . This means that the transformed *x* and *y* vectors are made up of a linear combination of both of the original vectors. The general formula for the transformation of *x* and *y* by a rotation is discussed in Section 4.7. For this rotation we obtain

$$x' = x \cos(120) - y \sin(120) = -\frac{1}{2}x - \frac{\sqrt{3}}{2}y \quad (5.56)$$

$$y' = x \sin(120) + y \cos(120) = \frac{\sqrt{3}}{2}x - \frac{1}{2}y \quad (5.57)$$

The angles are given in degrees and primes have been added to indicate the basis vectors after the C_3^1 rotation.

Table 5.16 Application of the reduction formula to $\Gamma(d)$ in O_h . In this case only the gerade irreducible representations need be considered, as each of the d-orbitals is gerade.

O_h	E	$8C_3$	$6C_2$	$6C_4$	$3C_2 (= C_4^2)$	i	$6S_4$	$8S_6$	$3\sigma_h$	$6\sigma_d$	$h=48$
$\Gamma(d)$	5	-1	1	-1		1	5	-1	-1	1	$\sum_c \frac{1}{h} \sum_c$
A_{1g}	5	-8	6	-6		3	5	-6	-8	3	6 0 0
A_{2g}	5	-8	-6	6		3	5	6	-8	3	-6 0 0
E_g	10	8	0	0		6	10	0	8	6	0 48 1
T_{1g}	15	0	-6	-6		-3	15	-6	0	-3	-6 0 0
T_{2g}	15	0	6	6		-3	15	6	0	-3	6 48 1

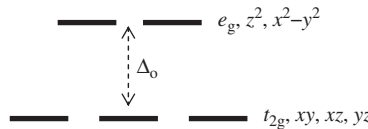


Figure 5.21 The d -orbital energy levels for the central atom of an O_h complex; the diagram to the right shows the reference axis system for the octahedron.

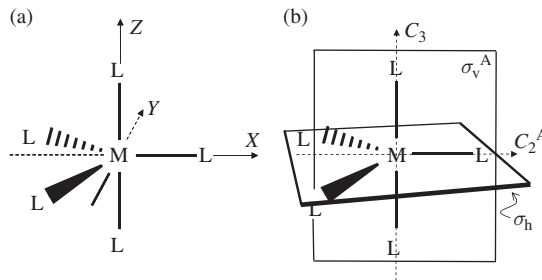


Figure 5.22 A complex with trigonal bipyramidal geometry belonging to the point group D_{3h} . (a) The structure and reference coordinate system. (b) The symmetry elements used in orbital analysis for this complex.

This is a new situation; in the previous examples the x, y, z basis has had only characters $+1, 0$ or -1 . In this case we find the p_x and p_y orbitals would be transformed into mixtures which each contain $-1/2$ of the original orbitals, *i.e.* a character of $-1/2$.

To find the transformed d -orbital functions we must take into account the full functional forms found for the single vectors. For example, the xy function will become

$$\begin{aligned} x'y' &= \left(-\frac{1}{2}x - \frac{\sqrt{3}}{2}y \right) \left(\frac{\sqrt{3}}{2}x - \frac{1}{2}y \right) \\ &= -\frac{\sqrt{3}}{4}x^2 + \frac{\sqrt{3}}{4}y^2 + \frac{1}{4}xy - \frac{3}{4}xy \\ &= -\frac{\sqrt{3}}{2} \left(\frac{1}{2}(x^2 - y^2) \right) - \frac{1}{2}xy \end{aligned} \quad (5.58)$$

so that the d_{xy} orbital after the transformation can be thought of as a mixture of the d_{xy} and $d_{x^2-y^2}$ orbitals. Notice that a factor of a half has been used for the $x^2 - y^2$ to account for the different normalization factors in the full functional forms of Equations (5.30). The mixture found in Equation (5.58) is not too surprising, as we have rotated the orbital in the XY plane and both d_{xy} and $d_{x^2-y^2}$ have lobes in this plane, but with different orientations relative to the X and Y reference directions. The rotation is just equivalent to mixing the two orbitals in the plane together in the correct proportions, as illustrated in Figure 5.23. Equation (5.58) gives us the character for the transformation of d_{xy} by the C_3^1 operation as $-1/2$.

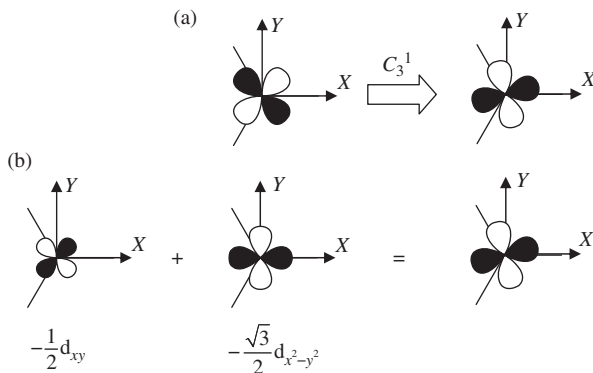


Figure 5.23 (a) The effect of a C_3^1 rotation on the d_{xy} orbital in a D_{3h} complex. The structure is viewed down the principal axis and one M–L bond is aligned with the X direction. (b) The same result obtained as a linear combination of d_{xy} and $d_{x^2-y^2}$.

Similarly, the $d_{x^2-y^2}$ orbital rotation can also be achieved by mixing it with the d_{xy} . To obtain the coefficients that control how they must be mixed, we simply write out the new function using the transformed x and y basis vectors:

$$\begin{aligned} \frac{1}{2} \left((x')^2 - (y')^2 \right) &= \frac{1}{2} \left(\left(-\frac{1}{2}x - \frac{\sqrt{3}}{2}y \right)^2 - \left(\frac{\sqrt{3}}{2}x - \frac{1}{2}y \right)^2 \right) \\ &= \frac{1}{2} \left(\frac{1}{4}x^2 + \frac{3}{4}y^2 + \frac{\sqrt{3}}{2}xy - \left(\frac{3}{4}x^2 + \frac{1}{4}y^2 - \frac{\sqrt{3}}{2}xy \right) \right) \quad (5.59) \\ &= -\frac{1}{2} \left(\frac{1}{2}(x^2 - y^2) \right) - \frac{\sqrt{3}}{2}xy \end{aligned}$$

The d_{xz} and d_{yz} orbitals will also be mixed by the C_3^1 rotation:

$$\begin{aligned} x'z' &= \left(-\frac{1}{2}x - \frac{\sqrt{3}}{2}y \right) z \\ &= -\frac{1}{2}xz - \frac{\sqrt{3}}{2}yz \quad (5.60) \end{aligned}$$

$$\begin{aligned} y'z' &= \left(\frac{\sqrt{3}}{2}x - \frac{1}{2}y \right) z \\ &= \frac{\sqrt{3}}{2}xz - \frac{1}{2}yz \quad (5.61) \end{aligned}$$

We should expect the d_{z^2} orbital not to be altered by a C_3^1 operation, since the major lobe of the orbital is orientated along the rotation axis. This is not obvious at first from the basis vectors, but if we insert the transformed x, y, z vectors into the full functional form of the d_{z^2} orbital we obtain

$$\begin{aligned} 2(z')^2 - (x')^2 - (y')^2 &= 2z^2 - \left(-\frac{1}{2}x - \frac{\sqrt{3}}{2}y\right)^2 - \left(-\frac{\sqrt{3}}{2}x - \frac{1}{2}y\right)^2 \\ &= 2z^2 - \left(\frac{1}{4}x^2 + \frac{\sqrt{3}}{2}xy + \frac{3}{4}y^2\right) - \left(\frac{3}{4}x^2 - \frac{\sqrt{3}}{2}xy + \frac{1}{4}y^2\right) \\ &= 2z^2 - x^2 - y^2 \end{aligned} \quad (5.62)$$

where we have left out the normalization factor for simplicity. The result is that the d_{z^2} function is unaltered by the C_3^1 rotation, as expected from its alignment with the principal axis.

The complete set of transformations using the symmetry elements illustrated in Figure 5.22b is given in Table 5.17. For most of the operations the derivation of these functions is straightforward. The improper S_3^1 rotation has the same effect on x and y as C_3^1 but it causes z to become $-z$, and so we can obtain the d-orbital functions for this operation by taking the C_3^1 results and replacing z with $-z$. The character for each orbital under each operation can be worked out from Table 5.17, remembering that what is required is the amount of the original function still present after each transformation. These characters are summarized in Table 5.18, which also gives the sums required for the reducible representations of the p- and d-orbital sets.

Application of the reduction formula to the reducible representations is detailed in Table 5.19, from which we obtain

$$\Gamma(p) = e' + a_2'' \quad (5.63)$$

and

$$\Gamma(d) = a_1' + e' + e'' \quad (5.64)$$

Remarkably, this analysis shows that the p_x and p_y orbitals are degenerate as they form the e' representation found in $\Gamma(p)$. This means that the interaction with the ligands for a p-orbital aligned with an M—L bond, along X in Figure 5.22a, is equivalent to that for a p-orbital along Y , not directly aligned with a ligand at all. In the X case, one lobe of the orbital is directed toward a ligand while the other is in the middle of the other two equatorial ligands and so has the lowest possible interaction. In the Y direction, both lobes interact less strongly than if they were directed straight at a ligand, but more strongly than if placed in between two equatorial ligands. The net effect is that the two environments are exactly equivalent.

This observation can also be made for the d-orbitals which Equation (5.64) shows are split into a single a_1' type (d_{z^2}) and two pairs of degenerate orbitals e' ($d_{x^2-y^2}, d_{xz}$) and e'' (d_{xz}, d_{yz}). The orbital energy levels are illustrated in Figure 5.24.

Table 5.17 The transformations of the p - and d -orbital functions under example symmetry operations from each class in D_{3h} . The symmetry elements that were used are those shown in Figure 5.22. The normalization factor for the d_{z^2} orbital has been omitted for the sake of clarity.

Table 5.18 The characters generated by the transformations of the *p*- and *d*-orbital functional forms under a symmetry operation from each class in D_{3h} and the summation giving the reducible representations for *p*- and *d*-orbitals.

D_{3h}	E	C_3^{-1}	C_2^A	σ_h	S_3^{-1}	σ_v^A
x	1	-1/2	1	1	-1/2	1
y	1	-1/2	-1	1	-1/2	-1
z	1	1	-1	-1	-1	1
$\Gamma(p)$	3	0	-1	1	-2	1
xy	1	-1/2	-1	1	-1/2	-1
xz	1	-1/2	-1	-1	1/2	1
yz	1	-1/2	1	-1	1/2	-1
$x^2 - y^2$	1	-1/2	1	1	-1/2	1
$2z^2 - x^2 - y^2$	1	1	1	1	1	1
$\Gamma(d)$	5	-1	1	1	1	1

Table 5.19 Application of the reduction formula to $\Gamma(d)$ in O_h . In this case only the gerade irreducible representations need be considered, as each of the *d*-orbitals is gerade.

D_{3h}	E	$2C_3$	$3C_2$	σ_h	$2S_3$	$3\sigma_v$	$h=12$
$\Gamma(p)$	3	0	-1	1	-2	1	
			$g_c \chi_i(C) \chi_{\Gamma}(C)$			\sum_c	$h^{-1} \sum_c$
A_1'	3	0	-3	1	-4	3	0
A_2'	3	0	3	1	-4	-3	0
E'	6	0	0	2	4	0	12
A_1''	3	0	-3	-1	4	-3	0
A_2''	3	0	3	-1	4	3	12
E''	6	0	0	-2	-4	0	0
$\Gamma(d)$	5	-1	1	1	1	1	
			$g_c \chi_i(C) \chi_{\Gamma}(C)$			\sum_c	$h^{-1} \sum_c$
A_1'	5	-2	3	1	2	3	12
A_2'	5	-2	-3	1	2	-3	0
E'	10	2	0	2	-2	0	12
A_1''	5	-2	3	-1	-2	-3	0
A_2''	5	-2	-3	-1	-2	3	0
E''	10	2	0	-2	2	0	12

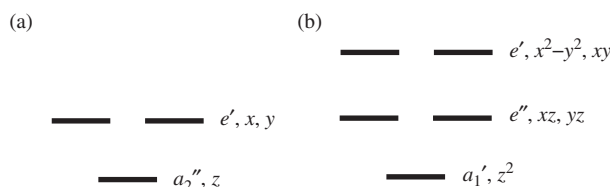


Figure 5.24 The orbital energy levels for (a) the *p*- and (b) the *d*-orbitals in a D_{3h} complex.

5.9 Linear Molecules: Groups of Infinite Order

When we try to find the irreducible representations for vibrations or orbitals in a group containing a C_∞ axis there is a stumbling block. The infinite axis gives rise to an infinite number of operations, since a rotation by any angle about the axis of a linear molecule is a symmetry operation. This means that the order of these groups, h , is infinity and so the $1/h$ term in the reduction formula is always zero. There are several approaches in the literature to coping with this problem. The most straightforward is to deduce the irreducible representations by inspection of the character set in the reducible representation. In this section we will see how this allows the elimination of sets of irreducible representations that are not consistent with the reducible character set. This process will result in only one sum which is able to give all the characters of the reducible representation.

The reducible representation in these groups can be assigned in the normal way. We consider the effect of an example operation on each member of the basis to assign a character for each class of operations in the group. To proceed with the reduction into the set of standard irreducible representations we return to the basic idea from which the reduction formula was derived in Section 5.5.

Equation (5.15) states that, within each class, the sum of the characters from the set of irreducible representations which make up a given reducible representation Γ sum to the character obtained for that Γ , $\chi_\Gamma(C)$. This sum must work for every class; so, once a particular alternative combination of irreducible representations is shown to be inconsistent with the $\chi_\Gamma(C)$ in any class, we need not consider that mix again.

For example, the linear molecule CO_2 belongs to the point group $D_{\infty h}$. If we wish to analyse the C=O stretching modes in this molecule then we can use the basis of the two bond vectors shown in Figure 5.25. There are two basis vectors, and so under the E operation of the reducible representation we must have a character of 2. Both vectors are on the axis of the molecule, and so any rotation around the C_∞ axis will have a character of 2 also. Likewise, the vertical mirror planes in the group each contain the molecular axis, leading to a character of 2 again. The remaining operations in the group, i , S_∞^Φ or any C_2 axis, will exchange the basis vectors, giving a character of 0. The resulting reducible representation is given in Table 5.20.



Figure 5.25 The $D_{\infty h}$ molecule CO_2 showing a suitable basis for the analysis of the C—O stretching modes.

Table 5.20 The reducible representation for the C—O stretching modes of CO_2 .

$D_{\infty h}$	E	C_∞^Φ	...	$\sigma_v(XZ)$	i	S_∞^Φ	...	$C_2(X)$
Γ	2	2	...	2	0	0	...	0

Now the standard character table is shown in Table 5.21, and so we have to look for combinations of irreducible representations that correspond to Γ . The first restriction is that the irreducible representations must give only two objects, because we have used

Table 5.21 The standard character table for the $D_{\infty h}$ point group.

two basis vectors. This limits our choice to any two (including two the same) of the Σ representations or a single Π or Δ type – by leaving the subscripts and superscripts out at this point we are leaving our options open.

Under the principal axis, the Π - or Δ -type representations give cosine functions of the angle of rotation. For our reducible representation, $\chi_{\Gamma}(C_{\infty}) = 2$, and so Π - or Δ -type representations do not fit at all.

The correct combination must be two Σ representations. At this point, any of these would be allowed because they each have character 1 under $2C_{\infty}$ in Table 5.21. However, under the $\infty\sigma_v$ class the Σ^- (both *gerade* and *ungerade* cases) have -1 . This means that the inclusion of these in our linear combination will lead to a total character of less than the required 2. So the set of irreducible representations we seek can only contain Σ^+ types.

Next, looking at the inversion centre column, in Γ we find 0, and since *gerade* representations have character 1 under i and *ungerade* -1 , the only possible combination of irreducible representations remaining is

$$\Gamma = \Sigma_g^+ + \Sigma_u^+ \quad (5.65)$$

So, the stretching vibration consists of one *gerade* and one *ungerade* Σ^+ representation. These are the linear molecule versions of the symmetric and unsymmetric stretch modes which were found for the O–H stretching modes of H_2O .

As a further example of the reduction procedure in groups containing a C_{∞} axis we will consider the symmetry labels for the 6p- and 5d-orbitals of the Au atom in the complex $\text{Au}(\text{CN})_2^-$. This cyanide complex of Au^+ is important in gold production because it is used in the recovery of the metal ion from aqueous solution formed using mineral ores. It is another linear molecule belonging to the $D_{\infty h}$ point group, as illustrated in Figure 5.26.

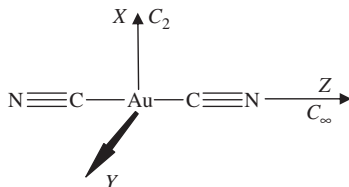


Figure 5.26 The $D_{\infty h}$ complex $\text{Au}(\text{CN})_2^-$ showing the reference axis system and symmetry axes used in the main text.

To derive the symmetry labels we will follow the same procedure as introduced earlier: forming the transformed p-orbital functions based on the x , y , z basis and then using the results to generate the transformed d-orbitals.

Table 5.22 summarizes the transformations of the x , y , z vectors for one example of an operation from each class of the $D_{\infty h}$ point group and Table 5.23 gives the resultant characters. Under E we must have 3, because the identity operator simply gives a count of the number of objects in the representation.

A rotation by Φ degrees around the principal C_{∞} will not change the p_z orbital, as this is aligned with the axis. However, the p_x and p_y orbitals are perpendicular to the axis, and

Table 5.22 The transformations of the x , y , z basis for the central atom in a $D_{\infty h}$ complex for an example operation from each class.

$D_{\infty h}$	E	C_{∞}^{Φ}	...	$\sigma_v(XZ)$	i	S_{∞}^{Φ}	...	$C_2(X)$
x	x	$x \cos(\Phi) - y \sin(\Phi)$...	x	$-x$	$x \cos(\Phi) - y \sin(\Phi)$...	x
y	y	$x \sin(\Phi) + y \cos(\Phi)$...	$-y$	$-y$	$x \sin(\Phi) + y \cos(\Phi)$...	$-y$
z	z	z		z	$-z$	$-z$		$-z$

these are rotated so that they make an angle Φ with their original direction. As we saw in Section 4.7, this means that the character for each of the p_x and p_y orbitals will be $\cos(\Phi)$, and so the total character for the p-orbital set is $1 + 2 \cos(\Phi)$.

For the vertical reflection plane we can choose any operation from the infinite set; it is convenient to pick a plane containing either X or Y . Taking the XZ plane reflection will not change either p_z or p_x , but p_y will be reversed, so we have a total character of 1.

The inversion centre reverses all three p-orbitals, and so we assign a character of -3 .

The improper rotation affects the p_x and p_y orbitals in an identical fashion to the simple rotation, but additionally p_z is reversed by the reflection through the horizontal plane, i.e. the required character is $-1 + 2 \cos(\Phi)$.

Finally, we can choose any axis perpendicular to the principal axis as an example C_2 symmetry element. Taking the X axis, the p_x orbital will not be affected by the rotation, but both p_y and p_z will be reversed, giving a total character of -1 .

So we have arrived at a reducible representation for the p-orbital set which is summarized of Table 5.23. There is no immediate match with any of the standard representations, and so this must be a reducible representation.

Table 5.23 The reducible representation derived for the p-orbitals of the central atom in a $D_{\infty h}$ complex.

$D_{\infty h}$	E	$2C_{\infty}^{\Phi}$...	$\infty\sigma_v$	i	$2S_{\infty}^{\Phi}$...	∞C_2
$\Gamma(p)$	3	$1 + 2 \cos(\Phi)$...	1	-3	$-1 + 2 \cos(\Phi)$...	-1

Now we will consider each class of operations to narrow down the possible standard irreducible representations that can be present until we arrive at only one option. The 3 under the E class reminds us that there are three orbitals being represented, and so our combination must consist of either three Σ -type representations or one Σ and one doubly degenerate representation. Under the inversion centre i the total character is -3 , and so all three orbitals must be reversed by the inversion. This means that any irreducible representation present must have *ungerade* symmetry; if we assigned a *gerade* representation, then it would contribute positively under i . This eliminates all *gerade* representations from further consideration.

Under the $2C_{\infty}^{\Phi}$ class we have $1 + 2 \cos(\Phi)$; the cosine term can only come from the Π_u representation because the Σ representations give $+1$ or -1 in this class, while the Δ representations have cosines of 2Φ . So, two of the orbitals fall into the Π_u representation; we know that these are the p_x and p_y orbitals from our derivation of the reducible representation. The remaining irreducible representation for p_z must be of Σ type. The two possible

alternatives, Σ_u^+ or Σ_u^- , each give the required 1 under $2C_\infty^\Phi$. However, they differ under the σ_v class; here, the Π_u representation has a 0 and so the reducible representation value of 1 can only come about by assigning p_z to Σ_u^+ . So we have assigned the irreducible representations for each of the p-orbitals unambiguously.

Problem 5.9: Check that the sum $\Pi_u + \Sigma_u^+$ gives the correct character for the reducible representation of the p-orbitals (Table 5.23) in all classes of the $D_{\infty h}$ group.

We can now find the transformed d-orbitals for each operation using the results for the x, y, z basis from Table 5.22. For the C_∞^Φ and S_∞^Φ a little algebra is required; for example:

$$\begin{aligned} x'y' &= [x \cos(\Phi) - y \sin(\Phi)] [x \sin(\Phi) + y \cos(\Phi)] \\ &= (x^2 - y^2)(\cos(\Phi) \sin(\Phi)) + xy(\cos^2(\Phi) - \sin^2(\Phi)) \\ &= \left(\frac{1}{2}(x^2 - y^2)\right) \sin(2\Phi) + xy \cos(2\Phi) \end{aligned} \quad (5.66)$$

in which we have made use of the trigonometric identities

$$\sin(2\Phi) = 2 \sin(\Phi) \cos(\Phi) \quad (5.67)$$

and

$$\cos(2\Phi) = \cos^2(\Phi) - \sin^2(\Phi) \quad (5.68)$$

Note that in Equation (5.66) the factor of 1/2 has been bracketed with $x^2 - y^2$ as this is the required normalization factor for mixing this orbital with xy (see Equations (5.30)). The relation holds for both operations, because the only difference between them is that S_∞^Φ reverses the z basis vector, and this will not affect d_{xy} .

Similarly, for the d_{z^2} orbital under C_∞^Φ we find

$$2(z')^2 - (x')^2 - (y')^2 = 2z^2 - [x \cos(\Phi) - y \sin(\Phi)]^2 - [x \sin(\Phi) + y \cos(\Phi)]^2 \quad (5.69)$$

We would expect the d_{z^2} orbital to be unaffected by the rotation as it is aligned with the principal axis. To see this from the algebra we need to expand the two brackets on the right-hand side of Equation (5.69):

$$[x \cos(\Phi) - y \sin(\Phi)]^2 = x^2 \cos^2(\Phi) + y^2 \sin^2(\Phi) - 2xy \cos(\Phi) \sin(\Phi) \quad (5.70)$$

and

$$[x \sin(\Phi) + y \cos(\Phi)]^2 = x^2 \sin^2(\Phi) + y^2 \cos^2(\Phi) + 2xy \cos(\Phi) \sin(\Phi) \quad (5.71)$$

If we remember the identity

$$\cos^2(\Phi) + \sin^2(\Phi) = 1 \quad (5.72)$$

then Equations (5.70) and (5.71) add to give

$$x^2 + y^2 \quad (5.73)$$

and so it has been shown that

$$2(z')^2 - (x')^2 - (y')^2 = 2z^2 - x^2 - y^2 \quad (5.74)$$

as required.

The transformed functions in Table 5.24 can each be obtained in this way.

Problem 5.10: Confirm the transformed functions for the yz , xz and $x^2 - y^2$ functions in Table 5.24 are correct.

The data given in Table 5.24 allow us to assign the characters for each orbital function, and these are laid out in Table 5.25. Inspection of the results for C_∞^Φ gives three alternatives: $\cos(2\Phi)$, $\cos(\Phi)$ and 1. Since these results occur for different irreducible representations in the standard $D_{\infty h}$ character table, we have only summed characters for functions with the same response to C_∞^Φ in the Γ rows of the table. Comparison with the standard character table shows we have recovered

$$\Gamma(xy, x^2 - y^2) = \Delta_g, \quad \Gamma(xz, yz) = \Pi_g, \quad \Gamma(z^2) = \Sigma_g^+ \quad (5.75)$$

These assignments agree with the rightmost column of the character table. Note that we have found only *gerade* symmetry labels, since d-orbitals are unaffected by inversion. In this case the d_{z^2} orbital is most strongly interacting with the ligands, followed by those of Π_g symmetry, with Δ_g the lowest in energy according to ligand field theory. The corresponding energy diagram is shown in Figure 5.27. One point to note about the CN^- ligands is that the π -antibonding orbital on the ligand will be able to interact with the Π_g orbitals on the metal. This kind of interaction is not well treated in ligand field theory, as the orbital structure of the ligands is ignored.

Table 5.24 The transformations of the d -orbital functions for the central atom in a $D_{\infty h}$ complex for an example operation from each class.

$D_{\infty h}$	E	$C_{\infty} \Phi$	\dots	$\sigma_i(XZ)$	i	$S_{\infty} \Phi$	\dots	$C_2(X)$
xy	xy	$\frac{1}{2}(x^2 - y^2)\sin(2\Phi) + xy\cos(2\Phi)$	\dots	$-xy$	xy	$\frac{1}{2}(x^2 - y^2)\sin(2\Phi) + xy\cos(2\Phi)$	\dots	$-xy$
xz	xz	$xz\cos(\Phi) - yz\sin(\Phi)$	\dots	xz	xz	$-xz\cos(\Phi) + yz\sin(\Phi)$	\dots	$-xz$
yz	yz	$xz\sin(\Phi) + yz\cos(\Phi)$	\dots	$-yz$	yz	$-xz\sin(\Phi) - yz\cos(\Phi)$	\dots	yz
$x^2 - y^2$	$x^2 - y^2$	$\frac{1}{2}(x^2 - y^2)\cos(2\Phi) + xy\sin(2\Phi)$	\dots	$x^2 - y^2$	$x^2 - y^2$	$\frac{1}{2}(x^2 - y^2)\cos(2\Phi) + xy\sin(2\Phi)$	\dots	$x^2 - y^2$
z^2	z^2	z^2	\dots	z^2	z^2	z^2	\dots	z^2

Table 5.25 The characters derived for the d -orbital functions for the central atom in a $D_{\infty h}$ complex.

$D_{\infty h}$	E	C_{∞}^{Φ}	...	$\sigma_v(XZ)$	i	S_{∞}^{Φ}	...	$C_2(X)$
xy	1	$\cos(2\Phi)$...	-1	1	$\cos(2\Phi)$...	-1
xz	1	$\cos(\Phi)$...	1	1	$\cos(\Phi)$...	-1
yz	1	$\cos(\Phi)$...	-1	1	$\cos(\Phi)$...	1
$x^2 - y^2$	1	$\cos(2\Phi)$...	1	1	$\cos(2\Phi)$...	1
z^2	1	1	...	1	1	1	...	1
$\Gamma(xy, x^2 - y^2)$	2	$2 \cos(2\Phi)$...	0	2	$2 \cos(2\Phi)$...	0
$\Gamma(xz, yz)$	2	$2 \cos(\Phi)$...	0	2	$2 \cos(\Phi)$...	0
$\Gamma(z^2)$	1	1	...	1	1	1	...	1

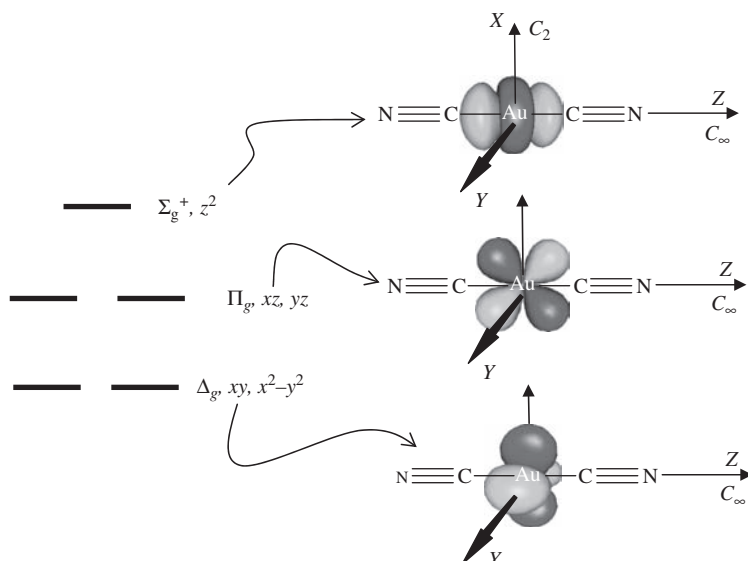


Figure 5.27 The ligand-field-derived energy diagram for the central metal atom d -orbital system of a $D_{\infty h}$ complex.

5.10 Summary

In this chapter we have covered the use of representations in symmetry analysis. The general approach to problems in symmetry can be written out as follows.

1. Decide on the point group of the molecule using the symmetry operations the atoms obey.
2. Decide on a basis for the analysis, using a suitable set of atom displacement vectors for vibrational modes or sets of atomic orbital (AO) functions for the description of

electronic states. The complete basis for vibrational modes is a set of three vectors on each atom, but sometimes a simpler basis will give information on specific vibrations.

3. Generate the reducible representation of the basis by inspection using example operations from each class in the point group.
4. Reduce the representation to its components using the reduction formula:

$$n_i = \frac{1}{h} \sum_c g_c \chi_{\Gamma}(C) \chi_i(C)$$

where n_i is the number of times the i th irreducible representation occurs in the reducible representation Γ , g_c is the number of operations in the C th class and h is the order of the point group. The character $\chi_{\Gamma}(C)$ is that found for the reducible representation for the chosen operation from class C and $\chi_i(C)$ is the character from the character table for the irreducible representation i in class C .

5. If a vibrational analysis using $3N$ displacement vectors is being carried out, then the representations that correspond to simple molecular translation or rotation must now be removed. In a character table, the irreducible representations for these degrees of freedom are indicated in the rightmost columns with the symbols x, y, z and R_x, R_y, R_z .
6. For the AOs at a central atom in a complex or molecule with a given geometry, the reducible representation for the p-orbitals can be constructed from a basis of x, y, z vectors initially aligned with the reference directions. For the d-orbitals, the five functions after a given transformation can be generated using products of the transformed x, y, z vectors. Characters are then assigned by direct inspection where possible, or by finding a linear combination of the original d-orbital set which reproduces the transformed function.

5.11 Self-Test Questions

1. In Section 5.6 we identified a third vibrational mode for H_2O with the A_1 symmetry representation. Draw a diagram showing the atom movements in this third mode and show that the set of vectors you use transforms correctly with each operation in the group.
2. Using the relationships listed as Properties 4 and 5, show:
 - (a) the B_1 representation in group C_{4v} is orthogonal to all the other representations in the group and gives a sum of squares which is the group order;
 - (b) each of the *gerade* representations in C_{2h} is orthogonal to all of the *ungerade* representations.
3. If one of the Cl^- ligands in the $[\text{CoCl}_4]^{2-}$ complex were replaced with F^- the point group would change to C_{3v} . Derive the irreducible representations for the p- and d-orbitals in this point group. What effect has the substitution had on the degree of degeneracy in the metal orbitals?

6

Applications in Vibrational Spectroscopy

6.1 Introduction

The Horsehead Nebula, shown in Figure 6.1a, is one of the most spectacular images of astronomy. The nebula is roughly 1500 light years distant and can be found in the constellation of Orion. Images of the quality shown here are only really possible using powerful telescopes, but the whole nebula can be seen with the naked eye as the central star in Orion's sword. The dark molecular cloud that forms the horse's head is visible only because its obscuring dust is silhouetted against a bright emission region of the nebula. The light from the emission region and of stars that are behind it as viewed from Earth must pass through the dust cloud. Any molecular species in the nebula will absorb light at characteristic frequencies, just like samples in a laboratory spectrometer. So we know the molecular composition of nebulae such as this one from the spectral analysis of light passing through them. The vibrational spectra of molecules in the cloud are identical to reference samples on Earth, and so is the symmetry of their vibrations. The spectra shown in Figure 6.1b are a fingerprint for the vibrational excitation of H₂ when this molecule is already above the vibrational ground state. So we not only know that H₂ is present, but that there is intense radiation in the area capable of exciting the diatomic molecule. This conclusion hinges on an understanding of symmetry. In this chapter we will find out how symmetry is used in the interpretation of molecular vibrational spectra.

The chapter is roughly divided into three sections. In the first (Sections 6.2 and 6.3) we look at the background theory of vibrational spectroscopy, including the selection rules for IR and Raman spectroscopy. We can already use reducible representations and the reduction formula to determine the symmetry labels for the vibrational modes of any molecule.

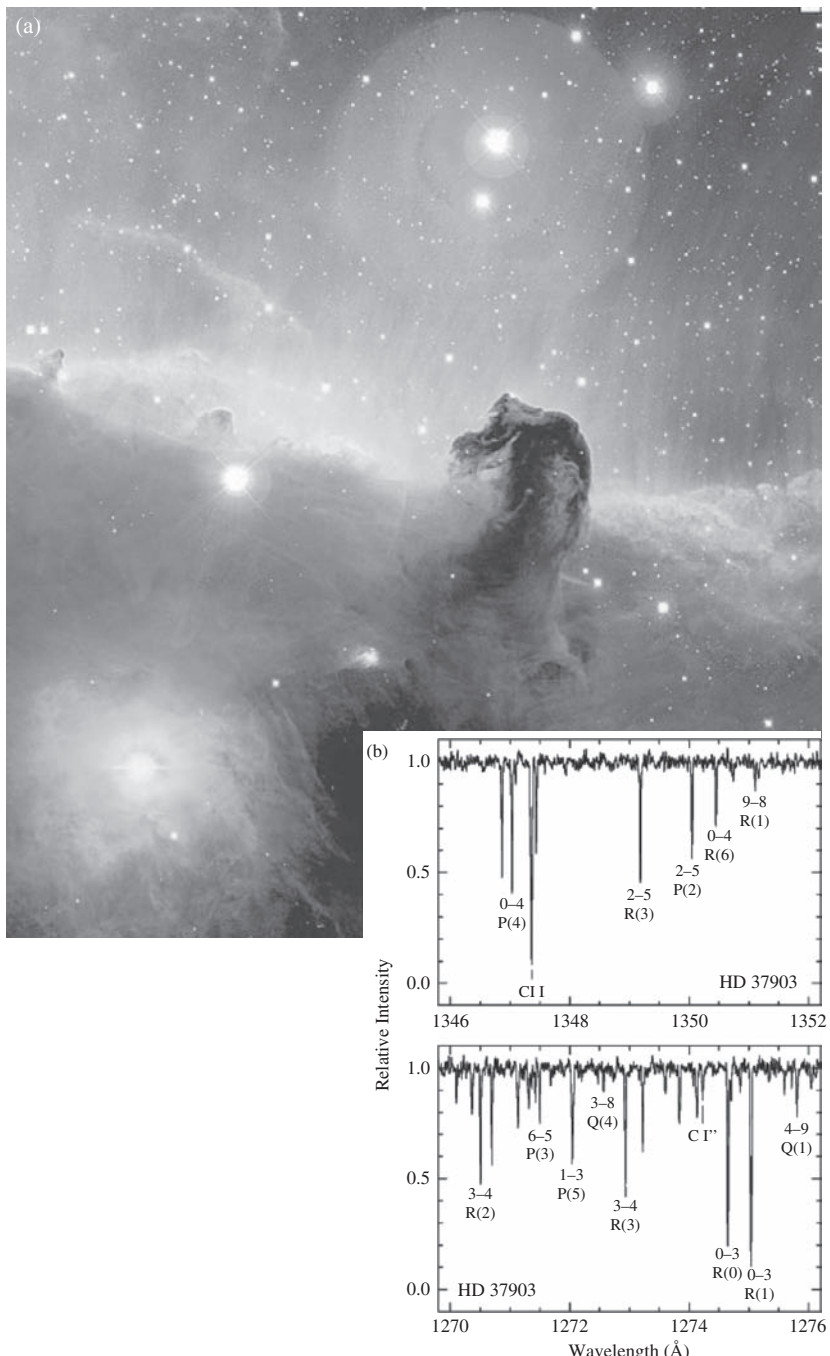


Figure 6.1 (a) The Horsehead Nebula in the constellation of Orion. (b) Hubble Space Telescope Imaging Spectrograph (STIS) observations of HD 37903 showing vibrational fine structure of the UV region of the spectrum. The observed lines are evidence of UV absorption by vibrationally excited H_2 . (Source: Meyer DM, Lauroesch JT, Sofia UJ, Draine BT, Bertoldi F (2001) *The Astrophysical Journal* **553**: L59–L62. Reproduced by permission of the AAS.)

The selection rules allow us to determine the number of bands to expect in vibrational spectra, since only vibrations belonging to certain irreducible representations lead to bands in the spectra.

In the second part (Sections 6.4–6.7) we will consider what the vibrations belonging to a given irreducible representation ‘look like’. This involves the construction of linear combinations of the basis of atomic movements that are consistent with the characters of the irreducible representation. These combinations are known as symmetry adapted linear combinations (SALCs). SALCs are a general way to visualize the molecular properties that correspond to the objects with the irreducible symmetries identified by the reduction formula. The method we shall use to obtain these SALCs is the projection operator, which is introduced in Section 6.6 and will also be employed in Chapter 7 to find molecular orbitals.

Finally, in Section 6.8, examples of vibrational analysis and its use in differentiating molecular isomers will be given.

6.2 Selection Rules

Selection rules are used in spectroscopy to determine whether a transition between two energy states within a molecule will show up in its spectrum. To be seen the transition has to be able to couple to the light which is used as a probe. This coupling is controlled by integrals over the initial and final states for the transition and the appropriate molecular property for the type of spectroscopy.

IR absorption occurs when the transition between two vibrational states of a molecule has an energy matching the photon energy of the probe radiation *and* the transition causes a change in the molecular dipole moment. If there is no change in molecular dipole moment during the vibration, then there will be no absorption and we say that the mode is not allowed by the selection rules.

Raman spectroscopy uses higher energy probe radiation and the spectrum is caused by the link between the vibrational and electronic states of the molecule through molecular polarizability. If the vibration causes no change in polarizability then the selection rule will not be satisfied and no spectral signature is observed for that vibration.

Symmetry controls the yes/no decision of the selection rules, determining which vibrations will lead to absorption and, hence, the number of bands to expect. However, symmetry does not allow the calculation of the band position (frequency) or intensity, as these are controlled by physical properties of a molecule such as bond strengths and the masses of the constituent atoms.

In the next two sections we consider the selection rules for IR and Raman spectroscopies in more detail.

6.2.1 Infrared Spectroscopy

When the irreducible representations for the vibrations of a molecule have been identified, the collective motions of the atoms that constitute each mode can be thought of as a simple oscillator to be described with quantum mechanics. As the molecule vibrates in a given mode it moves through a potential energy surface that is set by the chemical bonds of the system. For small displacements, which are all that occur at room temperature, we

usually assume that the potential energy surface is harmonic, i.e. the change of energy as the molecule vibrates is proportional to the square of the displacement from the minimum energy point.

To picture this we can define a coordinate q for any vibrational state which is a single value to indicate how far from equilibrium the oscillation has moved. An example for the symmetric stretch in H₂O is shown in Figure 6.2. Here, the vibrational motion involves the H atoms moving from/toward the O atom in phase with one another while the O atom moves only along the C₂ axis. The idea of the normal mode coordinate q is that it describes where in this collective motion the atoms are at any given time. In the harmonic approximation the potential energy for this vibrational motion is proportional to q^2 .

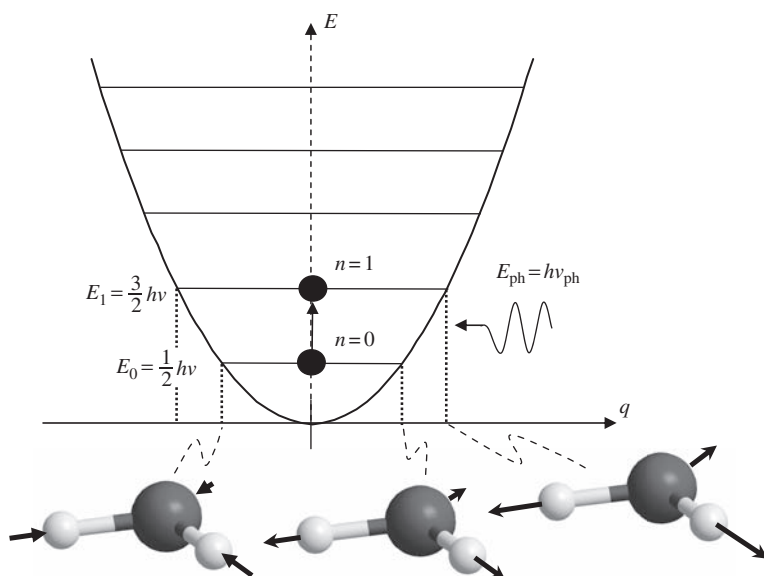


Figure 6.2 The normal mode coordinate for the symmetric stretch mode (A_1) of water.

The illustrations in Figure 6.2 show that for q negative, to the left of the minimum in the potential energy curve, the H atoms are moving toward the O, while for q positive they are moving away.

Each mode has a set of energy levels that form a regular ladder of states, with energies E_n given by

$$E_n = \left(n + \frac{1}{2}\right)h\nu \quad (6.1)$$

Here, n is a quantum number taking values 0, 1, 2 . . . etc., the vibrational frequency, ν , is in s⁻¹ units of the mode and h is the Planck constant (6.626×10^{-34} J s). The lowest energy state ($n = 0$) and the first excited state ($n = 1$) differ in energy and in the amplitude of the oscillation. In the higher energy state the atoms can move further from the minimum point before bond strain forces cause them to return.

In Appendix 6 it is shown that the simple form of Equation 6.1 is a direct consequence of the harmonic approximation, and anharmonic corrections are required for the most accurate spectroscopic analysis. However, the harmonic model is perfectly adequate for most cases in which spectroscopy is used to identify polyatomic molecules, and so we will continue to use it here.

Any given molecule in isolation will have a quantum number n for each of its vibrational modes and will remain in the same state indefinitely, unless some external factor intervenes so these vibrational states are referred to as stationary states. To move between stationary states we must supply energy to the system, and one way to do this is by exposing the molecule to light. The light wave used as a probe in a spectrometer can be thought of as a stream of photons each with an energy E_{ph} given by

$$E_{\text{ph}} = h\nu_{\text{ph}} \quad (6.2)$$

where ν_{ph} (s^{-1}) is the frequency of the oscillating electromagnetic field that constitutes the light beam.

A photon can be absorbed if the photon energy is exactly right to excite the oscillator into a higher vibrational level, as shown schematically in Figure 6.2. This is simply an example of the conservation of energy; the photon is being lost by exciting the vibration and so the photon energy must exactly match the difference in energy of the two vibrational states:

$$\begin{aligned} E_{\text{ph}} &= (n + 1 + \frac{1}{2})\hbar\nu - (n + \frac{1}{2})\hbar\nu \\ &= \hbar\nu \end{aligned} \quad (6.3)$$

If the photon is absorbed, then the light intensity at the frequency corresponding to the molecular vibration will be reduced, which is observed as an absorption band in the spectrum. In Appendix 6 we show that, within the harmonic approximation, absorption from state n to state $n + 1$ can occur, but not to higher energy states. For a molecular vibration in the ground state ($n = 0$), absorption may occur to the first excited state (subject to the selection rules discussed below) when the photon energy matches the vibration energy. However, even if the light frequency is 2ν , the $n = 0$ to $n = 2$ will not be seen. In practice, absorptions at frequencies near 2ν , referred to as overtones, can sometimes be observed because molecular bonds are not perfectly harmonic. The absorption due to overtones is generally weaker than that at ν .

Matching of the photon energy to the vibrational transition is not the only requirement for an absorption to be seen. The light must also be able to cause the transition by coupling the ground and excited states. The strongest effect that can give a transition is the interaction of the electric field of the light wave and the change in molecular dipole moment caused by the vibration of the molecule. An outline of the physics behind this coupling can be found in Appendix 6, but the key result from a symmetry point of view is that the strength of the coupling depends on the transition dipole moment M_{01} , given by

$$M_{01} = \int_{-\infty}^{\infty} \psi_1 \underline{\mu} \psi_0 \, d\tau \quad (6.4)$$

where $\underline{\mu}$ is the dipole moment operator, (ex , ey , ez); this is a vector because the dipole moment has X , Y and Z components. In the integrand, ψ_0 is the initial stationary state, which we take to be the ground state ($n = 0$), and ψ_1 the excited state. Strictly, we should use the complex conjugate of ψ_1 , but Appendix 6 shows that the harmonic oscillator wavefunctions are real (as $\sqrt{-1}$ does not appear) and so the function and its complex conjugate are the same.

In Equation (6.4) the volume of an infinitesimal region required for the integration is written $d\tau$.

The integral for the transition dipole moment M_{01} is taken from $-\infty$ to $+\infty$, i.e. over all space. This ensures that we capture all possible positions of the atoms and associated electron density during the vibration. For the selection rules, we will never have to evaluate M_{01} , just find out if it has to be zero by symmetry or not. No matter what the point group of the molecule, if the integrand in M_{01} belongs to anything other than the totally symmetric representation (usually A_1) then the integral will be zero. In any other irreducible representations there will be some operation that reverses the sign of the integrand, and this automatically implies the integral will be zero. For example, if the irreducible representation of the integrand has a -1 character for a reflection, then the two ‘halves’ of the function on either side of the corresponding mirror plane will have opposite signs and so the integration of one half will cancel the other. An example function with B_2 symmetry for the C_{2v} point group is shown in Figure 6.3. An integration over all space implies the range $y = -\infty$ to $y = \infty$ and clearly the result from the left- and right-hand sides of the $\sigma_v(XZ)$ plane will cancel for a B_2 function.

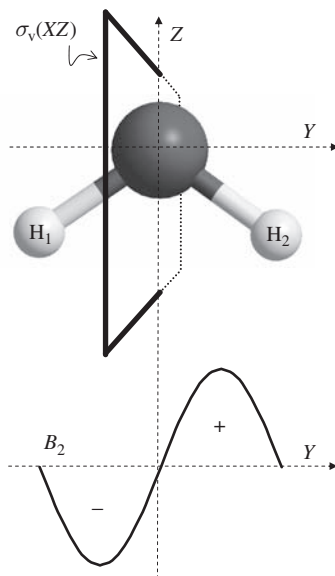


Figure 6.3 An example of a function with the correct behaviour for the $\sigma_v(XZ)$ plane in the B_2 irreducible representation of the C_{2v} point group.

The IR selection rule depends on the fact that the transition dipole moment integral must be nonzero in order to observe the transition as an IR absorption band. This means that the integrand for M_{01} must have A_1 symmetry.

To use this definition, we require the symmetry of the integrand $\psi_1 \mu \psi_0$. As explained in Appendix 6, the ground state will always belong to the A_1 irreducible representation. The first excited state vibration will have the same irreducible representation as the underlying vibrational motion, described by the normal coordinate q .

The dipole moment operator has three components with the same symmetry as the simple x , y and z functions, and these are usually noted in the right-hand columns of character tables.

To identify those vibrations which cannot have a finite transition dipole moment and so exclude them from the assignment of spectroscopic bands, we will use the idea of direct products (introduced in Chapter 4) to look at the symmetry of the integrand in Equation (6.4) for a few examples.

H_2O , C_{2v}

We have already found that the symmetric vibration of H_2O , illustrated in Figure 6.2, belongs to the A_1 irreducible representation. The symmetry representations for the components of the dipole operator are the same as x , y and z from the C_{2v} character table in Appendix 12 the right-hand columns tell us that these belong to the B_1 , B_2 and A_1 irreducible representations. The three components of the dipole operator each give an integrand; for the symmetric stretch these are

$$\begin{aligned}\psi_1 \mu_x \psi_0 &\Rightarrow A_1 \times B_1 \times A_1 = B_1 \\ \psi_1 \mu_y \psi_0 &\Rightarrow A_1 \times B_2 \times A_1 = B_2 \\ \psi_1 \mu_z \psi_0 &\Rightarrow A_1 \times A_1 \times A_1 = A_1\end{aligned}\tag{6.5}$$

To obtain these products, we multiply, class by class, the characters of the irreducible representations and then look for a match between the result and a row of the character table. In these examples, A_1 has character 1 for all classes, and so the solutions are straightforward.

Equation (6.5) says that, to get the y -component of M_{01} , we have to integrate a function with B_2 symmetry from $-\infty$ to $+\infty$, which Figure 6.3 shows must give zero because the function will have opposite signs either side of the $\sigma_v(XZ)$. Similarly, the B_1 integrand generated by μ_x has a -1 character under $\sigma_v'(YZ)$ and so will lead to a zero integral. For the H_2O symmetric stretch, only μ_z gives an A_1 integrand.

This is sufficient for us to conclude that the symmetric stretch will lead to an absorption band and also that this absorption is due to a transition dipole moment aligned with the Z -axis in the standard symmetry setting. The physical interpretation of this result can be understood from a diagram of H_2O in the standard setting, such as Figure 6.3. As O is more electronegative than H, both O—H bonds will have local dipole moments pointing from O toward H. In the A_1 vibration the O—H bonds move in phase, and so the Y -components of these dipoles, which are in opposite directions to one another, always cancel out. However,

the Z-components are in the same direction, so we see a changing dipole moment aligned with the Z-axis in the A_1 vibration.

The antisymmetric stretch mode of water has a B_2 irreducible representation, so now the three components of the integrand have the following symmetry:

$$\begin{aligned}\psi_1 \mu_x \psi_0 &\Rightarrow B_2 \times B_1 \times A_1 = A_2 \\ \psi_1 \mu_y \psi_0 &\Rightarrow B_2 \times B_2 \times A_1 = A_1 \\ \psi_1 \mu_z \psi_0 &\Rightarrow B_2 \times A_1 \times A_1 = B_2\end{aligned}\tag{6.6}$$

Here, the only direct product which gives an A_1 representation is μ_y , and so we conclude that the antisymmetric stretch is an IR-active mode because the vibration has a changing dipole in the standard Y-direction.

Problem 6.1: The direct product required for the μ_x component of the dipole in Equation (6.6) is shown fully in Table 6.1. Check the other direct products in Equation (6.6) are correct. The fact that the characters of the A_1 representation are all 1 means that this acts like the number 1 in ordinary multiplication; it leaves the representation product unchanged. Accordingly, each product requires at most two representations to be multiplied.

Table 6.1 The direct product for the μ_x component of Equation (6.6).

$\mu_x (C_{2v})$	E	C_2	$\sigma_v(XZ)$	$\sigma_v'(YZ)$
B_2	1	-1	-1	1
B_1	1	-1	1	-1
A_1	1	1	1	1
$B_2 \times B_1 \times A_1 = A_2$	1	1	-1	-1

Problem 6.2: Show that in a group containing the inversion centre the dipole moment components must have *ungerade* representations. Hence, demonstrate that M_{01} must be zero for any *gerade* representation.

Because the ground-state vibration always has A_1 symmetry, the triple product required for the selection rules only depends on the symmetry of the vibrational mode and the related axis. Any product of a simple nondegenerate irreducible representation with itself will give A_1 , and any product of two different irreducible representations cannot give A_1 . So the selection rule for choosing IR-active modes can be restated simply as follows:

To be IR active a vibrational mode must belong to an irreducible representation which matches that of one of the Cartesian axes, x , y or z .



The statement of the selection rules given above also applies to degenerate modes of vibration. For example in Section 5.7 we show that the C=O vibrational modes of the D_{3h} complex $[Fe(CO)_5]$ have the irreducible representations:

$$2A_1' + E' + A_2'' \quad (6.7)$$

Inspection of the character table in Appendix 12 shows that the simplified selection rule gives the A_2'' mode as IR active for a transition dipole moment in the Z-direction and the E' doubly degenerate modes as both active: one for a transition dipole moment along X and the other along Y. The two A_1' modes would not give rise to absorption and so would not be seen as bands in the IR spectrum.

To check that the E' representation conforms to the earlier statement of the selection rule we need to form the products for the integrands:

$$\begin{aligned} \psi_1\mu_x\psi_0, \psi_1\mu_y\psi_0 &\Rightarrow E' \times E' \times A_1 \\ \psi_1\mu_z\psi_0 &\Rightarrow E' \times A_2'' \times A_1 \end{aligned} \quad (6.8)$$

We have grouped the μ_x and μ_y cases together because they form a degenerate pair within the E' representation. The first direct product is set out in Table 6.2. Under the identity operator we have generated the character 4; since no irreducible representation contains 4 under this column, this product must be reducible. In Table 6.3, the reduction formula is applied in the normal way to obtain

$$E' \times E' = A_1' + A_2' + E' \quad (6.9)$$

Table 6.2 The direct product of E' with itself in point group D_{3h} .

$\mu_x, \mu_y (D_{3h})$	E	$2C_3$	$3C_2$	σ_h	$2S_3$	$3\sigma_v$
E'	2	-1	0	2	-1	0
$E' \times E' =$	4	1	0	4	1	0

Table 6.3 Application of the reduction formula to the $E' \times E'$ direct product from D_{3h} .

$\mu_x, \mu_y (D_{3h})$	E	$2C_3$	$3C_2$	σ_h	$2S_3$	$3\sigma_v$		$h = 12$
$\Gamma(E' \times E')$	4	1	0	4	1	0		
			$g_c \chi_i(C) \chi_{\Gamma}(C)$				\sum_c	$h^{-1} \sum_c$
A_1'	4	2		4	2		12	1
A_2'	4	2		4	2		12	1
E'	8	-2		8	-2		12	1
A_1''	4	2		-4	-2		0	0
A_2''	4	2		-4	-2		0	0
E''	8	-2		-8	2		0	0

This reduction procedure shows that the $E' \times E'$ product contains the A_1' representation, i.e. the totally symmetric representation (all characters equal to 1) in D_{3h} . So we can say that both of the vibrations in E' will be IR active, but because they are degenerate they will occur at exactly the same frequency, giving rise to only one spectral band.

Problem 6.3: By forming the direct product $E' \times A_2''$, show that the E' vibrational modes will not give a transition dipole moment in the Z-direction for the $[\text{Fe}(\text{CO})_5]$ carbonyl stretching modes.

$\text{HF}, C_{\infty v}$

Diatom molecules, such as HF, are having only a single vibrational mode. HF belongs to the point group $C_{\infty v}$, and in the standard symmetry the axis of the molecule is set along the Z-axis. For the single bond stretch mode the two atoms move out of phase with one another and we can derive the irreducible representation by inspection with reference to Figure 6.4.



Figure 6.4 The bond stretch mode of a diatomic molecule such as HF.

The two classes of operation in this group, other than the identity, are $2C_\infty^\Phi$, which is rotation around the molecular axis, and $\infty\sigma_v$, reflection through any plane containing the two atoms (see Appendix 12). Neither of these sets of operations would change the appearance of the stretching mode, and so we conclude that it is fully symmetric in the group with irreducible representation Σ^+ . This symbol is part of the special nomenclature for linear molecules and is equivalent to A_1 in other groups, having character 1 for all classes of operations. From the character table we see that this will also be the representation for the Z-component of the transition dipole operator, and so the mode is confirmed as IR active.

$\text{H}_2, D_{\infty h}$

If we carry out the same analysis on a homonuclear diatomic, such as H_2 , then additional operations are present because the molecule is now in $D_{\infty h}$ and so is unaltered if the two atoms swap over. This introduces the inversion centre i at the middle of the bond and the improper rotation class $2S_\infty^\Phi$. However, the vibration remains totally symmetric, so that for H_2 the stretching mode belongs to the irreducible representation Σ_g^+ .

Problem 6.2 shows that the components of the dipole operator in a group containing the inversion centre will always belong to *ungerade* representations. This is an important result which leads to the following statement:

In point groups containing the inversion centre, only vibrations which belong to *ungerade* irreducible representations *can* be IR active.

An immediate consequence is that the vibration of a homonuclear diatomic will not be IR active.

6.2.2 Infrared Absorption and the Greenhouse Gases

IR absorption by gases in the atmosphere is thought to be responsible for climatic warming effects. Sunlight in the visible and ultraviolet (UV) parts of the spectrum that arrives at the surface of the Earth is absorbed and partially re-emitted in the IR region. The Earth's atmosphere is roughly 78% nitrogen, 21% oxygen, 0.93% argon, 0.04% carbon dioxide (CO_2), along with small amounts of methane (CH_4) and water vapour. Nitrogen and oxygen are present as homonuclear diatomic molecules and so, as we have seen, their bond vibrations will not absorb IR radiation. The atomic argon component is similarly benign and so if only these three gases were present the heat radiated by the Earth would escape back into space.

However, CO_2 , CH_4 and water all have IR-active vibrations. Hence, these relatively minor constituents of the atmosphere will absorb IR radiation, trapping some of the radiated energy and warming the planet. With these gases present the atmosphere acts in a similar way to the glass of a greenhouse: visible wavelength radiation can pass through the glass into the greenhouse where it is absorbed by the plants and soil and is partially re-emitted at IR wavelengths. Glass is practically opaque in the IR and so the re-emitted energy is trapped, warming the interior of the greenhouse. The absorption of energy by IR-active vibrations of atmospheric components causes heating in a similar way.

To some extent the Earth's greenhouse effect is a good thing; the surface temperature of the moon varies between -233 and $+123^\circ\text{C}$. The moon's lack of an atmosphere means that all the radiation from the sun reaches the surface during the daytime and heat emitted by the surface is rapidly lost to space during the night. On the Earth these extremes are tempered by the atmosphere with the 'greenhouse' gases helping to hold the heat radiated by the planet's surface through the night-time. However, since the amount of heat retained by the atmosphere is dependent on the concentration of relatively minor components, increases in the average amounts of CO_2 , CH_4 and other IR-active molecular species will lead to additional warming of the planet.

H_2O , C_{2v}

We can now show that the three main greenhouse gases are IR active as a result of their molecular symmetry. For the case of water, we have already found in Section 5.6 that the irreducible representations are

$$\Gamma(\nu) = 2A_1 + B_2 \quad (6.10)$$

The two A_1 modes are the symmetric stretch and bending motions and the B_2 vibration is the asymmetric stretch. By reference to the standard character table in Appendix 12 for C_{2v} , we find that all three modes are IR active, because Z belongs to A_1 and y to B_2 .

CO_2 , $\text{D}_{\infty h}$

CO_2 is a linear triatomic molecule belonging to the point group $\text{D}_{\infty h}$. A basis which gives three degrees of freedom to each atom is shown in Figure 6.5a. This basis can be split into

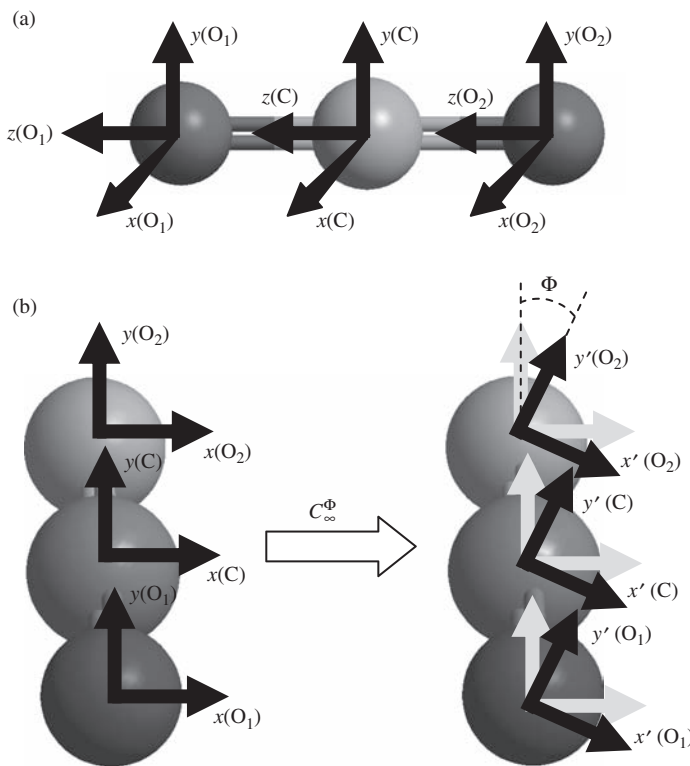


Figure 6.5 (a) The full basis for the vibrational modes of CO_2 with three degrees of freedom per atom. (b) The effect of a C_∞^Φ operation on the x and y components of the basis.

two sets according to their response to a C_∞^Φ rotation. The three z vectors are aligned with the principal axis, and so each has a character 1 for this operation. However, the x and y vectors rotate through an angle Φ (Figure 6.5b) and so, as we saw in Section 4.7, they each have a character of $\cos(\Phi)$. It makes sense to form one reducible representation for the three z vectors and one for the six x and y vectors. The full set of characters for these two reducible representations is given in Table 6.4.

Table 6.4 The reducible representations for the z and (x, y) vectors of CO_2 .

$D_{\infty h}$	E	$2C_\infty^\Phi$...	$\infty\sigma_v$	i	$2S_\infty^\Phi$...	∞C_2
$\Gamma(z)$	3	3	...	3	-1	-1	...	-1
$\Gamma(x, y)$	6	$6 \cos(\Phi)$...	0	-2	$2 \cos(\Phi)$...	0

Problem 6.4: Confirm the character assignments in Table 6.4 using the basis shown in Figure 6.5a. Remember that the improper S_∞^Φ rotation swaps the two O atoms over, whereas the C_∞^Φ rotation does not.

Application of the reduction formula to the groups of infinite order ($D_{\infty h}$ and $C_{\infty v}$) is problematic because the order of these groups $h = \infty$. In this book we have used an approach based on the equation from which the reduction formula was obtained in Section 5.5:

$$\chi_{\Gamma}(C) = \sum_j n_j \chi_j(C) \quad (6.11)$$

This equation says that any reducible representation can be constructed, character by character, from the irreducible representations of the group. This can be used to deduce the irreducible representations present by working through the reducible character set and eliminating combinations that are logically impossible. The process for the two reducible representations for the vibrations of CO_2 is laid out in Figures 6.6 and 6.7, along with checks that the irreducible representations determined give the correct character sums.

$D_{\infty h}$	E	$2C_{\infty}^{\Phi}$...	$\infty\sigma_v$	i	$2S_{\infty}^{\Phi}$...	∞C_2
$\Gamma(z)$	3	3	...	3	-1	-1	...	-1

No 'cos' terms,
so must be
from Σ reps

Must be from
 $3 \times (+1)$, so only
 Σ^+ reps possible

Must be from $2 \times (-1) + 1$,
so have $\Gamma(z) = 2\Sigma_u^+ + \Sigma_g^+$

$D_{\infty h}$	E	$2C_{\infty}^{\Phi}$...	$\infty\sigma_v$	i	$2S_{\infty}^{\Phi}$...	∞C_2
Σ_g^+	1	1	...	1	1	1	...	1
Σ_u^+	1	1	...	1	-1	-1	...	-1
$2\Sigma_u^+ + \Sigma_g^+$	3	3	...	3	-1	-1	...	-1

$\Gamma(z)$

Figure 6.6 The reduction procedure for $\Gamma(z)$ of the z vectors of CO_2 .

$D_{\infty h}$	E	$2C_{\infty}^{\Phi}$...	$\infty\sigma_v$	i	$2S_{\infty}^{\Phi}$...	∞C_2
$\Gamma(x, y)$	6	$6 \cos(\Phi)$...	0	-2	$2 \cos(\Phi)$...	0

Six basis vectors can
only give $6 \cos(\Phi)$ if we
only have Π reps. These
are the doubly
degenerate reps, so we
have three irreducible
reps to find

Must be from $2 \times (-2)$
+ 2, so have
 $\Gamma(x, y) = 2\Pi_u + \Pi_g$

$D_{\infty h}$	E	$2C_{\infty}^{\Phi}$...	$\infty\sigma_v$	i	$2S_{\infty}^{\Phi}$...	∞C_2
Π_g	2	$2 \cos(\Phi)$...	0	2	$-2 \cos(\Phi)$...	0
Π_u	2	$2 \cos(\Phi)$...	0	-2	$2 \cos(\Phi)$...	0
$2\Pi_u + \Pi_g$	6	$6 \cos(\Phi)$...	0	-2	$2 \cos(\Phi)$...	0

$\Gamma(x, y)$

Figure 6.7 The reduction procedure for $\Gamma(x, y)$ of the (x, y) vectors of CO_2 .

By this elimination procedure, the reducible representations are found to be:

$$\Gamma(z) = 2\Sigma_u^+ + \Sigma_g^+ \quad \text{and} \quad \Gamma(x, y) = 2\Pi_u + \Pi_g \quad (6.12)$$

A full basis of three vectors per atom has been used, and so some of these irreducible representations will be for simple motion of the whole molecule and its rotation. The character table shows that movement in x and y belongs to Π_u . This is a doubly degenerate representation, so that only one instance need be removed from $\Gamma(x, y)$.

Similarly, rotations about X and Y axes are degenerate in Π_g . Note that R_z , the symbol for rotation around Z , has not appeared, for any linear molecule rotation around the molecular axis has no effect on the atom coordinates and so is not a degree of freedom for the molecule.

Motion in the Z -direction, on the other hand, is a degree of freedom and has the representation Σ_u^+ . So we are left with the vibrations

$$\Gamma(z) = \Sigma_u^+ + \Sigma_g^+ \quad \text{and} \quad \Gamma(x, y) = \Pi_u \quad (6.13)$$

So, for this linear molecule, we have found four vibrational modes. Σ_g^+ and Σ_u^+ are the symmetric and antisymmetric stretch modes, similar to those found for H_2O . There are also two bending modes, which are degenerate with one another, bending in the XZ plane and bending in the YZ plane. The character table indicates that the antisymmetric stretch and the bending modes are IR active, and so CO_2 can absorb IR radiation from the surface of the Earth.

In this analysis of the linear triatomic CO_2 we have found one more vibration than was obtained for the nonlinear H_2O case. This is due to the loss of the rotational degree of freedom around the molecular axis. Instead of the rotation and single bending mode for H_2O , we find two degenerate bending modes for the linear triatomic case. For a linear molecule containing N atoms there will always be $3N - 5$ vibrational modes, one more than the $3N - 6$ for the nonlinear case.

Problem 6.5: The other greenhouse gas mentioned above is CH_4 , which belongs to the T_d point group. Using the basis shown in Figure 6.8, demonstrate that the C—H stretching modes of this molecule have the reducible representation shown:

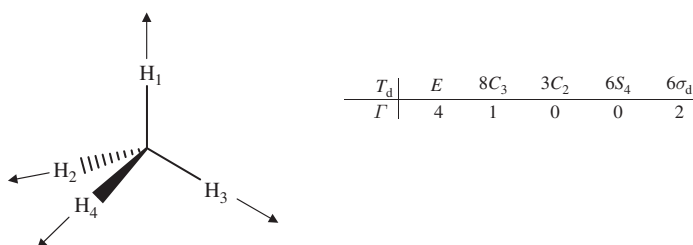


Figure 6.8 A basis of the four C—H bonds for obtaining the reducible representation for the stretching modes of CH_4 . The corresponding reducible representation is shown to the right.

Then apply the reduction formula to show that

$$\Gamma = A_1 + T_2$$

This basis is the four vectors along the C—H bonds and so only vibrational modes due to C—H stretches will be found. This means there is no need to remove translations or rotations after the reduction procedure.

In Problem 6.5 you found that the triply degenerate T_2 modes are contained in the reducible representation for the C—H stretches. In the standard character table this representation has all three of x , y , z , indicating that IR absorption due to the C—H stretching mode will be possible.

6.2.3 Interstellar H₂

In Section 6.2.1 we pointed out that the vibration of a homonuclear diatomic will not be IR active. So where does this leave the spectral bands shown in Figure 6.1 for H₂ from the observations of the Horsehead Nebula in the introduction to this chapter?

It should be remembered that most of the discussion in this chapter is aimed at laboratory analysis under ‘normal’ conditions. We assume that the selection rules are to be applied for molecules initially in the ground vibrational state in an IR spectrometer, so that M_{01} is the important coupling factor and the symmetry of the initial state of the vibration excited by the IR radiation is always totally symmetric. This has led to the simple selection rule that a vibration must have a symmetry representation that matches one of the dipole moment operator components to be IR active.

The H₂ bands observed in the interstellar spectra are actually features of excitation from the electronic ground state for which the effect of vibrations can be seen in the fine structure. The primary excitation is electronic rather than vibrational, and so a different set of selection rules will apply. The origin of vibrational fine structure can be understood in terms of the Franck–Condon approach to electronic excitations discussed in Appendix 9.

The spectra shown in Figure 6.1 require 14 excited vibrational states of the ground electronic state to be taken into account to explain all the fine structure that is seen. The researchers analysing the spectra conclude that H₂ in this interstellar region is being formed on dust particles and then dissociated by intense UV radiation. So the spectra have yielded information on the conditions in this region of space, the presence of dust and the composition of the interstellar gas in chemical terms.

The vibrational fine structure of electronic transitions is also responsible for Raman spectra used in the laboratory. In the next section we discuss the appropriate selection rules for this particular analytical tool.

6.2.4 Raman Spectroscopy

Raman spectroscopy probes the vibrational states of a molecule in a very different way to IR. The photon energy used is much higher (in the visible or UV part of the spectrum) and so causes an electronic rather than vibrational excitation. The light source will be

monochromatic, typically a laser, so that the probe frequency ν_o is set by the experimenter. As light passes through the sample, a small fraction (typically 1/1000th) of the incident beam will be scattered by interaction with the molecular species present. In Raman spectroscopy, the scattered light is sampled and its frequency compared with the probe frequency.

The ability of Raman spectroscopy to give information on the vibrational states of a molecule depends on the role of the vibrational states during the relaxation processes that occur during the scattering event. We will see in the rest of this section that the energy of the scattered photon can differ from that of the incident radiation by an amount linked to the energy of the vibrational states of the molecule. In Raman spectroscopy, the measured frequency differences correspond to the frequencies of the vibrations of the molecules. Of course, not all vibrational modes will be observed since there is a selection rule that controls which modes of a molecule are Raman active.

Electronic Excitation and Molecular Structure

The scattering of light does not require an electronic transition between electronic energy levels to occur, so that the incident light frequency used in Raman spectroscopy need not coincide with the energy required for such a transition. If a tuneable laser is used, then the frequency can be adjusted to give an electronic transition for the molecule of interest; the technique is then referred to as resonance Raman and an increased scattering intensity is observed. In this discussion we will refer to the electronically excited state. In resonance Raman this will also be a stable electronic state of the molecule; in the more usual case of working, off-resonance excitation causes transition to a ‘virtual’ state that only exists for the short time of the scattering event.

To begin, we consider the effect of an electronic excitation on the bonding forces between the atoms of a molecule. It is useful to first consider this as a simple diatomic. The bonding forces can be pictured by drawing a graph of the molecular energy versus bond length, which typically has the shape of a Morse curve, e.g. the lower curve of Figure 6.9a. The lowest energy point on the curve gives the optimum bond length for the molecule.

Compressing the bond leads to a rapid increase in energy, as the nuclear repulsion between the two atom centres overrides the attraction between them due to the electronic bonding states. The origin of these bonding states will be covered in more detail in Chapter 7.

If the molecule is stretched relative to the Morse curve minimum point, the energy again rises as the atoms begin to separate and their bonding interactions weaken. At large separations the two atoms would not be bonding at all and the Morse curve goes to zero.

So far, our description of the molecule depends only on the electronic states and the nuclear repulsion. Molecules are constantly vibrating due to thermal motion, and we have seen that this leads to vibrational states with energies quantized into levels given by Equation (6.1). In the Morse curves of Figure 6.9 this is represented by overlaying the vibrational states on the Morse curve as a series of horizontal lines. This representation was also used with the harmonic approximation to the Morse curve in Figure 6.2.

We can now show how the vibrational states can affect relaxation after an electronic excitation. If an electron is excited by the absorption of a photon it will move to a higher electronic state (be that real or ‘virtual’) and so interact differently with the nuclei and other

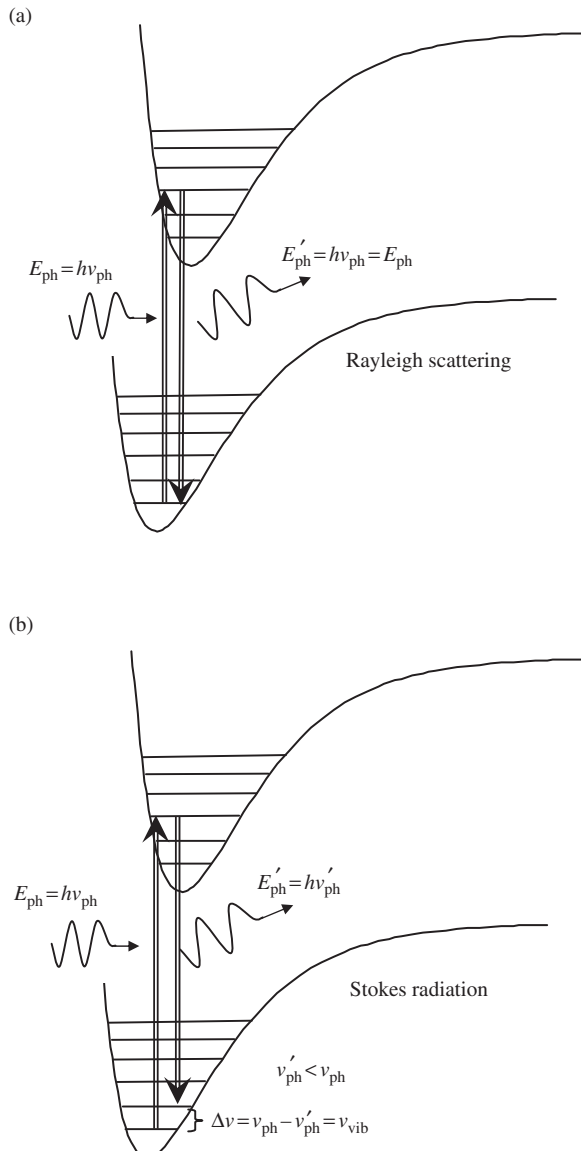


Figure 6.9 (a) Illustration of the Franck—Condon principle for a vertical excitation and re-emission at the same frequency; Rayleigh scattering. (b) The origin of Stokes lines in Raman bands: on relaxation, the emitted photon frequency differs from that absorbed by an amount dependent on the vibrational energy levels. In each diagram, the lower Morse curve represents the electronic ground state with vibrational levels included as a ladder of states. The excited state has a different Morse curve, being higher in energy and shifted to right to indicate longer bonds in the excited state. An electronic excitation is shown vertically on the diagram giving a vibrationally excited molecule in the higher electronic state. (Used with permission from the Journal of Chemical Education (1967) 44:1, page 4; Copyright 1967, Division of Chemical Education, Inc.)

electrons. This will alter the bonding forces discussed above; in particular, the optimum geometry will be different in the electronic excited state to that in the ground state. The excited state is higher in energy than the ground state, and so the excited-state Morse potential is drawn above the ground state in Figure 6.9a.

The difference in energy levels for the electronic states is usually much greater than that for the molecular vibrational states; hence the need for higher energy photons for the excitation! This also means that the two Morse curves are separated further than the spacing between the vibrational energy levels they contain. We think of each electronic state as having a subset of vibrational states. To define the state of the molecule fully we would need to specify the electronic and the vibrational states.

The effect of excitation on the geometry of the molecule is also represented in Figure 6.9a. In the electronic excited state the nuclei will be less strongly bound than the ground state, so that the optimum structure will tend to be expanded by the excitation. This is shown in the figure by placing the optimum of the potential in the excited state to the right of that in the ground state.

The Absorption Process

Since electrons have much lower mass than the nuclei of the molecule, the photon absorption and electron transition can occur much faster than the molecular geometry can respond. Hence, the system will ‘arrive’ in the excited state at the ground-state molecular geometry, as shown by the vertical arrow in Figure 6.9a; indeed, such a process is often referred to as a vertical transition. The idea that electronic transitions occur without an initial change in the molecular geometry is called the *Franck–Condon principle*.

A treatment of the excitation process based on a quantum model is given in Appendix 7. Here, we use the result that, because the excited state Morse curve is shifted to the right in Figure 6.9, the vertical transition implies that it is relatively easy for the molecule to have a vibrational state with a quantum number greater than zero in the electronic excited state. After absorption, the electronic structure will relax back to the ground state and must release the excess energy. The most probable process is to emit a single photon that allows relaxation directly back to the ground state. It is easy to see that this photon will have the same energy, and so the same frequency, as the absorbed photon (Figure 6.9a). This process is referred to as Rayleigh scattering, and the direction in which the photon is emitted is random.

Raman spectroscopy depends on alternative relaxation processes to Rayleigh scattering, for which the energy released as a photon by a molecule during relaxation back to the ground state is different to the energy of the exciting photon. The difference occurs because emission is accompanied by a change in the vibrational state of the molecule.

In Figure 6.9b we see that the molecule starts in an $n = 0$ vibrational state but is returned to the $n = 1$ state. The difference between the exciting photon energy and the photon emitted in the relaxation process is simply the difference in energy between the two vibrational levels; $h\nu_v$. Here the subscript ‘v’ in ν_v is used to emphasize that this is the frequency of the molecular vibrational mode. In the illustration of Figure 6.9b the emitted photon is lower in energy than the exciting photon. This is observed as a band shifted downward in frequency relative to the Rayleigh scattered light; such processes are referred to as Stokes absorptions.

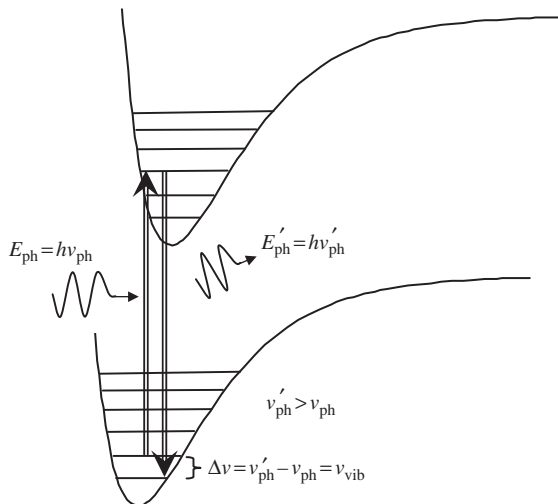


Figure 6.10 Illustration of an absorption leading to an anti-Stokes Raman band. Note that the molecule is initially in a vibrationally excited state.

Anti-Stokes absorptions can also occur; these give a band with higher frequency than the incident light source. However, this requires the system to have initially been in a vibrationally excited state, as shown in Figure 6.10. The thermal population of the excited vibrational states is usually low at normal laboratory temperatures, and so the anti-Stokes bands have lower intensity than the Stokes bands.

Figure 6.11 shows the Raman spectrum for tetrachloromethane. The intensity of the central Rayleigh scattered peak is off the scale: the Raman peaks are only about 1/1000th of the scattered light intensity. For each Stokes peak to the left of the centre there is a corresponding anti-Stokes band to the right. The anti-Stokes bands have lesser intensity, reflecting the low number of molecules in the electronic ground state which are vibrationally excited.

The Selection Rule for Raman Spectroscopy

Figures 6.9 and 6.10 illustrate the energy balance for the Raman process but do not tell us about the selection rules that must be applied. To illustrate how the selection rules come about, a classical, non-quantum, picture is actually quite useful as a starting point. Figure 6.12 shows the classical picture of a molecule of urea as a light wave of UV frequency passes.

The light wave causes oscillations in the electromagnetic field and the diagram illustrates how the electrons respond to the electric component. In the quantum model we have used the Franck–Condon principle, which states that the electronic transition occurs on a much shorter timescale than any nuclear motion. Correspondingly, at the UV/visible frequency, in this classical approach the nuclei of the molecule are too slow to respond, but the electron density will move in sympathy with the frequency of the light. The charge densities illustrated in Figure 6.12 show this effect. In this illustration, when the phase of the

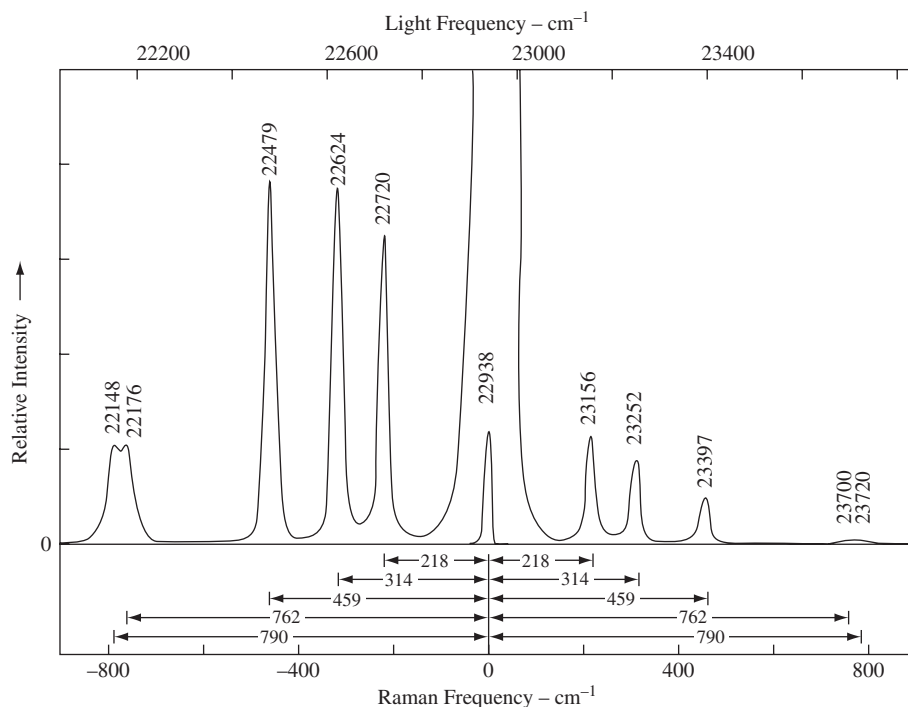


Figure 6.11 Raman spectrum of tetrachloromethane (carbon tetrachloride) taken using the blue line of a mercury arc lamp to give an exciting frequency of $22\ 938\ \text{cm}^{-1}$. The top scale shows the wavenumber of the radiation detected, the Rayleigh line is shown in the centre of the diagram and the bottom scale shows the relative frequency shift. Stokes lines occur at lower frequencies to the left of the Rayleigh line and anti-Stokes to the right. (Used with permission from the Journal of Chemical Education 77:5 (1967). Copyright 2000, Division of Chemical Education, Inc.)

electric field is positive, movement of the electron density to the right occurs, whereas the charge cloud moves to the left with a negative field. So the dipole moment of the molecule will be constantly changing because the negative charge of the electrons is shifting at the frequency of the exciting radiation. The effect of the field is opposed by the presence of the charged nuclei, which try to restore the charge density to the zero field situation.

The induced dipole μ_{ind} will depend on the particular molecule under consideration, and the controlling molecular property is called the polarizability α of the molecule:

$$\mu_{\text{ind}} = \alpha E \quad (6.14)$$

where E is the electric field of the light wave. The polarizability α is constant for the molecule fixed at its equilibrium geometry, and so the induced dipole oscillates at the frequency of the light and re-emits that frequency in all directions (except the direction of the induced dipole vector itself). This gives rise to the Rayleigh scattering line at the centre of all Raman spectra. However, as the molecule vibrates, the relationship between

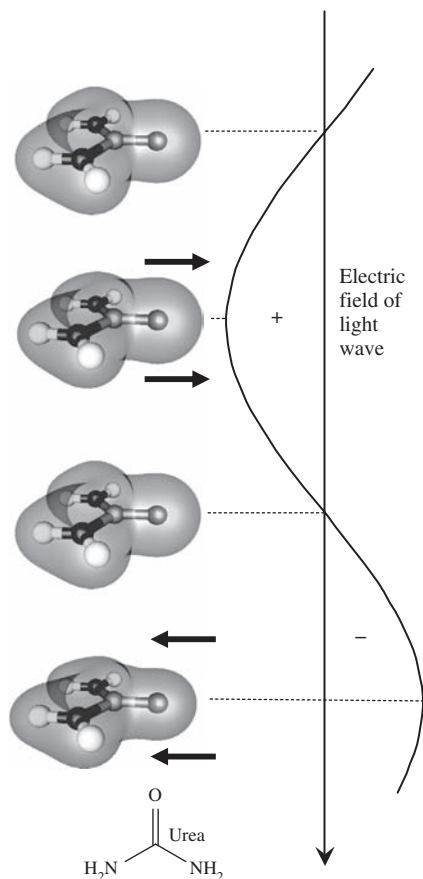


Figure 6.12 An illustration of the polarization of electron density by a light wave in the classical picture. The electric field variation is shown to the right and plots of the electron density of urea at various points in the oscillation of the electric field are illustrated to the left. When the phase of the electric field is positive, the electron density moves to the right; when the phase is negative, the density moves to the left. These changes of the molecular dipole moment through polarization of the electron density require energy, which is absorbed from the light wave. The chemical structure of urea (CN_2OH_4) is shown bottom left.

the nuclei and the electron density is changing and so, potentially, the polarizability of the molecule will be changed by the molecular vibration. We show in Appendix 8 that this change of polarizability can lead to shifts in the emitted light frequencies giving the Stokes/anti-Stokes bands if the vibration causes a change in the polarizability of the molecule. Moving back to the quantum picture, this gives the coupling factor:

$$M_{01} = \int_{-\infty}^{\infty} \psi_1 \Delta\alpha \psi_0 \, d\tau \quad (6.15)$$

where $\Delta\alpha$ is the change in the molecular polarizability when the vibrational state shifts from $n = 0$ to $n = 1$, i.e. from ψ_0 to ψ_1 . The selection rules are now based on the fact that

only vibrations belonging to certain irreducible representations can have nonzero values of the coupling integral, Equation (6.15).

So far, the induced dipole moment has been treated as a simple number. However, a dipole has a definite size and direction, i.e. it is a vector quantity, as is the electric field of the light wave. In general, α must be a matrix which relates the three components of E to the three components of μ_{ind} :

$$\begin{pmatrix} \mu_x \\ \mu_y \\ \mu_z \end{pmatrix} = \begin{pmatrix} \alpha_{xx} & \alpha_{xy} & \alpha_{xz} \\ \alpha_{yx} & \alpha_{yy} & \alpha_{yz} \\ \alpha_{zx} & \alpha_{zy} & \alpha_{zz} \end{pmatrix} \begin{pmatrix} E_x \\ E_y \\ E_z \end{pmatrix} \quad (6.16)$$

The matrix allows for the dipole due to polarization being in a different direction to the field of the radiation. For instance, an electric field in the x -direction may induce a dipole in the y - or z -directions. The matrix is symmetric, so $\alpha_{xy} = \alpha_{yx}$, etc., and there are only six independent coefficients. If the molecular vibration causes a change in any of the components of α we will see a band in the Raman spectrum. Just as in the case of the IR selection rules, we find that only vibrations whose irreducible representations match one or more of the representations appropriate to the components of α can have nonzero coupling elements.

The three diagonal elements of the Cartesian polarization matrix can be simplified to two in spherical polar coordinates in a similar way to the d-orbital functions considered in Section 5.8. So, in the character tables, functions used for the d-orbitals can also be used to identify Raman-active vibrational modes. Thus, the Raman selection rule can be stated as follows.

Raman bands arise for molecular vibrations which alter the polarizability of a molecule. The polarizability coefficients transform as $z^2, x^2 - y^2, xy, xz, yz$ and so are in the same representations as the products of axes shown in the right-hand column of a character table for the molecular point group. A vibration must have one of these representations to be Raman active.

6.2.5 Comparison of Infrared and Raman Selection Rules

We have now discovered that the selection rules for Raman and IR spectra are different. The IR selection rule requires a vibration to belong to the same irreducible representation as x, y, z , whereas vibrations are Raman active if they belong to irreducible representations for the products of axes. This means that vibrations that show up in IR spectra need not be present in Raman and vice versa.

In particular, if a molecule belongs to a point group containing the inversion centre, then IR active vibrations must be *ungerade*. We can now see that Raman-active modes in the same situation must be *gerade* because the products of x, y, z will be unchanged by the inversion operation. For example, in Section 6.2.1 we found the *gerade* representation Σg^+ for the single vibrational mode of a homonuclear diatomic molecule. In the standard character table the right-hand column shows that this representation is also used for the function z^2 . So the bond stretch of homonuclear diatomic molecules is Raman active.

For more complex molecules in point groups with the inversion, centre vibrations that are IR active will also have irreducible representations that are *ungerade* while Raman-active modes will be *gerade*. Since different vibrations will usually occur at different frequencies, it is unlikely that bands in the two spectra will appear to be coincident. For example, *trans*-1,2-dichloroethene has an inversion centre as it belongs to the point group C_{2h} , the IR and Raman spectra for this molecule are compared in Figure 6.13a. This molecule has six atoms, and so $3 \times 6 - 6 = 12$ vibrational modes. The total number of bands in the Raman and IR spectra is fewer than 12 because some vibrations are too low frequency to be detected in the range shown. However, it can be seen that the Raman and IR frequencies are indeed different to one another.

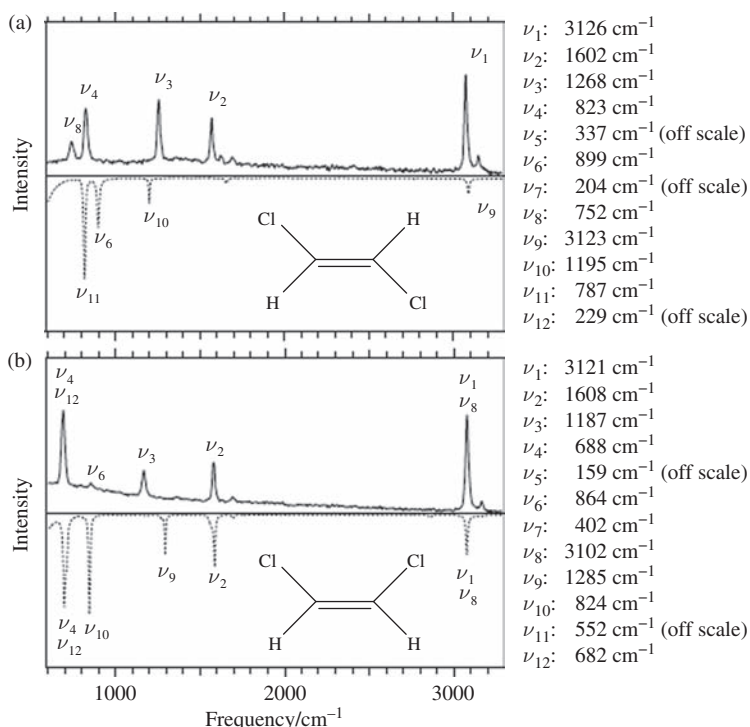


Figure 6.13 Comparison of IR and Raman spectra for the isomers: (a) *trans*-1,2-dichloroethene (C_{2h}); (b) *cis*-1,2-dichloroethene (C_{2v}). Raman spectra are shown as solid lines and IR spectra are shown as dotted lines with peaks pointing downward (the measured transmittance T was converted to absorbance A using $A = -\log T$). The listed vibrational frequencies were estimated using a computer modelling package; those marked ‘off scale’ are below the range of the experimental spectrometers. Peaks marked as two vibrations have distinct frequencies but cannot be resolved by this apparatus. (Source: McClain BL, Clark SM, Gabriel RL, Ben-Amotz D (2000) Journal of Chemical Education 77: 654.)

This is not the case for molecules that belong to other point groups. For example, the *cis* isomer of 1,2-dichloroethene belongs to the C_{2v} point group. Here, the character table

in Appendix 12 shows that the A_1 irreducible representation has both z and z^2 assigned to it, and so a totally symmetric vibration will be present in both IR and Raman spectra. The spectra for *cis*-1,2-dichloroethene are shown in Figure 6.13b, and several bands can be seen to be coincident.

6.3 General Approach to Analysing Vibrational Spectroscopy

We are now in a position to predict the bands that may exist in the vibrational spectra (IR or Raman) for a given molecule. A few examples have already been covered, but the steps that should be followed can be summarized as follows:

1. Decide on the point group of the molecule using the symmetry operations the atoms obey.
2. Decide on a basis for the vibrations of interest. The complete basis for vibrational modes is a set of three vectors on each atom, but a simpler basis may be more convenient to give information on specific vibrations.
3. Generate the reducible representation Γ of the basis by assigning characters for each basis vector according to the effect of an example operation from each class. If a basis vector is unaffected by the operation, then it contributes 1 to Γ ; if it is reversed, then it gives -1 ; and if it changes completely (e.g. if the atom on which the basis vector is sited moves), then a contribution of 0 results. Intermediate values occur for rotated basis vectors, as discussed in Section 4.7. Γ is then the sum of the characters obtained for the members of the basis set; one summation for each class of operations in the point group.
4. (a) For a nonlinear molecule, reduce the representation to its components using the reduction formula:

$$n_i = \frac{1}{h} \sum_c g_c \chi_{\Gamma}(C) \chi_i(C) \quad (6.17)$$

which gives the number of times n_i that representation i (A_1 , A_2 , etc.) occurs in the reducible representation Γ . The summation is across the classes of the point group and contains terms which are the product of the number of operations g_c in class C , with the characters from the reducible and irreducible representations for that class, $\chi_{\Gamma}(C)$ and $\chi_i(C)$ respectively. The order of the group h is the total number of operations in the group which can be obtained by summing the values of g_c from the column headings for the group classes. It is useful to carry out this process using tables to lay out the terms in the summation.

(b) Linear molecules will belong to either the $C_{\infty v}$ or $D_{\infty h}$ point groups, both of which have $h = \infty$. To carry out the reduction step we make use of the relationship

$$\chi_{\Gamma}(C) = \sum_i n_i \chi_i(C) \quad (6.18)$$

That is, the character of the reducible representation in any class of the point group will be the sum of the characters from its component irreducible representations. This must be true for all classes, and so we can work across the columns of the character table eliminating combinations that do not comply until a unique solution is found.

This approach was used in our discussion of the IR absorption properties of CO₂ in Section 6.2.2.

5. If the basis captures molecular movement or rotation, then remove the corresponding representations. For example, if three vectors per atom are used for a full vibrational analysis of a nonlinear molecule, then we will find six irreducible representations that do not describe vibration, one each from the group's standard representations for x , y , z and R_x , R_y , R_z . For a linear molecule, rotation around the molecular axis R_z is not a degree of freedom and an additional vibrational mode will be found.
6. Use the character table to decide which modes are IR and which Raman active. The IR-active modes will be the remaining representations that have labels corresponding to those of x , y or z in the character table. The Raman-active modes will be those belonging to the representations for products of x , y , z usually written as z^2 , $x^2 - y^2$, xy , xz and yz .

In the following section we cover an example of the application of this recipe.

6.3.1 Example: the C—H Stretch Bands of 1,4-Difluorobenzene

With the addition of the selection rules we now have enough tools to use symmetry to decide on the irreducible representations for the vibrations of a particular molecule and then pick out those modes which are IR and/or Raman active. In this example we will apply the general approach above to the C—H stretching modes of 1,4-difluorobenzene.

1. *Symmetry point group assignment.* The structure of 1,4-difluorobenzene is shown in Figure 6.14a. This molecule is a simple substituted benzene. In benzene there is a C_6 axis through the centre of the ring perpendicular to the molecular plane. However, because of the two fluorine atom substituents, this is not a symmetry element for 1,4-difluorobenzene; the corresponding axis is only C_2 . There are two other C_2 axes present in the plane of the molecule, one joining the fluorine atoms and the other perpendicular, bisecting the (H)C—C(H) bonds.

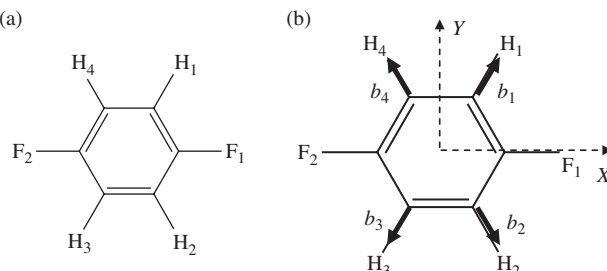


Figure 6.14 (a) The structure of 1,4-difluorobenzene and (b) a suitable basis for the analysis of the C—H stretching modes of this molecule; the Z -axis is perpendicular to the plane of the molecule pointing out of the page.

The choice of principal from the three C_2 axes is arbitrary, but it is common to take Z perpendicular to the molecular plane. In Figure 6.14b, X is then taken to be collinear with the C—F bonds and Y is set to give a right-handed axis system (turning from X to

Y will take a right-handed screw in the Z -direction). The rotation axes are then labelled according to the direction in space with which they are aligned: $C_2(X)$, $C_2(Y)$, $C_2(Z)$.

There are also three mirror planes, $\sigma(XY)$, $\sigma(YZ)$ and $\sigma(XZ)$; so, whichever axis we choose as principal, one of these will be a horizontal mirror plane σ_h . Following the flow chart given in Figure 3.29, we assign the point group D_{2h} and note that the molecule must also have an inversion centre i .

2. *Basis set choice.* In this example we are only interested in the C—H stretching frequencies. These will be distinct from other modes because the small mass of the H atoms results in relatively high-frequency vibrations (around 3000 cm^{-1}). There are four C—H bonds, and so the four basis vectors $b_1 - b_4$ in Figure 6.14b will form the basis set.
3. *Generate the reducible representation.* By carrying out an example operation from each class of the point group we can examine the effect on the basis vectors, remembering that a basis vector that does not change contributes a character of 1 and a basis vector that is reversed gives a character -1 . The movement of a basis vector to a different position in the molecule implies off-diagonal elements in the operation matrix and a zero on the diagonal, i.e. a character of 0. Applying this to the case of the $b_1 - b_4$ basis in Figure 6.14b gives the results of Table 6.5.

Table 6.5 The reducible representation for C—H stretch modes of 1,4-difluorobenzene.

D_{2h}	E	$C_2(Z)$	$C_2(Y)$	$C_2(X)$	i	$\sigma(XY)$	$\sigma(XZ)$	$\sigma(YZ)$
Γ	4	0	0	0	0	4	0	0

4. *Reduce the representation.* The sums formed in the application of the reduction formula are given in Table 6.6. In this table the symmetry classes that have reducible representation characters of 0 are omitted as they will not contribute to the totals in any irreducible representation. The order of the D_{2h} point group $h = 8$, so that the reduction process yields

$$\Gamma = A_g + B_{1g} + B_{2u} + B_{3u} \quad (6.19)$$

5. *Remove molecular movement/rotation.* This basis is designed to include only specific bond vibrations, so no molecular translations or rotations need to be removed.

Table 6.6 Reduction of the reducible representation for C—H stretch modes of 1,4 difluorobenzene: (a) gerade and (b) ungerade irreducible representations. Note that only classes with nonzero character for Γ from Table 6.5 are considered here.

(a)			(b)		
D_{2h}	E	$\sigma(XY)$	D_{2h}	E	$\sigma(XY)$
Γ	4	4	Γ	4	4
	$g_c \chi_i(C) \chi_\Gamma(C)$	\sum_C		$g_c \chi_i(C) \chi_\Gamma(C)$	\sum_C
A_g	4	4	A_u	4	-4
B_{1g}	4	4	B_{1u}	4	-4
B_{2g}	4	-4	B_{2u}	4	4
B_{3g}	4	4	B_{3u}	4	4

6. Identify IR- and Raman-active modes. From the standard D_{2h} character table in Appendix 12, the right-hand columns indicate the following:

- IR active – B_{2u} and B_{3u} , which correspond to transition dipole moments in y and x respectively. Note that the basis is confined to the XY plane and so does not capture C–H out-of-plane bending modes, which would be at much lower frequencies than the stretching modes of interest here.
- Raman active – A_g and B_{1g} , which have x^2 , y^2 , z^2 and xy respectively in the rightmost column.

This is an example of a point group with an inversion centre and so we have found only *ungerade* modes as IR active and only *gerade* modes as Raman active. Even though there are four vibrational states, we will only see two absorption bands in the IR and two in the Raman spectra, and the IR and Raman band frequencies are not likely to coincide.

Problem 6.6: The structure of 1,2-difluorobenzene is shown in Figure 6.15. This isomer belongs to the C_{2v} point group. Using a basis of the four C–H bonds, demonstrate that the reducible representation in this case is that shown in Table 6.7 and apply the reduction formula to show that

$$\Gamma = 2A_1 + 2B_2 \quad (6.20)$$

Using the standard character table, identify those modes which will be IR active and those that will be Raman active. In this case, there is no inversion operation in the point group and so a vibration may be both IR and Raman active.

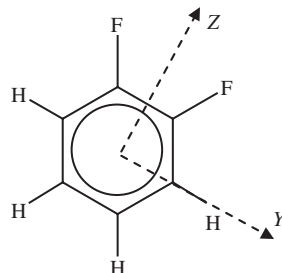


Figure 6.15 The structure of 1,2-difluorobenzene.

Table 6.7 The reducible representation for C–H stretch modes of 1,2-difluorobenzene.

C_{2v}	E	C_2	$\sigma_v(XZ)$	$\sigma_v'(YZ)$
Γ	4	0	0	4

The above example and problem cover the symmetry analysis of two isomers of difluorobenzene. We find that the 1,4-isomer has only two bands in each of the IR and Raman spectra and that these bands will not coincide. In contrast, the 1,2-isomer has all four C–H vibrations active in both IR and Raman spectra and so, clearly, there will be bands common to both techniques.

This sort of analysis provides a powerful use of spectroscopy to aid in the identification of molecular structure through the application of symmetry. If we had made a sample of difluorobenzene and believed it to be a pure isomer of either the 1,4- or 1,2-form, vibrational spectroscopy would provide one way to distinguish which isomer we had made.

Problem 6.7: Figure 6.13 shows the experimental spectra of two isomers of 1,2-dichloroethene. The set of basis arrows shown in Figure 6.16 is one possible choice of the three arrows per atom for a complete basis. This choice has the advantage that each atom has one basis arrow perpendicular to the molecular plane and one aligned with a bond.

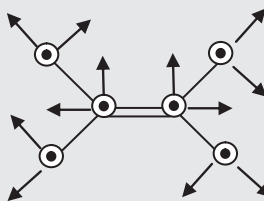


Figure 6.16 One choice for a complete basis set for either isomer of 1,2-dichloroethene. The \odot symbol is used to imply an arrow coming out of the page.

1. Show that the irreducible representations for the 12 vibrational modes are:

$$C_{2h} : \Gamma = 5A_g + B_g + 2A_u + 4B_u \quad (6.21)$$

$$C_{2v} : \Gamma = 5A_1 + 2A_2 + B_1 + 4B_2 \quad (6.22)$$

(remember to align Z-direction with the principal axis, with Y in the molecular plane for C_{2v}).

How many IR and Raman bands would you expect to see in the spectra of each isomer of 1,2-dichloroethene? Is your prediction higher or lower than seen in the experimental spectra?

2. For *cis*-1,2-dichloroethene, some bands are too weak to be detected in the experimental spectra. However, all active modes in the frequency range of the spectrometer can be seen for *trans*-1,2-dichloroethene (Figure 6.13a). The modes that are off scale in Figure 6.13 have the atom displacements shown in Figure 6.17. Assign irreducible representations to each of these modes and hence decide on their IR or Raman activity. Using this information, confirm the number of modes predicted in part (1) is correct.

6.4 Symmetry-Adapted Linear Combinations

The preceding sections have shown how to use symmetry analysis on a basis of vectors to determine the irreducible representations for molecular vibrations. In building the reducible representation the basis vectors are treated as individual objects to which characters are assigned. This makes the total character for the basis easy to calculate by summing the results for each of the basis vectors in isolation.

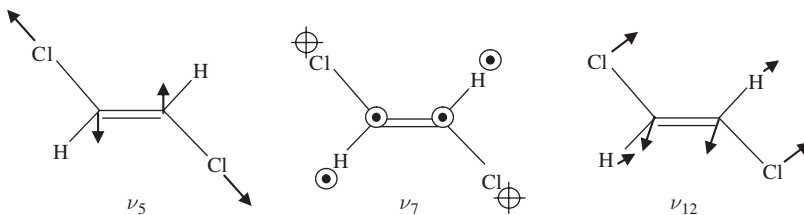


Figure 6.17 The atomic motions in the ‘off-scale’ vibrations of *trans*-1,2-dichloroethene from Figure 6.13. The \odot symbol is used to imply motion out of the page \oplus and indicates motion into the page. These symbols are placed to the side of the atom labels to avoid obscuring them. In these diagrams the C–Cl bonds are shown to be longer than the C–H or C=C bonds, as they are.

We have also looked at specific examples of the molecular vibrations themselves; these are usually collective motions of the atoms. For example, the symmetric and antisymmetric stretch modes of H_2O are shown as $\nu(A_1)$ and $\nu(B_2)$ in Figure 5.3, and Figure 6.17 shows three modes of *trans*-1,2-dichloroethene to which single symmetry labels were assigned as part of Problem 6.7.

What is now required is a method which can be applied after the reduction process to give the collective motion of each irreducible representation in terms of the basis automatically. This is the job of the projection operator, which is explained in the next section. Here, the use of the basis to describe collective motions of the atoms of a molecule is discussed so that it is clear what the projection operator is aiming for.

Collective functions formed from the basis which belong to a particular irreducible representation are referred to as symmetry adapted linear combinations (SALCs). In essence, each SALC can be thought of as a sum over all the basis functions:

$$\phi_i = \sum_j c_{ij} b_j \quad (6.23)$$

where ϕ_i is the i th SALC function, b_j is the j th basis function and c_{ij} is a coefficient which controls how much of b_j appears in ϕ_i . The values of c_{ij} can be positive, negative or even zero. The projection operator is used to find the coefficients consistent with each irreducible representation.

As a simple example, the O–H stretching modes of H_2O could be obtained from the basis of the two O–H bonds shown in Figure 6.18a.

Problem 6.8: Confirm that the basis of Figure 6.18a leads to the reducible representation shown in Table 6.8 and, hence, that

$$\Gamma = A_1 + B_2 \quad (6.24)$$

In the symmetric stretch (A_1) mode, shown in Figure 6.18b, the two H atoms move in phase with one another while in the antisymmetric (B_2) motion the H atoms are out of phase. This can be captured by setting

$$\phi(A_1) = b_1 + b_2 \quad (6.25)$$

and

$$\phi(B_2) = b_1 - b_2 \quad (6.26)$$

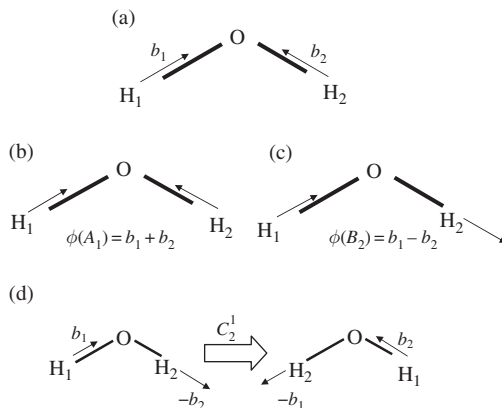


Figure 6.18 (a) A simplified basis of the two O–H bond vectors for the stretching modes of H_2O . (b) The SALC for the symmetric stretch mode and (c) the SALC for the antisymmetric stretch mode. (d) The effect of a C_2^1 rotation on the B_2 mode; note that after the operation the basis vectors are labelled relative to the original setting of (a).

Table 6.8 The reducible representation for the O–H bond vectors in H_2O .

C_{2v}	E	C_2	$\sigma_v(XZ)$	$\sigma_v'(YZ)$
Γ	2	0	0	2

These are linear combinations of the type suggested by Equation (6.23). The symmetric mode (Equation (6.25)) has been arbitrarily chosen as mode 1, so we have $c_{11} = c_{12} = 1$, and the asymmetric mode as mode 2 has $c_{21} = 1, c_{22} = -1$. In this way the individual modes can be thought of as sets of coefficients for the basis functions. Because the basis is simplified to two bond vectors, this analysis does not give the O atom motion that is shown in Figure 5.3; however, since the symmetry analysis for these two modes does not require this part of the motion, we will ignore it for now.

To see how these SALCs conform to the symmetry irreducible representations, it is interesting to consider the affect of the C_{2v} symmetry operations on the functions themselves. For example, after a C_2^1 operation the two H atoms swap over and so do the basis vectors. However, the mode is a function of both vectors, and it is the symmetry of the overall function that determines the value of its character. Looking at the result for each function as a whole, there are still vectors at H₁ and H₂. For the symmetric mode, b₁ and b₂ will have swapped but the function looks identical: it is still $b_1 + b_2$, so has a character of 1. In terms of the old basis, b₁ has become b₂ and vice versa.

For the antisymmetric mode, b₁ and b₂ would also be swapped by a C_2^1 rotation, but the sign of b₂ was opposite to b₁ so the function changes sign, i.e.

$$\phi(B_2) = b_1 - b_2 \xrightarrow{C_2^1} b_2 - b_1 = -\phi(B_2) \quad (6.27)$$

Now the function as a whole has a character of -1 , as required by the B_2 irreducible representation. Note that in doing this comparison the vector which has ‘arrived’ at the original H_1 position is compared with the original b_1 , i.e. we are expressing the transformed basis in terms of the original vectors, as shown in Figure 6.18d.

Problem 6.9: The results each of the operations in C_{2v} on $\phi(A_1)$ and $\phi(B_2)$ are summarized in Table 6.9. Confirm that the set for $\phi(B_2)$ are correct using the method described for the C_2 example above.

Table 6.9 The results and corresponding characters of C_{2v} operations on the symmetric (A_1) and antisymmetric (B_2) modes derived from the O–H bond basis.

C_{2v}	E	C_2	$\sigma_v(XZ)$	$\sigma_v'(YZ)$
$\phi(A_1) = b_1 + b_2$	$b_1 + b_2$	$b_1 + b_2$	$b_1 + b_2$	$b_1 + b_2$
Character	1	1	1	1
$\phi(B_2) = b_1 - b_2$	$b_1 - b_2$	$-b_1 + b_2$	$-b_1 + b_2$	$b_1 - b_2$
Character	1	-1	-1	1

6.5 Normalization

Symmetry cannot tell us about the frequency of a vibration or the amplitude of oscillation, because these are determined by physical factors such as the bond strengths and atomic masses for the particular molecule being studied. Symmetry does give information on the phase pattern for each fundamental vibrational mode of the molecule, i.e. the relative directions of motion of atoms. It is useful to separate this factor from the physical factors by choosing the coefficients in Equation (6.23) so that the length of the vector of coefficients is 1. Then, if some other method is available to calculate the magnitude of the vibration, we simply multiply the mode produced from symmetry analysis by that magnitude. The basis set vectors themselves are chosen to represent directions of motion, and so their lengths can also be taken as 1.

To find the magnitude of any vector we can make use of the vector dot product, defined as

$$\mathbf{a} \cdot \mathbf{b} = |\mathbf{a}| |\mathbf{b}| \cos \theta \quad (6.28)$$

where the vertical lines indicate the length or magnitude of a vector and θ is the angle between the two vectors. This gives the apparently trivial result that

$$\mathbf{b}_1 \cdot \mathbf{b}_1 = \mathbf{b}_2 \cdot \mathbf{b}_2 = 1 \quad (6.29)$$

i.e. the vector dot product of any basis vector with itself is the square of the magnitude of the vector (since $\cos(0) = 1$). This will be useful when we come to find the magnitude of a linear combination of vectors (see below).

The basis vectors have also been chosen so that they are independent of one another, i.e. the motion of H_1 can only be described using b_1 and the motion of H_2 can only

be described using b_2 . This means the basis vectors are orthogonal to one another, and so

$$\mathbf{b}_1 \cdot \mathbf{b}_2 = 0 \quad (6.30)$$

This result is not based on the geometry of the problem: \mathbf{b}_1 and \mathbf{b}_2 are not at 90° ; it is simply a consequence of the independence of the basis vectors.

For the fundamental modes represented as SALCs, normalization requires a magnitude of 1. Taking the dot product of a whole SALC with itself will give the square of the magnitude (from Equation (6.28) with $\theta = 0^\circ$), which must also be 1. To ensure that any arbitrary mode has this property, we choose a factor, called the normalization factor N , and scale the vibrational mode to fulfil this constraint. Writing

$$\phi_i = N \sum_j c_{ij} b_j \quad (6.31)$$

the normalization factor can be worked out by taking the dot product of the function with itself and then finding N in terms of the coefficients of the basis vectors. For instance, in our H₂O stretching mode example, we require

$$\phi_1 \cdot \phi_1 = N^2 (\mathbf{b}_1 + \mathbf{b}_2) \cdot (\mathbf{b}_1 + \mathbf{b}_2) = 1 \quad (6.32)$$

Since \mathbf{b}_1 and \mathbf{b}_2 are orthogonal and normalized, we can use Equations (6.29) and (6.30) to multiply out the brackets to give

$$2N^2 = 1 \quad (6.33)$$

and so find

$$N = \frac{1}{\sqrt{2}} \quad (6.34)$$

The same factor also applies to the antisymmetric vibration, and so the normalized modes are written as follows:

symmetric stretch	$\phi(A_1) = \frac{1}{\sqrt{2}}(\mathbf{b}_1 + \mathbf{b}_2)$
antisymmetric stretch	$\phi(B_2) = \frac{1}{\sqrt{2}}(\mathbf{b}_1 - \mathbf{b}_2)$

(6.35)

This dot product example shows that, provided the basis set is orthogonal and normalized, the normalization factor for the i th linear combination of basis functions will be simply related to the corresponding coefficients, i.e.

$$N_i = \frac{1}{\sqrt{\sum_{j=1}^n c_{ij}^2}} \quad (6.36)$$

Problem 6.10: One of the fundamental modes for the N—H stretch in ammonia (C_{3v}) is a symmetric stretch, which can be written

$$\phi = N(b_1 + b_2 + b_3) \quad (6.37)$$

using the basis vectors defined in Figure 4.6. Calculate the normalization factor N in this case, assuming b_1 – b_3 are orthogonal and normalized.

6.6 The Projection Operator Method

The projection operator method for obtaining a picture of the motion represented by each of the irreducible representations begins by considering the effect of each operation in the group on one, or a subset, of the basis vectors for the symmetry-related atoms.

Let us illustrate the method by finding SALCs equivalent to Equations (6.25) and (6.26), which were simply stated in Section 6.4, using the two-vector basis for the O—H stretching modes of water shown in Figure 6.18a. If we take the b_1 basis vector, which is along the O—H₁ bond, and apply each of the C_{2v} operations, the results obtained are as given in the first row of Table 6.10. The E and $\sigma_v'(YZ)$ operations (the plane of the molecule) do not affect the positions of the basis vectors, and so b_1 is simply transformed into itself. In contrast, the C_2 and $\sigma_v(XZ)$ operations swap over b_1 and b_2 ; these two basis functions are linked by the operations of the group.

Table 6.10 The result of each of the C_{2v} operations on the generating vector b_1 and the resulting functions using the characters from each irreducible representation as coefficients in linear combinations.

C_{2v}	E	C_2	$\sigma_v(XZ)$	$\sigma_v'(YZ)$	Sum
b_1	b_1	b_2	b_2	b_1	
A_1	b_1	b_2	b_2	b_1	$2(b_1 + b_2)$
A_2	b_1	b_2	$-b_2$	$-b_1$	0
B_1	b_1	$-b_2$	b_2	$-b_1$	0
B_2	b_1	$-b_2$	$-b_2$	b_1	$2(b_1 - b_2)$

Table 6.10 also shows the result of multiplying the result of each operation by a character in an irreducible representation and then summing the results to give a function of b_1 and b_2 . The sums for the irreducible representations A_1 and B_2 generate the functions of the same symmetry we have already seen, give or take a numerical scaling factor. The sums for the other irreducible representations are zero.

This very useful result is the basis of the projection operator method. The ‘projection’ is the use of the operations from the group to give the effect for a particular ‘generating’ basis vector, e.g. a C_2 rotation transforms b_1 into b_2 . The character multiplications give the correct relationship between the original and projected vector for the particular irreducible representation. In a B_2 vibration (Figure 6.18c), the vector actually present at H₂ is in the opposite direction to the C_2 projection of b_1 , and the multiplication by the appropriate

character from B_2 gives the required minus sign. Summation of the results collects together a linear combination of basis vectors that is bound to follow the irreducible representation. If this summation gives zero, then there is no projection of the generating basis vector that conforms to the irreducible representation.

The two nonzero sums have the same relationship between b_1 and b_2 as was found earlier; normalization, as set out in Section 6.5, would yield the standard forms of Equation (6.35).

In this example, we have used a basis of two vectors and constructed two SALCs, so the job is done; both modes that the basis can represent have been obtained from a single generating vector. We will see below that this is not always the case.

Problem 6.11: Show that using b_2 as the generating vector would lead to conclusions equivalent to those drawn from Table 6.10. Remember that the SALCs only tell us about the *relative* motion of the two O—H bonds.

For the general case, the projection method automates this process through the application of the equation

$$P_i = \sum_j \chi_i(j) T_j v \quad (6.38)$$

where i refers to an irreducible representation in the point group for the molecule and j is an index indicating a symmetry operation in the group. T_j is the j th symmetry operation and it acts on the generating vector v . The character for the i th irreducible representation under the j th operation is given the symbol $\chi_i(j)$. Note that, unlike the reduction formula, the sum is over *all* the operations of the group, rather than the classes of operations.

6.6.1 Projection Operator Applied to the C—H Stretches of 1,4-Difluorobenzene

The relative motions can be more complex when we have a larger set of basis vectors; however, the idea of using the basis to build up the fundamental modes using the projection operator can still be used. Each mode will be described by a symmetry adapted linear combination (SALC) of the basis vectors used in the symmetry analysis.

As an example application of the projection operator to a slightly more complex case, we will return to the C—H stretch vibrations of 1,4-difluorobenzene that were first met in Section 6.3.1. There, the basis vectors were labelled b_1 to b_4 for the C—H₁ to C—H₄ bonds (Figure 6.14b). Applying the reduction formula to this basis yielded

$$\Gamma = A_g + B_{1g} + B_{2u} + B_{3u} \quad (6.39)$$

To apply the projection operator, we arbitrarily select b_1 as the generating vector and then consider the result of each operation of the point group in turn. This is laid out in Table 6.11 along the row labelled $T_j b_1$. T_j is used in the projection operator to represent the j th operation of the group. So here, $j = 1$ would mean the E operation, $j = 2$ the $C_2(Z)$ rotation, etc. This first row of the table lists the transformed b_1 vector in terms of the original basis in each case. So, for example, reflection in the $\sigma(XZ)$ would send b_1 to the b_2 position.

Table 6.11 Application of the projection operator to the irreducible representations found for the C—H stretch modes of 1,4-difluorobenzene. For basis set and reference axis system see Figure 6.14b.

D_{2h}	E	$C_2(Z)$	$C_2(Y)$	$C_2(X)$	i	$\sigma(XY)$	$\sigma(XZ)$	$\sigma(YZ)$	$\mathbf{P}_i b_1 = \sum_j \chi_i(j) \mathbf{T}_j b_1$
$T_j b_1$	b_1	b_3	b_4	b_2	b_3	b_1	b_2	b_4	
$A_g T_j b_1$	b_1	b_3	b_4	b_2	b_3	b_1	b_2	b_4	$2(b_1 + b_2 + b_3 + b_4)$
$B_{1g} T_j b_1$	b_1	b_3	$-b_4$	$-b_2$	b_3	b_1	$-b_2$	$-b_4$	$2(b_1 - b_2 + b_3 - b_4)$
$B_{2u} T_j b_1$	b_1	$-b_3$	b_4	$-b_2$	$-b_3$	b_1	$-b_2$	b_4	$2(b_1 - b_2 - b_3 + b_4)$
$B_{3u} T_j b_1$	b_1	$-b_3$	$-b_4$	b_2	$-b_3$	b_1	b_2	$-b_4$	$2(b_1 + b_2 - b_3 - b_4)$

Application of the projection operator (Equation (6.38)) for a particular irreducible representation involves multiplying these results by the correct character for the operation and then summing the results. The terms generated for the four irreducible representations for the C—H stretch modes from Equation (6.39) are also given in Table 6.11 with the resulting sums in the final column. In general, the projection operator will give the functional form, but without normalization. The method of Section 6.5 allows normalization factors to be determined, and the resulting normalized SALCs are given in Figure 6.19 alongside illustrations of the vibrations.

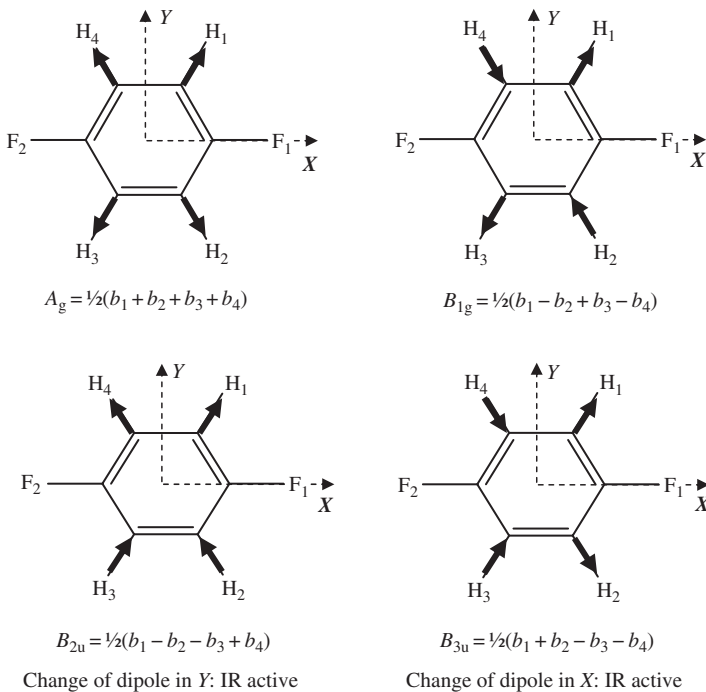


Figure 6.19 The SALCs for the C—H stretch modes of 1,4-difluorobenzene.

The modes give a further illustration of the selection rules derived at the beginning of the chapter. In Section 6.3.1 it was shown that we expect only the B_{2u} and B_{3u} to be IR active. The C—H bonds in 1,4-difluorobenzene will have local dipole moments with a $\delta+$ charge on H and $\delta-$ charge on C: as a C—H bond shortens, the local dipole will decrease; and as the bond lengthens, the local dipole will increase. The motion of the A_g and B_{1g} modes does not give IR activity because the changes in local dipoles opposite one another cancel out. For the B_{2u} and B_{3u} modes, the changes in local dipoles opposite to one another reinforce and the net effect is a changing dipole moment in the Y -direction for B_{2u} and in X for B_{3u} . This was predicted from the rightmost columns of the D_{2h} character table in Section 6.3.1. The origin of Raman selectivity is more difficult to visualize, as it depends on the properties of the polarization matrix.

6.6.2 The Projection Operator and Degenerate Representations

The choice of the generating vector for a point group without degenerate states is quite straightforward. In the examples so far we have simply taken the first basis vector in the list and used this as the generating vector. In Problem 6.11 it was found that selecting any of the other vectors in the basis would give equivalent results.

If the reduction formula has given degenerate representations then we expect two vibrations for each E representation and three for each T representation. But the projection of a single vector will give only a single mode, and so we must find an alternative generating function for the others.

Ammonia, NH₃, C_{3v}

As an example we will look at the N—H stretching modes in ammonia. The basis of N—H bonds in ammonia was used in Chapter 4 as part of the development of matrices in symmetry. We can now use this basis (defined in Figure 4.7) to consider degenerate vibrations of a molecule. The reducible representation and the application of the reduction formula for the three-vector basis is shown in Table 6.12. Once the totals are divided by the order of the group ($h = 6$ in C_{3v}), we find

$$\Gamma = A_1 + E \quad (6.40)$$

So the three basis vectors give rise to a vibration of A_1 symmetry and two degenerate vibrations conforming to the E irreducible representation. From the character table we expect the A_1 and E modes to be both IR and Raman active.

Table 6.12 Application of the reduction formula to the ammonia N—H bond basis defined in Figure 4.7.

C_{3v}	E	$2C_3$	$3\sigma_v$	$h = 6$
Γ	3	0	1	
		$g_c \chi_i(C) \chi_\Gamma(C)$		$\sum_C g_c \chi_i(C) \chi_\Gamma(C)$
A_1	3		3	6
A_2	3		-3	0
E	6		0	6

To find the linear combinations of the basis vectors for A_1 and the first part of the E representation we can apply the projection method arbitrarily taking b_1 (the N—H₁ vector) as the generating vector. The results are summarized in Table 6.13, where the three mirror planes in the $3\sigma_v$ class are considered separately using A, B and C superscripts to refer to planes containing the N—H₁, N—H₂ and N—H₃ bonds respectively.

Table 6.13 Application of the projection operator method to the ammonia N—H bond basis. The vertical mirror planes have been labelled A, B and C to signify the planes which, in the initial configuration, contain the basis vectors b_1 , b_2 and b_3 respectively.

C_{3v}	E	C_3^1	C_3^2	σ_v^A	σ_v^B	σ_v^C	$\mathbf{P}_i b_1 = \sum_j \chi_i(j) \mathbf{T}_j b_1$
$A_1 \mathbf{T}_j b_1$	b_1	b_2	b_3	b_1	b_3	b_2	$2(b_1 + b_2 + b_3)$
$E \mathbf{T}_j b_1$	$2b_1$	$-b_2$	$-b_3$	0	0	0	$2b_1 - b_2 - b_3$

For the A_1 case we end up with a function in which the b vectors are present with the same sign and same weight. This represents a vibration of the molecule in which the three N—H bonds oscillate with the same amplitude and in phase with one another, akin to the symmetric stretch mode of H₂O. The normalization factor for the A_1 mode was found in Problem 6.10, so we know that this function with unit length would be

$$\phi(A_1) = \frac{1}{\sqrt{3}}(b_1 + b_2 + b_3) \quad (6.41)$$

This vibration is illustrated in Figure 6.20a.

In Table 6.13, projection of b_1 using the E irreducible representation produces a mode in which the N—H₁ vector oscillates out of phase with the other two vectors and with twice the amplitude (Figure 6.20b).

Problem 6.12: Show that the normalized form for this first of the E representation functions can be written as

$$\phi_1(E) = \frac{1}{\sqrt{6}}(2b_1 - b_2 - b_3) \quad (6.42)$$

To generate the second mode of the E representation requires the projection of a different function of the basis set. Choosing b_2 or b_3 alone will only produce an analogous mode to that found in Table 6.13, but with a different vector playing the role of b_1 . The three H atoms in ammonia are indistinguishable, so these would merely be alternative ways to write down the mode already identified. What is needed is a function orthogonal to the E mode described by Equation (6.42) which we can use in the projection method to generate the partner E -type vibration. There are two functions which can be written down easily that have the required orthogonality property.

The first is

$$b_1 + b_2 + b_3 \quad \text{because} \quad (b_1 + b_2 + b_3)(2b_1 - b_2 - b_3) = 2b_1^2 - b_2^2 - b_3^2 = 0 \quad (6.43)$$

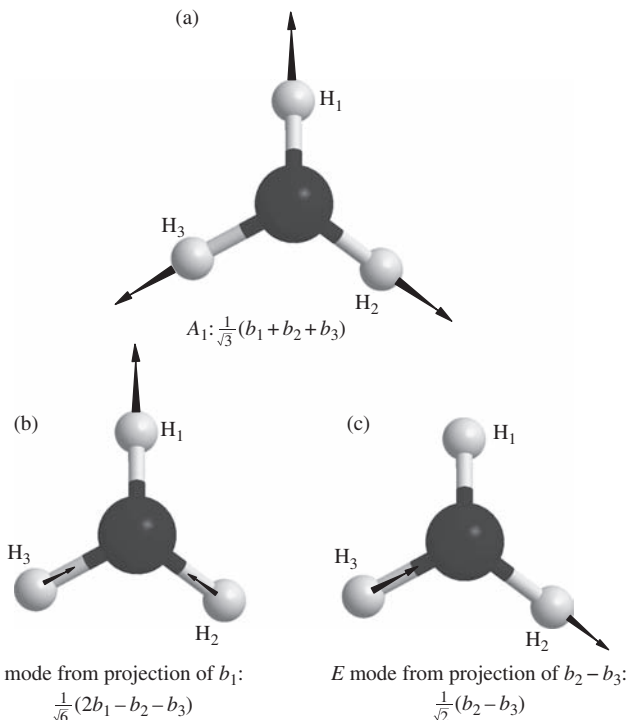


Figure 6.20 The N–H stretching modes of ammonia shown as SALCs of the three-bond vector basis. (a) The A_1 symmetric stretch mode; (b) and (c) the degenerate pair of modes for the E irreducible representation.

and we have assumed b_1 , b_2 and b_3 are orthogonal to one another and normalized (Equations (6.29) and (6.30)). This is just the same as the A_1 mode in Table 6.13, and so is not a good candidate as a generating vector.

The second orthogonal function is

$$b_2 - b_3 \quad \text{because} \quad (b_2 - b_3)(2b_1 - b_2 - b_3) = -b_2^2 + b_3^2 = 0 \quad (6.44)$$

Problem 6.13: Show that $b_2 - b_3$ is also orthogonal to $b_1 + b_2 + b_3$.

The projection operator for the E representation of this new function is shown in Table 6.14. The function is unaltered by the process other than a scaling factor; after normalization we obtain

$$\phi_2(E) = \frac{1}{\sqrt{2}}(b_2 - b_3) \quad (6.45)$$

The form of this vibration is shown in Figure 6.20c. It should be remembered that $\phi_1(E)$ and $\phi_2(E)$ form a degenerate pair which are found in this form because of our choice of b_1 as the initial projection operator. They look like very different motions, but symmetry tells us that they belong to the same degenerate irreducible representation and so must have the same vibrational frequency.

Table 6.14 The projection operator applied to the proposed generating function ($b_2 - b_3$).

C_{3v}	E	C_3^1	C_3^2	σ_v^A	σ_v^B	σ_v^C	$P_i(b_2 - b_3) = \sum_j \chi_i(j) T_j(b_2 - b_3)$
$ET_j(b_2 - b_3)$	$2(b_2 - b_3)$	$-(b_3 - b_1)$	$-(b_1 - b_2)$	0	0	0	$3(b_2 - b_3)$

To check that the $\phi_1(E)$ and $\phi_2(E)$ vibrations give the correct characters for the E representation we have to consider the effect of a symmetry operation from each class of the C_{3v} point group and deduce the relevant characters. This is difficult to do based on diagrams alone, but the procedure introduced for d-orbitals in Section 5.8 can also be brought to bear here.

If the C_3^1 rotation operation is carried out for the two E vibration functions shown in Figure 6.20b and c we find

$$\begin{aligned}\phi_1(E) &\rightarrow \frac{1}{\sqrt{6}}(2b_2 - b_3 - b_1) \\ \phi_2(E) &\rightarrow \frac{1}{\sqrt{2}}(-b_1 + b_3)\end{aligned}\quad (6.46)$$

Now, to find the character we need the amount of each original vibration still present in the transformed functions in each case. So, the transformed functions are written as a linear combination of the original functions with coefficients to be determined. For $\phi_1(E)$ this means

$$\frac{1}{\sqrt{6}}(2b_2 - b_3 - b_1) = \frac{p}{\sqrt{6}}(2b_1 - b_2 - b_3) + \frac{q}{\sqrt{2}}(b_2 - b_3) \quad (6.47)$$

where p and q are unknown constants and by finding p we will obtain the amount of the original $\phi_1(E)$ function required to construct the transformed version, i.e. its character.

For Equation (6.47) to work there must be equal numbers of each basis set on the left- and right-hand sides of the equation. Comparing the b_1 coefficients gives

$$\frac{-1}{\sqrt{6}} = \frac{2p}{\sqrt{6}} \quad \text{so that} \quad p = -\frac{1}{2} \quad (6.48)$$

This is the contribution to the character under the $2C_3$ class for the first mode in the pair of E vibrations.

For the second, we again write down a linear combination of the original functions, but this time we are looking for coefficients to give the transformed $\phi_2(E)$ vibration, i.e.

$$\frac{1}{\sqrt{2}}(-b_1 + b_3) = \frac{p}{\sqrt{6}}(2b_1 - b_2 - b_3) + \frac{q}{\sqrt{2}}(b_2 - b_3) \quad (6.49)$$

This time the value of q gives the required character since the left-hand side of the equation is the transformed $\phi_2(E)$ function. Unfortunately, on the right-hand side of Equation (6.49) there are no basis vectors which only have q in their coefficients, and so we must solve for p first using the b_1 vector:

$$\frac{-1}{\sqrt{2}} = \frac{2p}{\sqrt{6}} \quad \text{or} \quad p = -\frac{\sqrt{6}}{2\sqrt{2}} \quad (6.50)$$

Note that p and q in this process are just being used as unknown variables and the values obtained depend on the transformed function being considered; there is no reason why Equations (6.50) and (6.48) should find the same value of p .

Using the result from Equation (6.50) in a comparison of the b_2 coefficients in Equation (6.49) now gives

$$0 = \frac{1}{2\sqrt{2}} + \frac{q}{\sqrt{2}} \quad \text{i.e.} \quad q = -\frac{1}{2} \quad (6.51)$$

which is the character required for the second function in the pair derived for the E irreducible representation.

The sum of the characters obtained for $\phi_1(E)$ and $\phi_2(E)$ is -1 , which agrees with the entry under the $2C_3$ class of the standard C_{3v} character table (Appendix 12). This, along with the solution to Problem 6.14, confirms that the two vibrations shown in Figure 6.20b and c as a pair are consistent with the E irreducible representation, at least for the $2C_3$ class.

Problem 6.14: Under the identity class of C_{3v} modes, $\phi_1(E)$ and $\phi_2(E)$ clearly give a character of 2. To complete the check that this pair of modes follows the characters of the E irreducible representation, use the above procedure for the $3\sigma_v$ class. Note: this is most easily done by using the σ_v^A plane (containing H_1 in Figure 6.20) as the example operation.

6.7 Linking Results for Symmetry-Inequivalent Sets of Atoms

The projection operator results provide SALCs for symmetry-related basis vectors. Because it depends on the symmetry operations of the point group, the method does not provide information on the relative motion of symmetry-*inequivalent* atoms. For example, the basis of four C—H bond vectors shown in Figure 6.21 could be used to investigate the C—H stretch modes of the C_{2v} molecule 1,2-difluorobenzene. The four basis vectors easily split into two subsets (b_1 with b_2 and b_3 with b_4) because none of the point-group operations interchange vectors between these pairs (e.g. b_1 and b_3 cannot be swapped by an operation). Projection of the b_1 vector would give the two functions already seen with the simple H_2O example:

$$\begin{aligned}\phi(A_1) &= \frac{1}{\sqrt{2}}(b_1 + b_2) \\ \phi(B_2) &= \frac{1}{\sqrt{2}}(b_1 - b_2)\end{aligned} \quad (6.52)$$

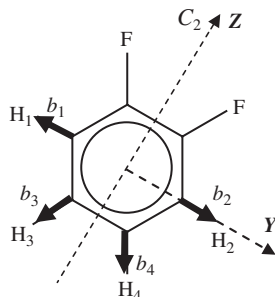


Figure 6.21 A basis of four C—H bond vectors for the C—H stretch modes of the C_{2v} molecule 1,2-difluorobenzene.

These do not involve b_3 or b_4 because these basis vectors are not symmetry related to b_1 .

Another two functions can be obtained by projection of, say, b_3 , to give

$$\begin{aligned}\phi(A_1) &= \frac{1}{\sqrt{2}}(b_3 + b_4) \\ \phi(B_2) &= \frac{1}{\sqrt{2}}(b_3 - b_4)\end{aligned}\quad (6.53)$$

To get the overall picture of the vibrations we need to link together the modes for the two sets of H atoms. This has to be done so that only modes of like symmetry are combined. This ensures that in, say, an A_1 mode for the molecule as a whole the movement of each subset of atoms must conform to the same irreducible representation.

However, the subsets may move in phase with one another or out of phase with one another. So, adding superscripts to indicate the subsets, the two pairs of basis functions give four possible results:

$$\begin{aligned}\phi_1(A_1) &= \phi^{12}(A_1) + \phi^{34}(A_1) = \frac{1}{\sqrt{2}}(b_1 + b_2 + b_3 + b_4) \\ \phi_2(A_1) &= \phi^{12}(A_1) - \phi^{34}(A_1) = \frac{1}{\sqrt{2}}(b_1 + b_2 - b_3 - b_4) \\ \phi_1(B_1) &= \phi^{12}(B_1) + \phi^{34}(B_1) = \frac{1}{\sqrt{2}}(b_1 - b_2 + b_3 - b_4) \\ \phi_2(B_1) &= \phi^{12}(B_1) - \phi^{34}(B_1) = \frac{1}{\sqrt{2}}(b_1 - b_2 - b_3 + b_4)\end{aligned}\quad (6.54)$$

Note that from a basis of four bond vectors we have again arrived at four vibrational modes. The addition of two normalized functions in Equation (6.54) gives new functions that are no longer of unit magnitude. However, it is straightforward to use the procedure of Section 6.5 to renormalize, i.e. scale by a factor which restores the magnitude to one.

The renormalized vibrations are given in Figure 6.22, along with illustrations of the modes. In contrast to 1,4-difluorobenzene, there is no cancellation of opposing dipoles for any of the modes; so, in line with the selection rules, all are IR active. The earlier analysis using the right-hand column of the character table also indicated that all four will also be Raman active.

Problem 6.15: Show, using the projection operator method, that combinations of the mode using different symmetries such as

$$\phi^{12}(A_1) + \phi^{34}(B_2) \quad (6.55)$$

are inconsistent with either irreducible representation.

Hint: write out the function explicitly in terms of the b vectors and tabulate the projection operator results for each irreducible representation.

6.7.1 Sets of Atoms Differing in Mass or Chemical Bond Strength

The sets of inequivalent C—H bonds in the above example are of very similar chemical character, and so it is a good approximation to renormalize the bond vibrations to give

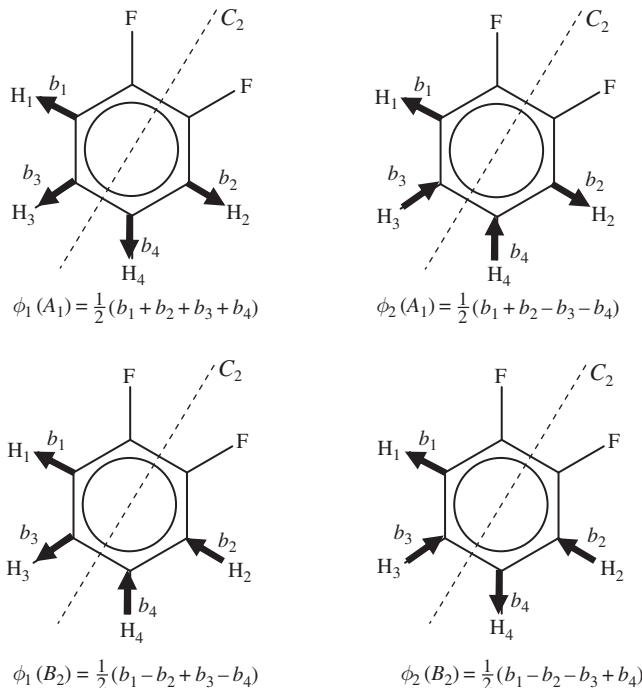


Figure 6.22 The four C–H stretching modes obtained for 1,2-difluorobenzene. Note that the Z-direction is along the principal axis and y is in the molecular plane.

the functions shown in Figure 6.22. This will not be the case when the atom masses or chemical bond strengths for atoms in different subsets are not the same, as the relative atom displacements will also depend on these factors. This means that renormalization is not possible on the basis of symmetry alone. However, the phase patterns that give us the relative motion of the atoms can still be obtained.

As a simple example we return once again to the stretching modes of H₂O. In Figure 6.18 we defined a simple basis set of vectors so that each of the H atoms had a basis vector pointing down their respective O–H bond. This choice of basis vectors leads to the H atom motions for the stretching modes with the normalized SALCs:

$$\begin{aligned}\phi(A_1) &= \frac{1}{\sqrt{2}}(b_1 + b_2) \\ \phi(B_2) &= \frac{1}{\sqrt{2}}(b_1 - b_2)\end{aligned}\tag{6.56}$$

The symmetry operations of the C_{2v} point group link the two H atoms, but the O atom is clearly always distinct; for a complete picture we need to add in the O atom motion. Each of the SALCs constructed for the H atoms has been given a symmetry label, and so in each case the O atom must move in a way that conforms to the symmetry of the H atom movement. In Section 5.2 it was shown that the O atom can only move along the direction defined by principal axis in an A₁ mode and only in the in-plane Y-direction in a

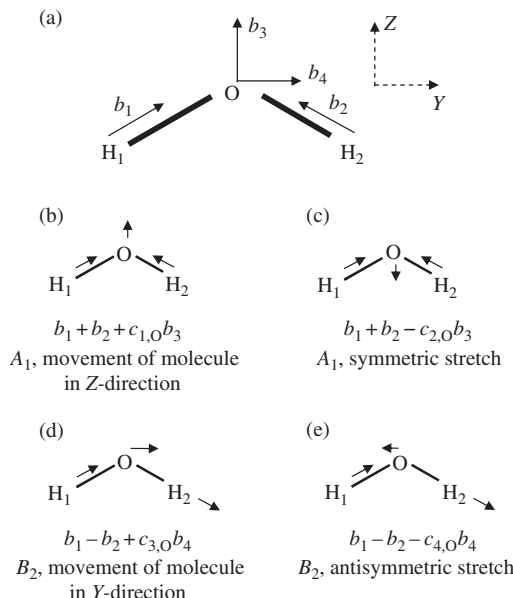


Figure 6.23 (a) A basis for including O motion in the vibrational analysis of H_2O stretching modes; (b, c) A_1 SALCs; (d, e) B_2 SALCs.

B_2 mode. So, to account for the O atom we need only add two more vectors to the basis (Figure 6.23a).

For the A_1 case there are only two possibilities for the O atom: either it moves in phase with the H atoms or out of phase with them in the direction defined by b_3 . So, there are two SALCs for the system as a whole that conform to the A_1 irreducible representation:

$$\begin{aligned}\phi_1(A_1) &= b_1 + b_2 + c_{1,0}b_3 \\ \phi_2(A_1) &= b_1 + b_2 - c_{2,0}b_3\end{aligned}\quad (6.57)$$

Here, the coefficients $c_{1,0}$ and $c_{2,0}$ are used to emphasize that the magnitude of the movement of the O atom will not be the same as for the H atoms. The absolute amplitude of the H and O atom displacements will not be determined here, so we have also abandoned the normalization factors from Equation (6.56). In fact, in a vibration, the O atom will move to ensure that the centre of mass of the molecule remains static as the atoms oscillate. The O atom is more massive than the H atoms, so its amplitude of oscillation will be smaller than that of its H neighbours.

The first A_1 function of Equation (6.57) involves all of the atoms moving in a similar direction (Figure 6.23b). This pattern of vectors will cause the centre of mass of the molecule to be displaced; so, it is not a vibration at all, but represents one of the translational degrees of freedom for the molecule as a whole. Figure 6.23c shows that the second SALC is a vibration; the O atom moves down the page as the H atoms move up; so, by choosing the correct value of $c_{2,0}$, the centre of mass of the molecule will remain stationary. This is the symmetric stretch of the H_2O molecule we first met at the beginning of Chapter 4.

The second linear combination from Equation (6.56) has B_2 symmetry and so can be accompanied by movement of the O only in the plane of the molecule perpendicular to the principal axis following b_4 . Again, this leads to two possibilities:

$$\begin{aligned}\phi_3(B_2) &= b_1 - b_2 + c_{3,O}b_4 \\ \phi_4(B_2) &= b_1 - b_2 - c_{4,O}b_4\end{aligned}\tag{6.58}$$

Figure 6.23d shows that the first of these has all the atoms moving to the right, so the centre of mass will be displaced and this function cannot represent a pure vibration.

The second function, Figure 6.23e gives an SALC with the correct phase pattern for the antisymmetric stretch of H_2O .

In this analysis, the basis vectors have been aligned to best represent the vibrational motion of the molecule, e.g. with b_1 and b_2 along O—H bonds. If it was our intention to study the movement of the molecule as a whole, then a better basis would have the vectors on H atoms aligned with the reference axis system, but then the vibrations would become more complex mixtures of basis vectors. Correspondingly, the functions we have discarded (Figure 6.23b and d) are not ‘pure’ translations; the A_1 example contains a mixture of translation and the symmetric vibration and the B_2 a mixture of translation and rotation around X. To some extent the alignment of the basis is arbitrary, but life is made easier if vectors are chosen that will give simple functions for the properties of interest.

A much more detailed discussion of the choice of basis for a quantitative description of molecular vibrations is given in the text by Bright Wilson *et al.* referenced in this chapter’s Further Reading section. This covers the use of mass-weighted coordinates and systems of internal coordinates based on bond vectors, bond angles and dihedral angles. Here, we are interested in the application of symmetry to vibrational spectroscopy to understand selection rules, and usually the much simpler basis of a few carefully chosen atom or bond displacements will suffice.

6.8 Additional Examples

To finish the chapter we will cover a few additional worked examples of the application of symmetry to molecular vibrations. The first is the case of the highly symmetric molecule benzene, which we noted in Chapter 1 has a surprisingly simple IR spectrum.

6.8.1 Benzene, D_{6h}

Benzene belongs to the group D_{6h} . In this example we will consider a complete basis covering the three degrees of freedom for the 12 atoms. The basis will be written with three vectors per atom, labelled u, v and z , and defined so that z is perpendicular to the molecular plane, each u is aligned with the atom’s C—H bond and each v perpendicular to u and z , i.e. in the molecular plane, as shown in Figure 6.24.

This basis has the z vectors on each atom aligned with the principal C_6 axis, which defines the Z-direction of the normal frame of reference. The u vectors are placed to represent the C—H stretch modes that we will find, and v is chosen to give the third degree of

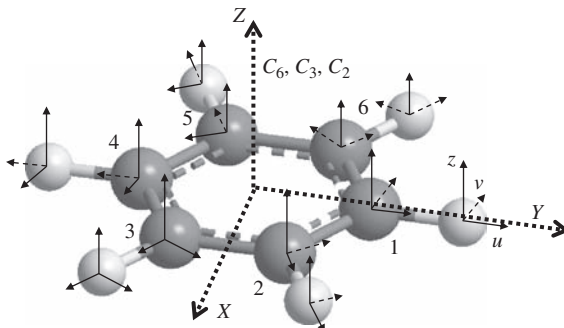


Figure 6.24 A basis of $3N$ vectors for the D_{6h} molecule benzene.

freedom of each atom. The X and Y directions are taken so that $C—H_1$ is aligned with Y ; this means that the u vectors of the atoms C_1 , H_1 , C_4 and H_4 are also along Y , but the other u basis vectors are not.

There are 36 basis vectors, and the effect of each operation of the D_{6h} group gives the reducible character set shown in Table 6.15. These characters are obtained by considering the effect of an example operation from each class in the point group on the basis.

Table 6.15 The reducible representation obtained for benzene with a basis of three vectors per atom.

D_{6h}	E	$2C_6$	$2C_3$	C_2	$3C_2'$	$3C_2''$	i	$2S_3$	$2S_6$	σ_h	$3\sigma_d$	$3\sigma_v$
Γ	36	0	0	0	-4	0	0	0	0	12	0	4

As usual, the identity operator E leaves all basis vectors unchanged and so simply counts the number of basis vectors.

The element for the rotations $2C_6$, $2C_3$ and $2C_2$ is the vertical axis through the centre of the molecule. Any rotation around this axis interchanges the atoms, and so all basis vectors are changed completely.

The $3C_2'$ axes, through opposite atoms, interchange all atoms except the four on the axis employed. For these four atoms the z and v are reversed but u is unaltered, giving character $-2 + 1 = -1$ per atom on the axis and so a total of -4 .

The operations in the classes $3C_2''$, i , $2S_3$ and $2S_6$ all interchange atoms so that none remains in its original position, giving a character of 0.

The σ_h operation is a reflection in the plane of the molecule; this leaves all atoms in place with all u and v basis vectors unaltered and each z is reversed, giving a character of 1 per atom, making a total of 12.

The mirror planes for the $3\sigma_d$ class contain the principal axis and dissect opposite bonds in the ring. Each σ_d operation swaps atoms with their images; hence the character is 0.

The $3\sigma_v$ planes each contain the principal and a C_2' axis; that is, on reflection, four atoms are left in place with u and z unaltered but their v reversed, giving a character of 1 per unaltered atom and so a total of 4.

Table 6.16 The application of the reduction formula to the reducible representation for the vibrational modes of benzene (Table 6.15). The classes with zero in Γ are omitted as they will not contribute to the summation. However, the order of the group h is set by the total number of operations in the complete D_{6h} character table.

D_{6h}	E	$3C_2'$	σ_h	$3\sigma_v$	$h = 24$
Γ	36	-4	12	4	
		$g_c \chi_i(C) \chi_{\Gamma}(C)$			
A_{1g}	$1 \times 36 \times 1$	$3 \times -4 \times 1$	$1 \times 12 \times 1$	$3 \times 4 \times 1$	$\sum_C g_c \chi_i(C) \chi_{\Gamma}(C)$
A_{2g}	$1 \times 36 \times 1$	$3 \times -4 \times -1$	$1 \times 12 \times 1$	$3 \times 4 \times -1$	48
B_{1g}	$1 \times 36 \times 1$	$3 \times -4 \times 1$	$1 \times 12 \times -1$	$3 \times 4 \times -1$	0
B_{2g}	$1 \times 36 \times 1$	$3 \times -4 \times -1$	$1 \times 12 \times -1$	$3 \times 4 \times 1$	48
E_{1g}	$1 \times 36 \times 2$	$3 \times -4 \times 0$	$1 \times 12 \times -2$	$3 \times 4 \times 0$	48
E_{2g}	$1 \times 36 \times 2$	$3 \times -4 \times 0$	$1 \times 12 \times 2$	$3 \times 4 \times 0$	96
A_{1u}	$1 \times 36 \times 1$	$3 \times -4 \times 1$	$1 \times 12 \times -1$	$3 \times 4 \times -1$	0
A_{2u}	$1 \times 36 \times 1$	$3 \times -4 \times -1$	$1 \times 12 \times -1$	$3 \times 4 \times 1$	48
B_{1u}	$1 \times 36 \times 1$	$3 \times -4 \times 1$	$1 \times 12 \times 1$	$3 \times 4 \times 1$	48
B_{2u}	$1 \times 36 \times 1$	$3 \times -4 \times -1$	$1 \times 12 \times 1$	$3 \times 4 \times -1$	48
E_{1u}	$1 \times 36 \times 2$	$3 \times -4 \times 0$	$1 \times 12 \times 2$	$3 \times 4 \times 0$	96
E_{2u}	$1 \times 36 \times 2$	$3 \times -4 \times 0$	$1 \times 12 \times -2$	$3 \times 4 \times 0$	48

To find the irreducible representations present requires the use of the reduction formula. It is worth noting that several of the classes have given a 0 in the character set for Γ , and so will not contribute to the sum in the reduction formula (Equation (6.17)). In this case, only the E , $3C_2'$, σ_h and $3\sigma_v$ classes need be considered. The application of the reduction formula is summarized in Table 6.16; even though only a few classes contribute, the order $h = 24$ is still the total number of operations in the full D_{6h} point group. From the final column in the table we find that

$$\Gamma = 2A_{1g} + 2A_{2g} + 2B_{2g} + 2E_{1g} + 4E_{2g} + 2A_{2u} + 2B_{1u} + 2B_{2u} + 4E_{1u} + 2E_{2u} \quad (6.59)$$

This means we have 12 singly degenerate vibrations (labelled A or B) and 12 doubly degenerate vibrations (labelled E), giving a total of 36, as required by the use of 36 basis vectors to describe the atomic motions. Of these, six will be simple movements or rotations of the molecule as a whole. We can find out which these are from the character table: the symbols x and y occur with the irreducible representation E_{1u} , z with A_{2u} and R_x , R_y and R_z with E_{1g} and A_{2g} , so the corresponding number of each irreducible representation needs to be removed from Γ , remembering that E states are doubly degenerate. This leaves the 30 modes

$$\Gamma(\text{vib}) = 2A_{1g} + A_{2g} + 2B_{2g} + E_{1g} + 4E_{2g} + A_{2u} + 2B_{1u} + 2B_{2u} + 3E_{1u} + 2E_{2u} \quad (6.60)$$

The character table indicates that IR-active modes will have symmetry A_{2u} and E_{1u} . These are present in $\Gamma(\text{vib})$ as $A_{2u} + 3E_{1u}$, i.e. there are seven vibrational modes that are IR active, but we only expect four bands in the IR spectrum, since six form degenerate pairs. Way back in Figure 1.5 we saw that the experimentally observed IR spectrum of benzene does indeed have only four bands. The products of axes in the character table follow A_{1g} , E_{1g}

and E_{2g} irreducible representations and all are present in $\Gamma(\text{vib})$. Equation (6.60) gives a total of 12 Raman-active vibrations with degeneracy, leading to seven bands.

Application of the projection operator with such a large number of operations is quite time consuming. However, it is possible to reduce the effort required by first considering only the rotational subgroup operations concerned with the C_6 axis. The classes E , $2C_6$, $2C_3$ and $2C_2$ form the C_6 subgroup of D_{6h} , because any products of operations of this smaller set are contained within it.

In addition, we can reduce the number of basis vectors that need to be used by noting that the A_{2u} vibration is expected to give a change of dipole moment in the Z -direction (from the character table), so projection of u or v basis vectors can be neglected. The projection using the H_1 atom z vector in the C_6 subgroup is given in Table 6.17 and simply gives

$$\phi(A) = z_1 + z_2 + z_3 + z_4 + z_5 + z_6 \quad (6.61)$$

Here, the subscripts refer to the atom positions around the ring as labelled in Figure 6.24. A quick check across the full list of operations for the D_{6h} group confirms that this function has the correct form for the A_{2u} representation. For example, the σ_h operation would reverse all the z -basis functions and so give the same result as -1 times the Equation (6.61) function. This is the character under the σ_h column of the D_{6h} point-group table for A_{2u} ; so, we have found the motion of the H atoms in the $\phi(A_{2u})$ mode.

Table 6.17 Projection of the z_1 basis vector in the A representation of the C_6 rotational subgroup. This provides a candidate function for the motion of the C or H set of atoms in the A_{2u} irreducible representation of D_{6h} benzene.

C_6	E	C_6^1	C_6^5	C_3^1	C_3^2	C_2	Total
A	1	1	1	1	1	1	
z_1	z_1	z_2	z_6	z_3	z_5	z_4	$z_1 + z_2 + z_3 + z_4 + z_5 + z_6$

The same analysis of the carbon atom basis would give a similar result, and so we obtain two possible SALCs that describe A_{2u} motion:

$$\phi(A_{2u}) = c_C \phi(A_{2u}) + c_H \phi(A_{2u}) \quad \text{or} \quad \phi(A_{2u}) = c_C \phi(A_{2u}) - c_H \phi(A_{2u}) \quad (6.62)$$

Here, the coefficients c_C and c_H refer to the C and H atoms respectively. The relative magnitudes of these coefficients will depend on the atomic masses, so we would expect the H atoms to move with greater amplitude than the C atoms.

In the first of these functions the C and H atoms move in phase along the Z -direction. This is not a vibration, but the translation of the molecule as a whole along Z which was removed by inspection of the character table in the change over from Γ to $\Gamma(\text{vib})$.

In the second SALC of Equation (6.62) the C atoms and H atoms move out of phase: as C atoms move downward, H atoms move upward, and vice versa. This is shown in Figure 6.25a, and it can be seen that this mode does result in the expected changing Z -dipole for the A_{2u} vibration.

The other IR-active modes have the E_{1u} representation, and the character table indicates that these give rise to transition dipole moments in the X or Y directions. For these modes,

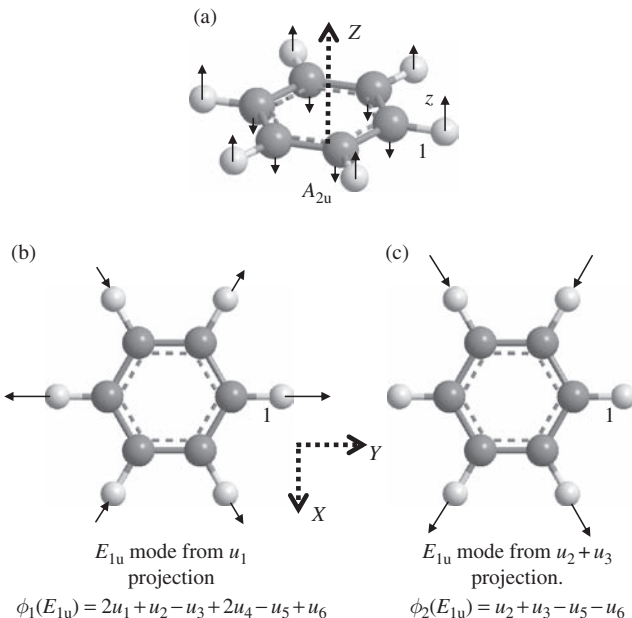


Figure 6.25 Example IR-active modes obtained using the projection operator method for benzene. (a) The A_{2u} mode giving a changing dipole moment along Z ; (b, c) degenerate $C-H$ stretching modes belonging to the E_{1u} representation.

displacement along the z vectors will not occur, and so the projection should concentrate on the u and v vectors only.

Table 6.18 shows projection of the u_1 vector, on H_1 in the C_6 rotational subgroup. This leads to the SALC

$$\phi_1(E_{1u}) = 2u_1 + u_2 - u_3 + 2u_4 - u_5 + u_6 \quad (6.63)$$

Note that only u -type vectors, i.e. those aligned with the $C-H$ bonds, have appeared in this projection. This mode will correspond to a collective stretching mode, which is illustrated in Figure 6.25b. By inspection, it is clear that this mode has *ungerade* symmetry (it changes sign with the i operation) and so is also the first part of $\phi_1(E_{1u})$ in the full D_{6h} point group of benzene. In the character table, E_{1u} has -2 under i , because both of the degenerate modes contribute to the characters. The transition dipole moment for this mode is aligned with the Y -direction.

Equation (6.63) gives the first of two degenerate vibrations; to obtain the second we need a new generating vector that is likely to lead to an orthogonal result. In $\phi_1(E_{1u})$, u_2 and u_3 occur with opposite sign, so that H_2 and H_3 move out of phase with one another. Accordingly, a possible choice of generating vector is one which forces these two atoms to move in phase with one another, the simplest form of which is

$$u_2 + u_3 \quad (6.64)$$

Table 6.18 Projection of the u_1 basis vector in the E_1 representation of the C_6 rotational subgroup.

C_6	E	C_6^1	C_6^5	C_3^1	C_3^2	C_2	Total
E_1	2	1	1	-1	-1	-2	
u_1	$2u_1$	u_2	u_6	$-u_3$	$-u_5$	$-2u_4$	$2u_1 + u_2 - u_3 - 2u_4 - u_5 + u_6$
$u_2 + u_3$	$2(u_2 + u_3)$	$u_3 + u_4$	$u_1 + u_2$	$-(u_4 + u_5)$	$-(u_6 + u_1)$	$-2(u_5 + u_6)$	$3u_2 + 3u_3 - 3u_5 - 3u_6$

Projection based on this function is also shown in Table 6.18 and yields the following SALC:

$$\phi_2(E_1) = u_2 + u_3 - u_5 - u_6 \quad (6.65)$$

The factor of 3 in the table is common to all vectors, and so removing it does not affect the relative motion of the atoms. The second E_{1u} mode is illustrated in Figure 6.25c, which shows a changing dipole moment along X .

For these stretching modes we could again find the corresponding projections for u vectors on the C atoms and take combinations of the H and C SALC functions. However, in stretching modes, the C atoms simply move out of phase with their own H atoms, and so the mode can be visualized based on Equations (6.64) and (6.65) alone.

Problem 6.16: (a) Confirm that the sum of the characters for $\phi_1(E_1)$ and $\phi_2(E_1)$ under the D_{6h} operations other than those in the C_6 subgroup, conform to the assignment of these modes to E_{1u} .

(b) Show that another pair of E_{1u} modes can be obtained from the set of v basis vectors.

We have used symmetry to identify the irreducible representations for the molecular vibrations and selection rules to decide how many of these should be IR active. The projection operator then shows us the pattern of atomic movements consistent with each mode. However, symmetry alone cannot determine which vibration goes with which band in the experimental spectrum (Figure 1.5). For that, some knowledge of the bond strength and effective masses involved is required. For example, Figure 6.25 shows that the E_{1u} modes are combinations of C—H stretch movements, whereas the A_{2u} mode is out-of-plane movement of the H atoms. Bond compressions usually occur at higher frequencies than bending or these out-of-plane motions, and so the E_{1u} modes will be associated with the high -frequency band (around 3000 cm^{-1}).

6.8.2 The *fac* and *mer* Isomers of Transition Metal Complexes

The vibrational spectra of metal complexes containing CO can be a useful probe of their structure and chemical bonding. The stretching vibration usually lies in the range $2100\text{--}1700\text{ cm}^{-1}$ and can usually be distinguished from the vibrations of other ligands. We will see in Chapter 7 that the C=O bond strength, and so its vibrational frequency, is affected by its bonding to a metal centre. This means that the IR spectra of complexes containing CO can give insight into molecular bonding.

In this section we will show how symmetry analysis can help decipher the spectrum by determining how many bands to expect for a given molecular geometry. This allows us to distinguish between possible isomers. For example, the general six-coordinate complex $\text{ML}_3(\text{CO})_3$ can occur in one of two isomeric forms:

- Figure 6.26 shows the facial (*fac*) isomer, in which all three CO ligands are on the same triangular face of the octahedron of metal coordination sites. This belongs to the C_{3v} point group.
- The meridian (*mer*) isomer, which has the three CO ligands in the same plane, is also shown in Figure 6.26 and gives a C_{2v} structure.

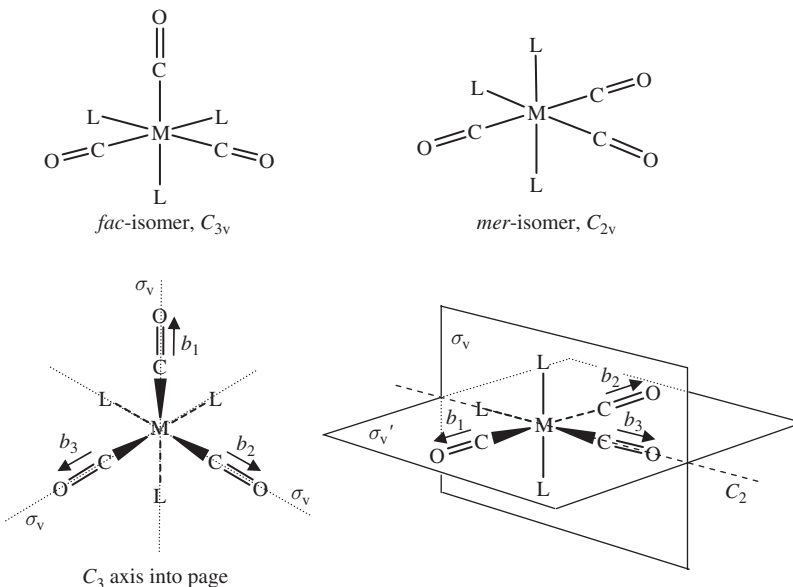


Figure 6.26 The facial (*fac*) isomer and meridian (*mer*) isomer of the general complex $ML_3(CO)_3$. In each case the upper diagram shows a sketch in the normal orientation for ‘octahedral’ complexes and the lower pictures use a view that should make the symmetry elements easier to see. The basis arrows along carbonyl bonds that are used in the vibrational analysis of carbonyl stretching modes are drawn slightly to the side of each ligand for clarity. Note that, for the C_{2v} *mer*-isomer, the basis vectors b_1 and b_2 are symmetry related to each other, but not to b_3 .

The analysis of the *fac*-isomer is identical to the ammonia N—H stretching modes example of Section 6.6.2, so that the three basis vectors give rise to three vibrational modes with irreducible representations:

$$\Gamma = A_1 + E \quad (6.66)$$

Vibrational modes following the A_1 and E representations will be IR active; however, because the two vibrations in the E representation are degenerate, only two IR bands would be expected. The pattern of CO bond stretches in these modes is analogous to the N—H stretching modes shown in Figure 6.20.

For the C_{2v} *mer*-isomer the σ_v' plane will be taken to be the one containing all three CO bonds, as drawn in Figure 6.26. The reducible representation for this isomer generated with this setting is shown at the top of Table 6.19. This table also shows that the application of the reduction formula gives

$$\Gamma = 2A_1 + B_2 \quad (6.67)$$

For the C_{2v} case we have found three irreducible representations, all of which are IR active.

Table 6.19 Application of the reduction formula to the three CO bond basis for the C_{2v} mer-isomer of $ML_3(CO)_3$.

C_{2v}	E	C_2	$\sigma_v(XZ)$	$\sigma_v'(YZ)$	$h = 4$	
Γ	3	1	1	3	\sum_C	n_i
			$g_c \chi_i(C) \chi_\Gamma(C)$			
A_1	3	1	1	3	8	2
A_2	3	1	-1	-3	0	0
B_1	3	-1	1	-3	0	0
B_2	3	-1	-1	3	4	1

Problem 6.17: For the C_{2v} isomer, the basis vectors b_1 and b_2 are symmetry related. Use the projection operator method to show that the A_1 and B_2 SALCs have the form

$$\begin{aligned}\phi(A_1) &= b_1 + b_2 \\ \phi(B_2) &= b_1 - b_2\end{aligned}\quad (6.68)$$

The C=O bond on the C_2 axis, with basis vector b_3 , is separate from b_1 and b_2 because it is not exchanged with them by any of the symmetry operations. b_3 lies on the symmetry axis, so it can only have an A_1 representation. This means it can only be involved in linear combinations with the A_1 function found for the b_1 and b_2 set, i.e.

$$\phi_1(A_1) = b_1 + b_2 + b_3 \quad (6.69)$$

and

$$\phi_2(A_1) = b_1 + b_2 - b_3 \quad (6.70)$$

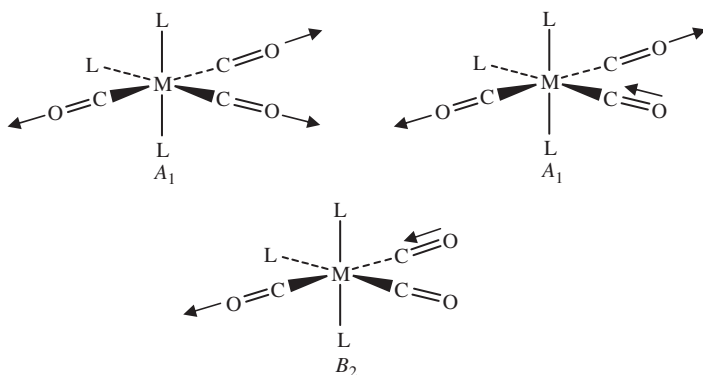


Figure 6.27 The three C=O stretching modes for the mer-isomer of $ML_3(CO)_3$. The arrows are drawn to show the motion of the O atom in the extension or compression of the individual ligands.

In the B_2 vibration, b_3 must have a zero coefficient, so that

$$\phi_3(B_2) = b_1 - b_2 \quad (6.71)$$

These three vibrations are illustrated in Figure 6.27. From the character table, all three modes are expected to be IR active.

The number of predicted bands is an important difference between the isomers. If a compound $ML_3(CO)_3$ is synthesized, then one clue to its structure will be the number of IR bands in the CO stretch region of the spectrum. If two bands are observed, then it would indicate the *fac*-isomer had been made, whereas three bands would be evidence pointing toward the *mer*-isomer.

6.9 Summary

Section 6.3 gave a summary of the application of the reduction formula to a basis to identify the irreducible representations for vibrations. The more general points covered in this chapter are as follows.

1. Symmetry can be used to identify the transitions between energy levels that will be unable to couple to the probe radiation in spectroscopic experiments and so predict those transitions that will not be observed. This is the basis of the selection rules.
2. Often, isomers of a molecule or complex will have different point groups and so may have different numbers of allowed transitions; symmetry analysis can then be used to interpret spectra and aid identification.
3. In quantum mechanics, the coupling between light and a molecule depends on integrals such as

$$M_{fi} = \int_{-\infty}^{\infty} \psi_f O \psi_i d\tau \quad (6.72)$$

where O is an operator, ψ_i is the wavefunction for the initial state and ψ_f the wavefunction for the excited state. Only if M_{fi} is finite will the transition from ψ_i to ψ_f be observable. This means the integrand $\psi_f O \psi_i$ must belong to the totally symmetric representation for the point group of the molecule (character 1 for all symmetry classes).

4. The irreducible representation of the integrand for Equation (6.72) can be calculated using the method of direct products.
5. For vibrational spectroscopy, under laboratory conditions, ψ_i will usually be the ground-state vibration, which always belongs to the totally symmetric irreducible representation. The excited-state vibrations will have the symmetries derived from the analysis of a suitable basis.

6. For IR spectroscopy, the appropriate operator is the transition dipole moment. This has components with the same symmetry as x , y and z . The selection rule for IR spectroscopy requires that a vibration must have the same irreducible representation as one of x , y and z .
7. For Raman spectroscopy, the appropriate operator is the molecular polarizability. This has components with the same symmetry as the products x^2 , y^2 , z^2 , xy , xz and yz or their linear combinations. The selection rule for Raman spectroscopy requires that a vibration must have the same irreducible representation as one of these products or their linear combinations.
8. The pattern of atom motion in a vibration can be pictured as an symmetry adapted linear combination (SALC) of the basis used to obtain the irreducible representations. The SALC as a whole must conform to one of the irreducible representations identified using the reduction formula.
9. The SALC for an irreducible representation can be determined using the projection operator method (Section 6.6). This builds the linear combination by considering the effect of each operation in the group on a generating vector with a coefficient assigned from the character of the irreducible representation. This process requires *all* symmetry operations for the point group to be considered, i.e. operations within the same class must be considered separately.
10. For groups containing large numbers of operations, the projection operator method should first be carried out with a rotational subgroup. The results can then be assigned to the correct irreducible representations by considering the behaviour of the resulting functions for the additional operations of the full point group.
11. For degenerate representations, the projection operator requires a different generating function for each of the equivalent vibrations. The first can simply be a single vector which will generate an SALC. The rest of the generating functions should be chosen so that they will give a result orthogonal to the first.
12. When the basis contains subsets of symmetry-related vectors, separate SALCs will be obtained for each subset. These can be combined by taking further linear combinations within which each subset has the same irreducible representation.

6.10 Self-Test Questions

1. In the benzene example, the projection of the z and u vectors from the basis in Figure 6.24 gave an A_{2u} and one pair of degenerate E_{1u} vibrations. Use the projection operator method and the v_1 vectors to derive the SALC for C—H group bending modes which have the E_{1u} representation and so can be IR active.
2. The carbonyl stretches of a square planar complex, $M(CO)_4$, can be derived from a basis made up of four vectors, one along each of the C—O bonds (pointing from C to O). From this basis, derive the reducible representation that makes up the C—O stretches and use the reduction formula to identify the irreducible representations it contains. Identify which vibrations will be IR active and which Raman active and use the projection operator method to sketch out each of the four vibrations.
3. The complex $MnI(CO)_5$ shows three IR and four Raman bands in the CO stretching region of spectra. Assign the point group of the six-coordinate complex, derive

the irreducible representations for the CO stretching modes and, hence, explain these observations.

4. Iron tetrinitrosyl, $\text{Fe}(\text{NO})_4$, has been synthesized from $\text{Fe}(\text{CO})_5$ by treatment with NO under pressure. It is a very reactive complex that decomposes even under an inert atmosphere. It has a suggested structure of $[\text{Fe}(\text{NO}^+)_3]\text{NO}^-$, supported by the observation that it shows two IR absorptions in the NO^+ stretch region. Possible structures for the $[\text{Fe}(\text{NO}^+)_3]$ complex include D_{3h} or C_{3v} point groups.
 - (a) Using a suitable basis, identify the irreducible representations for NO^+ stretching vibrations that are IR active for each complex geometry and so identify the most likely geometry.
 - (b) For each of the irreducible representations you have identified, sketch the motion of the NO^+ atoms during the corresponding vibration. Explain your answer in terms of compliance with the characters of the representation and the spectroscopic selection rules.
5. (a) Explain why molecules which belong to point groups having centres of inversion will have IR-active vibrations with only *ungerade* representations.
 - (b) Using a basis of six C—H vectors, identify the representations for all the *ungerade* C—H stretching vibrations of benzene.
 - (c) Two of the *ungerade* C—H stretch vibrations of benzene lead to observable IR absorption; explain why only one band is seen experimentally.
 - (d) Using the projection operator, obtain a normalized SALC representation of the vibrational motion of the C—H stretch mode of benzene which is *ungerade* but *not* IR active. Based on your SALC, illustrate the relative phases of motion of the C—H bonds in this vibration using the basis from (b). Why does this mode not give a transition dipole moment?
6. In Section 6.3.1 and Problem 6.6 the irreducible representations for C—H stretching modes of 1,4- and 1,2-difluorobenzene are derived.
 - (a) Using the projection operator method, find normalized SALC representations for all modes in each case. Confirm that your functions have the expected behaviour for the group operations by deriving the characters for each mode and comparing with the relevant irreducible representation. *Note:* for degenerate modes, the characters for the individual vibrations should be summed.
 - (b) Show that the SALC functions you have derived for the C—H stretching modes are orthogonal to one another.

Further Reading

For a full discussion of quantitative vibrational analysis, see:

Bright Wilson E, Decius JC, Cross PC (1980) *Molecular Vibrations: the Theory of Infrared and Raman Vibrational Spectra*, new edition, Dover Publications (ISBN: 0-486-6394-X).

7

Symmetry in Chemical Bonding

7.1 Introduction

In earlier chapters we classified the symmetry of atomic orbitals (AOs) in a number of example molecules. It is now time to develop the ideas of molecular orbital (MO) theory and use it to describe chemical bonding. Symmetry classifications help in the MO description of chemical bonding because symmetry controls how the AOs on neighbouring atoms mix together. MOs are the wavefunctions for electrons in the complex field of the many nuclei and other electrons that make up a molecule. The complexity of MOs can be dealt with by constructing them from the AOs of the isolated atoms. The MOs are formed by mixing the AOs based on the idea of interference described by the superposition of waves: when waves come together in the same phase they reinforce one another, whereas waves of opposite phase will tend to cancel each other out.

In this chapter we will find that only AOs of the same symmetry can mix by superposition to give MOs. To construct MOs, the symmetry of the AOs for the interacting atoms are first established and then each matching set is used to produce SALCs which predict the shapes of the MOs. This is simply an application of symmetry analysis to a basis of AOs, and so we will always be able to construct the same number of MOs as there are AOs in the basis.

Symmetry cannot tell us the relative energies of these orbitals, and so we also review some ideas in chemical bonding and atomic electronegativity to allow the energetic ordering of MOs to be judged. We begin, in the next section, by outlining the idea of interference and superposition of waves. Then we will discuss the link between MOs and the electron density that is probed in experiment. The approach is to overview the general concepts of MO theory using some quite complex-looking examples. Then, in later sections, a more detailed analysis of chemical bonding and MO theory will be undertaken using simpler cases in greater depth.

7.1.1 Wave Phenomena and Interference

Everyday life offers many opportunities to observe wave-like phenomena and the interference patterns formed between waves. When raindrops hit the surface of a puddle or pond, circular patterns of surface waves are sent out from the points of impact. A typical scene is shown in Figure 7.1a. Interference occurs where the waves meet: for points on the surface of the pond at which waves arrive in phase, the disturbance of the surface is greater than for either wave alone; in contrast, where they arrive out of phase, the peaks and troughs tend to cancel out, resulting in less local disturbance. This gives rise to the cross-hatch pattern visible in the close-up of two particular drop impacts in Figure 7.1b.

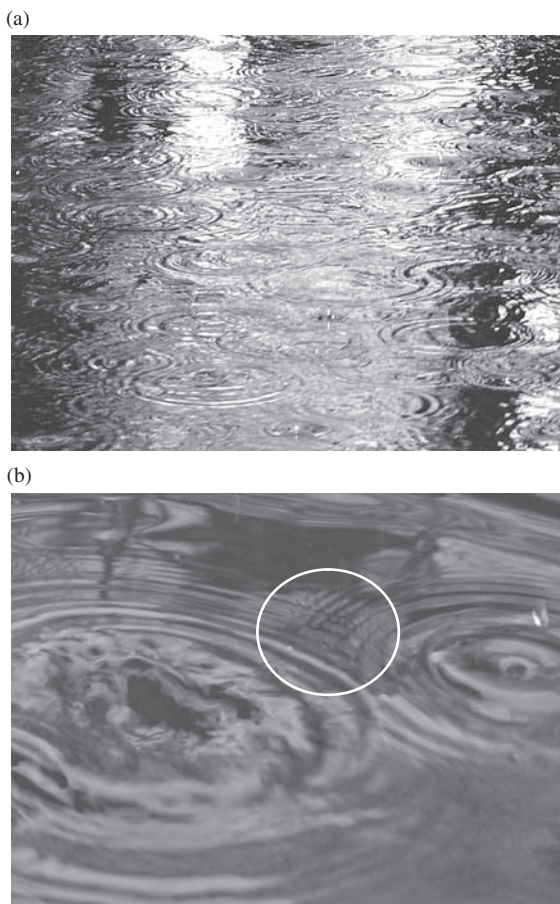


Figure 7.1 (a) The pattern of surface waves caused by raindrops hitting the surface of a pond. (b) A close-up of two particular circular waves; in the space between the impact sites the pattern due to interference can be seen, particularly in the region highlighted by the white circle. This pattern arises from superposition of the waves, so that two peaks arriving at the same point reinforce one another while a peak and a trough will cancel out.

To obtain the disturbance at any point we have to add together contributions from all the waves generated by the rain drops; that is, we have to use superposition of the individual waves.

The idea of the superposition of waves is useful to bear in mind when we deal with chemical bonding: the individual waves are akin to the AOs and their superposition gives the MOs of sets of atoms. We should expect regions where the AOs are in phase to result in a relatively large wavefunction amplitude, while regions where opposite phases come together will give a low, or even zero, amplitude.

However, the analogy with water waves can only be taken so far. For example, the water waves travel away from the impact centre until the disturbance falls to zero, whereas the MOs are stationary solutions of the Schrödinger equation: the attraction to the atomic nuclei holds the electrons in place and the wavefunctions describe how electrons may distribute themselves around the nuclei. They will remain undisturbed in these patterns indefinitely unless acted upon by some external agent, such as light of sufficient photon energy to cause an electronic excitation (see Appendix 7). In addition, there is only one interference pattern on the surface of the pond in Figure 7.1, while there will be as many MOs as there are AOs. This follows because the AOs are a basis from which the MOs are constructed as symmetry adapted linear combinations (SALCs).

Figure 7.2 shows an example MO for the polycyclic aromatic molecule phenanthrene. Here, the MO is formed from the C atom p-orbitals that are perpendicular to the molecular plane. In areas in which these AOs are in phase, constructive superposition occurs and

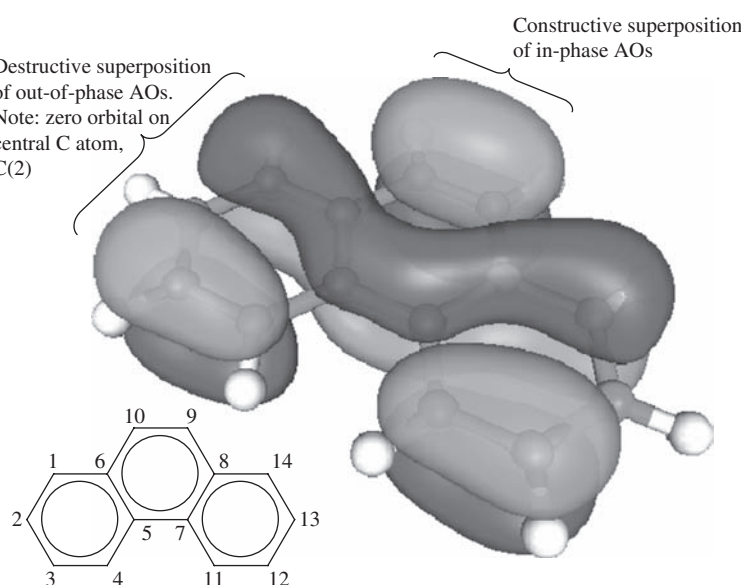


Figure 7.2 An example MO from the aromatic molecule phenanthrene ($C_{14}H_{10}$). This MO is formed from a linear combination of the $C(2p)$ orbitals which are perpendicular to the molecular plane. Areas of constructive and destructive superposition of AOs are indicated. The chemical structure of phenanthrene is shown bottom left.

the p-orbitals join up across the molecule. In regions where the p-orbitals meet out of phase, destructive interference results in zeros in the wavefunction, which means that the AOs of some atoms (e.g. C(2)) make no contribution to this particular orbital. This MO is part of a set that gives the delocalized π -electron density of aromatic molecules such as phenanthrene. The H(1s) atom basis functions are not involved in this MO because their symmetry does not match that of the p-orbitals perpendicular to the plane.

Problem 7.1: In this problem we will look at the symmetry of the MO shown in Figure 7.2. The whole orbital should be thought of as a single object in your analysis.

1. What is the point group of phenanthrene?
2. Write down the characters for the MO of Figure 7.2 for each class of operation in the point group. (Remember, if an operation appears to leave the orbital unchanged then the character is 1; if it swaps positive and negative phases, then the character is -1 .)
3. Compare your characters with the standard table in Appendix 12 and, hence, assign an irreducible representation to the MO.

Computer packages capable of calculating MOs, such as those in Figure 7.2, are now widely available and have been used for some of the figures in this chapter. These programs produce the SALC MOs that we will discuss. Having a computer to generate the shapes of the MOs is very useful, but their description and properties are still best understood with the insight gained from symmetry.

7.1.2 The Born Interpretation of the Wavefunction

In quantum mechanics, the wavefunction itself is not an ‘observable’ quantity. This means that it cannot be directly measured by experiment. What we can measure is the electron density. For example, the intensity distribution of X-rays in the diffraction pattern from a crystalline material depends on the electron density of the sample. In low-resolution X-ray diffraction experiments, the pattern is used to identify the high electron density concentrated at the atom centres, and so X-ray diffraction is often used to determine molecular structure. However, high-resolution X-ray diffraction can map out the electron density in some detail; for example, Figure 7.3 shows data taken for (*Z*)-*N*-methyl-*C*-phenylnitronite. Nitrones are a class of organic molecules containing the $\text{C}=\text{N}(+)-\text{O}(-)$ group which are used as radical trapping agents. They are able to interact with short-lived radical species to produce much longer lived nitroxide radicals that can be observed using electron spin resonance.

The map in Figure 7.3 shows the difference between the charge density found in the molecular crystal and that expected for the same set of atoms with no chemical bonding interactions. Solid contours indicate regions in which electronic density has been increased by chemical bond formation, while dotted contours are used to show electron densities that have been lowered. In general, charge has accumulated in the internuclear regions at the expense of areas remote from the nuclei, so that the spherical isolated atom charge is rearranged in a molecule by building up electron density in the chemical bonds. Around the

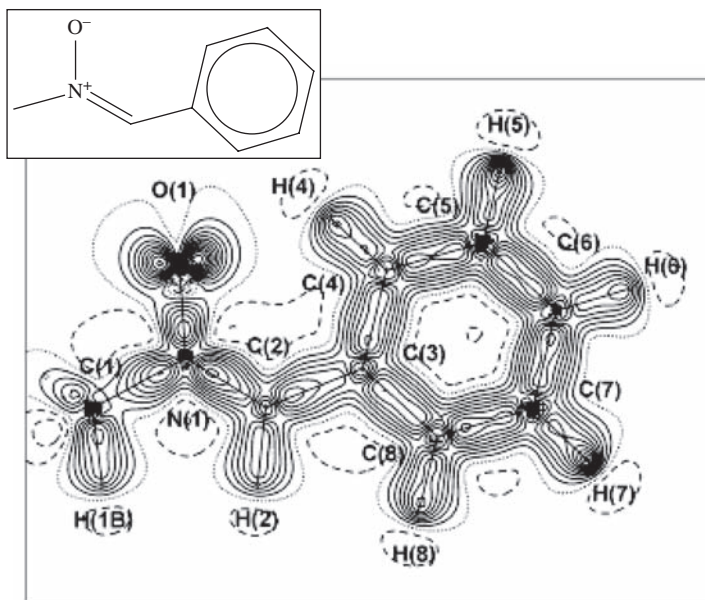


Figure 7.3 An example experimental electron density difference map for (Z)-N-methyl-C-phenylnitrone. The solid (dashed) contours are for an increased (decreased) electron density compared with a simple sum of noninteracting atomic densities. The inset in the top left shows a chemical structure of the same molecule in roughly the orientation in the contour plot. (Source: Hibbs DE, Hanrahan JR, Hursthouse MB, Knight DW, Overgaard J, Turner P, Piltz RO, Waller MP (2003) *Organic & Biomolecular Chemistry* **1**: 1034–1040.)

oxygen atom O(1) the charge density has also increased in two distinct lobes at roughly 120° to the N(1)–O(1) bond. This is an image of the ‘lone pair’ density at the oxygen atom, showing that the surplus electrons that are not used in chemical bonding tend to concentrate in regions orientated in definite directions with respect to the chemical bonds.

The experiments that generate charge density maps show us how the electrons as a whole are distributed in a molecule, but do not show the orbitals they occupy. In the Born interpretation, the electron density $\rho(r)$ at a point r is linked to the set of occupied MOs $\phi_i(r)$ by a summation of the wavefunction magnitudes squared:

$$\rho(r) \, d\tau = \sum_{i=1}^{N_{occ}} n_i \phi_i^*(r) \phi_i(r) \, d\tau \quad (7.1)$$

where $d\tau$ is an infinitesimal volume element of space around the point r and n_i is the number of electrons occupying MO i . We can ignore empty orbitals in this calculation, and so the sum is over all occupied orbitals N_{occ} . The asterisk on the first wavefunction in the sum indicates that the complex conjugate of the orbital should be used. This is one consequence of the fact that wavefunctions cannot be observed directly; and so they may contain imaginary numbers. The role of imaginary numbers in wavefunctions is outlined in

Appendix 9; for now, though, we just note that the product of a function with its own complex conjugate gives a real (nonimaginary) value that is the magnitude of the wavefunction squared; the wavefunctions may contain imaginary numbers, but the density will be real and so observable.

So the product in the summation in Equation (7.1) can be interpreted as the square of the ‘size’ of the wavefunction at the point r . The square of the wavefunction will be positive even when the phase of the wavefunction is locally negative. However, the phase of the wavefunction is important in chemical bonding since it determines the interference pattern when MOs are constructed from two or more AO functions, as we saw in Figure 7.2.

The relationship in Equation (7.1) is illustrated in Figure 7.4, which shows an example set of MOs calculated for the polyaromatic molecule phenanthrene ($C_{14}H_{10}$). The four

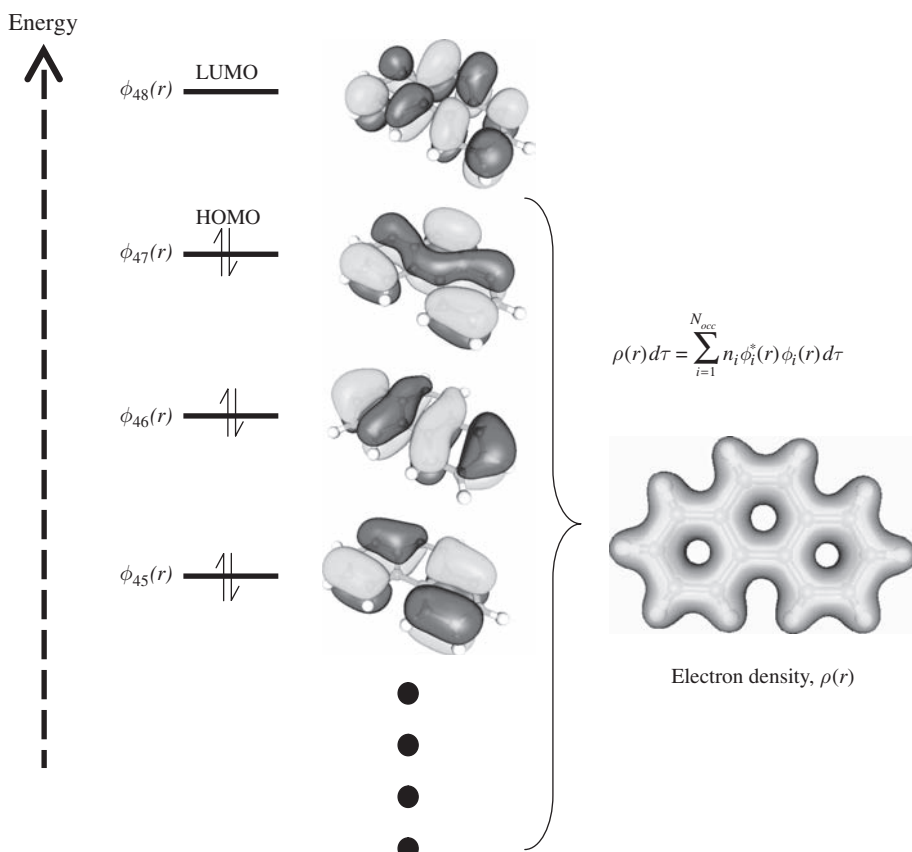


Figure 7.4 The relationship of the electron density to the occupied MOs using the example of phenanthrene. The MO diagram on the left of the figure is drawn with the convention that orbital energy increases up the page. In the ground state, MOs are filled from the lowest to the highest by pairs of electrons. For phenanthrene, the highest occupied MO (HOMO) is number 47, leaving number 48 empty and so the lowest unoccupied MO (LUMO). The Born convention gives the formula, shown to the right (Equation (7.1)), to relate the observable electron density to the underlying MOs.

MOs (numbers 45–48) are set out in order of energy, with the lines on the left of the diagram indicating their energy levels. Each energy level is a quantum state that differs in the spatial pattern of the MO. In addition, the electrons can have their spin in one of two possible orientations: spin up and spin down. This means that each MO can accommodate up to two electrons, as indicated by the pair of arrows in each occupied energy level. Working out which orbitals will be occupied requires the number of electrons in the molecule to be calculated: neutral carbon atoms have the electronic configuration $1s^2\ 2s^2\ 2p^2$ and hydrogen atoms have $1s^1$, so that the energy levels in phenanthrene must accommodate $6 \times 14 + 1 \times 10 = 94$ electrons. The lowest energy state for the system is obtained by filling the energy levels from the bottom up, so in Figure 7.4 all orbitals from 1 to 47 are occupied and those from 48 upward are empty. This is the ground-state configuration for the molecule, which gives the electron distribution with the lowest energy. The ground state is used to discuss chemical bonding for molecules free of external influences (such as excitation by photons). For phenanthrene, Equation (7.1) states that the observed electron density distribution is the sum of the squares of the amplitudes for MOs 1–47 with each having an occupation number $n_i = 2$.

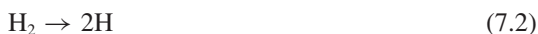
In the ground state, the HOMO contains the most weakly bound electrons and so will be important for intermolecular interactions that involve donation to another molecule. Likewise, the LUMO can be thought of as available to receive donated electrons.

7.2 Bond Energies

The MOs discussed above give the distribution of electrons around the nuclei, and we will spend most of this chapter looking at the energy levels this creates for the electrons. The electrons and nuclei of the molecule have opposite charges; thus, they will have attractive Coulomb interactions that depend on the way the electrons are distributed, and so on the wavefunctions. In addition, we will also see that the electron kinetic energy is determined by the shape of the MOs. In this section we will outline how the MO energies fit in with the idea of bond energy.

If we think about a simple diatomic molecule, the MOs formed from the two sets of AOs may have lower or higher energy than the constituent AOs. Those with lower energy are referred to as ‘bonding’ orbitals and those with higher energy as ‘antibonding’ orbitals.

For a diatomic molecule, such as H_2 , the concept of the bond energy is well defined and we would like to relate the MO energies to this experimentally measurable quantity. For a diatomic molecule the bond energy is the energy that must be supplied to dissociate the bond, separating the atoms so that they no longer interact:



Experimental measurements will actually give the bond enthalpy change ΔH for this process, which is related to the change of internal energy ΔU for an experiment taking place at constant pressure P by

$$\Delta H = \Delta U + P\Delta V \quad (7.3)$$

Clearly, the change of volume for Equation (7.2) will be considerable, as 1 mol of a diatomic gas is being converted to 2 mol of monatomic gas. This effect is subtracted out

in most references to give the change of internal energy, which is more relevant to the chemical bond dissociation energy.

From a molecular perspective we can think of plotting the bond potential energy as a function of the internuclear separation, as illustrated in Figure 7.5. The low point on this plot corresponds to a minimum energy D_e . This is marked in this figure as the energy difference between the bottom of the potential well (at R_o) and the atoms separated to large R .

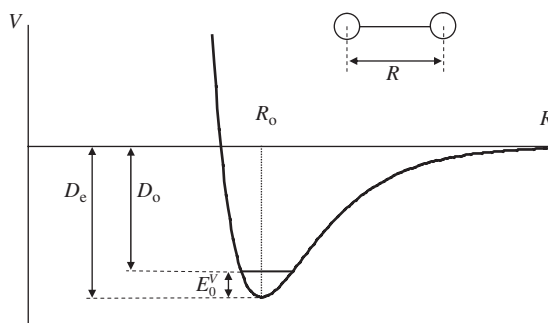


Figure 7.5 The potential energy of two atoms as a function of their internuclear distance. The potential energy minimum is at the optimal bond length R_o and defines the minimum bond potential energy D_e . The observed bond dissociation energy is smaller by an amount equal to the zero-point vibrational energy E_0^v .

The potential energy curve in Figure 7.5 is the Morse curve we first met in Section 6.2.4. There, the discussion of vibrational motion concentrated on the region near the potential minimum and the vibrational energy levels E_n^v were described with the harmonic approximation

$$E_n^v = (n + \frac{1}{2})\hbar\nu \quad (7.4)$$

with n a quantum number taking values $0, 1, 2, \dots, v$ (s^{-1}) the vibrational frequency of the mode and \hbar the Planck constant. The superscript v has been added to E_n^v to distinguish it from the electronic energy levels discussed in the rest of this chapter.

The harmonic approximation is valid because the movement of the atoms around the optimal bond length R_o in a vibration is small. However, Equation (7.4) tells us that a molecule can never quite attain the minimum energy on the bond potential curve because it will always have vibrational energy of at least the $n = 0$ vibrational state, i.e. $E_0^v = \frac{1}{2}\hbar\nu$. This quantity is the zero-point energy (ZPE) for the bond. Figure 7.5 shows that the experimentally observed bond dissociation energy D_o will always be less than estimates based on the minimum potential energy by an amount equal to E_0^v .

The dissociation process involves the atoms moving from R_o to become noninteracting atoms and so D_e and D_o are quoted as positive values. The effect of the ZPE on bond energies is small, but significant. For example, Table 7.1 quotes the experimental bond dissociation energy D_o for H_2 as 432 kJ mol^{-1} ; the vibrational frequency of H_2 is 4160 cm^{-1} , so the bottom of the potential energy well would be 25 kJ mol^{-1} lower, giving $D_e = 457 \text{ kJ mol}^{-1}$, due to the ZPE.

Table 7.1 The bond lengths and bond dissociation energies for the diatomic species H_2 , H_2^+ and He_2^+ . Values for bond dissociation energies are taken from Linde DR (ed.) (2005–6) CRC Handbook of Chemistry and Physics, 86th edition, Taylor and Francis, adjusted to 0 K.

Molecule	Bond length/ Å	Bond dissociation energy $D_e/ \text{kJ mol}^{-1}$
H_2	0.74116	432
H_2^+	1.06	255
He_2^+	1.08	230

Problem 7.2: The vibrational frequency of D_2 is 2990 cm^{-1} . Assuming that the chemical bond in D_2 is identical to that of H_2 , show that there will be a difference between the observed dissociation energy and potential minimum of 18 kJ mol^{-1} .

For polyatomic molecules, the bond dissociation energy refers to one particular bond cleavage event, while the bond energy is the average for the series of bond dissociations required to separate the molecule into atoms. For example, for H_2O :



So, it is harder to remove the first H than the second. The bond energy for H_2O is the average of these two, i.e. 459 kJ mol^{-1} . Note that in these expressions we have separated the bonds into neutral radicals, hence the ‘•’ symbol. The bond energies refer to these homolytic cleavage processes, rather than to the heterolytic splitting of H_2O to produce an anionic hydroxyl and proton.

In our analysis of the MO picture of the chemical bond we tend to ignore the ZPE effect. Although it is important, it is easier to work with the larger energy changes that occur due to the rearrangement of electrons and nuclei during bond formation and then reintroduce vibrational energy differences if comparison with experiment is needed.

The energy of the electronic system E_{el} , as estimated by MO calculations, is simply a sum over all the occupied orbital energies:

$$E_{\text{el}} = \sum_{i=1}^{N_{\text{occ}}} n_i E_i \quad (7.5)$$

So, we can estimate the contribution of the electronic states to the bond dissociation energy if we know the orbital energy levels E_i for the reactant and product sides of reactions such as in Equation (7.2). In the next few sections we outline the application of the Schrödinger equation to the simplest of molecules H_2^+ and H_2 . This will allow us to obtain the orbital energy levels for these molecules. We will also see how the shapes of the orbitals and the way they are built from an AO basis can give insight into their relative energies. This

means we can roughly estimate the contribution of an orbital to the stability of a molecule without recourse to complex calculations.

The Schrödinger equation used to develop MO theory should contain potential energy terms for the interaction energy of the electrons with nuclei and electrons with each other. The bond energy also requires the change in internuclear repulsion to be quantified: the repulsion between the nuclei in the molecule is not present in the separated atoms of Equation (7.2), and so there must be an unfavourable nuclear contribution to the bond energy. However, as the nuclei are well represented as point charges, this term is quite easy to calculate.

The interactions of electrons and nuclei largely depend on Coulomb's law, which says that the interaction energy between charges depends on the reciprocal of their separation. If the separation becomes infinite, then the calculated potential energy tends to zero. As opposite charges interact (e.g. nuclei and electrons), the result is a negative energy. Accordingly, MO calculations usually give negative energies, and when they are used in bond energy calculations, along with an estimate of the internuclear repulsion, it is the bond formation energy $-D_e$ that is obtained.

7.2.1 The Symmetry-Adapted Linear Combinations for the Molecular Orbitals of H_2^+ and H_2

The dihydrogen cation H_2^+ is the simplest molecular species we can study; it has only one electron, and so the corresponding Schrödinger equation can actually be solved exactly. This makes it an ideal subject for considering the concept of a chemical bond at a fundamental level. In Appendix 10 we cover the question of why H_2^+ should be stable with respect to a separated H atom and H^+ cation in some detail. The study of H_2^+ gives us insight into the contributions that make up the stabilization energy from the various interactions between electrons and nuclei. We will comment on these contributions to bonding after setting up the relevant MOs.

In the linear combination of AOs model, the MOs are built from the AOs derived for H-like atoms (see Appendix 9). The H atom in isolation has the simple electronic structure $1s^1$, and so in the H_2 molecule, or its cation, we are interested in SALCs of the two atomic s-orbitals centred on the two H nuclei.

H_2^+ , H_2 and any other homo-diatomic molecule belong to the point group $D_{\infty h}$. Taking the two s-orbitals as sketched in Figure 7.6a as a basis, any operation which does not swap the atoms over will have character 2, while any operation which interchanges the atoms will have character 0. It is then easily shown (Problem 7.3) that this reducible representation gives two SALCs:

$$1\sigma_g^+ = N_{1g}(s(\text{H}_1) + s(\text{H}_2)) \quad (7.6)$$

$$2\sigma_u^+ = N_{2u}(s(\text{H}_1) - s(\text{H}_2)) \quad (7.7)$$

where N_{1g} and N_{2u} are normalization constants. The convention in chemical bonding is to use lower case symmetry labels for MOs and to number those of the same symmetry sequentially from the lowest energy SALC to the highest. In the case of molecules belonging to the $D_{\infty h}$ group, the distinction of *gerade* (g) and *ungerade* (u) orbitals in this

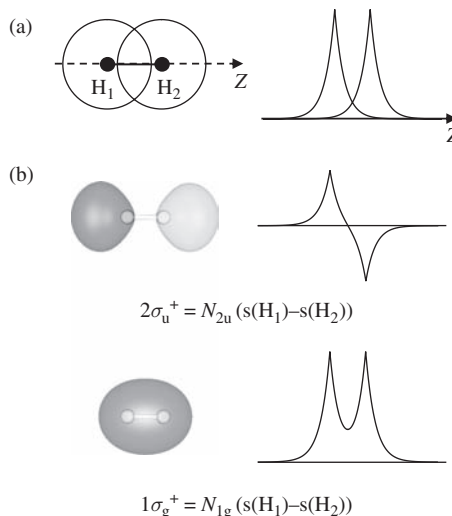


Figure 7.6 (a) The two 1s orbitals for the H_2 molecule sketched as noninteracting orbitals, to the right is a plot of the radial decay of the 1s orbitals away from the nuclear centres. (b) The MOs for the H_2 molecule. In the $1\sigma_g^+$ SALC the AOs reinforce one another in the internuclear region, building up negative charge between the two positive nuclei. In the $2\sigma_u^+$ combination the two s-orbitals have opposite phase and cancel each other at the bond centre.

numbering scheme is neglected. This will make the comparison between homonuclear diatomic ($D_{\infty h}$) and related heteronuclear diatomic ($C_{\infty v}$) molecules more straightforward.

Problem 7.3: Write out the reducible representation for the basis of two H(1s) orbitals in the H_2 molecule. Then use the elimination method introduced in Section 6.2.2 to confirm that the irreducible representations σ_g^+ and σ_u^+ are correct for the SALCs in Equations (7.6) and (7.7).

Figure 7.6a shows sketches of the two basis function orbitals drawn as noninteracting spheres around the H atoms. The illustration to the right shows the radial profile of the basis functions. In the molecule, the two orbitals overlap, and so the MO will be affected by the interference of the s-orbital functions in this internuclear region. Both s-orbitals have the same phase for the $1\sigma_g^+$ SALC, so in the overlap region they reinforce one another, leading to an increased charge density compared with that of either s-function alone. The $2\sigma_u^+$ MO, on the other hand, has destructive interference in the internuclear region, leading to a reduced wavefunction amplitude which falls to zero at half the bond length and gives a negative phase orbital around H_2 , as indicated by the SALC in Equation (7.7).

For the corresponding electron density we can make use of the Born interpretation of the wavefunction again. This states that the product of the wavefunction and its own complex conjugate gives the probability per unit volume of finding an electron occupying the orbital

at a given point in space. In this case, the 1s basis functions are real (they contain no imaginary part); so, if we choose any point r , the probability becomes

$$P_{\text{lg}}(r)\delta\tau = (1\sigma_g^+(r))^2 \delta\tau \quad (7.8)$$

where $1\sigma_g^+(r)$ is the value of the wavefunction at point r and $\delta\tau$ is a small volume around r . We can never define the probability of the electron being exactly at r , only within this small volume centred on r .

Writing the $1\sigma_g^+$ MO as its SALC of the basis functions from Equation (7.6) gives the probability in terms of the basis functions:

$$P_{\text{lg}}(r)\delta\tau = N_{\text{lg}}^2 s_1^2 \delta\tau + N_{\text{lg}}^2 s_2^2 \delta\tau + 2N_{\text{lg}}^2 s_1 s_2 \delta\tau \quad (7.9)$$

where the shorthand $s_i = s(r, H_i)$, i.e. the value of the i th s-orbital at position r , has been introduced.

Applying the same procedure to the $2\sigma_u^+$ MO from Equation (7.7) gives

$$P_{\text{lu}}(r)\delta\tau = N_{\text{lu}}^2 s_1^2 \delta\tau + N_{\text{lu}}^2 s_2^2 \delta\tau - 2N_{\text{lu}}^2 s_1 s_2 \delta\tau \quad (7.10)$$

Equations (7.9) and (7.10) say that the electron density associated with the $1\sigma_g^+$ or $2\sigma_u^+$ MO at any point is actually made up of two types of contribution. The first two terms contain s_1^2 and s_2^2 , and so involve only single basis functions; but the third term, $s_1 s_2$, is a mixture of basis functions, so we will now look at how these terms contribute to the total density.

To imagine the shape of the density it is useful to simplify the three-dimensional function defined for $P(r)$ by reducing to one dimension in some way. A $D_{\infty h}$ molecule is conventionally taken to be aligned with its principal C_∞ axis along the Z-direction; it must also have cylindrical symmetry, and so the density will be constant around any circle centred on the molecular axis and parallel to the XY plane. So one way to simplify $P(r)$ is to integrate over planes perpendicular to the molecular axis and then plot these values as a function of z . This is like taking slices through the molecule and then plotting the total density from each slice at its z coordinate. More detail of the required procedure is given in Appendix 10. The results for the $1\sigma_g^+$ and $2\sigma_u^+$ SALCs are illustrated in Figure 7.7a and b respectively. For the $1\sigma_g^+$ MO the first two terms are added to the contribution from the basis overlap $2N_{\text{lg}}^2 s_1 s_2$, and this leads to a high value for the density in the internuclear region for $(1\sigma_g^+)^2$. In the $2\sigma_u^+$ case the overlap contribution is subtracted from the first two terms, and so there is a lowering of the density in between the nuclei. In Appendix 9 it is shown that the H 1s orbital follows an exponential function:

$$s_i = A \exp\left(-\frac{r_i}{a_0}\right) \quad \text{with} \quad A = \frac{1}{\sqrt{\pi}} \left(\frac{1}{a_0}\right)^{3/2} \quad (7.11)$$

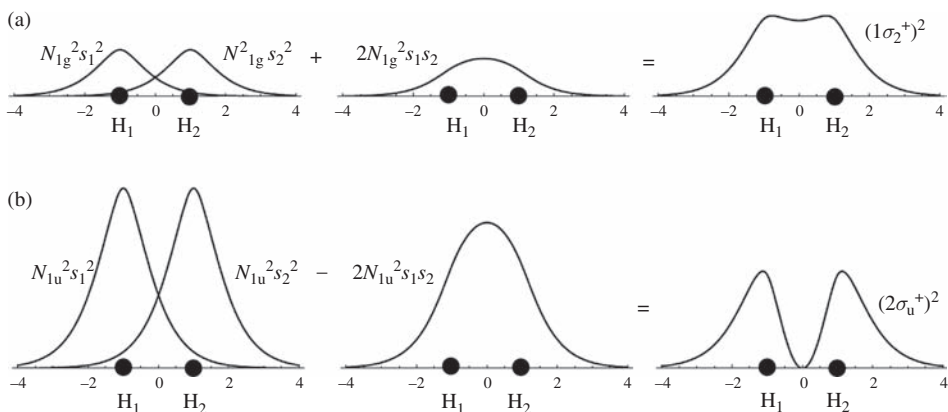


Figure 7.7 The components of the bond density from different basis products calculated for H_2^+ in (a) the $1\sigma_g^+$ and (b) $2\sigma_u^+$ linear combinations. In these diagrams, the density in planes perpendicular to the z -coordinate has been integrated to give a one-dimensional plot.

where r_i is the distance from the i th nucleus and a_0 is the Bohr radius. For the plane on the bond centre all points are equidistant from the two nuclei; so $r_1 = r_2$, meaning that

$$s_1^2 = s_2^2 = A^2 \exp\left(-\frac{2r_1}{a_0}\right)$$

and

$$s_1 s_2 = A^2 \exp\left(-\frac{r_1}{a_0}\right) \exp\left(-\frac{r_2}{a_0}\right) = A^2 \exp\left(-\frac{2r_1}{a_0}\right) \quad (7.12)$$

on the bond centre plane. This ensures that the density of the $2\sigma_u^+$ orbital is always zero at the bond centre whatever the internuclear distance.

The density plots of Figure 7.7 have been drawn with appropriate normalization constants for the experimental bond length in H_2^+ . To find these normalization constants, the Born interpretation of the one-electron wavefunctions has been applied to an integration ‘over all space’ of the MOs. The density plots give the probability of finding the electron on a given z -plane. If we integrate all along the molecular axis, we sum $(1\sigma_g^+)^2$ or $(2\sigma_u^+)^2$ through all space and must find a total probability of 1. This is the normalization condition for one-electron wavefunctions: integrating the probability over all space must result in a unit probability.

We will use a simple shorthand for such ‘all space’ integration; for example, for the $(1\sigma_g^+)^2$ integration we write

$$\int_{-\infty}^{\infty} P(r) dr = \int_{-\infty}^{\infty} (1\sigma_g^+)^2 dr = N_{1g}^2 \left(\int_{-\infty}^{\infty} s_1^2 dr + \int_{-\infty}^{\infty} s_2^2 dr + 2 \int_{-\infty}^{\infty} s_1 s_2 dr \right) = 1 \quad (7.13)$$

The full three-dimensional integrations are laid out in various coordinate systems in Appendices 9 and 10. The first two integrals here are over the squares of AO basis functions. We can reasonably expect these to be normalized, and so the first two integrals are each 1. The third integral arises from the orbital overlap and accordingly is referred to as the overlap integral S_{12} :

$$S_{12} = \int_{-\infty}^{\infty} s_1 s_2 \, d\tau \quad (7.14)$$

We did not meet this sort of term in Chapter 6 because all basis vectors in the vibrational analysis were taken to be orthogonal to one another, so that such terms integrate to zero. However, we cannot assume that the basis functions are orthogonal here. Orthogonality would imply that the basis functions are completely independent, but Figure 7.6b shows that the two basis functions of the AOs interact strongly, particularly in the overlap region. So, to work out N_{1g} from Equation (7.13), the integral over the product of s_1 and s_2 has to be retained. We can only calculate the normalization factor based on this overlap integral:

$$2N_{1g}^2(1 + S_{12}) = 1 \quad \text{so that} \quad N_{1g} = \frac{1}{\sqrt{2(1 + S_{12})}} \quad (7.15)$$

For the $1\sigma_g^+$ orbital the overlap integral quantifies the build up of charge in the internuclear region. When the nuclei are far apart, S_{12} will tend to zero and N_{1g} becomes $1/\sqrt{2}$, the value found for two equally weighted orthogonal functions in Chapter 6. As the nuclei approach, some of the density is described by the overlap integral, and so N_{1g} is reduced to ensure the wavefunction remains correctly normalized.

Problem 7.4: Show that for the antibonding MO $2\sigma_u^+$ the normalization factor is

$$N_{2u} = \frac{1}{\sqrt{2(1 - S_{12})}} \quad (7.16)$$

Problem 7.4 shows that the overlap integral appears with a negative sign in the $2\sigma_u^+$ MO normalization factor. In the density plot, it can be seen that the overlap contribution is now subtracted from the single basis function components. As the overlap becomes significant, the normalization factor has to increase to ensure the overall density remains normalized. Note that since S_{12} is in the range 0–1, a negative sign cannot appear in the square root of the denominator of Equation (7.16).

7.2.2 The Chemical Bond Energy from Molecular Orbitals

Figure 7.5 implies that for atoms to come together in a molecule the total energy must be lower than for the atoms in isolation. So, to get an idea of what a chemical bond is, we need to estimate the energy of the MOs using the Schrödinger equation.

In Appendix 10 we look in detail at the simplest molecular system, the dihydrogen cation H_2^+ . This is a molecule with only one electron, and so only electron–nuclear and nuclear–nuclear interactions need be considered. Here, we summarize the findings of Appendix 10 and identify the contributions to the total energy of the molecule in terms of the basis functions.

To estimate the MO energies we turn to the Schrödinger equation applied to the MO SALCs, which is simply written thus:

$$H\phi_i = E_i\phi_i \quad (7.17)$$

Here, the subscript i is used to label the MO, ϕ_i ; for this H_2^+ example, taking $i = 1$ would set ϕ_i to $1\sigma_g^+$. The MO is a function that, as we have seen, describes how an electron is distributed over space. In Equation (7.17), H is the Hamiltonian, which contains the operators to obtain the energy of the electron averaged over its distribution; the result is the orbital energy E_i , which is a simple number.

The chemical bond formation energy is the energy gained when the H atom and H^+ cation come together to form the molecular cation in its ground state. We can work out the energies of the two orbitals $1\sigma_g^+$ and $2\sigma_u^+$ from Equation (7.17) as outlined below. As a first estimate of the chemical bond energy with the electron in one or other of these orbitals, we then just need to add the internuclear repulsion energy and remove the H $1s^1$ energy of the atomic state. The results are plotted as a function of internuclear separation in Figure 7.8.

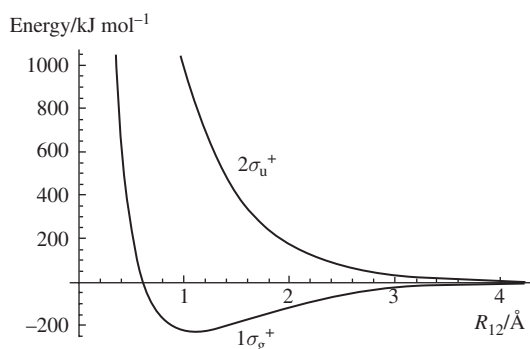


Figure 7.8 The potential energy of H_2^+ as a function of the internuclear distance. The MO occupied by the single electron is indicated next to each curve.

To obtain Figure 7.8, the Hamiltonian for the electron states was first split into electronic kinetic T and potential V operators:

$$(T + V)\phi_i = E_i\phi_i \quad (7.18)$$

Appendices 9 and 10 discuss the forms of the T and V operators for the hydrogen-like AOs and H_2^+ MOs respectively. The potential depends on the particular system; for the H atom there is just the field of the single proton, while the electrostatic interaction of the

electron with the two nuclei is needed for H_2^+ . Here, we are talking about the potential energy of the electron rather than the potential energy of the whole molecule, and this depends on the way the MO that the electron occupies is distributed around the nuclei. The kinetic energy of an electron in an MO is related to the second derivative, or curvature, of ϕ_i with respect to its coordinates.

It should be expected that the MOs are normalized, so we can obtain an equation for E_i by multiplying both sides of Equation (7.18) by ϕ_i^* (the complex conjugate of ϕ_i) and then integrating over all space:

$$E_i = \int_{-\infty}^{\infty} \phi_i^*(T + V)\phi_i \, d\tau = \int_{-\infty}^{\infty} \phi_i^* T \phi_i \, d\tau + \int_{-\infty}^{\infty} \phi_i^* V \phi_i \, d\tau = \langle T(\text{H}_2^+)_i \rangle + \langle U(\text{H}_2^+)_i \rangle \quad (7.19)$$

The MO normalization condition has been used to set the integral formed on the E_i side of the equation to 1. The integral on the H side cannot be dispensed with so simply, because $H (= T + V)$ is an operator rather than a simple number like E_i . These integrals give the kinetic and potential energy of the electron averaged over the electron distribution in orbital i . These averaged properties are commonly called ‘expectation values’, and the fact that the averaging has been carried out is indicated by the angular brackets $\langle \rangle$. So, we will denote the expectation value of the kinetic energy as $\langle T(\text{H}_2^+)_i \rangle$ and that of the potential as $\langle U(\text{H}_2^+)_i \rangle$. The individual contributions to the bond formation energy are obtained by subtracting the corresponding expectation values for the atomic H state from which the molecular ion has been formed. Since Equation (7.19) only deals with the electronic states, we also have to add in the nuclear–nuclear repulsion V_{nn} given by

$$V_{nn} = \frac{e^2}{4\pi \varepsilon R_{12}} \quad (7.20)$$

where ε is the permittivity of free space ($8.854 \times 10^{-12} \text{ C}^2 \text{ N}^{-1} \text{ m}^{-2}$). The calculated interatomic bond potential for H_2^+ , along with the kinetic and potential energy contributions, is plotted for the electron ground-state $1\sigma_g^+$ MO in Figure 7.9. Units of kilojoules per mole have been used to allow comparison with the experimental bond dissociation value. The minimum on this curve gives an estimate for the bond formation energy of -225 kJ mol^{-1} , which compares reasonably well with the measured bond dissociation energy of 255 kJ mol^{-1} from Table 7.1. More accurate calculations can be made by extending the basis set on the atoms to p- and d-orbitals (see Further Reading section of this chapter).

Figure 7.9 shows how both the kinetic and potential expectation values are important in bond formation. The major attraction between the centres at large nuclear separations is a lowering of the electron kinetic energy as it spreads out in the molecular bonding orbital, reducing the curvature of the orbital. The potential energy is actually greater than the atomic state for separations above about 1.9 \AA , but below this it falls rapidly and is the dominant negative term at the equilibrium geometry.

For the simplest of examples, i.e. H_2^+ , Appendix 10 shows that there are three important contributions to the bond formation energy which can be understood in terms of the orbital and density plots for the $1\sigma_g^+$ and $2\sigma_u^+$ molecular orbitals (Figure 7.7):

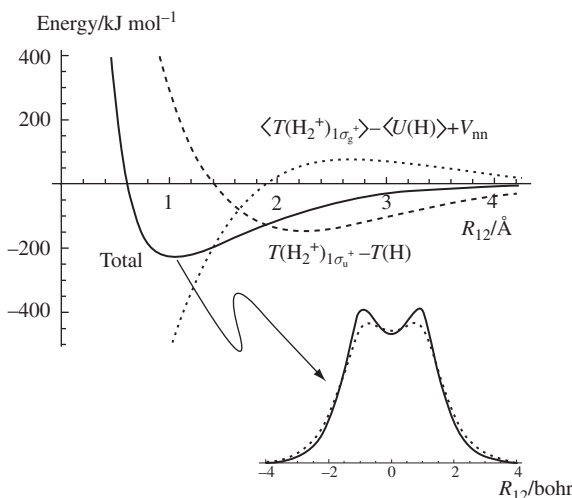


Figure 7.9 The contributions of the electron kinetic and potential energy expectation values to the interatomic potential curve for H_2^+ . The internuclear term is also added to ensure the potential goes to zero at large R_{12} . The inset plot (bottom right) shows the electron density integrated over planes perpendicular to the bond axis with the basis set decay factor optimized at the potential minimum; the dotted curve shows the density that would be obtained using the decay factor for an isolated H atom.

1. The kinetic energy. The build up of electron density between the nuclei in $1\sigma_g^+$ means that the wavefunction along the $\text{H}-\text{H}$ bond has a more gradual variation with internuclear distance than would be the case for either atom in isolation. This makes the second derivative, and so the kinetic energy, lower in this region than at a similar position in the orbital of the isolated atom. In contrast, the $2\sigma_u^+$ SALCs falls more rapidly, passing through zero at the bond centre. A zero in a wavefunction such as this is referred to as a node and, in general, the kinetic energy increases with the number of nodes (see Appendix 10). This is a contributing factor to the order of the energy levels for the wavefunctions of, for example, phenanthrene (shown in Figure 7.4).
2. The potential energy. The two nuclei have the same positive charge and so will tend to repel each other. The constructive interference in the $1\sigma_g^+$ orbital will increase the density in the internuclear region and so place some negative charge between them, countering the internuclear interaction and so lessening its destabilizing effect. Taking these together, the electron density can be thought of as shielding the nuclei from one another. This is often seen as a signature for a chemical bond; for example, in the electron density plot of Figure 7.3 there is a build-up of density between neighbouring atoms, and this signifies chemical bonding.

However, the density plots in Figure 7.7a show that the probability of finding the electron in H_2^+ occupying $1\sigma_g^+$ outside of the internuclear region is still considerable, and so the shielding must be incomplete. For H_2^+ , the net effect of nuclear–nuclear and electron–nuclear interactions based on AOs is to destabilize the molecule. The shielding

effect in the $2\sigma_u^+$ orbital is clearly less, as the internuclear region actually has reduced electron density compared with noninteracting atoms at the same separation.

3. If we limited ourselves to basis functions which are optimized for the atomic state we would have to conclude that the bond formation energy in H_2^+ comes from the decrease in kinetic energy as the electron moves from an atomic to a molecular bonding orbital. However, it would be surprising if the radial decay of the s-orbitals remained the same in the H_2^+ molecule as in the H atom, because the nuclear potential has been changed by the inclusion of a second nucleus. The inset in Figure 7.9 gives a plot of the electron density in the bonding orbital and shows that the changing environment as the electron moves from the AO to the MO causes a contraction around the nuclei. On average, the electron spends more time close to the nuclei than it would if we use the 1s orbital basis with the decay constants from the atomic states. The expectation value for the potential energy is lowered by this effect, making it the stabilizing term in the bond formation energy.

This final point is a subtle effect that we will not consider again; the qualitative picture can be obtained without it. However, in calculations using computer packages (such as the H_2O example given in Appendix 11), the basis set usually contains more than one basis function for each AO to account for such changes of shape. The idea is to have functions that decay differently with distance from the nuclei. If we have one function that goes toward zero faster than the atomic 1s function and one that decays more slowly, then a linear combination can give any behaviour in between. This gives the basis set in a calculation the flexibility to reproduce the contraction effect discussed in point (3) and so give a lower bonding orbital energy than would be found for just a single basis function for each atomic orbital.

7.2.3 The Molecular Orbital Energy

To appreciate the MO picture of chemical bonds, the level of detail given above is not actually required. We will not usually even be concerned with separating the Hamiltonian into its kinetic and potential components. However, we do need to consider the role of the overlap of basis functions in the chemical bond energy. Using the example of H_2 with the SALC representation for the bonding orbital $1\sigma_g^+$ (Equation (7.6) with N_{1g} from Equation (7.15)), we can estimate the orbital energy from the expectation value of the Hamiltonian:

$$\begin{aligned} E_{1g} &= \frac{1}{2(1 + S_{12})} \int_{-\infty}^{\infty} (s_1 + s_2) H(s_1 + s_2) d\tau \\ &= \frac{1}{2(1 + S_{12})} \left(\int_{-\infty}^{\infty} s_1 H s_1 d\tau + \int_{-\infty}^{\infty} s_2 H s_2 d\tau + \int_{-\infty}^{\infty} s_1 H s_2 d\tau + \int_{-\infty}^{\infty} s_2 H s_1 d\tau \right) \end{aligned} \quad (7.21)$$

The first two terms here involve only a single basis function; these represent the energy an electron would have if confined to either of the single s functions; to simplify the discussion, the value of such integrals will be written as Q . The second two integrals involve both

basis functions and are only nonzero when the H atoms are interacting. These are referred to as resonance integrals β and are the major part of the chemical bonding energy of the system; with these substitutions we obtain

$$E_{1g} = \frac{Q + \beta}{1 + S_{12}} \quad (7.22)$$

Similarly, substitution of the SALC for $2\sigma_u^+$ results in

$$E_{2u} = \frac{Q - \beta}{1 - S_{12}} \quad (7.23)$$

When the H atoms are well separated, and so not interacting, both S_{12} and β become zero. E_{1g} and E_{2u} each reduce to Q , the energy of an isolated H atom. However, as the internuclear distance decreases, the orbitals overlap and the electron originally on H_1 can lower its energy by also interacting with the nucleus of H_2 . Similarly, the electron originally with H_2 can also feel the influence of the H_1 proton. These interactions result in a negative resonance integral β , and so we find $E_{1g} < E_{2u}$. The more the overlap between the orbitals, the greater is the magnitude of β , which stabilizes $1\sigma_g^+$ and destabilizes $2\sigma_u^+$ with respect to the free atoms, as illustrated in Figure 7.10. In this type of MO diagram we concentrate on the MO energies at one particular internuclear distance and how they differ from the reference atomic states. The separation chosen will usually be the optimum bond length, and so the electronic contribution to the bond formation energy can be estimated from the sum of the individual electron energies as given by the orbital energies. We concluded from Figure 7.8 that $1\sigma_g^+$ is a bonding orbital and $2\sigma_u^+$ antibonding. The same information can be drawn from the MO diagram: the $1\sigma_g^+$ level is below the atomic reference and the $2\sigma_u^+$ is above. Equations (7.22) and (7.23) also indicate that the energy increase incurred by occupying the $2\sigma_u^+$ orbital will outweigh the decrease from occupying the bonding $1\sigma_g^+$ level.

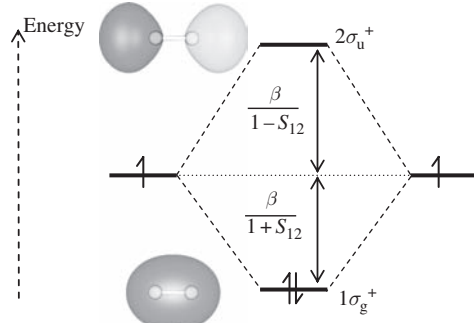


Figure 7.10 An MO diagram for H_2 , showing the formation of bonding $1\sigma_g^+$ and antibonding $2\sigma_u^+$ orbitals. The $2\sigma_u^+$ orbital is higher in energy, as destructive interference between the nuclei would lead to a low charge density. However, in H_2 , only the bonding orbital is occupied, stabilizing the molecule with respect to the separated atoms.

Figure 7.10 shows electrons as half arrows, with the arrow direction indicating the electron spin. In isolation each H atom has a $1s^1$ configuration; in the molecule, the $1\sigma_g^+$ MO

has a lower energy than the $2\sigma_u^+$, and so both electrons are placed in the $1\sigma_g^+$ level with antiparallel spins. This means that only the energy lowering state is occupied and so the molecule is stabilized by its electronic structure.

In the H_2 molecule there will, of course, also be electron–electron interactions, which tend to be repulsive; but for a large class of molecules, a working, qualitative, understanding of bonding can be obtained by assuming that the nuclear–electron interaction is dominant.

7.2.4 Bond Order

The MO picture gives an easy appreciation of the concept of the bond order of a chemical bond. The bond order quantifies the degree of covalent bonding between atoms. A simple estimate of bond order between two atoms, A and B, can be gained from a simple inspection of the MO diagram using the definition

$$B_{AB} = \frac{1}{2}(n_{\text{bond}} - n_{\text{anti}}) \quad (7.24)$$

where n_{bond} and n_{anti} are the number of electrons in the bonding and antibonding MOs respectively. For H_2 , placing the two available electrons into the stabilizing MO, $1\sigma_g^+$, leads to a bond order of 1. If an electron is removed from H_2 to produce the molecular cation H_2^+ , then the bond order will reduce to 1/2. The effect of this can be seen in Table 7.1. The bond length of H_2 is around 0.74 Å and the energy to separate the molecule into its constituent atoms, the bond dissociation energy, is 432 kJ mol⁻¹. The bond length of H_2^+ is 0.32 Å longer than H_2 and the bond energy 177 kJ mol⁻¹ less. So, the lower bond order gives a weaker chemical bond. Table 7.1 also gives data for the He_2^+ molecular ion, which has the electron configuration $(1\sigma_g^+)^2 (2\sigma_u^+)^1$. The data for He_2^+ is similar to H_2^+ , which may be expected since it also has a bond order of 1/2.

The hypothetical molecule He_2 would have a bond order of 0. In fact, the overlap integral in the denominator of the energy-level equations, Equations (7.22) and (7.23), means that the *ungerade* symmetry MO destabilizes this system slightly more than the stabilization gained by filling the $1\sigma_g^+$ level. Accordingly, He_2 is unstable with respect to isolated He atoms, and so helium is a monatomic gas.

The bond order from Equation (7.24) is a useful ‘rule of thumb’ estimate of the relative bond strengths to expect from MO diagrams. However, it does not take into account several factors which are important for estimating actual bond energies.

First, the effect of the overlap integral in Equations (7.22) and (7.23) is ignored. In the comparison of H_2 and H_2^+ , the longer bond length of the molecular cation will lead to a smaller overlap integral between the two H(1s) AOs forming the bond. This makes the orbital intrinsically less bonding, since the resonance integral β will be less negative.

Second, electron–electron repulsion is not taken into account. From the relative bond orders of H_2 and H_2^+ we would expect H_2^+ to have around half the bond energy of H_2 , with the longer bond length of the cation indicating an even weaker bond. However, from the data in Table 7.1, H_2^+ actually has a bond energy 0.59 that of H_2 , i.e. the cation has a stronger bond than expected. H_2^+ has only a single electron in the $1\sigma_g^+$ bonding orbital, and so there is no electron–electron interaction, as is present in H_2 , which leads to the neutral molecule being less stable than expected based only on the bond order estimate.

These are important points; for any quantitative work, electron–electron interactions must be taken into account, and the theories underpinning computation of MOs do this at various levels of accuracy. Approaches such as Hartree–Fock or density functional theory adapt the Hamiltonian operator to include electron–electron terms in an averaged way so electrons see the Coulomb field of each other averaged over the calculated density associated with each MO (see the Further Reading section in this chapter).

In the H_2 example, the atoms coming together in the molecule are identical. This results in MOs in which the electrons are evenly spread between the two nuclei (as illustrated for H_2^+ in Figure 7.7). Bonds formed through sharing of electrons between nuclei are termed covalent. In later sections we will consider cases in which the electrons are not evenly shared between the nuclei, so that the electronic charge is polarized toward one or other of the atoms. In extreme cases this will lead to charge transfer from one atom to the other, giving an anion and cation pair in an ionic bond.

Moving beyond the H_2 example, we will need to consider higher angular momentum AOs (p, d, etc.). One aspect of constructing MO diagrams like Figure 7.10 for heavier atoms is how to place the reference AOs correctly, i.e. where are the p-orbitals relative to s? For bonds between different types of atom we will also have to estimate the relative energies of the contributing AOs. These aspects are dealt with in the following two sections.

Four important generalizations can be made from this section:

1. An energy level in an MO diagram gives the energy an electron occupying that state would have. The total electronic energy is obtained by summing over the occupied energy levels.
2. The resonance integral, representing the bonding interaction, is negative and increases in magnitude with the overlap between the AOs.
3. Filling bonding orbitals with electrons stabilizes a chemical bond, but this is offset if the corresponding antibonding orbital is also occupied.
4. A simple definition of the bond order is the number of electrons in bonding orbitals minus the number in antibonding orbitals, divided by two. Hence, H_2 has a bond order of 1 while He_2 would have a bond order of 0.

7.3 The Relative Energies of Hydrogen-Like Atomic Orbitals

7.3.1 Radial Behaviour of Atomic Orbitals

The basis functions used in constructing MOs are the AOs based on the hydrogen atom solutions of the Schrödinger equation discussed in Appendix 9, with the proviso that accurate energies will require flexibility in the radial decay constants. Before moving on to molecules more complex than H_2 , it is worth looking at the shapes of the AOs relevant for the first row of the periodic table. We have already used the shapes of s-, p- and d-functions to discuss the symmetry of particular AOs (e.g. the d-orbitals of the central metal atom in transition metal complexes were covered in Section 5.8). These shapes are based on the

angular part of the AOs, i.e. how the orbital changes as we move around the atom centre. The s-functions are independent of the angular coordinates, whereas a p-function has a preferred direction (X , Y or Z) and has opposite phases on opposite sides of the atom. For bonding we will need to consider the mixing of these functions on neighbouring atoms, and so the decay of the functions away from the nuclear centres is also important.

Figure 7.11a shows the radial functions $R(r)$ for the H atom 1s, 2s and 2p orbital functions defined in Appendix 9. The 1s orbital is a simple exponential decay with distance from the nucleus r (Equation (7.11)). The 2s function looks similar at small r values but passes through zero and becomes negative at just over 1 Å. This, and any other point on the radial plot, actually represents a whole set of points at that radius defining a sphere centred on the nucleus. A zero in a wavefunction is referred to as a node; this is the radial node in the 2s function.

A 2p orbital has a radial part which is zero at $r = 0$ and has a maximum near to 1 Å, with no radial node. In the angular function, as it must pass through zero to move between

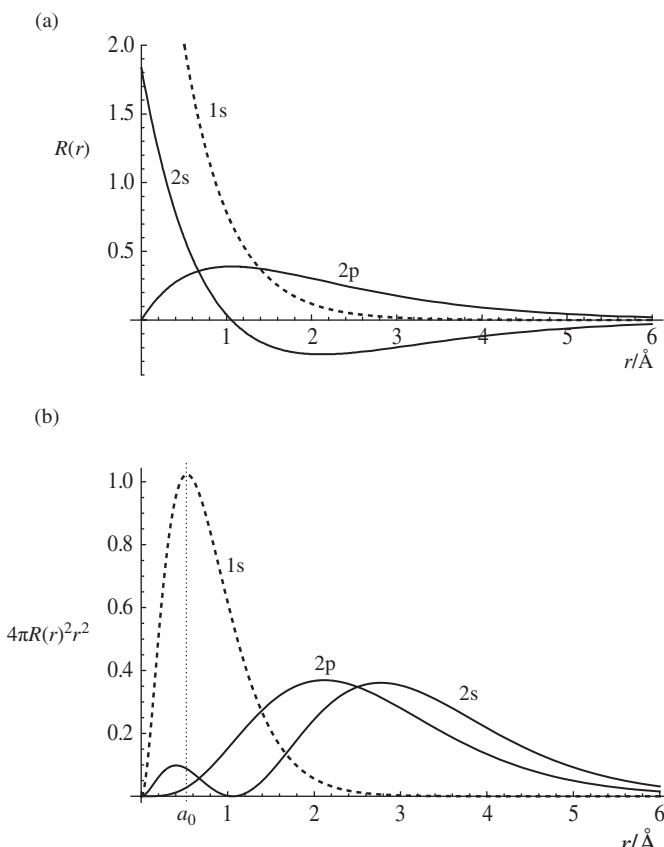


Figure 7.11 (a) The radial part of the H atom AOs $R(r)$ for 1s, 2s and 2p functions plotted against distance from the nucleus r . (b) The radial probability functions for the same set of AOs.

the positive- and negative-phase lobes, so the orbital stands perpendicular to an angular nodal plane.

All three radial functions decay toward zero at large r , with the 1s orbital approaching this limit more quickly than the 2s or 2p. This shows that electrons occupying these states would be localized by attraction to the positive atomic core, since the probability of finding an electron in such a state a long way from the nucleus will be vanishingly small.

The wavefunction can be used to obtain the probability of finding an electron at any particular distance from the nucleus by integrating over the surface of the sphere at that distance. As can be seen from Figure 7.12, the infinitesimal volume concerned depends on the surface area of the sphere of radius r . The mathematics of this is discussed in more detail in Appendix 9, but here we note that the relevant function for the radial probability is actually $4\pi r^2 R(r)^2$. The $4\pi r^2$ factor arises because the infinitesimal volume at a particular distance from the nuclear centre increases with r^2 . So there is four times more volume at 2 Å from the nucleus than at 1 Å. The plots of the probability function for 1s, 2s and 2p orbitals are shown in Figure 7.11b.

The 1s function shows a peak at around 0.529 Å; this is known as the Bohr radius a_0 and is the basic unit of distance used in the atomic units system discussed in Appendices 9 and 10. The same value was derived by Bohr as the radius for the orbit of the electron based on a classical physics analysis of the electrostatic interaction between the electron and nucleus in a hydrogen atom.

Figure 7.11b shows that the 1s orbital of a second-row element is much more compact than the 2s or 2p functions and so it is usually thought of as part of the atom core; it remains atomic-like even in molecules, while the 2s and 2p orbitals can become mixed into MOs. This leads to the idea of the valency of an atom, which is the number of electrons in these outer orbitals. As we progress down the periodic table, laying out all the occupancies of the

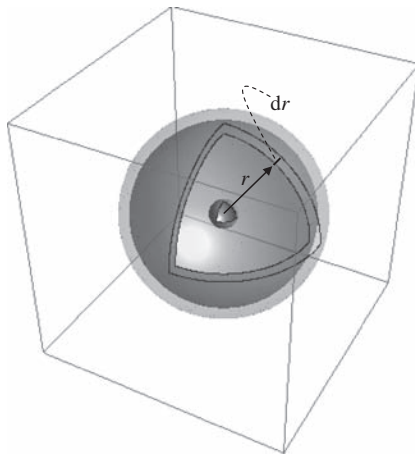
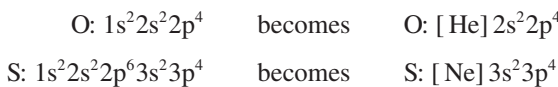


Figure 7.12 The infinitesimal volume at a distance r from the nucleus is the product of the surface area of a sphere of radius r and an infinitesimal change of radius dr . The surface area of the sphere has the effect of introducing a $4\pi r^2$ factor into the probability of finding the electron at that distance (see Figure 7.11b).

core orbitals becomes tiresome, and so it is common practice to list the equivalent ideal gas symbol for the core electrons and then only quote the detail of the valence orbitals, so that:



and



This makes it easier to recognize why atoms from the same group of the periodic table, such as these examples, have similar chemical properties.

The radial node in the 2s function gives it a minor peak in the probability density below the Bohr radius, which is not present for 2p. This means that a 2s electron will spend more time close to the nuclear centre than will one in a 2p atomic orbital. This, in turn, implies that the 2s orbital has a lower energy than the 2p orbital. The main peak in 2s is at just under 3 Å, a little beyond the peak in the 2p radial function; so, despite its lower energy, it is still available to mix with orbitals from neighbouring atoms in molecules.

These pictures of the orbital radial probabilities will be useful in understanding the relative energies of the AOs in the next section.

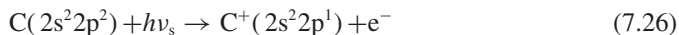
7.3.2 The Relative Energies of Atomic Orbitals in Different Elements

For the MO diagram of H₂ in Figure 7.10 the atomic energy levels for the two atoms are drawn at the same level, since they are identical atoms. For molecules containing atoms of different types we must estimate the relative energy of the constituent atomic states.

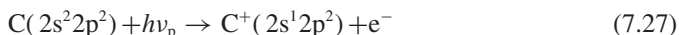
There are experimental probes of the electronic energy levels of atoms and molecules. Perhaps the simplest is provided by the ionization energies of the elements which have been obtained by determining the photon energies required to eject electrons from essentially isolated (gas-phase) atoms. The photon energy is simply related to the light frequency ν (s⁻¹) by the Planck constant h . For example, by measuring the lowest frequency radiation with which it is possible to ionize Li atoms, we are probing the ionization event



To a first approximation, the lowest photon energy hf at which ionization occurs gives a direct estimate of the energy of the orbital from which the photoelectron was ejected. For atoms with occupied 2p orbitals there are two primary ionization energies; for example, carbon can be ionized as follows:



or,



where the subscripts s and p indicate that the required energy to ionize from a 2s state will be different from that required to ionize a 2p electron.

Table 7.2 The atomic configurations and ionization potentials (eV) for the first two rows of the periodic table. For boron and heavier elements it is possible to ionize from either 2s or 2p states, and so this data gives an estimate of the energy differences between these orbitals.

Atom	Z	Atomic config.	1s	2s	2p	2s – 2p
H	1	1s ¹	13.6	—	—	—
He	2	1s ²	24.6	—	—	—
Li	3	[He]2s ¹ 2p ⁰	—	5.4	—	—
Be	4	[He]2s ² 2p ⁰	—	9.3	—	—
B	5	[He]2s ² 2p ¹	—	14.0	8.3	5.7
C	6	[He]2s ² 2p ²	—	19.4	10.6	8.8
N	7	[He]2s ² 2p ³	—	25.6	13.2	12.4
O	8	[He]2s ² 2p ⁴	—	32.3	15.8	16.5
F	9	[He]2s ² 2p ⁵	—	40.2	18.6	21.6
Ne	10	[He]2s ² 2p ⁶	—	48.5	21.6	26.9

The ionization energies for the first two rows of the periodic table are given in Table 7.2. Figure 7.11 shows that for second-row elements the two electrons that occupy the 1s energy level remain close to the nucleus, and so the 1s energy level is much lower than the 2s or 2p states. Electrons in the 2s and 2p states of first-row elements spend most of their time outside the inner shell volume; so, on average, they experience a nuclear charge which is shielded by the core electrons. The shielding has an effect on the atomic energy levels of the outer or valence electrons, so that, for example, the ionization energy of Li (1s²2s¹) at 5.3917 eV is actually lower than that of H, which is 13.5984 eV, despite the 3+ nuclear charge of Li. The core electrons of Li shield the valence orbitals so that the effective nuclear charge, as far as the 2s and 2p orbitals are concerned, is around the same as the 1+ of the H nucleus. The H 1s¹ electron is in a state closer to the positive charge, so is lower in energy and more difficult to ionize than the Li 2s¹ electron.

The small peak in the 2s probability function shown in Figure 7.11b exposes an electron in this state to the unshielded nuclear charge slightly more often than a 2p electron, and so the 2s state is always the lower in energy. Hence, for all elements with both 2s and 2p electrons in Table 7.2 the ionization energy for 2s is greater than for 2p. As we move from left to right across the periodic table the nuclear charge increases and this difference becomes larger. Figure 7.13 extends this comparison to the third and fourth rows of the periodic table. The same trend, of the gap between *ns* and *np* orbitals becoming wider across the row, can be seen lower down the table. However, the range of values observed for rows 3 and 4 is less than for the second row, as the higher principal quantum number for these levels places the electrons, on average, further from the core of the atoms.

It is also notable from the values in Table 7.2 that the ionization potential of He is not quite twice that of H. This is due to the electron–electron repulsion between the two 1s electrons confined to the same spatial orbital in He. In the equations discussed so far, the electron–electron repulsion has not been explicitly included. In the H₂ example we simply assume that this effect is outweighed by the attractive interaction between the electrons and nuclei, so that it is favourable to put both electrons in the bonding MO despite the resulting electron–electron repulsion. The MOs obtained give the correct qualitative picture, but a more accurate account of the electron–electron interaction is required to

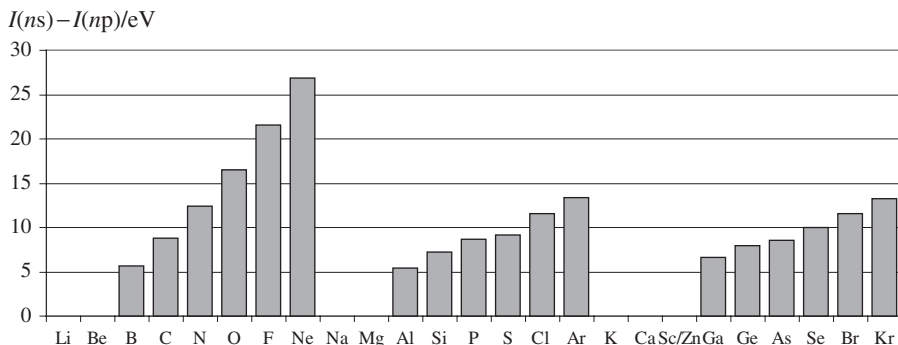


Figure 7.13 The difference in the ionization potentials for ejection of electrons from the ns and np states of the main-group elements Li–Kr.

generate accurate values for the orbital energies. In the remainder of this chapter we will continue with the qualitative approach, and so no actual energy scales appear on the MO diagrams. The graphical images of MOs are obtained within the Hartree–Fock approximation, which does include electron–electron interactions through averaging over the electron distribution corresponding to each occupied MO.

7.3.3 The Relative Energies of Atomic Orbitals from Electronegativity

LiH and HF

In the previous example of H_2 we saw that the covalent bond lowers the electronic energy by allowing the electrons to interact with more than one nucleus. In diatomic molecules with $D_{\infty h}$ symmetry (i.e. composed of a single element), the sharing of electron density must be even between the two nuclei. When atoms of different elements form a diatomic molecule, the relevant symmetry will be $C_{\infty v}$ because the symmetry elements which interchange the nuclei are no longer valid. In addition, the nuclear charges will be unequal, and so we may expect the electron density to be biased toward the more attractive of the two atomic cores.

One measure of the relative attractive power is the ionization potential discussed in the previous section. The higher the energy required to remove an electron from an atom, the more strongly the electrons must be attracted to the atomic core. So, we should expect that the greater the difference between the atomic ionization potentials of the atoms in a diatomic molecule, the more ionic the bond will be.

As examples of very polar bonds we will consider LiH and HF. Table 7.2 shows that the ionization potential of Li is 5.4 eV while that of H is 13.6 eV, and F has an even higher value of 18.6 eV. Hence, in the LiH molecule, we can already see that bonding electrons will be able to lower their energy by spending more time close to the H nucleus. Similarly, in HF, a lower energy will be obtained if the valence electrons are biased toward the F centre.

However, an atom in a molecule is not quite the same as one in isolation. We have seen, for example, that the wavefunction for H_2^+ is more compact than we would expect from the AO decay constants (inset in Figure 7.9). For the relative energies of atomic states used to sketch MO diagrams, some estimate of an atom's ability to draw bonding electrons

towards itself when in a molecule is required. This atomic property is known as the atomic electronegativity. Unfortunately, measuring the property of one atom within a molecule is a difficult task, and so estimates of electronegativity are obtained indirectly.

In the first attempt to quantify the electronegativity of atoms in molecules, Pauling compared the bond dissociation energies of heteronuclear diatomics such as HF with that of the homonuclear diatomics of the constituent atoms. In the homonuclear cases we expect to see an equal sharing of electron density in a covalent bond, typified by the H₂ example covered earlier. In the covalent bond, stability arises from the electron–nuclear interaction, as represented by the resonance integral. The strength of this interaction depends on the type of nuclei, but if a heteronuclear diatomic molecule forms with a mainly covalent interaction, then it is reasonable to expect that the bond energy should be close to the average of the homonuclear diatomics of the constituent atoms. There are cases where this appears to be the case; for example, taking values from Table 7.3:

Table 7.3 The bond lengths and bond dissociation energies for a range of diatomic molecules. Values for bond dissociation energies are taken from Linde DR (ed.) (2005–6) CRC Handbook of Chemistry and Physics, 86th edition, Taylor and Francis, adjusted to 0 K.

Molecule	Bond length/Å	Bond dissociation energy $D_o/\text{kJ mol}^{-1}$	Molecule	Bond length/Å	Bond dissociation energy $D_o/\text{kJ mol}^{-1}$
H ₂	0.74116	432	LiH	1.5953	230
Li ₂	2.672	110	BH	1.2325	336
B ₂	1.589	274	CH	1.1202	334
Bi ₂	—	195	NH	1.045	335
C ₂	1.2425	602	OH	0.9706	426
N ₂	1.0976	942	HF	0.9168	566
O ₂	1.20741	494	HCl	1.2744	427
F ₂	1.417	155	HBr	1.4145	362
Na ₂	3.078	72	HI	1.609	295
Cl ₂	1.988	239	BrCl	2.138	215
K ₂	3.923	49	BF	1.262	728
Br ₂	2.2809	190	BN	1.281	385
I ₂	2.6666	149	BO	1.2043	805
			CO	1.128	1072
			NO	1.151	627

$$D_o(\text{HI}) = 295 \text{ kJ mol}^{-1}$$

whereas

$$(D_o(\text{H}_2) + D_o(\text{I}_2)) / 2 = (432 + 149) / 2 = 290.5 \text{ kJ mol}^{-1}$$

So, in the HI molecule, the bond energy is close to the average for H₂ and I₂.

However, there are many contrary examples:

$$D_o(\text{HF}) = 566 \text{ kJ mol}^{-1}$$

whereas

$$(D_o(\text{H}_2) + D_o(\text{F}_2)) / 2 = (432 + 155) / 2 = 293.5 \text{ kJ mol}^{-1}$$

meaning that the HF bond is much stronger than we would expect from a purely covalent model. We have already noted that the ionization potential of F is considerably greater than that of H, so the bonding electrons in HF will tend to locate nearer to the F atom than to the H centre. Stabilization is achieved by charge transfer between the nuclei rather than by sharing of electron density between them.

In LiH, the bond energy is actually lower than expected for a purely covalent interaction, since

$$D_o(\text{LiH}) = 230 \text{ kJ mol}^{-1}$$

whereas

$$(D_o(\text{Li}_2) + D_o(\text{H}_2)) / 2 = (106 + 432) / 2 = 269 \text{ kJ mol}^{-1}$$

This makes LiH difficult to observe as a diatomic molecule because it is unstable with respect to homoatomic molecules of its constituent elements.

Pauling suggested that these comparisons of bond dissociation energies can be used to build up a relative scale of electronegativity, a measure of the attraction of an atomic core to draw electron density toward itself when part of a molecule.

The Pauling values are reproduced in Table 7.4. We see that the electronegativity of H, at 2.10, is greater than that of Li (0.98) but less than that of F (3.98), because the bond energies of LiH and HF differ greatly from the average of the relevant homonuclear diatomics. In LiH the valence electrons loiter around the H atom, whereas in HF the F atom is more attractive. This is reflected in the names of the molecules, lithium hydride contains hydrogen as a negative centre, while in hydrogen fluoride it is the F atom that is the more negative of the two atoms in the molecule. The electronegativity of I at 2.66 is much closer to the H value than either F or Li, because the bond dissociation energies suggest that the bond in HI is largely covalent.

Many other attempts have been made to quantify electronegativity. For example, Allred and Rochow developed a scale based directly on the atomic radii of atoms in molecules. They argued that the electronegativity should be proportional to the electric field at an atom's surface within the molecule. The position of this atomic surface was estimated using covalent radii R_c , and the electric field at this distance then depends on the effective nuclear charge Z_{eff} of the atom. In their scheme, the electronegativity χ_{AR} is calculated via

$$\chi_{\text{AR}} = 0.744 + \frac{0.3590 Z_{\text{eff}}}{R_c^2} \quad (7.28)$$

The inverse dependence on the square of the radius comes directly from the electric field of a point charge.

A third definition of electronegativity was put forward by Mulliken. In his work, the average of the ionization potential I and electron affinity A_e of the isolated atoms was used:

$$\chi_M = \frac{1}{2}(I + A_e) \quad (7.29)$$

Table 7.4 Electronegativities defined on the Pauling scale.

He	
H 2.10	
Li 0.98	Be 1.57
Na 0.93	Mg 1.31
K 0.82	Ca 1.00
Rb 0.82	Sr 0.95
Cs 0.79	Ba 0.89
He	
B 2.04	C 2.55
Al 1.61	Si 1.90
Fe 1.83	Co 1.88
Mn 1.55	Ni 1.91
V 1.63	Cu 1.90
Ti 1.54	Zn 1.65
Sc 1.36	Ga 1.81
Y 1.22	Ge 2.01
Zr 1.33	As 2.18
Nb —	Se 2.55
Tc —	Br 2.96
Mo 2.16	In 2.18
Rh —	Te —
Pd 2.28	Sb 2.05
Ag 1.93	Te —
Ir —	Bi 2.02
Os —	Po —
Re —	At —
Tl —	Rn —
Hg —	Xe 2.67
	Kr 3.00

The electron affinity is the energy gained when an electron is added to a neutral gas-phase atom, and so Mulliken's electronegativities average the ability of a neutral atom to retain its outermost electrons and its ability to attract an additional electron to form an anion.

The Allred and Rochow and the Mulliken scales place the atoms of the periodic table in roughly the same order as the Pauling scale; so, for our placement of the AOs in an MO diagram, the values in Table 7.4 will suffice. The other definitions help to highlight different approaches to the concept of electronegativity.

We can now use the electronegativity values to place the AO levels at the correct relative energies before drawing an MO diagram. The LiH case is shown in Figure 7.14; because H is more electronegative than Li, the H(1s) AO is drawn lower than the 2s or 2p orbitals of Li. The trend seen in the ionization potentials across the first row in Figure 7.13 suggests that the 2s and 2p states of Li will be relatively close together, and these levels are placed accordingly.

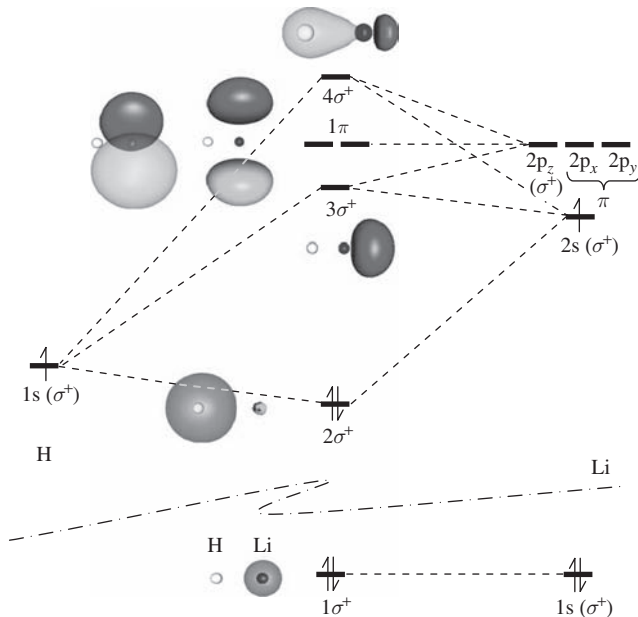


Figure 7.14 The orbitals of LiH. The AOs of H are drawn lower than those of Li due to the difference in electronegativity. This makes the occupied $2\sigma^+$ orbital predominantly H-like. In the MO diagrams, the position of H is shown with a white sphere and that of Li by a dark grey sphere.

There are no operations which swap atoms over in $C_{\infty v}$ symmetry, there is only the identity E , the infinite number of operations associated with the C_∞ axis and the infinite number of vertical mirror planes that contain the molecular axis. Conventionally, we align the Z axis with the principal axis, along the molecular bond. The character table in Appendix 12 shows that 1s, 2s and $2p_z$ AOs belong to the σ^+ irreducible representation, while $2p_x$ and $2p_y$ are degenerate, belonging to the π representation.

When the AOs interact to form bonding and antibonding MOs, part of the bonding density is described by the overlap integral (see Figure 7.7). There are now two choices for the symmetry of the orbitals on the Li centre, giving two possible types of overlap integral to consider:

$$S_{12} = \int_{-\infty}^{\infty} \chi_H^{\sigma^+} \chi_{\text{Li}}^{\sigma^+} d\tau \quad (7.30)$$

which is a totally symmetric integrand, and

$$S_{12} = \int_{-\infty}^{\infty} \chi_H^{\sigma^+} \chi_{\text{Li}}^{\pi} d\tau \quad (7.31)$$

which does not have a totally symmetric integrand.

In the first case, when the orbital on H and that on Li have the same symmetry, the totally symmetric integrand can give a finite overlap and so a mixed MO can be created. For the second case, Equation (7.31), we are proposing to take an integral over the product of two functions which belong to orthogonal irreducible representations. Their product will not belong to the totally symmetric representation of the group, so this overlap integral has to be zero.

This observation greatly simplifies the construction of MOs, since only the AOs of matching symmetry on the two atoms will mix. Figure 7.14 shows the construction of the MOs for LiH. The lowest energy orbital is just the Li 1s state, labelled $1\sigma^+$. Although this has the correct symmetry to interact with the H 1s AO, it is in the Li core and so has only a small overlap with the neighbouring atom (see Figure 7.11). The energy level for this MO is drawn at the same level as the Li 1s reference, as it is only weakly affected by the presence of the H atom. The next level, $2\sigma^+$, is formed by the interaction of H 1s and Li 2s and $2p_z$ states, although the lower energy H 1s AO is the major contributor: the MO plot shows a large lobe on the H centre and only a minor component on the Li atom. This orbital is lower in energy than any of the contributing AOs, and so is bonding in nature.

The strong bias of the occupied $2\sigma^+$ toward H corresponds to the difference in electronegativities between Li and H. In the MO diagram, the H 1s state is closer in energy to the $2\sigma^+$ MO and so dominates the SALC formed from mixing the available valence orbitals of σ^+ symmetry. The distribution of the occupied $2\sigma^+$ orbital leads to a net negative charge on H, because the MO contains two electrons and so these are concentrated around the single proton. Correspondingly, the Li centre is positively charged and the chemical bond is largely electrostatic in nature, making LiH an ionic compound.

Since Li contributes three electrons and H only one, there are four electrons to accommodate in the MO scheme; so, only $1\sigma^+$ and $2\sigma^+$ are filled and all higher energy states are empty. Moving up to the unoccupied MOs, we find $3\sigma^+$, again formed from the valence σ^+ symmetry AOs, but now with Li 2s and $2p_z$ dominant, as these AOs are closer in energy to the MO than is H(1s). This orbital is higher in energy than the H 1s and Li 2s AOs, and so is antibonding in nature. The MO plot shows that, if occupied, it would move charge density to the Li atom and out of the internuclear region, destabilizing the ionic bond formed by $2\sigma^+$.

The next level up is 1π , a degenerate pair of states formed from the Li $2p_x$ and $2p_y$ AOs. There are no orbitals of corresponding symmetry on the H atom in this energy range, so these orbitals remain Li-like and are neither bonding nor antibonding. These are nonbonding states by symmetry, and their energies are practically the same as in the isolated Li atom. Accordingly, the energy levels are drawn at the same level as the reference AOs. The final state is $4\sigma^+$, a linear combination of H 1s and Li 2s and $2p_z$.

It has been noted that LiH is actually very difficult to prepare as a gas-phase diatomic molecule. We have seen that the very polar nature of the Li...H interaction produces essentially the lithium cation Li^+ and the hydride anion H^- . These species attract one another electrostatically, and so a mixture of Li and H can form an ionic solid having the rock-salt structure (typified by NaCl). In this solid phase, each ion has six neighbours of the opposite charge and so the total binding energy per atom in the solid is much greater than for the gas-phase dimer. The electron affinity of the H atom is quite low, and so complete electron transfer to produce a hydride with this degree of ionicity is only really possible for the easily ionized Group 1 metals. In addition, LiH is liable to rapid decomposition in the presence of any source of H^+ , even H_2O .

At the other end of the second row of the periodic table, fluorine also forms a diatomic molecule with hydrogen. HF also belongs to the $C_{\infty v}$ point group. The MOs for HF are

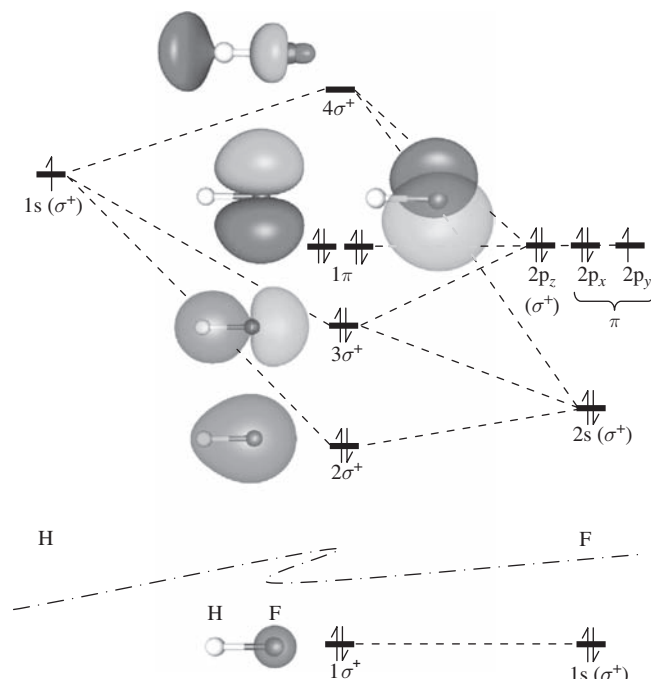


Figure 7.15 The orbitals of HF. The AOs of H are drawn higher than those of F due to the difference in electronegativity. In the MO diagrams, the position of H is shown with a white sphere and that of F by a dark grey sphere.

shown in Figure 7.15 and are labelled similarly to those of LiH. However, F is much more electronegative than H, and so the reference AOs for F are drawn lower than those of H. The first valence MO, $2\sigma^+$, is correspondingly dominated by the F atom, 2s orbital.

We are now at the right-hand end of the second row of the periodic table; F has seven valence electrons to place in the MO scheme so that, with the single H(1s) electron, there are a total of eight. Figure 7.15, therefore, has all MOs up to the degenerate 1π pair occupied. The electronegativity difference between H and F is actually greater than that between H and Li. However, the $3\sigma^+$ orbital in HF, which contains a significant contribution from the H(1s) orbital, is occupied. Accordingly, HF is a polar molecule with F negatively charged, but the charge transfer is not as complete as seen in the LiH example. The first unoccupied state is $4\sigma^+$, which is an antibonding orbital, with the expected large H(1s) component.

The HF molecule is stable with respect to the associated elemental diatomics. However, in the solid or liquid phase the polarity of the HF bond gives rise to intermolecular interactions between each positively charged H atom and the negatively charged F atom of a neighbouring molecule. In the solid state this results in chains of molecules with an angle between adjacent molecular axes of around 116° . These H-bonding interactions have a large electrostatic component, and so the density, rather than particular MOs, should be used to explain the directional preference. Density is a sum over occupied orbitals. Here, $2\sigma^+$ is largely spherical around F, $3\sigma^+$ has a large lobe to the side of the F atom along the molecular axis, and the 1π orbitals are at 90° to the axis. The directionality of the charge distribution around the F atom comes from the sum of $3\sigma^+$ and 1π orbitals, which results in the observed directional intermolecular bonding. This type of nonuniform electron distribution is often referred to as lone pair density.

The lone pair density observed in the (*Z*)-*N*-methyl-C-phenylnitrone example discussed in Section 7.1.2 (Figure 7.3) shows a similar nonspherical distribution of charge around the O atom of the N—O[−] group. MO calculations on the nitrone would give nonbonding orbitals similar to those found here for the simpler example of HF.

Points to note from this section:

1. The reference AOs in MO diagrams should be placed according to the atomic electronegativities; a high electronegativity gives a low-lying orbital.
2. Only AOs of the same symmetry can mix to form bonding and antibonding MOs.
3. AOs which do not match the symmetry of orbitals on neighbouring atoms, such as the F(2p_x) and F(2p_y) states in Figure 7.11, are nonbonding by symmetry.
4. MOs formed from energetically different AOs have SALCs whose largest contribution is from the energetically closest AO. At the extreme, this leads to practically nonbonding states for very different AO energies, e.g. the core states of second-row elements.
5. The electron density is important for understanding intermolecular interactions. In an orbital picture, the density arises from a sum over occupied orbitals.

7.4 The Molecules Formed by Other Second-Row Elements with Hydrogen

7.4.1 BeH₂, Beryllium Hydride

BeH₂ is a linear molecule belonging to the $D_{\infty h}$ point group. For this triatomic molecule the two H atoms are related to one another by symmetry. We cannot assign symmetry labels to each H 1s orbital, as has been done for the LiH and HF diatomic examples, because some of the symmetry operations swap over s(H₁) and s(H₂). To get around this, we first of all form symmetry adapted linear combinations (SALCs) of the H 1s orbitals and then see how these combined orbitals interact with the central Be atom. Finding the SALCs for the H atoms is an identical problem to the H₂ MOs, and the results are drawn to the right of Figure 7.16. In BeH₂, the H atoms are quite far apart and so the σ_u^+ combination is only marginally higher in energy than the σ_g^+ .

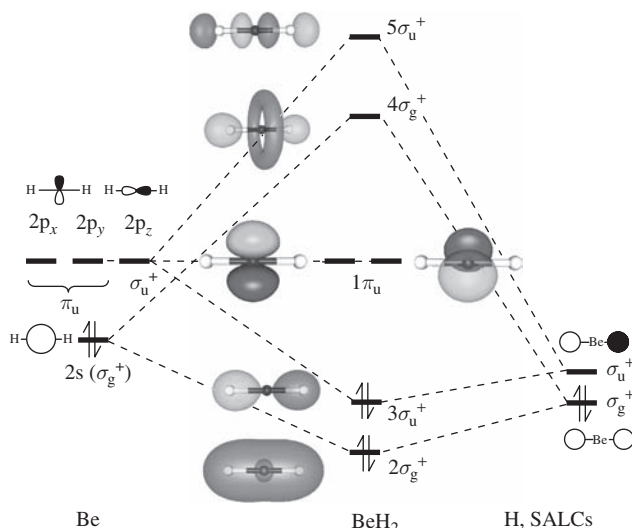


Figure 7.16 The orbitals of the $D_{\infty h}$ molecule BeH₂. The two H(1s) orbitals are taken as the SALCs shown to the right and the valence orbitals of Be are shown to the right.

Table 7.4 gives the electronegativity of H as 2.10 compared with the Be value of 1.57. Accordingly, the H SALCs are drawn lower than the Be valence AOs in the reference levels of the MO diagram. The Be atom has an [He]2s²2p⁰ ground-state electronic configuration; so, we cannot directly obtain the separation of 2s and 2p orbitals from the ionization potentials discussed in Section 7.3.2 because the p-orbitals are empty. However, we can estimate that this gap is quite small based on extrapolation of the trend shown in Figure 7.13, the ionization energy difference across the row of the periodic table. So, in Figure 7.16, the Be 2s and 2p levels are drawn closer together than the corresponding orbitals for F in Figure 7.15.

As usual, the principal symmetry axis is taken to be aligned with Z , and so the Be 2s and $2p_z$ AOs belong to the σ_g^+ and σ_u^+ representations respectively, while $2p_x$ and $2p_y$ are degenerate, belonging to π_u .

The MOs for BeH_2 are shown in the centre of Figure 7.16. The lowest lying valence orbital is $2\sigma_g^+$ formed from the interaction of Be(2s) and the σ_g^+ linear combination of H(1s) AOs (the $1\sigma_g^+$ is the core 1s state on Be that is not shown). In the graphic of this orbital, a small lobe centred on the Be atom can be seen; this is caused by the radial node in the Be 2s AO.

The next orbital is $3\sigma_u^+$, which contains the Be $2p_z$ and σ_u^+ SALC of H(1s) orbitals. This is the HOMO, as there are only four electrons to accommodate in BeH_2 . The LUMOs are the degenerate pair of Be π_u orbitals; there are no corresponding H orbitals low enough in energy to form a significant interaction, and so these are nonbonding states.

The linear structure of BeH_2 maximizes the overlap between the Be $2p_z$ and the σ_u^+ combination of the H 1s orbitals in the HOMO state. Since only occupied orbitals contribute to the energy of the molecule, this is preferred in this case over a bent (C_{2v}) triatomic molecule, which we will see in considering H_2O . The C_{2v} geometry does allow more mixing between the 2p orbitals on the central atom and H SALCs, but with less efficient overlap in each of the MOs formed.

7.4.2 BH_3 , Boron Hydride

The next element across the second row is B with an $[\text{He}]2s^22p^1$ electronic ground state. In its simplest form the compound BH_3 is a planar, D_{3h} , molecule. To orientate the molecule we take the Z -axis to be along the principal, C_3 , axis and place the X -axis along B—H₁. From the standard character table in Appendix 12, the B valence orbital symmetries are

$$2s: a_1', \quad 2p_z: a_2'' \quad \text{and} \quad 2p_x, 2p_y: e'$$
 (7.32)

So we have a degenerate pair of 2p orbitals in the molecular plane.

The three H atoms are interchangeable by the symmetry operations of the group; so, before drawing up the MO diagram, SALCs of the H(1s) states will be constructed.

Problem 7.5: Using the basis shown in Figure 7.17 and an example of one operation from each of the classes given in the D_{3h} character table (Appendix 12), find the reducible representation for the basis of three H(1s) orbitals in BH_3 . The answer can be checked against the reducible representation Γ in Table 7.5.

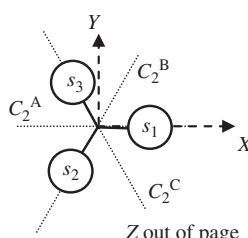


Figure 7.17 A basis of three H(1s) orbitals for construction of the H atom SALCs in BH_3 .

Table 7.5 The reduction of the reducible representation for the three H(1s) AOs in BH_3 .

D_{3h}	E	$2C_3$	$3C_2$	σ_h	$2S_3$	$3\sigma_v$	$h = 12$	
Γ	3	0	1	3	0	1	\sum_c	$h^{-1} \sum_c$
				$g_c \chi_i(C)$	$\chi_\Gamma(C)$			
A_1''	3		3		3		12	1
A_2''	3		-3	3		-3	0	0
E''	6		0	6		0	12	1
A_1'	3		3	-3		-3	0	0
A_2'	3		-3	-3		3	0	0
E'	6		0	-6		0	0	0

From the reducible representation we must identify the irreducible representations for the H(1s) orbitals so that those that match with the B atom orbital symmetries listed above can be identified. The reduction is laid out in Table 7.5.

In this table there are zeros for the reducible representation under the symmetry classes $2C_3$ and $2S_3$, because rotations around the principal axis interchange the H(1s) orbitals. In the reduction, the corresponding columns are left blank because they cannot contribute to the sums required by the reduction formula:

$$n_i = \frac{1}{h} \sum_c g_c \chi_i(C) \chi_\Gamma(C) \quad (7.33)$$

We first met this formula in Section 5.5; h refers to the order of the group, g_c is the number of operations under class C , $\chi_\Gamma(C)$ is the character for the reducible representation of the basis (obtained in Problem 7.5) and $\chi_i(C)$ is the standard character for the i th irreducible representation in class C from the character table.

Table 7.5 shows that the SALCs for the three H(1s) orbitals belong to the A_1' and E' irreducible representations. To obtain the orbital patterns for these we use the projection operator method introduced in Section 6.6. To simplify the process, it is useful first to work with the rotational subgroup D_3 , which is part of the D_{3h} operator set. This is self-contained, because the product of any two operations is still within the subgroup. When the SALC functions with the symmetry of the subgroup have been obtained we will just need to check which irreducible labels they conform to in the full D_{3h} point group.

The use of the projection operator in D_3 is shown in Table 7.6. The easiest approach when using the projection operator is to take one of the basis functions alone as the generating vector and work out the functional form for each irreducible representation in turn. In Table 7.6 we use s_1 as the generating vector. This gives an a_1 MO which has all the H(1s) orbitals in phase with one another. In D_{3h} the a_1' representation also has character 1 under both types of mirror plane and the improper rotation classes. The sum of all H(1s) orbitals in phase is easily seen to conform to this.

Projection of s_1 for the E irreducible representation of the D_3 group gives the SALC:



Table 7.6 The projection operator method for finding the SALCs for H(1s) orbitals in BH_3 , using the D_3 rotational subgroup of D_{3h} . The assignment of the horizontal C_2 axes follows the convention that C_2^A , C_2^B and C_2^C are through $B-\text{H}_1$, $B-\text{H}_2$ and $B-\text{H}_3$ respectively, as shown in Figure 7.13.

D_3	E	C_3^1	C_3^2	C_2^A	C_2^B	C_2^C	$\mathbf{P}_i \mathbf{v} = \sum_j \chi_i(j) \mathbf{T}_j \mathbf{v}$
$A_1 \mathbf{T}_j s_1$	s_1	s_2	s_3	s_1	s_3	s_2	$2(s_1 + s_2 + s_3)$
$E \mathbf{T}_j s_1$	$2s_1$	$-s_2$	$-s_3$	0	0	0	$2s_1 - s_2 - s_3$
$E \mathbf{T}_j (s_2 - s_3)$	$s_2 - s_3$	$s_3 - s_1$	$s_1 - s_2$	0	0	0	$2(s_2 - s_3)$

The relative size of the coefficients shows that the lobe on H_1 is twice as large as those on H_2 and H_3 and has the opposite phase, as illustrated. Note that, since the X -axis is aligned with $\text{B}-\text{H}_1$, this orbital is complementary to the $\text{B}(2\text{p}_x)$ part of the e degenerate pair of the B atom, but orthogonal to $\text{B}(2\text{p}_y)$.

Before checking that $\phi_1(e)$ from the D_3 projection is the right form for $\phi_1(e')$ in D_{3h} , we need to find the second of the pair of SALCs for e . This should be able to form a bonding orbital to $\text{B}(2\text{p}_y)$ and be orthogonal to $\phi_1(e)$. In the SALC of Equation (7.34) the s_2 and s_3 contributions are in phase (they both appear with a negative sign). As we expect $\phi_1(e)$ and $\phi_2(e)$ to be orthogonal to one another, a good guess at the generating function for the second of the e pair is $s_2 - s_3$, in which the orbitals are out of phase. This is used in the final line of Table 7.6 and confirms that this is a combination that conforms to the E representation.

Problem 7.6: (a) If the small overlap between the H(1s) orbitals in BH_3 is ignored, then the SALCs identified in Table 7.6 for the e representation can be written with normalization factors as follows:

$$\phi_1(e) = \frac{1}{\sqrt{6}}(2s_1 - s_2 - s_3) \quad (7.35)$$

and

$$\phi_2(e) = \frac{1}{\sqrt{2}}(s_2 - s_3) \quad (7.36)$$

Assuming that each s function is itself normalized, confirm that the normalization factors in these equations are correct and that the two SALCs are orthogonal to one another.

(b) We have used the rotational subgroup D_3 to derive the functional forms for the two degenerate e SALCs. Using the normalized forms given above, show that they also behave correctly for the e' representation of D_{3h} by checking the characters are correct for the remaining operations.

Approach. To check that the functions are correct we need to find the character for their transformations with each operation in the group. To do this we first apply an

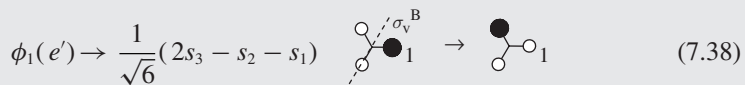
operator and work out the transformed function. This can then be equated to a linear combination of $\phi_1(e)$ and $\phi_2(e)$ with unknown coefficients to obtain the character for the transformation, i.e. the amount of the original function still present after the transformation.

This technique was applied to find characters for d-orbitals in various symmetries in Section 5.8. Here, we must remember that the two functions are degenerate and so the character in the standard D_{3h} table should be the sum of the two we derive.

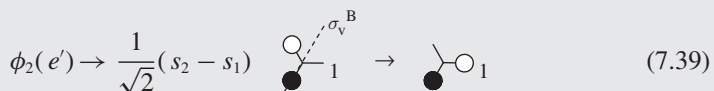
Example. For the σ_v^B operation, reflection through a mirror plane perpendicular to the molecule and including the B—H₂ bond gives

$$s_1 \rightarrow s_3 \quad s_2 \rightarrow s_2 \quad s_3 \rightarrow s_1 \quad (7.37)$$

so that the functions become



and



To find the characters for this operation we have to construct the new functions from the original SALCs; for the transformed $\phi_1(e')$ we write

$$\frac{1}{\sqrt{6}}(2s_3 - s_2 - s_1) = \frac{a}{\sqrt{6}}(2s_1 - s_2 - s_3) + \frac{b}{\sqrt{2}}(s_2 - s_3) \quad (7.40)$$

where a and b are coefficients that control the mixing of the SALCs. Comparing s_1 coefficients:

$$\frac{-1}{\sqrt{6}} = \frac{2a}{\sqrt{6}} \quad \text{and so} \quad a = -\frac{1}{2} \quad (7.41)$$

a is the amount of the original $\phi_1(e')$ still present after the σ_v^B transformation, i.e. the character for the first function of the e' pair.

For $\phi_2(e')$ we write

$$\frac{1}{\sqrt{2}}(s_2 - s_1) = \frac{a}{\sqrt{6}}(2s_1 - s_2 - s_3) + \frac{b}{\sqrt{2}}(s_2 - s_3) \quad (7.42)$$

Again, the coefficients of s_1 can be used to find a :

$$\frac{2a}{\sqrt{6}} = -\frac{1}{\sqrt{2}} \quad \text{or} \quad a = -\frac{\sqrt{3}}{2} \quad (7.43)$$

The character in this case is the value of b . Now we know the value of a , comparing coefficients for s_3 gives

$$\frac{\sqrt{3}}{2\sqrt{6}} - \frac{b}{\sqrt{2}} = 0 \quad \text{so that} \quad b = \frac{1}{2} \quad (7.44)$$

This shows that

$$\frac{1}{\sqrt{2}}(s_2 - s_1) = -\left(\frac{\sqrt{3}}{2}\right)\frac{1}{\sqrt{6}}(2s_1 - s_2 - s_3) + \left(\frac{1}{2}\right)\frac{1}{\sqrt{2}}(s_2 - s_3) \quad (7.45)$$

$$\text{Diagram: } \begin{array}{c} \text{---} \\ | \\ \text{---} \end{array} \text{ } \begin{array}{c} \text{---} \\ | \\ \text{---} \end{array} = -\left(\frac{\sqrt{3}}{2}\right) \begin{array}{c} \text{---} \\ | \\ \text{---} \end{array} \text{ } \begin{array}{c} \text{---} \\ | \\ \text{---} \end{array} + \left(\frac{1}{2}\right) \begin{array}{c} \text{---} \\ | \\ \text{---} \end{array} \text{ } \begin{array}{c} \text{---} \\ | \\ \text{---} \end{array}$$

The pictorial equation contains the same information as the algebra; when trying to image the effect of the coefficients on the orbital images it is useful to remember that the negative sign of the first term will reverse the phases of the orbital shown.

So, from Equations (7.41) and (7.44) the characters for $\phi_1(e')$ and $\phi_2(e')$ for the σ_v^B operation are $-1/2$ and $+1/2$ respectively, giving a total character for the e' pair of 0, as expected from the $3\sigma_v$ class of the standard character table.

Note. The algebra is much simpler if we choose the σ_v^A mirror plane as an example from this class, because then the functions are not mixed and the characters can be obtained by inspection. σ_v^B was chosen in this example to help with cases for which the algebra cannot be avoided, e.g. S_3^{-1} .

The solution to Problem 7.6 demonstrates that the functions found to have e symmetry in the D_3 projection do indeed have e' symmetry in D_{3h} . The three H(1s) SALCs have practically the same energy, as there is negligible overlap between H(1s) orbitals. However, on the right-hand side of the BH_3 MO in Figure 7.18 they are shown with the a_1' combination slightly lower than the two degenerate e' orbitals for clarity of presentation.

Table 7.4 gives an electronegativity for B of 2.04, which is less than the 2.10 of H, but closer than was the case for Li. This means that the 2p AOs of B are drawn slightly higher than the three linear combinations of H 1s orbitals. The valence AOs of B were assigned symmetry labels, by reference to the right-hand column of the standard character table in Appendix 12, in Equation (7.32).

To form MOs, all that needs to be done is to match the symmetry of the B valence orbitals to the H SALCs, and Figure 7.18 shows the resultant MOs in the central part of the diagram.

Ignoring the B core 1s state, the lowest lying valence orbital is $2a'$ formed between the B(2s) and the H SALC in which all H atoms have the same phase. In the graphic of the MO, the radial node of the B(2s) orbital gives rise to a small inner sphere around the B nucleus.

The next two orbitals are a degenerate pair, formed from the e' H SALCs and the two B(2p) orbitals that are in the plane. These are the highest occupied levels for the molecule.

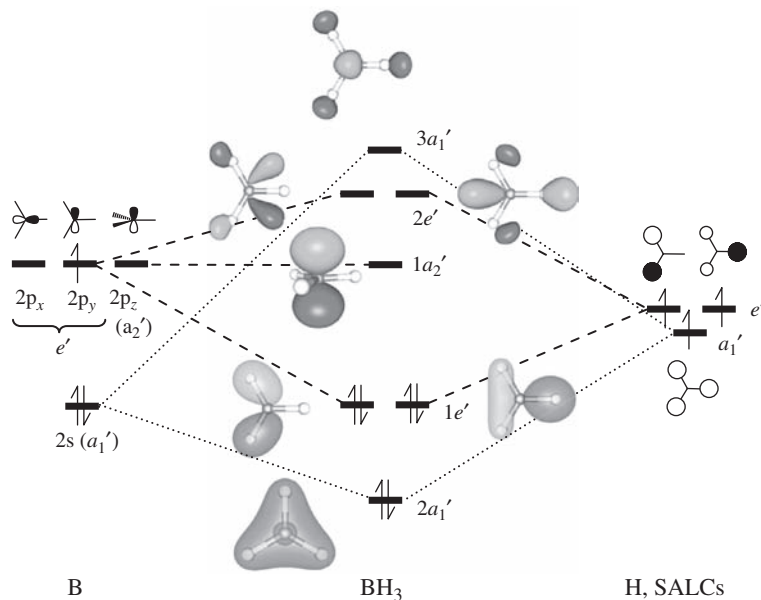


Figure 7.18 The MO diagram for the D_{3h} molecule BH_3 . For clarity, the dotted lines for the a_1' orbitals are drawn in a different style to those for the others.

The lowest unoccupied orbital is $B(2p_z)$, which has no partner in the H SALC set and so is the nonbonding state, $1a_2'$.

The six bonding electrons are shared between three $B-H$ bonds, and so each has a bond order of 1. The valence count around the B atom falls short of the octet required to complete the atomic shell, and so BH_3 is electron deficient. The empty $1a_2'$ MO readily accepts donation of electrons from other molecules, and so makes BH_3 a Lewis acid. It also allows BH_3 to dimerize to give a structure with four-coordinate B atoms sharing two of the six H atoms in a bridging motif similar to the $Al_2(CH_3)_3$ structure discussed in Chapter 1 (Figure 1.26).

The higher energy MOs, $2e'$ and $3a'$ are antibonding complements to the bonding orbitals already discussed; they are higher in energy than the original atomic states and so would destabilize the molecule if occupied by electrons. Note the change of relative phase of the central B atom orbitals with respect to the H SALCs, leading to nodes between the atom centres.

7.4.3 CH₄, Methane

Methane, CH₄, has T_d symmetry. The C atom sits on a special point at the centre of the molecule, which is contained in all symmetry elements, and so we can simply read the irreducible representations for its valence orbitals from the standard character table (Appendix 12):

$$C(2s): a_1, \quad C(2p_x), C(2p_y) \text{ and } C(2p_z): t_2 \quad (7.46)$$

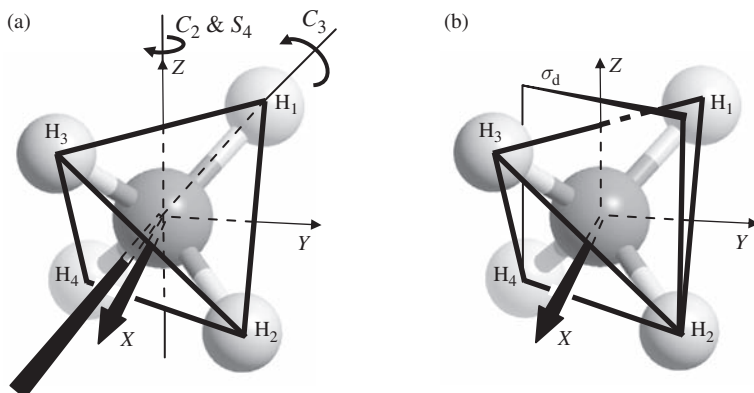


Figure 7.19 (a) The axis system used for a tetrahedral molecule such as methane, showing the positions of some symmetry axes. (b) One of the six σ_d mirror planes in T_d .

The paper model given in Appendix 3 shows the arrangement of the X , Y and Z axes for the geometry of the cube and the related tetrahedron; the axes are also overlaid on a model of CH_4 in Figure 7.19, along with some example symmetry elements. The C_3 axes run along the C—H bonds, while the C_2 and collinear S_4 axes bisect the bond angles and are aligned with X , Y and Z directions. The mirror planes, e.g. σ_d in Figure 7.19b, each contain two of the C—H bonds and act to reflect the other two H atoms into one another.

The choice of axes system given in Figure 7.19 means that the X , Y and Z directions are each on a line passing through the centres of opposite edges in the tetrahedron. This setting places each $\text{C}(2\text{p})$ orbital along the line in between opposite pairs of H atoms (on the C_2 and S_4 axes), emphasizing the fact that they are degenerate, with all three assigned together to the T_2 representation.

Problem 7.7: Using a basis of the four H(1s) orbitals in CH_4 , obtain the reducible representation Γ given at the top of Table 7.7.

Table 7.7 The reducible representation for the four H(1s) orbitals of CH_4 and the application of the reduction formula.

T_d	E	$8C_3$	$3C_2$	$6S_4$	$6\sigma_d$		$h = 24$
Γ	4	1	0	0	2	\sum_C	$h^{-1} \sum_C$
				$g_c \chi_i(C)$	$\chi_{\Gamma}(C)$		
A_1	4	8			12	24	1
A_2	4	8			-12	0	0
E	8	-8			0	0	0
T_1	12	0			-12	0	0
T_2	12	0			12	24	1

For the four H(1s) orbitals we can obtain the irreducible representations by applying the reduction formula to the reducible representation. Table 7.7 shows that this process results in

$$\Gamma = a_1 + t_2 \quad (7.47)$$

Projection using the s_1 orbital as a generating vector with the rotational subgroup T is laid out for these two irreducible representations in Table 7.8. For A_1 , a function with all the H AOs present with equal weight and with the same phase is obtained:

$$a_1 = s_1 + s_2 + s_3 + s_4 \quad (7.48)$$

where we have dropped the multiplier found in the table and stick to the convention that lower case letters are used for MO labels. This MO will form bonding and antibonding states with the central C atom 2s orbital, which has the same symmetry.

The projection operation for the T representation using s_1 gives a function in which the generating AO has a coefficient three times the other H(1s) AOs and with the opposite phase:

$$\phi(t) = 3s_1 - s_2 - s_3 - s_4 \quad (7.49)$$

This function is not suited to interact with any particular C(2p) orbital because it is ‘aligned’ with the C—H₁ bond, rather than any of the C_2 axes.

Let us take a step back and construct a generating function designed to interact only with 2p_z. In Figure 7.19a, H₁ and H₃ are equidistant from the positive Z-axis and so we would expect s_1 and s_3 to have the same phase as one another. A possible generating function that could lead to this is

$$s_1 + s_3 \quad (7.50)$$

This function is also projected for the T irreducible representation in Table 7.8 to give

$$\phi_1(t) = s_1 - s_2 + s_3 - s_4 \quad (7.51)$$

which is clearly suited to interact with the C(2p_z) orbital, which would be vertical in the sketch. However, its interaction with C(2p_x) and C(2p_y) orbitals would be zero, since they are along the other two C_2 axes, which each have one positive- and one negative-phase H(1s) orbital to either side. Similar generating functions can be used to produce SALCs aligned with 2p_x and 2p_y, and Table 7.8 shows that these are

$$\phi_2(t) = s_1 - s_2 - s_3 + s_4 \quad \phi_3(t) = s_1 + s_2 - s_3 - s_4 \quad (7.52)$$

Table 7.8 Projection of generating functions to obtain a_i and t SAlCs for the $H(1s)$ orbitals of CH_4 . The C_3 axes are labelled A, B, C and D for elements passing through $C-H_1$, $C-H_2$, $C-H_3$ and $C-H_4$ respectively. For the $8C_3$ class in group T (and T_d), the characters for T representations are 0. The C_2 axes are labelled A, B and C for elements bisecting H_1-C-H_2 , H_1-C-H_3 and H_1-C-H_4 respectively.

T subgroup of T_d	E	$C_3^{1(A,B,C,D)}$	$C_3^{2(A,B,C,D)}$	$C_2^{(A,B,C)}$	C_2	$\mathbf{P}_{S_1} = \sum_i \chi_i(j) \mathbf{T}_j S_1$
$A_1 \mathbf{T}^{S_1}$	S_1	S_1, S_4, S_2, S_3	S_1, S_3, S_4, S_2	S_2, S_3, S_4	$-S_2, -S_3, -S_4$	$3(S_1 + S_2 + S_3 + S_4)$
$TT_j S_1$	$3S_1$	0	0			$3S_1 - S_2 - S_3 - S_4$
$TT^i_j(S_1 + S_3)$	$3(S_1 + S_3)$	0	0	$-(S_3 + S_1), -(S_2 + S_4), -(S_4 + S_2)$	$2(S_1 - S_2 + S_3 - S_4)$	
$TT^i_j(S_1 + S_4)$	$3(S_1 + S_4)$	0	0	$-(S_3 + S_2), -(S_2 + S_3), -(S_4 + S_1)$	$2(S_1 - S_2 - S_3 + S_4)$	
$TT^i_j(S_1 + S_2)$	$3(S_1 + S_2)$	0	0	$-(S_3 + S_4), -(S_2 + S_1), -(S_4 + S_3)$	$2(S_1 + S_2 - S_3 - S_4)$	

The sketches use the same atom layout as Figure 7.19, and so it should be clear that they each complement a single C(2p) AO.

Problem 7.8: Show that the three SALCs found in Equations (7.51) and (7.52) are orthogonal to one another.

The simple projection of the s_1 orbital in Table 7.8 does result in a function that could be taken as one of an alternative set of three SALCs. However, we decided to abandon it because it was not suitably aligned to bond to a single C(2p) orbital in the axis system of Figure 7.19. Now we can see that it is related to the three t_2 SALCs found by deliberately constructing linear combinations aligned with the axis system at the bottom of Table 7.8. Inspection of the formulae shows that

$$\phi_1(t) + \phi_2(t) + \phi_3(t) = 3s_1 - s_2 - s_3 - s_4 \quad (7.53)$$

i.e. the first function found is a linear combination of the final three SALCs and so is not orthogonal to them. The three basic functions we have found are well suited to the MO construction because they are aligned with the axes that are used to define the direction of the C(2p) orbitals.

The MO diagram for CH₄ is shown in Figure 7.20; in this instance, C has a higher electronegativity than H (Table 7.4) and so its AOs are drawn lower than the H(1s) SALCs. The lowest energy MO formed from the valence AOs is $2a_1$, which is a linear combination of C(2s) and the totally symmetric H(1s) SALC. This is lower in energy than the t_2 MOs

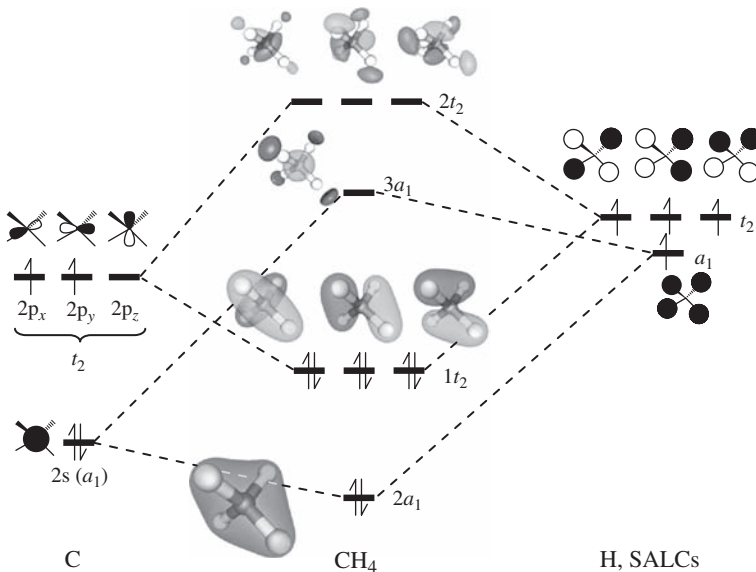


Figure 7.20 The MO diagram for CH₄ in the T_d point group.

largely because the C(2s) state is below the C(2p) orbitals. Next are the three degenerate t_2 states which involve each of the C(2p) orbitals and the corresponding H(1s) SALC constructed in Table 7.8. Since there are eight valence electrons in CH₄, these t_2 states are the highest occupied orbitals. The lowest unoccupied state is $3a_1$, the antibonding counterpart to $2a_1$.

In this description of CH₄, all eight valence electrons are in bonding MOs, and so Equation (7.24) gives a bond order of 4. Since there are also four C—H bonds and the orbitals distribute the electron density evenly between them, we consider each to be a single bond. In the MO picture, the bond order arises from equal contributions from each of the low-lying $2a_1$ and $1t_2$ MOs to each C—H bond; no particular pair of electrons is associated with a particular bond.

A common approach for the discussion of bonding to tetrahedral carbon centres, as typified by CH₄, is to introduce hybridization of the C atom orbitals to give four equivalent sp³ combinations. This does account for the fact that the four C—H bonds are equivalent; however, it predicts four degenerate energy levels for the electron orbital states, and we see below that this is difficult to reconcile with photoelectron spectroscopy data.

The experimental photoelectron spectrum (PES) of CH₄ is shown in Figure 7.21. Here, light is used to eject electrons from the molecule and the spectrum is based on the kinetic energy of the electrons emitted. To a first approximation the electron kinetic energy is the difference between the incident photon energy and the electron binding energy. So the spectrum shows peaks that correspond to the ionization energies for the MOs. Two well-separated photoelectron emission regions are seen in the spectrum. The lower energy region contains three broad peaks that merge together, centred at 13.6 eV, 14.4 eV and one, giving the shoulder, at 15.0 eV. These are accompanied by sharper features which decorate the broad peaks. This area of the spectrum contains signals due to excitation from the $1t_2$ level of CH₄. The sharp features are caused by coupling of the ionization event with the vibrational states of the molecule and cation formed after ionization. The origin of the three peaks is dealt with in the questions at the end of this chapter, and is related to the triple degeneracy of the t_2 MOs.

At the higher binding energy end of the spectrum, a single broad feature is seen at around 23 eV, again overlaid with sharp peaks due to vibrational coupling. The vibrational origin of these features is evidenced by their regular spacing, as expected from the energy

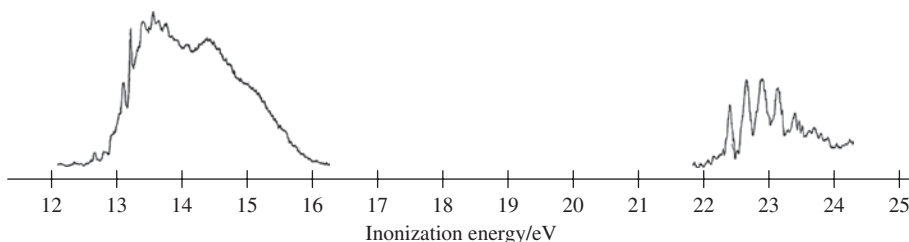


Figure 7.21 The PES of the valence orbital region of CH₄. The original spectra were reported in two sections (from 12 to 16.3 eV and from 21.9 to 24.2 eV) and are brought together here on a single energy scale. The vertical axis is photoelectron intensity in arbitrary units. Adapted from Potts A.W., Price W.C. (1972) *Proceedings of the Royal Society of London, Series A* **326**: 165–179. With permission from the Royal Society.

levels of the harmonic oscillator (Equation (7.4)) used to describe vibrational modes in Chapter 6 and related appendices. This feature is consistent with ionization of the $2a_1$ MO of CH_4 : it is at higher energy than the $1t_2$ band as the orbital is lower lying. Its intensity is actually notably less than the $1t_2$ ionization feature, and by more than the factor of 3 expected from the relative degeneracies. This is likely due to the compact nature of the $2a_1$ orbital compared with each of the three $1t_2$ MOs, as the former contains a dominant component from the C(2s) AO. So the $2a_1$ level presents a smaller ‘target’ for the incident photons to strike.

This spectral data seems difficult to understand using an sp^3 hybridization model, but arises naturally from the MO approach used here.

7.4.4 NH_3 , Ammonia

Ammonia has a pyramidal structure with the N centre above the plane of the three H atoms. The molecule belongs to the C_{3v} point group, and reference to the standard character table in Appendix 12 shows that, with the principle axis aligned with Z, the N valence orbitals have the following irreducible representations:

$$2s, 2p_z : a_1; \quad 2p_x, 2p_y : e \quad (7.54)$$

For the H(1s) irreducible representations we can make use of the fact that C_{3v} shares a rotational subgroup with D_{3h} , namely C_3 . We have already derived the SALCs for our analysis of BH_3 MOs in the more complex D_3 subgroup, and the same combinations can be used here:

$$a_1 = \frac{1}{\sqrt{3}}(s_1 + s_2 + s_3) \quad (7.55)$$

and the degenerate pair:

$$\phi_1(e) = \frac{1}{\sqrt{6}}(2s_1 - s_2 - s_3) \quad \phi_2(e) = \frac{1}{\sqrt{2}}(s_2 - s_3) \quad (7.56)$$

A check of the characters for these functions in C_{3v} should confirm the irreducible representation assignments. For the e representation, the methodology of Problem 7.6 should be followed.

The MO diagram for NH_3 is shown in Figure 7.22. Nitrogen has a higher electronegativity than H (Table 7.4), and so in the MO diagram its valence orbitals are drawn lower than the H SALCs. In addition, the separation of the 2s and 2p states is greater than in diagrams for elements earlier in the period because of the increased core charge as we move across the row of the periodic table. This trend was quantified in the discussion of ionization potentials (see Figure 7.13).

As before, the lowest energy orbital in this system is actually the core 1s state of the heavy atom, labelled $1a_1$ in the molecule. However, we are only interested in chemical bonding, so this is not shown in Figure 7.22. The first MO formed from valence AOs is $2a_1$. There are three orbitals which can contribute: N(2s), N(2p_z) and the a_1 SALC of the H(1s) AOs. The N(2s) orbital is the closest in energy to the $2a_1$ MO and so is the dominant component. The next two MOs are the degenerate $1e$ states formed from the combination

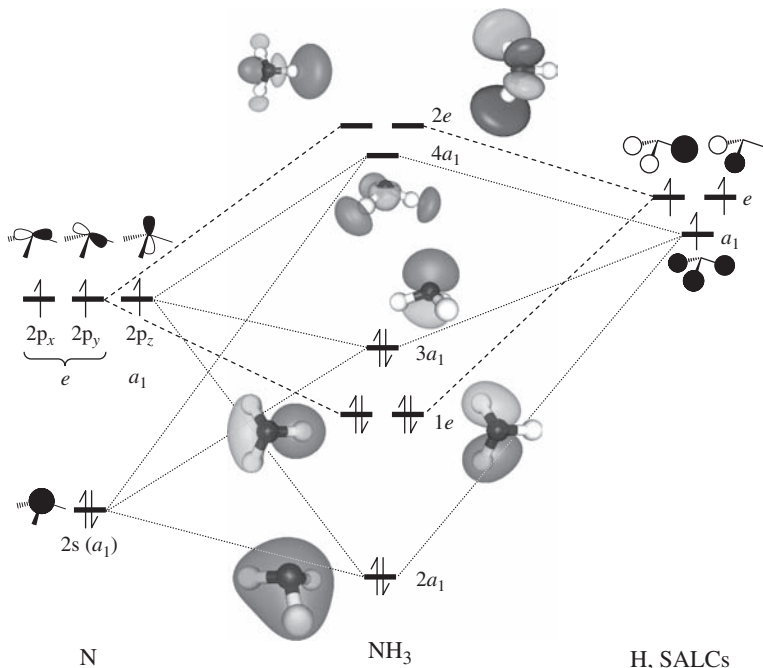


Figure 7.22 The MO diagram for the C_{3v} molecule NH_3 . For clarity, the dotted lines for the a_1 orbitals are drawn in a different style to those for the others.

$\text{N}(2\text{p}_x)$ and $\text{N}(2\text{p}_z)$ with their corresponding $\text{H}(1\text{s})$ SALCs. The final occupied orbital, $3a_1$, has a large $\text{N}(2\text{p}_z)$ character with only weak interaction with the $\text{H}(1\text{s}) a_1$ SALC.

The unoccupied orbitals begin at $4a_1$, which has a larger contribution from the $\text{H}(1\text{s}) a_1$ SALC than the earlier a_1 MOs. Finally, the $2e$ antibonding doubly degenerate levels are the highest energy MOs.

In the case of NH_3 , a hybridization picture can be useful in understanding the bonding scheme. We have found three a_1 valence MOs formed from linear combinations of the functions: $\text{N}(2\text{s})$, $\text{N}(2\text{p}_z)$ and the a_1 SALC of the $\text{H}(1\text{s})$ AOs. We can view these linear combinations as the result of first mixing the N-centred AOs, to form sp hybrids, and then dealing with the interaction between these hybrids and the H atom SALC. This is consistent with the irreducible representations on the N atoms, as it will produce hybrid orbitals that have the same a_1 symmetry. The linear combinations forming the hybrids have to be orthogonal to one another and normalized. This can be achieved by linking the coefficients c_1 and c_2 used in the hybrids so that

$$h_1(a_1) = N_h(c_1\text{s} + c_2\text{p}_z) \quad (7.57)$$

and

$$h_2(a_1) = N_h(c_2\text{s} - c_1\text{p}_z) \quad (7.58)$$

where N_h is a normalization constant. This nomenclature for the hybrid orbitals emphasizes that the new functions still have a_1 symmetry, because they are linear combinations of a_1 AOs.

Problem 7.9: Assuming that the original s and p_z AOs are normalized and orthogonal, show that:

1. Any choice of coefficients c_1 and c_2 leads to orthogonal hybrid functions.
2. The normalization constant will be

$$N_h = \frac{1}{\sqrt{c_1^2 + c_2^2}} \quad (7.59)$$

In Figure 7.23a, the case of hybrids formed from s and p states of the same energy results in equal contributions to form degenerate hybrids. The result of the mixing of an s and a p state on the same atom results in this way is a skewed distribution around the nuclear centre. A larger lobe is generated where the phases match (constructive interference), while a reduced lobe is seen where s and p phases are opposite to one another (destructive interference). When the energies of the s and p orbitals differ, the degree of mixing in the hybrids will depend on the energy separation between the AOs. It is more likely that the s orbital will be lower in energy than the p, as shown in Figure 7.23b. Here, the lower energy hybrid orbital will be of mainly s character, while the higher energy one

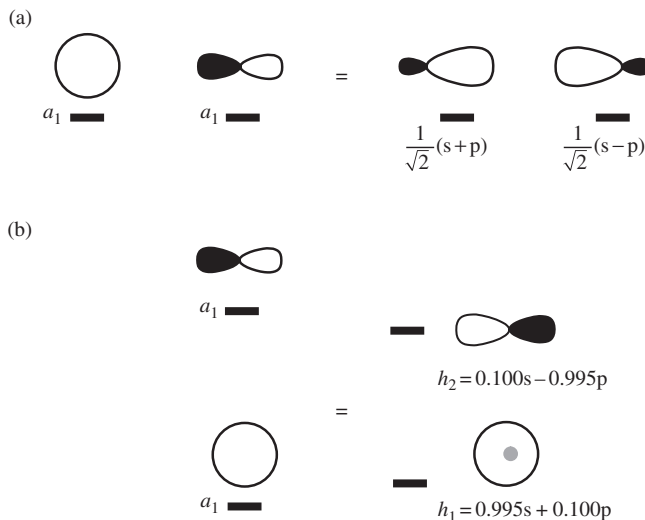


Figure 7.23 Examples of sp hybrid orbitals constructed from AOs which belong to the same irreducible representation. (a) AOs of the same energy would contribute equally to give degenerate hybrids. (b) When the energy separation between s and p states is larger, the hybrid orbitals are no longer equivalent. The grey spot in the h_1 orbital indicates the position of the nucleus, showing that mixing in $0.1p$ has polarized the s-orbital.

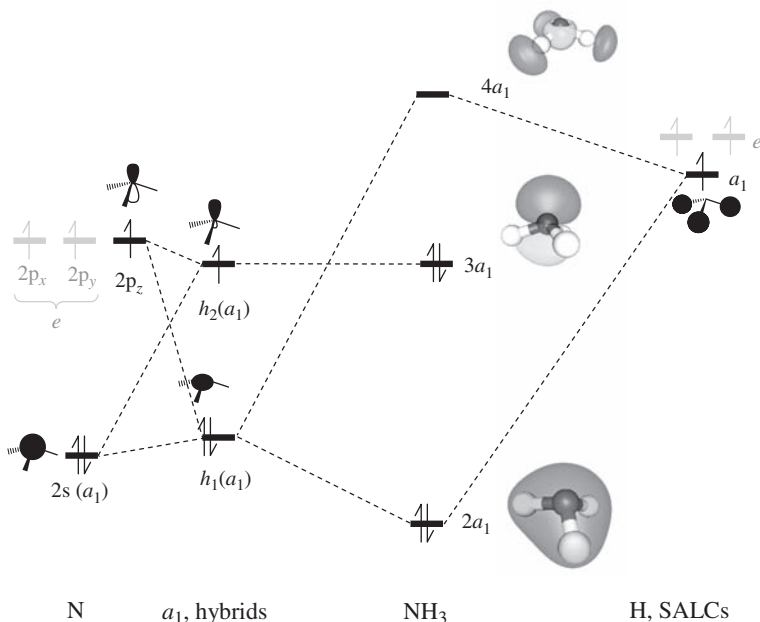


Figure 7.24 The use of a_1 hybrid orbitals to understand the origin of the three NH_3 MOs of a_1 symmetry.

is dominated by the p-orbital. In this illustration we have arbitrarily taken $c_1 = 0.1$; in general, the greater the difference in energy between the two AOs; the smaller c_1 will be. With such unequal weightings; each hybrid closely resembles the atomic state to which it is nearest in energy.

The two hybrids for NH_3 are shown to the right of the original N AOs in Figure 7.24, where their use in constructing the a_1 symmetry MOs for NH_3 is illustrated. The $2s$ - $2p$ separation for N is quite large and so the hybrids follow Figure 7.19b. The difference between the hybrid states is that the lobe of $h_1(a_1)$ is skewed downward toward the H atom plane, and so this orbital has strong overlap with the a_1 H(1s) SALC, forming the bonding $2a_1$ and antibonding $4a_1$ MOs. In contrast, the larger lobe of $h_2(a_1)$ is orientated away from the H atoms, resulting in a $3a_1$ MO that is practically nonbonding, through poor orbital overlap with the H(1s) a_1 SALC.

The use of hybrids of symmetry-matched AOs in this way is really just a change of the choice of basis set. It does not change the resulting electron density calculated for the molecule, as the sum over all occupied states (Equation (7.1)) will give the same result irrespective of the way the SALCs are formed.

The hybrid scheme is clearer for estimating the bond order for NH_3 . Since the $3a_1$ level is nonbonding it does not contribute to our calculation of bond order (Equation (7.24)). So, we are left with three doubly occupied bonding orbitals ($2a_1$ and the pair of $1e$ MOs). There are also three N—H bonds, so that each bond is single order.

From the MO diagram, with or without the use of hybrids, the highest occupied state ($3a_1$) in NH_3 has a large lobe above the N atom and away from the plane of the H atoms. This orbital is available to interact with other molecules and gives NH_3 its Lewis basic

character. The electrons occupying the $3a_1$ are commonly referred to as the NH_3 molecule's 'lone pair'.

We have now seen two molecules of formula AH_3 : the planar BH_3 belongs to the D_{3h} point group and the pyramidal NH_3 has C_{3v} symmetry. The structure adopted by any molecule should be that which minimizes its total energy. Once we have drawn the MO diagram, the electronic contribution to the total energy can be estimated by considering the occupied orbitals (Equation (7.5)). The total electronic energy is the sum of the occupied energy levels weighted according to the number of electrons they contain.

Figure 7.25 shows how the atomic N states are related to the occupied MOs from Figure 7.22 and how these in turn are related to the orbitals that would be obtained for NH_3 in a planar D_{3h} geometry. The C_{3v} MOs are lower in energy than the atomic states, so that molecule formation is favourable. If we imagine moving from the pyramidal NH_3 structure to a planar geometry, then the $2a_1$ state would actually increase in energy. This is because in the C_{3v} structure the hybrid orbital $h_1(a_1)$ overlaps with the H(1s) orbitals more effectively than would the 2s orbital alone. The 2s and 2p are hybridized in C_{3v} , but in D_{3h} symmetry they have different irreducible representations and so must be considered separately. However, the overlap of the p_x and p_y orbitals with the corresponding H(1s) SALCs in D_{3h} is much better than in C_{3v} , since the H atoms, and their 1s orbitals, are in the same plane as the central atom. The $3a_1$ orbital in the C_{3v} structure is the second MO that uses an sp hybrid. The hybridization has lowered the reference AO with respect to the pure p_z state that forms the nonbonding $1a'_2$ orbital in D_{3h} . Figure 7.25 shows that this orbital increases in energy as we move from the C_{3v} NH_3 structure to a planar D_{3h} version. Overall, NH_3 has a lower total energy in the C_{3v} geometry because of the stabilization of $3a_1$ and $1a'_2$ compared with the planar alternative. In the BH_3 molecule, $1a'_2$ is an empty orbital, and so the planar geometry is preferred due to the lower energy of the $1e'$ levels compared with the $1e$ of C_{3v} .

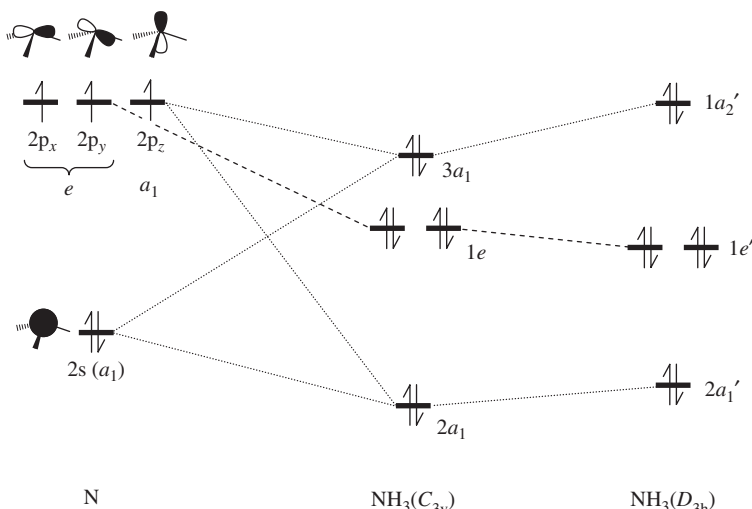


Figure 7.25 The relationship between the N valence orbitals and the NH_3 MOs in C_{3v} and D_{3h} symmetries. In the MOs, an additional three electrons are supplied by the H atoms.

In general, molecules adopt geometries, and so point groups, which minimize their total energy. An MO diagram can be used to judge the electronic contribution to the total energy from the occupied states. A comparison of the occupied states for alternative geometries can help explain the observed structures.

7.4.5 H₂O, Water

The C_{2v} structure of H₂O has served as an illustrative example many times in earlier chapters. In Section 4.2 we went through the designation of the O valence orbitals in detail, and the results are used to label the AOs to the left of Figure 7.26. They are also drawn lower than the H(1s) SALCs because the electronegativity of O (3.44) is considerably higher than that of H (2.10). Table 7.2 also shows that the 2s–2p separation for O is larger than for earlier elements in the second row of the periodic table, and so the valence states of O are drawn further apart than, for example, those of N in NH₃ (Figure 7.22). The SALCs formed from the two possible combinations of the H(1s) phases are easily assigned to the a₁ and b₂ representations, shown to the right of the MO diagram.

The lowest energy valence MO is the 2a₁ level, which has a large contribution from the low-lying O(2s) AO. The coefficients for the a₁ H(1s) SALC in this orbital are relatively minor, since they are at considerably higher energy. This can be seen in the accompanying

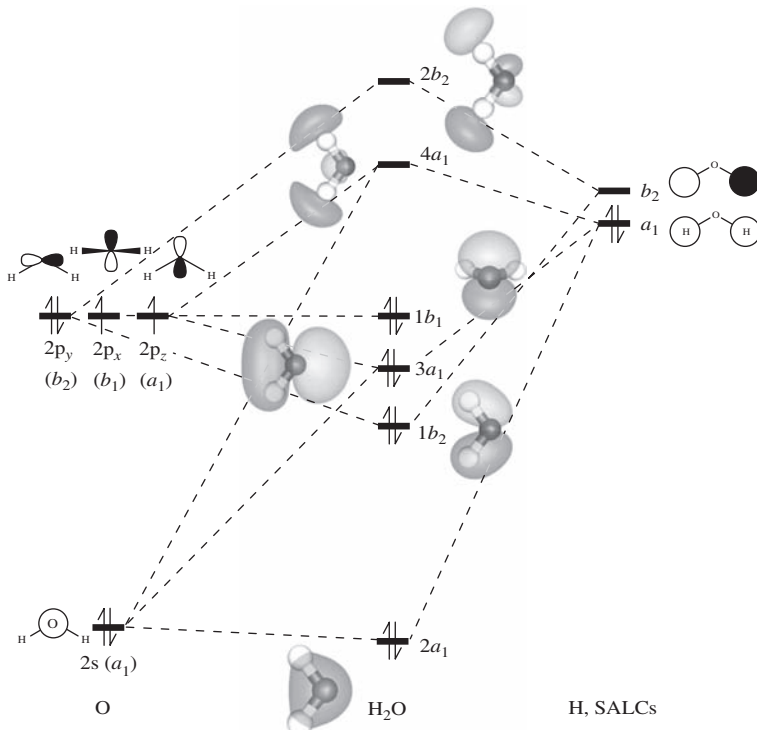


Figure 7.26 The MO diagram for H₂O.

graphic, as the spheres used to mark the H atom positions are largely outside of the orbital contour. The next level, $1b_2$, does contribute to bonding, being formed from the $2p_y$ and the b_2 H(1s) SALC, which are much closer to one another. Similarly, the $3a_1$ level contains significant contributions from both the O($2p_z$) orbital and H(1s) a_1 SALC.

The HOMO is the nonbonding $1b_1$ level. This is the O($2p_x$) AO, which is perpendicular to the plane of the molecule. The unoccupied orbitals are the antibonding $4a_1$ and $2b_2$ levels.

The weak involvement of the H(1s) orbitals in the $2a_1$ state leads to a bond order estimate of 2 split evenly over the two O—H bonds so that each is a single bond.

Water is an essential component of biological systems and has many interesting physical properties. For example, the density of ice at 0 °C is actually less than that of the liquid state, and so the solid floats. This is unusual, since for most other molecules the intermolecular forces cause a denser packing in the solid state. However, the intermolecular bonding for H_2O is directional in nature due to hydrogen bonding. The electronegativity of O is higher than H, and so the OH bonds are polarized to give positively charged H atoms and a negatively charged O. In addition, the nonbonding electrons on O lead to an anisotropic distribution of electron density at O, commonly referred to as the O lone pairs. To obtain optimal intermolecular H bonding the structure that ice adopts is quite open, leading to a low density compared with the liquid state.

Problem 7.10: In Figure 7.25 we compare the energy levels for NH_3 in C_{3v} and D_{3h} geometries. Here, H_2O is taken to be C_{2v} , whereas we have seen that BeH_2 is a linear $D_{\infty h}$ molecule with the MO diagram given in Figure 7.16. Draw a diagram linking the O atomic states in the alternative geometries and so demonstrate that the H_2O structure is preferred when the $3a_1$ state is occupied.

7.5 The Second-Row Diatomic Molecules

7.5.1 Homonuclear Diatomics

All the molecules considered so far have had H as one of the participants in the bonding scheme. In this section we will start to consider the MOs produced for interactions between heavier atoms, beginning with homonuclear diatomics, A_2 , of second-row elements. General MO diagrams for these diatomics will be constructed and then used to discuss the relative stability of those that are observed experimentally: N_2 , O_2 and F_2 and those that are not found under normal circumstances, Li_2 , Be_2 , B_2 and C_2 . In common with H_2 , these molecules all belong to the $D_{\infty h}$ point group and so the 2s valence orbitals will be linked together as σ_g^+ and σ_u^+ SALCs:

$$\sigma_g^+ = \frac{1}{\sqrt{2}}(s_1 + s_2) \quad (7.60)$$

$$\sigma_u^+ = \frac{1}{\sqrt{2}}(s_1 - s_2) \quad (7.61)$$

The orbitals will be numbered as we construct the MO diagram following the convention that σ -symmetry orbitals are numbered without regard to the ‘g’ or ‘u’ labels. This time we will also need to cope with the p-orbitals on the two atoms in the diatomic. We have dealt with the symmetry of p and d-orbitals on the central Au atom in the $D_{\infty h}$ complex $\text{Au}(\text{CN})_2^-$ in Section 5.9. There, it was noted that the p_z orbital (aligned with the molecular axis) belongs to a separate irreducible representation to p_x and p_y . For the diatomic molecules we must now take SALCs of p-orbitals on the two equivalent atoms. This means that it is not possible to assign symmetry labels to the individual AOs, only to their linear combinations.

The reducible representation for the p_z orbitals is given in the first line of Table 7.9. The operations which do not swap the two atoms over leave this basis unchanged, and so a character of 2 is found, while for operations that exchange the atoms we find 0. This is identical to the reducible representation for the s-orbitals discussed in Section 7.3, so that the same reducible representations must be present:

$$\sigma_g^+ = \frac{1}{\sqrt{2}}(p_{z1} - p_{z2}) \quad (7.62)$$

$$\sigma_u^+ = \frac{1}{\sqrt{2}}(p_{z1} + p_{z2}) \quad (7.63)$$

Table 7.9 The reducible representations for the $2p$ valence orbitals of a second-row diatomic molecule. The p_x and p_y orbitals (perpendicular to the molecular axis) are degenerate forming Π_g and Π_u combinations.

$D_{\infty h}$	E	$2C_\infty^\Phi$...	$\infty\sigma_v$	i	$2S_\infty^\Phi$...	∞C_2
p_z	2	2	...	2	0	0	...	0
p_x, p_y	2	$4 \cos(\Phi)$...	0	0	0	...	0
Π_g	2	$2 \cos(\Phi)$...	0	2	$-2 \cos(\Phi)$...	0
Π_u	2	$2 \cos(\Phi)$...	0	-2	$2 \cos(\Phi)$...	0

These linear combinations for the s and p_z orbitals are shown in Figure 7.27a. Notice that the σ_g^+ SALC of the p_z orbitals contains ‘ $-p_{z2}$ ’, Equation (7.62), while that for the s-orbitals has ‘ $+s_2$ ’, Equation (7.60). This comes about because the inversion operation, which moves an s_1 or p_{z1} orbital to atom 2 in the molecule, also reverses the phase of the p_z orbital, as shown in Figure 7.24b. For both types of orbital the σ_g^+ SALC is bonding and the σ_u^+ is antibonding.

The reducible character set for the p_x and p_y orbitals is given on the second line of Table 7.9. We could proceed with the reduction following the elimination method covered in Section 6.2.2, but for brevity the result is given at the bottom of the table and a simple summation of the characters confirms that

$$\Gamma(p_x, p_y) = \pi_g + \pi_u \quad (7.64)$$

The corresponding SALCs are shown in Figure 7.27c. This time, the *ungerade* π_u combination gives bonding orbitals and the π_g are antibonding.

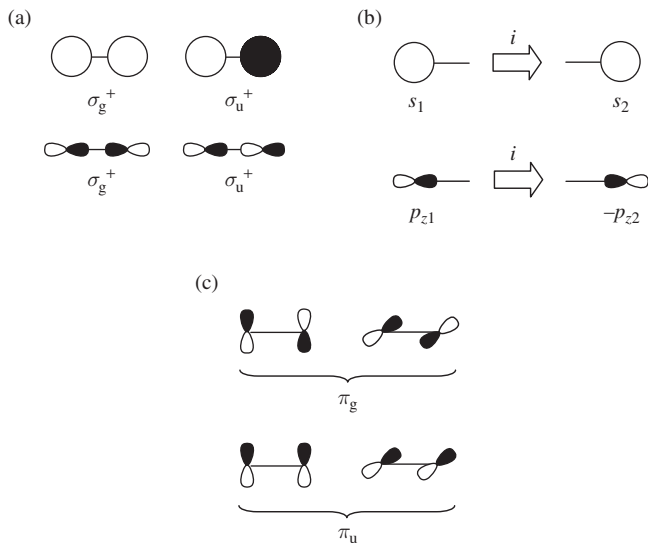


Figure 7.27 The SALCs for s and p states of a diatomic $D_{\infty h}$ molecule. (a) The σ_g^+ and σ_u^+ combinations of s and of p_z AOs. (b) The action of the inversion operation for s_1 and p_{z1} . (c) The π_g and π_u degenerate pairs formed from p_x and p_y orbitals.

Figure 7.28 shows a general MO diagram based on the SALCs we have generated. In this picture it is assumed that the σ -symmetry MOs formed from the s -AOs do not mix with their counterparts of the same symmetry from p_z . This will be the case if the energy

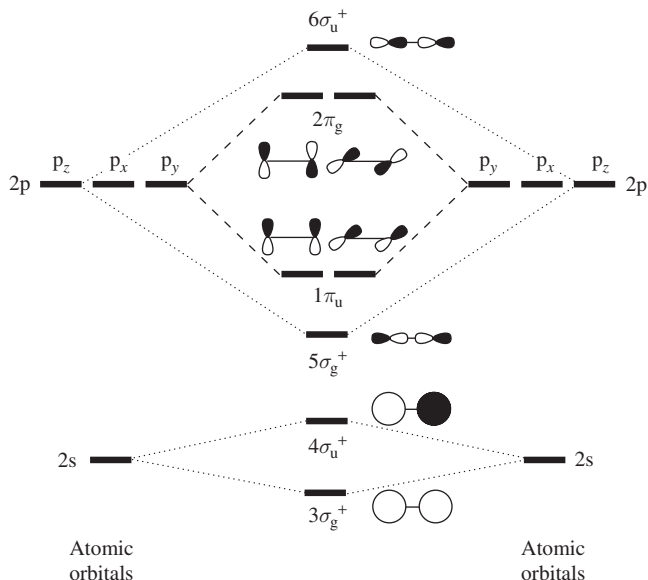


Figure 7.28 A general MO diagram for diatomic molecules A_2 for second-row elements. This diagram assumes no hybridization of the σ_g^+ or σ_u^+ combinations of s and of p_z AOs.

difference between the s and p states is large, i.e. for elements from the right-hand end of the second row (see Figure 7.13).

If the s and p states are closer in energy, then mixing of the MOs formed from s and p_z can occur. Figure 7.29 shows how this affects the MO diagram for the diatomic molecule. The lowest energy valence orbital, $3\sigma_g^+$, is shifted down in energy because mixing with the p_z -orbitals in $5\sigma_g^+$ leads to an increased orbital overlap in the hybrid state. The antibonding counterpart, $4\sigma_u^+$, is also shifted down in energy since the sp hybridization gives a weaker overlap in the internuclear region and so this orbital becomes only weakly antibonding.

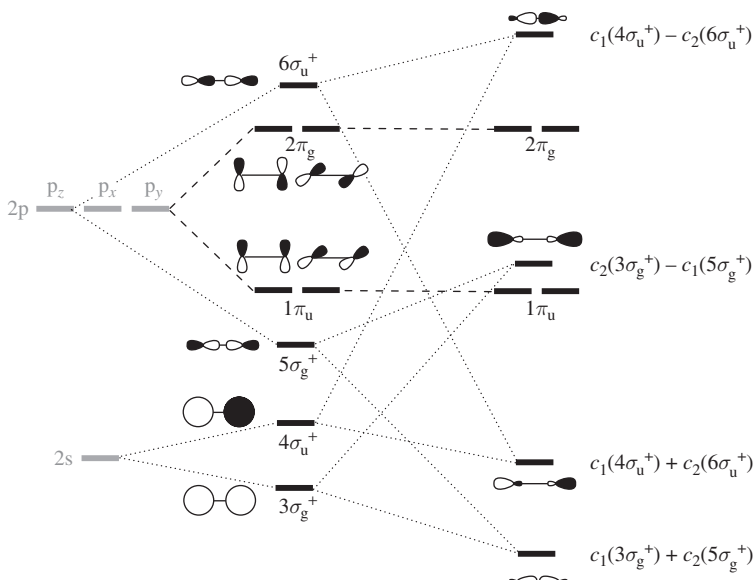


Figure 7.29 The effect of hybridization on the MO diagram of A_2 molecules. The orbital labels of the σ hybrids are referred to using the same numbering system as for the nonhybrid case, i.e. starting from $3\sigma_g^+$ as the lowest energy state; they are numbered in order of energy.

A similar effect can be seen for the $5\sigma_g^+$ state, but, since this is bonding when formed purely from p_z -orbitals, the loss of overlap density causes its energy to increase. Finally, the antibonding character of the $6\sigma_u^+$ is increased on sp-hybridization.

The coefficients in the hybrids shown in Figure 7.29 will depend on the energy difference between the orbitals of matching symmetry. This, in turn, depends on the separation of the AOs in the atomic states shown in grey in Figure 7.29. For closely spaced s and p orbitals, coefficient c_2 will be relatively large and sp-mixing gives the MO diagram to the right of the figure. When the AOs of the parent atoms are widely spaced, c_2 will tend to zero and we recover the MO diagram in the centre of Figure 7.29 (remember that multiplying the entire MO by -1 does not change the energy of the orbital, only reverses the phase pattern).

Perhaps the most important effect from hybridization is the change in the relative positioning of $5\sigma_g^+$ and $1\pi_u$. Symmetry alone cannot determine which molecules will have the orbital ordering with $5\sigma_g^+$ above $1\pi_u$ (significant sp-hybrids) and which will have $5\sigma_g^+$

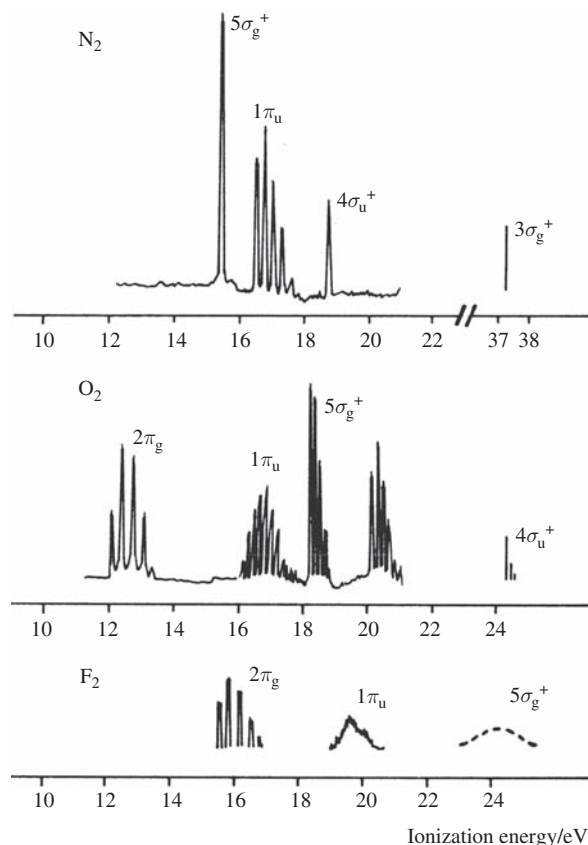


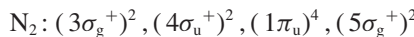
Figure 7.30 The PESs for the diatomics N_2 , O_2 and F_2 . Adapted with permission from Brundle C.R. and Baker A.D. (1977) *Electronic Spectroscopy: Theory, Techniques and Applications*, vol. 1, Academic Press (ISBN 0-12-137801-2). Copyright Elsevier.

below $1\pi_u$ (independent s and p_z SALCs). One way to obtain this information is from the PESs, which are shown for the stable molecules N_2 , O_2 and F_2 in Figure 7.30.

The spectra show sets of peaks that can be assigned to ionization from each MO. Several closely spaced peaks are seen in most cases because of vibrational effects as the photoelectron leaves the molecule. For example, removing an electron from a bonding state will tend to weaken the molecular bond and so the nuclei will move apart, initiating vibration. These effects are different for σ - and π -symmetry bonds and so actually help in the assignment of spectral bands.

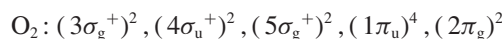
From the relative atomic ionization energies the 2s and 2p orbitals in N are closer in energy than they are in O or F; so, if sp-hybrids are important for any of these molecules, then they will be for N_2 . The PES for N_2 is consistent with the hybrid MO diagram. The lowest energy ionization is assigned to the $5\sigma_g^+$ state, and so the corresponding MO must be above the $1\pi_u$ level. Also, the PES line for the $4\sigma_u^+$ level is roughly 6.9 eV lower than the atomic N 2s ionization energy (25.6 eV, Table 7.2), whereas the $3\sigma_g^+$ band is 11.6 eV higher in energy. This indicates that the stabilization of the chemical bond from

the $3\sigma_g^+$ MO outweighs the antibonding influence of $4\sigma_u^+$ by almost a factor of 2. The hybrid scheme easily explains this, because the overlap in the $4\sigma_u^+$ antibonding orbital is weakened on hybridization. Accordingly, the full valence electron configuration of N_2 is



where the orbitals are written in order of stability left to right. Of these MOs, only $4\sigma_u^+$ is antibonding, and so N_2 is assigned a triple-bond order. This gives N_2 the shortest bond length and highest bond energy of the second-row diatomics (Table 7.3).

The O_2 PES in Figure 7.30 shows that the ionization energy for the $1\pi_u$ is now lower than that for $5\sigma_g^+$, so that sp-hybrids are much less important than for N_2 . Table 7.2 gives the $2s - 2p$ energy difference in atomic O as 16.5 eV, compared with 12.4 eV for N. So both the PES and ionization potential data are consistent with an O_2 electronic configuration:



A calculated MO diagram which agrees with this experimental ordering of the energy levels for O_2 is shown in Figure 7.31. Note that the highest occupied level $2\pi_g$ is antibonding and so lies above the atomic p-states from which it is formed. This makes the threshold ionization energy for O_2 lower than for N_2 , despite the higher core-charge on the atoms,

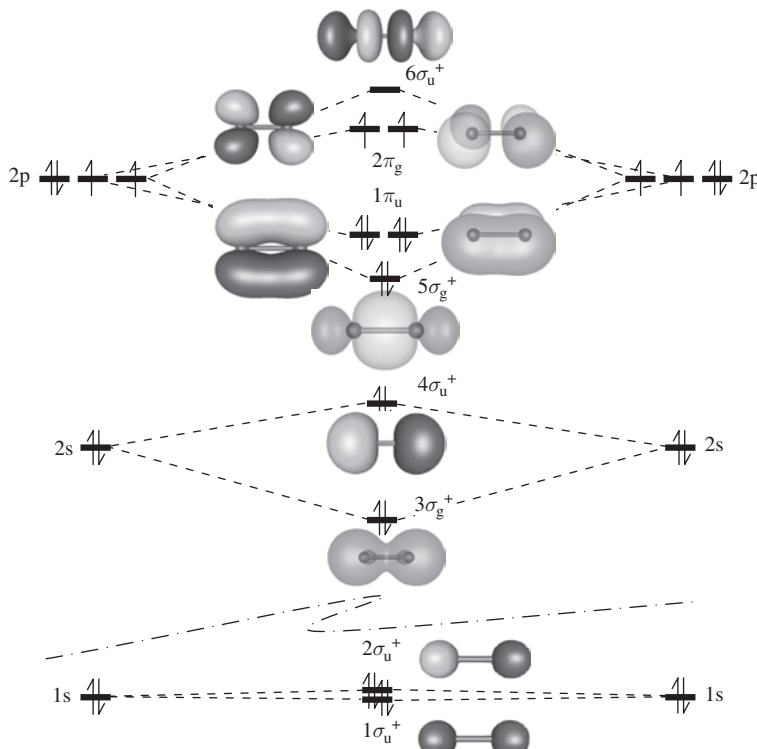


Figure 7.31 The MO diagram for O_2 .

and also leads to an O_2 bond order of 2. The $2\pi_g$ level is also doubly degenerate, and so the two electrons can reside in different spatial orbitals with their spins aligned, making O_2 paramagnetic.

In the PES of O_2 the $5\sigma_g^+$ band is split in two (Figure 7.30). This results from the two alternative spin states for the O_2^+ cation that is formed on ionization; referring to Figure 7.31, removing the spin-down electron from $5\sigma_g^+$ will give a cation with three unpaired spins, while removing the spin-up electron will give a cation with only one unpaired spin. The difference in the energies of these alternative cation spin states leads to the observed splitting. A similar effect does occur for ionization from the $1\pi_u$, but the splitting is smaller and it is masked by the broad spread of the vibrational peaks for ionization from this orbital.

The third spectrum in Figure 7.30 is for F_2 ; this has the same ordering of peaks as O_2 but considerably more spread out. Now the antibonding $2\pi_g$ state contains four electrons, so that the bond order is 1 and the molecule is diamagnetic. The first ionization of F_2 requires more energy than O_2 because of the higher effective core charge of the F atoms.

The PESs show that sp-hybridization is important for the diatomics from Li_2 up to N_2 . So we can predict the ground-state electronic configurations of the unstable diatomics from the early part of the second row:

$Li_2: (3\sigma_g^+)^2$	A single bond.
$Be_2: (3\sigma_g^+)^2, (4\sigma_u^+)^2$	Formally no net bonding, although the sp-hybrid scheme does suggest a weak interaction because both $3\sigma_g^+$ and $4\sigma_u^+$ are lowered by hybridization.
$B_2: (3\sigma_g^+)^2, (4\sigma_u^+)^2, (1\pi_u)^2$	A single bond. This would also give a triplet ground state because the two electrons in the $1\pi_u$ level occupy different orbitals.
$C_2: (3\sigma_g^+)^2, (4\sigma_u^+)^2, (1\pi_u)^4$	A double bond with no unpaired electrons.

Table 7.3 does list data for Li_2 , B_2 and C_2 , but, as expected from above, Be_2 is very difficult to observe experimentally. Li_2 has a weak single bond with an estimated energy of 106 kJ mol^{-1} . This is much lower than the bond energy of H_2 because of the larger radius of the 2s orbitals compared with 1s and the repulsion between the core states on the two Li atoms. This also leads to a very long bond length.

The single bond of B_2 is considerably stronger; as we have seen, the $4\sigma_u^+$ antibonding character is reduced by hybridization. The bond energy of C_2 is the highest in the set of these ‘unusual’ diatomics. In fact, B_2 and C_2 both have bond energies considerably higher than that of the more familiar F_2 molecule. However, under normal conditions, the electron-deficient nature of these elements, early in the second row, leads to a preference for forming metallic solids (Li , Be) or insulating solids consisting of extended covalent arrays (B , C).

7.5.2 Heteronuclear Diatomics of Second-Row Elements

When the two atoms in a diatomic are different, the molecule belongs to the $C_{\infty v}$ point group. There are several important diatomics from second-row elements; CO and NO , for example, are important in inorganic chemistry as ligands in inorganic complexes. The strong binding of CO to metal centres also makes it capable of inhibiting the Fe(haem)

component of haemoglobin, making it a dangerous asphyxiate. NO has an odd number of electrons and so is a free radical. As an atmospheric pollutant, NO is one of the agents that can cause ozone depletion. These molecules are products of incomplete oxidation present in car exhausts. The need to protect our environment has led to the development of multicomponent catalytic converters that effectively remove NO (through reduction to N₂ and O₂) and CO (through oxidation to CO₂).

The two atoms in the heteronuclear diatomics are not related by any symmetry operation, and so we can assign symmetry labels to the individual AOs and then match up symmetry-related sets in the MO diagram. The assignments are straightforward, taking the molecular axis as Z:

- 2s and 2p_z are unaffected by any symmetry operation and so will be σ⁺.
- 2p_x and 2p_y are perpendicular to the molecular axis and degenerate, giving π symmetry.

The relative electronegativities of the two atoms in the molecule will give one set of AOs a lower energy than the other.

The example of CO is shown in Figure 7.32. The ordering of the orbitals is similar to the hybrid scheme used for the homonuclear diatomics up to N₂, with the 5σ⁺ orbital in

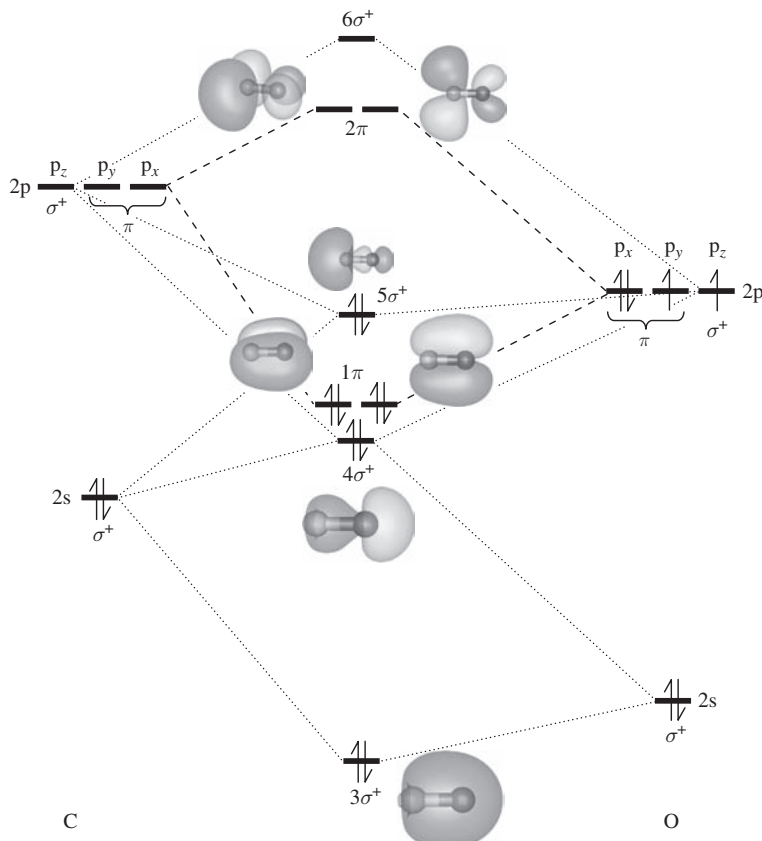


Figure 7.32 The MO diagram for CO.

between the 1π and 2π levels. In fact, the $5\sigma^+$ orbital shows more significant hybridization on the C side of the bond than the O, since this MO is much closer in energy to the C(2s) orbital than to the O(2s). The difference in electronegativities also means that the bonding 1π orbitals are polarized toward O. Correspondingly, the antibonding (and empty) 2π orbitals have larger lobes on C than on O. The NO molecule has one additional electron to CO and so this must occupy one of the degenerate 2π orbitals.

Problem 7.11: The bond length of NO^+ (1.062 \AA) is shorter than that of NO by 0.089 \AA , whereas CO^+ has a bond length (1.115 \AA) only -0.013 \AA shorter than CO. Use the MO diagram of Figure 7.32 to explain these observations.

7.6 More Complex Polyatomic Molecules

In Section 7.4 we considered the molecules formed by second-row elements with H. In each case there was only one heavy atom situated at the junction of all the symmetry elements, i.e. at the ‘point’ of the point group. This allows the symmetry labels for the p-orbitals of this atom to be taken directly from the right-hand column of the standard character table in Appendix 12. To form the MO diagram, we then considered the SALCs for the H(1s) orbitals and matched symmetry labels to identify the MOs that will give bonding–antibonding interactions.

In this section we introduce more complex molecules in which there are multiple heavy atoms. We now need to identify SALCs for the sets of atoms that are related by symmetry operations. The MO diagram is then constructed by matching irreducible representations for the SALCs.

7.6.1 Ethene

As a first example we consider the D_{2h} molecule C_2H_4 . The two C atoms form one set of atoms and the four H atoms another. In the D_{2h} point group there are three mutually perpendicular C_2 axes, labelled $C_2(X)$, $C_2(Y)$ and $C_2(Z)$. Figure 7.33 shows the axis system used in this analysis, which places X along the C=C bond and Z out of the molecular plane. The figure also gives the basis of four H(1s) orbitals for the SALC construction for this set of atoms.

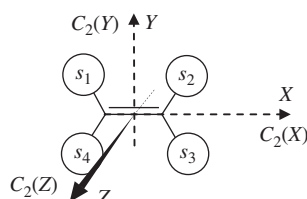


Figure 7.33 The axis system and basis used to obtain SALCs for the H(1s) orbital set in the D_{2h} molecule ethene.

Table 7.10 The reducible representation for the H(1s) orbitals of ethene (D_{2h}). In the application of the reduction formula (lower table) only the nonzero characters from $\Gamma(H(1s))$ need be considered. However, the order of the group (the total number of operations) is $h = 8$, irrespective of zeros in the reducible representation.

D_{2h}	E	$C_2(Z)$	$C_2(Y)$	$C_2(X)$	i	$\sigma(XY)$	$\sigma(XZ)$	$\sigma(YZ)$
$\Gamma(H(1s))$	4	0	0	0	0	4	0	0
D_{2h}	E	$\sigma(XY)$						
$\Gamma(H(1s))$	4	4						
		$g_c \chi_i(C) \chi_\Gamma(C)$	\sum_C					
A_g	4	4	8					
B_{1g}	4	4	8					
B_{2g}	4	-4	0					
B_{3g}	4	-4	0					
A_u	4	-4	0					
B_{1u}	4	-4	0					
B_{2u}	4	4	8					
B_{3u}	4	4	8					

The reducible representation for the H(1s) AOs is easily obtained, since only E and $\sigma(XY)$ operations leave the atoms in place to give a total character of 4, while all other operations interchange the atoms resulting in a character of 0. The application of the reduction formula is given in Table 7.10, where it is emphasized that the operation classes for which $\chi_\Gamma = 0$ need not be considered. The calculations give

$$\Gamma(H(1s)) = a_g + b_{1g} + b_{2u} + b_{3u} \quad (7.65)$$

Problem 7.12: Use the projection operator to obtain the normalized SALC H(1s) functions and show that your answers correspond to the orbital phase patterns below:



You can check your assignments of irreducible representation labels to these diagrams with the right-hand side of the MO diagram shown in Figure 7.36.

For the C atom orbital set we have to consider the eight C atom valence orbitals: 2s and $2p_{x,y,z}$ on each atom. Table 7.11 shows the reducible representation for a basis of all eight orbitals; any operation which swaps the two carbon atoms has a zero entry. The $C_2(X)$ rotation does not swap the atoms, but it does reverse the p_z and p_y orbitals on each atom while leaving s and p_x unchanged, so the total character is 0. Application of the reduction formula based on the three classes with nonzero entries gives

$$\Gamma(C(2s, 2p)) = 2a_g + b_{1g} + b_{2g} + b_{1u} + b_{2u} + 2b_{3u} \quad (7.66)$$

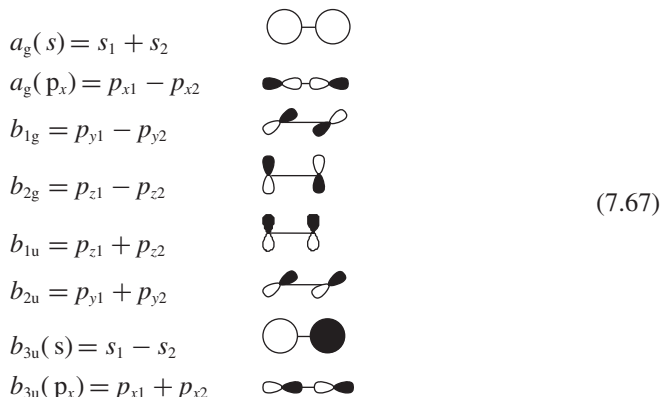
Table 7.11 The reducible representation for the valence orbitals of the carbon atoms of ethene (D_{2h}). In the application of the reduction formula (lower table) only the nonzero characters from $\Gamma(C(2s, 2p))$ need be considered.

D_{2h}	E	$C_2(Z)$	$C_2(Y)$	$C_2(X)$	i	$\sigma(XY)$	$\sigma(XZ)$	$\sigma(YZ)$
$\Gamma(C(2s, 2p))$	8	0	0	0	0	4	4	0

D_{2h}	E	$\sigma(XY)$	$\sigma(XZ)$	
$\Gamma(C(2s, 2p))$	8	4	4	
		$g_c \chi_i(C) \chi_{\Gamma}(C)$	\sum_c	
A_g	8	4	4	16
B_{1g}	8	4	-4	8
B_{2g}	8	-4	4	8
B_{3g}	8	-4	-4	0
A_u	8	-4	-4	0
B_{1u}	8	-4	4	8
B_{2u}	8	4	-4	8
B_{3u}	8	4	4	16

The SALCs that these represent are obtained using the projection operator with the rotational subgroup D_2 in Table 7.12. Here, we use the observation that the symmetry operations only link AOs of the same type on atoms 1 and 2, s_1 with s_2 , p_{x1} with p_{x2} , etc. This allows the required functions to be obtained by projecting each orbital of atom 1 in turn.

There is no inversion centre in the D_2 subgroup, so the ‘u’ and ‘g’ labels are assigned by inspection of the behaviour of each of the SALCs under the inversion operation. As usual, the scaling factors obtained from the projection can be ignored, and so we have the following functional forms:



The molecule orientations in the sketches accompanying these equations are the same as shown in the inset in Figure 7.34. The main part of Figure 7.34 shows how these SALCs are derived from the AOs and their relative energies. The energies are estimated based on the degree of bonding/antibonding; for example, the $3a_{1g}$ orbital contains a bonding interaction for the p_{x1} orbitals which are aligned with the molecular axis. The overlap of

Table 7.12 The projection operator method applied to the C=C orbital set for ethene. The rotational subgroup D_2 is used to simplify the process and ‘u’ and ‘g’ labels required for the full D_{2h} point group are assigned in the text. The generating functions are the 2s and 2p orbitals of atom 1.

D_2	E	$C_2(Z)$	$C_2(Y)$	$C_2(X)$	$\mathbf{P}_i b_1 = \sum_j \chi_i(j) \mathbf{T}_j b_1$
$\mathbf{T}_j s_1$	s_1	s_2	s_2	s_1	
$A\mathbf{T}_j s_1$	s_1	s_2	s_2	s_1	$2(s_1 + s_2)$
$B_1 \mathbf{T}_j s_1$	s_1	s_2	$-s_2$	$-s_1$	0
$B_2 \mathbf{T}_j s_1$	s_1	$-s_2$	s_2	$-s_1$	0
$B_3 \mathbf{T}_j s_1$	s_1	$-s_2$	$-s_2$	s_1	$2(s_1 - s_2)$
D_2	E	$C_2(Z)$	$C_2(Y)$	$C_2(X)$	$\mathbf{P}_i b_1 = \sum_j \chi_i(j) \mathbf{T}_j b_1$
$\mathbf{T}_j p_{x1}$	p_{x1}	$-p_{x2}$	$-p_{x2}$	p_{x1}	
$A\mathbf{T}_j p_{x1}$	p_{x1}	$-p_{x2}$	$-p_{x2}$	p_{x1}	$2(p_{x1} - p_{x2})$
$B_1 \mathbf{T}_j p_{x1}$	p_{x1}	$-p_{x2}$	p_{x2}	$-p_{x1}$	0
$B_2 \mathbf{T}_j p_{x1}$	p_{x1}	p_{x2}	$-p_{x2}$	$-p_{x1}$	0
$B_3 \mathbf{T}_j p_{x1}$	p_{x1}	p_{x2}	p_{x2}	p_{x1}	$2(p_{x1} + p_{x2})$
D_2	E	$C_2(Z)$	$C_2(Y)$	$C_2(X)$	$\mathbf{P}_i b_1 = \sum_j \chi_i(j) \mathbf{T}_j b_1$
$\mathbf{T}_j p_{y1}$	p_{y1}	$-p_{y2}$	p_{y2}	$-p_{y1}$	
$A\mathbf{T}_j p_{y1}$	p_{y1}	$-p_{y2}$	p_{y2}	$-p_{y1}$	0
$B_1 \mathbf{T}_j p_{y1}$	p_{y1}	$-p_{y2}$	$-p_{y2}$	p_{y1}	$2(p_{y1} - p_{y2})$
$B_2 \mathbf{T}_j p_{y1}$	p_{y1}	p_{y2}	p_{y2}	p_{y1}	$2(p_{y1} + p_{y2})$
$B_3 \mathbf{T}_j p_{y1}$	p_{y1}	p_{y2}	$-p_{y2}$	$-p_{y1}$	0
D_2	E	$C_2(Z)$	$C_2(Y)$	$C_2(X)$	$\mathbf{P}_i b_1 = \sum_j \chi_i(j) \mathbf{T}_j b_1$
$\mathbf{T}_j p_{z1}$	p_{z1}	p_{z2}	$-p_{z2}$	$-p_{z1}$	
$A\mathbf{T}_j p_{z1}$	p_{z1}	p_{z2}	$-p_{z2}$	$-p_{z1}$	0
$B_1 \mathbf{T}_j p_{z1}$	p_{z1}	p_{z2}	p_{z2}	p_{z1}	$2(p_{z1} + p_{z2})$
$B_2 \mathbf{T}_j p_{z1}$	p_{z1}	$-p_{z2}$	$-p_{z2}$	p_{z1}	$2(p_{z1} - p_{z2})$
$B_3 \mathbf{T}_j p_{z1}$	p_{z1}	$-p_{z2}$	p_{z2}	$-p_{z1}$	0

the two p-orbitals in this ‘end-on’ arrangement is greater than the $1b_{1u}$ or $1b_{2u}$ SALCs, which have ‘side-on’ overlap, and so $3a_{1g}$ is drawn lower.

In Figure 7.35, orbital sp-hybridization involving the matched symmetry 2s and $2p_x$ SALCs is also indicated, most notably for the $3a_{1g}$ orbital which lies at an energy between the atomic 2s and $2p_x$ levels. This hybridization shows how the bonding character of the $3a_{1g}$ level is actually enhanced compared with either the 2s or $2p_x$ orbitals alone.

Figure 7.35 shows the C=C energy levels in the D_{2h} point group and in the absence of the four H atoms. In this hypothetical situation the $1b_{1u}$ and $1b_{2u}$ orbitals have the same energy, as do the $1b_{1g}$ and $1b_{2g}$ SALCs. A comparison with the general MO scheme for homonuclear diatomics in Figure 7.28 shows that these would be the degenerate π -symmetry orbitals for C_2 while $3a_{1g}$ would be a σ -type MO. In Figure 7.36 we bring together the C=C and H(1s) SALCs to form the MO diagram of ethane, and it is found

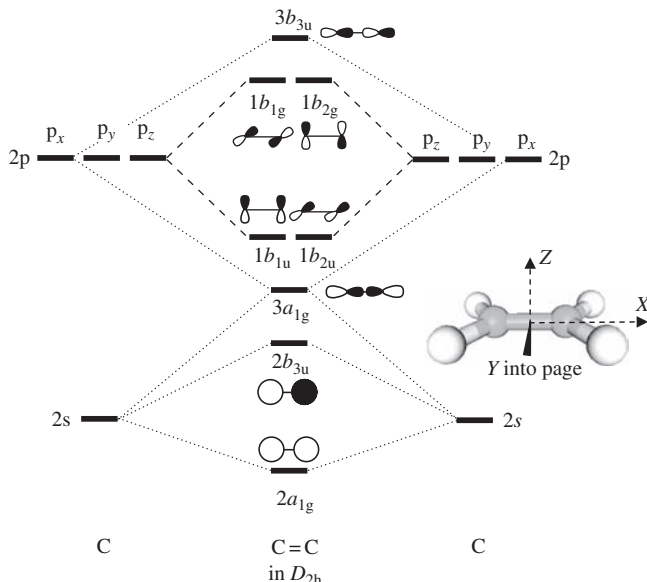


Figure 7.34 The MO diagram for the D_{2h} molecule ethene, without forming hybrid orbitals.

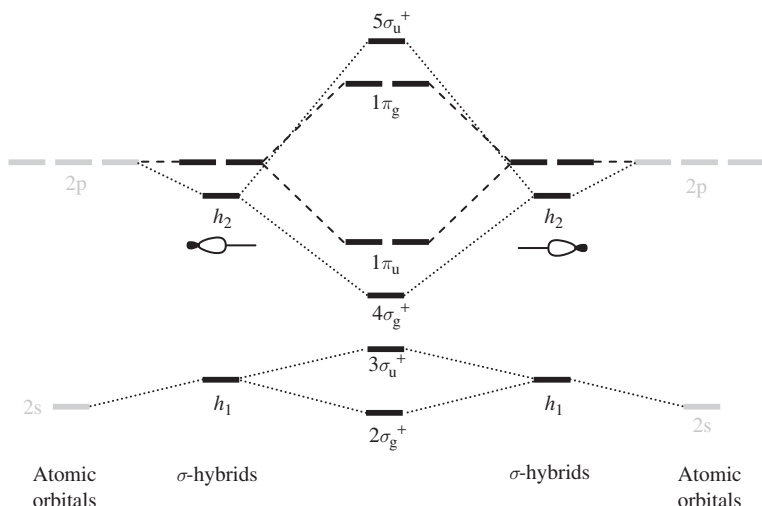


Figure 7.35 The hybrid orbitals for the symmetry-related carbon atoms in ethene.

that the $\text{C}=\text{C}$ orbitals derived from p_y have partners in the $\text{H}(1s)$ SALCs but those from p_z orbitals do not. Hence, the degeneracy expected for the π irreducible representations in $D_{\infty h}$ is lost. The comparison of atom–atom bonds with the diatomic case leads to the commonly used classification of MOs which include bonding/antibonding character as ‘ σ ’ or ‘ π ’, even in quite complex, nonlinear, structures. For example, the single b_{1u} MO formed here from the $\text{C}(p_z)$ orbitals in ethene is commonly referred to as a π -bonding MO.

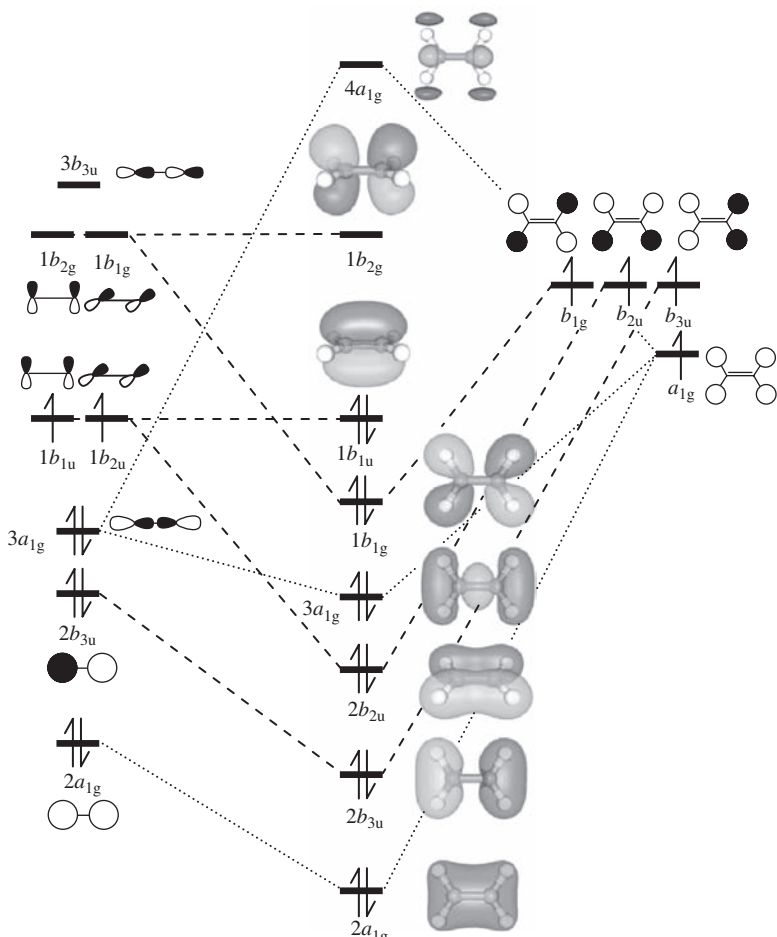
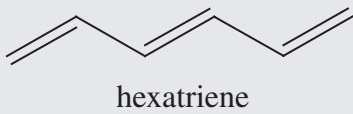


Figure 7.36 The MO diagram for the D_{2h} molecule ethene, using hybrid orbitals.

In the MO diagram of Figure 7.36 the H orbitals are placed higher in energy than the bonding SALCs of the C=C set since the electronegativity of C is greater than H (Table 7.4). The basis of AOs now contains 12 functions, and so there will be 12 MOs formed. However, to keep the diagram simple, only the six occupied valence orbitals and two lowest unoccupied levels are shown in Figure 7.36. The first five orbitals contain bonding C=C and C–H interactions, while the highest occupied level is the bonding C=C $1b_{1u}$ that is nonbonding for C–H.

Problem 7.13: In the example of ethene, the two p_z orbitals perpendicular to the molecular plane form orbitals of a π -bonding nature. For more complex alkenes we can treat the σ -orbital system and π -orbitals separately, as they will not mix by symmetry. The π -orbitals usually also contain the chemically important frontier (HOMO and LUMO) orbitals. In this problem we will treat just the p_z -orbitals of hexatriene and derive the relevant MOs.

1. Assign the point group of hexatriene from the chemical drawing shown below:



- Derive the reducible representation for the relevant set of p-orbitals; one per C atom perpendicular to the molecular plane.
- Apply the reduction formula (Equation 7.33)) to the reducible representation found in part (2) and list the irreducible representations for the π -orbitals.
- Figure 7.37 shows the calculated MO diagram for the π -system of hexene. Assign symmetry labels to the energy levels by identifying the irreducible representations of the orbitals illustrated.

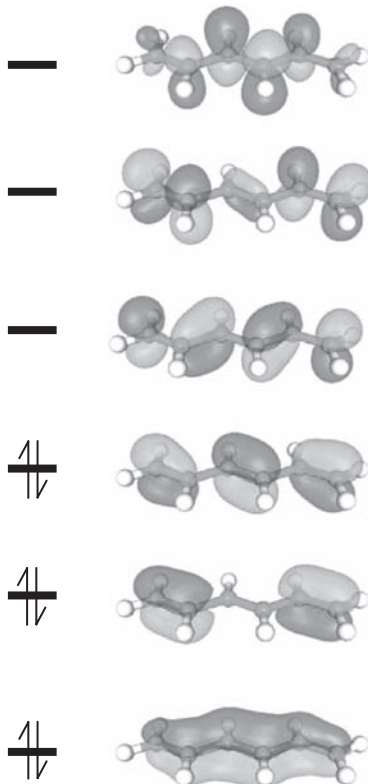


Figure 7.37 The MOs forming the π -system of hexatriene.

7.7 Metal Complexes

7.7.1 Complexes Containing σ -Donor Ligands

The irreducible representations for the p- and d-orbitals for a central metal atom in some common transition metal complex geometries were discussed in Section 5.8. We are now

in a position to understand how these orbitals interact with the ligand orbitals to give MOs with which to describe bonding in these complexes. We will concentrate on complexes in which the metal–ligand interaction is that of a σ -donor ligand, i.e. in the isolated ligand the orbitals would be filled and the metal is sufficiently electronegative to receive charge.

O_h Symmetry Complexes

Octahedral complexes have six ligands equidistant from a metal centre at the corners of an octahedron. In this class we include hexaaqua complexes such as $[\text{Ni}(\text{H}_2\text{O})_6]^{2+}$ shown in Figure 3.32a or $[\text{Mn}(\text{H}_2\text{O})_6]^{2+}$ in Figure 5.19a. The σ -donor orbitals from the H_2O molecules can be thought of as the $1b_1$ levels in the MO diagram for isolated H_2O (Figure 7.26). These are the highest occupied states for H_2O and so will most readily donate electron density to vacant orbitals on the metal centre. Formally, the symmetry of the complex is lower than O_h , since the H atoms of the H_2O cannot be arranged to conform to all of the point group operations. However, even at low temperature, the H_2O molecule orientation around metal–ligand bond will be randomized by thermal motion. For example, the H_2O molecules will be able to spin around the metal–ligand axis without disturbing the σ -donor interaction with the metal.

A simplified basis of just the σ -donor orbitals from H_2O is shown in Figure 7.38, along with some example symmetry axes from the O_h rotational classes. Appendix 12 gives the rotational subgroup given for O_h as O .

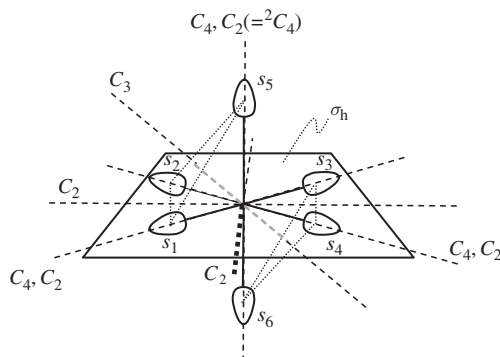


Figure 7.38 The basis of σ -donor orbitals for a six-coordinate complex in O_h symmetry. The ligand donor orbitals are represented by the s_1 – s_6 basis placed on the coordinate axis system. Also shown are some examples of the symmetry axes present and one of the horizontal mirror planes. The full set of operations is illustrated in Figure 3.28.

Problem 7.14: The reducible representation for the six σ -donor orbitals of Figure 7.38 in the O rotational subgroup is given in Table 7.13. Adding up the total number of operations for O from the character table in Appendix 12 gives an order $h = 24$. Using the reduction formula (Equation (7.33)), show that

$$\Gamma = a_1 + e + t_1 \quad (7.68)$$

Table 7.13 The reducible representation for the six σ -donor orbitals shown in Figure 7.38, within the rotational subgroup O .

O	E	$8C_3$	$3C_2 (= C_4^2)$	$6C_4$	$6C_2$
Γ	6	0	2	2	0

For the central metal atom we can read the irreducible representations for the s-, p- and d-orbitals directly from the functional forms quoted in the right-hand columns of the O character table:

$$\begin{aligned} M(nd_{xy}), M(nd_{yz}) \text{ and } M(nd_{xz}): & t_2 & M(nd_{z^2}) \text{ and } M(nd_{x^2-y^2}): & e \\ M((n+1)p_x), M((n+1)p_y) \text{ and } M((n+1)p_z): & t_1 & M((n+1)s): & a_1, \end{aligned} \quad (7.69)$$

Rotational subgroup symbols are always linked to the longer list of irreducible representations in the parent group. So, in this case, reading from the O_h character table we find

$$\begin{aligned} M(nd_{xy}), M(nd_{yz}) \text{ and } M(nd_{xz}): & t_{2g} & M(nd_{z^2}) \text{ and } M(nd_{x^2-y^2}): & e_g \\ M((n+1)p_x), M((n+1)p_y) \text{ and } M((n+1)p_z): & t_{1u} & M((n+1)s): & a_{1g}. \end{aligned} \quad (7.70)$$

The ‘g’ and ‘u’ labels can be understood from the effect of the inversion operation i on the AOs; d-orbitals are *gerade* and p-orbitals *ungerade*.

For the ligand orbitals, we can deduce the phase pattern of the SALCs for each of the irreducible representations identified in Equation (7.68) through thinking about the bonding/antibonding orbitals that will be formed with the metal centre. These are shown to the right of the ligand reference levels in the MO diagram of Figure 7.39.

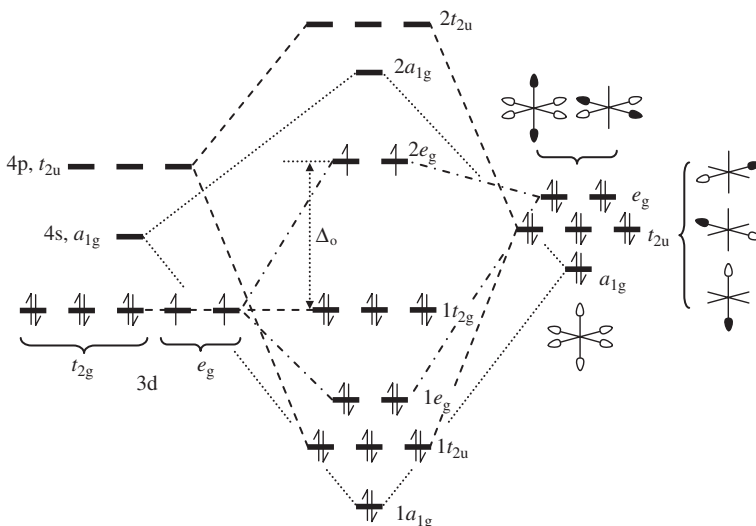


Figure 7.39 The MO diagram for an O_h symmetry complex with σ -donor orbitals.

In the MO diagram, the ligand SALCs are drawn higher in energy than the metal d-states, because donation of electron density from the ligands to the metal is expected. The different symmetries for the ligand reference states have been separated out, but this is really just to allow clear illustration; the SALCs should be thought of as practically isoenergetic. All of the ligand SALCs match with metal-centred orbitals, and so there are six bonding orbitals: $1a_{1g}$, $1t_{2u}$ and $1e_g$. These are closer in energy to the metal d-orbitals, signifying that the bond density will be polarized toward the metal, as we would expect for a σ -donor interaction.

The next set of levels is the three nonbonding t_{2g} MOs derived from the metal d-orbitals that have no symmetry match with the ligands. There are then six antibonding orbital complements to the bonding set: $2e_g$, $2a_{1g}$ and $1t_{2u}$.

As the ligand orbitals are initially filled, we can think of the six bonding states as taking up the ligand electrons. The metal d-electrons then enter the t_{2g} and possibly the e_g levels. This is, of course, an arbitrary choice, but gives a nice parallel to the ligand field approach in Chapter 5, where the ligand electrons were only present via their ‘field’ at the metal centre. The orbital filling shown in Figure 7.39 is representative of the d^8 complex $[\text{Ni}(\text{H}_2\text{O})_6]^{2+}$ with the configuration $(t_{2g})^6(e_g)^2$. The two e_g electrons are drawn in separate energy levels to minimize electron–electron repulsion.

On the MO diagram, the crystal field splitting parameter is indicated by the symbol Δ_o . In the MO picture, this is interpreted as the separation between the nonbonding t_{2g} states and the antibonding $2e_g$ levels.

7.7.2 The Jahn–Teller Effect

The MO diagram for O_h symmetry complexes has its highest filled MOs in degenerate states for most transition metals. The Jahn–Teller effect is a change of geometry due to an uneven filling of such degenerate states. For example, Cu^{2+} in the hexaaqua complex $[\text{Cu}(\text{H}_2\text{O})_6]^{2+}$ has a d^9 configuration, one more than shown in Figure 7.39. This results in a filling of all MOs up to the e_g states, with three electrons to be placed in these two MOs. In O_h symmetry there would be two choices: place two electrons in the e_g level derived from the metal d_{z^2} orbital and one in that from the $d_{x^2-y^2}$ or two in $d_{x^2-y^2}$ and only one in d_{z^2} . When such an imbalance is present, a shift of the complex geometry to a lower symmetry can give a more stable system.

In this case, two *trans*- H_2O ligands have longer $\text{Cu}\dots\text{O}$ distances than the four equatorial ligands. So, the $[\text{Cu}(\text{H}_2\text{O})_6]^{2+}$ complex has D_{4h} symmetry, as shown in Figure 7.40, and we will now show how this distortion is driven by MO energy by comparing the O_h and D_{4h} MO diagrams for d^9 systems.

D_{4h} Symmetry Complexes

The reducible representation and the application of the reduction formula for the D_{4h} complex are set out in Table 7.14. This shows that the six σ -donor ligand orbitals give SALCs with the following irreducible representations:

$$\Gamma = 2a_{1g} + b_{1g} + a_{2u} + e_u \quad (7.71)$$

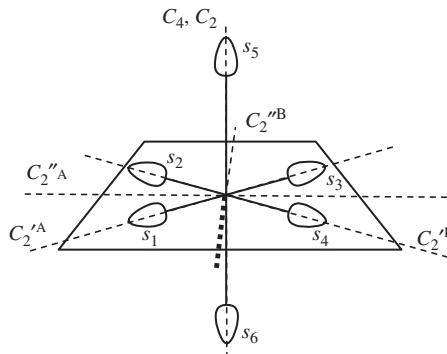


Figure 7.40 The basis of σ -donor orbitals for a six-coordinate complex after a distortion to D_{4h} symmetry. The axial ligands represented by s_5 and s_6 are further from the metal centre than the equatorial ligands. Also shown are the axes used in the projection operator calculations: the principal C_4 , collinear C_2 and the four horizontal C_2 axes.

Table 7.14 The reducible representation and application of the reduction formula for the six σ -donor orbitals in D_{4h} , $[Cu(H_2O)_6]^{2+}$.

D_{4h}	E	$2C_4$	C_2	$2C_2'$	$2C_2''$	i	$2S_4$	σ_h	$2\sigma_v$	$2\sigma_d$		$h = 16$
Γ	6	2	2	2	0	0	0	4	4	2		
							$g_c \chi_i(C) \chi_\Gamma(C)$				\sum_C	$h^{-1} \sum_C$
A_{1g}	6	4	2	4				4	8	4	32	2
A_{2g}	6	4	2	-4				4	-8	-4	0	0
B_{1g}	6	-4	2	4				4	8	-4	16	1
B_{2g}	6	-4	2	-4				4	-8	4	0	0
E_g	12	0	-4	0				-8	0	0	0	0
A_{1u}	6	4	2	4				-4	-8	-4	0	0
A_{2u}	6	4	2	-4				-4	8	4	16	1
B_{1u}	6	-4	2	4				-4	-8	4	0	0
B_{2u}	6	-4	2	-4				-4	8	-4	0	0
E_u	12	0	-4	0				8	0	0	16	1

The projection operator method for the a_{1g} representation will give functions having the same phase at symmetry-related positions, because it has character 1 for all classes. In the D_{4h} basis shown in Figure 7.40 there are actually two separate groups of σ -donor orbitals. The operations in the group do not swap the axial with the equatorial ligands, so the orbitals s_1 to s_4 form one symmetry-related set and the axial orbitals, s_5 and s_6 , are another. Accordingly, the two a_{1g} SALCs are the combinations of the two sets in phase and out of phase with one another, i.e.

$$a_{1g} = s_1 + s_2 + s_3 + s_4 + s_5 + s_6 \quad \text{and} \quad a_{1g} = s_1 + s_2 + s_3 + s_4 - s_5 - s_6 \quad (7.72)$$

For the b_{1g} representation we can use the projection operator method along with the D_4 rotational subgroup of D_{4h} as laid out in Table 7.15. The rotational subgroup does not contain the inversion centre, and so the *gerade* (g) and *ungerade* (u) labels do not appear.

Table 7.15 The projection operator method applied for the irreducible representations found from the reduction in Table 7.14 using the D_4 rotational subgroup. The designations of A and B axes are shown in Figure 7.40.

D_4	E	C_4^1	C_4^3	$C_2 (= C_4^2)$	$C_2'^A$	$C_2'^B$	$C_2''A$	$C_2''B$	$\mathbf{P}_i V = \sum_j \chi_i(j) \mathbf{T}_j V$
$B_1 \mathbf{T}_j s_1$	s_1	$-s_2$	$-s_4$	s_3	s_1	s_3	$-s_2$	$-s_4$	$2(s_1 - s_2 + s_3 - s_4)$
$B_1 \mathbf{T}_j s_5$	s_5	$-s_5$	$-s_5$	s_5	s_6	s_6	$-s_6$	$-s_6$	0
$A_2 \mathbf{T}_j s_1$	s_1	s_2	s_4	s_3	$-s_1$	$-s_3$	$-s_2$	$-s_4$	0
$A_2 \mathbf{T}_j s_5$	s_5	s_5	s_5	s_5	$-s_6$	$-s_6$	$-s_6$	$-s_6$	$4(s_5 - s_6)$
$E \mathbf{T}_j s_1$	$2s_1$	0	0	$-2s_3$	0	0	0	0	$2(s_1 - s_3)$
$E \mathbf{T}_j s_2$	$2s_2$	0	0	$-2s_4$	0	0	0	0	$2(s_2 - s_4)$
$E \mathbf{T}_j s_5$	$2s_5$	0	0	$-2s_5$	0	0	0	0	0

After the projection, we can assign these labels that are required by the full point group by considering the effect of the inversion operation. The B_1 projection in D_4 with the s_1 orbital as a generating function gives

$$b_1 = s_1 - s_2 + s_3 - s_4 \quad (7.73)$$

The projection based on the axial ligand orbital, s_5 , gives a zero result, and so the axial σ -orbitals cannot take part in a SALC with b_1 symmetry. Under the inversion operation of the full D_{4h} point group, s_1 swaps with s_3 and s_2 with s_4 ; this leaves the function in Equation (7.73) unchanged, so we assign *gerade* symmetry to give b_{1g} .

Table 7.15 shows that the projection of the s_1 orbital for the A_2 representation in D_4 results in it visiting each equatorial position, but also that the resulting sum gives a function that is zero. This means that the equatorial σ -donor orbitals cannot participate in the a_{2u} SALC. On the other hand, the projection of the axial s_5 orbital gives a functional with a_2 symmetry in D_4 in which the axial ligand orbitals have opposite sign. For the inversion operation of the full D_{4h} point group this would have a character of -1, and so we can assign

$$a_{2u} = s_5 - s_6 \quad (7.74)$$

A quick check with the other operations in the full D_{4h} group confirms that this function has the full set of characters required for the a_{2u} representation.

Finally, for the e_u representation required from the reduction result (Equation (7.71)), Table 7.15 contains the projection based on the s_1 orbital with the e representation of the D_4 group. This is also an *ungerade* function when we consider the i operation of the full point group, and so one of the pair of e_u functions will be

$$\phi_1(e_u) = s_1 - s_3 \quad (7.75)$$

In this case, the characters of the E_u representation are zero for any operation that moves s_1 to either s_2 or s_4 . So, a new function can be obtained simply by projecting s_2 to give

$$\phi_2(e_u) = s_2 - s_4 \quad (7.76)$$

However, if we try a projection of the axial orbital, s_5 , a zero is obtained, meaning that the axial ligands do not take part in the e_u SALCs.

These results are used to label the ligand orbitals in the MO diagram of Figure 7.41. The relative energies of the ligand orbitals are exaggerated to allow clear presentation in the diagram; the various SALCs would have practically the same energy as one another. The relative positions of the molecule orbitals for the D_{4h} complex have been judged from the degree of overlap between each ligand SALC and its symmetry-matching metal-centred orbitals. In this case, both the $3d_{z^2}$ and $4s$ orbitals have a_{1g} symmetry, and so we could construct sd hybrids in a similar way to the sp hybrids considered in Figure 7.23. However, there is a clear match of the lower a_{1g} ligand orbital with $4s$ and the other a_{1g} SALC with $3d_{z^2}$. These involve all six σ -donor orbitals, and so have been assumed to give the lowest energy MOs.

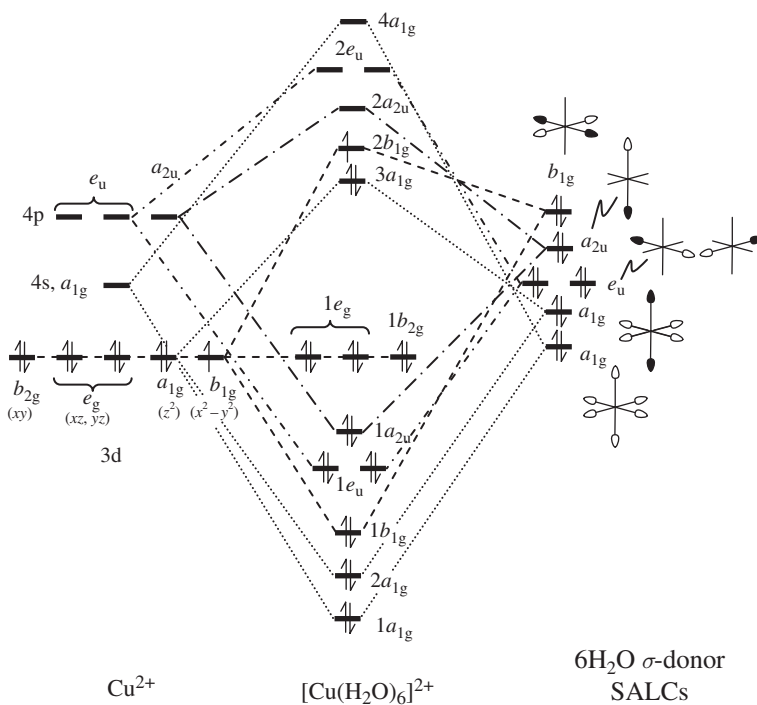


Figure 7.41 The MO diagram for the D_{4h} complex $[Cu(H_2O)_6]^{3+}$.

The $1b_{1g}$ bonding orbital is a combination of $d_{x^2-y^2}$ and four of the ligand orbitals, and so is drawn next. In the D_{4h} structure of $Cu(H_2O)_6$, the axial ligands are further away from the metal centre than the equatorial ligands, and so the $1e_u$ level is below the $1a_{2u}$. This gives six bonding molecule orbitals into which can be placed the 12 electrons from the donor molecules. The first levels used for metal electrons are the nonbonding $1e_g$ and $1b_{2g}$ orbitals. In the crystal field discussion of Chapter 5, the $1e_g$ set of orbitals was taken to be slightly lower in energy than the $1b_{2g}$ state, since the ligand field from the axial ligands is

weaker than from the equatorial ligands. However, the MO treatment simply sees these as nonbonding states which are drawn at the same level as the metal 3d orbitals. The next two levels are the antibonding $3a_{1g}$ and $2b_{1g}$ states. The longer M—O distances for the axial ligands means a smaller overlap for the metal and ligand orbitals in the $3a_{1g}$ arrangement, and so this antibonding orbital is the lower in energy.

For Cu^{2+} with its d^9 configuration, the $1e_g$, $1b_{2g}$ and $3a_{1g}$ levels are all filled, but the $2b_{1g}$ orbital has only a single electron.

Figure 7.42 compares the d-orbital configurations for the $[\text{Cu}(\text{H}_2\text{O})_6]^{2+}$ complex with O_h and D_{4h} symmetries. In the D_{4h} case the $3a_{1g}$ orbital has a lower energy than the O_h $2e_g$ levels, as it is less antibonding because the axial ligands have moved away from the metal centre. Correspondingly the $2b_{1g}$ orbital is higher in energy because the equatorial ligands are closer. However, since $2b_{1g}$ contains only a single electron, the effect is outweighed by the increased stability of its doubly occupied partner. So, the Jahn–Teller distortion results in a lowering of the total MO energy.

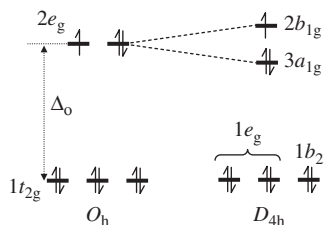


Figure 7.42 A comparison of the MOs with large d-orbital character in $[\text{Cu}(\text{H}_2\text{O})_6]^{3+}$ in the hypothetical O_h point group and the observed D_{4h} symmetry.

7.7.3 Complexes Containing Ligand Orbitals of π -Symmetry

The Δ_o parameter marked on Figure 7.39 marks the separation of the t_{2g} and e_g orbitals in an octahedral complex. These will usually be partially filled, and transitions of electrons between the states can be observed in the UV-visible region of the spectrum. Spectra of d^1 or d^9 complexes show a single broad transition, which is a measure of the orbital separation. An example for the d^1 complex, $[\text{Ti}(\text{H}_2\text{O})_6]^{3+}$, is shown in Figure 7.43, and

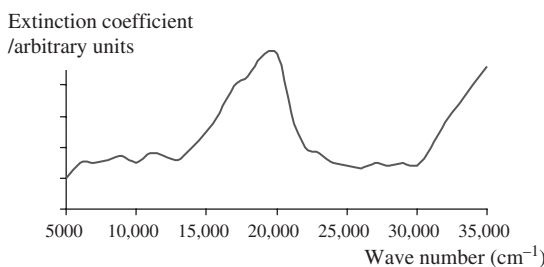


Figure 7.43 Absorption spectrum of the $[\text{Ti}(\text{H}_2\text{O})_6]^{3+}$ ion in the UV-visible range.

Table 7.16 The peak of the absorption band for some Ti^{3+} d^1 complexes.

Complex	Observed band/cm ⁻¹
$[TiCl_6]^{3-}$	13 000
$[TiF_6]^{3-}$	18 900
$[Ti(H_2O)_6]^{3+}$	20 300
$[Ti(CN)_6]^{3-}$	22 300

Table 7.16 gives the main peak position as $20\ 300\text{ cm}^{-1}$. The position of the peak is sensitive to the metal centre and ligand present. Table 7.16 also shows values for three other complexes containing Ti^{3+} . These indicate that the energy separation of the t_{2g} and e_g levels increases in the order



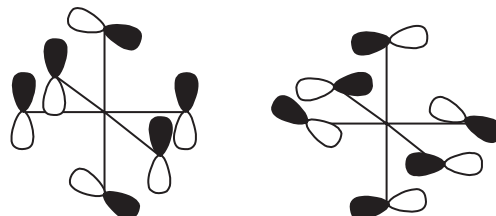
Interpretation of spectra for complexes with different d-orbital configurations is complicated by multi-electron effects; this requires a ‘term state’ approach to carry out the analysis, which is beyond the scope of this book. However, the results for the ligand effect are consistent with Equation (7.77) and have led to the development of the spectrochemical series for ligands which ranks them in order of observed Δ_o parameter:



Ligands to the left in this list have a small Δ_o parameter value and are called weak field ligands, while those toward the right have a larger Δ_o parameter value and are called strong field ligands. This terminology comes directly from the ligand or crystal field approach used in Chapter 5. To some extent the ligand field model predicts the observed trend. Thus, within the halogens, the more compact F^- anion has a stronger field ligand than the large I^- ligand. However, it is not clear why the neutral ligands H_2O and NH_3 are actually stronger field ligands than these anions, nor why CN^- and CO should give the strongest ligand fields.

To understand the ordering in the spectrochemical series, we have to consider π -symmetry ligand orbitals.

In the halogens, the anions have filled p-orbitals that are perpendicular to the metal-ligand bonds. A suitable basis for studying the interaction of these with the metal centre is shown in Figure 7.44. For clarity, the basis is drawn as two sets of six orbitals, as each

**Figure 7.44** A basis of ligand orbitals with π -symmetry for an O_h symmetry complex.

ligand will have two p-orbitals perpendicular to the metal–ligand bond. However, we will treat this as a single set of 12 basis orbitals.

The reducible representation in the rotational subgroup, O , is given in Table 7.17. These characters are obtained using the usual rules. A basis orbital that is unchanged by an operation from the class contributes 1, an orbital that is transformed into a different basis contributes 0 and one that is reversed contributes -1 . In particular, a rotation from the $6C_4$ class leaves two of the ligands in place (those on the axis). However, the p-orbitals on each of the coordinating atoms on the rotation axis are rotated through 90° and so change to a different basis function. This means that a total character of 0 results under $6C_4$.

Table 7.17 The reducible representation and application of the reduction formula to the basis of 12 π -symmetry ligand orbitals.

O	E	$8C_3$	$3C_2 (= C_4^2)$	$6C_4$	$6C_2$		$h = 24$
Γ	12	0	-4	0	0	$\sum_c g_c \chi_i(C) \chi_{\Gamma}(C)$	$\sum_c h^{-1} \sum_c$
A_1	12		-12			0	0
A_2	12		-12			0	0
E	24		-24			0	0
T_1	36		12			48	2
T_2	36		12			48	2

The application of the reduction formula laid out in Table 7.17 shows that, in the O subgroup, we have

$$\Gamma = 2t_1 + 2t_2 \quad (7.79)$$

In the full O_h point group of the complex we can obtain either a *gerade* or *ungerade* version of t_1 or t_2 from this basis. For example, Figure 7.45a shows how four of the p-orbitals can be used to form one of the t_{2g} patterns and there will clearly be a set of three equivalent such linear combinations. We know that this t_{2g} arrangement of the p-orbitals will be able to mix with the t_{2g} d-orbitals that are nonbonding in the σ -donor MO diagram of Figure 7.39. One such interaction is illustrated in Figure 7.45a. Looking at each

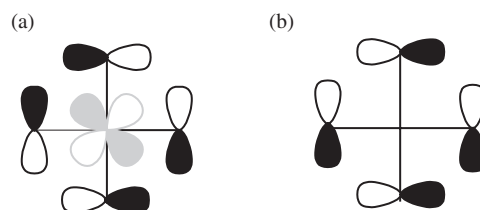


Figure 7.45 (a) One of three t_{2g} arrangements of the p-orbital basis of Figure 7.44. The bonding interaction with a metal d-orbital is shown. (b) The corresponding t_{2u} arrangement that cannot form bonds to metal d-orbitals.

metal–ligand part of this MO we can classify it as a π -bonding interaction by the same type of comparison with the diatomic MO scheme used in our discussion of ethene. In Figure 7.45b, the same pair of basis functions are shown in a t_{2u} arrangement. These are unsuitable to interact with the metal d-states.

So, orbitals with ‘ π -symmetry’ perpendicular to the metal–ligand bonds will generate a set of three t_{2g} SALCs. These will form bonding and antibonding combinations with the metal t_{2g} d-orbitals that are nonbonding for complexes with only σ -donor ligands. Figure 7.46 shows the effect of this for the d-states of an octahedral complex with a d^6 configuration.

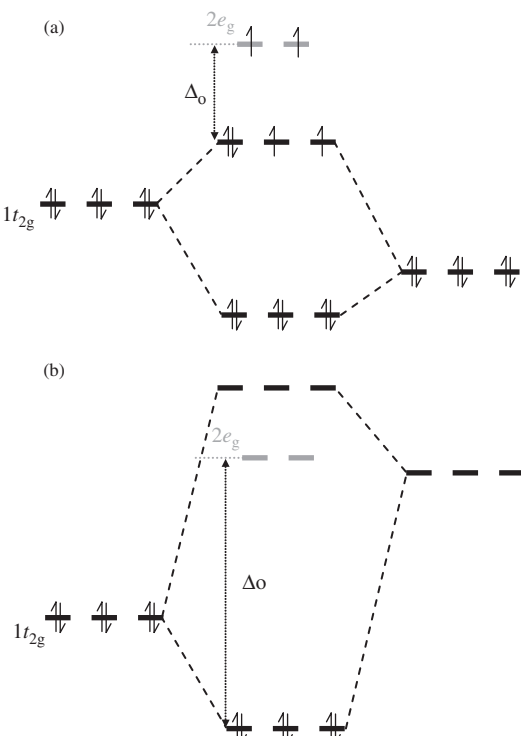


Figure 7.46 The effect of the t_{2g} set of ligand orbitals with π -symmetry for an O_h complex. Two cases are shown: (a) low-lying filled ligand orbitals; (b) high-lying empty ligand orbitals.

In the case of halogen ligands, the p-orbitals will be occupied and low lying in energy (Figure 7.46a). The bonding orbitals that are formed through mixing with the complementary d-orbitals will then be filled by the ligand electrons. The antibonding orbitals are moved up relative to the pure σ -donor complex, and so the Δ_o parameter is reduced. In this example we have assumed that the ligand field is now so weak that the $t_{2g} - e_g$ gap is smaller than the electron pairing energy. A lower energy configuration can then be obtained by prompting two of the electrons to the e_g levels. The high spin arrangement shown is common in complexes with weak field ligands for this reason.

Figure 7.46b shows the case of a ligand with empty high-lying states of π -symmetry. This is typified by complexes containing CO ligands. The MO diagram of CO in isolation (Figure 7.32) has a highest filled orbital ($5\sigma^+$) which gives it σ -donor character. The lowest unoccupied orbitals are the 2π pair; these will clearly act like the basis of Figure 7.44 in a metal complex environment. Note that the larger lobes of both the $5\sigma^+$ and 2π CO orbitals are on the C-atom, which gives the ligand the best overlap with metal orbitals when bonded to a metal centre via the carbon atom. In the metal complex, the t_{2g} set of these π -symmetry ligand orbitals will be high lying and empty, so Figure 7.46b shows that in this case the metal electrons move into the bonding orbitals created. Since these are lower than the nonbonding t_{2g} set in the reference σ -donor complex, the Δ_o parameter appears to be larger. The electron pairing energy is now likely to be smaller than the energy to promote an electron to the e_g level, and so we find a low-spin complex.

These MO diagrams, including the effect of π -symmetry ligand orbitals account for the observed spectrochemical series (Equation (7.78)) quite well. The lowest field ligands have low-lying filled π -symmetry orbitals which result in a small Δ_o parameter. The molecular ligands in the centre of the series (H_2O and NH_3) have no suitable π -symmetry orbitals, and so only interact with metals as σ -donors; and finally, the strongest field ligands have high-lying empty orbitals of π -symmetry, and so lower the energy of the metal t_{2g} orbitals, increasing the Δ_o parameter.

7.8 Summary

In this chapter we have reviewed some ideas in chemical bonding theory to show how AOs can be combined to generate MOs. The main goal was to give the reader confidence in building MO diagrams. The general approach should now be clear:

1. Identify the parts of the molecule that the MO diagram will require for the reference states. This may be simply single atoms (e.g. for the MO diagram of diatomics) or sets of symmetry-related atoms (e.g. the H atoms of ethene).
2. Assign the irreducible representations of the reference states. For atoms at the centre of a molecule contained by all symmetry elements, these can simple be read from the relevant character table. For sets of symmetry-related atoms, the irreducible representations will require a reducible representation Γ to be defined and the application of the reduction formula.
3. For sets of symmetry-related atoms, the orbital patterns for each irreducible representation should be drawn out using the SALCs obtained by the projection operator, where possible it is easier to work in a rotational subgroup initially.
4. The relative energies of the reference states should be estimated based on the electronegativity of the atoms involved or with knowledge of the type of chemical interaction (e.g. the donation from a Lewis acid to a base as in metal-ligand interactions).
5. MOs are then generated by joining sets of reference state orbitals that have the same symmetry. There will always be as many MO states generated as AOs used in this process.

6. The polarization of an MO will favour the energetically nearest AO reference orbital. In bonding orbitals, this usually favours the more electronegative element.
7. When two reference orbitals match in symmetry but differ greatly in energy, the degree of polarization means that the MO will be practically nonbonding. For example, the core states of an atom may match in symmetry with the valence levels of a neighbour, but the energies will be very different.
8. Reference orbitals that do not match any of the irreducible representations for the other atom or set of atoms are nonbonding by symmetry.

Along the way we have also covered the idea of hybridization and taken the rather strict approach that only orbitals of the same symmetry should take part in hybridization. This makes it much easier to follow the symmetry arguments for building bonding/antibonding orbitals. We have also seen how the idea of σ and π -symmetry bonding derived from diatomic molecules in the $D_{\infty h}$ point group is generally extended to molecules in other point groups, and even to metal complexes. In a similar way, the idea of hybridization to discuss structure is often used outside of the restrictions imposed by symmetry.

7.9 Self-Test Questions

1. In Table 7.3, both BO and NO have a longer bond length and lower bond dissociation energy than CO. Explain this observation based on the MO diagram for CO (Figure 7.32).
2. The PES for CH_4 shown in Figure 7.21 shows two distinct peaks and a shoulder. To explain this it is useful to consider the final state of the cation formed after ionization. The electronic structure of the CH_4^+ cation in T_d geometry would contain a t_2 level with five electrons; show that distortion to D_{2d} symmetry will lower the system energy. Explain how this structural distortion gives rise to the observed multiple peaks through alternative arrangements of the electrons in the final state.
3. The ionization potential for the 3s state of Cl is 25.3 eV and that for the 3p is 13.7 eV. Using this information, construct an MO diagram for Cl_2 . Table 7.3 gives the bond length of Cl_2 as 1.988 Å and the bond dissociation energy as 239 kJ mol⁻¹. The molecular cation Cl_2^+ actually has a shorter bond (1.8917 Å) and a bond dissociation energy of 415 kJ mol⁻¹. Explain the differences between Cl_2 and Cl_2^+ based on your MO diagram.
4. The six p-orbitals that are perpendicular to the plane of benzene (D_{6h}) are the basis for the π -symmetry orbitals of the molecule.
 - (a) Derive a reducible representation for this basis and apply the reduction formula to obtain the irreducible representations for the π -symmetry six MOs.
 - (b) Apply the projection operator method to obtain the pattern of AOs in each of the MOs from (a).
 - (c) Based on your sketches, estimate the relative energy of the MOs and, hence, obtain the MO diagram for the π -symmetry orbitals of benzene. From your diagram you should be able to explain why the HOMO state of benzene is doubly degenerate.
5. Derive the MO diagram for a tetrahedral metal complex with σ -donor ligands. For the ligand SALCs, reference to the case of methane (in Section 7.4) may be useful here;

the symmetry of metal d-states in T_d was covered in Section 5.8. Complexes of Cr^{2+} usually have tetrahedral geometries, while those of Cr^{3+} are more likely square planar. Explain why this should be the case by comparing your T_d MO diagram with the D_{4h} example in the text.

6. In CO_2 and in SO_2 the two O atoms are related by symmetry. Derive MO diagrams for each molecule. Why should CO_2 be linear while SO_2 is not?

Further Reading

Physical data, such as ionization potentials and reference spectra can be obtained from the US National Institute of Standards and Technology (NIST), at <http://physics.nist.gov/>.

References for electronegativity scales can be found in the following:

Pauling P (1932) The nature of the chemical bond. IV. The energy of single bonds and the relative electronegativity of atoms. *Journal of the American Chemical Society* **54**: 3570.

Pauling P (1970) *General Chemistry*. Dover Publications, New York (ISBN 0-486-65622-5).

Allred AL (1961) Electronegativity values from thermochemical data. *Journal of Inorganic Nuclear Chemistry* **17**: 215.

A very comprehensive coverage of chemical bonding with examples from relevant experimental data is given in:

DeKock RL, Gray HB (1989) *Chemical Structure and Bonding*. University Science Books, Mill Valley, CA (ISBN 0-935702-61-X).

The quantum chemistry of atomic states and bond formation is discussed in more detail by:

Atkins PW, Friedman RS (1997) *Molecular Quantum Mechanics*. Oxford University Press (ISBN 0-19-855947-X).

Calculation of the bond energy of H_2^+ with larger basis sets, and much more detailed coverage of quantum chemistry in general, can be found in:

McQuarrie DA (2008) *Quantum Chemistry*. University Science Books, Mill Valley, CA (ISBN 978-1-891389-50-4).

A fuller discussion of MO theory applied to transition metal complexes can be found in:
Kettle SFA (1998) *Physical Inorganic Chemistry: A Coordination Chemistry Approach*. Oxford University Press (ISBN 0 19 850404 7).

A full discussion of the experimental electron density plot of Figure 7.3 can be found in:
Hibbs DE, Hanrahan JR, Hursthouse MB, Knight DW, Overgaard J, Turner P, Piltz RO, Waller MP (2003) *Organic & Biomolecular Chemistry* **1**: 1034–1040.

Appendix 1

H₂O Models for Identifying the Results of Symmetry Operation Products

The following page contains eight images of H₂O set out in pairs, either side of the vertical line. You should cut out each pair so that you keep the label above each set with it, as indicated by the dotted lines. Then fold each strip of paper along the vertical line and glue the two sides together using paper adhesive. Additional copies of these model templates can be obtained from the Web site associated with this book.

Each model is viewed from the side on which the label can be read correctly. On this side the middle of each atom has a small white circle, pierce a small hole through the middle of the circle on the oxygen atom and then insert a burnt match so that the burnt end is away from the paper. This match represents the *x*-vector on the atom and the burnt end represents its direction. You should insert the matches so that:

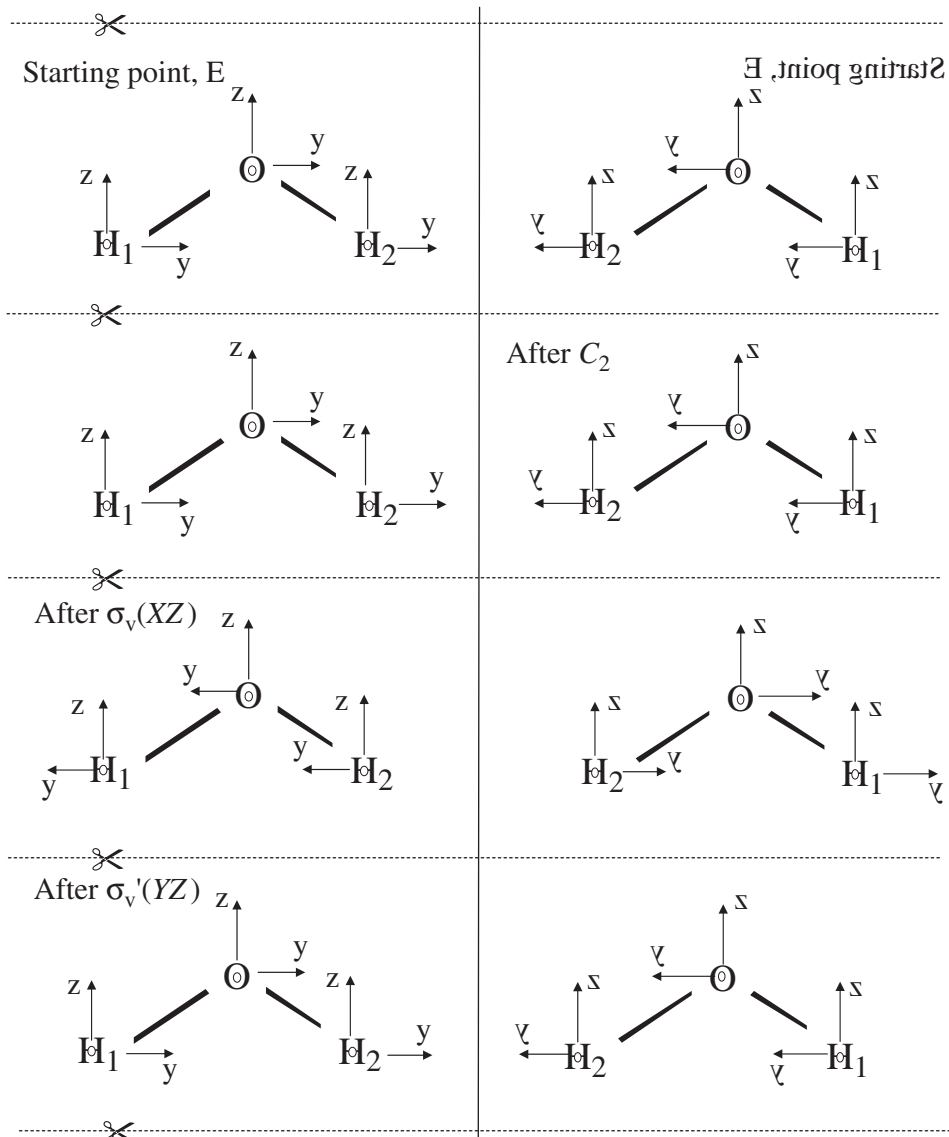
1. The ‘Starting point, *E*’, model and ‘After $\sigma_v(XZ)$ ’, models – burnt ends toward you.
2. The ‘After C_2 ’ and ‘After $\sigma_v(YZ)$ ’, models – burnt ends away from you, i.e. the match is pushed almost right through the paper because the *x*-vector is reversed.

There is a model for each of the operations in the point group of H₂O. To perform a product of two operations, start by picking up the model which represents the first part of the product and hold it with the labelled side toward you. To carry out the second operation, do one of the following:

1. *E*: do nothing. This just demonstrates the $XE = EX = X$, where *X* is any operation. This follows from the definition of *E*.
2. C_2 : rotate the model by 180° about the Z-axis.

3. $\sigma'_v(YZ)$: take out the match, reverse it and put it back in the hole at the oxygen atom so that the burnt end is again away from the paper. This effectively reverses the x -vector to show it has been reflected in the plane of the molecule. The y and z vectors are in the YZ plane, and so reflection through the plane does not affect them.
4. $\sigma_v(XZ)$: imagine the model you are holding with the y -vector reversed. In this case the x and z vectors are in the mirror plane and so are unaffected by the operation.

After completing the second operation, compare the model you have with the ones left over. Your new model should be identical to one of the other three, and this identical model provides the single symmetry operation corresponding to the product.



Appendix 2

Assignment of Chiral Centre Handedness using Cahn–Ingold–Prelog Rules

A centre of symmetry at a four-coordinate centre can be defined as left or right handed using a convention introduced by Cahn, Ingold and Prelog. The method is based on assigning a priority to each of the groups attached to the chiral centre. Figure A2.1 shows a generic tetrahedral centre with four attached groups *a*–*d* and illustrates the process of assigning the *R* (rectus, right) and *S* (sinister, left) labels to each of the two enantiomers.

The molecule is classified as *R* or *S* according to the following steps:

1. Number the groups according to their priority, 1 for highest down to 4 for lowest priority; in the examples in Figure A2.1 we have assumed that the priority runs $a > b > c > d$. There is more detail on assigning priorities to groups below.
2. Orientate the molecule so that the highest priority groups are toward you and the molecule is viewed down the bond from the chiral centre to the lowest priority group.
3. The handedness is assigned according to the order of the priority read around the chiral centre in this orientation. If the 1–3 priority atoms are arranged in a clockwise fashion, then the chiral centre is *R*; if they are read in order in an anticlockwise fashion, then the centre is *S*.

The most difficult part of the process is the assignment of the group priorities, for which the following rules are employed:

1. Assign the priority of the atoms directly bonded to the chiral centre based on their atomic numbers, with atoms further down the periodic table having the higher priority. If a lone pair forms one of the groups, then it has the lowest priority. For unambiguous

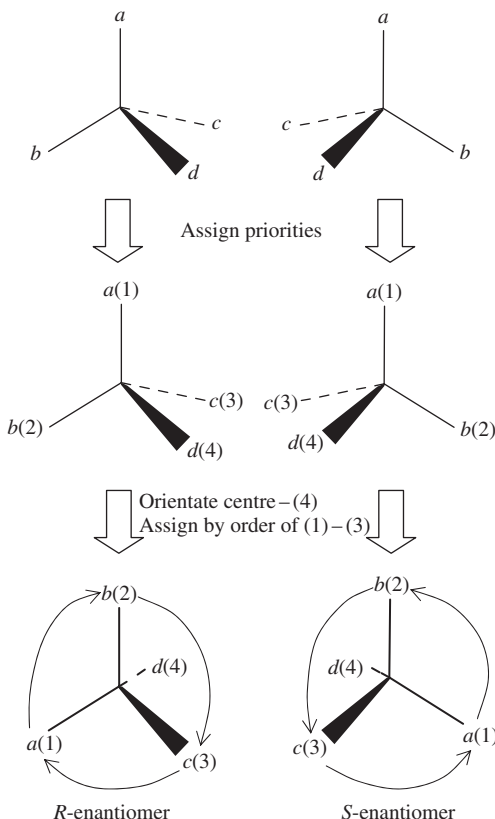
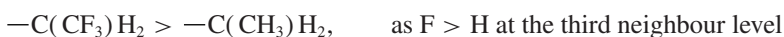
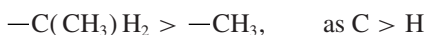


Figure A2.1 General approach to assignment of handedness to a molecule with a chiral centre. In this example the groups are assumed to have priority $a > b > c > d$.

cases, in which the four atoms joined to the chiral centre are different, this will suffice, as shown in Figure A2.2 for the example of 1-chloro-1-fluoroethane.

- If there are two or more atoms of equal priority, then move out to the next set of neighbours. There are now more possibilities, since there may be more than one atom at a second neighbour position along a given branch away from the chiral centre. Choose the highest priority from the set of second neighbours for each first neighbour and use those to decide. If there is no resolution, go out to further sets of neighbours until a difference is found. This means that the following group priorities would apply:



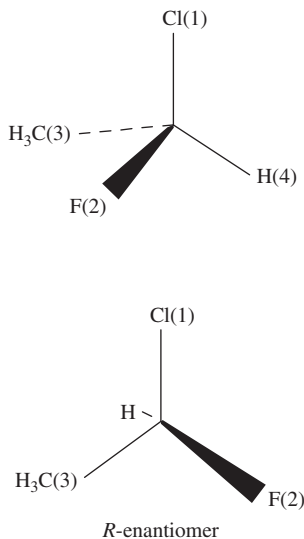
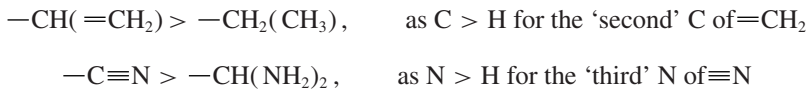


Figure A2.2 Example of 1-chloro-1-fluoroethane, a molecule whose chirality is determined solely by the atoms neighbouring the chiral centre.

In addition, if there is a double or triple bond present, then it is treated as if there were two or three of that atom type present. For example:



A good illustration of applying the priority rules to higher order neighbours is provided by the example of limonene given in Chapter 2; the assignment is shown in Figure A2.3. Starting from the chiral centre, the hydrogen atom has the lowest atomic number of the immediate neighbours and so is assigned priority 4. The other three neighbours are C atoms, and so we have to move to second neighbours. The double bond of the isopropyl group gives the *exo*-cyclic group a higher priority than either of the routes around the ring. The other two groups, from the two sides of the ring, each have C as the highest priority second neighbour to the chiral centre; so, to distinguish these, we move out to third-order neighbours. Here, the side of the cyclohexene ring with the double bond is assigned the higher priority, since the double-bonded carbon atom takes precedence. Looking down the chiral centre to the hydrogen atom bond, the priority 1–3 groups are arranged in an anticlockwise fashion around the chiral centre, and so this structure is the *S*-enantiomer of limonene.

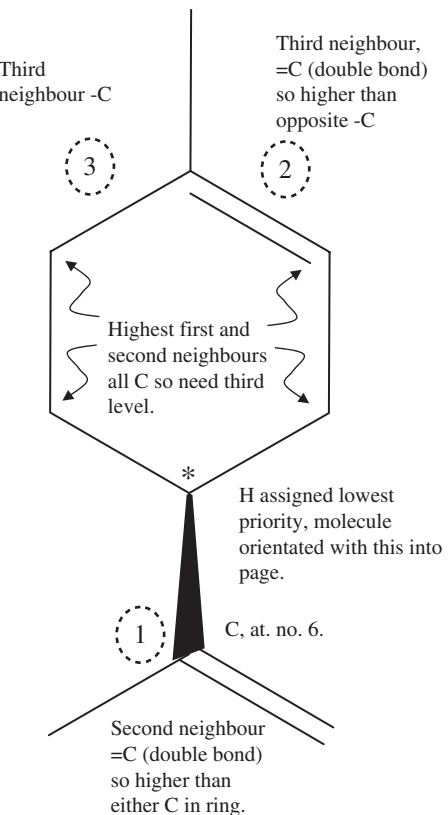


Figure A2.3 Assignment of handedness for *S*-limonene, the chiral centre is marked with a ‘*’. To realize that this example is a left-handed molecule requires neighbours out to third order.

Appendix 3

Model of a Tetrahedron and the Related Cube

This appendix contains templates for paper models of a tetrahedron and a cube. The final shapes are shown in Figure A3.1a. The cube dimensions are set so that the tetrahedron will just fit inside, as shown in Figure A3.1b. Additional copies of the model templates can be obtained from the Web site associated with this book.

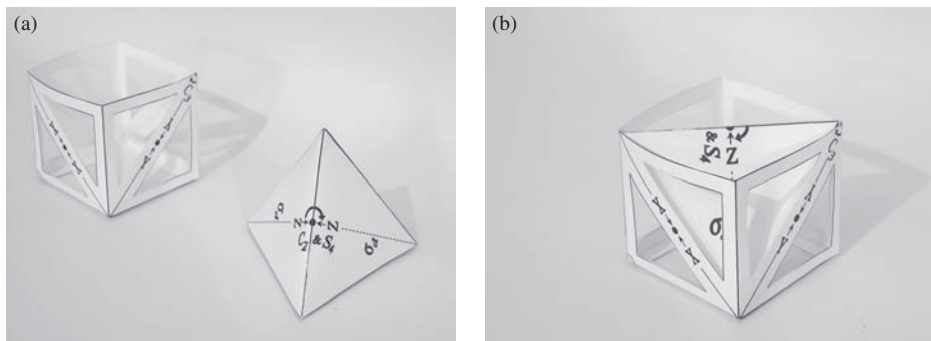


Figure A3.1 The completed tetrahedral and cube models: (a) shown separately; (b) with the tetrahedron inserted into the cube showing the relationship between the two shapes.

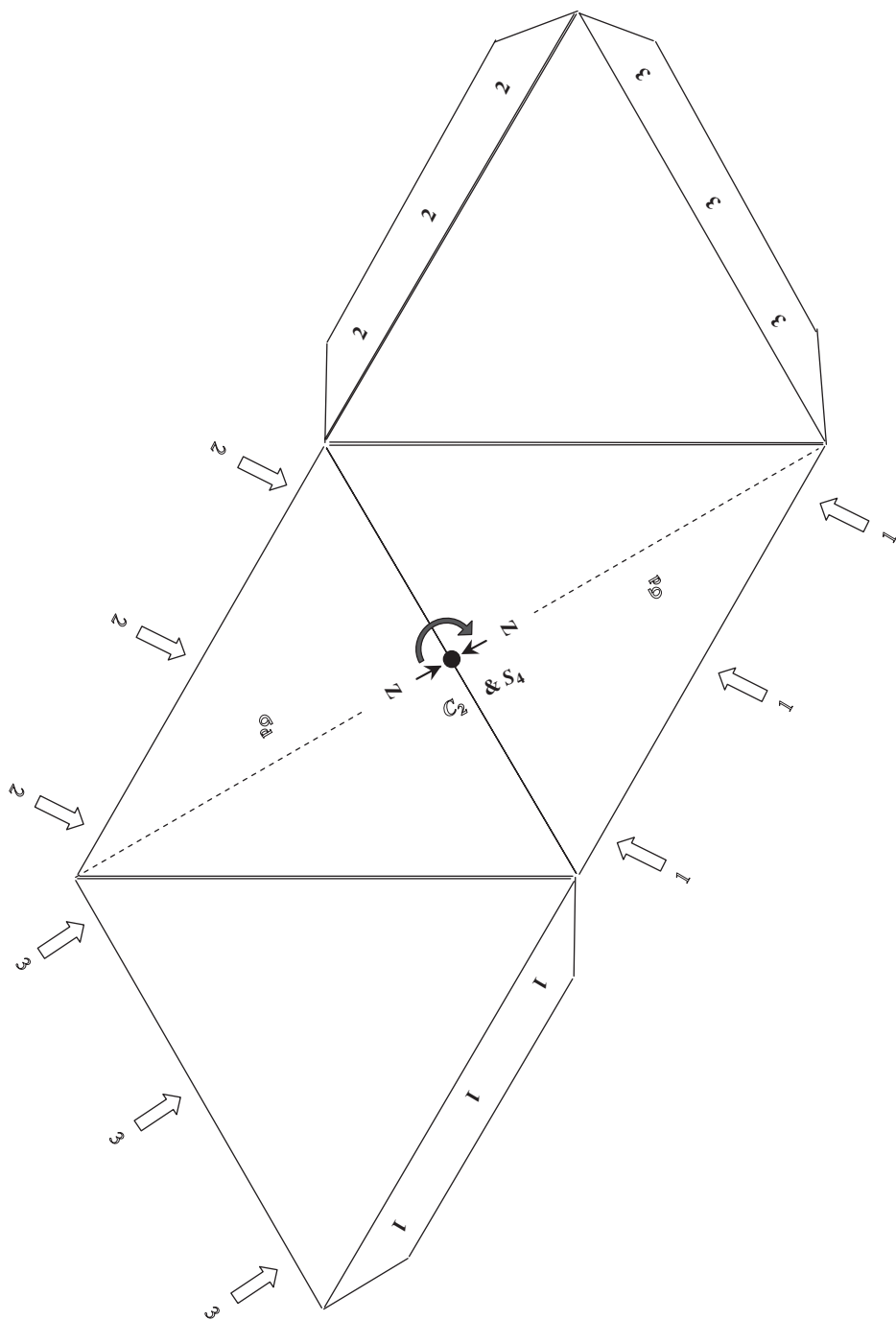
To construct the tetrahedron model:

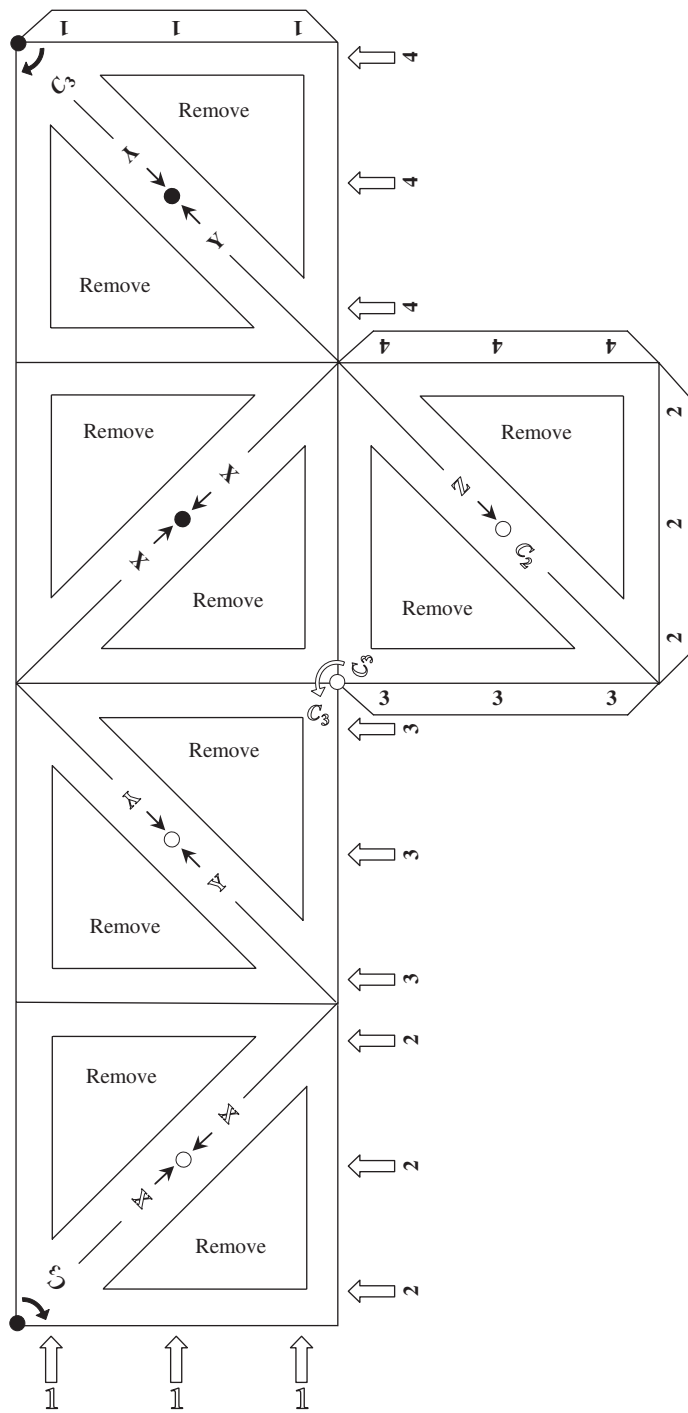
1. Cut around the outline of the pattern, including the flaps.
2. With the printed side of the template downward, fold along all the solid lines; after folding each of the flaps, push it flat again.

3. Apply glue to each of the flaps and glue them under the side with the corresponding number indicated on the template. Flap 1 is to be glued in place first; flaps 2 and 3 should then be glued together with light pressure applied to the outside of the tetrahedral shape formed.

To construct the cube model:

1. Cut around the outline of the pattern, including the flaps.
2. With the printed side of the template downward, fold along all the solid lines that outline the squares, including the flaps; after folding each of the flaps, push it flat again.
3. Cut out the triangular areas marked ‘Remove’ using a sharp craft knife; it may help to place a ruler next to each line as the cut is made. Push out each triangle, taking care not to crease the remaining paper in the model.
4. Apply glue to each of the flaps and glue them under the side with the corresponding number indicated on the template. Flap 1 is to be glued in place first; flaps 2, 3 and 4 should then be glued together. One side of the cube is left open, and so pressure can be applied to these flaps from inside the box shape formed.





Appendix 4

Model of an Octahedron

This appendix contains a template for a model of an octahedron. The final shape is shown in the photographs in Figure A4.1. The folding up of the template is quite straightforward, but to help you the destination of each flap to be glued is indicated on the template. Make sure you understand how the template folds up into the octahedron before cutting it out. Construction follows the steps set out below. Additional copies of the model template can be obtained from the Web site associated with this book.

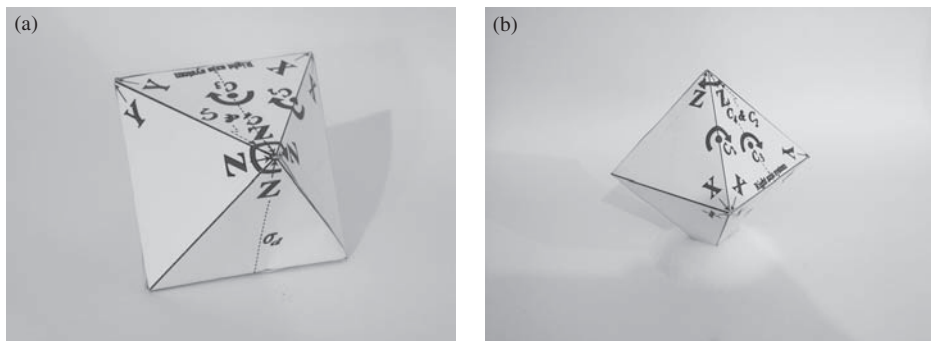
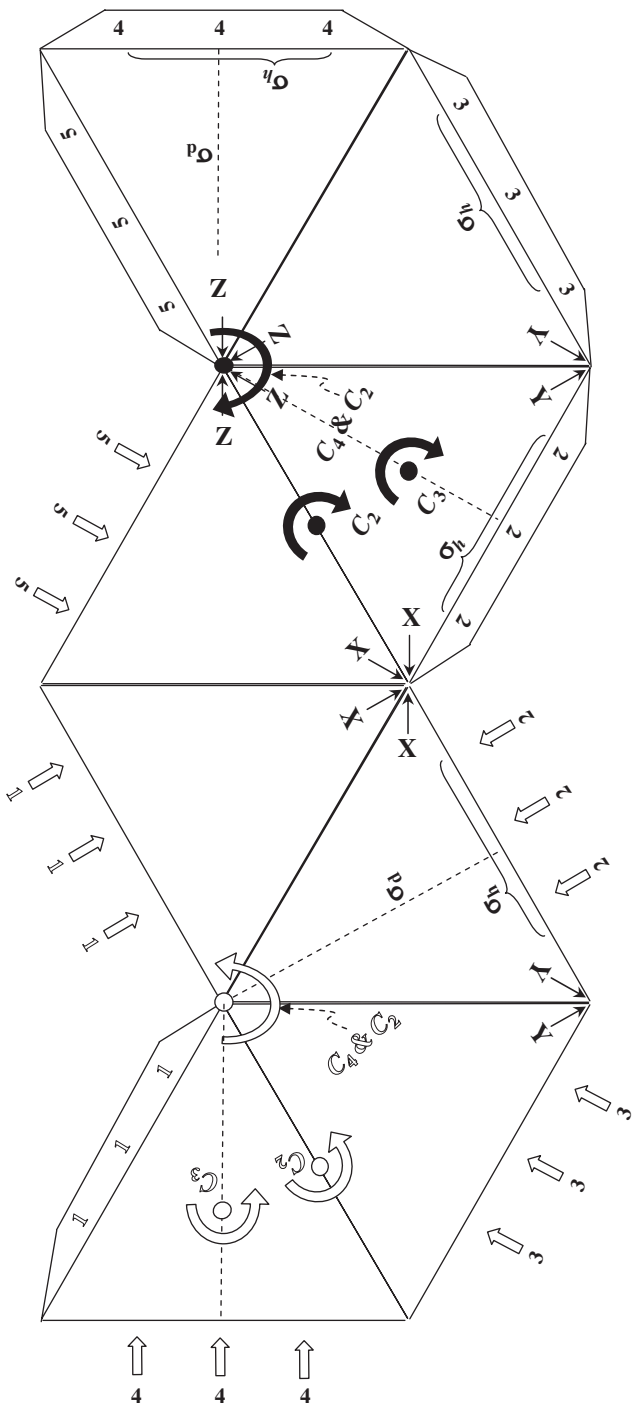


Figure A4.1 Two views of the completed octahedron model: (a) with a C_3 axis vertical; (b) with a C_4 axis vertical.

1. Cut out around the shape outline.
2. With the printed side of the template downward, fold all solid lines; after folding each flap, push it back flat again.
3. Apply glue to all flaps from the printed side of the template.

4. Take flap number 1 and inserted it underneath the edge indicated on the template. You should make sure that the two solid lines are aligned at the join.
5. Following the same procedure, glue the flaps in place in the order as numbered. Flaps 4 and 5 should be glued at the same time, applying light pressure from outside of the octahedron.

The markings on the octahedron show some examples of axes and mirror planes that are symmetry elements for the octahedron. Not all the elements are marked, since the model would become too complex. For example, there are four C_3 axes which pass through the centre of opposite triangular faces, but only one is marked. The geometry of the octahedron is discussed in more detail in Section 3.9.



Appendix 5

Matrices and Determinants

The idea of a matrix crops up a number of times in the mathematics of symmetry, both as a way to represent symmetry operations and in the solution of problems to which symmetry may be applied. In the Futher Reading section of this appendix, some references to detailed discussions of the mathematics of matrices and the related determinants are given; here, we cover the essential elements required to understand the more mathematical aspects of the discussion in the main text.

A5.1 Matrices as Representations of Symmetry Operators

In Chapter 4 we introduce the idea of a matrix representation for symmetry operations. The matrix is a compact way of writing several simultaneous equations in one go. For example, the effect of the C_2 operation on basis vectors x and y in the C_{2v} point group is given by Equation (4.3):

$$\begin{aligned}x' &= -1 \times x + 0 \times y \\y' &= 0 \times x + -1 \times y\end{aligned}\tag{A5.1}$$

These equations say that the new position of the x basis vector is in the opposite direction to the original one and that the y basis vector is also reversed. In matrix notation, x and y are grouped into a single column vector and the coefficients of the two equations in Equation (A5.1) are used to form a square matrix:

$$\left(\begin{array}{c} x' \\ y' \end{array} \right) = \left(\begin{array}{cc} -1 & 0 \\ 0 & -1 \end{array} \right) \left(\begin{array}{c} x \\ y \end{array} \right)\tag{A5.2}$$

To recover the equations we can multiply the vector by the matrix. The multiplication is carried out following the convention that the first element on the left is given by summing the products of the first row of the matrix with the column vector on the right-hand side:

$$\begin{pmatrix} x' \\ y' \end{pmatrix} = \begin{pmatrix} -1 & 0 \\ 0 & -1 \end{pmatrix} \begin{pmatrix} x \\ y \end{pmatrix} \text{ gives } x' = -1 \times x + 0 \times y \quad (\text{A5.3})$$

Similarly, the second element on the left-hand side is a sum of products of the second row of the matrix and the column vector on the right-hand side:

$$\begin{pmatrix} x' \\ y' \end{pmatrix} = \begin{pmatrix} -1 & 0 \\ 0 & -1 \end{pmatrix} \begin{pmatrix} x \\ y \end{pmatrix} \text{ gives } y' = 0 \times x + -1 \times y \quad (\text{A5.4})$$

Since the matrix represents a symmetry operation, the act of multiplying the vector by the matrix is often referred to as an operation, i.e. the matrix operates on the vector.

Larger systems of basis vectors can be dealt with in much the same way. For example, in Section 4.5 we considered the effect of a C_3^1 rotation on a basis of the three N—H bonds of ammonia in the C_{3v} point group. As before, to carry out the multiplication the column b_1, b_2, b_3 (representing N—H bonds 1–3) is multiplied by the top row of the matrix to give the vector now in the b_1 direction, then by the middle row to get the new term in b_2 and finally by the bottom row to get the new b_3 :

$$\begin{array}{c} \begin{pmatrix} 0 & 0 & 1 \\ 1 & 0 & 0 \\ 0 & 1 & 0 \end{pmatrix} \begin{pmatrix} b_1 \\ b_2 \\ b_3 \end{pmatrix} = \begin{pmatrix} b_3 \\ b_1 \\ b_2 \end{pmatrix} \text{ giving } b_1 \text{ now replaced by } b_3 \\ \begin{pmatrix} 0 & 0 & 1 \\ 1 & 0 & 0 \\ 0 & 1 & 0 \end{pmatrix} \begin{pmatrix} b_1 \\ b_2 \\ b_3 \end{pmatrix} = \begin{pmatrix} b_3 \\ b_1 \\ b_1 \end{pmatrix} \text{ giving } b_2 \text{ now replaced by } b_1 \\ \begin{pmatrix} 0 & 0 & 1 \\ 1 & 0 & 0 \\ 0 & 1 & 0 \end{pmatrix} \begin{pmatrix} b_1 \\ b_2 \\ b_3 \end{pmatrix} = \begin{pmatrix} b_3 \\ b_1 \\ b_2 \end{pmatrix} \text{ giving } b_3 \text{ now replaced by } b_2 \end{array} \quad (\text{A5.5})$$

A5.1.1 Products of Matrices

We can extend the algebra of matrices to include products formed by multiplying two matrices together. The product of the matrices must give a third matrix, since we know, for example, that the combined $C_2\sigma_v$ operation in the C_{2v} point group is equivalent to the other vertical reflection σ_v' . The multiplication of the two matrices can be carried out by treating the columns of the second matrix as vectors and multiplying each one by the rows

of the first matrix in turn. The row and column for each element in the resulting matrix is set by the row and column used in the multiplication.

In the example of the combined $C_2\sigma_v$ operation this gives

$$\begin{aligned}
 & \left(\begin{array}{cc} -1 & 0 \\ 0 & -1 \end{array} \right) \left(\begin{array}{cc} 1 & 0 \\ 0 & -1 \end{array} \right) = \left(\begin{array}{cc} -1 & 0 \\ 0 & -1 \end{array} \right) \quad \text{from } -1 \times 1 + 0 \times 0 = -1 \\
 & \left(\begin{array}{cc} -1 & 0 \\ 0 & -1 \end{array} \right) \left(\begin{array}{cc} 1 & 0 \\ 0 & -1 \end{array} \right) = \left(\begin{array}{cc} -1 & 0 \\ 0 & -1 \end{array} \right) \quad \text{from } -1 \times 0 + 0 \times -1 = 0 \\
 & \left(\begin{array}{cc} -1 & 0 \\ 0 & -1 \end{array} \right) \left(\begin{array}{cc} 1 & 0 \\ 0 & -1 \end{array} \right) = \left(\begin{array}{cc} -1 & 0 \\ 0 & 0 \end{array} \right) \quad \text{from } 0 \times 1 + -1 \times 0 = 0 \\
 & \left(\begin{array}{cc} -1 & 0 \\ 0 & -1 \end{array} \right) \left(\begin{array}{cc} 1 & 0 \\ 0 & -1 \end{array} \right) = \left(\begin{array}{cc} -1 & 0 \\ 0 & 1 \end{array} \right) \quad \text{from } 0 \times 0 + -1 \times -1 = 1
 \end{aligned} \tag{A5.6}$$

Checking the product matrix against Table 4.5 confirms that the matrix product acts just like the symmetry operations, since we have generated σ_v' from the product $C_2\sigma_v$.

A5.1.2 Products of Matrices, Expressed as Summations

For the simple 2×2 matrices used above the product is quite easy to write out in full. However, as the number of basis functions increases, it can become cumbersome to write out the full matrix and we may prefer to write out formulae for obtaining a general element of the product matrix. Products of matrices are obtained using the multiplication procedure of taking rows from the first matrix with columns from the second. To extend this to the 3×3 case and beyond, we will look at the general matrix product:

$$P = AB = \left(\begin{array}{ccc} a_{11} & a_{12} & a_{13} \\ a_{21} & a_{22} & a_{23} \\ a_{31} & a_{32} & a_{33} \end{array} \right) \left(\begin{array}{ccc} b_{11} & b_{12} & b_{13} \\ b_{21} & b_{22} & b_{23} \\ b_{31} & b_{32} & b_{33} \end{array} \right) \tag{A5.7}$$

Here, A and B are any two 3×3 matrices whose elements are denoted a and b with subscripts giving the row and column of the element in that order. The product of A and B is the 3×3 matrix P . To generate the product, each column of the matrix B is treated like the vectors in the earlier calculations, being multiplied element by element with a row from the A matrix and then summed. Each row of the A matrix is used in turn, so that the three rows of A and the three columns of B form the nine sums of elemental products needed to generate a 3×3 matrix as the result. The product matrix elements are labelled by the row of A and column of B used in the multiplication. For example, element 1,2 of the result p_{12} is found by multiplying each element of the second column in matrix B

by the corresponding element of row 1 from matrix A and then summing the three terms generated:

$$\begin{pmatrix} p_{11} & \boxed{p_{12}} & p_{13} \\ p_{21} & p_{22} & p_{23} \\ p_{31} & p_{32} & p_{33} \end{pmatrix} = \begin{pmatrix} a_{11} & a_{12} & a_{13} \\ a_{21} & a_{22} & a_{23} \\ a_{31} & a_{32} & a_{33} \end{pmatrix} \begin{pmatrix} b_{11} & \boxed{b_{12}} & b_{13} \\ b_{21} & b_{22} & b_{23} \\ b_{31} & \boxed{b_{32}} & b_{33} \end{pmatrix} \quad p_{12} = a_{11}b_{12} + a_{12}b_{22} + a_{13}b_{32} = \sum_{k=1}^3 a_{1k}b_{k2} \quad (\text{A5.8})$$

Similarly, element p_{31} is calculated from row 3 of matrix A and column 1 of matrix B :

$$\begin{pmatrix} p_{11} & p_{12} & p_{13} \\ p_{21} & \boxed{p_{22}} & p_{23} \\ p_{31} & p_{32} & p_{33} \end{pmatrix} = \begin{pmatrix} a_{11} & a_{12} & a_{13} \\ a_{21} & a_{22} & a_{23} \\ a_{31} & a_{32} & a_{33} \end{pmatrix} \begin{pmatrix} b_{11} & b_{12} & b_{13} \\ b_{21} & \boxed{b_{22}} & b_{23} \\ b_{31} & b_{32} & b_{33} \end{pmatrix} \quad p_{31} = a_{31}b_{11} + a_{32}b_{21} + a_{33}b_{31} = \sum_{k=1}^3 a_{3k}b_{k1} \quad (\text{A5.9})$$

In this way, each of the nine elements of the product can be built from the elements of the A and B matrices. The sums that are written out for the particular cases shown in Equations (A5.8) and (A5.9) have an index k which defines the column index of the a element and the row index of the b element used in each term of the sum. This index disappears in the final answer for the product element produced and only the fixed indices remain to define p . For an arbitrary product element p_{ij} we can use the formula

$$p_{ij} = \sum_{k=1}^3 a_{ik}b_{kj} \quad (\text{A5.10})$$

which embodies the idea of producing the i,j element of the P matrix as a sum of products of the i^{th} row of A and j^{th} column of B .

A matrix product formed in this way can be used to generate matrices for the operator products we need when considering compound operations. For example, in the NH₃ case of Figure 4.6, a C₃² rotation can be generated by applying the C₃¹ matrix twice. This can be done by applying the C₃¹ matrix once and then using the intermediate column vector in a second application:

$$\begin{pmatrix} 0 & 0 & 1 \\ 1 & 0 & 0 \\ 0 & 1 & 0 \end{pmatrix} \begin{pmatrix} 0 & 0 & 1 \\ 1 & 0 & 0 \\ 0 & 1 & 0 \end{pmatrix} \begin{pmatrix} b_1 \\ b_2 \\ b_3 \end{pmatrix} = \begin{pmatrix} 0 & 0 & 1 \\ 1 & 0 & 0 \\ 0 & 1 & 0 \end{pmatrix} \begin{pmatrix} b_3 \\ b_1 \\ b_2 \end{pmatrix} = \begin{pmatrix} b_2 \\ b_3 \\ b_1 \end{pmatrix} \quad (\text{A5.11})$$

But we can also use the matrix product to generate a matrix for the C_3^2 operation and then apply this as a single operation, giving the same result:

$$\begin{pmatrix} 0 & 0 & 1 \\ 1 & 0 & 0 \\ 0 & 1 & 0 \end{pmatrix} \begin{pmatrix} 0 & 0 & 1 \\ 1 & 0 & 0 \\ 0 & 1 & 0 \end{pmatrix} \begin{pmatrix} b_1 \\ b_2 \\ b_3 \end{pmatrix} = \begin{pmatrix} 0 & 1 & 0 \\ 0 & 0 & 1 \\ 1 & 0 & 0 \end{pmatrix} \begin{pmatrix} b_1 \\ b_2 \\ b_3 \end{pmatrix} = \begin{pmatrix} b_2 \\ b_3 \\ b_1 \end{pmatrix} \quad (\text{A5.12})$$

So, as we found for the case of the simpler basis in H_2O , the matrix representation of symmetry operations allows products of operations to be considered algebraically. This matrix product approach can be extended to matrices of any size and so for any size of basis.

A5.2 Matrices for Solving Sets of Linear Equations

Matrices also appear in the solution of problems in linear algebra because they provide a compact way of discussing sets of equations. For example if we have three unknowns, x_1 , x_2 and x_3 which conform to the simultaneous equations:

$$\begin{aligned} a_{11}x_1 + a_{12}x_2 + a_{13}x_3 &= d_1 \\ a_{21}x_1 + a_{22}x_2 + a_{23}x_3 &= d_2 \\ a_{31}x_1 + a_{32}x_2 + a_{33}x_3 &= d_3 \end{aligned} \quad (\text{A5.13})$$

where a_{ij} and d_i are constants; the equivalent matrix equation is

$$\begin{pmatrix} a_{11} & a_{12} & a_{13} \\ a_{21} & a_{22} & a_{23} \\ a_{31} & a_{32} & a_{33} \end{pmatrix} \begin{pmatrix} x_1 \\ x_2 \\ x_3 \end{pmatrix} = \begin{pmatrix} d_1 \\ d_2 \\ d_3 \end{pmatrix} \quad (\text{A5.14})$$

for which we can use the shorthand

$$Ax = d \quad (\text{A5.15})$$

This allows any algebraic manipulation to be carried out in the shorthand notation. For example, if we wish to find the values of x_i in Equation (A5.13), then we can see from Equation (A5.15) that, if we can find the inverse matrix of A , the solution will be straightforward because

$$A^{-1}Ax = A^{-1}d \quad \text{gives} \quad x = A^{-1}d \quad (\text{A5.16})$$

because $A^{-1}A = E$, the identity matrix.

To find the inverse matrix requires the introduction of the determinant. The determinant is related to the square matrices we use as representations for symmetry operations, but is a simple number formed in a systematic way from the elements of the matrix. To distinguish the determinant from a matrix it is written enclosed in straight lines, rather

than the brackets used to signify a matrix. So the determinant for the matrix A would be written

$$|A| = \begin{vmatrix} a_{11} & a_{12} & a_{13} \\ a_{21} & a_{22} & a_{23} \\ a_{31} & a_{32} & a_{33} \end{vmatrix} \quad (\text{A5.17})$$

The evaluation of the determinant requires its simplification into sets of 2×2 sub-determinants, which can then be evaluated using the following prescription:

$$\begin{vmatrix} a_{11} & a_{12} \\ a_{21} & a_{22} \end{vmatrix} = a_{11}a_{22} - a_{12}a_{21} \quad (\text{A5.18})$$

To evaluate a higher order determinant we choose a row of the determinant and form the product of each element with its co-factor. The co-factor is the sub-determinant formed by blocking the row and column for a given element and forming a determinant from the visible elements. For example, to form the co-factor c_{11} of the a_{11} element in Equation (A5.17):

$$\begin{vmatrix} a_{11} & a_{12} & a_{13} \\ a_{21} & a_{22} & a_{23} \\ a_{31} & a_{32} & a_{33} \end{vmatrix} \quad \text{gives } c_{11} = \begin{vmatrix} a_{22} & a_{23} \\ a_{32} & a_{33} \end{vmatrix} \quad (\text{A5.19})$$

When working out the value of the 3×3 determinant, a sign is also added to the co-factor following the chessboard pattern:

$$\begin{vmatrix} + & - & + \\ - & + & - \\ + & - & + \end{vmatrix} \quad (\text{A5.20})$$

The co-factor takes the sign in the position corresponding to the element used to generate the co-factor. This means that the result for a_{11} in Equation (A5.19) is given a positive sign, but if we require the co-factor for a_{12} we would use

$$\begin{vmatrix} a_{11} & a_{12} & a_{13} \\ a_{21} & a_{22} & a_{23} \\ a_{31} & a_{32} & a_{33} \end{vmatrix} \quad \text{gives } c_{12} = - \begin{vmatrix} a_{21} & a_{23} \\ a_{31} & a_{33} \end{vmatrix} \quad (\text{A5.21})$$

Since we have blocked one row and one column, the co-factor is always simpler than the parent determinant. The 3×3 determinant from Equation (A5.17) can now be simplified to the evaluation of three 2×2 determinants:

$$\begin{aligned} |A| &= \begin{vmatrix} a_{11} & a_{12} & a_{13} \\ a_{21} & a_{22} & a_{23} \\ a_{31} & a_{32} & a_{33} \end{vmatrix} = a_{11} \begin{vmatrix} a_{22} & a_{23} \\ a_{32} & a_{33} \end{vmatrix} - a_{12} \begin{vmatrix} a_{21} & a_{23} \\ a_{31} & a_{33} \end{vmatrix} + a_{13} \begin{vmatrix} a_{21} & a_{22} \\ a_{31} & a_{32} \end{vmatrix} \\ &= a_{11}(a_{22}a_{33} - a_{23}a_{32}) - a_{12}(a_{21}a_{33} - a_{23}a_{31}) + a_{13}(a_{21}a_{32} - a_{22}a_{31}) \end{aligned} \quad (\text{A5.22})$$

We now have all the elements required to construct an inverse for a matrix. The inverse of a matrix has a more complex definition than that for simple numbers; for a matrix A :

$$A^{-1} = \frac{\text{Co}^T(A)}{|A|} \quad (\text{A5.23})$$

where $\text{Co}(A)$ is the determinant formed from the complete set of co-factors. This means that a co-factor is formed for each element using the row and column blocking method described above and the value of the co-factor is then placed at the position of the element used in the blocking process. The co-factors also require the signs given by the chessboard pattern of Equation (A5.20). The superscript ‘T’ implies the matrix is transposed (rows and columns interchanged) after it is formed.

As an example, consider the C_4^1 rotation matrix used in Section 4.9:

$$C_4^1 = \begin{pmatrix} 0 & -1 & 0 \\ 1 & 0 & 0 \\ 0 & 0 & 1 \end{pmatrix} \quad (\text{A5.24})$$

This type of matrix is referred to as orthogonal, since its columns (or rows) are a set of mutually perpendicular vectors. In this case, the first column is aligned with Y , the second with $-X$ and the third with Z , but any arrangement which makes the columns at right angles to one another will give an orthogonal matrix. Orthogonal matrices have the property that their inverses are simply the transposed matrix, and we will show that this is the case here by forming the inverse in the standard way and then comparing with the transposed matrix.

The matrix of co-factors is quite straightforward in this case:

$$\text{Co}(C_4^1) = \begin{pmatrix} 0 & -1 & 0 \\ 1 & 0 & 0 \\ 0 & 0 & 1 \end{pmatrix} \quad \text{so} \quad \text{Co}^T(C_4^1) = \begin{pmatrix} 0 & 1 & 0 \\ -1 & 0 & 0 \\ 0 & 0 & 1 \end{pmatrix} \quad (\text{A5.25})$$

The determinant can be evaluated using Equation (A5.22). Many of the terms will be zero; the only co-factor required corresponds to the second element of the first row, and so has a negative sign.

$$|C_4^1| = 1 \left| \begin{array}{cc} -1 & 0 \\ 0 & 1 \end{array} \right| = 1 \quad (\text{A5.26})$$

The fact that the determinant is 1 is another general property of matrices which represent symmetry operations. This ensures that the symmetry operation does not affect the size of any basis vectors on which it operates.

So, we have found that the inverse of the C_4^1 rotation matrix is given by

$$(C_4^1)^{-1} = \begin{pmatrix} 0 & 1 & 0 \\ -1 & 0 & 0 \\ 0 & 0 & 1 \end{pmatrix} \quad (\text{A5.27})$$

Comparing this with Equation (A5.24), you will see that, as stated earlier, the inverse is simply the transpose of the original matrix. This is also a general property of matrices which represent symmetry operations, and it makes finding these inverses much easier than following this standard formula route. You should also be able to see that the inverse matrix is the same as the matrix we defined for C_4^3 in the main text, i.e. the inverse matrix correctly gives the inverse symmetry operation.

As a check of the calculation, we form the product of the matrix and its inverse:

$$(C_4^1)^{-1} C_4^1 = \begin{pmatrix} 0 & 1 & 0 \\ -1 & 0 & 0 \\ 0 & 0 & 1 \end{pmatrix} \begin{pmatrix} 0 & -1 & 0 \\ 1 & 0 & 0 \\ 0 & 0 & 1 \end{pmatrix} = \begin{pmatrix} 1 & 0 & 0 \\ 0 & 1 & 0 \\ 0 & 0 & 1 \end{pmatrix} = E \quad (\text{A5.28})$$

so the inverse multiplied into the matrix gives the identity matrix as required.

Further Reading

- Steiner E (1996) *The Chemistry Maths Book*. Oxford Science Publications (ISBN 0 19 855913 5).
 Lambourne R, Tinker M (2000) *Basic Mathematics for the Physical Sciences*, Wiley (ISBN 0 471 82507 4).
 Lambourne R, Tinker M (2000) *Further Mathematics for the Physical Sciences*, Wiley (ISBN 0 471 86723 3).

Appendix 6

The Mathematical Background to Infrared Selection Rules

In the main text we introduced the selection rules for IR spectroscopy via the transition dipole moment integral. This appendix gives a little more detail on the origin of the selection rules, with explicit formulae for the vibrational wavefunctions. This also allows a more complete explanation of the observation that absorption due to transitions involving neighbouring levels (e.g. $n = 0$ to $n = 1$) are more easily observed than overtones which involve transitions to higher levels in the ladder of vibrational states.

The diatomic molecule is a good place to start a discussion of molecular vibrations. There are six degrees of freedom: three translations of the molecule, two rotations and, so, only a single vibration, which is the bond stretch. In this appendix we will consider a diatomic molecule belonging to the $C_{\infty v}$ using H—F as an example. It is conventional in symmetry problems to align the principal axis with the Z-direction. However, we have decided to break with convention here and align with X, because the variable x is more often used in mathematics.

A6.1 Model Based on Classical Mechanics

Figure A6.1a illustrates the vibrational motion of our model H—F molecule in the harmonic approximation. Here, the bond between the two atoms is thought of as a simple spring with spring constant k and equilibrium length l_0 . The potential energy V stored in the spring is then proportional to the square of the extension or compression x with the constant of proportionality being k (Figure A6.1b):

$$V = \frac{1}{2}kx^2 \tag{A6.1}$$

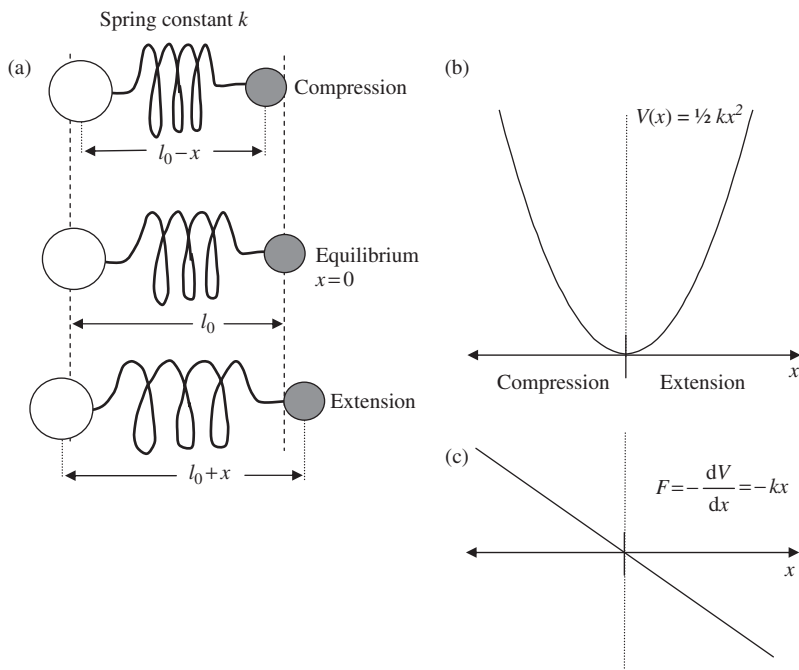


Figure A6.1 (a) Model of a diatomic molecule such as HF with the chemical bond represented by a spring; (b) the potential $V(x)$ versus bond extension x in the harmonic approximation; (c) the classical force versus x .

The factor of one-half arises from the usual choice of k based on Hooke's law; the restoring force due to the extension of a spring is directly proportional to that extension. So, following classical mechanics:

$$F = -\frac{dV}{dx} = -kx \quad (\text{A6.2})$$

This relationship is plotted in Figure A6.1c and shows that any distortion of the bond will generate a force which tends to move the atoms back toward the equilibrium bond length. At the equilibrium bond length the potential and the force are both zero.

At any nonzero temperature the classical atoms of the molecule will also be moving; if the H atom has a velocity v with respect to the F atom, then the kinetic energy T to do with the bond distortion is

$$T = \frac{1}{2}\mu_m v^2 = \frac{1}{2}\mu_m \left(\frac{dx}{dt}\right)^2 \quad (\text{A6.3})$$

where t is the time variable and μ_m is the reduced mass of the two-atom system:

$$\frac{1}{\mu_m} = \frac{1}{m_H} + \frac{1}{m_F} \quad (\text{A6.4})$$

with m_H and m_F the masses of the H and F atoms respectively.

At all times the total energy (sum of potential and kinetic) E will have a constant value, and so we can use the conservation of energy to write

$$T + V = E \quad \text{or} \quad \frac{1}{2}\mu_m \left(\frac{dx}{dt} \right)^2 + \frac{1}{2}kx^2 = E \quad (\text{A6.5})$$

This equation is readily simplified to give

$$\left(\frac{dx}{dt} \right)^2 + \frac{k}{\mu_m} x^2 = \frac{2E}{\mu_m} \quad (\text{A6.6})$$

This is a differential equation for the bond extension x as a function of time. It tells us that the squares of the first derivative and the extension itself are linked. For this classical model of masses and a spring we should expect an oscillating solution, and so a good starting guess for the solution is

$$x = A \cos(\omega t) \quad \text{for which} \quad \frac{dx}{dt} = -A\omega \sin(\omega t) \quad (\text{A6.7})$$

In this proposed formula for x , A will set the amplitude of the oscillation. The parameter ω is related to the frequency f of oscillation in reciprocal time units. The period over which the cosine function repeats is 2π radians and the period over which the extension completes a cycle of its oscillation is $1/f$, so the two are related via

$$\omega = 2\pi f \quad (\text{A6.8})$$

The quantity ω is referred to as the angular frequency of the oscillation.

We will now check that the proposed function for x in Equation (A6.7) is a solution of Equation (A6.6) and show how the angular frequency depends on the reduced mass and spring constant.

Using the results of Equation (A6.7) in Equation (A6.5) we find

$$A^2 \left[\omega^2 \sin^2(\omega t) + \frac{k}{\mu_m} \cos^2(\omega t) \right] = \frac{2E}{\mu_m} \quad (\text{A6.9})$$

For an arbitrary choice of ω the left-hand side is still an oscillating function of time, while the right-hand side is a constant. The only way this equation can work for all t is if the two terms in the bracket give the same sum for any value of t . Remembering the trigonometric identity (see the end note to Appendix 9)

$$\cos^2(\theta) + \sin^2(\theta) = 1 \quad (\text{A6.10})$$

it is clear that this will only occur if

$$\omega^2 = \frac{k}{\mu_m} \quad \text{i.e.} \quad \omega = \sqrt{\frac{k}{\mu_m}} \quad (\text{A6.11})$$

So the frequency of oscillation is proportional to the square root of the spring constant (the stiffer the spring is, the more rapid the oscillation is) and inversely proportional to the square root of the reduced mass (the heavier the atoms are, the slower the oscillation is).

The amplitude of the oscillation can now be related to the total energy by substituting our result for ω back into Equation (A6.9):

$$A = \sqrt{\frac{2E}{k}} \quad (\text{A6.12})$$

So the amplitude is inversely proportional to the square root of the spring constant and proportional to the total energy available. This means that (for the same total energy) the stiffer the spring is, the lower the amplitude of vibration is; this is because the potential energy increases more sharply with the bond extension.

We have shown that, in the classical picture, distortions due to atom motion that extends the bond will increase the potential energy and cause a restoring force that tends to shorten it. Also, if the bond is compressed, then the potential energy again increases, but the restoring force now favours extension of the bond. The result is oscillation with energy constantly switching between kinetic and potential. At the equilibrium point, the potential energy is zero and the kinetic energy is equal to the total. At the maximum extension/compression ($x = \pm A$) the kinetic energy is zero but the potential energy is equal to the total (to show this, try substituting Equation (A6.7) with A from Equation (A6.12) into Equation (A6.1)).

The total energy itself can take on any value; under thermal equilibrium, the range of total energies available to each molecule would be set by the Boltzmann distribution and depends on the temperature of the system.

A6.2 Model Based on Quantum Mechanics

The classical model works well when describing macroscopic systems of masses and springs. However, we run into difficulties when trying to apply the same mechanics to problems at the scale of atoms and electrons. For example, in the vibrating H–F molecule in Figure A6.1 the dipole moment of the molecule would be changing over the cycle of the oscillation. Such an oscillating dipole should radiate electromagnetic waves. In fact, this is how radio and television signals are broadcast; the transmitting aerials set up macroscopic oscillating fields from which radio waves emanate. If the same rules applied to the H–F molecule then it should spontaneously emit radiation at the frequency of the bond vibration, losing energy until the atoms come to rest. From experimental observation we know that this is not the case: molecules can vibrate without radiating energy and their atoms are never at rest.

Quantum mechanics gives us a way to deal with the behaviour of matter at the molecular level. In this approach, molecular vibrations are stable only in specific stationary states which define energy levels for the system. While in a stationary state the vibration still takes place, but no radiation is emitted. Radiation is only emitted or absorbed on transition between energy levels (see Figure 6.2). The state of a system, such as a vibrating molecule, is described in quantum mechanics by a wavefunction, and we will see below how the use of a wave-like description naturally gives discrete energy levels.

Following the motion of the oscillating bond in a stationary state, as we did for the classical model, no longer makes any sense in a wavefunction picture. All we can look for is the probability that an observation of the bond will see a particular extension. The probability of finding any particular value of x should be expected to depend on the value sought. For example, extensions of the bond which give a potential energy greater than the total should be very unlikely. The wavefunction ψ gives the probability that the bond is between x and $x + dx$ as the square of the wavefunction magnitude, $|\psi(x)|^2 dx$, and so we must expect ψ to be a function of x that approaches zero at large x .

To obtain ψ we solve the time-independent Schrödinger equation for the system:

$$\left(-\frac{\hbar^2}{2\mu_m} \frac{d^2}{dx^2} + \frac{1}{2} kx^2 \right) \psi = E\psi \quad (\text{A6.13})$$

This equation is another statement that the total energy E is the sum of the kinetic energy and potential energy, but in this case there is no time dependence. These two contributions must be drawn from the wavefunction, and Schrödinger demonstrated that the kinetic energy should be a function of its second derivative with respect to position, the first term on the left of Equation (A6.13). A mathematical tool for extracting information from the wavefunction is called an operator, so this first term is the kinetic energy operator.

The potential energy depends on the particular system. For the harmonic oscillator we can use the same form as the classical potential, Equation (A6.1), in Equation (A6.13). This is now the potential energy operator, since it is ‘operating’ on the wavefunction. The inclusion of the wavefunction will allow us to average the potential energy across all bond extension values weighted according to their probability.

In Equation (A6.13), \hbar is related to the Planck constant via

$$\hbar = \frac{h}{2\pi} \quad (\text{A6.14})$$

It is useful to rearrange Equation (A6.13) in such a way that the second differential in x has no multiplying coefficient and to group the constants on the left-hand side into a single symbol:

$$\frac{d^2\psi}{dx^2} - \alpha^2 x^2 \psi = -\frac{2\mu_m E}{\hbar^2} \psi \quad \text{where } \alpha^2 = \frac{\mu_m k}{\hbar^2} \quad (\text{A6.15})$$

Solutions of Equation (A6.15) will require us to ‘try out’ or trial functional forms for ψ which have a hope of balancing the left and right sides; on taking the second derivative and simplifying the left-hand side we must end up with just a number multiplying ψ . Our trial function must also conform to any boundary conditions of the problem. Here, we know that at large positive or negative x the wavefunction must tend to zero, and so this is the required boundary condition.

We can make a start using a basic property of the exponential function; the derivative is the same as the function itself:

$$\text{if } y = A \exp(\beta x) \quad \text{then} \quad \frac{dy}{dx} = A\beta \exp(\beta x) = \beta y \quad \text{and} \quad \frac{d^2y}{dx^2} = \beta^2 y \quad (\text{A6.16})$$

Here, A and β are constants that give us some flexibility in defining the function y . This property gives us a promising lead, because the second derivative of y is just a number times y . However, such a simple exponential of x for ψ in Equation (A6.15) will not work, because x can take on both positive and negative values (extension and compression of the bond) and the boundary conditions require ψ to tend to zero at either extreme. An exponential function does tend to zero at large negative x , but it increases indefinitely for positive x .

An exponential-type function that does have the correct behaviour for the boundary conditions is the Gaussian:

$$\psi_{\text{tr}} = N \exp\left(-\frac{\beta x^2}{2}\right) \quad (\text{A6.17})$$

The subscript ‘tr’ is added here to indicate that this is a ‘trial’ wavefunction, i.e. it has a promising functional form, but there is some way to go yet. The constants N and β control the height and width respectively of the Gaussian, and we need to see if there are values of these constants that allow ψ_{tr} to satisfy Equation (A6.15).

To use ψ_{tr} in Equation (A6.15), its second derivative is needed. Here, the rules for differentiating a function of a function can help, so that if we write

$$u = \frac{\beta x^2}{2} \quad (\text{A6.18})$$

then we can take the derivative of ψ_{tr} as follows:

$$\frac{d\psi_{\text{tr}}}{dx} = \frac{du}{dx} \frac{d}{du} N \exp(-u) = -N\beta x \exp(-u) = -x\beta\psi_{\text{tr}} \quad (\text{A6.19})$$

The second derivative can then be obtained:

$$\frac{d^2\psi_{\text{tr}}}{dx^2} = \frac{d}{dx}(-x\beta\psi_{\text{tr}}) = -\beta\psi_{\text{tr}} - x\beta \frac{d\psi_{\text{tr}}}{dx} = (\beta^2 x^2 - \beta)\psi_{\text{tr}} \quad (\text{A6.20})$$

The left-hand side of Equation (A6.15) now becomes

$$\frac{d^2\psi_{\text{tr}}}{dx^2} - \alpha^2 x^2 \psi_{\text{tr}} = (\beta^2 x^2 - \beta)\psi_{\text{tr}} - \alpha^2 x^2 \psi_{\text{tr}} \quad (\text{A6.21})$$

The right-hand side of Equation (A6.15) contains only numbers multiplying ψ_{tr} , and so for this solution to work we must not have any x^2 terms remaining. The only way to achieve this is to set

$$\beta = \alpha \quad (\text{A6.22})$$

With this value for β , our trial wavefunction has satisfied the equation because the operators on the left-hand side have produced the trial wavefunction multiplied by a constant, and Equation (A6.15) becomes

$$-\alpha\psi_{\text{tr}} = -\frac{2\mu_m E}{\hbar^2}\psi_{\text{tr}} \quad (\text{A6.23})$$

The operators have now been dealt with and the wavefunction will cancel on both sides. This shows that we have found the value for β that makes our trial function into a working solution for the harmonic oscillator Schrödinger equation.

Cancelling ψ_{tr} in Equation (A6.23) and rearranging gives the energy corresponding to our trial wavefunction as

$$E = \frac{\alpha\hbar^2}{2\mu_m} \quad (\text{A6.24})$$

Taking the expression for α defined in Equation (A6.15), we find

$$E = \frac{\hbar}{2} \sqrt{\frac{k}{\mu_m}} \quad (\text{A6.25})$$

The square-root term is just the angular frequency obtained from a classical analysis of the vibration of two masses joined by a spring (Equation (A6.11)). So we have shown that the energy of the proposed Gaussian wavefunction is simply

$$E = \frac{1}{2}\hbar\omega \quad (\text{A6.26})$$

An alternative way to write this energy is using the frequency in terms of oscillations per second ν ; since $\omega = 2\pi\nu$, we have

$$E = \frac{1}{2}\hbar\nu \quad (\text{A6.27})$$

where the definition of \hbar has been used to cancel the factors of 2π .

There is an apparent sleight of hand here; at the beginning of this section we stated that, in a stationary state, it was not worth thinking about following the motion of the atoms as a function of time, yet here we bring back the classical frequency of oscillation. Remember that the energy is linked to the spring constant and reduced mass by Equation (A6.25), so that it can be defined in terms of molecular properties. This equation happens to contain the expression for the angular frequency assigned from the classical model, and in the remainder of this appendix we will show that this is also related to the photon energy required to cause a transition between stationary states. For this reason, the use of ‘frequency’ to discuss changes in energy in spectroscopy is common.

The particular solution for the quantum harmonic oscillator is the first of a set of solutions; in fact, we have defined the ground state of the oscillator and the minimum energy that any vibrational mode can have: the zero-point energy. In the quantum picture, the atoms can never come to rest because the bond vibration energy can never be lower than that given by Equation (A6.27).

In finding this solution we have set one of the variables, β , in the trial wavefunction; for the other (N in Equation (A6.17)) we can make use of the interpretation of the wavefunction in terms of a probability. The probability of finding the molecule with a particular value of the bond extension in between x and $x + dx$ is given by

$$P(x) = \psi^*\psi \, dx \quad (\text{A6.28})$$

The asterisk refers to the complex conjugate of the wavefunction. If the wavefunction contains a real part a and an imaginary part b , then the complex conjugate is the same function but with i ($i = \sqrt{-1}$) replaced by $-i$. Then, $\psi^*\psi = (a - ib)(a + ib) = a^2 + b^2 = |\psi|^2$; note that although the wavefunction may contain imaginary numbers, the probability will always be purely a real number.

Clearly, the bond must have some value of x , and so if we look over all possible values of x the probability of finding the correct bond extension is unity. This is often referred to as the normalization condition and can be stated mathematically as

$$\int_{-\infty}^{\infty} \psi^* \psi \, dx = 1 \quad (\text{A6.29})$$

For the ground-state wavefunction of the bond vibration we have found a real function (i.e. no imaginary part), and so the integrand is simply the wavefunction squared:

$$N^2 \int_{-\infty}^{\infty} \exp(-\alpha x^2) \, dx = 1 \quad (\text{A6.30})$$

This integral is the total area under the Gaussian curve, a standard result, so we can write

$$N^2 \sqrt{\frac{\pi}{\alpha}} = 1 \quad \text{and,} \quad N = \left(\frac{\alpha}{\pi}\right)^{1/4} \quad (\text{A6.31})$$

which allows us to complete the trial wavefunction definition:

$$\psi_0 = \left(\frac{\alpha}{\pi}\right)^{1/4} \exp\left(-\frac{\alpha x^2}{2}\right) \quad \text{with} \quad \alpha = \frac{1}{\hbar} \sqrt{\mu_m k} \quad (\text{A6.32})$$

This function is plotted as state $n = 0$ in Figure A6.2a. The line showing the level for the zero-point energy is also used as the zero line for the wavefunction plot. Where this

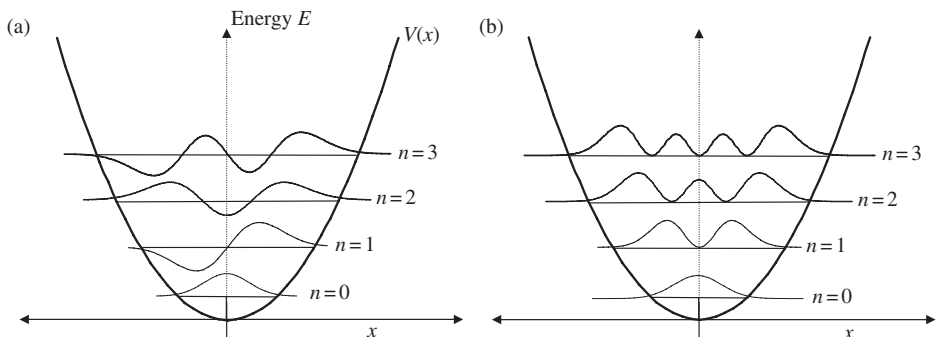


Figure A6.2 (a) The first four wavefunctions of the harmonic oscillator; (b) the squares of the wavefunctions, which give the probability of finding the bond at a particular extension x .

line intercepts the potential energy curve defines the amplitude of the classical oscillator. The wavefunction is decaying at this point, but there is a finite probability that extensions greater than the classical limit will be observed.

A6.3 Excited Vibrational States

We have found the ground state for the oscillator, but there are also other functions that can satisfy the Schrödinger equation. These will represent the excited states of the oscillator and become important when the molecule absorbs energy from the light used in IR spectroscopy. The complete set of solutions for the wavefunctions of the harmonic oscillator are actually a product of the Gaussian function discussed above and a Hermite polynomial H_n which ensures that the cancellation of the x^2 function we forced by one choice of β in Equations (A6.21)–(A6.23) also occurs for the excited states. The general solution for state n of the harmonic oscillator is then

$$\psi_n = N_n H_n(x\sqrt{\alpha}) \exp\left(-\frac{\alpha x^2}{2}\right)$$

with

$$N_n = \left(\frac{\alpha}{\pi}\right)^{1/4} \frac{1}{2^n n!} \quad (\text{A6.33})$$

Here, n is an integer quantum number for the states of the oscillator; n can only have positive values, 0, 1, 2, N_n is the normalization factor for the n th vibrational level and $H_n(x\sqrt{\alpha})$ is the corresponding Hermite polynomial; a standard set of polynomials for which we use $x\sqrt{\alpha}$ as the argument.

Explicitly, for the first four functions we obtain

$$\begin{aligned} \psi_0 &= \left(\frac{\alpha}{\pi}\right)^{1/4} \exp\left(-\frac{\alpha x^2}{2}\right) & \psi_1 &= \left(\frac{4\alpha^3}{\pi}\right)^{1/4} x \exp\left(-\frac{\alpha x^2}{2}\right) \\ \psi_2 &= \left(\frac{\alpha}{4\pi}\right)^{1/4} (2\alpha x^2 - 1) \exp\left(-\frac{\alpha x^2}{2}\right) & \psi_3 &= \left(\frac{\alpha^3}{9\pi}\right)^{1/4} (2\alpha x^3 - 3x) \exp\left(-\frac{\alpha x^2}{2}\right) \end{aligned} \quad (\text{A6.34})$$

These wavefunctions are all real functions, and so the probability of finding the oscillator with a particular value of x when it is in one of these stationary states is just proportional to the square of the wavefunction at that value of x . The four functions and their squares are plotted in Figure A6.2a and b respectively. Each of these functions is normalized in the same way as ψ_0 , so that an integral over all x will give 1.

The vibrational state wavefunctions are also orthogonal to one another, meaning that an integral over all space of two different functions will yield zero. As an example, Figure A6.3a shows the product $\psi_1 \psi_2$ as a function of x ; because this has equal area above and below the x -axis, an integral over all values of x must give zero.

The energy of any vibrational state in the harmonic approximation is given by

$$E_n = (n + \frac{1}{2}) h\nu \quad (\text{A6.35})$$

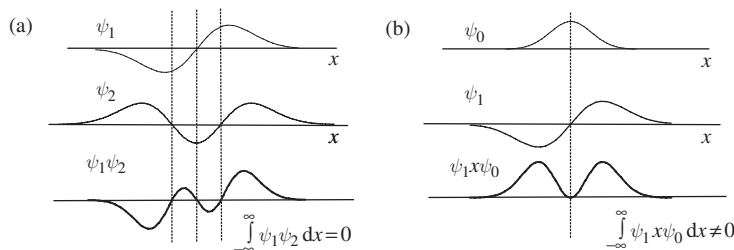


Figure A6.3 (a) The product $\psi_1\psi_2$ gives a function whose integral over all x is zero and so these wavefunctions are orthogonal. (b) The product $\psi_1x\psi_0$ gives a function which is positive everywhere and so has a finite integral.

This equation for the state energy is obtained by substituting the general expression for the n th wavefunction from Equation (A6.33) into the Schrödinger equation, Equation (A6.15). Applying the kinetic and potential energy operators and then rearranging for E , as we did for the ground state, will then give this result. n is a quantum number; stationary states must have an integer value of n , and so Equation (A6.35) tells us that the energy levels are discrete, or quantized, with a separation between states of $h\nu$.

It is worth making a brief comparison of these wavefunctions derived from quantum mechanics and the behaviour of a classical harmonic oscillator such as discussed at the beginning of this appendix. A classical harmonic oscillator is undergoing a constant interchange of kinetic and potential energy. At the maximum displacement the spring in such a system would be under tension, all the energy of the system would be stored in the spring and the mass would be instantaneously stationary as it turns back toward the zero displacement point. As the mass moves, the tension in the spring would be reduced until at zero displacement there is no potential energy. At this point the mass has its highest velocity, i.e. all the potential energy has been converted to kinetic energy. The total energy of the system is always constant: at the extremes of motion we have all potential and no kinetic energy, and at the central point there is only kinetic energy present and no potential energy. In this classical picture, the maximum displacement is set by the total energy of the system, and the particle spends less time at the central point than at the extremes, since its kinetic energy, and so its speed, is a maximum at the centre.

In the quantum picture, illustrated in Figure A6.2, the wavefunction at a given energy level is more or less confined by the points at which the energy level cuts the potential curve. This would be the maximum displacements possible in the classical oscillator, since the total energy set by the energy level is then the same as the potential energy. The quantum model does allow for a finite possibility of movement beyond these limits, a tunnelling effect, but is essentially confined to the same region of space. The biggest difference between the quantum and classical models can be seen at low values of n , especially the $n = 0$ state. The classical oscillator spends more time at the extremes of motion than at the centre. In contrast, the $n = 0$ state of the quantum oscillator has a peak at the centre, indicating the probability of being at the centre is higher than at the extremes of motion. As n increases (e.g. $n = 3$), peaks near the extremes become larger than those at the centre, and at very large n the classical picture would be recovered.

A6.4 Vibrational Modes for Polyatomic Molecules

We have illustrated harmonic motion using a simple diatomic molecule for which the bond displacement is x . As described in the main text, the vibrations of polyatomic molecules are often quite complex mixtures of individual atom displacements. The patterns that are possible for the fundamental vibrations of a molecule can be classified by the irreducible representations. The oscillation in any of these modes can then be analysed using a normal-mode coordinate (generally given the symbol q), which should be thought of as a single variable describing the extent of motion in a given vibration.

The coordinate q carries the symmetry of the vibrational mode and will play the same role as x in our diatomic example. Classically, this would mean that all vibrations have the irreducible representation of the pattern of atomic movements. However, referring to Equation (A6.34), the quantum picture is different. In the ground state, q will only appear as its square; since the direct product of any nondegenerate irreducible representation with itself is A_1 , this means that the ground state of any vibrational mode will also be A_1 . The first excited state will contain q in the Hermite polynomial, and so does have the same symmetry as the irreducible representation of the classical picture of the vibration.

In an IR spectroscopy experiment we introduce light, an electromagnetic wave, which interacts with a molecule by disturbing the local electric field E_F . In general, the electric field is a vector quantity, but here we will simplify matters by only dealing with the X -component (an arbitrary choice). The molecule can couple to the field through its dipole moment. For our diatomic molecule from Figure A6.1, the perturbation energy for an excitation from the $n = 0$ to $n = 1$ states will be given by

$$E_{Fx} \int_{-\infty}^{\infty} \psi_1 \mu_x \psi_0 \, dx \quad (\text{A6.36})$$

The integral is just our definition of the transition dipole moment M_{01} in Equation (6.4) of the main text.

As a simplification, we can imagine the molecular dipole is due to charges located on the atom centres. The two atoms have different electronegativities, so this molecule will have a charge separation with F and H carrying equal and opposite charges, F (δ^-) and H (δ^+). Such a separation of charge gives rise to a dipole moment, which is the product of the charge and the distance between the charge centres.

The bond length extension is distributed according to the harmonic oscillator wavefunctions, and so μ_x in Equation (A6.36) is itself a function of x . If we take the dipole moment of the molecule at its equilibrium bond length as μ_0 and the extension of the bond as x , then we can write the dipole moment at any extension as

$$\mu_x = \mu_0 + \left(\frac{d\mu_x}{dx} \right) x + \frac{1}{2} \left(\frac{d^2\mu_x}{dx^2} \right) x^2 \dots \quad (\text{A6.37})$$

For small extensions the first two terms in this series will be all we need to worry about, so that the transition between states will depend on the coupling integral

$$M_{01} = \int_{-\infty}^{\infty} \psi_1 \left[\mu_0 + \left(\frac{d\mu_x}{dx} \right) x \right] \psi_0 dx \quad (\text{A6.38})$$

Now, μ_0 is just the permanent dipole of the molecule, which does not depend on x , and so can be treated here as a simple number, which means we can write

$$M_{01} = \mu_0 \int_{-\infty}^{\infty} \psi_1 \psi_0 dx + \left(\frac{d\mu_x}{dx} \right) \int_{-\infty}^{\infty} \psi_1 x \psi_0 dx \quad (\text{A6.39})$$

We know that the vibrational state wavefunctions are orthogonal to one another, and so the first term is zero. This tells us that the permanent dipole moment of a molecule does not influence the absorption event required for IR spectroscopy. The integrand of the second term is plotted in Figure A6.3b; the inclusion of the operator x in this integral gives a function which is positive everywhere, and so the integral is nonzero. From a symmetry point of view, the ψ_0 function is totally symmetric, and so $\psi_0(-x) = \psi_0(x)$. In contrast, $\psi_1(-x) = -\psi_1(x)$, so that in the $C_{\infty v}$ point group it has Σ_u^+ symmetry (in the standard setting used in the character tables of Appendix 12 the molecular axis is aligned with Z). This is the same behaviour as the function x itself, and so the second integral in Equation (A6.39) has a totally symmetric integrand and so can be finite.

A6.5 Generalization to Arbitrary Transitions

So far, and in the main text, we have concentrated on absorption due to molecules initially in the ground state. This will be the case for most general laboratory analysis of samples at low temperature for the high-frequency modes of chemical functional groups. This is because the spacing of the energy levels for these vibrations is sufficiently large compared with the thermal energy $k_B T$ (where k_B is the Boltzmann constant) that only the ground state will be significantly populated. For lower frequency modes, such as the skeletal vibrations of polyatomic molecules, it is possible to have a distribution of molecules in the different vibrational states to begin with. To finish this appendix we will generalize Equation (A6.39) to consider these cases.

We can take the second term in Equation (A6.39) and substitute in the general solutions for the harmonic oscillator discussed earlier (Equation (A6.33)). For a transition between two arbitrary states m and n the coupling matrix term would be

$$M_{mn} = \left(\frac{d\mu}{dx} \right) N_m N_n \int_{-\infty}^{\infty} H_m x H_n \exp(-\alpha x^2) dx \quad (\text{A6.40})$$

We have stuck with the x -direction to simplify the discussion but have dropped the subscript on the dipole moment, as now the molecular dipole for the polyatomic molecule need not be along X . There will also be transition dipole moments for y and z which should be taken into account in the same way.

The Hermite polynomials have the following useful recurrence relationship:

$$2\frac{x}{\alpha}H_n = H_{n+1} + 2nH_{n-1} \quad (\text{A6.41})$$

This can actually be used to derive all the polynomials from H_0 and H_1 by using the $n = 1$ case to derive H_2 and then the $n = 2$ case to get H_3 and so on. You may like to test that this expression holds for the polynomials in the first few wavefunctions given earlier in Equation (A6.34).

In the consideration of selection rules, Equation (A6.41) allows us to transform the M_{mn} expression into integrals that only contain products of Hermite polynomials without the intervening x factor; that is, because

$$xH_n = \frac{\alpha}{2}H_{n+1} + \alpha n H_{n-1} \quad (\text{A6.42})$$

we may write

$$M_{mn} = N_m N_n \int_{-\infty}^{\infty} H_m \left(\frac{\alpha}{2} H_{n+1} + \alpha n H_{n-1} \right) \exp(-\alpha x^2) dx \quad (\text{A6.43})$$

Now, we have seen that the wavefunctions form an orthonormal set, and so this integral can only be nonzero if

$$m = n \pm 1 \quad (\text{A6.44})$$

This is an additional selection rule for allowed transitions in an IR absorption event; the vibrational quantum number can only change by ± 1 . It should be remembered that this selection rule is based on the properties of the Hermite polynomials, which are only part of the wavefunctions under the harmonic approximation.

A6.6 Summary of Selection Rules

Equation (A6.44) will also apply to the particular case of transitions from the ground state, and so together with Equation (A6.39) forms the basis of the selection rules for IR absorptions within the harmonic oscillator approximation. In general, we can now say that an IR absorption will be observed if:

1. The photon energy matches the spacing between harmonic oscillator energy levels, i.e. the photon frequency equals the classical frequency of vibration. This gives a transition involving only a unit change of quantum number: $m = n \pm 1$.

2. The dipole moment of the molecule changes during the course of a transition between the states in such a way that its derivative with respect to the atomic displacements is not zero.
3. The excited vibrational state has the same symmetry as x , y or z in the molecular point group.

Further Reading

The mathematics of the IR selection rules and the use of the time-dependent Schrödinger equation to discuss the actual transition event between the stationary states is covered in: McQuarrie DA (2008) *Quantum Chemistry*, 2nd edn. University Science Books, Sausalito, CA (ISBN 978-1-891389-50-4).

The standard properties of a whole host of mathematical functions, such as the Hermite polynomials, are covered in:

Abramowitz M, Stegun IA (eds) (1970) *Handbook of Mathematical Functions*, Dover (ISBN 0-486-61272-4).

Appendix 7

The Franck–Condon Principle

We have seen how Raman spectra depend on an initial electronic excitation followed by re-emission at a shifted frequency. In the main text this is explained with the aid of a diagram (Figure 6.9) showing how each electronic level of a molecule can be thought of as having a subset of vibrational energy levels. The Franck–Condon principle says that the electronic excitation will be vertical in such a diagram because the nuclei respond to the change of electronic structure on a much longer timescale than the electronic transition itself. In this appendix we will look at this in more detail and show how the vibrational states of the molecule enter into the integral controlling the electronic transition, making the electronically excited state likely to be also vibrationally excited.

In our treatment of IR selection rules (Appendix 6) we have written wavefunctions for the harmonic oscillator without reference to the electronic state of the molecule. In fact, all the detail of the electronic states is assumed to be contained within the spring constant for the bond. To characterize the molecule fully we would need to take into account the nuclear and electronic coordinates when defining the potential energy. Rotational and translational degrees of freedom could also be included, adding more coordinates to describe the molecular motion of the system. However, we will only consider the internal structure of molecules, and so these additional factors will be left to one side.

The wavefunction with the required information for the electronic and vibrational aspects of a molecule would depend on the coordinate set of the electrons r to account for the multi-electronic state and those of the nuclei R to account for the vibrational state. As a shorthand, the combined picture is referred to as a vibronic state. We use the symbol Ψ to refer to states that contain information about multiple particles and write $\Psi(r, R)$ to mean that the state is a function of both electron and nuclear coordinates.

The mass of a proton is 1836 times that of an electron, and so the electron has a much smaller mass than even the H atom nucleus. This difference allows the functional form of the total wavefunction to be simplified by treating the electronic and vibrational states separately. The separation of the nuclear and electronic degrees of freedom in this way is

known as the Born–Oppenheimer approximation and gives the following apparently trivial equation:

$$\Psi(r; R) = \Psi_e(r; R) \Psi_N(R; \Psi_e) \quad (\text{A7.1})$$

The semicolon here is used to separate the coordinates which enter directly into the functional form of the wavefunction from other factors on which the wavefunction depends. So, under the Born–Oppenheimer approximation:

- | | |
|---------------------|--|
| $\Psi_e(r; R)$ | This means that the electronic part of the wavefunction is a function of the electronic coordinates only, but that these depend on the particular arrangement of the nuclei. The nuclei provide a potential in which the electrons move; changing the nuclei positions does change $\Psi_e(r; R)$, but only through the effect of this potential on the electron coordinates. |
| $\Psi_N(R; \Psi_e)$ | This means that the nuclear part of the wavefunction is a function of the nuclear coordinates only, but it does depend on the particular electronic state. On the timescale of the nuclear motion the electrons appear smeared out over a distribution defined by Ψ_e . They create forces acting on the nuclei, e.g. controlling the value of the spring constant in the harmonic oscillator formulae. However, these are effectively averaged over the electronic wavefunction, and so the electron coordinates do not explicitly appear. A change in the electronic state will influence $\Psi_N(R; \Psi_e)$ through a change of these averaged effects. |

For electronic excitations, Equation (A7.1) is extremely useful. Consider the sort of excitation shown in Figure 6.7:

$$\Psi_{e0}(r; R) \Psi_{N0}(R; \Psi_{e0}) \rightarrow \Psi_{e1}(r'; R) \Psi_{Nn}(R; \Psi_{e1}) \quad (\text{A7.2})$$

That is, a molecule originally in the ground vibronic state absorbs a photon with the correct energy to move to the first electronic excited state with a shift in the electronic coordinates from r to r' . This also places the molecule in the n th vibrational state of the electronically excited molecule. The Franck–Condon principle appears here since we assume that the nuclear coordinates R remain constant during the transition.

As we have seen, for light to be absorbed, a change in dipole moment must occur so that the coupling matrix element between the two states is nonzero. In this case, we must consider both the nuclear contributions μ_N and electronic contributions μ_e to the transition dipole moment operator, so that the required matrix element is

$$M_{1n:00} = \int \Psi_{e1}^*(r'; R) \Psi_{Nn}^*(R; \Psi_{e0}) (\mu_N + \mu_e) \Psi_{e0}(r; R) \Psi_{N0}(R; \Psi_{e0}) dr dr' dR \quad (\text{A7.3})$$

where the integration is over all space for all electron and nuclear coordinates. Keeping the electron and nuclear contributions to the transition dipole moment operator separate reminds us that μ_N will only operate on nuclear wavefunctions, $\Psi_N(R; \Psi_e)$, and

μ_e will only operate on electronic wavefunctions, $\Psi_e(r; R)$. So the Born–Oppenheimer approximation allows Equation (A7.3) to be rearranged to give

$$M_{1n:00} = \int \Psi_{e1}^*(r'; R) \Psi_{e0}(r; R) dr dr' \int \Psi_{Nn}(R; \Psi_{e1}) \mu_N \Psi_{N0}(R; \Psi_{e0}) dR + \int \Psi_{Nn}^*(R; \Psi_{e1}) \Psi_{N0}(R; \Psi_{e0}) dR \int \Psi_{e1}^*(r'; R) \mu_e \Psi_{e0}(r; R) dr dr' \quad (\text{A7.4})$$

The first term here contains an integral over the ground and excited electronic states. But we see in Chapter 7 that these will always be orthogonal to one another, so the first term is simply zero, leaving

$$M_{1n:00} = \int \Psi_{Nn}(R; \Psi_{e1}) \Psi_{N0}(R; \Psi_{e0}) dR \int \Psi_{e1}^*(r'; R) \mu_e \Psi_{e0}(r; R) dr dr' \quad (\text{A7.5})$$

This expression contains the transition dipole moment for the electronic states (the second integral) and symmetry rules will apply to this in the same way as we have seen for the vibrational states in the main text and in Appendix 6. That is, to be nonzero, the electronic transition must be such that the integrand has A_1 symmetry. How this comes about for electronic transitions we will not cover here.

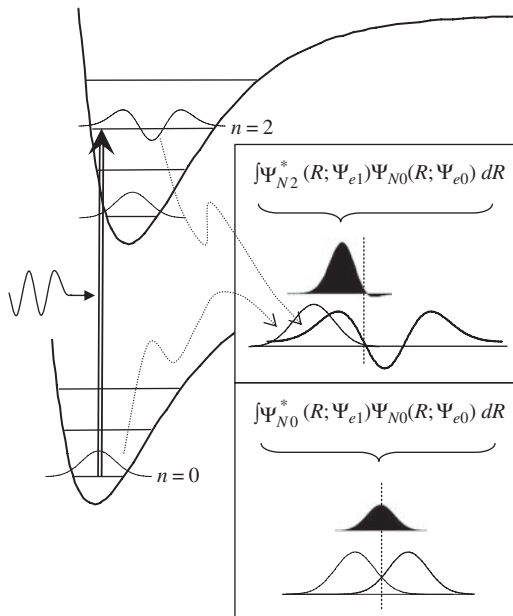


Figure A7.1 The overlap integral for the ground-state vibration with the $n = 2$ vibration in the electronically excited state. The displacement to the right of the Morse curve in the excited state makes the overlap with the excited vibrational states larger than that for the ground state, and so the transitions to vibrationally excited states are more likely.

Interestingly, the vibrational states still affect the electronic transition. The integral over the n th vibrational state of the electronically excited molecule with the ground-state vibration appears as the first integral in Equation (A7.5). This is the overlap between the ground state and excited vibrational wavefunctions illustrated in Figure A7.1.

In Appendix 6 we show that the vibrational states are orthogonal to one another for a given bond potential. Figure A7.1 shows that the integral in Equation (A7.5) is slightly different: the ground-state vibration is in the potential from the electronic ground state and the vibrationally excited state is in the potential of the excited electronic state. In the electronically excited state the minimum of the potential has shifted to longer bond lengths and the spring constant will also have changed. The two sets of vibrational states are not orthogonal to one another, and so the first integral in Equation (A7.5) can have a nonzero value.

Within the harmonic approximation, the Hermite polynomial factors in the vibrational wavefunctions (Equation (A6.33) and Figure A6.2) lead to a peak at the potential minimum for the ground-state vibration and near the maximum bond compression/extension for states with higher n values. These peak patterns, together with the shift in the bond potentials shown in Figure A7.1, make the overlap integral between the ground state vibration, $\Psi_{N0}(R; \Psi_{e0})$, and excited-state vibrations such as $\Psi_{N2}(R; \Psi_{e1})$ greater than that with $\Psi_{N0}(R; \Psi_{e1})$. This makes it more likely that an electronic transition will result in a vibrationally excited molecule.

In Figure A7.1, and throughout this text, we have retained the harmonic approximation to the bond potential even though we have drawn these as Morse curves. Wavefunctions taking into account the shape of the Morse potential can also be obtained, and the general conclusion that a vibrationally excited molecule is likely to be generated is still valid.

Appendix 8

Classical Treatment of Stokes/Anti-Stokes Absorption

The classical picture of the absorption of light of UV-visible frequencies is illustrated in the main text (Figure 6.12) using the polarization of a molecule of urea by the electric field of a light wave as an example. In this appendix we develop the mathematics that describe the response of the molecule to the light wave and show that the Stokes and anti-Stokes lines observed experimentally in Raman spectra follow from the modulation of the molecular polarizability by its vibrational motion.

Any external electric field E will produce a change in the electric dipole of a molecule due to the rearrangement of the electron density in response to the field. We will begin by considering the electric field to be a simple scalar quantity; this is generalized to an electric field vector in the main text. In this simplified model, the induced dipole μ_{ind} is proportional to the electric field and the proportionality constant is the molecular polarizability α , so that

$$\mu_{\text{ind}} = \alpha E \quad (\text{A8.1})$$

The electric field of a light wave will be oscillating at the frequency ν of the radiation with amplitude E_0 , so that

$$E = E_0 \cos(2\pi\nu t) \quad (\text{A8.2})$$

where t is time measured from a positive maximum in the field. Equations (A8.1) and (A8.2) say that the induced dipole moment varies as

$$\mu_{\text{ind}} = \alpha E_0 \cos(2\pi\nu t) \quad (\text{A8.3})$$

This just means that electron density of the molecule is forced to oscillate at the frequency of the incident light.

Molecular polarizability depends on the geometry and atom types that make up the molecule. So, the polarizability itself will be time dependent, changing as the molecule vibrates. If the molecule has a mode with frequency ν_0 , then the polarizability will change as

$$\alpha = \alpha_0 + (\Delta\alpha) \cos(2\pi\nu_0 t) \quad (\text{A8.4})$$

where $\Delta\alpha$ is the maximum deviation of the polarizability.

The combined result of the vibration and field oscillation is given by substituting from Equation (A8.4) into Equation (A8.3) to give

$$\mu_{\text{ind}} = [\alpha_0 + (\Delta\alpha) \cos(2\pi\nu_0 t)] [E_0 \cos(2\pi\nu t)] \quad (\text{A8.5})$$

To interpret this formula we can make use of an identity from standard trigonometry:

$$\cos A \cos B = \frac{1}{2} [\cos(A + B) + \cos(A - B)]$$

which allows Equation (A8.5) to be written thus:

$$\mu_{\text{ind}} = \alpha_0 E_0 \cos(2\pi\nu t) + \frac{\Delta\alpha}{2} E_0 \{ \cos[2\pi(\nu + \nu_0)t] + \cos[2\pi(\nu - \nu_0)t] \} \quad (\text{A8.6})$$

So the induced dipole oscillates at a combination of the exciting frequency and the exciting frequency plus/minus the vibrational frequency of the molecule.

In a classical model, any oscillating dipole emits radiation, and this is the source of the scattered light. Scattering at the incident frequency ν is referred to as Rayleigh scattering, scattering at a lower frequency, $\nu - \nu_0$, is called Stokes radiation and scattering at a higher frequency, $\nu + \nu_0$, is called anti-Stokes radiation.

Equation (A8.6) shows that the Stokes/anti-Stokes lines depend on the change of molecular polarizability $\Delta\alpha$ for the vibrational modes of the molecule. This allows us to develop the selection rules for Raman spectroscopy in Section 6.2.4.

In the main text we arrive at the same conclusion regarding the possible frequency shifts based on a qualitative discussion of vibronic states. The complete quantum model of Raman spectroscopy also has to take into account the change of polarizability accompanying the transition between stationary vibrational states, which leads to the coupling factor in Equation (6.15).

Appendix 9

The Atomic Orbitals of Hydrogen

The discussion of chemical bonding in the main text depends on the description of molecular orbitals as linear combinations of atomic orbitals. In this appendix we show how solutions of the Schrödinger equation for H-like atoms give us the atomic orbitals that are used as the building blocks in this approach. We will also take the opportunity to cover some basic ideas in quantum mechanics.

By ‘H-like’ we mean that a solitary electron moves in the field of a positively charged nucleus. This avoids the complication of considering electron–electron interactions. For a qualitative insight into chemical bonding, these can be reintroduced later.

To calculate wavefunctions for any stationary state of an H-like atom we would like solutions to the Schrödinger equation:

$$-\frac{\hbar^2}{2m_e} \nabla^2 \chi_p + V \chi_p = E_p \chi_p \quad (\text{A9.1})$$

where \hbar is the Planck constant divided by 2π , m_e the electron mass and χ_p the wavefunction for an electron experiencing the potential V with total energy E_p ; p is just an index to allow us to tell the many possible solutions apart from one another. As we go through outlining the solution of Equation (A9.1) we will replace p with the quantum numbers for the atomic orbitals. In this appendix we will assume that the nuclear mass is so much greater than the electron mass that it can be treated as a stationary point around which the electron moves. The effects of removing this assumption and introducing the reduced mass of the system are very minor.

Equation (A9.1) assumes nothing about the units of the quantities used. If we switch to atomic units (au) then the manipulation and solution of this formula becomes clearer because we remove the clutter of the physical constants. In au $\hbar = 1$, $m_e = 1$ and the electron charge $e = 1$, i.e. these quantities are used to define the units of angular momentum, mass and charge respectively. These units are actually derived from the solution of the H

atom problem, and so the unit of length is the bohr ($0.529\ 177\ \text{\AA}$), which, as we will see, turns out to be the most probable distance between electron and proton in the H 1s orbital. The Schrödinger equation in au is written thus:

$$-\frac{1}{2}\nabla^2\chi_p + V\chi_p = E_p\chi_p \quad (\text{A9.2})$$

The left-hand side of Equation (A9.2) should be thought of as a mathematical operator acting on the wavefunction to give the kinetic energy (first term) and potential energy (second term) for the wavefunction. The equation itself just states that these contributions must sum to the total state energy.

The first term in Equation (A9.2) is the kinetic energy operator, which contains the Laplacian ∇^2 ('del squared'). This is the three-dimensional equivalent to the one-dimensional kinetic energy operator we met for the harmonic oscillator in Appendix 6. In Cartesian coordinates, the Laplacian operator is defined as

$$\nabla^2 = \frac{\partial^2}{\partial x^2} + \frac{\partial^2}{\partial y^2} + \frac{\partial^2}{\partial z^2} \quad (\text{A9.3})$$

i.e. the sum of the second derivatives with respect to the each of the components of the coordinate system.

The second term in Equation (A9.2) is the potential energy operator acting on the wavefunction. This will depend on the system under consideration. For the atomic orbitals of H it is the Coulomb interaction between the electron and the nucleus. The dimensions of the nucleus are much smaller than the atom itself, and so we can treat it as a point and it is convenient to place it at the origin of coordinates. The potential energy of an electron at r is then simply

$$V = -\frac{Z_{\text{eff}}}{r} \quad \text{with} \quad r = \sqrt{x^2 + y^2 + z^2} \quad (\text{A9.4})$$

where, again, the use of atomic units gives a particularly simple form. The potential depends only on the effective charge on the nucleus Z_{eff} and the electron's distance from the nucleus. For H itself $Z_{\text{eff}} = 1$, the proton charge, but for heavier atoms the electron sees the potential of the nucleus and the other electrons. Some idea of the effect of electrons that are closer to the nucleus than the one under consideration can be obtained by assuming that the effective potential is lower than that of the bare nucleus. For example, the 1s electrons in an Li atom are closer to the nucleus than the 2s electron. The 2s electron experiences the attraction of the nucleus and the repulsion of the 1s electrons and so 'sees' $Z_{\text{eff}} < 3$.

The wavefunctions for the one-electron states of an H-like atom is a problem that is soluble analytically. We will not go all the way through the solution here, but we will examine the results that are available from other texts and show that they comply with the Schrödinger equation. We can then relate the solutions to the standard orbitals in common usage, such as 1s, 2s, 2p_x, 2p_y, 2p_z, 3d_{xy}, 3d_{yz}, etc.

A9.1 Choice of Coordinate System

From Equation (A9.4) we see that the electron potential energy will have the same value at any point a distance r from the nucleus, i.e. any point on the surface of a sphere of radius r . Equation (A9.4) also shows that, in Cartesian coordinates, r actually depends on all three components of the axis system, which makes the direct solution of the Schrödinger equation quite difficult. However, if we transform to the spherical polar coordinate system illustrated in Figure A9.1, then the distance from the origin r becomes a single coordinate. In our problem, the potential energy of the electron is then a much simpler function than in the Cartesian case.

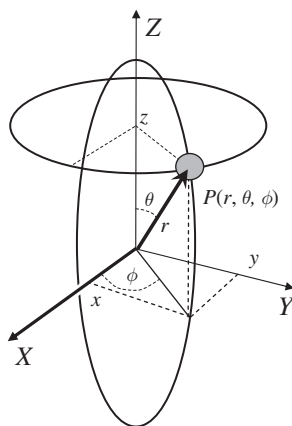


Figure A9.1 The spherical polar coordinate system. Any point P is defined by its distance from the origin r , the rotation angle ϕ away from the X -axis and the rotation angle θ away from the Z -axis.

In spherical polar coordinates the r -coordinate of any point in space, such as P in Figure A9.1, sets the radius of the sphere on which the point lies. Pinning down the point to a particular location on the surface of this sphere is akin to finding a location on the surface of any globe, such as the surface of the Earth. Accordingly, the other two coordinates are angles which define the point's longitude ϕ and latitude θ , although 'latitude' in the coordinate system is measured from the pole rather than the equator.

The Laplacian operator in spherical polar coordinates becomes

$$\nabla^2 = \frac{1}{r^2} \frac{\partial}{\partial r} \left(r^2 \frac{\partial}{\partial r} \right) + \frac{1}{r^2 \sin(\theta)} \frac{\partial}{\partial \theta} \left(\sin(\theta) \frac{\partial}{\partial \theta} \right) + \frac{1}{r^2 \sin^2(\theta)} \frac{\partial^2}{\partial \phi^2} \quad (\text{A9.5})$$

To make the manipulation of equations involving the Laplacian easier, we will define more compact operators which contain differentials with respect to radial and angular degrees of freedom:

$$\nabla^2 = \frac{1}{r^2} \nabla_r^2 + \frac{1}{r^2} \Lambda_{\theta\phi}^2 \quad (\text{A9.6})$$

Direct comparison of Equations (A9.5) and (A9.6) gives the functional forms of the new operators; subscripts have been included to show which variables they included.

A9.2 Separation of Variables

The spherical polar expression for the Laplacian operator appears much more foreboding than the Cartesian coordinate version. However, this is not really the case, since now the Schrödinger equation can be split into radial and angular equations that can be solved separately. To see this, we first write the wavefunction as a product of a function that only depends on r and a function that only depends on the angles θ and ϕ :

$$\chi_p(r, \theta, \phi) = R_p(r) Y_p(\theta, \phi) \quad (\text{A9.7})$$

The first function, $R_p(r)$, will control the behaviour of the function on any line moving directly away from the nuclear centre, while the second gives the angular behaviour as we move around the nucleus. The Schrödinger equation for the H atom problem can now be written:

$$\frac{1}{R_p} \nabla_r^2 R_p - 2Vr^2 + 2E_p r^2 + \frac{1}{Y_p} \Lambda_{\theta\phi}^2 Y_p = 0 \quad (\text{A9.8})$$

This formula is derived by substituting from Equation (A9.7) into Equation (A9.2) with the Laplacian in spherical polar form (Equation (A9.6)). The energy term is moved to the left and the whole equation multiplied through by -2 and by r^2 ; this removes the r dependence in the angular part of the Laplacian operator. Finally, dividing through by $R_p Y_p$ gives some terms that depend only on r and some that depend only on the angles θ and ϕ . In Equation (A9.8), like terms have then been gathered together. The potential is only a function of r , as we saw in Equation (A9.4), and the total energy E_p appears with the radial part of the equation because of our multiplication through by r^2 .

Notice that in the first set of terms the angular function has been cancelled when we divide by $R_p Y_p$ but the radial function survived. This is because the angular function is not affected by the radial operators and so can be written to the left of them and cancelled. The radial function cannot be moved so easily, because it will be affected by the differential operators in the first term. A similar rearrangement has been used to cancel R_p from the angular term.

Equation (A9.8) has to be true at all points in space, meaning every set of values of r , θ and ϕ . Imagine taking the value of the radial and angular parts at one particular set of coordinates and then just altering r while leaving θ and ϕ alone. The value of the angular term in Equation (A9.8) would remain unchanged; so, if the value of the radial term were to alter, the equation would be violated. The only way to always keep the balance between the terms is if they always have equal and opposite constant values.

So, Equation (A9.8) can be separated into a radial equation

$$\frac{1}{R_{pl}} \nabla_r^2 R_{pl} - 2Vr^2 + 2E_{pl} r^2 = l(l+1) \quad (\text{A9.9})$$

and an angular equation

$$\frac{1}{Y_{lp}} \Lambda_{\theta\phi}^2 Y_{lp} = -l(l+1) \quad (\text{A9.10})$$

We have chosen to write the constant that ensures Equation (A9.8) is obeyed as $l(l+1)$, because this preempts the solution of the angular equation in which l will be shown to be the angular momentum quantum number. The solutions to Equations (A9.9) and (A9.10) will depend on the particular value of l , and so this has been added as a subscript to the R_{pl} and Y_{lp} functions. These two equations can now be solved separately.

A9.3 The Angular Equation

The angular equation can be rearranged to give a form that looks very like a Schrödinger equation with only a kinetic term:

$$-\Lambda_{\theta\phi}^2 Y_{lp} = l(l+1) Y_{lp} \quad (\text{A9.11})$$

This is understandable; if we sit at a fixed radius and just vary the angular degrees of freedom, then the potential will be constant. The kinetic energy in this case is to do with the electron motion around the nucleus.

The angular equation can be further subdivided into two differential equations, one involving only θ and one for ϕ , by writing

$$Y_{lp} = \Theta_{lp}(\theta) \Phi_p(\phi) \quad (\text{A9.12})$$

Writing out $\Lambda_{\theta\phi}^2$ explicitly, we obtain

$$-\frac{1}{\Theta_{lp}} \sin(\theta) \frac{\partial}{\partial \theta} \left(\sin(\theta) \frac{\partial \Theta_{lp}}{\partial \theta} \right) - l(l+1) \sin^2(\theta) - \frac{1}{\Phi_p} \frac{\partial^2 \Phi_p}{\partial \phi^2} = 0 \quad (\text{A9.13})$$

from Equation (A9.11). Again, this equation can only work if the terms involving only θ give a simple constant which is equal and opposite to a constant from terms depending on ϕ alone. This constant is usually written as m_l^2 , which will define the second quantum number for the angular functions.

Setting the term in Equation (A9.13) involving ϕ to $-m_l^2$ and those depending on θ to m_l^2 , after some rearrangement, the two differential equations are

$$\frac{\partial^2 \Phi_{ml}}{\partial \phi^2} + m_l^2 \Phi = 0 \quad (\text{A9.14})$$

and

$$\frac{1}{\sin \theta} \frac{\partial}{\partial \theta} \left(\sin \theta \frac{\partial \Theta_{lm_l}}{\partial \theta} \right) + \left[l(l+1) - \frac{m_l^2}{\sin^2 \theta} \right] \Theta_{lm_l} = 0 \quad (\text{A9.15})$$

The angular functions have to conform to boundary conditions; if we go right round the atom and return to the same point, then we must find the same value for the function. This means that

$$\Theta_{lm_l}(\theta + 2\pi) = \Theta_{lm_l}(\theta) \quad \text{and} \quad \Phi_{m_l}(\phi + 2\pi) = \Phi_{m_l}(\phi) \quad (\text{A9.16})$$

In Section A9.11 we show that Equation (A9.14) for Φ_{m_l} is related to an equation used by Euler to demonstrate the relationship

$$\exp(i m_l \phi) = \cos(m_l \phi) + i \sin(m_l \phi) \quad (\text{A9.17})$$

in which $i = \sqrt{-1}$; so these solutions are expressed as functions containing imaginary numbers. The solutions have the required periodic nature, since both cosine and sine repeat once every 2π radians. The real (nonimaginary) parts are plotted out in Figure A9.2 for some choices of m_l . For $m_l = 1, 2, 3$ we see that tracing the wavefunction around the nucleus gives a continuous wave. However, if we take a value that is a noninteger, such as the example of 1.5 in Figure A9.2d, then the wavefunction must break somewhere. A discontinuous function of this type cannot be a stationary solution of the Schrödinger equation and will not be seen in atomic orbitals. So Equation (A9.17) provides a solution for $\Phi_{m_l}(\phi)$ provided m_l is an integer. Not shown in Figure A9.2 is the $m_l = 0$ solution, as this is just a constant, giving the same value for any position around the equatorial ring used in the figure.

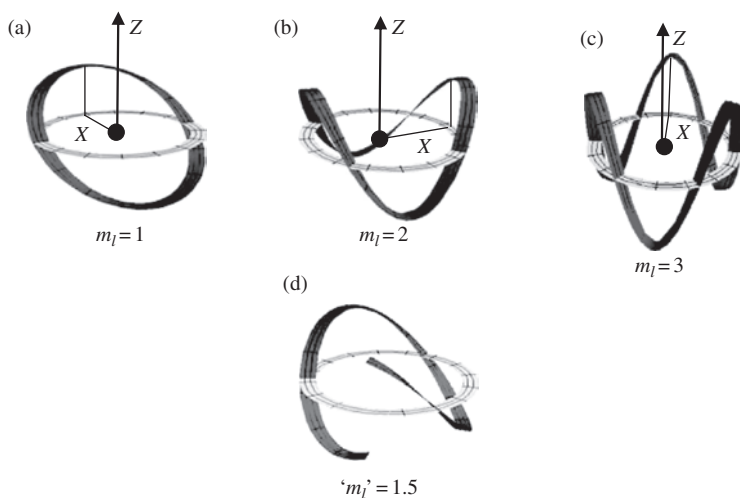


Figure A9.2 Example real components of the solutions for the $\Phi_{m_l}(\phi)$ part of the angular equation. (a)–(c) Continuous solutions for $m_l = 1, 2$ and 3 . (d) A discontinuous function is found for a noninteger value of m_l . In each case the function is plotted around an equatorial ring with the value indicated as a Z-displacement.

As we have seen before, the quantization of the solution comes about when we impose the boundary conditions; because the electron is confined to move around the nucleus, it can only occupy particular states: those with an integer m_l quantum number.

Equation (A9.17) provides the functional form for $\Phi_{m_l}(\phi)$, but we usually work with normalized wavefunctions. Since the overall wavefunction is a product of angular and radial functions, normalizing each term individually will ensure a normalized function when they are brought together.

We can obtain the normalization factor N_ϕ for $\Phi_{m_l}(\phi)$ from the integral

$$\int_{-\pi}^{\pi} \Phi^* \Phi \, d\phi = N_\phi^2 \int_{-\pi}^{\pi} \exp(-im_l\phi) \exp(im_l\phi) \, d\phi = 1 \quad (\text{A9.18})$$

where the limits are chosen to give a complete revolution around the Z-axis. This is a straightforward integral to do because the product of exponentials must give 1 for any value of m_l . So we have

$$N_\phi^2 \int_{-\pi}^{\pi} d\phi = 1 \quad \text{which gives} \quad N_\phi = \frac{1}{\sqrt{2\pi}} \quad (\text{A9.19})$$

The normalized solution can then be written as

$$\Phi_{m_l} = \frac{1}{\sqrt{2\pi}} \exp(im_l\phi) \quad (\text{A9.20})$$

The direct solution of Equation (A9.15), for $\Theta_{lm_l}(\theta)$, is much more involved and we leave that to texts dedicated to quantum mechanics, some of which are referenced in the Further Reading section of this appendix. The normalized solutions are

$$\Theta_{lm_l}(\theta) = \sqrt{\left(\frac{2l+1}{2}\right) \left[\frac{(l-|m_l|)!}{(l+|m_l|)!}\right]} P_l^{|m_l|}(\cos\theta) \quad (\text{A9.21})$$

Here, $P_l^{|m_l|}$ are the associated Legendre polynomials, which can be obtained from the sources in the Further Reading section of this appendix. We go this far to note that Θ_{lm_l} is only defined for l being an integer and $|m_l| \leq l$, since, while $0!$ is taken to be 1, the factorial of a negative number is not defined.

The combination of Θ_{lm_l} and Φ_{m_l} to give the angular part of the wavefunction defines the spherical harmonic functions, $Y_{lm_l} = \Theta_{lm_l} \Phi_{m_l}$, which are the solutions to the full angular equation. The first six spherical harmonics are sufficient for us to develop H atom wavefunctions up to d-orbitals, and these are listed in Table A9.1 along with the real combinations that are in common usage, which are described later. Notice that all these functions conform to both of the angular boundary conditions given in Equation (A9.16), and so the spherical harmonics give continuous functions in θ and ϕ .

A general property of the spherical harmonic functions is that

$$-\Lambda_{\theta\phi}^2 Y_{lm_l} = l(l+1) Y_{lm_l} \quad (\text{A9.22})$$

Table A9.1 The solutions for the angular equation, Equation (A9.11), for angular momentum quantum number l from 0 to 2. For $m_l \neq 0$ the linear combinations can be taken to give real functions whose Cartesian forms follow the familiar orbital labels.

l	m_l	$Y_{lm_l}(\theta, \phi)$	Real combinations of $Y_{lm_l}(\theta, \phi)$	Equivalent real combinations in Cartesian coordinates
0	0	$\frac{1}{2\sqrt{\pi}}$	$\frac{1}{2\sqrt{\pi}}$	$\frac{1}{2\sqrt{\pi}}$
1	0	$\frac{1}{2} \left(\frac{3}{\pi} \right)^{1/2} \cos(\theta)$	$\frac{1}{2} \left(\frac{3}{\pi} \right)^{1/2} \cos(\theta)$	$\frac{1}{2} \left(\frac{3}{\pi} \right)^{1/2} \frac{z}{r}$
± 1		$\mp \frac{1}{2} \left(\frac{3}{2\pi} \right)^{1/2} \sin(\theta) \exp(\pm i\phi)$	$\frac{1}{\sqrt{2}} (Y_{1,-1} - Y_{1,1}) = \frac{1}{2} \left(\frac{3}{\pi} \right)^{1/2} \sin(\theta) \cos(\phi)$ $\frac{i}{\sqrt{2}} (Y_{1,-1} + Y_{1,1}) = \frac{1}{2} \left(\frac{3}{\pi} \right)^{1/2} \sin(\theta) \sin(\phi)$	$\frac{1}{2} \left(\frac{3}{\pi} \right)^{1/2} \frac{x}{r}$ $\frac{1}{2} \left(\frac{3}{\pi} \right)^{1/2} \frac{y}{\sqrt{x^2 + y^2 + z^2}}$
2	0	$\frac{1}{4} \left(\frac{5}{\pi} \right)^{1/2} [3 \cos^2(\theta) - 1]$	$\frac{1}{4} \left(\frac{5}{\pi} \right)^{1/2} [3 \cos^2(\theta) - 1]$	$\frac{1}{4} \left(\frac{5}{\pi} \right)^{1/2} \frac{2z^2 - x^2 - y^2}{x^2 + y^2 + z^2}$
± 1		$\mp \frac{1}{2} \left(\frac{15}{2\pi} \right)^{1/2} \cos(\theta) \sin(\theta) \exp(\pm i\phi)$	$\frac{1}{\sqrt{2}} (Y_{2,-1} - Y_{2,1}) = \frac{1}{2} \left(\frac{15}{\pi} \right)^{1/2} \cos(\theta) \sin(\theta) \cos(\phi)$ $\frac{i}{\sqrt{2}} (Y_{2,-1} + Y_{2,1}) = \frac{1}{2} \left(\frac{15}{\pi} \right)^{1/2} \cos(\theta) \sin(\theta) \sin(\phi)$	$\frac{1}{2} \left(\frac{15}{\pi} \right)^{1/2} \frac{xz}{r^2}$ $\frac{1}{2} \left(\frac{15}{\pi} \right)^{1/2} \frac{yz}{r^2}$
± 2		$\frac{1}{4} \left(\frac{15}{2\pi} \right)^{1/2} \sin^2(\theta) \exp(\pm 2i\phi)$	$\frac{i}{\sqrt{2}} (Y_{2,-2} - Y_{2,2}) = \frac{1}{4} \left(\frac{15}{\pi} \right)^{1/2} \sin^2(\theta) \sin(2\phi)$ $\frac{1}{\sqrt{2}} (Y_{2,-2} + Y_{2,2}) = \frac{1}{4} \left(\frac{15}{\pi} \right)^{1/2} \sin^2(\theta) \cos(2\phi)$	$\frac{1}{2} \left(\frac{15}{\pi} \right)^{1/2} \frac{xy}{r^2}$ $\frac{1}{4} \left(\frac{15}{\pi} \right)^{1/2} \frac{(x^2 - y^2)}{r^2}$

This property is consistent with the solution of the angular part of the Schrödinger equation, since using the operator on the function gives back the same function multiplied by a number. The number in this case is always $l(l+1)$, and this is the reason that the separation constant used to split the complete H atom Schrödinger equation into radial and angular parts takes this value.

As an example demonstration that spherical harmonics are working solutions of the angular part of the Schrödinger equation, we will substitute $Y_{1,-1}$ back into the angular equation, Equation (A9.11), and show that Equation (A9.22) is valid in this case. Using the function from Table A9.1, the left-hand side of Equation (A9.12) becomes

$$-\Lambda_{\theta\phi}^2 Y_{1,-1} = -A \Lambda_{\theta\phi}^2 \sin(\theta) \exp(-i\phi) \quad \text{with } A = \frac{1}{2} \left(\frac{3}{\pi} \right)^{1/2} \quad (\text{A9.23})$$

Lumping together a group of constants into the factor A greatly simplifies the ensuing algebra, and we will keep redefining an ‘ A ’ factor for each problem tackled in this appendix.

The operator $\Lambda_{\theta\phi}^2$ contains separate differential operators for θ and ϕ (see Equations (A9.5) and (A9.6)). For the θ operator part, the $\exp(-i\phi)$ function can be written to the left of the operator to show it is not affected by differentiation with respect to θ .

Concentrating on the θ operator part of $\Lambda_{\theta\phi}^2 Y_{1,-1}$, we then have

$$\begin{aligned} \exp(-i\phi) \left[\frac{1}{\sin(\theta)} \frac{\partial}{\partial \theta} \left(\sin(\theta) \frac{\partial}{\partial \theta} \right) \right] \sin(\theta) &= \exp(-i\phi) \frac{1}{\sin(\theta)} \frac{\partial}{\partial \theta} (\sin(\theta) \cos(\theta)) \\ &= \exp(-i\phi) \frac{1}{\sin(\theta)} (\cos^2(\theta) - \sin^2(\theta)) = \exp(-i\phi) \frac{1}{\sin(\theta)} (1 - 2 \sin^2(\theta)) \end{aligned} \quad (\text{A9.24})$$

where the differentiation of a product and the trigonometric identity $\cos^2(\theta) + \sin^2(\theta) = 1$, discussed in Section A9.11, have been used.

For the ϕ operator part of $\Lambda_{\theta\phi}^2 Y_{1,-1}$, $\sin(\theta)$ can be written to the left of the operator so that

$$\left(\frac{\sin(\theta)}{\sin^2(\theta)} \frac{\partial^2}{\partial \phi^2} \right) \exp(-i\phi) = -i \left(\frac{1}{\sin(\theta)} \frac{\partial}{\partial \phi} \right) \exp(-i\phi) = -\frac{\exp(-i\phi)}{\sin(\theta)} \quad (\text{A9.25})$$

where the last step makes use of $i^2 = -1$.

We can now use these results (Equations (A9.24) and (A9.25)) in Equation (A9.23):

$$\begin{aligned} -\Lambda_{\theta\phi}^2 Y_{1,-1} &= -A \left[\frac{1}{\sin(\theta)} (1 - 2 \sin^2(\theta)) - \frac{1}{\sin(\theta)} \right] \exp(-i\phi) \\ &= 2A \sin(\theta) \exp(-i\phi) \\ &= 2Y_{1,-1} \end{aligned} \quad (\text{A9.26})$$

We chose a spherical harmonic function with $l = 1$, which gives $l(l + 1) = 2$, so Equation (A9.22) has been validated.

It is a useful exercise to demonstrate that a few of the other spherical harmonics listed in Table A9.1 also conform to Equation (A9.22).

A9.4 Physical Interpretation of the Angular Equation Solutions

Concentrating on the mathematical solutions of the Schrödinger equation, we can easily lose touch with the physical problem that is being considered. We will now recap the classical picture of the electron motion in an orbit around the nucleus so that we can try to relate the solutions found for the angular equation to this more tangible model. This will also allow the differences between the classical and quantum pictures of matter at the atomic scale to be highlighted.

In the classical H-like atom the electron is bound by its electrostatic attraction to the positively charged nucleus. The potential energy of the electron at a distance r from the nucleus was quoted in atomic units in Equation (A9.4); in SI units we would have

$$V = -\frac{Z_{\text{eff}}e^2}{4\pi\varepsilon_0 r} \quad (\text{A9.27})$$

where ε_0 is the permittivity of free space. The force acting due to this potential is given by the negative of the potential gradient:

$$F_r = -\frac{dV}{dr} = -\frac{Z_{\text{eff}}e^2}{4\pi\varepsilon_0 r^2} \quad (\text{A9.28})$$

This force acts along the radial vector, and the minus sign tells us that the attractive Coulomb force acts to try to reduce r . The potential energy and force are plotted as a function of r in Figure A9.3, which shows that both energy and force become increasingly negative as r decreases.

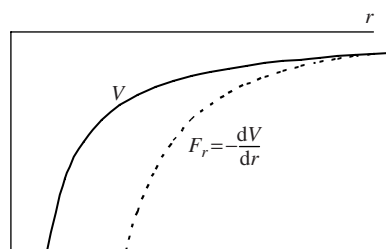


Figure A9.3 The Coulomb potential V and radial force F_r as a function of the electron-nuclear separation r .

Figure A9.4a illustrates the classical mechanics model of an electron circling a fixed, positively charged nucleus. The electron moving on an orbit around the nucleus has a velocity which continually changes direction but not magnitude. A changing velocity

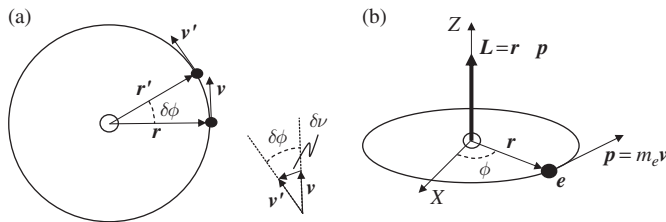


Figure A9.4 (a) The classical picture of an electron moving around a nucleus showing the relationship between the changing velocity δv and angular displacement $\delta\phi$. (b) The linear momentum \mathbf{p} and angular momentum \mathbf{L} for the orbiting electron.

implies acceleration, and so we will next obtain an expression for the electron acceleration a and use Newton's law ($F = ma$) to link this to the Coulomb force.

Figure A9.4a shows that for two points a small distance apart along the electron's path the change of velocity is related to the angular displacement $\delta\phi$. At very small displacements the curvature of the path can be ignored, and the definition of angles in radian units then gives

$$\delta v = v\delta\phi \quad (\text{A9.29})$$

If this displacement takes place in the short time δt , then we have the acceleration:

$$a = -\frac{\delta v}{\delta t} = -v \frac{\delta\phi}{\delta t} \quad \text{or taking } \delta t \rightarrow 0, \quad a = -v \frac{d\phi}{dt} \quad (\text{A9.30})$$

Figure A9.4a also shows that this acceleration will be directed along the radius toward the proton, i.e. the negative r direction. Because r is our reference direction, a negative sign appears in Equation (A9.30).

The differential of the angular displacement can be used to define an angular velocity:

$$\omega = \frac{d\phi}{dt} \quad (\text{A9.31})$$

The electron will sweep out 2π radians per revolution while it actually moves a distance of $2\pi r$, and so the angular velocity is related to the linear velocity via

$$v = \omega r \quad (\text{A9.32})$$

which means

$$a = -\frac{v^2}{r} \quad (\text{A9.33})$$

The acceleration is a response to the Coulomb force, so we can use Newton's law to relate Equations (A9.28) and (A9.33):

$$\frac{Z_{\text{eff}}e^2}{4\pi\epsilon_0 r^2} = \frac{m_e v^2}{r} \quad (\text{A9.34})$$

The term on the right is the force along the radius that causes the electron to move around the orbit; this is referred to as the centripetal force.

Equation (A9.34) can give us the classical kinetic energy as a function of the radius of the orbit:

$$T = \frac{1}{2}m_e v^2 = \frac{Z_{\text{eff}} e^2}{8\pi\epsilon_0 r} \quad (\text{A9.35})$$

The total energy of the system is

$$E = T + V = -\frac{Z_{\text{eff}} e^2}{8\pi\epsilon_0 r} \quad (\text{A9.36})$$

So the total energy of the electron is negative, consistent with a bound state. In the classical model there is no quantization, and so no energy levels to describe the spectra of atomic H. To account for the observed spectral lines, Bohr postulated that only certain radii give rise to stable orbits that do not radiate electromagnetic energy. The energies of these orbitals can be obtained from the ionization potential and electronic spectra of H. For example, in Table 7.2 we give the ionization energy of H as 13.6 eV. This means that the lowest lying orbital must have an energy of -13.6 eV; Equation (A9.36) then gives a classical orbital radius of 0.529 Å. This radius of the lowest lying H orbital is now used to define the natural length scale of the atomic units system: the Bohr radius.

A9.5 Angular Momentum

In the above discussion we introduced the idea of angular velocity as the rate of change of the angular coordinate ϕ . To describe the rotational motion of the electron, such angular, rather than linear, quantities can actually be used more widely.

Figure A9.4b shows that the electron has linear momentum $\mathbf{p} = m_e \mathbf{v}$; we can also define an angular momentum \mathbf{L} given by

$$\mathbf{L} = \mathbf{r} \times \mathbf{p} \quad \text{or in Figure A9.4b as} \quad \mathbf{L} = rp \sin\left(\frac{\pi}{2}\right) \mathbf{z} = rpz \quad (\text{A9.37})$$

Here, we have begun to write vector quantities using bold type, both linear and angular momentum have size and direction, and so are vectors, the magnitudes of vector quantities are shown in italics. In fact, the velocity, acceleration and force used in the preceding section are all vectors. However, since the Coulomb and centripetal forces both act along the radius vector, the effect of direction simply involves keeping track of the sign of the forces relative to the \mathbf{r} -direction.

In Equation (A9.37), \mathbf{r} is the position vector for the electron and \mathbf{p} its linear momentum tangential to the circle on which it moves around the nucleus; the angle between them is always 90° ($\pi/2$ radians), and so the sine of the angle between \mathbf{r} and \mathbf{p} is always unity. The product used to define \mathbf{L} is a vector cross product, which says that the angular momentum is perpendicular to both the electron coordinate and the linear momentum of the electron. In this classical model, we choose the XY plane to coincide with the circle in which the

electron moves and then the angular momentum is aligned with Z. In the second expression given in Equation (A9.37) this is indicated by the z term, which is a unit vector along the Z-direction.

The angular momentum is a constant of the orbital motion of the electron, whereas its linear momentum is constantly changing. The definitions in Equation (A9.37) recognize that what is constant is the magnitude of the momentum and the plane in which the electron moves. Hence, the angular momentum is defined as a vector perpendicular to the plane of motion.

Equation (A9.32) allows the kinetic energy and magnitude of the angular momentum to be written in terms of the angular velocity:

$$T = \frac{1}{2}m_e r^2 \omega^2 \quad \text{and} \quad L^2 = (m_e r^2 \omega)^2 \quad (\text{A9.38})$$

These equations include the distance r of the electron from the nucleus, because, for the same angular velocity, an electron placed further from the nucleus would be moving faster.

The quantity $m_e r^2$ is the moment of inertia I of the electron, which plays much the same role in angular motion as does mass in linear problems. So we can convert these equations to read

$$T = \frac{1}{2}I\omega^2 \quad \text{and} \quad L^2 = (I\omega)^2 \quad \text{or} \quad L^2 = 2IT \quad (\text{A9.39})$$

Angular momentum is a conserved quantity in both classical and quantum mechanics. In classical mechanics, this means that the angular momentum of a system will remain unchanged indefinitely unless acted upon by an external force (or strictly a torque for angular motion).

In the quantum picture, the angular wavefunction will be a stationary state as defined by the quantum numbers l and m_l . Angular momentum can still be defined, but we need an appropriate operator to obtain its value. The angular kinetic energy operator is defined by using the angular part of the Laplacian from Equation (A9.6) in the kinetic energy operator from Equation (A9.1):

$$\hat{T}_{\theta\phi} Y_{lm_l} = -\frac{\hbar^2}{2m_e} \frac{1}{r^2} \Lambda_{\theta\phi}^2 Y_{lm_l} \quad (\text{A9.40})$$

where a ‘hat’ over a symbol is used to distinguish an operator from a number when the same symbol is used. We have also reverted to the Schrödinger equation with explicit constants for comparison with our classical model.

The denominator of Equation (A9.40) contains the definition for the moment of inertia. Using this and the result from Equation (A9.22) for $-\Lambda_{\theta\phi}^2 Y_{lm_l}$ we have

$$\hat{T}_{\theta\phi} Y_{lm_l} = \frac{\hbar^2}{2I} l(l+1) Y_{lm_l} \quad (\text{A9.41})$$

By analogy with the classical analysis result, Equation (A9.39), we can also obtain an operator for the square of magnitude of the angular momentum:

$$\hat{L}^2 Y_{lm_l} = 2I\hat{T}_{\theta\phi} Y_{lm_l} = \hbar^2 l(l+1) Y_{lm_l} \quad \text{and} \quad L = \sqrt{l(l+1)}\hbar \quad (\text{A9.42})$$

So the magnitude of the angular momentum is quantized and set by the quantum number l . This result also confirms that the natural unit for angular momentum is the Planck constant over 2π .

In the spherical polar coordinate system the angle ϕ sets the position away from the X-axis measured parallel to the XY plane (Figure A9.1). The normal to this plane is clearly the Z-axis. So the ϕ angle can be used to describe that part of the rotation which is about the Z-axis, i.e. the Z-component of the angular momentum L_z . The angular wavefunction must also obey the differential equation

$$-i\hbar \frac{\partial}{\partial \phi} Y_{lm_l} = L_z Y_{lm_l} \quad (\text{A9.43})$$

The left-hand side is the operator for the L_z component of the angular momentum acting on the spherical harmonic function (see Further Reading section of this appendix). We can apply this operator to the general form of the spherical harmonic solutions:

$$-i\hbar \frac{\Theta}{\sqrt{2\pi}} \frac{\partial}{\partial \phi} \exp(im_l\phi) = \hbar m_l \frac{\Theta}{\sqrt{2\pi}} \exp(im_l\phi) = \hbar m_l Y_{lm_l} \quad (\text{A9.44})$$

so that

$$L_z = m_l \hbar \quad (\text{A9.45})$$

In the quantum description we have found the magnitude of the angular momentum and its Z-component. This gives a set of planes on which the electron can be thought to move, as illustrated in Figure A9.5a. The direction of the angular momentum can never be pinned down precisely; this is one manifestation of the uncertainty principle. The relationship

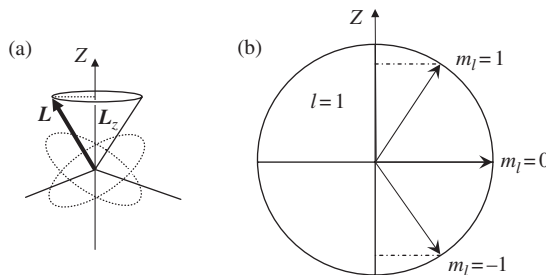


Figure A9.5 (a) In quantum mechanics the angular momentum vector can be orientated anywhere on a cone around the Z-axis, so that the plane in which the electron moves is not fixed. (b) The magnitude of the angular momentum is controlled by the quantum number l , while the magnetic quantum number m_l determines the Z-component of the angular momentum.

between the l and m_l quantum numbers is now seen to be a consequence of the vector nature of the angular momentum, as shown in Figure A9.5b. Because l defines the magnitude of the vector it must always be zero or a positive integer; m_l controls the Z-component, which can be negative, but can never exceed the magnitude of the vector itself, so that $-l \leq m_l \leq l$.

A9.6 The Radial Equation

To complete the solution of the Schrödinger equation we return to the radial equation in atomic units, Equation (A9.9), which can be rearranged to give

$$-\frac{1}{2r^2} \nabla_r^2 R_{nl} + \left[\frac{l(l+1)}{2r^2} - \frac{Z_{\text{eff}}}{r} \right] R_{nl} = E_{nl} R_{nl} \quad (\text{A9.46})$$

Here, we have introduced the final quantum number we need for this three-dimensional problem. This is the principal quantum number and is usually written as n . In this form we have what looks like a normal Schrödinger equation: the first term on the left being the radial part of the kinetic energy operator (see Equations (A9.6) and (A9.2)), the term in brackets a potential energy operator and on the right-hand side we have the state energy multiplying the wavefunction R_{nl} .

The potential includes the Coulomb interaction, which has been written explicitly in terms of the effective nuclear charge. But it also includes a term that depends on the angular quantum number l . This tells us that the effective potential in which the electron moves depends on the magnitude of its angular momentum. This observation is analogous to the centrifugal effect experienced by a macroscopic rotating body.

In the classical description we showed how the centripetal force is generated by the Coulomb interaction and keeps the electron on its orbit. If we could instantaneously remove the electron–nuclear attraction the electron would continue along the tangential direction, flying away from the nucleus. This means that the electron motion is continually acting to separate the particles but this is counteracted by the nuclear attraction. This aspect of the angular momentum is often called the centrifugal effect.

In the quantum mechanics model, if the electron has angular momentum ($l \neq 0$), then the additional potential represents the centrifugal effect and becomes increasingly positive as the electron approaches the nucleus. At very short separations it overrides the attractive Coulomb potential, and so the wavefunction for the electron tends to zero as it approaches the nucleus.

If an electron has no angular momentum ($l = 0$) then only the Coloumb potential operates and we see a finite value for the wavefunction at the nucleus (see Figure 7.11 in the main text). The idea of a stationary state for an electron that has no angular momentum is a purely quantum effect. In the classical picture, it is the angular momentum that prevents the electron being pulled into the nucleus. In the quantum picture, zero angular momentum is possible because the uncertainty principle will prevent the coordinate of the electron being fixed at that of the nucleus. After establishing the radial part of the wavefunction we will return to this point to show that, although the wavefunction is positive, the probability of the electron visiting the nucleus is still zero.

The general solution of the radial equation is not straightforward. We are interested in solutions for which the electron is in a stationary state bound to the nucleus. This gives a boundary condition that $R_{nl}(r) \rightarrow 0$ at large r values. The set of functions that satisfy Equation (A9.46) is then a product of an associated Laguerre polynomial, $L_{n+1}^{2l+1}(\rho r)$, and a decaying exponential that ensures this boundary condition is met:

$$R_{nl}(r) = -\sqrt{\left(\frac{2Z_{\text{eff}}}{n}\right)^3 \left\{ \frac{(n-l-1)!}{2n[(n+1)!]^3} \right\}} L_{n+1}^{2l+1}(\rho r) \exp\left(-\frac{\rho}{2}r\right) \quad \text{with } \rho = \frac{2Z}{na_0} \quad (\text{A9.47})$$

From this general expression the factorial terms tell us that n must be a positive integer and that $l \leq n-1$. n is the principal quantum number, which determines which electronic shell the orbital belongs to.

The first few radial functions are listed in Table A9.2; for completeness, the length scale is shown in these functions by including the Bohr radius a_0 explicitly.

Table A9.2 The solutions for the radial equation, Equation (A9.7), for principle quantum number n from 1 to 3. Note: Z_{eff} is the effective nuclear charge, a_0 is the Bohr radius (0.529 177 Å), r is the radial coordinate, and $\rho = (2Z_{\text{eff}}/na_0)$.

n	l	$R_{nl}(r)$
1	0 (1s)	$\left(\frac{Z_{\text{eff}}}{a_0}\right)^{3/2} 2e^{-(\rho/2)r}$
2	0 (2s)	$\left(\frac{Z_{\text{eff}}}{a_0}\right)^{3/2} \frac{1}{2\sqrt{2}}(2-\rho r)e^{-(\rho/2)r}$
	1 (2p)	$\left(\frac{Z_{\text{eff}}}{a_0}\right)^{3/2} \frac{1}{2\sqrt{6}}\rho r e^{-(\rho/2)r}$
3	0 (3s)	$\left(\frac{Z_{\text{eff}}}{a_0}\right)^{3/2} \frac{1}{9\sqrt{3}}(6-6\rho r+\rho^2 r^2)e^{-(\rho/2)r}$
	1 (3p)	$\left(\frac{Z_{\text{eff}}}{a_0}\right)^{3/2} \frac{1}{9\sqrt{6}}(4-\rho r)\rho r e^{-(\rho/2)r}$
	2 (3d)	$\left(\frac{Z_{\text{eff}}}{a_0}\right)^{3/2} \frac{1}{9\sqrt{30}}\rho^2 r^2 e^{-(\rho/2)r}$

To test out these solutions we will substitute some examples back into Equation (A9.46), remembering that this equation is in atomic units and so takes $a_0 = 1$.

To obtain the kinetic energy term for R_{10} we will need

$$\begin{aligned} \nabla_r^2 R_{10} &= A \frac{\partial}{\partial r} \left(r^2 \frac{\partial}{\partial r} \right) \exp\left(-\frac{\rho}{2}r\right) \\ &= -\frac{A\rho}{2} \frac{\partial}{\partial r} \left[r^2 \exp\left(-\frac{\rho}{2}r\right) \right] \end{aligned}$$

$$\begin{aligned} l &= -\frac{A\rho}{2} \left(-\frac{\rho r^2}{2} + 2r \right) \exp\left(-\frac{\rho}{2}r\right) \\ &= \left(\frac{\rho^2 r^2}{4} - \rho r \right) R_{10} \end{aligned} \quad (\text{A9.48})$$

where $A = 2(Z_{\text{eff}}/a_0)^{3/2}$. Equation (A9.46) for this function now becomes

$$\left(-\frac{\rho^2}{8} + \frac{\rho}{2r} - \frac{Z_{\text{eff}}}{r} \right) R_{10} = E_{10} R_{10} \quad (\text{A9.49})$$

Substituting back for ρ from the formula in Table A9.2, we find that the r dependence of the left-hand side is removed and it becomes a simple number. This can then be equated to the state energy, in atomic units:

$$E_{10} = -\frac{Z_{\text{eff}}^2}{2} \quad (\text{A9.50})$$

So, for the H atom case ($Z_{\text{eff}} = 1$) the energy of the lowest lying orbital is half the potential energy at the Bohr radius, as found for the classical atom (Equation (A9.36)). A full comparison of the classical and quantum models required an estimate of the Bohr radius based on the quantum results, which gives the Z_{eff}^2 term in Equation (A9.50). We will see how to obtain these estimates in the next section.

Following the same procedure for the general R_{nl} function, the energy of an H-like atom state with quantum numbers n and l is given by

$$E_{nl} = -\frac{Z_{\text{eff}}^2}{2} \frac{1}{n^2} \quad \text{or in SI units} \quad E_{nl} = -\frac{Z_{\text{eff}}^2 m_e e^4}{32\pi^2 \epsilon_0 n^2} \frac{1}{n^2} \quad (\text{A9.51})$$

Equation (A9.51) is able to account for the observed series of atomic spectral lines for atomic H. For the H atomic orbitals we have shown that the energy is independent of l . However, for atoms with more electrons, shielding of the nucleus is important. To a first approximation this can be introduced by changing Z_{eff} , and we see in the main text that different values are appropriate for orbitals with the same principal quantum number but differing in l . This gives rise to different energies for atomic ns and np orbitals and explains how the energy difference between these varies across the periodic table.

A9.7 The Complete Atomic Orbitals

We now have all three quantum numbers for defining atomic orbitals: the principal quantum number n , the angular momentum quantum number l and the magnetic quantum number m_l . We have also seen how the possible values of the quantum numbers are interrelated. These are summarized in Table A9.3, which also covers the common nomenclature for atomic orbitals. This gives the principal quantum number followed by a letter indicating the angular momentum quantum number, with s, p, d, ... referring to $l = 0, 1, 2, \dots$

Table A9.3 The quantum numbers for the first few energy levels of an H atom. These show how the atomic orbital shells are built according to the principal n , angular momentum l , and magnetic m_l quantum numbers.

n	l	Orbital label	Values of m_l	No. of orbitals
1	0	1s	0	1
2	0	2s	0	1
	1	2p	-1, 0, 1	3
3	0	3s	0	1
	1	3p	-1, 0, 1	3
	2	3d	-2, -1, 0, 1, 2	5
4	0	3s	0	1
	1	3p	-1, 0, 1	3
	2	3d	-2, -1, 0, 1, 2	5
	3	4f	-3, -2, -1, 0, 1, 2, 3	7

For any atomic orbital quoted in this way there may be a level of degeneracy because the m_l quantum number can have $2l + 1$ values. Since the radial equation does not contain m_l , its value does not generally affect the orbital energy (unless the atom is in a magnetic field). So, orbitals occur in degenerate sets, i.e. all three 2p atomic orbitals have the same orbital energy $E_{2,1}$.

The orbital functions are formed as a product of the radial and angular solutions:

$$\chi_{nlm_l} = R_{nl} Y_{lm_l} \quad (\text{A9.52})$$

As we have seen before, the wavefunction itself is not an experimentally observable quantity, but it is related to the probability of finding an electron in the orbital at a particular point in space. The probability P_e of finding the electron that is occupying a given wavefunction in an infinitesimal volume $d\tau$ is given by

$$P_e = \chi_{nlm_l}^* \chi_{nlm_l} d\tau \quad (\text{A9.53})$$

Figure A9.6 shows that a small volume element can be defined in spherical polar coordinates using small increments in the coordinates. This gives an infinitesimal volume:

$$d\tau = r^2 \sin(\theta) dr d\theta d\phi \quad (\text{A9.54})$$

The probability depends on the complete wavefunction with its radial and angular parts combined. For example, if we wish to find the probability that the electron is at a distance r from the nucleus then we have to integrate over the angular degrees of freedom:

$$P_e(r) \delta r = \left(\int_{-\pi}^{\pi} \int_0^{\pi} \chi_{nlm_l}^* \chi_{nlm_l} r^2 \sin(\theta) d\theta d\phi \right) \delta r \quad (\text{A9.55})$$

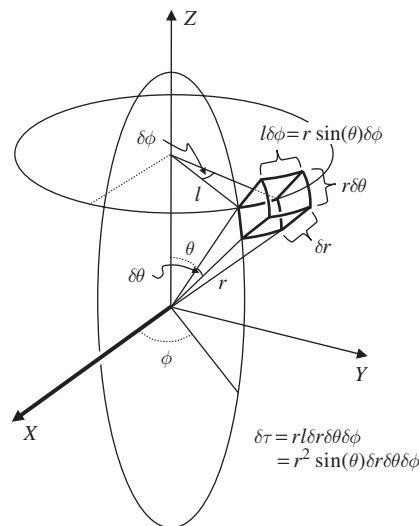


Figure A9.6 Geometry required to define a small volume element $\delta\tau$ in spherical polar coordinates according to the small changes δr , $\delta\theta$ and $\delta\phi$. The sides of the small element shown can be found using the definition of radians as the ratio of the arc length subtended by the angle and the radius.

In effect, this procedure sums the probability around a thin spherical shell of radius r and thickness δr , as illustrated in Figure 7.12. The limits of the integrals in this equation can be understood with reference to Figure A9.1. The θ derivative runs from 0 to π (or 180°) sweeping out a half circle with its diameter on the Z -axis. Then, the ϕ integral covers a full circle from $-\pi$ to π , ensuring that the half circle defined by θ is swept through a full sphere.

Our atomic orbital functions are products of radial and angular terms, and so this type of multiple integral can be treated as a product of integrals over each of the coordinates. For the 1s orbital, for example:

$$P_{100}(r) \delta r = \left(\int_{-\pi}^{\pi} \int_0^{\pi} \chi_{100}^* \chi_{100} r^2 \sin(\theta) \, d\theta \, d\phi \right) \delta r \quad (\text{A9.56})$$

Taking the angular and radial functions from Tables A9.1 and A9.2:

$$P_{100}(r) \delta r = A^2 r^2 \exp(-\rho r) \delta r \int_{-\pi}^{\pi} d\phi \int_0^{\pi} \sin(\theta) \, d\theta \quad \text{with} \quad A = \frac{1}{\sqrt{\pi}} \left(\frac{Z_{\text{eff}}}{a_0} \right)^{3/2} \quad (\text{A9.57})$$

These angular integrals are straightforward, with the integral over ϕ giving 2π and that over θ a factor of 2. So that a factor of $4\pi r^2$ arises in the probability function to give the surface area of the integration sphere and we have:

$$P_{100}(r)\delta r = 4\pi r^2 A^2 \exp(-\rho r) \delta r \quad (\text{A9.58})$$

This probability is plotted as a function of r in Figure 7.11b, where we find that, although the wavefunction itself is finite at the nucleus ($r = 0$), this probability falls to zero as the volume available vanishes.

The probability distribution for the 1s orbital also shows a maximum value which we can now determine mathematically. Taking derivatives with respect to r and remembering that δr is just the shell thickness and so is constant, we obtain

$$\frac{dP_{100}}{dr}\delta r = 4\pi A^2 (2r - \rho r^2) \exp(-\rho r) \delta r \quad (\text{A9.59})$$

So the gradient of the probability function is zero for $r = 0$, where we know $P_{100}(r)\delta r = 0$, or

$$r = \frac{2}{\rho} \quad \text{for the 1s orbital} \quad \rho = \frac{2Z_{\text{eff}}}{a_0} \quad \text{and so} \quad r = \frac{a_0}{Z_{\text{eff}}} \quad (\text{A9.60})$$

For H itself, $Z_{\text{eff}} = 1$, so we have found that the most probable distance for the electron is the Bohr radius that was determined from the classical approach. For heavier elements the value of Z_{eff} will be greater, giving a smaller radius to the 1s orbital due to the increased nuclear attraction felt by the electron.

A9.8 Expectation Values

An atomic property such as the electron position, or momentum, will vary with the electron coordinate. In an experiment we rarely examine one atom, or if we do we observe it for some time. This means that experimental results are averages of the property over all possible electron positions according to the probability that the electron visits each coordinate. We now know that $\chi_{nlm_l}^* \chi_{nlm_l} d\tau$ is the probability of finding the electron at a particular coordinate, and so if we wish to find the value of a property that can be compared with experimental results we should integrate its value over all possible electron coordinates with this probability weighting taken into account. The resulting averaged properties are referred to as expectation values, as they give an estimate of the value to expect from experiments that average over many observations. Expectation values are written using angled brackets, to indicate that the average process has been carried out.

To calculate a property we require the corresponding operator. In this appendix we have seen operators for kinetic and potential energy, as well as operators for the magnitude and Z-component of the angular momentum.

For example, $\langle r_{100} \rangle$, the average radial position for an electron in an H-like atom 1s orbital, can be found using the simple operator r and the appropriate atomic orbital functions. To calculate the expectation value we would write

$$\langle r_{100} \rangle = \int_{-\pi}^{\pi} \int_0^{\pi} \int_0^{\infty} \chi_{100}^* r \chi_{100} r^2 \sin(\theta) dr d\theta d\phi = A^2 \int_{-\pi}^{\pi} d\phi \int_0^{\pi} \sin(\theta) d\theta \int_0^{\infty} r^3 \exp(-\rho r) dr \quad (\text{A9.61})$$

As we saw earlier, the limits for the angular integrals give the surface of a sphere; the additional radial integral then ensures that we visit every point in space. Note that; although this integral is out to infinity; the decaying exponential in the integrand ensures a finite result is obtained.

The angular integrals, again, give a factor of 4π :

$$\langle r_{100} \rangle = 4\pi A^2 \int_0^{\infty} r^3 \exp(-\rho r) dr \quad (\text{A9.62})$$

The radial integral is less straightforward, but does crop up regularly in these sorts of problem and can be solved by repeated application of the integration by parts method. The general result (for arbitrary power of r) is given in Table A9.4, which also lists the first few cases. Taking the value of the integral from the table:

$$\langle r_{100} \rangle = 4\pi \frac{A^2}{\rho^4} = 24 \left(\frac{Z_{\text{eff}}}{a_0} \right)^3 \frac{a_0^4}{16 Z_{\text{eff}}^4} = \frac{3}{2} \frac{a_0}{Z_{\text{eff}}} \quad (\text{A9.63})$$

Table A9.4 The first few integrals of the type required for the integration of the radial functions. The $n = 0$ case is straightforward and the other solutions are obtained by repeated application of the method of integration by parts. Note with the limits shown the result is $I_n = n/\rho^{n+1}$.

Solutions for integrals of the type $I_n = \int_0^{\infty} r^n e^{-\rho r} dr$

n	Analytical integral	Application of limits
0	$-\frac{e^{-\rho r}}{\rho}$	$\frac{1}{\rho}$
1	$-(1 + \rho r) \frac{e^{-\rho r}}{\rho^2}$	$\frac{1}{\rho^2}$
2	$-(2 + 2\rho r + \rho^2 r^2) \frac{e^{-\rho r}}{\rho^3}$	$\frac{2}{\rho^3}$
3	$-(6 + 6\rho r + 3\rho^2 r^2 + \rho^3 r^3) \frac{e^{-\rho r}}{\rho^4}$	$\frac{6}{\rho^4}$
4	$-(24 + 24\rho r + 12\rho^2 r^2 + 4\rho^3 r^3 + \rho^4 r^4) \frac{e^{-\rho r}}{\rho^5}$	$\frac{24}{\rho^5}$

so that the average value of the radial position for the electron in the H 1s orbital is actually one and a half times the Bohr radius. Looking again at the probability plot in Figure 7.11b shows that the distribution beyond a_0 shows a tailing toward large r ; this explains why the average value is beyond the most probable.

We can use the same approach to compare the average radial distance of 2s and 2p functions.

For the 2s function, Tables A9.1 and A9.2 give

$$\chi_{200} = R_{20} Y_{00} = A(2 - \rho r) \exp\left(-\frac{\rho}{2}r\right) \quad \text{with} \quad A = -\frac{1}{4\sqrt{2\pi}} \left(\frac{Z_{\text{eff}}}{a_0}\right)^{3/2} \quad (\text{A9.64})$$

So the expectation value for the radial coordinate of the electron in this case is

$$\begin{aligned} \langle r_{200} \rangle &= A^2 \int_{-\pi}^{\pi} d\phi \int_0^{\pi} \sin(\theta) d\theta \left[4 \int_0^{\infty} r^3 \exp(-\rho r) dr \right. \\ &\quad \left. - 4\rho \int_0^{\infty} r^4 \exp(-\rho r) dr + \rho^2 \int_0^{\infty} r^5 \exp(-\rho r) dr \right] \end{aligned} \quad (\text{A9.65})$$

The angular integrals are the same as before, but we now require three of the standard radial integrals from Table A9.4:

$$\langle r_{200} \rangle = 4\pi A^2 \left[4 \left(\frac{6}{\rho^4} \right) - 4\rho \left(\frac{24}{\rho^5} \right) + \rho^2 \frac{120}{\rho^6} \right] = 4\pi A^2 \left(\frac{48}{\rho^4} \right) \quad (\text{A9.66})$$

Remembering that ρ depends on the principal quantum number (see Table A9.2), and substituting back for A , we obtain

$$\langle r_{200} \rangle = 6 \frac{a_0}{Z_{\text{eff}}} \quad (\text{A9.67})$$

So an electron in a 2s orbital is, on average, much further from the nucleus than a 1s electron.

For the 2p function we will take $n = 2$, $l = 1$ and $m_l = 1$. Hence, reading the corresponding functions from Tables A9.1 and A9.2:

$$\begin{aligned} \chi_{211} &= R_{21} Y_{11} = Ar \exp\left(-\frac{\rho}{2}r\right) \sin(\theta) \exp(i\phi) \quad \text{with} \\ A &= -\frac{1}{4\sqrt{6}} \left(\frac{Z_{\text{eff}}}{a_0}\right)^{3/2} \left(\frac{3}{2\pi}\right)^{1/2} \rho \end{aligned} \quad (\text{A9.68})$$

The expectation for the average electron position in this orbital is then

$$\begin{aligned}\langle r_{211} \rangle &= A^2 \int_{-\pi}^{\pi} \int_0^{\pi} \int_0^{\infty} \chi_{211}^* r \chi_{211} r^2 \sin(\theta) dr d\theta d\phi \\ &= A^2 \int_{-\pi}^{\pi} d\phi \int_0^{\pi} \sin^3(\theta) d\theta \int_0^{\infty} r^5 \exp(-\rho r) dr\end{aligned}\quad (\text{A9.69})$$

Here, the use of the complex conjugate leads to a cancellation of the ϕ -dependant complex exponential in the integrand.

The integral of $\sin^3(\theta)$ can be carried out using the integration by parts method (see *The Chemistry Maths Book* from the Further Reading section in this appendix).

The radial integral is one of the standard forms obtained from the general result in Table A9.3, and so we have

$$\int_{-\pi}^{\pi} d\phi = 2\pi \quad \int_0^{\pi} \sin^3(\theta) d\theta = \frac{4}{3} \quad \int_0^{\infty} r^5 \exp(-\rho r) dr = \frac{120}{\rho^6} \quad (\text{A9.70})$$

Bringing these results together with the definition of A for this orbital,

$$\langle r_{211} \rangle = 5 \frac{a_0}{Z_{\text{eff}}} \quad (\text{A9.71})$$

So, on average, electrons in both the 2s and 2p orbitals are further from the nucleus than the 1s orbital. In heavy atoms this means that the 1s² shell will effectively shield the $n = 2$ states, making the Z_{eff} value smaller than the nuclear charge by almost 2. Within a shell, the situation for estimating shielding is more complex. Our calculations show that the 2s electron is, on average, further from the nucleus than the 2p. However, the radial node in the 2s state gives an inner peak in the probability plot of Figure 7.11b that is not seen for the 2p orbitals. This is close in to the nucleus and so lowers the energy of the 2s states and increases the shielding for the 2p, with the result that the 2s orbitals have lower energies than the 2p for all elements of the second row.

9.9 Real Combinations to Form the Familiar Atomic Orbitals

The solutions for the angular part of the Schrödinger equation in Table A9.1 contain imaginary parts ($i = \sqrt{-1}$). Although we have shown that these cause no problems in describing atomic orbitals, we more often prefer to deal with real functions which can be drawn using the familiar pictures of p_x , p_y and p_z , etc. These are easily obtained when we notice that the angular solutions for $m_l \neq 0$ are found in pairs, so that the m_l solution is always the complex conjugate of that for $-m_l$ and the $m_l = 0$ solution is always real.

The radial functions in Table A9.2 are already real functions and are common factors for the orbitals from which we will take linear combinations, and so we will concentrate on the spherical harmonic solutions of the angular equation in this section.

For example, the two p-orbital angular functions

$$Y_{11} = -A \sin(\theta) \exp(i\phi) \quad \text{and} \quad Y_{1-1} = A \sin(\theta) \exp(-i\phi) \quad (\text{A9.72})$$

with $A = (3/2\pi)^{1/2}/2$, are solutions for quantum numbers $l = 1$ and $m_l = +1$ and -1 respectively.

A useful point to note is that, as well as being normalized, these functions are orthogonal to one another. To see this we extend the use of the $\langle \rangle$ expectation value brackets with no operator to mean the overlap between the functions:

$$\langle Y_{11} | Y_{1-1} \rangle = -A^2 \int_{-\pi}^{\pi} \exp(-2i\phi) d\phi \int_0^{\pi} \sin^2(\theta) d\theta \quad (\text{A9.73})$$

Now the integral over ϕ contains a nontrivial integrand. The solution of this is clearer if we make use of the mathematical identity in Equation (A9.17):

$$\int_{-\pi}^{\pi} \exp(-2i\phi) d\phi = \int_{-\pi}^{\pi} \cos(2\phi) d\phi - i \int_{-\pi}^{\pi} \sin(2\phi) d\phi = 0 \quad (\text{A9.74})$$

These integrals are easily shown to be zero, as the limits are over a complete cycle of the cosine and sine functions. Straight away we have shown that

$$\langle Y_{11} | Y_{1-1} \rangle = 0 \quad (\text{A9.75})$$

which means the functions are orthogonal.

Any of the allowed solutions given in the first column of Table A9.1 satisfy the angular equation (Equation (A9.11)). This also means that any linear combination of the solutions will also be a valid solution. For example, taking the sum $Y_{11} + Y_{1-1}$:

$$-\Lambda_{\theta\phi}^2(Y_{11} + Y_{1-1}) = l(l+1)(Y_{11} + Y_{1-1}) \quad (\text{A9.76})$$

is just

$$-\Lambda_{\theta\phi}^2 Y_{11} - \Lambda_{\theta\phi}^2 Y_{1-1} = l(l+1) Y_{11} + l(l+1) Y_{1-1} \quad (\text{A9.77})$$

So any linear combination can be split up to give matching terms on the left and right sides of the equation. This means we are at liberty to take combinations of the solutions and will look for ways to convert the imaginary solutions to real functions which do not have imaginary parts.

In this case the combinations are

$$\begin{aligned} Y_{11c} &= N_c(Y_{1,-1} - Y_{1,1}) & Y_{11s} &= iN_s(Y_{1,-1} + Y_{1,1}) \\ &\quad \text{and} & & \quad (A9.78) \\ &= AN_c 2 \sin(\theta) \cos(\phi) & & = AN_s 2 \sin(\theta) \sin(\phi) \end{aligned}$$

where the second construction depends on the fact that $i^2 = -1$ and we have made further use of Equation (A9.17). The subscripts refer to l , the magnitude of m_l and the type of linear combination used: ‘c’ signifies that $\cos(\phi)$ survives and ‘s’ that $\sin(\phi)$ is present.

The imaginary functions were normalized so that the integration over all space of the corresponding probability gives 1, but this will not be the case for the linear combinations in Equation (A9.78). So we have included normalization constants N_c and N_s which must be determined. This can be done quite neatly by making use of the orthogonality of the spherical harmonic functions. We require

$$\langle Y_{11c}|Y_{11c} \rangle = 1 \quad (A9.79)$$

The left-hand side can be written in terms of the imaginary spherical harmonics:

$$\begin{aligned} \langle Y_{11c}|Y_{11c} \rangle &= N_c^2 \langle (Y_{1,-1} - Y_{1,1}) | (Y_{1,-1} - Y_{1,1}) \rangle \\ \langle Y_{11c}|Y_{11c} \rangle &= N_c^2 (\langle Y_{1,-1}|Y_{1,-1} \rangle + \langle Y_{1,1}|Y_{1,1} \rangle - \langle Y_{1,1}|Y_{1,-1} \rangle - \langle Y_{1,-1}|Y_{1,1} \rangle) \end{aligned} \quad (A9.80)$$

But we know that the original functions are normalized and orthogonal, so the overlap of like functions is one and overlap between functions is zero, so we have

$$2N_c^2 = 1 \quad \text{and so} \quad N_c = \frac{1}{\sqrt{2}} \quad (A9.81)$$

The same argument can be used to show that N_s takes the same value. These normalization constants have been included in Table A9.1.

A9.10 Cartesian Forms of the Real Angular Functions

Now, functions in the spherical polar coordinate system can be referenced back to the Cartesian coordinates via the relationships

$$\begin{aligned} x &= r \sin(\theta) \cos(\phi) \\ y &= r \sin(\theta) \sin(\phi) \\ z &= r \cos(\theta) \\ r^2 &= x^2 + y^2 + z^2 \end{aligned} \quad (A9.82)$$

which can be shown from the geometry of Figure A9.1. Looking at the linear combinations of Equation (A9.78), conversion to Cartesian coordinates gives

$$Y_{11c} = 2N_c \left(\frac{3}{2\pi} \right)^{1/2} \frac{x}{\sqrt{x^2 + y^2 + z^2}} \quad \text{and} \quad Y_{11s} = 2N_s \left(\frac{3}{2\pi} \right)^{1/2} \frac{y}{\sqrt{x^2 + y^2 + z^2}} \quad (A9.83)$$

The denominator in both of these expressions is simply the distance from the origin, and so does not affect the angular behaviour of the functions. The first combination has an angular dependence which depends on the x -component of the Cartesian coordinate. This has its maximum value along the X -axis at a given distance from the origin. The second function has an orientation along the Y -axis, i.e. these are our familiar p_x and p_y orbitals. Table A9.1 also shows that the solution with $l = 1$ and $m_l = 0$ is related directly to the p_z orbital angular function.

A9.11 Endnote on Imaginary Numbers

In Appendix 6 we made a quick note that our wavefunctions may turn out to contain imaginary numbers, i.e. they may contain $i = \sqrt{-1}$. For the electron wavefunction problems studied in this appendix, imaginary numbers become more important, and so this section will give a brief overview to show how they should be handled.

The wavefunction may be imaginary, but the probability of finding the electron at a given location is a real number between 0 and 1. To ensure this is the case we use the complex conjugate in the probability definition, Equation (A9.53). For every wavefunction we can find a complex conjugate by simply replacing i with $-i$. This gives an easy route to the square of the magnitude of the wavefunction and demonstrates that a real value is always ensured:

$$\begin{aligned} \text{if } \chi &= (a + ib) \quad \text{then} \\ |\chi|^2 &= \chi^* \chi = (a - ib)(a + ib) \\ &= a^2 + b^2 + i(ab - ba) \\ &= A^2 + b^2 \end{aligned} \tag{A9.84}$$

All that is needed here is to remember that $i^2 = -1$.

In this appendix we go a little further and use the complex exponential in some of the wavefunctions. We are used to the idea that an exponential function describes rapidly increasing or rapidly decaying behaviour. Now we have to accept that a complex exponential is actually a periodic function, since it obeys the identity

$$\exp(i\phi) = \cos(\phi) + i \sin(\phi) \tag{A9.85}$$

This is actually the way we identify the real and imaginary parts of the complex exponential.

The usual method to explain Equation (A9.85) is to use the standard Taylor expansions of the three functions and show that they are equivalent to one another (see Further Reading section in this appendix). In this section we will just look at a few examples that confirm Equation (A9.85) is correct and that $\exp(i\phi)$ is periodic.

First, using the complex conjugate approach to obtain the square of the magnitude of $\exp(i\phi)$ gives

$$\begin{aligned}
 |\exp(i\phi)|^2 &= \exp(i\phi)\exp(-i\phi) \\
 &= \exp[i(\phi - \phi)] \\
 &= \exp(0) \\
 &= 1
 \end{aligned} \tag{A9.86}$$

Thinking of a number raised to a negative power as meaning ‘one over’ the same number raised to a positive power makes this simplification clear. Note that we have obtained a real number as the result again, even though the real and imaginary parts are not clearly laid out in $\exp(i\phi)$.

The same procedure for the right-hand side of Equation (A9.85) follows:

$$\begin{aligned}
 |\cos(\phi) + i\sin(\phi)|^2 &= [\cos(\phi) - i\sin(\phi)][\cos(\phi) + i\sin(\phi)] \\
 &= \cos^2(\phi) + \sin^2(\phi) + i[\cos(\phi)\sin(\phi) - \sin(\phi)\cos(\phi)] \\
 &= \cos^2(\phi) + \sin^2(\phi) = 1
 \end{aligned} \tag{A9.87}$$

The last step here is a trigonometric identity, which can actually be seen from the definitions of cosine and sine in a right-angled triangle:

$$\begin{aligned}
 \sin(\phi) &= \frac{\text{opp}}{\text{hyp}} & \text{adj} \\
 \cos(\phi) &= \frac{\text{adj}}{\text{hyp}} & \text{opp}
 \end{aligned} \tag{A9.88}$$

So

$$\cos^2(\phi) + \sin^2(\phi) = \frac{\text{opp}^2 + \text{adj}^2}{\text{hyp}^2} = \frac{\text{hyp}^2}{\text{hyp}^2} = 1$$

i.e. this is just a restatement of Pythagoras’s theorem.

So far we have just shown that the two sides of Equation (A9.85) have the same size, so they could be the same thing, but there are lots of functions that have unit size and are not equivalent to one another.

To show that they behave in the same way as functions we will solve a simple differential equation:

$$\frac{d^2y}{d\phi^2} + y = 0 \quad \text{boundary conditions : } y(0) = 2 \text{ and } \left. \frac{dy}{d\phi} \right|_{\phi=0} = 0 \tag{A9.89}$$

This is a second-order differential equation, but slightly less complicated than the Schrödinger equation tackled in the main part of the appendix. It is also a problem considered by Leonhard Euler when complex exponentials were emerging in the world of mathematics.

To find a functional form for y we need to propose functions that could be differentiated twice and give back a similar function. Euler chose trigonometric and exponential functions as good candidates for trial solutions of this differential equation:

$$y = A \cos(\alpha\phi) \quad \text{or} \quad y = A \sin(\alpha\phi) \quad \text{or} \quad y = B[\exp(\beta\phi) + \exp(-\beta\phi)] \quad (\text{A9.90})$$

where A , B , α and β are constants that need to be determined to fit with the differential equation and its boundary conditions. Notice that, for this second-order differential equation, we have two constants in each trial function. A second-order differential equation requires two ‘integrations’ to be carried out, each of which introduces an undetermined constant. The values of the constants will be found from the two boundary conditions. Any more or any less constants in the function would not be satisfactory.

For this particular set of boundary conditions we can immediately eliminate the second option because $\sin(0) = 0$, but either of the others will work if we take $A = 2$ and $B = 1$.

Taking derivatives:

trial function 1	trial function 3
$\frac{dy}{d\phi} = -2\alpha \sin(\alpha\phi)$	$\frac{dy}{d\phi} = \beta[\exp(\beta\phi) - \exp(-\beta\phi)]$

(A9.91)

Both functions comply with the second boundary condition, that the derivative at $\phi = 0$ is also zero. The result for trial function 3 depends on the sum of two exponentials originally proposed, and so was probably obtained after realizing that a simple exponential would fail at this hurdle.

On to the second derivatives:

trial function 1	trial function 3
$\frac{d^2y}{d\phi^2} = -2\alpha^2 \cos(\alpha\phi)$	$\frac{d^2y}{d\phi^2} = \beta^2[\exp(\beta\phi) + \exp(-\beta\phi)]$
$= -\alpha^2 y$	$= \beta^2 y$

(A9.92)

so that the original differential equation becomes

$$-\alpha^2 y + y = 0 \quad \beta^2 y + y = 0 \quad (\text{A9.93})$$

Function 1 clearly works if we take $\alpha = 1$. Function 3 can also satisfy the equation, but only if we allow $\beta^2 = -1$, which means that $\beta = \sqrt{-1} = i$.

The first solution of this equation shows that the answer is periodic; the second shows that an equally good solution contains complex exponentials. After solving the differential equation with these trial functions, Euler proposed that

$$2 \cos(\phi) = \exp(i\phi) + \exp(-i\phi) \quad (\text{A9.94})$$

The solution of the differential equations alone is not a proof of this relationship; we have just found two functions each of which solve the equation. To fully confirm the

equality we also need the Taylor expansion proof mentioned above and available in the references of the Further Reading section in this appendix.

Euler's equality fits with Equation (A9.85) because the right-hand side is a sum of complex conjugates; so, if we use the earlier identity

$$\exp(i\phi) + \exp(-i\phi) = \cos(\phi) + i \sin(\phi) + \cos(\phi) - i \sin(\phi) = 2 \cos(\phi) \quad (\text{A9.95})$$

then Equation (A9.89) with the boundary conditions

$$y(0) = 2 \quad \text{and} \quad \left. \frac{dy}{d\phi} \right|_{\phi=0} = 2 \quad (\text{A9.96})$$

along with the trial functions

$$y = A \sin(\alpha\phi) \quad \text{and} \quad y = B[\exp(\beta\phi) - \exp(-\beta\phi)] \quad (\text{A9.97})$$

can also be used to show that

$$2i \sin(\phi) = \exp(i\phi) - \exp(-i\phi) \quad (\text{A9.98})$$

Euler's analysis provided us with the complex exponential to use in the place of trigonometric functions in problems giving periodic functions. After a little practice it is often much easier to manipulate than sines and cosines. A useful exercise is to obtain Equation (A9.98) from the boundary conditions in Equation (A9.96) and trial functions in Equation (A9.97) following the same route.

Euler's problem is very close to the equation for the function of ϕ we obtained by separating variables for the angular equation:

$$\frac{\partial^2 \Phi}{\partial \phi^2} + m_l^2 \Phi = 0 \quad (\text{A9.99})$$

The only difference is that now we have a coefficient for the Φ term. Looking back at Equation (A9.93) shows that our choice of β would stem from $\beta^2 = -m_l$, so the solutions that will now be found are

$$\Phi = \exp(im_l\phi) \quad (\text{A9.100})$$

In the main text, the boundary conditions are then imposed to stipulate allowed values of m_l .

Further Reading

The classical mechanics of rotating bodies is fully covered in:

Goldstein H, Poole C, Safko J (2002) *Classical Mechanics*, 3rd edition. Pearson (ISBN 0321-188977).

The H atom problem and the concept of angular momentum are dealt with in several texts, including:

Atkins PW, Friedman RS (1997) *Molecular Quantum Chemistry*, third edition. Oxford University Press (ISBN 0 19 855947 X).

Brink DM, Satchler GR (1993) *Angular Momentum*. Oxford University Press (ISBN 0 19 851759 9)

The general treatment of differential equations, including the H atom problem, along with a more detailed look at imaginary numbers can be found in:

Steiner E (1997) *The Chemistry Maths Book*, Oxford Science Publications (ISBN 0 19 855913 5).

A very readable discussion of the history and application of complex numbers is given in:

Nahin PJ (1998) *An Imaginary Tale, The Story of $\sqrt{-1}$* . Princeton University Press (ISBN 0-691-02795-1).

The properties of spherical harmonics and the associated Legendre functions are given in:

Abramowitz M, Stegun IA (eds) (1970) *Handbook of Mathematical Functions*. Dover (ISBN 0-486-61272-4).

There are also sophisticated computer packages that can deal with the analytical mathematics required for some of the problems in this appendix. Most notable are *Mathematica* (<http://www.wolfram.com/>) and *Matlab* (<http://www.mathworks.com/>).

Appendix 10

The Origin of Chemical Bonding in H_2^+

In Chapter 7 of the main text we outline the various contributions to the stabilization energy of the simplest of all molecules: the H_2^+ cation. The main goal there is to introduce the concepts of MO theory to use in more complex molecules. In this appendix, some additional notes are given on the role of the various components of the kinetic and potential energy terms that contribute to the chemical bond energy of the H_2^+ cation.

We will begin by following the general idea that a linear combination of AOs can be used to form MOs by taking the 1s functions of the H atom derived in Appendix 9 as our basis. Half way through this discussion we will come to the conclusion that chemical bonds decrease the electron's kinetic energy but increase its potential energy. However, we will find that the energies calculated violate an important theorem in the expected balance of average kinetic and potential energy for the molecular ion.

This demonstrates that the linear combination of AOs using the radial decay factors for atoms cannot give a complete picture of chemical bond formation. The radial profiles of the orbitals also have to be allowed to adapt to account for the changing environment the electron experiences on moving from the AOs to MOs. Once this is done, the potential energy is decreased and the kinetic energy increased due to the contraction of the orbitals around the nuclei.

The flexibility of the radial shape of the AOs used in the description of MOs is an important one in theoretical chemistry and will be discussed further in Appendix 11.

A10.1 Chemical Bond Formation

The formation of a molecule from atomic hydrogen and an H⁺ cation can be thought of as the reaction



The chemical bond formation energy is just the energy change for this reaction. We would expect a stable bond to have a lower energy than that of the atoms or ions that are involved. So the chemical bond energy here should be negative.

As discussed in the main text, Equation (A10.1) is the reverse of the usual experimental situation in which the energy required to dissociate from the molecular state is usually measured. However, for calculations, the association of the reactants is easier to consider, as at large separation the interaction terms that we will outline below all tend to zero.

In the following sections we will use the Schrödinger equation to obtain the energy of the reactant and product side of Equation (A10.1) and so estimate the bond formation energy. In this analysis we ignore the zero-point vibrational energy of the molecular ion and so are calculating the molecular energy as if the structure could be frozen at the bottom of the interaction potential-well plotted in Figure 7.5. The addition of the zero-point energy based on the ground state of the harmonic oscillator ($h\nu/2$) is a straightforward and relatively small correction.

As H₂⁺ has only one electron, the potential energy can be analysed using only nuclear-electron and nuclear–nuclear interaction terms, which can be calculated reasonably easily. In more complex molecules the electron–electron interaction must also be accounted for, which is a more difficult task. Indeed, the quest for methods to evaluate the electron–electron interaction accurately is still an active area of research in theoretical chemistry.

A10.2 H Atom and H⁺ Cation

The reactant side of Equation (A10.1) has the H atom and an H⁺ cation. The H atom consists of a negatively charged electron moving in the electrostatic potential of the nucleus, a single positively charged proton. The total energy of the H atom is referenced to the electron and proton separated, so that they no longer interact, and most of this section is concerned with obtaining the atom's total energy in the lowest energy state. The cation on the reactant side of Equation (A10.1) is a completely isolated proton, and so its energy will be taken as zero.

The H AOs and their related orbital energy values have been discussed in some detail in Appendix 9 (see Tables A9.1 and A9.2 and Equations (A9.51) and (A9.52)).

The discussion of Appendix 9 also introduces the atomic unit (au) system, and we will use that again for our discussion of bonding. The atomic unit system takes the Bohr radius (1 bohr = 0.529 177 Å) as the unit of length and uses the electron mass and charge to define the mass and charge fundamental units. The energy unit in this system is the hartree (1 Ha = 4.359 744 × 10⁻¹⁸ J) and we will see how this arises in the solution of the H atom ground state. Chemical energies are often quoted in per mole units; for example, the bond energies given in Tables 7.1 and 7.3 are given in kilojoules per mole units. It is useful to note that

$1 \text{ Ha} \times N_a = 2.62546 \times 10^6 \text{ J}$, and so $1 \text{ Ha mol}^{-1} = 2625.46 \text{ kJ mol}^{-1}$

in which N_a is the Avagadro constant ($6.02205 \times 10^{23} \text{ mol}^{-1}$).

In everyday chemical transformations the hartree is a very large unit. Even the strong CO bond quoted in Table 7.3 as 1072 kJ mol^{-1} corresponds to a bond energy for each CO molecule of only 0.4075 Ha . However, the interactions between electrons and nuclei in atoms and molecules are in the hartree range, and so it is a sensible unit of choice.

Adoption of the atomic unit system simplifies the Schrödinger equation for the H atom to

$$-\frac{1}{2} \nabla^2 \chi_p - \left(\frac{1}{r} \right) \chi_p = E_p \chi_p \quad (\text{A10.2})$$

In this equation, the first term gives the kinetic energy χ_p of an electron in the p th orbital using the Laplacian differential operator ∇^2 . The Laplacian operator is written out in full for the spherical polar coordinate system in Equation (A9.5).

The second term in Equation (A10.2) contains the potential energy operator, which just defines the Coulomb interaction between proton and electron at separation r . It is useful to think of r as the electron radial coordinate relative to the proton fixed at the origin. On the right-hand side is the total energy of the p th orbital E_p .

For the comparison of atomic and molecular systems in their respective ground states in Equation (A10.1) we will only need the 1s orbital, i.e. χ_0 , which in atomic units is simply

$$|s\rangle = \frac{1}{\sqrt{\pi}} \exp(-r) \quad (\text{A10.3})$$

Here, we have also switched to the bra and ket notation that was introduced by Dirac to deal with wavefunctions in an elegantly compact manner. In Dirac notation, a wavefunction is denoted by a ket; i.e. the 1s orbital has been written $|s\rangle$ and the corresponding complex conjugate would be shown as $\langle s|$. If a bra and ket appear in the right order to complete a ‘bracket’, then integration is implied; for example:

$$\langle s|s\rangle = \int_{-\pi}^{\pi} \int_0^{\pi} \int_0^{\infty} \frac{1}{\pi} \exp(-2r) r^2 \sin(\theta) dr d\theta d\phi \quad (\text{A10.4})$$

The right-hand side is the standard mathematical form for integration over all space discussed in Appendix 9.

The 1s function depends only on the distance from the origin, and so the two angular integrals in Equation (A10.4) give a value of 4π , and

$$\langle s|s\rangle = 4 \int_0^{\infty} r^2 \exp(-2r) dr = 1 \quad (\text{A10.5})$$

where the standard result from Table A9.4 has been used, and we find that the ket $|s\rangle$ defined in Equation (A10.3) is correctly normalized.

In Dirac notation, the Schrödinger equation for the H atom becomes

$$-\frac{1}{2}\nabla^2|s\rangle - \left(\frac{1}{r}\right)|s\rangle = E|s\rangle \quad (\text{A10.6})$$

Multiplying from the left by the complex conjugate $\langle s|$ we obtain

$$-\frac{1}{2}\langle s|\nabla^2|s\rangle - \langle s|\left(\frac{1}{r}\right)|s\rangle = E\langle s|s\rangle \quad (\text{A10.7})$$

Here, numbers are written outside of the integration brackets, but operators need to remain inside, as they affect the functional form of the wavefunctions.

We have just shown that the 1s orbital is normalized and so the integral $\langle s|s\rangle$ on the right-hand side of Equation (A10.7) is just unity. Because of this we can use Equation (A10.7) as another method for calculating the total energy for the ground state of the atom complementary to the solution of the radial equation used in Appendix 9.

The integrals to the left of Equation (A10.7) have the form of expectation values (a concept we met in Appendix 9); they are integrals over all space for the $|s\rangle$ wavefunction containing operators for the kinetic and potential energy of the electron. Equation (A10.7) simply says that the total energy is calculated by summing the expectation values for the kinetic energy T and potential energy U components:

$$E = \langle T \rangle + \langle U \rangle = -\frac{1}{2}\langle s|\nabla^2|s\rangle - \langle s|\left(\frac{1}{r}\right)|s\rangle \quad (\text{A10.8})$$

The 1s orbital has no angular dependence, and so we can consider the contributions as a simple function of r . The implied integrations over the three spherical polar coordinates are best taken in two steps: an integration over the angular coordinates, θ and ϕ , at fixed r , followed by an integration for all r values from zero to infinity. In the angular part of this process we are integrating over a spherical shell around the nucleus over which T and

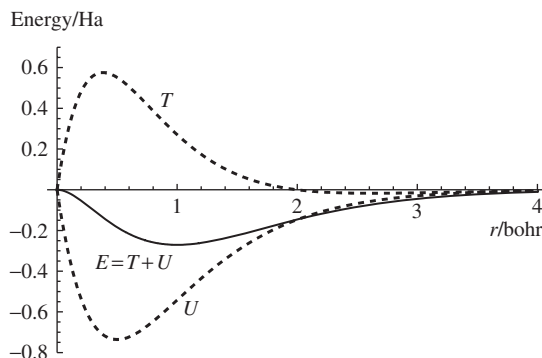


Figure A10.1 The contributions to the kinetic energy T , potential energy U and total energy E of an electron in the 1s orbital of atomic H as a function of the electron–nuclear separation r .

U will be constant. Figure A10.1 gives the result of this intermediate integration over the angular coordinates as a function of r so that we can picture the behaviour of the kinetic and potential energy as a function of the electron–proton separation. On the figure we are plotting T and U before the averaging over the r coordinate required for Equation (A10.8), and so the expectation value brackets $\langle \rangle$ have been dropped.

Figure A10.1 shows that the kinetic energy of the electron is positive below around 2 bohr and increases as the electron approaches the nucleus, because the attraction of the positive charge becomes stronger. There is a peak around 0.4 bohr, below which the lower volume available to the electron wins out over the increasing speed and the contribution to the kinetic energy falls off.

Interestingly, the kinetic energy is negative above 2 bohr. From a classical point of view this makes no sense; kinetic energy is proportional to the particle speed squared and so should not be negative. A classical particle must balance its kinetic and potential energy at every point on its trajectory so that the total energy remains constant. In quantum mechanics, however, particles must only maintain this balance ‘on average’; hence the integrals in Equation (A10.8). This means the electron can move into classically forbidden regions in which their kinetic energy is negative, an effect referred to as quantum tunnelling. Here, the electron is classically confined to a sphere of radius 2 bohr centred on the proton but it can tunnel to greater distances, as indicated by the exponential decay of the wavefunction.

The potential energy U in Figure A10.1 is negative for all values of r , giving a minimum around 0.5 bohr.

The average kinetic $\langle T \rangle$ and potential energy $\langle U \rangle$ integrals can be calculated by integrating the curves in Figure A10.1 from $r = 0$ to ∞ to complete the integration over all space implied by the bra-ket pairs in Equation (A10.8). We find

$$\langle T \rangle = -\frac{1}{2} \langle s | \nabla^2 | s \rangle = \frac{1}{2} \quad \langle U \rangle = -\langle s | \left(\frac{1}{r} \right) | s \rangle = -1 \quad (\text{A10.9})$$

To check these results you will need the standard integrals from Table 9.4 and the Laplacian operator in spherical polar terms (Equation (A9.5)) with the s -function defined in Equation (A10.3). You should also remember that only the radial differential of the Laplacian needs to be applied, because the s -function has no angular dependence.

The atomic units system is built around the H atom problem, and so it is no surprise that the potential energy should be -1 Ha .

A10.3 The Virial Theorem

Equation (A10.9) shows that the values of the kinetic and potential energy for the 1s electron are related by a factor of -2 . This result is an example of the virial theorem. The virial theorem is a very general concept which says that for a particle moving in a potential that follows a power law, such as the Coulomb potential, the average kinetic and potential energy will be linked by a simple numerical factor.

For a power law in which $U = ar^n$, with a the proportionality constant, the virial theorem states

$$\langle T \rangle = \frac{n}{2} \langle U \rangle \quad (\text{A10.10})$$

This very powerful idea is valid for both classical and quantum systems. In cases described by quantum mechanics it only works when we have correctly identified a stationary state of the system, and so can be a useful test of results.

Equation (A10.9) shows that $\langle T \rangle = -\frac{1}{2}\langle U \rangle$, which is the correct result for the Coulomb power law ($n = -1$). That the virial theorem is obeyed is also confirmation that the exponent in the $|s\rangle$ function (Equation (A10.3)) has the optimum form: we are correct to use $\exp(-r)$ rather than some other radial decay, such as $\exp(-\zeta r)$ with $\zeta \neq 1$, as will be checked in Problem A10.1. The electron is distributed as a function of r , so the decay constant affects the averaging process and so is important in calculating the expectation values of the energies.

The virial theorem links the form of the potential the electron experiences to the balance between average kinetic and potential energies in the ground state. Figure A10.1 shows that the electron is more or less confined to a region 2 bohr from the centre of the atom, where its kinetic energy is positive. If the potential field for the electron were to change (e.g. by an increase of the nuclear charge), then both $\langle T \rangle$ and $\langle U \rangle$ would alter: $\langle U \rangle$ would become more negative due to the increased Coulomb interaction and $\langle T \rangle$ would become more positive because the wavefunction would be more strongly confined by the new potential. However, the virial theorem says that the balance would still give $\langle T \rangle = -\frac{1}{2}\langle U \rangle$ in the new ground state and the shape of the wavefunction would have to alter to ensure this.

The sum of $\langle T \rangle + \langle U \rangle$ from Equation (A10.9) is -0.5 Ha , so the system is more stable with the electron in the 1s orbital than with the electron and proton separated. Figure A10.1 indicates that at the Bohr radius the total energy has its minimum value, but the total required for inclusion in the bond formation energy has to take into account the integral of the energy over the entire wavefunction, as indicated by the use of expectation values in Equation (A10.8).

Problem A10.1: We can use the virial theorem to obtain the exponential decay constant in the 1s orbital function. To do this, consider the general form of a trial s -function with a decay constant ζ and then we try to prove that only $\zeta = 1$ gives a wavefunction that satisfies the virial theorem. The Greek letter ‘zeta’ is widely used to describe the decay constants for basis sets in computational chemistry, and so we have adopted that convention here. The normalized trial function $|s_{\text{tr}}\rangle$ will be

$$|s_{\text{tr}}\rangle = \frac{\zeta^{3/2}}{\sqrt{\pi}} \exp(-\zeta r) \quad (\text{A10.11})$$

1. Confirm that $|s_{\text{tr}}\rangle$ is normalized for any choice of ζ .
2. Using the approach laid out in Section A9.8, show that the expectation value for the potential energy is

$$\langle U \rangle = -\langle s_{\text{tr}} | \left(\frac{1}{r} \right) | s_{\text{tr}} \rangle = -\zeta \quad (\text{A10.12})$$

You will need to make use of the standard integrals from Table A9.4 for the radial part of Equation (A10.12), and remember that the integration over θ and ϕ will give a factor of 4π .

3. To obtain the expectation value of the kinetic energy it is useful to first apply the Laplacian (Equation (A9.5)) to $|s_{\text{tr}}\rangle$. Remembering that the trial function has no angular dependence, and so any differential with respect to θ or ϕ will be zero, confirm that

$$\nabla^2|s_{\text{tr}}\rangle = \frac{-\zeta^{5/2}}{\sqrt{\pi}} \left(\frac{2}{r} - \zeta \right) \exp(-\zeta r) \quad (\text{A10.13})$$

4. With the result from Equation (A10.13), show that the expectation value for the kinetic energy of our trial wavefunction is

$$\langle T \rangle = -\frac{1}{2} \langle s_{\text{tr}} | \nabla^2 | s_{\text{tr}} \rangle = \frac{1}{2} \zeta^2 \quad (\text{A10.14})$$

5. The wavefunction for the H atom 1s state must obey the virial theorem for the Coulomb central potential, i.e. we must have $\langle T \rangle = -\frac{1}{2}\langle U \rangle$. Show that only $\zeta = 1$ gives a 1s function obeying the virial theorem.

Problem A10.1 shows that the expectation values for the kinetic and potential energy components for any trial wavefunction $|s_{\text{tr}}\rangle$ are dependent on the exponential decay factor ζ . The decay factor controls how the electron is distributed along the radial coordinate and so affects the averages taken to produce the expectation values.

We can also think about this problem in another way by asking the question: What is the optimum decay factor that gives the lowest energy for the H atom?

Equations (A10.12) and (A10.14) give the total energy as

$$E = \langle T \rangle + \langle U \rangle = \frac{1}{2} \zeta^2 - \zeta \quad (\text{A10.15})$$

This dependence of the energy components and the calculated total on ζ is shown in Figure A10.2. Notice that the total energy passes through a minimum value at $\zeta = 1$, which is just the parameter value we show is required for the virial theorem in Problem A10.1. This means that a trial wavefunction that obeys the virial theorem will also give the lowest total energy.

A10.4 H_2^+ Molecule

The product side of Equation (A10.1) is a $D_{\infty h}$ molecule, for which we take a linear combination of AOs to give a bonding and antibonding combination:

$$|1\sigma_g^+\rangle = N_{1g}(|s_1\rangle + |s_2\rangle) \quad |2\sigma_u^+\rangle = N_{2u}(|s_1\rangle - |s_2\rangle) \quad (\text{A10.16})$$

The $|1\sigma_g^+\rangle$ combination gives rise to a build-up of electron density between the nuclei, and so is expected to have a lower energy than the $|2\sigma_u^+\rangle$ state. For H_2^+ we have only to accommodate one electron, so in the ground state it is placed in $|1\sigma_g^+\rangle$, leaving $|2\sigma_u^+\rangle$

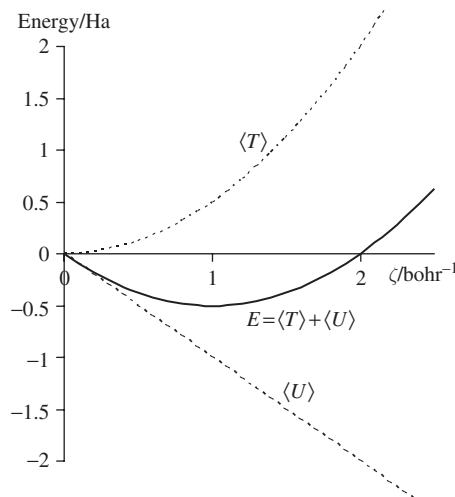


Figure A10.2 The variation of the total energy E and its components, the kinetic energy $\langle T \rangle$ and potential energy $\langle U \rangle$ with the decay constant ξ of a trial $1s$ -like function for the H atom.

empty (refer to Figure 7.10). Moving the electron to the $|2\sigma_u^+\rangle$ orbital would then give the first excited state of the molecule.

Here, we will look more closely at the terms contributing to the bond formation energy by attempting to quantify the various interactions. Initially we will use exactly the same function for the s-orbitals as defined for the H atom in the above discussion, but we will soon discover that this is not the best choice of basis functions for the molecular state.

In Section 7.2 of the main text we show that the normalization constants N_{1g} and N_{2u} depend on the overlap integral between the AO on atom 1 with that on atom 2. This can be written using bra-ket notation as

$$S_{12} = \langle s_1 | s_2 \rangle \quad (\text{A10.17})$$

From the main text we know that the normalization constants of the MOs N_{1g} and N_{2u} are given by

$$N_{1g} = \frac{1}{\sqrt{2(1 + S_{12})}} \quad N_{2u} = \frac{1}{\sqrt{2(1 - S_{12})}} \quad (\text{A10.18})$$

The wavefunctions from Equation (A10.16) with these normalization constants are plotted for the experimental $H-H$ separation in H_2^+ in Figure A10.3a and c. The $|s_1\rangle$ orbital has been overlaid on the left-hand atom at the same scale to allow a comparison of the AOs and MOs. These plots are simply the value of the wavefunctions at each point along the C_∞ axis, and we see the same picture as used in the main text: The $|1\sigma_g^+\rangle$ orbital has constructive interference with a build-up of charge between the nuclei, while destructive interference in this region in the $|2\sigma_u^+\rangle$ case leads to depletion of charge compared with the isolated atom.

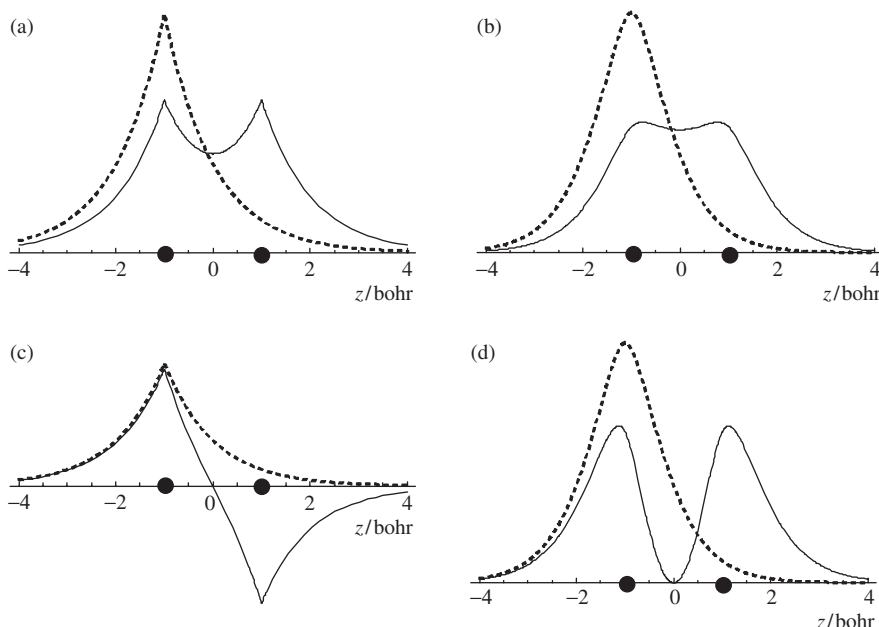


Figure A10.3 The (a) $|1\sigma_g^+\rangle$ and (c) $|2\sigma_u^+\rangle$ wavefunctions of H_2^+ . These functions are plotted along the line of the C_∞ axis with the bond centre at the origin. The $H-H$ distance is set at 2.00 bohr, which is the observed value from Table 7.1. The dotted line shows the atomic $1s$ function of the atom to left of centre. The other two diagrams show the integrated density for planes perpendicular to the Z -direction plotted against z , with (b) representing $\langle 1\sigma_g^+ | 1\sigma_g^+ \rangle$ and (d) $\langle 2\sigma_u^+ | 2\sigma_u^+ \rangle$.

For the energy terms we will need to carry out integrals over these MOs to quantify the electron–nuclear interactions. However, for the H_2^+ molecule the spherical polar coordinate system becomes quite clumsy, because only one nucleus can be at the origin.

A10.5 Choice of Coordinate System for H_2^+ : Cylindrical Polar Coordinates

To make progress we will switch to cylindrical polar coordinates with the axis of the molecule along the Z -direction and the bond midpoint at the origin. This scheme is illustrated in Figure A10.4a. The coordinates are the distance from the molecular axis u , the angle ϕ , measured in a plane perpendicular to the molecular axis, and the position along the molecular axis z . The cylindrical polar system is convenient because the $|1\sigma_g^+\rangle$ and $|2\sigma_u^+\rangle$ MOs have cylindrical symmetry; these functions have a constant value around any circle in a plane perpendicular to the molecular axis, as does the charge density shown in Figure A10.4b. We will use this property to plot the values of the various integrals over u and ϕ , at each value of z , so that we can illustrate how contributions to the various expectation values depend on position along the molecular axis.

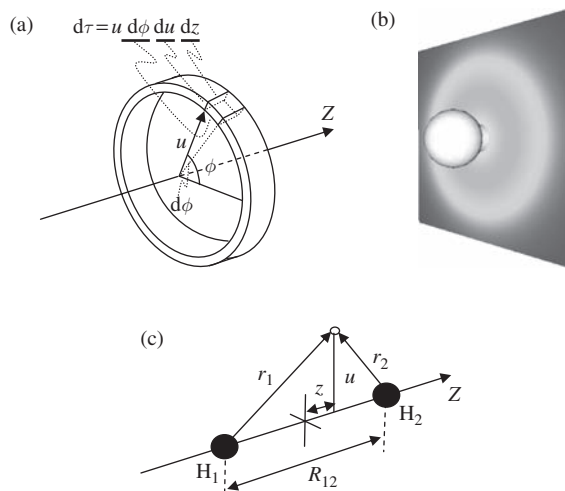


Figure A10.4 (a) The coordinate system and definition of an infinitesimal volume $d\tau$ for cylindrical polar coordinates, the factor u enters $d\tau$ because of the definition of an arc length using angles measured in radians. (b) A slice through the H–H bond showing the charge density on a plane perpendicular to the $\text{H}_2^+\text{C}_\infty$ axis. (c) The geometry used to obtain the distances r_1 and r_2 from each nuclear centre; these are the variables used in the s-orbital basis functions, since they define the nuclear–electron separations.

The analytical integrals required to obtain expectation values for the H_2^+ kinetic and potential energy contributions are still formidable; a better choice of coordinates for pen-and-paper solutions would actually be elliptical polar (see Further Reading section in this appendix). However, for the integrals required we will use numerical results generated using the *Mathematica* program, which also allows the plots of integrals over planes to be plotted against z . Powerful mathematics computer programs such as *Mathematica* take away the drudgery of long derivations for the integration or differentiation of complex functions and allow us to concentrate on the physical interpretation of results. While it is not essential to use *Mathematica* to follow the discussion here, familiarity with such a package can greatly increase your ability to play around with the equations used.

As an example of integration in cylindrical polar coordinates we will calculate the total probability density for the $|1\sigma_g^+\rangle$ MO using the integral

$$\langle 1\sigma_g^+ | 1\sigma_g^+ \rangle = N_{1g}^2 \int_{-\pi}^{\pi} d\phi \int_{-\infty}^{\infty} \int_0^{\infty} (s_1 + s_2)(s_1 + s_2) u \, du \, dz \quad (\text{A10.19})$$

The integral over the angle ϕ is written separately because we know the orbitals have cylindrical symmetry, i.e. they do not depend on ϕ but will vary with u and z . To cover all space we will have to integrate right around the molecular axis, and so the limits of the ϕ integral cover the range of 2π from $-\pi$ to π . The radial coordinate u is the distance from the molecular axis and can range from zero to infinity. The third coordinate in the

cylindrical polar system is the position along the axis z , which can take any value from $-\infty$ to $+\infty$. Figure A10.4a also shows that the infinitesimal volume for this coordinate system is $u \, d\phi \, du \, dz$.

The s -functions for the two atomic centres still follow the form given in Equation (A10.3), but we must express the distance from each nuclear centre in terms of the cylindrical polar coordinates. Figure 10.4c shows a general point (open circle) and the vectors required to find the distance from each H atom nucleus. It is straightforward to show that

$$r_1 = \left[\left(\frac{R_{12}}{2} + z \right)^2 + u^2 \right]^{1/2} \quad \text{and} \quad r_2 = \left[\left(\frac{R_{12}}{2} - z \right)^2 + u^2 \right]^{1/2} \quad (\text{A10.20})$$

where r_i is the distance of the general point from nucleus i and R_{12} is the internuclear separation. These expressions assume we have placed the molecule with the bond centre at the origin.

The angular integral in Equation (A10.19) simply gives 2π , and so

$$(1\sigma_g^+ | 1\sigma_g^+) = 2N_{1g}^2 \pi \int_{-\infty}^{\infty} \int_0^{\infty} (s_1 + s_2)(s_1 + s_2) u \, du \, dz \quad (\text{A10.21})$$

These integrals are carried out in the *Mathematica* sheet for this appendix available from the Website. As a check that we obtain unity for the normalized molecular orbital in the new coordinate system. The integrals over ϕ and u involve taking all contributions from planes perpendicular to the molecular axis at a particular z value, such as the plane illustrated in Figure 10.4b. By carrying out these integrations first we can plot the total for each plane against z and so obtain a picture of the contributions to the integral along the molecular axis. For this example, Figure 10.3b and d show a comparison of the calculated total density on each plane as a function of z for the bonding and antibonding MOs. Each plot includes a comparison with the same calculation for an isolated H atom at the position of the leftmost nucleus (H_1).

The bonding orbital shows a build-up of density compared with the isolated atom, while the antibonding orbital gives rise to a lower total density in the internuclear region, going to zero at the bond centre. This interpretation was also drawn from the plots of the wavefunctions along the molecular axis (Figure 10.3a and c). However, as we are now integrating over an entire slice of density at each z -coordinate, the curves in Figure A10.3b and d are smoother and do not show the cusps (sudden change in gradient as we pass through the nuclei) that are seen in the plots along the molecular axis. Notice also that the dip in the density between the nuclei in the bonding orbital is much less than for the axial plot (Figure A10.3b compared with Figure A10.3a), showing that the total density integrated over planes between the H nuclei in the bonding orbital is almost constant.

In the remainder of this appendix we will use this type of plot to illustrate the contributions to the calculated expectation values from planes perpendicular to the molecular axis.

A10.6 H_2^+ : the Electron Kinetic Energy

The kinetic energy for an electron in the $|1\sigma_g^+\rangle$ bonding orbital will be given by

$$\langle T \rangle_{1\sigma_g^+} = -\frac{1}{2} \langle 1\sigma_g^+ | \nabla^2 | 1\sigma_g^+ \rangle = N_{1g}^{-2} \pi \int_{-\infty}^{\infty} \int_0^{\infty} (s_1 + s_2) [\nabla^2(s_1 + s_2)] u \, du \, dz \quad (\text{A10.22})$$

And with the electron in the antibonding $|2\sigma_u\rangle$ orbital we would have

$$\langle T \rangle_{2\sigma_u^+} = -\frac{1}{2} \langle 2\sigma_u^+ | \nabla^2 | 2\sigma_u^+ \rangle = N_{2u}^{-2} \pi \int_{-\infty}^{\infty} \int_0^{\infty} (s_1 - s_2) [\nabla^2(s_1 - s_2)] u \, du \, dz \quad (\text{A10.23})$$

Now, we are in cylindrical polar coordinates and so must use the appropriate form of the Laplacian:

$$\nabla^2 = \frac{1}{u} \frac{\partial}{\partial u} \left(u \frac{\partial}{\partial u} \right) + \frac{1}{u^2} \frac{\partial^2}{\partial \phi^2} + \frac{\partial^2}{\partial z^2} \quad (\text{A10.24})$$

We have chosen cylindrical polar coordinates to exploit the cylindrical symmetry of the H_2^+ molecular ion. In the application of the Laplacian there will be no variation in the wavefunctions with the angular coordinate, so the differential with respect to ϕ will give zero and so only the derivatives with respect to u and z need be considered. The results still have to be integrated with respect to the ϕ , it is just that the same value of the integrand will occur at any point on a circle centred on the molecular axis and in a plane perpendicular to it. This has already been exploited in Equations (A10.22) and (A10.23) with the integration ϕ giving 2π as before. The full detail of applying the Laplacian to the molecular orbitals is set out in the *Mathematica* sheet accompanying this appendix available from the Website.

The kinetic energy integrated over planes perpendicular to the molecular axis is plotted in Figure A10.5. The bonding orbital (Figure A10.5a) shows a lower kinetic energy

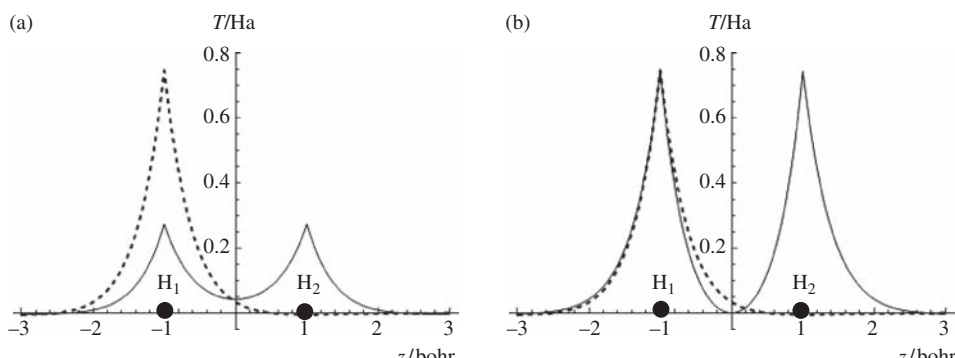


Figure A10.5 Plot of the kinetic energy integrated over planes perpendicular to the molecular axis against the z coordinate for (a) $|1\sigma_g^+\rangle$ and (b) $|2\sigma_u^+\rangle$. The dashed lines in each case show the same data for an isolated H atom placed at the H_1 position.

than for the reference atomic orbital state (shown as a dotted line). The lower kinetic energy corresponds to the smooth density plotted in Figure A10.3b, which has a low second derivative. The total integrated area under this curve gives an expectation value for the kinetic energy of $\langle T \rangle_{1\sigma_g^+} = 0.3863$ Ha, compared with the 0.5 Ha we found for the atomic case above. So the kinetic energy of the electron has been reduced on bond formation, and in this AO-based model this is one contribution to the stabilization of the H_2^+ ion.

The kinetic energy for the antibonding orbital is plotted in Figure A10.5b. The overlay of the atomic result in this case shows that the kinetic energy distribution in the $|2\sigma_u^+\rangle$ orbital has a very similar shape to the reference atomic plot for the H_1 atom in isolation. In the molecule, the second nucleus is equivalent, and so the electron kinetic energy has another peak associated with the part of the wavefunction near to this nucleus. The net effect is that the antibonding molecular orbital of the H_2^+ ion has a much higher electronic kinetic energy than the reference atomic state, $\langle T \rangle_{2\sigma_u^+} = 0.9363$ Ha. So, an electron occupying the antibonding orbital would have a higher kinetic energy than for the atomic state.

Figure A10.3 shows that the bonding MO, $|1\sigma_g^+\rangle$, has no node – it does not pass through zero – whereas the antibonding $|2\sigma_u^+\rangle$ wavefunction has a node at the bond centre. The observation that the orbital with a node feature has the higher kinetic energy is quite general, and we use it in the main text when discussing the MOs of phenanthrene (Chapter 7). The node introduces a greater degree of curvature, leading to significant second-derivative values as the wavefunction twists around to pass through the zero point.

A10.7 H_2^+ : the Electronic Potential Energy

The potential energy of an electron in a molecular orbital involves interactions of the electron with the two nuclei; for the bonding orbital this is

$$\langle 1\sigma_g^+ | (V_1 + V_2) | 1\sigma_g^+ \rangle = N_{1g}^{-2} (\langle s_1 | + \langle s_2 |) (V_1 + V_2) (\langle s_1 | + \langle s_2 |) \quad (A10.25)$$

where V_1 and V_2 are the potential energy operators for an electron due to its interaction with nuclei 1 and 2 respectively, i.e.

$$V_1 = -\frac{1}{r_1} \quad \text{and} \quad V_2 = -\frac{1}{r_2} \quad (A10.26)$$

The negative signs in these expressions arise from the opposite charges on the electron and nuclei.

The molecular potential energy must also take into account the nuclear–nuclear interaction, which is simply the Coulomb energy of the two protons:

$$V_{nn} = \frac{1}{R_{12}} \quad (A10.27)$$

Since these are to be treated as fixed point particles, this gives the potential energy of the nuclear–nuclear term directly.

The symmetry of the molecule means that any integral involving V_1 will have an equivalent from the V_2 potential; for example, $\langle s_1 | V_1 | s_1 \rangle = \langle s_2 | V_2 | s_2 \rangle$. This allows the set of integrals obtained on multiplying out Equation (A10.24) to be reduced to just three terms:

$$\langle 1\sigma_g^+ | (V_1 + V_2) | 1\sigma_g^+ \rangle = 2N_{1g}^2 (\langle s_1 | V_1 | s_1 \rangle + \langle s_2 | V_1 | s_2 \rangle + 2\langle s_1 | V_1 | s_2 \rangle) \quad (\text{A10.28})$$

The electronic potential energy of the single H atom on the reactant side of Equation (A10.1) is $\langle s_1 | V_1 | s_1 \rangle$, and so we can write down the potential energy change for the electron moving from the atomic 1s to the $1\sigma_g$ orbital of the cationic molecule as

$$\begin{aligned} \langle U(H_2^+) \rangle_{1\sigma_g^+} - \langle U(H) \rangle &= (2N_{1g}^2 - 1) \langle s_1 | V_1 | s_1 \rangle + 2N_{1g}^2 (\langle s_2 | V_1 | s_2 \rangle \\ &\quad + 2\langle s_1 | V_1 | s_2 \rangle) + \frac{1}{R_{12}} \end{aligned} \quad (\text{A10.29})$$

This is the potential energy change most relevant to bond formation, as it compares the molecular ion in its electronic ground state with the atomic reference, which is also an electronic ground state.

A similar procedure for the antibonding MO gives the energy difference between the molecular ion in its first excited state and the H atom reference as:

$$\begin{aligned} \langle U(H_2^+) \rangle_{2\sigma_u^+} - \langle U(H) \rangle &= (2N_{2u}^2 - 1) \langle s_1 | V_1 | s_1 \rangle \\ &\quad + 2N_{2u}^2 (\langle s_2 | V_1 | s_2 \rangle - 2\langle s_1 | V_1 | s_2 \rangle) + \frac{1}{R_{12}} \end{aligned} \quad (\text{A10.30})$$

Comparing results from Equations (A10.29) and (A10.30) would allow us assess the effect of exciting the molecular ion, e.g. by irradiating with light of a specific frequency.

The first three terms in these expressions give the contributions to the change in the potential energy of the electron as it moves from the atomic 1s orbital to either of the molecular orbitals:

Term 1,
 $(2N_{1g}^2 - 1) \langle s_1 | V_1 | s_1 \rangle$

Equation (A10.18)
 says:

$$N_{1g} = \frac{1}{\sqrt{2(1 + S_{12})}}$$

The origin of the integral $\langle s_1 | V_1 | s_1 \rangle$ is illustrated in the plot of Figure A10.6b. It involves the interaction between a nucleus and the part of the electron density described by the associated s-orbital, which is attractive and so gives a negative result. The thin solid line in Figure A10.6a shows the integral over planes plotted as a function of z . The corresponding integral for the atomic $|s\rangle$ orbitals is shown as a dotted line on the same figure and is split evenly between the two nuclei for comparison. In the bonding MO the electron population is lower than in the atomic state because the electron is now shared with the other nucleus. This results in the positive difference shown as the thick black line in Figure A10.6a.

We can also see that a positive value should occur for this term from the form of the normalization coefficient in Equation (A10.18). The overlap integral S_{12} can only be positive, so that $2N_{1g}^2 \leq 1$ (see Figure A10.7), which means that term 1 in Equation (A10.29) gives a positive, destabilizing, contribution to the bond formation energy.

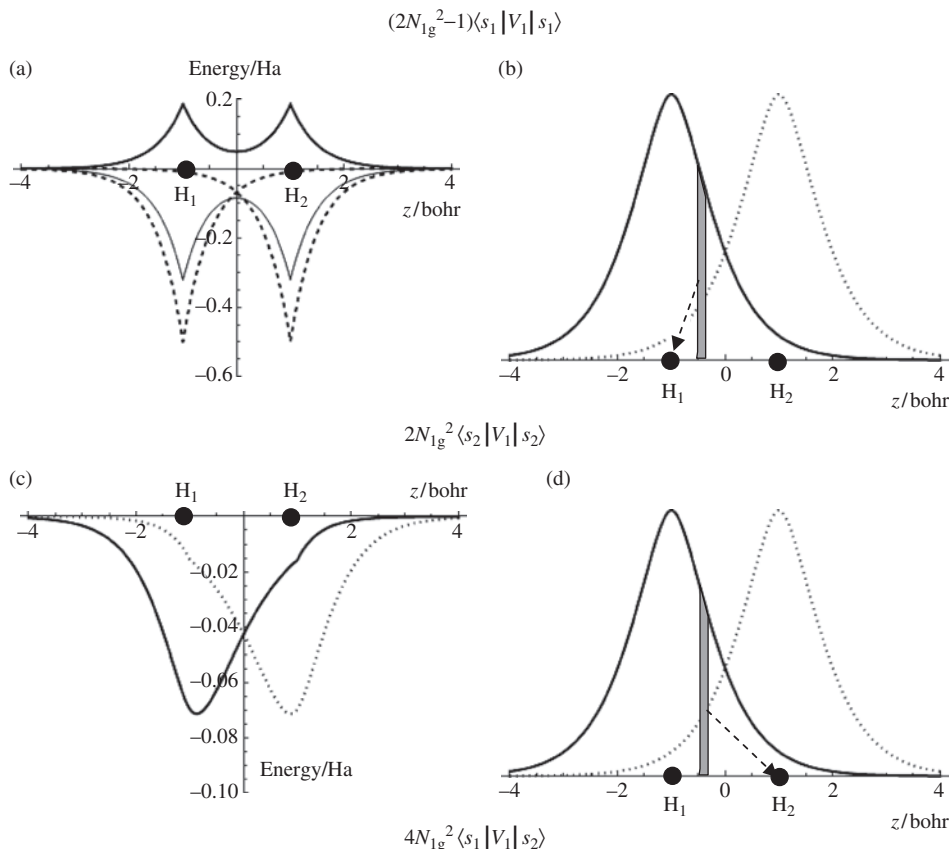
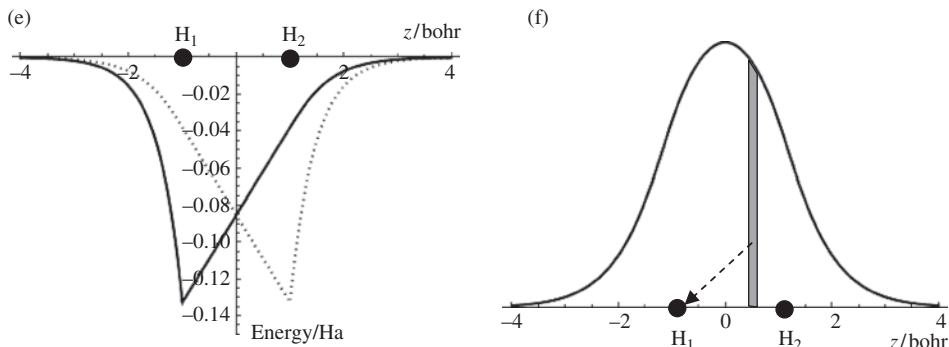
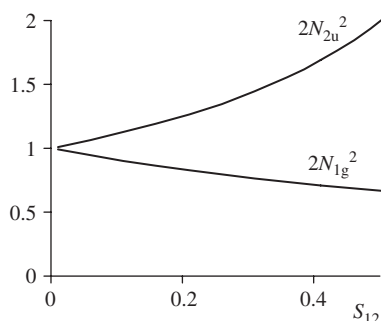


Figure A10.6 The contributions to the three terms for the electron–nuclear potential energy difference between H_2^+ with the electron in $|1\sigma_g^+\rangle$ and H integrated over planes perpendicular to the molecular axis. (a) The interaction of the density described by each $|s_i\rangle$ basis function with the corresponding nuclear centre (thin line) is compared with the same interaction for the isolated atoms scaled by a factor of 0.5 (dashed line); the difference gives a positive contribution to the bond formation energy (thick line). An illustration of the origin of this interaction is given in (b). (c) The interaction of the density described wholly by the $|s_1\rangle$ basis function with the potential due to the H_2 nucleus, as illustrated in (d), the corresponding integral for $|s_2\rangle$ with H_1 is shown as a dotted line. (e, f) The integral value versus z and its origin from the overlap density for term 3 of the electron–nuclear potential energy discussed in the text.

**Figure A10.6** (continued).**Figure A10.7** The dependence of the prefactor in the potential energy terms on the overlap integral S_{12} .

$$(2N_{2u}^2 - 1) \langle s_1 | V_1 | s_1 \rangle$$

Equation (A10.18) says:

$$N_{1g} = \frac{1}{\sqrt{2(1 + S_{12})}}$$

$$\text{Term 2, } 2N_{1g}^2 \langle s_2 | V_1 | s_2 \rangle$$

For the antibonding case we have a very similar first term in Equation (A10.29). Figure A10.3d shows that the lower density in the internuclear region actually means that an electron is more likely to be closer to its own nucleus than in the reference state in which the electron is split evenly between noninteracting atoms. This makes the potential energy from this term more negative than in the atomic reference state (Figure A10.8a) and so a stabilizing contribution is obtained.

This time the normalization constant has $-S_{12}$ in the denominator and so $2N_{2u}^2 \geq 1$, confirming that this term gives an overall negative contribution to the bond formation energy for an H_2^+ molecular ion with the electron in the antibonding orbital.

In the MOs the electron population described wholly by $|s_2\rangle$ interacts with centre 1 and that wholly described by $|s_1\rangle$ interacts with centre 2. These interactions are not present in the atom; since electron–nuclear interactions will be attractive, this

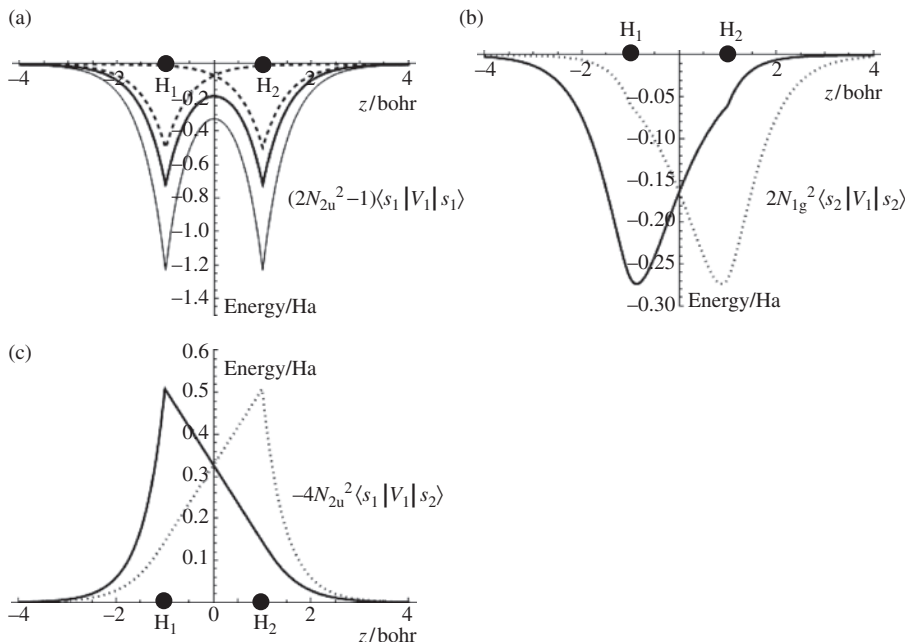


Figure A10.8 The contributions to the three terms for the electron–nuclear potential energy difference between H_2^+ in the first excited state, with the electron in $|2\sigma_u^+\rangle$ and H integrated over planes perpendicular to the molecular axis. (a) The interaction of the density described by each $|s_i\rangle$ basis function with the corresponding nuclear centre (thin line) is compared with the same interaction for the isolated atoms scaled by a factor of 0.5 (dashed line); the difference gives a negative contribution to the bond formation energy (thick line). (b) The interaction of the density described wholly by the $|s_1\rangle$ basis function with the potential due to the H_2 nucleus; the corresponding integral for $|s_2\rangle$ with H_1 is shown as a dotted line. (c) The integral value versus z from the interaction of the overlap density with H_1 ; the interaction with H_2 is shown as a dotted line.

tends to stabilize the molecule. Figure A10.6d shows the origin of this term and Figure A10.6c illustrates the contributions averaged over planes along the molecular axis for the bonding MO. A small kink feature can be seen for the integral over planes for each s-orbital at the z coordinate of the nucleus. At this point the centre of the integration plane gives a zero distance between the elemental charge and the nuclear centre.

$$2N_{2u}^2 \langle s_2 | V_1 | s_2 \rangle$$

In the antibonding orbital we again have a negative contribution from the second term in Equation (A10.30). Comparison of Figures A10.6c and A10.8b shows that the integrals over planes of this term for $|2\sigma_u\rangle$ are larger than for $|1\sigma_g\rangle$ at the same z . This is due to the behaviour of the $2N_{2u}^2$ factor as a function of the overlap integral S_{12} (Figure A10.7).

Term 3, $4N_{1g}^2 \langle s_1 | V_1 | s_2 \rangle$

The electron density described by the overlap $\langle s_1 | s_2 \rangle$ integral will have a Coulomb interaction with centre 1; this will be attractive. The factor of 4 arises from an identical contribution of the $\langle s_2 | s_1 \rangle$ density with centre 1 and both overlaps with centre 2. Figure A10.6e and f shows the integral and the overlap density respectively for the bonding MO. The overlap builds up charge between the centres, but this charge is spread wider than the bond separation and so contributions to this term also occur further out. The ‘shielding’ of the internuclear interaction is really the sum of these terms and the nucleus–nucleus potential given by Equation (A10.26), and so this may be less effective than we might expect. In the energy integrals there are, again, sharp turning points at the nuclear centre used in the potential operator.

$-4N_{2u}^2 \langle s_1 | V_1 | s_2 \rangle$

In the antibonding orbital the overlap integrals correspond to the loss of electron density from the internuclear region and a minus sign appears for this contribution in Equation (A10.28). The integral still evaluates to a negative value, and so this becomes a positive term as plotted in Figure A10.8c. Once again, the difference in the normalization constant means that this term has a greater magnitude than that for the bonding orbital.

An important check on the potential energy contributions suggested by Equations (A10.29) and (A10.30) is to consider what happens as R_{12} becomes large, i.e. we break the molecular bond. In the limit of separated, noninteracting, nuclei the overlap S_{12} must become zero, and so term 3 vanishes, because it gives the interaction of the density described by S_{12} with the nuclei. With no overlap we also obtain $N_{1g}^2 = N_{2u}^2 = \frac{1}{2}$ from Equations (A10.18), and so term 1 becomes zero. Term 2 involves an interaction between centre 1 and the remote charge density on atom 2, which will also be vanishingly small due to the inverse power dependence of Coulomb’s law. So, at the limit of large R_{12} there is no difference between the potential energies of either MO and an isolated H atom infinitely separated from H^+ , as required.

However, the $H + H^+$ system contains two different species and so cannot conform to $D_{\infty h}$ symmetry. At some point, as the bond is stretched, the electron must decide ‘which way to jump’, and this will destroy the molecular symmetry. By sticking to $D_{\infty h}$ we are forced to have a dissociated state of two $H^{0.5+}$ ions. This has the same energy as the ‘real’ reactants, but is not a correct physical picture.

The contributions to the total potential energy of the H_2^+ cation as a function of the internuclear distance R_{12} with the electron in the ground-state MO, $|1\sigma_g^+\rangle$, are shown in Figure A10.9a. In the bonding orbital, the total potential energy is always positive and so tends to favour dissociation of the molecule into its constituent atom and ion at all internuclear separations.

In contrast, Figure A10.9b shows that if we place the electron in the first excited state, $|2\sigma_u\rangle$, then the total potential energy appears to be negative when this antibonding MO is

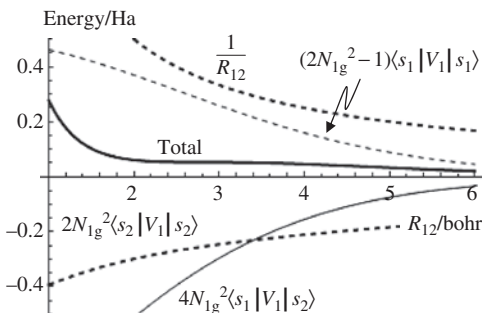
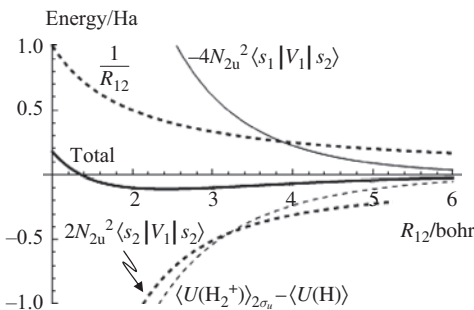
(a) Contributions to ground-state potential energy $\langle U(H_2^+) \rangle_{1\sigma_g} - \langle U(H) \rangle$ (b) Contributions to first excited-state potential energy $\langle U(H_2^+) \rangle_{2\sigma_u} - \langle U(H) \rangle$ 

Figure A10.9 The various terms in the electron–nuclear potential energy plotted as a function of internuclear separation R_{12} for (a) H_2^+ in the ground state, with the electron in $|1\sigma_g^+\rangle$, and (b) H_2^+ in the first excited state, with the electron in $|2\sigma_u^+\rangle$. In each case the internuclear repulsion energy is also shown, and the solid lines marked ‘Total’ are estimates for the bond formation energy at each R_{12} value. In these calculations, the decay constant of the basis functions is fixed at the AO value ($\zeta = 1$).

occupied. This occurs because in the antibonding MO the contributions from the integrals involving only a single s-orbital are both negative and outweigh the unfavourable effect from the overlap integral. In the antibonding combination the electron density is, on average, closer to the nuclei because of the node at the bond centre than in the reference atomic state (Figure A10.3d).

A10.8 The Chemical Bond Formation Energy Based on Rigid Atomic Orbitals

The above discussion of the potential energy should be unsettling: we have found that it is the kinetic energy in H_2^+ that stabilizes the chemical bond with the electron in the ground state, while the potential energy is destabilizing. This seems to contradict the commonly proposed picture of the chemical bond, in which the overlap density stabilizes the

molecule through the resulting attractive interaction with the nuclei. This interaction is attractive (term 3 above), but, for H_2^+ at least, the electron density in the internuclear region will always be less than unity and will be insufficient to overcome the repulsive terms, particularly that of the two nuclei.

We will find that the potential energy is important and stabilizing the bond. The fault lies in the use of the AOs to construct MOs. We have treated these as rigid entities with a radial decay set for the atomic state, but this is not appropriate to the molecular environment.

To show how the rigid orbital model fails, we will estimate the bond formation energy using the terms described above and test the validity of the result with the virial theorem.

Using the experimental H_2^+ bond length of 2 bohr from Table 7.1, we find

$$\langle T(\text{H}_2^+) \rangle_{1\sigma_g^+} - \langle T(\text{H}) \rangle = 0.3863 - 0.5000 = -0.1137 \text{ Ha}$$

For Equation (A10.29), working through the integrals with *Mathematica* gives

$$\text{Term 1 : } (2N_{1g}^2 - 1) \langle s_1 | V_1 | s_1 \rangle = 0.3697 \text{ Ha}$$

$$\text{Term 2 : } 2N_{1g}^2 \langle s_2 | V_1 | s_2 \rangle = -0.2979 \text{ Ha}$$

$$\text{Term 3 : } 4N_{1g}^2 \langle s_1 | V_1 | s_2 \rangle = -0.5118 \text{ Ha}$$

which leads to a change in electron–nuclear interaction energy on bond formation of

$$\langle U(\text{H}_2^+) \rangle_{1\sigma_g^+} - \langle U(\text{H}) \rangle = -0.4400 \text{ Ha}$$

The nuclear–nuclear repulsion term from Equation (A10.29) is 0.5 and, as expected from Figure A10.9, this wins out to give a slightly positive (0.0600 Ha) contribution to the bond energy. Adding the kinetic and potential energy contributions together, we have an estimate for the bond energy of H_2^+ of -0.0537 Ha or -141 kJ mol^{-1} .

This is 114 kJ mol^{-1} lower in magnitude than the experimental bond energy (255 kJ mol^{-1} given in Table 7.1; remember that experimental bond energies give the energy required to sever the bond, while we calculate the energy change on forming it).

Perhaps a more serious problem is uncovered if we test the virial theorem for the bonding orbital. Using the AOs as basis functions we have found that the kinetic energy is $\langle T(\text{H}_2^+) \rangle_{1\sigma_g^+} = 0.3863 \text{ Ha}$ and the potential energy $\langle U(\text{H}_2^+) \rangle_{1\sigma_g^+} = -0.9400 \text{ Ha}$. The virial theorem requires that the ratio of kinetic to potential energy for this system should be $-1/2$, but this data gives

$$\frac{\langle T(\text{H}_2^+) \rangle_{1\sigma_g^+}}{\langle U(\text{H}_2^+) \rangle_{1\sigma_g^+}} = -\frac{0.3863}{0.9400} = -0.4110$$

In fact, if we plot the expectation values for kinetic and potential energies as a function of the bond length, then the optimum value of the total energy using the atomic functions occurs around 2.49 \AA , as shown in Figure A10.10. This is significantly longer than the

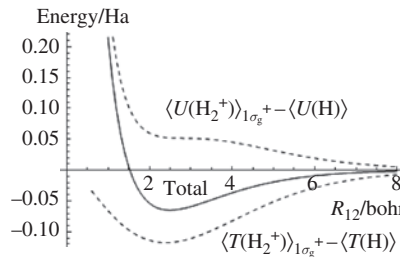


Figure A10.10 The bond formation energy (labelled ‘Total’) for H_2^+ in the electronic ground state estimated using rigid basis functions ($\zeta = 1$) as a function of R_{12} . The contributions from the expectation values of the kinetic ($\langle T(H_2^+) \rangle_{1\sigma_g^+} - \langle T(H) \rangle$) and potential ($\langle U(H_2^+) \rangle_{1\sigma_g^+} - \langle U(H) \rangle$) energies are shown as dashed lines.

experimental value. At this geometry the $\langle T(H_2^+) \rangle_{1\sigma_g^+} = 0.3827$ Ha and $\langle U(H_2^+) \rangle_{1\sigma_g^+} = -0.9475$ Ha, a ratio of -0.4039 , so the virial theorem for the electron is still not obeyed.

For the antibonding state, working through the integrals from Equation (A10.30) with *Mathematica* gives

$$\text{Term 1 : } (2N_{2u}^2 - 1) \langle s_1 | V_1 | s_1 \rangle = -1.4181 \text{ Ha}$$

$$\text{Term 2 : } 2N_{2u}^2 \langle s_2 | V_1 | s_2 \rangle = -1.1426 \text{ Ha}$$

$$\text{Term 3 : } -4N_{2u}^2 \langle s_1 | V_1 | s_2 \rangle = 1.9635 \text{ Ha}$$

These sum to produce a change in electron–nuclear interaction energy on bond formation, if the electron were to occupy the antibonding molecular orbital of

$$\langle U(H_2^+) \rangle_{2\sigma_u^+} - \langle U(H) \rangle = -0.5972 \text{ Ha}$$

Once again, the nuclear–nuclear repulsion term is 0.5 Ha, and so we now find a slightly negative (-0.0972 Ha) contribution to the bond formation energy with the electron in the antibonding MO. This would be more than offset by the kinetic energy, which contributes 0.4363 Ha to the bond formation energy with the electron in the $|2\sigma_u^+\rangle$ orbital. However, it still appears counterintuitive that the antibonding orbital should have a lower potential energy than the bonding orbital.

The lack of a virial theorem for the molecule with the electron in $|1\sigma_g^+\rangle$, and the strange behaviour of the potential energy term, implies that we have not really found the true ground-state wavefunction.

The picture is not yet complete, and Problem A10.1 indicates why. The s-orbitals used to construct the bonding and antibonding combinations have radial decays optimized for the atomic state. In the H_2^+ ion there are two nuclei, and so there is no reason why this decay factor should be suited to describe the MO. To address this we will optimize the energy with respect to the radial decay of the basis functions.

A10.9 Optimal Radial Decay of Molecular Orbitals

In Problem A10.1 we proposed a trial form for the 1s orbital in which the decay with distance from the nucleus is controlled by a parameter ζ :

$$|s_{\text{tr}}\rangle = \frac{\zeta^{3/2}}{\pi} \exp(-\zeta r) \quad (\text{A10.31})$$

It was also shown that the decay constant that was consistent with the virial theorem gave the lowest total energy for the atomic 1s orbital. We can now apply this to the molecular case by recalculating the kinetic, potential and total energies for the electron in the $|1\sigma_g^+\rangle$ orbital in H_2^+ fixed at the experimental bond length but for a range of decay constants. The result is shown in Figure A10.11.

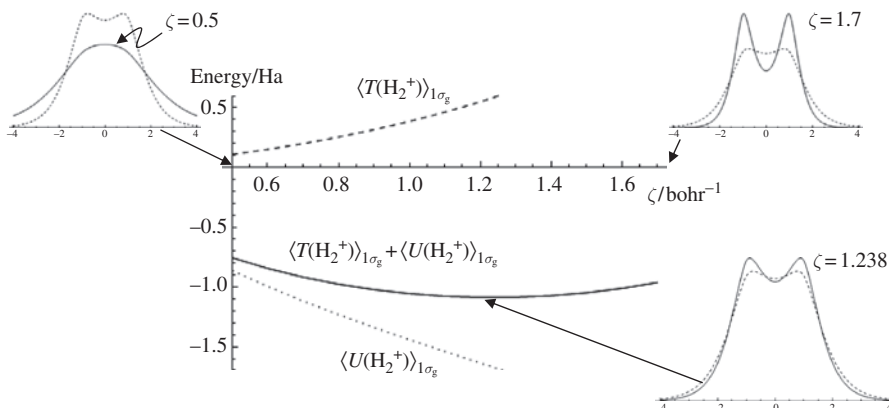


Figure A10.11 Plot of expectation values for the potential energy $\langle U(\text{H}_2^+) \rangle_{1\sigma_g}$, kinetic energy $\langle T(\text{H}_2^+) \rangle_{1\sigma_g}$ and total energy of an electron in the $|1\sigma_g^+\rangle$ MO of H_2^+ at a nuclear separation of $R_{12} = 2$ bohr against the basis function decay factor ζ . The diagrams inset to the side of the plot show the MO density at the ζ values indicated compared with the $\zeta = 1$ distribution (dashed lines).

For $\zeta < 1 \text{ bohr}^{-1}$, the $|1\sigma_g^+\rangle$ orbital becomes more spread out; this has the effect of reducing the kinetic energy, as the MO has less curvature than when we use the AO decay constant in the basis. The more diffuse orbital also increases the potential energy, as the electron spends more time away from the nuclei. This wins out and the energy increases compared with the $\zeta = 1$ reference.

For $\zeta > 1 \text{ bohr}^{-1}$, the $|1\sigma_g^+\rangle$ orbital becomes more compact and the potential energy goes down. Of course, this also confines the electron more closely and increases the curvature of the wavefunction, and thus the kinetic energy. Near to unity the net effect is a lowering of the total energy, and a minimum is found for $\zeta = 1.238 \text{ bohr}^{-1}$. At higher values of the decay constant the kinetic energy increases more rapidly than the potential falls.

With this value of ζ at a bond length of 2 bohr we find

$$\langle T(H_2^+) \rangle_{1\sigma_g^+} = 0.5871 \text{ Ha} \quad \langle U(H_2^+) \rangle_{1\sigma_g^+} = -1.1726 \text{ Ha Ha}$$

and so for the virial test we have

$$\frac{\langle T(H_2^+) \rangle}{\langle U(H_2^+) \rangle} = -\frac{0.5871}{1.1726} = -0.5003$$

For the optimized decay constant, the virial theorem is satisfied within the significance of the data. The total energy is also lower than that obtained with the rigid orbital model and we now have an estimated bond formation energy of -0.0855 Ha or -224 kJ mol^{-1} . This is now remarkably close to the 255 kJ mol^{-1} for the bond energy given in Table 7.1, considering that we have neglected the zero-point vibrational energy and the basis is still quite simple (see Appendix 11).

Note that now the electron kinetic energy is greater than the atomic reference state and stability is provided by the lower potential energy. The shrinking of the AOs around the nuclei increases the electron–nuclear favourable interactions and now outweighs the nuclear–nuclear repulsion.

A plot of the bond formation energy as a function of the nuclear separation with the decay constant optimized is given in Figure A10.12a. The minimum for the total energy has now shifted to 2 bohr and the potential well is deeper than for the same calculation with the AO value of ζ . However, at large separation the potential is now incorrect, as the decay constant is too large for the atomic state.

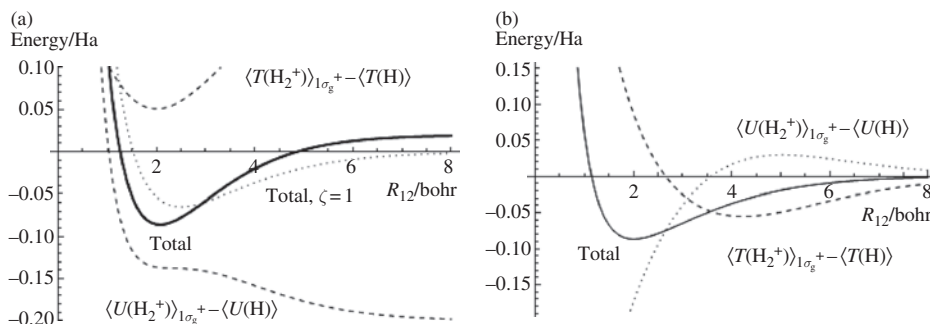


Figure A10.12 (a) Plot of kinetic energy, potential energy contributions and the total bond formation energy as a function of R_{12} using basis functions optimized at $R_{12} = 2$ bohr, i.e. rigid orbitals with $\zeta = 1.238$; the total energy plot for the rigid atomic basis functions ($\zeta = 1$) is included for comparison. (b) Plot of the energy contributions and total with the basis decay constant obtained by minimizing the total energy at each R_{12} value.

A more accurate picture can be obtained by optimizing the value of ζ for each internuclear separation so that the electron wavefunction responds to the changing environment as the molecule is formed. This has been done in Figure A10.12b, which shows that the

correct behaviour is obtained at large R_{12} . We can also see from this plot that, at relatively large separations (above 3.5 bohr), the main attraction results from a decrease in the electron's kinetic energy which acts against the repulsion generated by the potential terms. Only as the bond length approaches the observed H_2^+ internuclear separation does the potential energy switch over to negative values, and the confinement of the electron gives a net positive kinetic energy. Thus, at the optimal bond length the attractive contribution to the bond formation energy comes from the potential energy terms.

The same procedure can be followed for the first excited state, and the energy components and total as function of R_{12} are shown in Figure A10.12. At each point the decay constant has been optimized to give the lowest possible energy for the electron in the antibonding $|2\sigma_u^+\rangle$ orbital. The total energy is positive everywhere, tending to zero only at large R_{12} . So, the excited state of H_2^+ is unstable with respect to dissociation. The potential energy is negative down to almost the H_2^+ bond length, where it is practically zero. The molecule is actually destabilized by the increased kinetic energy in the antibonding state.

The value obtained for the optimal decay constant reflects the electron response to the potential of the nuclei. Since the electron distribution in the antibonding orbital is quite different to that in the bonding state, we obtain different basis function decay constants for the two orbitals. The optimal values of ζ as a function of the internuclear separation is plotted in Figure A10.13. We have already seen that for the ground state the basis functions in the $|1\sigma_g^+\rangle$ orbital contract as the molecule is formed, leading to a lowering of the potential energy. In the excited state, the values of ζ that minimize the total energy in the $|2\sigma_u^+\rangle$ orbital for R_{12} below around 4 bohr are less than 1 bohr $^{-1}$. This corresponds to an expansion of the MO compared with that obtained with the atomic basis functions, which will tend to decrease the kinetic energy by confining the electron less closely.

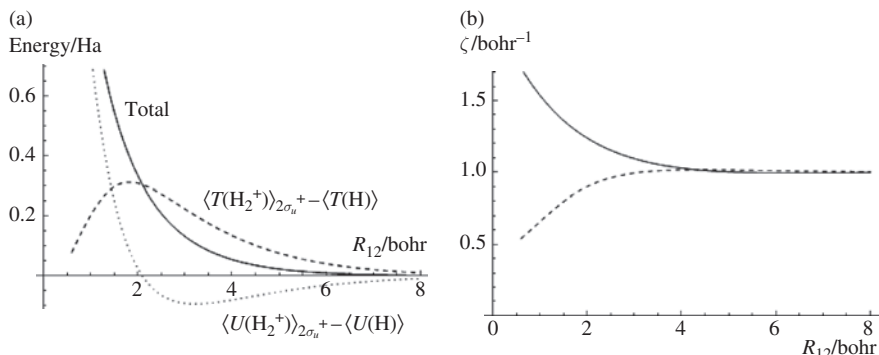


Figure A10.13 The optimized values of the basis decay factor ζ as a function of internuclear separation R_{12} for the $|1\sigma_g^+\rangle$ (solid line) and $|2\sigma_u^+\rangle$ (dashed line) MOs.

An important point to note from this study of a relatively simple system is that the AO functions as derived for isolated atoms are not the ideal basis for constructing MOs. In ‘real’ molecular systems the orbital shape adapts to the potential it experiences. For quantitative work we require basis sets that can reproduce this by responding to the potential

of the nuclei and, for larger problems, to the potential of the other electrons. This has led to the development of multiple ζ basis sets which can provide the required flexibility by mixing several functions of the same angular momentum but with differing radial decay constants.

In this example, we could have taken the linear combination of one function with $\zeta = 1 \text{ bohr}^{-1}$ and another with $\zeta = 1.238 \text{ bohr}^{-1}$ and used that as the basis function on each H atom. By adjusting the coefficient of each function in this linear combination so that the total energy is always minimized, we could then reproduce the ‘ideal’ orbital shape at all R_{12} values from the optimal bond length to larger separations. The idea of multiple ζ basis sets is encountered again in Appendix 11.

Further Reading

The use of the bra-ket notation is fully discussed in:

Dirac PAM (1981) *The Principles of Quantum Mechanics*. Oxford Science Publications (ISBN 0-19-852011-5).

The solution of the H_2^+ problem using elliptical polar coordinates and with more elaborate sets of basis functions can be found in:

McQuarrie DA (2008) *Quantum Chemistry*. University Science Books (ISBN 978-1-891389-50-4).

The *Mathematica* program is marketed by Wolfram Research, see: <http://www.wolfram.com/>.

Appendix 11

H₂O Molecular Orbital Calculation in C_{2v} Symmetry

The MOs plotted for molecules containing main-group elements in Chapter 7 were produced using restricted Hartree–Fock (RHF)-level calculations. In this approach the electron–nuclear and electron–electron interactions are taken into account in the Hamiltonian through Coulomb and exchange integrals, as described in the Further Reading section at the end of this appendix. The term ‘restricted’ means that spin-up and spin-down electrons must occupy identical spatial orbitals.

The inclusion of the electron–electron interaction in these calculations involves terms in the Hamiltonian for each MO which depend on the current shape of all the other occupied states. The shapes of the orbitals, in turn, are controlled by the sets of coefficients in the SALCs that describe the MOs in terms of basis functions. The optimization of the SALCs involves finding the set of coefficients which minimize the total energy of the molecule. Each electron experiences the potential of all the others, and so the MOs affect one another’s energies. The problem must be solved in such a way that the electron-generated potentials and MOs are consistent with one another.

The results of such self-consistent field (SCF) calculations appear as coefficients for the linear combination of basis functions used in the calculations. In Chapter 7 we used a simple basis consisting of only one function per AO. However, we have seen in Appendix 10 that these minimal basis sets do not give reliable energies even for the simple problem of H₂⁺ unless the basis function decay constants ζ are adjusted. In calculations for larger molecules of the type discussed here, this is accommodated by the use of more complex basis sets. These allow the orbital radial flexibility to be described by combining several basis functions with differing, but fixed, values of ζ .

In this appendix we will look in detail at the results for the H₂O example from Chapter 7, which employed a set of basis functions developed by Pople and co-workers with the code name 6-31G. This code tells us about the types and numbers of functions used in the

calculations. The letter ‘G’ says that Gaussian-type functions are used for the radial part of the AOs; that is, for a Cartesian basis set the functions used are

$$\chi_G = Nx^a y^b z^c \exp(-\zeta r^2) \quad (\text{A11.1})$$

where N is a normalization coefficient and the values of a , b and c are set by the angular momentum quantum number of the orbital. A set of basis functions for a particular angular momentum take all positive values of a , b and c for which $l = a + b + c$. For example, the set p-orbitals have $l = 1$ and p_x , p_y and p_z are generated by taking $a = 1$, $b = 1$ and $c = 1$ in turn with the other two powers set to zero. The radial decay of Equation (A11.1) is controlled by the value of the ζ (zeta) parameter; the larger this is, the more slowly the function decays with the distance r from the nuclear centre.

Gaussian functions have the useful property that the product of two neighbouring functions can be expressed as another Gaussian whose position and shape are easily related to the parent functions. Hartree–Fock calculations require a large number of integrals over products of basis functions. These generate accurate expectation values for the energy (kinetic, electron–nuclear, including the resonance integral and electron–electron) and overlap integrals mentioned in Section 7.2. The process of calculating these integrals is greatly speeded up by the use of Gaussian functions. However, in Appendix A9 we found that the radial solutions to the Schrödinger equation for the H atom decay with the exponential of r and not r^2 . So, using a single Gaussian per AO will give a poor representation of the radial form of the AOs. To counter this, each basis function is generated from a set of Gaussian functions:

$$\phi = \sum_{p=1}^n d_p \chi_G(\zeta_p) \quad (\text{A11.2})$$

The basis functions used in the calculation of MOs are these linear combinations of n Gaussian functions. The mixing of the Gaussians is controlled by the contraction coefficients d_p , which are determined as part of the basis set parameterization.

The Pople code tells us the level of contraction (value of n) for each component of the basis set. In 6-31G the core basis functions are built from six Gaussians, while each valence shell AO has one basis function consisting of three Gaussians and one single Gaussian. This means that, in the valence region, each atom has two sets of basis functions for each AO, allowing additional flexibility in the optimization of the radial decay of the functions for each particular MO. In an MO, all three functions can play a role. For example, the contribution of the C s-type basis functions to the $2a_1$ MO of methane (see Figure 7.20) is shown in Figure A11.1c. All three functions are used to represent the C(2s) AO, optimized for the environment of the molecule.

The H_2O calculation for the discussion in the main text was carried out within the C_{2v} point group symmetry and the calculated coefficients for the MOs pictured in Figure 7.26 are given in Tables A11.1 (for a_1 MOs), A11.2 (for b_2 MOs) and A11.3 (for b_1 MOs). Each table gives the energy and occupancy of the MO along with the coefficients of the constituent basis functions, reporting only those functions of the correct symmetry to take part in the orbital. Figure A11.2a shows the coordinate system that was used in the calculation with the principal axis along Z and the molecule lying in the YZ plane. To judge

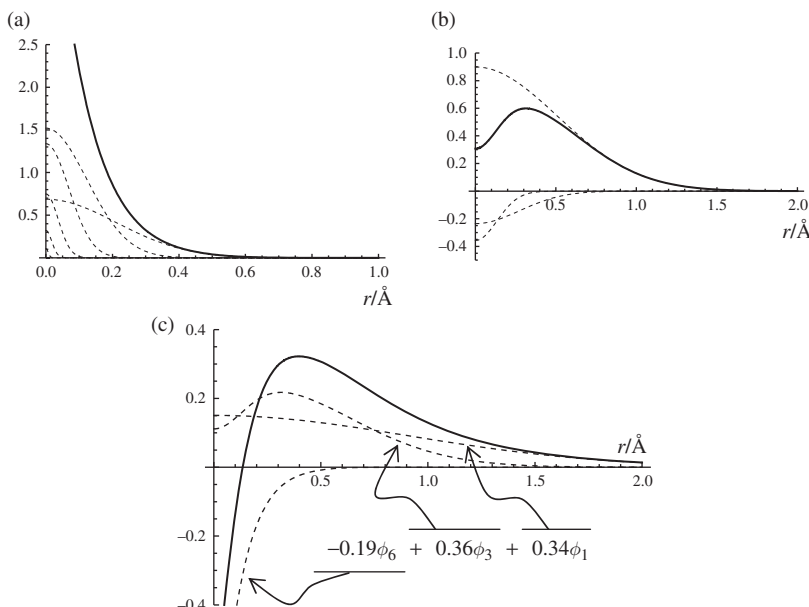


Figure A11.1 The radial functions used with s-type basis functions for C atoms in the 6-31G basis set. a) The six primitive Gaussians (dashed lines) are shown scaled by their contraction coefficients (d_p in equation A11.2). Their sum gives the contracted function (solid bold line) used for the core region. b) The three primitive Gaussians (dashed lines) scaled by the contraction coefficients and the contracted function (solid bold line) used for the valence region. c) Example use of all three basis functions to form the C(2s) atomic orbital in the 2a₁ molecular orbital of methane. The three basis functions are shown as dashed lines scaled by the SCF coefficients given in the formula. The resulting summed radial function is shown as the bold solid line.

the effects of the coefficients on the MOs, Figure A11.2 also shows examples of a_1 basis functions. The valence functions on H are linked together, as either a_1 or b_2 representation. This means that only a single coefficient is needed in each MO for H atom 1s functions and in an a_1 MO they will always appear with the same phase. When the MO coefficient for this basis is positive we show white 1s orbitals (Figure A11.1b); a negative coefficient will reverse the orbital phase, and so shading is included in Figure A11.1c. The same shading is carried through to an O(2p_z) basis function in Figure 11.1d and e, which can also contribute to a_1 symmetry MOs.

Since each atom has two valence basis functions, there are two coefficients for H(s) in Tables A11.1 and A11.2. Similarly, the O valence basis contains two coefficients per MO, one for the contraction of three Gaussians and one for the single Gaussian basis function. In addition, the O core basis function is a contraction of six Gaussians, and we note that only a single s-symmetry core function is required.

The lowest lying MO is 1a₁, which is simply the O(1s) core state, and so the only significant coefficient corresponds to the core basis function. This is much lower in energy than the valence shell orbitals (by almost 19 eV) and so is not involved in bonding and was

Table A11.1 The calculated energy, occupancy and basis function coefficients for H_2O MOs of a_1 symmetry. The value in square brackets under each basis function indicates the level of contraction in the 6-31G basis set.

	Energy (eV)	Occ.	$H(s)$ [3]	$H(s)$ [1]	$O(s)$ [6]	$O(s)$ [3]	$O(s)$ [1]	$O(p_z)$ [3]	$O(p_z)$ [1]
$1a_1$	-20.55	2	0.00	0.00	1.00	0.02	-0.01	0.00	0.00
$2a_1$	-1.35	2	0.20	-0.01	-0.21	0.47	0.48	0.11	0.06
$3a_1$	-0.55	2	0.19	0.11	0.07	-0.17	-0.29	0.56	0.42
$4a_1$	0.21	0	0.09	1.42	0.09	-0.11	-1.21	-0.22	-0.45

Table A11.2 The calculated energy, occupancy and basis function coefficients for H₂O MOs of b₂ symmetry. Values in square brackets indicate the level of contraction in the 6-31G basis set.

	Energy (eV)	Occ.	H(s) [3]	H(s) [1]	O(p _y) [3]	O(p _y) [1]
1b ₂	-0.726	2	-0.375	-0.162	0.504	0.262
2b ₂	0.303	0	0.045	1.966	0.330	0.844

Table A11.3 The calculated energy, occupancy and basis function coefficients for H₂O MOs of b₁ symmetry. Values in square brackets indicate the level of contraction in the 6-31G basis set.

	Energy (eV)	Occ.	O(p _x) [3]	O(p _x) [1]
1b ₁	-0.498	2	0.640	0.512

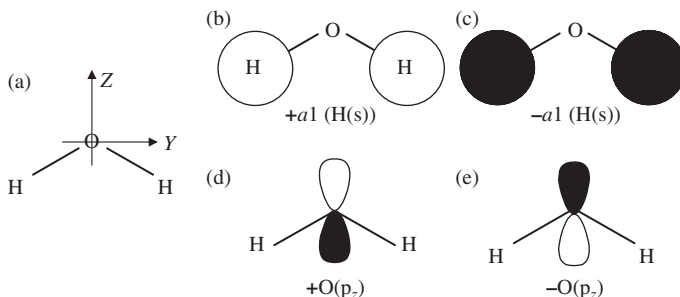


Figure A11.2 a) The orientation of the H₂O molecule in the reference axis system used in the calculation. b) The a₁ SALC of the H(s) basis functions and c) the affect of a negative coefficient in a molecular orbital. d) An O(p_z) basis function and e) the affect of a negative coefficient on this.

not drawn on the MO diagram of Figure 7.21. The first valence level MO is 2a₁, which is a bonding orbital since the H(1s) functions and the valence O(s) all appear with coefficients of the same sign; the small coefficient on O(p_z) shows that there is some mixing of the 2s and 2p_z AOs even though they are well separated energetically.

The linear combination for the 3a₁ MO is illustrated in Figure A11.3. Here, the H(1s) a₁ linear combination is out of phase with the O 2s and 2p_z orbitals and so an antibonding MO results. The mixing of the O(2s) and O(2p_z) in this way also diminishes the positive lobe of the O(2p_z) orbital in the MO to the extent that it does not show up at the contour level used in the graphic. Table A11.1 indicates that this orbital is not occupied, so that, despite its clear antibonding character, it does not contribute to the bond energy of the molecule.

The remaining occupied orbitals are 1b₂ (Table A11.2) and 1b₁ (Table A11.3). The 1b₂ orbital is bonding between the O(2p_y) orbital and the b₂ combination of the H(1s) orbitals while 1b₁ is the O(2p_x) AO which is perpendicular to the molecular plane and nonbonding by symmetry. For this reason, only the O(p_x) basis functions appear in Table A11.3.

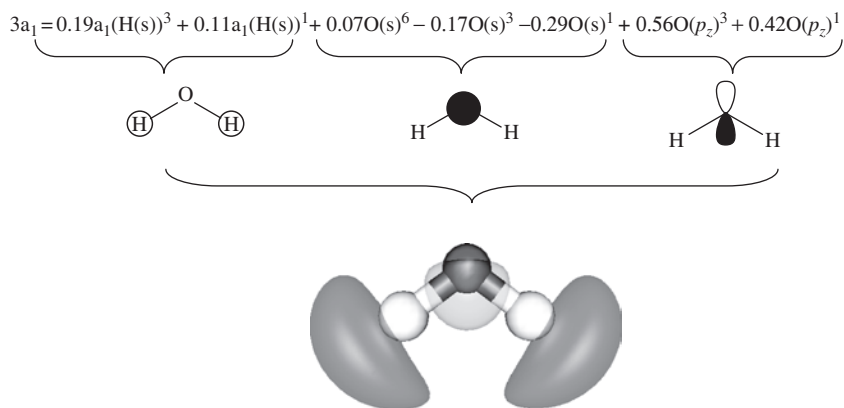


Figure A11.3 The composition of the $3a_1$ molecular orbital in H_2O . The basis functions are distinguished by superscripts giving the level of contraction in the 6-31G scheme, with the SALC of the $H(s)$ functions indicated as a_1 . The sketches under each set of terms give the atomic orbitals represented and then these are combined into the molecular orbital.

Further Reading

A good general introduction to quantum theory and its use in chemistry is provided by:
 Atkins PW, Friedman RS (1997) *Molecular Quantum Mechanics*. Oxford University Press (ISBN 0-19-855947-X).

The background theory and implementation of electronic structure theory is treated in even greater depth in:

Szabo A, Ostland NS (1982) *Modern Quantum Chemistry, Introduction to Advanced Electronic Structure Theory*. McGraw-Hill (ISBN 0-07-062739-8).

Appendix 12

Character Tables

This appendix lists the standard character tables for the point groups met in the main text. The right-hand columns indicate the irreducible representations for common functions of x, y, z and rotations around the Cartesian axes, R_x, R_y and R_z . Parentheses are used to show degenerate sets of these functions.

A12.1 Non-Axial Groups

C_s	E	σ_h		
A'	1	1	x, y, R_z	x^2, y^2, z^2, xy
A''	1	-1	z, R_x, R_y	yz, xz

A12.2 Axial Groups

These groups contain one or more rotational axes with no equivalent axes of order higher than 2. The first set, the C_n groups, form the smallest rotational subgroups of the corresponding C_{nv} , C_{nh} , D_{nd} and D_{nh} groups. These should be used to simplify the projection operator method for C_{nv} and C_{nh} , while the D_n groups listed later should be employed for projections in D_{nd} and D_{nh} groups.

A12.2.1 C_n Groups

C_2	E	C_2		
A	1	1	z, R_z	x^2, y^2, z^2, xy
B	1	-1	x, y, R_x, R_y	xz, yz

C_3	E	$2C_3$		
A	1	1	z, R_z	$x^2 + y^2, z^2$
E	2	-1	$(x, y), (R_x, R_y)$	$(x^2 - y^2, xy), (xz, yz)$

C_4	E	$2C_4$	C_2		
A	1	1	1	z, R_z	$x^2 + y^2, z^2$
B	1	-1	1		$x^2 - y^2, xy$
E	2	0	-2	$(x, y), (R_x, R_y)$	(xz, yz)

C_5	E	$2C_5$	$2C_5^2$		
A	1	1	1	z, R_z	$x^2 + y^2, z^2$
E_1	2	$2 \cos 72^\circ$	$2 \cos 144^\circ$	$(x, y), (R_x, R_y)$	(xz, yz)
E_2	2	$2 \cos 144^\circ$	$2 \cos 72^\circ$		$(x^2 - y^2, xy)$

C_6	E	$2C_6$	$2C_3$	C_2		
A	1	1	1	1	z, R_z	$x^2 + y^2, z^2$
B	1	-1	1	-1		
E_1	2	1	-1	-2	$(x, y), (R_x, R_y)$	(xz, yz)
E_2	2	-1	-1	2		$(x^2 - y^2, xy)$

A12.2.2 S_n Groups

S_4	E	$2S_4$	C_2		
A	1	1	1	R_z	$x^2 + y^2, z^2$
B	1	-1	1	z	$x^2 - y^2, xy$
E	2	0	-2	$(x, y), (R_x, R_y)$	(xz, yz)

S_6	E	$2C_3$	i	$2S_6$		
A_g	1	1	1	1	R_z	$x^2 + y^2, z^2$
E_g	2	-1	2	-1	(R_x, R_y)	$(x^2 - y^2, xy), (xz, yz)$
A_u	1	1	-1	-1	z	
E_u	2	-1	-2	1	(x, y)	

A12.2.3 C_{nv} Groups

C_{2v}	E	C_2	$\sigma_v(XZ)$	$\sigma'_v(YZ)$		
A_1	1	1	1	1	z	x^2, y^2, z^2
A_2	1	1	-1	-1	R_z	xy
B_1	1	-1	1	-1	x, R_y	xz
B_2	1	-1	-1	1	y, R_x	yz

C_{3v}	E	$2C_3$	$3\sigma_v$			
A_1	1	1	1	z		$x^2 + y^2, z^2$
A_2	1	1	-1	R_z		
E	2	-1	0	$(x, y), (R_x, R_y)$		$(x^2 - y^2, xy), (xz, yz)$

C_{4v}	E	$2C_4$	C_2	$2\sigma_v$	$2\sigma_d$		
A_1	1	1	1	1	1	z	$x^2 + y^2, z^2$
A_2	1	1	1	-1	-1	R_z	
B_1	1	-1	1	1	-1		$x^2 - y^2$
B_2	1	-1	1	-1	1		xy
E	2	0	-2	0	0	$(x, y), (R_x, R_y)$	(xz, yz)

C_{5v}	E	$2C_5$	$2C_5^2$	$5\sigma_v$			
A_1	1	1	1	1	z		$x^2 + y^2, z^2$
A_2	1	1	1	-1	R_z		
E_1	2	$2 \cos 72^\circ$	$2 \cos 144^\circ$	0	$(x, y), (R_x, R_y)$	(xz, yz)	
E_2	2	$2 \cos 144^\circ$	$2 \cos 72^\circ$	0		$(x^2 - y^2, xy)$	

C_{6v}	E	$2C_6$	$2C_3$	C_2	$3\sigma_v$	$3\sigma_d$		
A_1	1	1	1	1	1	1	z	$x^2 + y^2, z^2$
A_2	1	1	1	1	-1	-1	R_z	
B_1	1	-1	1	-1	1	-1		
B_2	1	-1	1	-1	-1	1		
E_1	2	1	-1	-2	0	0	$(x, y), (R_x, R_y)$	(xz, yz)
E_2	2	-1	-1	2	0	0		$(x^2 - y^2, xy)$

A12.2.4 C_{nh} Groups

C_{2h}	E	C_2	i	σ_h		
A_g	1	1	1	1	R_z	x^2, y^2, z^2, xy
B_g	1	-1	1	-1	R_x, R_y	xz, yz
A_u	1	1	-1	-1	z	
B_u	1	-1	-1	1	x, y	

C_{3h}	E	$2C_3$	σ_h	$2S_3$		
A'	1	1	1	1	R_z	$x^2 + y^2, z^2$
E'	2	-1	2	-1	(x, y)	$(x^2 - y^2, xy)$
A''	1	1	-1	-1	z	
E''	2	-1	-2	1	(R_x, R_y)	(xz, yz)

C_{4h}	E	$2C_4$	C_2	i	$2S_4$	σ_h		
A_g	1	1	1	1	1	1	R_z	$x^2 + y^2, z^2$
B_g	1	-1	1	1	-1	1		$x^2 - y^2, xy$
E_g	2	0	-2	2	0	-2	(R_x, R_y)	(xz, yz)
A_u	1	1	1	-1	-1	-1	z	
B_u	1	-1	1	-1	1	-1		
E_u	2	0	-2	-2	0	2	(x, y)	

C_{5h}	E	$2C_5$	$2C_5^2$	σ_h	$2S_5$	$2S_5^3$		
A'	1	1	1		1 1	1	R_z	$x^2 + y^2, z^2$
E_1'	2	$2 \cos 72^\circ$	$2 \cos 144^\circ$		2 2	$\cos 72^\circ$	$2 \cos 144^\circ$	(x, y)
E_2'	2	$2 \cos 144^\circ$	$2 \cos 72^\circ$		2 2	$\cos 144^\circ$	$2 \cos 72^\circ$	$(x^2 - y^2, xy)$
A''	1	1	1		-1 -1	-1	z	
E_1''	2	$2 \cos 72^\circ$	$2 \cos 144^\circ$		-2 -2	$\cos 72^\circ$	$2 \cos 144^\circ$	(R_x, R_y)
E_2''	2	$2 \cos 144^\circ$	$2 \cos 72^\circ$		-2 -2	$\cos 144^\circ$	$2 \cos 72^\circ$	(xz, yz)

C_{6h}	E	$2C_6$	$2C_3$	C_2	i	$2S_3$	$2S_6$	σ_h	
A_g	1	1	1	1	1	1	1	R_z	$x^2 + y^2, z^2$
B_g	1	-1	1	-1	1	-1	1	-1	
E_{1g}	2	1	-1	-2	2	1	-1	-2	(R_x, R_y)
E_{2g}	2	-1	-1	2	2	-1	-1	2	$(x^2 - y^2, xy)$
A_u	1	1	1	1	-1	-1	-1	-1	z
B_u	1	-1	1	-1	-1	1	-1	1	
E_{1u}	2	1	-1	-2	-2	-1	1	2	(x, y)
E_{2u}	2	-1	-1	2	-2	1	1	-2	

A12.2.5 D_n Groups

The D_n groups are rotational sub-groups of the D_{nd} and D_{nh} groups that include the horizontal C_2 axes. These should be used to simplify the projection operator method for D_{nd} and D_{nh} .

D_2	E	$C_2(z)$	$C_2(y)$	$C_2(x)$		
A	1	1	1	1		x^2, y^2, z^2
B_1	1	1	-1	-1	z, R_z	xy
B_2	1	-1	1	-1	y, R_y	xz
B_3	1	-1	-1	1	x, R_x	yz

D_3	E	$2C_3$	$3C_2$		
A_1	1	1	1		$x^2 + y^2, z^2$
A_2	1	1	-1	z, R_z	
E	2	-1	0	$(x, y), (R_x, R_y)$	$(x^2 - y^2, xy), (xz, yz)$

D_4	E	$2C_4$	$C_2 (= C_4^2)$	$2C_2'$	$2C_2''$		
A_1	1	1	1	1	1		$x^2 + y^2, z^2$
A_2	1	1	1	-1	-1	z, R_z	
B_1	1	-1	1	1	-1		$x^2 - y^2$
B_2	1	-1	1	-1	1		xy
E	2	0	-2	0	0	$(x, y), (R_x, R_y)$	(xz, yz)

D_5	E	$2C_5$	$2C_5^2$	$5C_2$		
A_1	1	1	1	1		$x^2 + y^2, z^2$
A_2	1	1	1	-1	z, R_z	
E_1	2	$2 \cos 72^\circ$	$2 \cos 144^\circ$	0	$(x, y), (R_x, R_y)$	(xz, yz)
E_2	2	$2 \cos 144^\circ$	$2 \cos 72^\circ$	0		$(x^2 - y^2, xy)$

D_6	E	$2C_6$	$2C_3$	C_2	$3C_2'$	$3C_2''$		
A_1	1	1	1	1	1	1		$x^2 + y^2, z^2$
A_2	1	1	1	1	-1	-1	z, R_z	
B_1	1	-1	1	-1	1	-1		
B_2	1	-1	1	-1	-1	1		
E_1	2	1	-1	-2	0	0	$(x, y), (R_x, R_y)$	(xz, yz)
E_2	2	-1	-1	2	0	0		$(x^2 - y^2, xy)$

A12.2.6 D_{nd} Groups

D_{2d}	E	$2S_4$	C_2	$2C_2'$	$2\sigma_d$			
A_1	1	1	1	1	1			$x^2 + y^2, z^2$
A_2	1	1	1	-1	-1	R_z		
B_1	1	-1	1	1	-1			$x^2 - y^2$
B_2	1	-1	1	-1	1	z		xy
E	2	0	-2	0	0	$(x, y), (R_x, R_y)$		(yz, xz)

D_{3d}	E	$2C_3$	$3C_2$	i	$2S_6$	$3\sigma_d$		
A_{1g}	1	1	1	1	1	1		$x^2 + y^2, z^2$
A_{2g}	1	1	-1	1	1	-1	R_z	
E_g	2	-1	0	2	-1	0	(R_x, R_y)	$(x^2 - y^2, xy), (xz, yz)$
A_{1u}	1	1	1	-1	-1	-1		
A_{2u}	1	1	-1	-1	-1	1	z	
E_u	2	-1	0	-2	1	0	(x, y)	

D_{4d}	E	$2S_8$	$2C_4$	$2S_8^3$	C_2	$4C_2'$	$4\sigma_d$		
A_1	1	1	1	1	1	1	1		$x^2 + y^2, z^2$
A_2	1	1	1	1	1	-1	-1	R_z	
B_1	1	-1	1	-1	1	1	-1		
B_2	1	-1	1	-1	1	-1	1	z	
E_1	2	$\sqrt{2}$	0	$-\sqrt{2}$	-2	0	0	(x, y)	
E_2	2	0	-2	0	2	0	0		$(x^2 - y^2, xy)$
E_3	2	$-\sqrt{2}$	0	$\sqrt{2}$	-2	0	0	(R_x, R_y)	(xz, yz)

D_{5d}	E	$2C_5$	$2C_5^2$	$5C_2$	i	$2S_{10}^3$	$2S_{10}$	$5\sigma_d$	
A_{1g}	1	1	1		1	1	1	1	$x^2 + y^2, z^2$
A_{2g}	1	1	1		-1	1	1	-1	R_z
E_{1g}	2	$2 \cos 72^\circ$	$2 \cos 144^\circ$	0	2	$2 \cos 72^\circ$	$2 \cos 144^\circ$	0	(R_x, R_y)
E_{2g}	2	$2 \cos 144^\circ$	$2 \cos 72^\circ$	0	2	$2 \cos 144^\circ$	$2 \cos 72^\circ$	0	(xz, yz)
A_{1u}	1	1	1		1	-1	-1	-1	
A_{2u}	1	1	1		-1	-1	-1	1	z
E_{1u}	2	$2 \cos 72^\circ$	$2 \cos 144^\circ$	0	-2	$-2 \cos 72^\circ$	$-2 \cos 144^\circ$	0	(x, y)
E_{2u}	2	$2 \cos 144^\circ$	$2 \cos 72^\circ$	0	-2	$-2 \cos 144^\circ$	$-2 \cos 72^\circ$	0	

D_{6d}	E	$2S_{12}$	$2C_6$	$2S_4$	$2C_3$	$2S_{12}^5$	C_2	$6C_2'$	$6\sigma_d$		
A_1	1	1	1	1	1	1	1	1	1		$x^2 + y^2, z^2$
A_2	1	1	1	1	1	1	1	-1	-1	R_z	
B_1	1	-1	1	-1	1	-1	1	1	-1		
B_2	1	-1	1	-1	1	-1	1	-1	1	z	
E_1	2	$\sqrt{3}$	1	0	-1	$-\sqrt{3}$	-2	0	0	(x, y)	
E_2	2	1	-1	-2	-1	1	2	0	0		$(x^2 - y^2, xy)$
E_3	2	0	-2	0	2	0	-2	0	0		
E_4	2	-1	-1	2	-1	-1	2	0	0		
E_5	2	$-\sqrt{3}$	1	0	-1	$\sqrt{3}$	-2	0	0	(R_x, R_y)	(xz, yz)

A12.2.7 D_{nh} Groups

D_{2h}	E	$C_2(z)$	$C_2(y)$	$C_2(x)$	i	$\sigma(xy)$	$\sigma(xz)$	$\sigma(yz)$		
A_g	1	1	1	1	1	1	1	1		x^2, y^2, z^2
B_{1g}	1	1	-1	-1	1	1	-1	-1	R_z	xy
B_{2g}	1	-1	1	-1	1	-1	1	-1	R_y	xz
B_{3g}	1	-1	-1	1	1	-1	-1	1	R_x	yz
A_u	1	1	1	1	-1	-1	-1	-1		
B_{1u}	1	1	-1	-1	-1	-1	1	1	z	
B_{2u}	1	-1	1	-1	-1	1	-1	1	y	
B_{3u}	1	-1	-1	1	-1	1	1	-1	x	

D_{3h}	E	$2C_3$	$3C_2$	σ_h	$2S_3$	$3\sigma_v$			
A'_1	1	1	1	1	1	1			$x^2 + y^2, z^2$
A'_2	1	1	-1	1	1	-1	R_z		
E'	2	-1	0	2	-1	0	(x, y)		$(x^2 - y^2, xy)$
A''_1	1	1	1	-1	-1	-1			
A''_2	1	1	-1	-1	-1	1	z		
E''	2	-1	0	-2	1	0	(R_x, R_y)		(xz, yz)

D_{4h}	E	$2C_4$	C_2	$2C_2'$	$2C_2''$	i	$2S_4$	σ_h	$2\sigma_v$	$2\sigma_d$	
A_{1g}	1	1	1	1	1	1	1	1	1	1	$x^2 + y^2, z^2$
A_{2g}	1	1	1	-1	-1	1	1	1	-1	-1	R_z
B_{1g}	1	-1	1	1	-1	1	-1	1	1	-1	
B_{2g}	1	-1	1	-1	1	1	-1	1	-1	1	$x^2 - y^2$
E_g	2	0	-2	0	0	2	0	-2	0	0	(R_x, R_y)
A_{1u}	1	1	1	1	1	-1	-1	-1	-1	-1	
A_{2u}	1	1	1	-1	-1	-1	-1	-1	1	1	z
B_{1u}	1	-1	1	1	-1	-1	1	-1	-1	1	
B_{2u}	1	-1	1	-1	1	-1	1	-1	1	-1	
E_u	2	0	-2	0	0	-2	0	2	0	0	(x, y)

D_{5h}	E	$2C_5$	$2C_5^2$	$5C_2$	σ_h	$2S_5$	$2S_5^3$	$5\sigma_v$		
A_1'	1	1		1	1	1	1	1		$x^2 + y^2, z^2$
A_2'	1	1		-1	1	1	1	-1	R_z	
E_1'	2	$2 \cos 72^\circ$	$2 \cos 144^\circ$	0	2	$2 \cos 72^\circ$	$2 \cos 144^\circ$	0	(x, y)	
E_2'	2	$2 \cos 144^\circ$	$2 \cos 72^\circ$	0	2	$2 \cos 144^\circ$	$2 \cos 72^\circ$	0		$(x^2 - y^2, xy)$
A_1''	1	1		1	-1	-1	-1	-1		
A_2''	1	1		-1	-1	-1	-1	1	z	
E_1''	2	$2 \cos 72^\circ$	$2 \cos 144^\circ$	0	-2	$-2 \cos 72^\circ$	$-2 \cos 144^\circ$	0	(R_x, R_y)	(xz, yz)
E_2''	2	$2 \cos 144^\circ$	$2 \cos 72^\circ$	0	-2	$-2 \cos 144^\circ$	$-2 \cos 72^\circ$	0		

D_{6h}	E	$2C_6$	$2C_3$	C_2	$3C_2'$	$3C_2''$	i	$2S_3$	$2S_6$	σ_h	$3\sigma_d$	$3\sigma_v$		
A_{1g}	1	1	1	1	1	1	1	1	1	1	1	1		$x^2 + y^2, z^2$
A_{2g}	1	1	1	1	-1	-1	1	1	1	1	-1	-1	R_z	
B_{1g}	1	-1	1	-1	1	-1	1	-1	1	-1	1	-1		
B_{2g}	1	-1	1	-1	-1	1	1	-1	1	-1	-1	1		
E_{1g}	2	1	-1	-2	0	0	2	1	-1	-2	0	0	(R_x, R_y)	(xz, yz)
E_{2g}	2	-1	-1	2	0	0	2	-1	-1	2	0	0		$(x^2 - y^2, xy)$
A_{1u}	1	1	1	1	1	1	-1	-1	-1	-1	-1	-1		
A_{2u}	1	1	1	1	-1	-1	-1	-1	-1	-1	1	1	z	
B_{1u}	1	-1	1	-1	1	-1	-1	1	-1	1	-1	1		
B_{2u}	1	-1	1	-1	-1	1	-1	1	-1	1	1	-1		
E_{1u}	2	1	-1	-2	0	0	-2	-1	1	2	0	0	(x, y)	
E_{2u}	2	-1	-1	2	0	0	-2	1	1	-2	0	0		

A12.3 Cubic Groups

A12.3.1 Tetrahedral, T_d

T_d	E	$8C_3$	$3C_2$	$6S_4$	$6\sigma_d$		
A_1	1	1	1	1	1		$x^2 + y^2 + z^2$
A_2	1	1	1	-1	-1		
E	2	-1	2	0	0		$(z^2, x^2 - y^2)$
T_1	3	0	-1	1	-1	(R_x, R_y, R_z)	
T_2	3	0	-1	-1	1	(x, y, z)	(xz, yz, xy)

A12.3.2 Rotational Subgroup of T_d , T

T	E	$8C_3$	$3C_2$		
A	1	1	1		$x^2 + y^2 + z^2$
E	2	-1	2		$(z^2, x^2 - y^2)$
T	3	0	-1	$(R_x, R_y, R_z), (x, y, z)$	(xz, yz, xy)

A12.3.3 Octahedral, O_h

O_h	E	$8C_3$	$6C_2$	$6C_4$	$3C_2 (= C_4^2)$	i	$6S_4$	$8S_6$	$3\sigma_h$	$6\sigma_d$		
A_{1g}	1	1	1	1	1	1	1	1	1	1		$x^2 + y^2 + z^2$
A_{2g}	1	1	-1	-1	1	1	-1	1	1	-1		$(z^2, x^2 - y^2)$
E_g	2	-1	0	0	2	2	0	-1	2	0		
T_{1g}	3	0	-1	1	-1	3	1	0	-1	-1	(R_x, R_y, R_z)	
T_{2g}	3	0	1	-1	-1	3	-1	0	-1	1		(xz, yz, xy)
A_{1u}	1	1	1	1	1	-1	-1	-1	-1	-1		
A_{2u}	1	1	-1	-1	1	-1	1	-1	-1	1		
E_u	2	-1	0	0	2	-2	0	1	-2	0		
T_{1u}	3	0	-1	1	-1	-3	-1	0	1	1	(x, y, z)	
T_{2u}	3	0	1	-1	-1	-3	1	0	1	-1		

A12.3.4 Rotational Subgroup of O_h , O

O	E	$8C_3$	$3C_2 (= C_4^2)$	$6C_4$	$6C_2$	
A_1	1	1	1	1	1	$x^2 + y^2 + z^2$
A_2	1	1	1	-1	-1	
E	2	-1	2	0	0	$(z^2, x^2 - y^2)$
T_1	3	0	-1	1	-1	$(x, y, z), (R_x, R_y, R_z)$
T_2	3	0	-1	-1	1	(xz, yz, xy)

A12.4 Groups for Linear Molecules

$C_{\infty v}$	E	$2C_\infty^\Phi$...	$\infty\sigma_v$		
$A_1 \equiv \sum^+$	1	1	...	1	z	$(x^2 + y^2), z^2$
$A_2 \equiv \sum^-$	1	1	...	-1	R_z	
$E_1 \equiv \Pi$	2	$2 \cos(\Phi)$...	0	$(x, y), (R_x, R_y)$	xz, yz
$E_2 \equiv \Delta$	2	$2 \cos(2\Phi)$...	0		$(x^2 - y^2), xy$
$E_3 \equiv v\Phi$	2	$2 \cos(3\Phi)$...	0		
...		

Index

- Abelian groups 50
Absorption
infrared (IR) 5, 165, 173–7, 187, 336, 337
in Raman spectroscopy 180–1
Stokes/anti-Stokes 180–1, 343–44
Absorption bands 5, 167, 169
Alkenes, epoxidation of 53
Allene 61
Allred and Rochow scale 246
'All space' integration 231
Amines 49
Ammonia
bending mode 126
bond order for 267
degenerate irreducible representations 98–100
as Lewis base 267–8
'lone pair' electrons in 267
matrix representations 85–8
multiplication table 29–31, 39, 43
N–H bonds 98–100, 126, 198, 199, 318
N–H stretching modes 195, 198–200, 213
reflection operation 87
structure of 7
symmetry elements 7, 29
symmetry operations 7
vibrational stretching modes 126
Angular equation 348–56, 368–9, 373
Angular frequency 327
Angular functions 368
Angular integrals 364–7
Angular momentum 356–9, 362
defining units of 345–6
higher 239
quantum number 349, 352, 361
Angular velocity 355, 356, 357
Anharmonic corrections 167
Anion and cation pair 239
Antibonding orbitals 225, 237–9, 249, 251
Anti-Stokes absorption 181, 182, 343–4
Anti-Stokes bands 181, 183
Anti-Stokes radiation 344
AOs *see* Atomic orbitals
Arbitrary states 336
Arbitrary transitions 336–7
Aromatic molecules 221, 222, 224
Asymmetric molecules 46
Atmospheric pollutants 277
Atomic displacements 334, 338
Atomic orbitals
comparison with water waves 221
functions 129, 160, 224
in heteronuclear diatomics 276–8
higher angular momentum 239
in homonuclear diatomics 270–6
of hydrogen 345–73
hydrogen-like 233, 239–51
linear combination model 228
molecular orbital energy and 225, 239–42, 248, 251, 295
in molecular orbital theory 219, 221, 295
nonbonding by symmetry 250, 296
out of phase 221, 222
in phase 221
radial behaviour of 239–42
reducible representations for 161
relative energies of 242–51
rigid 393–95
see also d-orbitals, p-orbitals, s-orbitals
Atomic unit system 241, 372, 375
Atoms
chemical bond strengths 204
chemically equivalent 19
degrees of freedom 110, 112, 122, 123, 125
heavy 278–84, 367
hydrogen-like 345, 354, 361, 365
masses of 193, 204, 326–8, 331, 334
neutral gas-phase 248
properties 364

- Atoms (*Continued*)
 relative motion 204
 symmetry-inequivalent 202–6
 valency 241–2
- Atropine 50
- Avagadro constant 377
- Axial groups 55–64, 407–13
- Basis functions 93, 118, 121, 236
 in basis sets 126, 236
 in computer packages 236
 in constructing molecular orbitals 239–40
 6–31G set 401–406
 in reducible representations 91
 operations on sets of 87, 102
 SALCs and 191
- Basis sets 126–8, 236, 399
- Basis vectors 119, 122, 190
 in basis sets 126
 characters 93
 generating 195, 196, 198
 in linear combinations 196
 multiplying by matrix 318
 orthogonal 194
 subsets 202, 203, 216
 symmetry-related 202
 use in matrix representations 82–8, 102
 vector dot product of 193
- Benzene 187
 C–H stretch modes 206, 210, 212
 degrees of freedom 5
 infrared (IR)-active modes 208, 210, 212
 infrared (IR) spectrum 3, 5, 206, 208–9
 mirror planes in 12
 molecular vibrations analysis 206–12
 structure of 4, 8, 9
 symmetry elements 8, 9
 symmetry operations 8, 9
 vibrational modes 5
- Beryllium hydride 252–3
- Bicyclo[2.2.2]octane 20
- Bimetallic complexes 50
- Bohr, Niels 356
- Bohr radius 231, 241, 360, 361, 364, 380
 as unit of length 356, 376
- Boltzmann constant 336
- Boltzmann distribution 328
- Bond compression/extension 212, 342
- Bond dissociation energy 226, 234, 238
 for diatomic molecules 244, 245, 246
 for polyatomic molecules 227
- Bond energies 225–39
- Bond enthalpy change 225
- Bond formation energy 228, 237, 380–2, 389
- Bonding
 chemical 6, 203–4, 212, 219–95, 375–99
 electronic 178
 orbitals 225, 236–9, 251, 255, 295
- Bonding–antibonding interactions 278
- Bond lengths 237, 238, 245
- Bond order 238–9, 267
- Bond strengths 193, 238
- Born–Oppenheimer approximation 340, 341
- Born interpretation 222–5, 229, 231
- Boron hydride 253–8
- Boron trifluoride
 character assignment 88–91
 improper rotation 36, 37
 rotational symmetry elements of 11
- Boundary conditions 350–1, 371–3
- Bowl of Fruit, Violin and Bottle 75, 76
- Bra-ket notation 377, 382
- Bra-ket pairs 379
- Buckminsterfullerene 65
- C_{2h} point group 117
- C_{2v} point group 204, 253
 character tables for 92, 123
 examples of 58
 guitar sound board comparison 106
 infrared (IR)-active modes 170, 173
 irreducible representations 116, 168
 matrix representations for symmetry
 operations 82–5, 91
- mer-isomers 213, 214
- multiplication tables for 81–2, 85
- operations 193, 195
- order of 116
- reducible representations 91–3
- symmetry representations and characters 75–81
- vibrational modes in 122–6
- C_{2v} symmetry, molecular orbital calculations in 401–406
- C_{3v} point group 198, 202, 264–5
 character table for 98
 degenerate irreducible representations 98–100
 examples of 58
 geometry of 265, 268
 matrix representations of symmetry operations 85–8
 reducible representations 9
 reflection operation 87
- $C_{\infty h}$ point group 229, 414
- $C_{\infty v}$ point group 65, 276, 336, 414
 symmetry 186, 244, 248
- Cahn–Ingold–Prelog rules 41, 303–6
- Carbon dioxide 154, 173–6, 187

- Carbon monoxide 276, 277, 278
 Carbonyl ligands 126–8
 Cartesian axis system 10–11, 130, 131
 Cartesian coordinates 346, 347, 348
 Centre of symmetry 13
 Centrifugal effect 359
 Centripetal force 356, 359
 Character representations 81–2, 119
 Character tables
 for $C_{\infty v}$ point groups 414
 for C_{nh} point groups 409–10
 for C_n point groups 407–8
 for C_{nv} point groups 408–9
 for $D_{\infty h}$ point groups 414
 for D_{nd} point groups 411–12
 for D_{nh} point groups 412–13
 for D_n point groups 410–11
 for non-axial groups 407
 for octahedral groups O_h 414
 for S_n point groups 408
 for tetrahedral groups T_d 413
 Charge density 222, 223
 Chemical bond energy 232–6, 233, 375, 376, 393–9
 Chemical bonding *see* Bonding
 Chemical shifts 18–22, 23
 Chessboard pattern 322, 323
 Chiral centre 42, 303–6
 Chirality 41–2, 46
 Chiral molecules 41–2
 1-chloro-1-fluoroethane 304, 305
 Chloroform 58
 Classes of operations 51, 93–6, 112–18
 Classical mechanics 325, 357, 373, 379
 Closed groups 26–37, 43, 47
 Co-factors 323
 Complex conjugates 373
 Complex exponentials 367, 370, 371, 372
 Contraction effect 236
 Coordinates
 Cartesian 346, 347, 348
 cylindrical polar 383–86
 electron 364
 elliptical polar 384
 spherical polar 347, 358, 362, 363, 369, 383
 systems 347, 358, 369, 383–5
 Coulomb energy 387
 Coulomb field 239
 Coulomb force 354, 355
 Coulomb integrals 401
 Coulomb interactions 225, 359, 377, 380, 392
 Coulomb potential 379
 Coulomb's law 228, 380, 392
 Coupling 165, 167
 factors 177, 183
 integral 336
 between light and molecule 215
 matrix 336, 340
 vibrational 263
 Covalent bonds 238, 244
 Crystal fields 290
 Crystal structures 6
 Crystal symmetry 24
 Cube
 model 308
 octahedron and 67–9
 symmetry of 65, 66, 68–9
 tetrahedron and 66–7, 137, 307
 Cubic groups 65–9, 413–14
 Cusps 385
 Cyanide complexes 156
 Cyclic groups 50–4, 407–8
 Cyclohexane 24, 69–72
 Cyclopentadiene ring 7
 Cyclopropane 112, 113
 Cylindrical polar coordinates 383–5
 Cylindrical polar systems 383
 D_{2h} point group 188, 189, 198, 278–83
 D_{3d} point group 61, 101, 115
 D_{3h} point group 147–53, 254, 257, 268
 carbonyl stretching modes 126–8
 character assignment 88–91
 complexes 171
 symmetry elements and operations 112–14, 270
 D_{4h} point group 119, 132–7
 applying reduction formula to 120–121
 character table 93
 classes of operations 93–6
 complexes 287–91
 degenerate irreducible representations 96–8
 symmetry elements and operations 114, 115
 D_{5h} point group 117, 118
 D_{6h} point group 206–12
 $D_{\infty h}$ point group 65, 154, 156, 173, 186, 228, 252, 270, 296
 character table 155
 d-orbitals in 156, 158, 159, 162, 184
 infrared (IR)-active vibrations 172
 p-orbitals in 157, 158
 symmetry 244, 392
 Decay constant 396–9, 403
 Degenerate representations 96–8, 100, 198, 263
 projection operator and 198–202, 216

- Degrees of freedom
 angular 347, 349, 362
 atomic 110, 122, 123, 125
 benzene and fluorobenzene 5
 in diatomic molecules 325
 electronic 339–40
 molecular 5, 107, 110, 122, 325
 nonlinear molecules and 5, 110
 nuclear 339
 radial 347
 rotational 339
 translational 339
- D-electrons 128
- Density functional theory 239
- Density plots 235
- Destructive interference 266
- Determinants 317–24
- Diagonal matrix elements 85–7
- Diatom gases 225
- Diatom molecules 163, 178, 296
 antibonding orbitals in 225
 bond dissociation energy of 245,
 246, 296
 bonding orbitals in 225
 bond lengths 245
 bond stretching mode 127
 in $C_{\infty v}$ and $D_{\infty h}$ point groups 65, 244
 degrees of freedom in 325
 electron density in 244
 heteronuclear 229, 245, 276–8
 ionization potentials 244
 lithium hydride as 246
 molecular vibrations in 325, 328
 of second-row elements 270–8
 symmetry axis in 48
see also Homonuclear diatomic
 molecules
- (1S, 2R)-1, 2-dichloro-1, 2-difluoroethane 50
 1, 2-dichloroethene 185, 186, 190, 191
 Dichlorofluoromethane 49
 Dichloromethane 47
 Di-cyclopentadienyl iron(II) *see*
 Ferrocene
- Differential equations 372, 374
- Difluorobenzene 24, 190
 1, 4-difluorobenzene 188
 C—H stretch modes of 188–9, 197–8, 202
 structure of 187, 189
- Dihedral mirror planes 12, 23
- Dihydrogen cations 233, 375–99
 bond formation energy 380–93
 chemical bonding in 375–99
 choice of coordinate system for 383–5
 electronic potential energy in 387–93
 electron kinetic energy in 386–7
- molecular orbitals of 228–32
 wavefunction for 244–5
- Dimethylcyclohexene 20, 21
 (1S, 2S)-1, 2-dimethylcyclopropane 52
 (E)-1, 2-diphenylethene 58, 59
- Dipole moment 216, 328, 335, 337, 340
 operator 168–9
see also Permanent dipole moment;
 Transition dipole moment
- Dirac notation 377, 378
- Dirac, Paul 377
- Direct products 79–81, 169, 170, 215
- Dissociation process 226
- D-orbitals 201, 245
 in complexes with O_h and D_{4h}
 symmetries 291
 in $D_{\infty h}$ point group 56, 158–61
 finding characters for 256
 functional forms of 129
 in transition metal complexes 128–53
- Electric dipole 343
- Electric fields 335, 343
see also Electromagnetic fields
- Electromagnetic energy 356
- Electromagnetic fields 167
see also Electric fields
- Electromagnetic waves 328, 335
- Electron density
 Born interpretation and 229–31
 chemical bonding and 235
 in diatomic molecules 244
 external electric field and 343
 intermolecular interactions and 251
 map 222, 223
 molecular orbitals and 219, 224
 in Raman spectroscopy 181–4
 in (Z)-N-methyl-C-phenylnitro 222,
 223, 257
see also Charge density; ‘Lone pair’ density
- Electronegativity, 244–51, 295, 335
- Electronic bonding *see* Bonding
- Electronic excitation 177–80, 221, 339, 340
see also Excited vibrational states
- Electronic spectroscopy 136
- Electronic states 162, 165–9, 177–81, 234,
 339–40
- Electronic transitions 180, 181, 341
- Electrons
 affinity 246, 250
 binding energy of 263
 coordinates 364
 d- 128
 kinetic energy of 234, 235, 263, 378, 379
 mass of 341, 372

- potential energy of 234, 235, 347, 378, 379
see also Electron density
 Electron spin resonance 222
 Elliptical polar coordinates 384
 Enantiomers 41, 42, 46
 Energy levels 166, 336
 atomic 242
 electrons and 225
 in MO diagrams 239
 in molecular systems 1
 orbital 227
 transitions 215, 336
 vibrational 226, 339
 Energy states 165, 167
 Epoxidation 53
 Equivalent atoms 37–8
 Equivalent axes 8
 Equivalent operations 37–8
 E representations 198
 Escher, M.C. 1
 Ethane 50, 60
 improper rotation operation 33–5
 methyl groups of 37
 mirror planes 12–13
 multiplication table 39, 40
 products of operations 39
 symmetry elements 31, 32, 39
 symmetry operations 31, 32, 33, 37, 39
 symmetry point group 31, 33
 Ethene 9–10, 62, 63, 278–84, 294
 Ethylene 65
 Euler, Leonard 371, 372, 373
 Euler's equality 350, 372, 373
 Exchange integrals 401
 Excited vibrational states 215, 263, 333, 339, 341, 342
see also Electronic excitation; Electronic states
 Expectation values 234, 364–7, 378
 Exponential decay factor 381
 Facial (*fac*) isomers 212–15
 Fern frond 3, 4
 Ferrocene 6, 7, 8, 62
 First-row elements 243
 Fish, Vignette 1, 2
 Fluorobenzene 3–5, 26, 58
 Franck–Condon principle 179–81, 339–41
 Free radicals 277
 Furan 58
 Gaussian functions 330, 331, 333, 402, 403
 Gerade 101, 228–9, 286
 Global axis system 29, 39, 43
 Global coordinate system 39, 291
 Gold production 156
 Greenhouse gases 173–7
 Ground states 168, 335, 337
 bonding forces 180, 225
 of electrons 234, 341
 molecular vibration in 167
 vibrations 215, 342
see also Electronic states
 Guitar sound board 105–7
 Haem 18, 276–7
 Haemoglobin 18, 277
 Halogens 292, 294
 Hamiltonian operator 233, 236, 239, 401
 Handedness 303–6
 Harmonic approximation 167, 226, 325, 333, 342
 Harmonic oscillator 329, 331, 336, 337, 376
 classical 332, 333
 energy levels of 264
 wavefunctions 168, 332, 335
 Hartree–Fock approximation 244
 Hartree–Fock calculations 401, 402
 Hartree–Fock theory 239
 Hartree (energy unit) 376, 377
 Hermite polynomials 333, 335, 337, 342
 Heteronuclear diatomic molecules 229, 245, 276–8
 Hexaaquo complexes 72–3, 285, 287
 Hexagons 1
 Hexatriene 283, 284
 H–F molecule 325–8
 Homolytic cleavage processes 227
 Homonuclear diatomic molecules
 atmospheric gases present as 173
 bond dissociation energies of 245
 bond stretch of 184
 comparison with heteronuclear molecules 229
 molecular orbitals in 270–6, 281
 of second-row elements 270–6
 HOMO orbitals 283
 Hooke's law 326
 Horizontal mirror planes 23
 Horsehead Nebula 163, 164, 177
 Hubble Space Telescope Imaging Spectrograph (STIS) 164
 Hybridization
 in ammonia 265
 of C atom orbitals 263
 in ethene 281
 in heteronuclear diatomics 277
 in homonuclear diatomics 272, 273, 276

- Hybrid orbitals
 in ammonia 265–8
 in ethene 282, 283
- Hybrid states 267
- Hydrogen
 atom 233, 234, 366, 376–9
 atomic orbitals of 345–73
 bond energy for 225
 bond order 238
 cation 375–99
 covalent bond in 244
 interstellar 177
 molecular orbitals 228–32, 242, 247
 stretching mode 172
 vibrational exciton 163, 177
 see also Hydrogen-like atoms; Hydrogen-like atomic orbitals
- Hydrogen cyanide 65
- Hydrogen fluoride 172, 244–51
- Hydrogen-like atomic orbitals 129, 233, 239–51
- Hydrogen-like atoms 345, 354, 361, 365
- Hydroxyl 227
- ice 270
- Identity matrix 321, 324
- Identity operation 28, 38, 43
- Imaginary numbers 223, 224, 332, 350, 370–1
- Imaginary parts 367, 368, 370
- Improper rotations 31–8
 axes 36, 42, 50, 52
 definition 32
 equivalences for 34–7
 of even order 34, 38
 inverse for 38–9
 of odd order 37, 38
- Infrared (IR) spectroscopy 163, 165–73, 184–6, 215, 325–36
- Infinity 154
- Infrared (IR) absorption 165, 172–7, 336, 337
- Infrared (IR)-active modes 184, 185, 187, 189
- Infrared (IR) radiation 173, 176, 177
- Infrared (IR) spectra 3, 5, 185, 186, 189, 212, 215
- Infrared (IR) spectrometer 177
- Inorganic complexes 276–7
- Insulating solids 276
- Integrals
 angular 364–5
 Coulomb 401
 exchange 401
 overlap 232, 238, 249, 341
 radial 365–7
 resonance 237, 239
- Integration by parts method 365
- Interaction energy 228
- Interference 219–22, 224
- Interstellar gas 177
- Inverses
 of matrices 323, 324
 of operations 38–9, 43
- Inversion centre 5–6, 13–15, 23, 42
- Inversion operations 14, 15, 17, 43
- Ionic bonds 239, 249
- Ionization energies
 for first-row elements 243
 in homonuclear diatomics 274–6
 for second-row elements 241, 243
- IR absorption *see* Infrared (IR) absorption
- Iron tetrinitrosyl 217
- IR radiation *see* Infrared (IR) radiation
- Irreducible representations 91–3, 102
 B representations 100–1
 definition 77
 degenerate 96–8, 100, 198–202
 deriving for water molecule 110
 E representations 100, 101
 gerade 101
 labelling of 100–1
 molecular vibrations and 107–9, 335–6
 nondegenerate 100, 335
 orthogonal 117, 118, 249
 properties of point groups and 112–18
 reduction formula and 118–122
 A representations 100, 102
 for single objects (nondegenerate) 100, 335
 of transition dipole moment integrand 168
 T representations 101, 102
 ungerade 172
 in vibrational spectroscopy 165
- Irreducible symmetries 165
- IR spectroscopy *see* (IR) Infrared spectroscopy
- Jahn–Teller effect 72, 287–91
- Kinetic energy 326–8, 340
 chemical bonds and 375
 in dihydrogen cation 381–3
 of electrons 225, 234, 235, 263, 378, 379
 operator 329, 334, 346, 359
- Ladder of states 166
- Laguerre polynomials 360
- Laplacian operator 357, 377
 applying to molecular orbitals 386
 in Cartesian coordinates 346
 in spherical polar coordinates 347, 348, 379
- Laser 178
- Legendre polynomials 351
- Lens optics 14

- Lewis acids 258, 295
 Ligands
 bonds with metals 142, 147, 151
 carbonyl 126–8
 cis-L 13
 fields 129, 161, 290–1, 292–5
 orbitals of 284–95
 salen 53
 tetra-dentate 17, 53
 in transition metal complexes 72–3, 126,
 291–5
 trans-L 12–13
 triphenylphosphine 53
 σ-donor 284–7, 294
 Light
 coupling with molecules 215
 electric field of 167
 exposure of molecules to 167
 frequency 242
 in IR spectroscopy 335
 molecular response to 343
 scattered 344
 ultraviolet (UV) 164, 177, 181,
 291, 343
 visible frequency 181
 see also Infrared (IR) radiation
 Limonene 41, 305, 306
 Linear combinations 190–3
 Linear equations 321–4
 Linear molecules 154–60, 172
 point groups for (C_{vv} and $D_{\infty h}$) 64–5, 414
 rotation around molecular axis 187
 Linear momentum 355–7
 Linear triatomic molecules 173, 176
 Lithium fluoride 244–51
 Lithium hydride 246, 248, 249
 ‘Lone pair’ density 223, 251, 268,
 270, 303
 LUMO orbitals 283
 Magnetic field 18
 Mathematica 384, 394, 395
 Matrices
 definition of 83
 elements of 85–7
 inverses of 321, 323, 324
 for operation products 320
 orthogonal 323
 products of 318–19
 as representations of symmetry operations
 82–5, 314–17, 323, 324
 for solving sets of linear equations 321–4
 square 317, 321
 trace of 87–8, 92, 102
 Meridian (*mer*) isomers 212–15
 Metal–ligand bonds 143, 147, 294
 Methane
 C–H bonds 258, 263
 C–H stretching modes 176–7
 as greenhouse gas 173
 infrared (IR) active modes 177
 molecular orbitals in 258–64
 photoelectron spectrum 263
 tetrahedral geometry of 65
 Methyl groups 21, 22
 (*Z*)-*N*-methyl-*C*-phenylnitrone 222–3, 251
 Minimum energy point 166
 Mirror planes 5–6, 17
 in axial groups 55–9
 chirality and 42
 dihedral 12, 23
 horizontal 11, 12, 23
 multiple 11
 simple 42
 vertical 11, 12, 23
 see also Planes of symmetry
 Molecular classification 45–7
 Molecular energy calculations 227, 228
 Molecular orbitals 51, 219, 221, 222, 227,
 228, 244
 antibonding 225, 237–9, 249, 251
 basis functions in construction of 239, 240
 in beryllium hydride 252–3
 bonding 228, 235, 237–9, 249, 251,
 282–3, 295
 in boron hydride 253–8
 chemical bond energy from 232–6
 constructing from atomic orbitals 219
 diagrams 244, 248, 252, 294
 in diatomic molecules 225, 270–6
 in dihydrogen cations 228–32
 electron density and 219, 224
 energy 236–7
 in ethene 278–83
 in hydrogen 228–32, 237
 of lithium hydride 248, 249
 in methane 258–64
 node feature in 387
 normalization condition 234
 occupied (HOMO) 223, 224, 225, 253
 in octahedral complexes 285–7
 optimal radial decay of 396–7
 ordering of 219
 polarization of 296
 in polyatomic molecules with multiple heavy
 atoms 278–84
 unoccupied (LUMO) 224, 225, 253

- Molecular vibrations
 classical mechanics analysis 325–8
 in diatomic molecules 325, 326
 in ground state 167
 independence of 118
 infrared absorption and 165
 quantitative description of 206
 quantum mechanics analysis 328–33
 representations 107–12, 190–1, 335
 in water 122
see also Vibrational modes
- Moment of inertia 357
- Momentum 239, 356–9, 364
- Monatomic gases 225–6, 238
- Morse curve 178, 179, 180, 226, 341
- Morse potential 180
- MOs *see* Molecular orbitals
- Mulliken, R.S. 100, 101
- Mulliken scale 246
- Multicomponent catalytic converters 277
- Multi-electron states (term states) 136
- Nebulae 163, 164, 177
- Neutral radicals 227
- Newton's law 355
- Nitrogen 173, 264
- Nitrogen (II) oxide (NO) 276, 278
- Nitrones 222, 251
- Nitroxide radicals 222
- NMR *see* Nuclear magnetic resonance
- Nodes 235, 240, 387, 393
- Nonaxial groups (C_s , C_i , C_1) 48–50, 69, 407
- Nonbonding states 250, 253
- Nondegenerate representations 100, 335
- Noninteger characters 88–91
- Nonlinear molecules 5, 110, 122, 186, 187
 degrees of freedom 5, 110
- Normalization 131–2, 193–5, 232, 333
see also Renormalization
- Normal-mode coordinate 335
- Nuclear magnetic resonance (NMR)
 bands 18
 chemical shifts 18–23
 experiments 19, 21
 machine 18
 spectra 18–19, 21
 spectroscopy 18, 37
- Nuclear mass 345
- Octahedral complexes
 σ -donor ligands in 284–7
 d-orbitals in 142–8, 284–7
 ligand orbitals of π -symmetry in 291–5
 molecular orbitals in 286
 normal orientation 213
- p-orbitals in 146–7, 284–6
 s-orbitals in 286
- Octahedral groups O_h 65–9, 114, 142–8, 414
- Octahedron
 cube and 67–9
 model 313–15
 reference axis system for 149
 symmetry of 68–9
- Off-diagonal matrix elements 85–7
- Operator products 320
- Orbital plots 235
- Orbitals
 antibonding 225, 237–9, 249, 251
 bonding 225, 236–9, 249, 251, 295
 calculation 89
 HOMO 283
 hybrid 265–8, 282, 283
 of ligands 284–95
 LUMO 283
 π - 283, 284
 reference 295, 296
 s - 129, 228, 229, 236, 266
 σ - 283, 285–90
See also Atomic orbitals, d-orbitals,
 Molecular orbitals; p-orbitals
- Orion 163, 164
- Orthogonality 117–19, 232
- Orthogonal matrices 323
- Oscillating fields 328
- Oscillation 327, 328, 331
- Out-of-plane movements 212
- Overlap integrals 232, 238, 249
- Overtones 167, 325
- Oxygen 17–18, 173
- Ozone depletion 277
- Pasteur, Louis 45, 46
- Pauling, Linus 245, 246
- Pauling scale 247, 248
- Periodic table 239, 241, 242, 250, 264
- Periodic systems 6
- Permanent dipole moment 336
see also Dipole moment
- PES *see* Photoelectron spectrum
- p-functions 240
- Phenanthrene 221, 222, 224, 225, 235
- Phenyl 53
- Phosphazenes 54
- Photoelectron spectrum (PES) 263, 274–6

- Photon energy
 angular frequency 331
 electron kinetic energy and 263
 in infrared absorption 165, 167, 337
 ionization energy and 243
 molecular orbitals and 221
 in Raman spectroscopy 177–8, 180
 in Rayleigh scattering 180
 relationship to light frequency 242
- Picasso, Pablo 75, 76
- π -antibonding orbital 159
- π -orbitals 283, 284
- π representation 248, 281
- π -symmetry 291–5
- Planar molecules 36, 37, 58, 62
- Planck constant 166, 226, 329, 345, 358
- Planes of symmetry 3, 5, 10–13, 42
see also Mirror planes
- Point groups 25–6, 45–103, 296
 assigning to molecules 69–73
 axial 55–64, 407–13
 character tables 45, 102
 classes of operations in 112–14
 cubic 65–9, 413–14
 cyclic 50–4, 407, 408
 definition 26
 families of 47
 identity operation in 38
 of infinite order 154–60, 175
 for linear molecules 64–5, 414
 nonaxial 48–50, 69, 407
 order of 115, 116
 properties of 112–18
 sets of operations for 42–3
 subgroups 47, 101
 symmetry elements 43
 of water 299–300
- Point of inversion 23
- Point of symmetry 5, 13
- Polar bonds 244
- Polarizability 165, 182–4, 216, 343, 344
- Polar molecules 251
- Polyatomic molecules
 bond dissociation energy for 227
 identification 167
 molecular dipole for 337
 molecular orbitals in 278–84
 with multiple heavy atoms 278–84
 skeletal vibrations in 336
 vibrational modes for 335–6
- Polynomials
 Hermite 333, 335, 337, 342
 Laguerre 360
 Legendre 351
 Pople code 402
- p-orbitals
 in ammonia 266
 in octahedral complexes 143–9
 reducible representations 162
 in square planar complexes 132
 in tetrahedral complexes 137, 141
 in transition metal complexes 128
 in trigonal bipyramidal complexes 151–2
- Porphyrins 17, 18
- Potassium bitartrate 45
- Potential energy 328–9, 334, 339, 346
 chemical bonds and 375
 in dihydrogen cation 387–93
 of electrons 234, 235, 347, 378, 379
 operator 329, 334, 346, 359
- Principal axis 7–8, 23
- Probe radiation 165, 215
- Projection operator 191, 195, 198–202, 216, 254
- Projection operator method 195–202, 216, 254
- Prop-1 2-diene 62
- Proper rotations 6–9, 23
- Pure rotation subgroup 101
- Pythagoras' theorem 371
- Quantum mechanics 165–6, 345–6
 angular momentum in 357, 358–9
 balance of energy in particles 379
 behaviour of matter in 328
 coupling between light and molecules in 215
 magnetic moment of a nucleus in 18
 virial theorem in 380
 wavefunction in 222
- Quantum oscillator 334
- Quantum tunnelling effect 334, 379
- Radial decay 396–9
- Radial equation 348, 359–61
- Radial functions 239–40
- Radial integrals 365–7
- Radiation 3, 163, 178, 182, 328
- Radicals
 free 277
 neutral 227
 nitroxide 222
- Radio-frequency waves 18
- Raman-active modes 184, 187, 189
- Raman spectra 177, 182–3, 185–6, 189, 339, 343

- Raman spectroscopy 177–86
 absorption process in 180–1
 quantum model of 344
 selection rules 163, 165, 181–6, 215, 344
- Rayleigh scattering 179, 180, 344
- Reducible representations 91–3, 102,
 107, 118
 definition 91
 finding 110–112
 reduction formula and 118–122
 simplification 119
- Reduction formula 112, 118–22, 161,
 165, 254
- Reference orbitals 296
- Reflection
 operations 13, 14, 16, 23, 25, 27, 43
 planes 23
 symmetry elements 42
- Relative energies
 estimation 295
 of hydrogen-like atomic orbitals 239–51
- Renormalization 204
- Representations *see* Irreducible representations;
 Reducible representations
- Resonance integrals 237, 239
- Resonance Raman 178
- Rock salt 250
- Rotational elements 6
- Rotational operations 6
- Rotational subgroups 216
- Rotation axes 6, 17, 21, 23
 equivalent 8
 infinite 154
 multiple 9, 11, 59–64
 operations 13, 38
 order of 7
 principal 7
 proper 23
- Rotations 6–10, 23, 31–8
see also Rotation axes
- Row and column blocking method 322, 323
- SALCs *see* Symmetry-adapted linear combinations
- Salen ligands 53
- SCF *see* Self-consistent field
- Schönflies, Arthur Moritz 46
- Schrödinger equation
 applications 227, 228, 232, 376–8
 for hydrogen atom 367, 376
 solutions 129, 333, 345–50, 353–354
- Second-row elements 241–3, 252–78
- Self-consistent field (SCF) 401
- s-functions 240
 σ -donor ligands 285, 294
 σ -donor orbitals 285–90
 σ -orbital system 283
- Sine and cosine functions 89, 90
- Skeletal vibrations 336
- Sodium ammonium tartrate 45, 46
- s-orbitals 129, 228, 229, 236, 266
- Spectra
 of d^1 and d^9 complexes 291
 infrared (IR) 3, 5, 185, 186, 189,
 212, 216
 of molecules 1, 3, 165, 167
 multi-electron effects and 292
 nuclear magnetic resonance 18, 19, 21
 Raman 177, 182–3, 185–6, 189, 339, 343
 vibrational 163, 165, 186
- Spectrometers 19, 163, 167, 177
- Spectroscopy
 electronic 136
 experiments 215
 molecular structure and 1
 nuclear magnetic resonance (NMR) 18, 37
 vibrational 6, 25, 163–217
- Spherical harmonic functions 351, 353, 354,
 358, 368–9
- Spherical harmonic solutions 358
- Spherical polar coordinates 347, 358, 362,
 363, 369, 383
- Springs 325–6, 331, 334
- Square matrices 317, 321
- Square planar complexes 13–14, 17, 114,
 134–7, 216
- Stationary states 167, 328, 331,
 323–4, 338
- STIS *see* Hubble Space Telescope Imaging Spectrograph
- Stokes absorption 180, 181, 343–4
- Stokes bands 181, 183
- Stokes radiation 344
- Sulfur 63
- Superposition of waves 219, 220, 221
- Symmetry-adapted linear combinations
 (SALCs) 191–7, 235
- basis functions 191
- derivation 252–91
- determination of 216
- explanation 165
- for symmetry-related basis vectors 202
- Symmetry elements 6–17, 22–3
see also Symmetry-equivalent elements
- Symmetry-equivalent elements 114
see also Symmetry elements
- Symmetry-inequivalent atoms 202–6
- Symmetry operations 6–17, 23, 317–19

- Tartaric acid 45, 46
 Taylor expansions 370, 373
 Term states *see* Multi-electron states
 Tetrachloromethane 181, 182
 Tetra-dentate ligands 17, 53
 Tetrahedral complexes 137–42
see also Tetrahedral groups
 Tetrahedral groups 65–70, 413
see also Tetrahedral complexes; Tetrahedral point group
 Tetrahedral molecules 65–70
 Tetrahedral point group 114, 137–43, 176, 262
see also Tetrahedral groups
 Tetrahedron
 cube and 66–7, 137, 307
 model 307–8
 reference axis system for 142
 symmetry of 65, 66
 1,3,5,7-tetramethylcyclooctatetraene 53–4
 Tetramethylsilane (TMS) 19
 Thermal energy 336
 TMS *see* Tetramethylsilane
 Total energy 268–9, 327–8, 334, 348, 378–9
 Transition dipole moment 167, 168–9, 210, 325, 335, 337, 340
see also Dipole moment
 Transition metal complexes
 bonding in 128–9
 carbonyl ligands stretching modes 126–8, 213
 containing ligand orbitals of π -symmetry 291–5
 containing σ -donor ligands 284–7
 d-orbitals in 128–53
 facial (fac) isomers 212–15
 infrared (IR)-active modes 215
 infrared (IR) spectra 212, 215
 Jahn–Teller effect 287–91
 meridian (mer) isomers 212–15
 p-orbitals in 129
 with six ligands 72–3
 s-orbitals in 129
 vibrational modes of 213–15
see also Octahedral complexes; Square planar complexes; Tetrahedral complexes; Trigonal bipyramidal complexes
 Transitions 325, 336–7, 341
 Translations 206
 T representations 198, 261
 Triatomic molecules 48, 173, 176, 252, 253
 1,1,1-trichloroethane 58
 Trichloromethane (chloroform) 47
 Trigonal bipyramidal complexes 127, 147–53
 Triphenylphosphine ligand 53
 Tropinone 49
 Tunnelling effect 334, 379
 Ultraviolet (UV) light 164, 173, 181, 291, 343
 Uncertainty principle 358
 Ungerade 101, 172, 228, 238, 286
 Urea 58, 181, 183, 343
 UV *see* Ultraviolet (UV) light
 Valency 241
 Vector dot product 193, 194
 Vertical mirror planes 23
 Vertical transition 180
 Vibrational energy levels 226, 339
 Vibrational excitation 163, 177–8
 Vibrational ground state 163
 vibrationally excited states 341, 342
 Vibrational modes
 basis for 186
 of benzene 5
 of carbon dioxide 176
 of fluorobenzene 5
 of molecules 5, 161, 163, 167, 335–6
 Vibrational spectra 163, 165, 186
 Vibrational spectroscopy 6, 25, 163–217
 Vibrational states 167, 177–81, 325, 339–40
 energy of 333
 stationary 344
 Vibrational wavefunctions *see* Wavefunctions
 Vibronic state 339
 Virial theorem 379–80, 394, 395–7
 Virtual state 178
 Visible frequency light 178
 Water
 absorption bands 169
 antisymmetric stretch 170, 191, 192, 194, 205, 206
 atomic degrees of freedom 110, 112, 122, 123, 125
 basis vectors 108, 110
 bending mode 125, 126, 173, 176
 bond energy for 227
 in hexaaqua complexes 285
 infrared (IR) active modes 169–70, 173
 ‘lone pair’ density 270
 matrix representation 83–6, 91
 molecular orbitals 269–70, 401–405
 motions of atoms 108–9
 multiplication table for 26–9, 40, 43
 O–H bonds in 109, 126, 169, 191, 206
 O–H stretching modes in 109, 156, 191
 O valence orbitals 78, 103, 269
 physical properties 269

- Water (*Continued*)
 planes of symmetry 10, 11
 products of operations 40, 299–300
 proper rotation operation 6
 reducible representation 91–3
 rigid-body movements 123, 125
 rotational degrees of freedom 124
 symmetric stretch 166, 169, 173, 191–2,
 194, 199, 205
 symmetry elements 6, 26, 76, 77
 symmetry operations 6, 27
 symmetry representations and characters
 75–9
 vibrational degrees of freedom 124, 125
 vibrational modes of 122–6
Wavefunctions 168, 225, 240, 244, 325, 335
 amplitude 221
 Born interpretation of 222–5, 229, 231
 for dihydrogen cations 244
 electronic 341
 energy levels for 235
 excited 342
 ground state 342
 for harmonic oscillator 339
 for hydrogen atoms 345, 346
 imaginary numbers in 223, 224, 369, 370
 nuclear 340
 one-electron 231, 346
 orthogonal 333, 334, 336, 341
 phase of 224
 in quantum mechanics 222, 328, 334
 vibrational 342
 zero in 240
Waves 220–2
 see also Wavefunctions
X-ray diffraction 222
Zero-point energy (ZPE) 226, 331, 332, 376